

DTIC FILE COPY



AGARD-LS-174

# AGARD

ADVISORY GROUP FOR AEROSPACE RESEARCH &amp; DEVELOPMENT

AD-A228 899

7 RUE ANCELLE 92200 NEUILLY SUR SEINE FRANCE

AGARD LECTURE SERIES No. 174

## New Light Alloys (Les Nouveaux Alliages Légers)

## DISTRIBUTION STATEMENT A

Approved for public release;  
Distribution UnlimitedS DTIC  
ELECTED  
NOV 26 1990  
C-E D

NORTH ATLANTIC TREATY ORGANIZATION

DISTRIBUTION AND AVAILABILITY  
ON BACK COVER

NORTH ATLANTIC TREATY ORGANIZATION  
ADVISORY GROUP FOR AEROSPACE RESEARCH AND DEVELOPMENT  
(ORGANISATION DU TRAITE DE L'ATLANTIQUE NORD)

AGARD Lecture Series No.174

## New Light Alloys

(Les Nouveaux Alliages Légers)



Accession For	
NTIS GRA&I <input checked="" type="checkbox"/>	
DTIC TAB <input type="checkbox"/>	
Unannounced <input type="checkbox"/>	
Justification	
By _____	
Distribution/	
Availability Codes	
Dist	Avail and/or Special
A-1	

This material in this publication was assembled to support a Lecture Series under the sponsorship of the Structures and Materials Panel of AGARD and the Consultant and Exchange Programme of AGARD presented on 15th—16th October 1990 in Madrid, Spain. 18th—19th October 1990 in Toulouse, France, and 29th—30th October 1990 in Monterey, United States.

# The Mission of AGARD

According to its Charter, the mission of AGARD is to bring together the leading personalities of the NATO nations in the fields of science and technology relating to aerospace for the following purposes:

- Recommending effective ways for the member nations to use their research and development capabilities for the common benefit of the NATO community;
- Providing scientific and technical advice and assistance to the Military Committee in the field of aerospace research and development (with particular regard to its military application);
- Continuously stimulating advances in the aerospace sciences relevant to strengthening the common defence posture;
- Improving the co-operation among member nations in aerospace research and development;
- Exchange of scientific and technical information;
- Providing assistance to member nations for the purpose of increasing their scientific and technical potential;
- Rendering scientific and technical assistance, as requested, to other NATO bodies and to member nations in connection with research and development problems in the aerospace field.

The highest authority within AGARD is the National Delegates Board consisting of officially appointed senior representatives from each member nation. The mission of AGARD is carried out through the Panels which are composed of experts appointed by the National Delegates, the Consultant and Exchange Programme and the Aerospace Applications Studies Programme. The results of AGARD work are reported to the member nations and the NATO Authorities through the AGARD series of publications of which this is one.

Participation in AGARD activities is by invitation only and is normally limited to citizens of the NATO nations.

The content of this publication has been reproduced  
directly from material supplied by AGARD or the authors.

Published September 1990

Copyright © AGARD 1990  
All Rights Reserved

ISBN 92-835-0588-3



Printed by Specialised Printing Services Limited  
40 Chigwell Lane, Loughton, Essex IG10 3TZ

# **Abstract**

The Lecture Series will review developments in research, manufacture and exploitation of new light alloys (based on Aluminium and Magnesium) for structural applications in aeronautics and space.

These new alloys exhibit significant potential for reducing structural weight and are gaining recognition as competitive materials within the aerospace industries.

Topics to be addressed in the lectures include: metal physics and processing aspects, properties of existing materials and prospects for future development and exploitation.

This Lecture Series, sponsored by the Structures and Materials Panel of AGARD, has been implemented by the Consultant and Exchange Programme.

# **Abrégé**

Ce cycle de conférences traitera des développements récents dans les domaines de la recherche, l'élaboration et l'exploitation des nouveaux alliages légers (à base de l'aluminium et de magnésium) pour des applications structurales dans les industries aérospatiales.

Ces nouveaux alliages sont prometteurs d'une réduction en poids des structures et leur compétitivité est de plus en plus reconnue par les industries aérospatiales.

Parmi les sujets qui seront abordés lors de la conférence on distingue: la physique des métaux et les traitements, les caractéristiques des matériaux existants et les perspectives pour le développement et l'exploitation futurs.

Ce cycle de conférences est présenté dans le cadre du programme des consultants et des échanges, sous l'égide du Panel AGARD des Structures et Matériaux.

# List of Authors/Speakers

**Lecture Series Director:** IGA P.Costa  
Directeur Scientifique des Matériaux  
ONERA  
29, Av. de la Division Leclerc  
92320 Châtillon/Bagneux  
France

## AUTHORS/SPEAKERS

**Dr D.J.Bray**  
RAE, Materials & Structures Dept.  
Farnborough, Hants GU14 6TD  
United Kingdom

**Prof. G.Champier**  
Institut Polytechnique de Lorraine  
Laboratoire de Physique du Solide  
Parc de Saurupt  
54042 Nancy Cedex  
France

**Dr Frazier**  
Naval Air Development Center  
Aerospace Materials  
Warminster, PA 18974  
United States

**Prof. S.Harris**  
Dept. of Metallurgy & Material Science  
University of Nottingham  
Nottingham Park  
Nottingham NG7 2RD  
United Kingdom

**Dr G.J.Hildenman**  
Alcoa Technical Center  
Alcoa Center, Pennsylvania 15069  
United States

**Prof. M.Koczak**  
Drexel University  
Dept. of Materials Engineering  
Philadelphia, PA 19104  
United States

**Dr C.J.Peel**  
RAE, Materials & Structures Dept.  
Farnborough, Hants GU14 6TD  
United Kingdom

**Dr W.E.Quist**  
Boeing Commercial Airplane Company  
P.O. Box 3707, M/S 73-43  
Seattle, Washington 98124  
United States

**Prof. E.A.Starke, Jr**  
School of Engineering & Applied Science  
University of Virginia  
Charlottesville  
Virginia 22901  
United States

**Dr J.F.Stohr**  
Direction des Matériaux  
ONERA  
29, Av. de la Division Leclerc  
92320 Châtillon/Bagneux  
France

# Contents

	Page
<b>Abstract/Abrégé</b>	iii
<b>List of Authors/Speakers</b>	iv
	<b>Reference</b>
<b>Introduction</b> by IGA P.Costa	<b>I</b>
<b>The Development of Aluminium Lithium Alloys: An Overview</b> by C.J.Peel	1
<b>The Microstructure and Properties of Aluminium-Lithium Alloys</b> by E.A.Starke, Jr and W.E.Quiest	2
<b>Les Composites à Matrice Métallique à Fibres Longues</b> par J.F.Stohr	3
<b>Developments in Particulate and Short Fibre Composites</b> by S.J.Harris	4
<b>Aluminum Powder Alloys — An Overview</b> by G.J.Hildenman and M.J.Koczak	5
<b>Physical Metallurgy of Aluminium Powder Alloys</b> by G.Champier	<b>6E</b>
<b>Métallurgie Physique des Alliages MP d'Aluminium</b> par G.Champier	<b>6F</b>
<b>Cast and Rapidly Solidified Magnesium Alloys</b> by D.J.Bray	7

## INTRODUCTION

by

**Paul Costa**  
 Materials Department, Head, ONERA  
 BP 72  
 F92322 Chatillon Cedex  
 France

The last fifteen years have been marked by considerable changes in aeronautical materials. One of the main areas of change has been a notable lightening of the structures employed in aircraft design, thereby increasing specific thrust, of principal concern in military aeronautics, for both aircraft and helicopters. Reduction in weight has been achieved in a number of ways; mainly through the increasing use of polymer matrix composites, from the initial small-scale applications involving mechanical parts with a low critical value to the more extensive applications in wings, as demonstrated with current designs for combat aircraft.

Within the last few years, in response to the development of the polymer matrix materials, the main producers of aluminium alloys have once again taken up the development of aluminium-lithium alloys in order to exploit their advantages of low density and high elastic modulus. In fact, these alloys had been known about for some thirty years but major investment was required for their development, especially in production technology. Work in this field has been particularly dynamic and productive. In less than a decade, a fairly low level of understanding of the field has been transformed into the industrial production of new optimised alloys (obtained using highly specialised casting techniques), the development of associated technologies such as superplastic forming and the adoption of these alloys for current aircraft design projects.

A great many meetings have been held on aluminium-lithium alloys over the last five years, but the AGARD Specialists' Meeting organised in Mierlo in October 1988 came at particularly opportune moment. For the first time, it enabled a comparison to be made between existing alloys on the basis of research and characterization studies. These studies were mostly carried out on a cooperative basis by alloy manufacturers and the major research establishments and provided a picture of the industrial developments planned by the aircraft manufacturers.

At the same Meeting, one session (out of five) was devoted to other light alloys. A number of materials have emerged concurrently in recent years: firstly, the aluminium and magnesium base alloys produced by powder metallurgy, often involving rapid solidification routes; secondly, particulate composite alloys (often produced via powder metallurgy routes) and intended for similar applications to the first group, and finally long fibre composites for use in space-flight structures of high dimensional stability, but which may also find a use in certain aeroengine parts or for second generation supersonic (and hypersonic) transport aircraft.

The Lecture Series on New Light Alloys has been organized on the same frame as this Meeting. The speakers have been chosen among the authors of Mierlo, who have of course been requested to update their contributions, due to the elapsed time (approximately two years). Beyond the total duration, which has been slightly reduced, the main difference between the two events lies in the general equilibrium between the various parts: the aluminium-lithium alloys will be this time treated as one of the considered alloy families - though undoubtedly the most important -, and Dr. C.J. Peel (Royal Aeronautical Establishment), who had formerly the task of giving a final synthesis of the contributions to the Specialists' Meeting, will give an overall review of the state of the art in this field, which will be followed by a talk by Pr. E.A. Starke Jr. (University of Virginia) more specifically devoted to the physical metallurgy of these alloys. Conversely, composites will be more extensively treated; half a day will be devoted to this subject, with a talk on long-fibre composites by Dr. J.F. Stohr (ONERA) and another one on particulate aluminium-matrix composites, materials which are along with aluminium-lithium alloys closest to application, due to their relatively low cost, by Pr. Harris (Nottingham University).

The second day will be exclusively devoted to powder-metallurgy aluminium and magnesium alloys with, for the first metal, an overall review by Pr. Koczak (Drexel University) and an account of some physical-metallurgy aspects by Pr. Champier (Institut Polytechnique de Lorraine, Nancy), and finally a presentation of the new magnesium alloys by Dr. D.J. Bray (Royal Aeronautical Establishment).

A round-table, interacting with the audience, will end this event.

## INTRODUCTION

par

**Paul Costa**

Ingénieur Général de l'Armement  
Directeur des Matériaux à l'ONERA (France)  
BP 72  
F92.322 Chatillon Cedex  
France

La période de quinze ans qui s'achève a été marquée par un renouvellement considérable des matériaux aéronautiques. L'une des lignes de force de cette modification est l'allègement des structures qui contribue à l'augmentation de la poussée spécifique, préoccupation centrale de l'aéronautique militaire, tant pour les avions que pour les hélicoptères. Diverses solutions sont apparues : application tout d'abord à des composites à matrice polymère à des parties d'importance croissante, dans un premier temps éléments peu critiques sur le plan mécanique, puis progressivement parties de la voilure, notamment dans les avions de combat actuellement en cours de conception.

A quelques années d'intervalle et en concurrence des matériaux précédents, les principaux producteurs d'alliages d'aluminium ont repris le développement des alliages aluminium-lithium, alliages de densité et de module d'élasticité très favorables. Ces alliages étaient connus depuis une trentaine d'années, mais leur mise au point et plus encore leur production exigeaient des investissements importants. Les études dans ce domaine ont été particulièrement actives et fructueuses puisque l'on a su, en guère plus de dix ans, parcourir tout le trajet séparant un niveau initial de connaissances assez fruste, de la production industrielle d'alliages nouveaux optimisés, obtenus par des technologies de coulée très particulières, du développement de technologies connexes comme le formage superplastique, et de l'insertion dans les projets en cours de nouveaux avions.

De nombreuses réunions se sont tenues au cours des cinq dernières années sur ce thème. La Réunion des Spécialistes qui s'est tenue dans le cadre de l'AGARD à Mierlo en octobre 1988 est intervenue à un moment tout à fait opportun, dans la mesure où elle a permis pour la première fois une comparaison entre les alliages existants, sur la base des recherches et des caractérisations, menées souvent sur le mode coopératif, par les industriels et les grands établissements de recherche, et de faire le bilan des développements industriels envisagés par les constructeurs aéronautiques.

Parallèlement, il a paru utile de consacrer une partie de la réunion - en fait une session sur cinq - à d'autres matériaux dérivant des alliages légers. Plusieurs autres familles sont en effet apparues concurremment au cours des dernières années : alliages d'aluminium ou de magnésium, produits par métallurgie des poudres, et relevant le plus souvent de techniques de refroidissement rapide, alliages composites particulaires, proches des précédents tant par la technologie (métallurgie des poudres) que par les applications, composites à fibres longues, applicables aux structures spatiales de grande stabilité dimensionnelle, mais qui peuvent également trouver un emploi pour certains éléments de moteurs aéronautiques, ou des avions de transport supersoniques de seconde génération - voire hypersoniques.

La Série de Conférences (Lecture Series) sur les nouveaux alliages légers a été organisée dans le droit fil de cette réunion. Les conférenciers ont été choisis parmi les intervenants de Mierlo, auxquels il a été demandé bien entendu d'actualiser leur exposé en raison du temps écoulé (deux ans environ). Outre la durée, un peu réduite, la différence principale entre les deux événements réside dans l'équilibre général entre les diverses parties : les alliages aluminium-lithium seront cette fois traités comme l'une des familles d'alliages envisagés - sans doute la plus importante -, et il a été demandé au Dr. C.J. Peel (Royal Aeronautical Establishment), à qui il était revenu précédemment de faire la synthèse des interventions lors de la réunion de spécialistes, de donner une revue globale de l'état de l'art dans ce domaine, revue qui sera suivie d'un exposé plus particulier du Pr. E.A. Starke Jr. (Université de Virginie) sur les aspects relevant de la physique métallurgique de ces alliages. A contrario, il a été prévu de s'étendre davantage sur les composites, auxquels sera consacrée une demi-journée avec un exposé sur les composites à fibres longues de M. J.F. Stohr (ONERA) et un autre exposé sur les composites particulaires, à matrice aluminium, qui sont sans doute avec les alliages Al-Li le matériau dont l'application est la plus proche, en raison de son coût relativement limité.

La seconde journée sera exclusivement consacrée aux alliages légers d'aluminium et de magnésium obtenus par métallurgie des poudres, avec pour le premier métal une revue de synthèse par le Pr. M. Koczak (Drexel University) et un exposé sur la physique métallurgique du Pr. Champier (Institut Polytechnique de Lorraine, Nancy), et enfin une présentation des nouveaux alliages de magnésium par le Dr. D.J. Bray (Royal Aeronautical Establishment).

Une table ronde, en interaction avec l'audience, terminera cette manifestation.

## THE DEVELOPMENT OF ALUMINIUM LITHIUM ALLOYS: AN OVERVIEW

C J PEEL

MATERIALS AND STRUCTURES DEPARTMENT  
ROYAL AEROSPACE ESTABLISHMENT  
FARNBOROUGH HANTS UK GU14 6TD

### INTRODUCTION

For the last decade the aluminium industry has been redeveloping aluminium-lithium alloys for aerospace use. Whilst not new in concept or in technology, these alloys would appear to offer the aircraft designer as much weight saving as non-metallic composite materials with the added advantage of the continued employment of well developed manufacturing routes supported by existing expensive equipment. It is clear that, were it not for significant technical and production difficulties, many of the airframes produced today would already be manufactured in aluminium-lithium alloy. This paper will attempt to highlight, not only the property advantages that enable very significant weight savings to be achieved, but those difficulties that are being slowly overcome by intensive effort. The scale of this effort can be judged by the fact that the last of the five International Conferences, held exclusively on aluminium-lithium alloys, produced over 1700 pages of print (1). It is far beyond the scope of this paper to comprehensively review this aggregated volume of work but an attempt is made to précis those aspects thought by the author to be most relevant to the successful outcome of the development.

### HISTORICAL DEVELOPMENTS

Lithium additions have been made to aluminium alloys since the 1920's. Early work included inconclusive evaluations of lithium as a strengthening addition to aluminium (2) and the effects of lithium as a trace addition in alloys hardened by other elements (3). However, the first known reference (4) to highlight the potentially attractive properties of alloys containing more than 2wt % lithium, i.e. with a major density reduction, did not appear in the United Kingdom until 1960, and was seemingly contemporary with Russian work on aluminium-magnesium-lithium alloys. The Russian work culminated in British and French patents in 1969 (5). In North America interest in the value of lithium additions had slowly developed around the perceived strengthening effects of small lithium additions to the aluminium-copper system with the 1942 patented example (6) of LeBaron illustrating the strengthening effects of a combination of approximately 1% lithium with a trace element such as cadmium, indium or tin. This theme was further investigated by Hardy and Silcock (7) and, in 1957, Alcoa introduced the commercial X2020 variant as an aerospace alloy exhibiting high compressive strength and stiffness with a modest reduction in density. This alloy achieved some limited application

and performed well (8), although the perception at the time was that the alloy was brittle. A new plot of contemporary data reveals that, although the 2020-T6 may have exhibited low toughness, it was being used in a very strong condition and not was not dissimilar in its relative performance to other high strength alloys [ Fig.1 ]. Activity in France at this time resulted in a patent by Pechiney covering a process to reduce oxidation during the melting of aluminium-lithium alloys. Work on both sides of the Atlantic continued in the 1960's with detailed investigations of the trace element strengthening effects of lithium additions, with a notable contribution (9) by Silcock, and began during the 1970's to emphasize the value of density reduction achieved with higher levels of lithium addition. By the late 1970's focussed alloy developments had been started with density reduction as a major theme with strong contributions funded by Industry and Government in North America and, to some extent in Europe. Developments during the 1980's have become increasingly commercial with the emergence of major new alloys based on the targets of the late 70's. The performance and characteristics of these new alloys is the major theme of this paper.

#### CONCEPTUAL DESIGN ASPECTS

##### Structural Design Concepts

With the realisation that aluminium-lithium alloys could be developed to directly exploit their reduced density, in contrast to the exploitation of elevated mechanical properties, it is noteworthy that the Russian alloy now designated 1420 was both early in its development and application and still exhibits one of the lowest densities available for a commercial alloy. Compositions and densities of some selected variants of these early alloys illustrate this point [ Table 1 ]. Considerable attention had been paid to design studies during the 1970's and these appeared to reinforce the concept of density reduction as the main driving force behind the development of aluminium-lithium alloys. This is typified by the Lockheed design data (10) [ Fig.2 ] which reveals that weight savings achieved with density reduction far outweigh the savings gained from a similar proportional increase in mechanical properties. Detailed design studies (11) predicted that aluminium-lithium alloys meeting predefined alloy development targets would be able to produce weight savings of the order of 8%-15% by a combination of density reduction and property enhancement [ Fig.3 ]. A retrospective study of these claimed potential weight savings compared to those actually achieved in demonstrator and prototype parts reveals that, in general terms, they were accurate and that savings of up to approximately 15% are achievable with aluminium-lithium alloys competitive with most advanced materials including the non-metallic composites.

Structural designs that were optimised to exploit aluminium-lithium alloys were found to require the new alloys to exhibit the same range in properties that had long since been developed in conventional alloys. This requirement allowed the concept of alloy

substitution to be developed. In this technique literal substitution of an aluminium-lithium alloy for a conventional alloy could be contemplated with, all things being equal, an immediate weight saving accrued from the density reduction. The concept could be further extended to new design in which a notional substitution, of a new alloy for the conventional, could be made to exploit both the reduction in density and also any property improvements.

Substitution, in this case, would be on the basis of alloy type for alloy type, i.e. a damage tolerant aluminium-lithium alloy would be chosen where, conventionally, a damage tolerant material such as 2024-T3 would have been used. Whilst, in design terms, this concept might well prove to be extremely effective allowing easy embodiment of the new alloys, it has the disadvantage of producing a requirement for the new alloys to meet many, quite different, alloy specifications. For example, aluminium alloys are used at relatively low strength levels, in a damage tolerant role, at intermediate strength levels as a general engineering material, where perhaps specific stiffness might be most important and, finally, there is a relatively wide range of high strength alloy variants.

The distribution of usage of alloys in these three categories is illustrated [ Table 2 ]. Because aluminium alloys are used in a variety of product forms including sheet, plate, extrusion, forgings and tubes etc. the problem is compounded into a requirement for all these product forms operating at the different property levels outlined. Additionally, individual aerospace companies, as potential users of the material, have raised their own house specifications often subtly different from those of their competitors. The complexity of the situation, as perceived for the UK alloys, is illustrated [ Fig.4 ] but the same mutiplicity of option faces all the other aluminium-lithium alloy suppliers, further compounding the problem of too many alloys in too many forms.

#### Cost of Material and Manufacture

The second major issue in conceptual design terms is the cost of manufacture using aluminium-lithium alloys. Conventional aluminium alloys have dominated in the manufacture of aircraft structure for decades perhaps because of their combination of good technical properties, low material cost and relative ease of manufacture. Whilst the debate will continue, as to the relative technical merits of non-metallic versus metallic airframe construction, ultimately decisions on the applications of these new materials will probably be based on cost of manufacture. In this respect advanced composites, both metallic and non-metallic, and aluminium-lithium alloys are intrinsically expensive materials. With the addition of up to 3% by weight lithium, these new alloys would appear to have to carry a premium of at least 100% in the cost of the raw material. It is clear that the efficiencies of production and of utilisation of this more expensive material must better those of conventional aluminium alloys, if at all possible, to attempt to offset the initial premium on material cost. At present

ingot sizes are relatively small and production routes somewhat specialised but, in principle, improvements in this area do not appear to be impossible since considerable attention has been given to fabrication processes during production, forming and finishing techniques and associated heat treatment practices. Moreover, the predicted relatively high cost of the aluminium-lithium alloys has concentrated attention on product forms that potentially can yield high levels of utilisation such as extrusions, sheet and die forgings and somewhat discouraged the development of thick plate.

Detailed considerations of the effects of material cost in the cost of aircraft manufacture reveal that, in addition to utilisation rate, the intrinsic value of the scrap that is produced is a major issue. Significant efforts have been made to generate a scrap recovery system for the emerging aluminium-lithium alloys and to develop cost effective technology for the reclamation of the valuable ingredients of the alloys for re-use (12). Considering that major airframe manufacturers may well convert half of the aluminium-lithium alloy that they purchase to scrap and that, if all continues successfully, they may well be purchasing thousands of tonnes of metal per year, it can be seen that this issue is of major importance. The scrap cycle is illustrated [ Fig.5 ] following the paper of Little (13).

#### ALLOY CHEMISTRY AND MANUFACTURING METHODOLOGIES

##### Alloy Chemistry

A range of new aluminium alloys containing lithium has slowly evolved over the last decade. In addition to the Al-Mg-Li alloys typified by the Russian development of 1420 alloy, the Al-Cu-Li alloy originally developed in North America as 2020 has been extended to greater lithium concentrations in the newer 2090 alloy. The Al-Cu-Mg-Li series was found to offer promise by research on both sides of the Atlantic and alloys such as 2091 and 8090 have developed, although the latter should be strictly described as an Al-Li-Cu-Mg alloy. The compositions of these alloys are listed [ Table 1 ] with their densities. It can be seen that the two development themes earlier identified have continued. Those, with a higher lithium addition such as 1420 or 8090, are aimed at maximising the density reduction by lithium addition, whilst those such as 2020 or Weldalite seek to exploit trace element effects of the addition of the lithium in perhaps inducing greater levels of precipitation. Whilst attention in this paper is focussed on registered alloys undergoing commercialisation it should be realised that they represent a very small selection from a very large body of candidate alloys, too large to be encompassed in detail in this paper.

Alloys developed specifically to suit manufacturing routes that can exploit rapid solidification technology and mechanical alloying practice should also be included and a limited selection is listed. Once again the list of experimental alloys disclosed in the literature is large.

Finally, it may be the case that future developments (14) might see the use of aluminium-lithium alloys as the basis of metal matrix composites reinforced with the addition of ceramic material in particulate or fibre forms.

### Ingot Manufacturing Technology

It should be understood that the new aluminium-lithium alloys have been primarily aimed at the bulk airframe manufacturing market which, inevitably, requires the routine production of large quantities of metal, often in relatively large pieces, that is an ingot manufacturing route is seemingly required. However, the high reactivity of lithium, especially when present in molten aluminium alloy, with atmospheric oxygen and water vapour has caused considerable production difficulties. These include very rapid reaction at melt surfaces with the potential for inclusion of oxides, nitrides and carbonates in the melt, the reaction of the melt with foundry materials, crucibles, linings and moulds and apparently an increased explosion risk (15). The manufacturers have clearly had to develop methods to control the reaction of lithium with the atmosphere in the casting process. The results of a large body of trial explosions conducted jointly by Alcan, RAE and the University of Aston to assess the sensitivity of the reactions between molten aluminium-lithium alloys and water must remain mainly proprietary, but the effect of lithium in reducing the surface tension of the molten alloy immersed in water can be seen [ Fig.6 ].

### Rapid Solidification Technology and Mechanical Alloying.

Alternative routes for production have also been developed (16-18) including spray and jet casting, powder metallurgy and mechanical alloying, in part to circumvent some of the ingot metallurgy production difficulties and partly to attempt to take some benefits from the extra alloying potential of rapid solidification and related techniques. In discussing the value of these more elaborate production techniques, two features seem to require investigation. Namely, whether the advanced production route circumvents production difficulties, such as the inclusion of flux or oxides in casting, or introduces more problems of its own such as the inclusion of oxide stringers derived from the particle surfaces for example. Secondly, whether the increase in cost normally associated with a more advanced technique is justified by an increase in properties of value to the structural designer. Some of the properties of the current alloys produced by these advanced techniques are included later and it can be seen that, in general terms, their balance of properties is somewhat similar to those of the ingot metallurgy material. i.e. whilst there may be some significant gains in the area, for example, of stress corrosion resistance (18) there are losses in fracture toughness or resistance to fatigue crack growth. Strength levels and density reductions appear to be aimed at the same levels for ingot metallurgy and rapid solidification materials.

Indeed, to some extent, the performance of the alloys can be judged to be independent of the method of manufacture such that there is some evidence (16), for example, that 8090 Al-Li-Cu-Mg alloy can be produced via the ingot metallurgy route or by spray casting to yield similar properties. It may be that, at least in the author's opinion, rapid solidification per se is of little intrinsic value in the aspect of increasing the lithium content in aluminium-lithium alloys because the limiting feature is not a lack of solid solubility but the damaging nature of the addition of lithium to the mechanical properties. That is ingot alloys already contain in the region of 10% lithium (atomic) at the tops of their composition ranges. To achieve significant density reductions by the addition of, for example, 15% lithium would produce major property reductions, particularly fracture toughness. Materials that are mechanically alloyed would appear to be optimised (18) for the process which is expected to include oxides and carbides in the material and possess natural limitations to the composition that may be successfully alloyed as a consequence of its processing route.

There remains the special issue as to the potential of the rapid solidification routes to improve the performance of aluminium-lithium alloys at elevated temperatures. This is addressed, to some extent, in the Section on elevated temperature properties.

Additionally, it may be the case that the combination of particulate reinforcement and an aluminium-lithium alloy matrix will produce a very high performance metal matrix composites, suitable for high temperature applications (14). These materials are judged to be beyond the scope of the present paper. Whatever route is chosen for production of the new aluminium-lithium alloys, it is imperative that the metallurgical quality of the ingot or billet is sound to enable premium quality aerospace materials to be produced. In the author's opinion, it is in this aspect that most problems have arisen.

### Oxidation and Lithium Loss

One of the root causes of many of the production difficulties would seem to remain the rapid oxidation of the lithium content of the molten alloy. Even in the solid state, loss of lithium by oxidation at the surface has posed problems. The combined reduction of lithium and magnesium contents at the surfaces of metal heat treated at high temperatures has led to the formation of what are now referred to as "lithium depletion zones" in which the grain structure of the alloys can be seen to be coarsened and the micro-hardness reduced [Fig.7]. The surface zone of reduced solute content and coarsened grain could well deleteriously affect the strength of thin sheet products and there have been several studies quantifying the rates of lithium depletion. The presence of water vapour in the atmosphere of the heat treatment furnace seemingly increases the rate of reaction considerably and can lead to the formation of lithium hydride (21). However, this understanding has

enabled thin sheet products to be produced and heat treated successfully without significant degradation in properties and, most encouragingly, there have been confirmed reports (22) that the presence of a lithium depleted zone does not apparently adversely affect the fatigue performance of the sheet metal. [ See Section on Damage Tolerance ]

A related concern, to those of claimed added explosion risks in the foundry and of lithium depletion, has been the performance of the materials in high temperature salt baths. Here it had been surmised that lithium contamination of the baths might produce a deleterious build-up of lithium salts in the bath or that the alloys might, in some way, cause an instability in the bath, even an explosion. Carefully staged trials (23) of aluminium-magnesium and aluminium-lithium alloys, the latter containing up to 10 wt% lithium addition, revealed that instability occurred in the baths when the bath temperature was sufficient to melt the alloy being heat treated. In the respect that the melting points of the aluminium-lithium alloys were significantly higher than those of the aluminium-magnesium alloys, the lithium-bearing alloys could be deemed safer than the conventional alloys. In the further respect that the melting points of the aluminium-lithium alloys exceed the safe maximum working temperatures prescribed for the nitrate salt baths, typically 550°C, it could be stated that no new problem had been uncovered beyond the normal requirements for the safe operation of heat treatment salt baths.

There remains the general concern in the aluminium alloy industry that contamination of conventional alloys by aluminium-lithium scrap will affect the properties of the conventional materials and a series of proprietary trials have investigated this point. Perhaps most at risk are special product forms such as welding wire, where the presence of lithium contamination could prove critical and sheet and foil with highly polished finishes that may prove to be vulnerable to blooming caused by the rapid oxidation of lithium contamination. These issues have been studied and are to some extent controlled by the management of lithium containing scrap and to some extent of less consequence than first feared.

#### PHYSICAL PROPERTIES

Three physical features of aluminium-lithium alloys require particular comment. Firstly, significant attributes are the reduction in density and the increase in elastic modulus achieved with the addition of lithium to aluminium alloys.

Currently, commercial alloys contain up to approximately 10% atomic concentrations of lithium (equating to approximately 2.75% by weight) producing a density reduction of approximately 10% because of the very low density of lithium ( 0.53 g/cc ).

To aid in the prediction of alloy density from composition or in checking alloy composition, in particular lithium content, from density, the author developed the following expression (24) for

alloy density by assuming that each elemental addition would contribute mass and volume in accord with its concentration and individual density:-

$$\text{Density, g/cc} = 2.71 - 0.079\text{Li} + 0.0245\text{Cu} - 0.010\text{Mg} + 0.018\text{Zn}$$

where the atomic symbols represent the concentration of those elements in weight percent. This formula has proved sufficiently accurate to predict densities to  $\pm 0.005$  g/cc and a plot of predicted densities against those determined practically is included [ Fig.8 ]. The great value, in terms of saving weight in new designs, by exploiting reduced densities should perhaps be restated, noting that alloy chemistries have been included in this plot that extend the density reduction beyond that achieved with 1420 or 8090 alloys.

The increase in modulus with lithium addition is also well documented and the mechanism of the increase has also been addressed to some extent (25). The levels of lithium addition achieved in practical alloys would appear to limit the achievable modulus to approximately 80 GPa [ Fig.9 ]. Further extensions beyond this level would appear to require the use of rapid solidification techniques or additions of ceramic reinforcements. It would appear that the elastic modulus of the aluminium-lithium alloys is reduced slightly and continuously by artificial ageing, consistent with the principal stiffening influence of the lithium addition being in solid solution form [ Fig.10 ] and by elevation of the test temperature.

The addition of 10% (atomic) lithium also has a marked effect on thermal and electrical conductivities [ Table.3, Figs.11 and 12 ]. The reduction of electrical conductivity to approximately half that of a conventional aluminium alloy (24) could potentially pose problems in the performance of structure struck by lightning. For example, if the minimum gauge of sheet permitted is controlled by electrical conductivity to withstand lightning strikes then the weight loss achieved with the application of aluminium-lithium may be lost by the need to increase gauge for conductivity reasons. Low thermal conductivity may also produce some difficulties in terms of the length of time required for heat treatment and in limiting gauges of metal that can be used without problems of quench sensitivity. The quench sensitivity of the current alloys has been studied in some detail and it would appear that the richer alloys are vulnerable to the precipitation of copious quantities of embrittling T1 phase amongst others (26,27).

#### MECHANICAL PROPERTIES

It was indicated previously that several categories of aluminium-lithium alloys could be selected on the basis of their mechanical properties i.e. low strength alloys with high toughness or damage tolerance, medium strength and high strength alloys. The necessity for this selection of categories arising from the natural inverse relationship of properties such as toughness and strength.

## Damage Tolerant Alloys

Two materials would appear to be contending in the important category of damage tolerant alloys suited for potential applications such as lower wing skins and fuselage skinning. These are both Al-Cu-Mg-Li alloys, 2091 and 8090, and both are seemingly capable of producing high toughness at modest strength levels (28,29). Additionally, both offer extremely good resistance to fatigue crack growth under representative conditions. This latter aspect being most important, being a major attraction of the incumbent 2024-T3 alloy which, if they are to be successful, the new alloys must replace. Two types of grain structure, with subtly different properties should be included. Sheet, would seem to offer the best combination of damage tolerance properties when recrystallised and in an under-aged condition. Thicker gauges, such as thin plate or extruded material would seem to be offered in an un-recrystallised and under-aged condition. The gauge at which the change in structure occurs is dependent upon the manufacturer and the alloy. Controlled stretching, before ageing, appears to be beneficial to the combination of strength and fracture toughness. Tensile properties for these two damage tolerant alloys are included [ Table.4 ] for the T81/T8151, stretched and aged conditions. However, it should be noted that, by accepting a reduction in strength level, 2091 can be used in a naturally aged condition to produce a high level of fracture toughness and relative ease of manufacture, potentially suitable for damage tolerant applications where strength is not critical. On the other hand, the lighter, more dilute 8090 (in terms of copper and magnesium contents) proves to be more stable enabling forming to be conducted in the T3 condition with greater ease.

The key aspects of fracture toughness, represented by the  $K_r$ , crack resistance curve, and the resistance to fatigue crack growth are summarised in comparison to the performance of clad 2024-T3 sheet [ Figs.13-16 ]. It can be seen (28-32) that both the selected aluminium-lithium alloys can offer, potentially, a very high resistance to fatigue cracking under constant amplitude conditions and to fast fracture of long cracks, i.e. good fracture toughness. The very high fracture toughness levels achieved in conventional damage tolerant alloys and in the new aluminium-lithium alloys has enforced the use of very large test pieces to attempt to obtain validity in Linear Elastic terms. Plane stress  $K_r$  curves have now been obtained by several independent bodies (33,34), including those for panels up to 2m in width obtained by RAE. Plane strain fracture toughness results are frequently found to be invalid because of the limitations imposed on test piece size by plate gauges, but  $K_g$  values can be quoted at representative gauges for potential applications.

It seems to be clearly established that the resistance of the aluminium-lithium alloys to fatigue crack growth under constant amplitude loading is significantly better than that exhibited by the conventional alloys. It is seemingly the case that the reasons

for this improved resistance to fatigue crack growth stem, in part, from the increased level of elastic modulus but, principally, from the propensity of the alloys to undergo plastic deformation in a planar slip mode (35-38). That is, in the fatigue crack growth process, the plastic deformation is concentrated on slip planes of preferred crystallographic orientations producing faceted fatigue crack fractures and crack growth at acute angles to the loading direction. This type of fracture occurs in a most pronounced manner at levels of stress intensity factor where the plastic zone size is of the order of the grain size of the alloy and seems to be maximised for the T-L stressing orientation. The tortuous crack path increases the likelihood of crack closure effects on the unloading portion of the fatigue cycle and as such the advantages of the lithium containing alloys over the conventional diminish at high mean stresses. The appearance of this tortuous crack path, crack closure and shielding effects therefore control the extent to which the aluminium-lithium alloys can outperform the conventional in fatigue crack growth resistance and features such as stress level and crack length, stress ratio, programme loading and environment will all prove important in controlling crack growth rates.

Of particular importance, in the author's opinion, is the resistance of the aluminium-lithium alloys to the growth of fatigue cracks at low levels of stress intensity factor, whether at long or short crack lengths. This is because in the practical situation of the initiation and growth of many small cracks at neighbouring fastener holes, the short crack growth behaviour will determine, to a large extent, the all-critical crack growth life. A distinction needs to be drawn between the short and long crack situations, since for long cracks the advantage of the lithium-bearing alloys is maintained whilst in the situation of short cracks, close to the origin, the crack deviation and shielding mechanisms do not necessarily produce such low crack growth rates (39,40). However, further work may well be required in this area because many studies of short crack growth behaviour naturally use field stresses that are high in relation to general levels of stress applied in practical structures and, for example the use of J integral rather than linear elastic fracture mechanics has been found to be more appropriate (40). Studies (41-44) have also been conducted into the resistance of these new alloys under programmed load conditions and in environments, more aggressive than the conventional laboratory air. It would seem that, to some extent, both the application of mixed loading levels, in the programmed load sequences, and the presence of an aggressive environment speed up the rates of fatigue crack growth relative to the 2024-T3 control alloy. However, in many cases, the aluminium-lithium alloys maintain an advantage over the existing alloys but perhaps on a reduced level. In the case of programmed loading, it can be seen from the constant amplitude loading data that the crack deviation effects are maximum at intermediate levels of stress intensity factor, associated with a critical size of plastic zone, and that a combination of programmed cycles at stress intensity levels above and below this critical regime, as well as in it, may well produce a crack straightening

effect. That is, in particular, occasional cycles of high range in stress intensity factor might well straighten a deviant crack, the effects of the application of many small cycles being less obvious. In this respect it is claimed (45) that the inclusion of single compressive overloads is significantly more damaging to the fatigue crack growth resistance of 2090 than to conventional alloys but that the response to tensile overloads is better. However, compression dominated programme loaded spectra can still show advantages for aluminium-lithium alloys against conventional control alloys.

It would appear that, in terms of resistance to fatigue crack growth, the aluminium-lithium alloys appear to possess a distinct advantage over the conventional damage tolerant materials, especially when the constant amplitude case is considered. It could be argued that it is this constant amplitude cycling that is most important in that it represents the ground-air-ground aircraft cycle which can produce a predominant contribution to the accumulation of aircraft fatigue damage.

Whilst, on a microscopical scale this effect of planar slip on the nature of fatigue crack growth has given the aluminium-lithium alloys a distinct advantage, the combination of the propensity to planar slip and a pronounced crystallographic texture would seem to give rise to longer range, macroscopic crack turning effects which may cause problems in structures, where a prediction of crack growth direction is of importance (46). That is examples have been produced, for all of the commercial alloys, of fatigue cracks that produce a major change in growth direction away from the normal to the applied stress. It would seem that the control of crystallographic texture can induce or prevent this effect in recrystallised sheet according to the strength of the texture. This is illustrated [ Fig.17 ] for three sheets of 8090-T81 alloy with selected crystallographic textures. Crack turning would seem to be related to the strength of the texture and techniques that reduce the textural intensity seem to prevent crack turning, but the exact mechanism of the phenomenon is still being sought.

In terms of conventional fatigue life, S-N data, which is dominated by crack initiation behaviour, aluminium-lithium alloys appear (47,48) to behave as any conventional aluminium alloy, that is their performance is controlled by aspects of surface quality and the acuity of surface stress concentrations [ Figs.18,19 ]. It would appear (49,50) that, in the respect of their sensitivity to local chemical attack during anodising or pickling for example, the aluminium-lithium alloys are less sensitive than some of their conventional counterparts. This, in practice, may well lead to small benefits in fatigue life for components given conventional workshop finishes. Similarly, the new alloys appear to respond to techniques such as cold working of the surface of notches or holes to improve fatigue resistance and they seem no more susceptible to fretting fatigue (51). Only a few studies of the performance of the alloys in joints are available (52,53) that of Zink et al indicates that that of damage tolerant 8090 can equal or better that of 2024.

In studying the effects of surface quality on fatigue life, several definitive studies (54-55) have been made on the effects of lithium depletion on fatigue life, stemming from concerns that soft surface layers, such as pure aluminium cladding on conventional alloys, significantly reduce fatigue strengths [ Fig.20 ]. These studies seem to show that lithium depletion does not significantly reduce fatigue strength, certainly in the case of tension-tension stressing, although there are some indications that, under the extreme conditions of bending stressing, some effects of the depletion layer can be detected. Nevertheless, it would appear to be the case that under notched or plain fatigue conditions, aluminium-lithium alloys are likely to perform as well, if not better, than conventional alloys. At present, it is not advised that fatigue working stresses are increased for aluminium-lithium alloys beyond the level that would be applied for conventional alloys despite their apparently increased fatigue performance.

#### Medium Strength, High Stiffness Alloys

A considerable proportion of an aircraft structure is constructed of medium strength general purpose alloy, typified by 2014-T6 or perhaps, 2024-T8. In many cases, stiffness is a critical property in this category as may also be the limitations imposed by minimum gauge. That is, with the thinner gauges of sheet material, structure may well become stiffness critical and strength levels and fatigue performance are unimportant, provided they exceed a certain minimum level. High strength levels may be of little use, because, to exploit very high strength levels, very thin metal may be required ( e.g. < 0.3mm thick ), thinner than can sensibly be manufactured or assembled into structure. With their reduced density and increased stiffness, aluminium-lithium alloys appear very attractive in this category. Comparison of the specific stiffness of some selected aluminium-lithium alloys with conventional alloys is made [ Fig.21 ] revealing a 25% advantage over conventional aluminium-zinc alloys. Advantage of the increased stiffness and low density can also be taken in structure that is prone to elastic buckling, where approximately 15% weight savings can be made.

Achievement of the required levels of strength in the medium strength category can be obtained from a range of alloys and heat treatment practices (56-58) [ Table.5 ]. Seemingly both recrystallised and un-recrystallised sheet and extrusion can produce the required performance, but plate and forgings would normally be unrecrystallised. The major requirement has been to attempt to balance the properties of these alloys to optimise the combination of strength, toughness and corrosion performance. In terms of the usual design properties such as strength and toughness in the longitudinal and transverse directions, few problems exist. However, a closer inspection reveals problems with pronounced anisotropy in property levels, particularly in unrecrystallised sheet, such that in extreme cases, a 100 MPa drop in strength can be observed (59) at angles in between the longitudinal and

transverse [ Fig.22 ]. This effect afflicts all the aluminium-lithium alloys produced by the ingot metallurgy route to variable extents that depend upon the degree of recrystallisation and precipitation. That is, it is once again the result of the combination of a propensity to planar slip and the presence of a strong crystallographic texture.

Recrystallisation reduces the anisotropy significantly in the case of sheet [ Fig.23 ] and heavy precipitation of phases such as the S phase ( $\text{Al}_2\text{CuMg}$ ) can be used to block planar slip producing isotropic behaviour. The use of stretching, before ageing, and duplex precipitation treatments (60) can encourage this type of desired precipitation and is the more effective in plate and extrusions, where stretching before ageing is virtually universally applied. The anisotropy of tensile properties and, to some extent, of fatigue properties has been checked in plate material both in terms of variation of properties in the plane of the plate and in terms of variation in planes tested at selected levels through the plate (61). In common with other thick section alloys grain refined with a zirconium addition, variations have been found, but, as with the conventional alloys the lowest property levels measured, appear to just achieve the specified minimum property levels required.

In thicker section materials further problems arise in the need to obtain high performance in the short transverse direction. Tensile ductility, fracture toughness and stress corrosion performance are the obvious measures of quality, but short transverse fatigue strength and fatigue crack growth resistance have also been checked. There seems little doubt that acceptably good levels of short transverse ductility have been reproducibly obtained [ Table.5 ] but also that, on occasions, the ductility in this direction falls to zero reflecting difficulties in obtaining the desired quality of material in the cast ingots. Poor ductility in this direction is associated with reduced strength as is common with all ductile metallic materials.

The fatigue strengths and resistance to fatigue crack growth in the short transverse direction do not seem to be deficient. Indeed, in comparison with conventional alloys produced and finished with representative pickling and anodising treatments, the aluminium-lithium alloys seem to be at least as good, if not better than the high strength aluminium-zinc alloys that provided a natural comparison [Fig.24 ]. In this respect, the low level of quench sensitivity exhibited by the dilute 8090 alloy has proved a major benefit. The situation with regard to short transverse fracture toughness is not so clearly satisfactory however. Whilst acceptable levels of S-L fracture toughness in excess of 18 MPa/m have been demonstrated and, on occasion, high levels approaching 30 MPa/m have proved possible, there remains the general consensus that the short transverse toughness of aluminium-lithium alloys is lower than that of the conventional alloys at the same strength level. In the author's opinion it would seem that obtaining high toughness in this direction has proved possible, establishing that there is no fundamental inadequacy in the aluminium-lithium alloy system, but

that the high level of variability demonstrated indicates a certain lack of understanding and metallurgical control. Some of this variability may well stem from data obtained with early cast material, in which the ingot quality might legitimately be questioned and in this particular circumstance poor toughness can be correlated with poor short transverse ductility. However, there remain problems even in plate with demonstrably good quality. Firstly, it can be seen that short transverse fracture toughness decays with artificial ageing. This is common to all high strength aluminium alloys that are precipitation hardened. After a period of ageing the S-L toughness appears to reach a low plateau value and little change occurs thereafter (62) [ Fig.25 ]. In this respect the aluminium-lithium alloys behave most like the aluminium-copper alloys. It would seem that the rapid initial decay in toughness is associated with the strengthening of the matrix and the concentration of deformation at the grain boundaries and that the very slow decay along the plateau with further ageing is associated with the slow precipitation of coarse particles of intermetallic phase on the grain boundaries. It has been discovered (63) that a short "reversionary" ageing treatment can demonstrate a startlingly powerful effect on the S-L toughness almost irresepective of the aged condition of the material to which it is applied [ Fig.26 ]. There are several explanations proffered for this phenomenon.

In addition to these recognised effects of ingot quality and precipitation, there has appeared a body of evidence (64-66) that suggests that the aluminium-lithium alloys are more prone, in some way, to embrittlement by alkali metal impurities additional to the deliberate lithium addition. The mechanism proposed for this effect is that of liquid metal embrittlement, in which phases containing, for example, sodium and potassium are in a molten state in the grain boundaries at room and slightly elevated temperatures. Low levels of alkali metal contamination are common to most aluminium alloys but it has been suggested that aluminium-lithium alloys could be both subject to increased levels because of the alkali contaminants in the lithium addition and because the elements such as silicon, that may normally bind the sodium in an innocuous form in conventional alloys, are now associated with the lithium addition, freeing the alkali impurities to concentrate on and embrittle the grain boundaries. It would certainly seem to be the case that deliberately added excesses of sodium or potassium can embrittle [ Fig.27 ]. However, it is not clear whether the low levels of residual impurity found in current commercial casts of the aluminium-lithium alloys such as 5 ppm sodium, are in any way deleterious. It would appear that by control of quality and heat treatment practice, adequate short transverse properties will be attained. It needs to be demonstrated that this can be done consistently.

Transverse properties are also most important in forged material. Considerable progress has been achieved in the development of aluminium-lithium forgings both in the closed die and hand forged varieties. A feature of particular significance is the slow response of the aluminium-lithium alloys to ageing and the

consequent need to employ cold work before ageing to optimise properties. This technique is naturally difficult in shaped die forgings, although successful examples can be found in the literature (67). Hand forgings are more readily cold worked before ageing and a large body of data now exists for selected alloys in this form. On one hand, it would seem that the dilute alloys such as 8090 or 905XL will be suitable for thick section application in that the quench sensitivity of these dilute alloys is low, on the other hand, it would seem that the richer alloys may well respond better to ageing without prior stretch and so be better candidates for the higher strength requirements. It has been demonstrated (68,69) that, both a delay before ageing, after quenching, and a slow heat-up to the ageing temperature can be beneficial to the balance between strength and fracture toughness. The properties (70) of selected current alloys in forged form are illustrated including data for very thick sections [ Table 6 ].

### High Strength Alloys

Undoubtedly the combination of low density, high stiffness and high strength would be of great value in many aerospace designs provided other properties such as fatigue and corrosion resistance are maintained at a viable level. For many applications, primarily loaded in compression, a reduction in the levels found in the medium strength categories for fracture toughness and possibly corrosion performance could be acceptable. Potential and commercial alloys meeting this category are represented by 2090, 8091 and CP276 with 2090 being singularly the most advanced [ Tables.1,7 ]. High strength alloys are required as sheet, thin plate, extrusions and, importantly, as die forgings. Whilst it has proved possible to obtain very high strength material in T8 tempers, once again product forms such as sheet and die forgings, where cold work may not always be employed, have proved difficult. It is presently the case that to obtain very high strength levels, unrecrystallised material is used which can introduce problems of anisotropy in properties (71). Whilst very high strengths have been reproducibly obtained, fracture toughness levels have proved to be at an acceptable level, especially in material aged with prior cold work (72). One explanation (73) for the relatively high level of fracture toughness obtained in the important L-T and T-L directions is that the relatively poor short transverse capability allows a controlled form of delamination to occur in the plane of the material, thereby effectively dividing the material into thinner gauge laminates and so toughening it. Whether this argument is accurate or not, as the short transverse properties slowly improve there is little evidence of a deterioration of the L-T and T-L values.

Relevant data (71) from a large compilation of results for 2090 have been included throughout this paper [ Table.7 ]. Compression performance is important in this category and a brief comparison is made of the contending aluminium-lithium alloys against aluminium-zinc alloys [ Table.8 ].

## CORROSION AND STRESS CORROSION

A major concern with all aluminium alloys used in aerospace applications is the prediction of long term service performance in real environments from accelerated laboratory testing. Accelerated tests, on occasions, have proved both pessimistic and dangerously optimistic. In many cases seemingly good corrosion resistance is destroyed by galvanic and crevice corrosion conditions. The forms of corrosion attack that have been reported for the ingot metallurgy aluminium-lithium alloys 2090, 2091 and 8090 are typical of high strength aerospace aluminium alloys and include pitting, crevice and intergranular corrosion, exfoliation and stress corrosion cracking. The susceptibility to attack in these forms depends upon the alloy in question, its grain structure and heat treated condition and the environmental regime in which it was tested as for all aluminium alloys. For example, comparison between sheet versions of aluminium-lithium alloys 8090 and 2091 and bare control alloys of the 2000 and 7000 series types revealed (75) that the aluminium-lithium alloys have a propensity to exfoliation and blistering attack as opposed to severe pitting in the case of the control alloys, reflecting the more laminar grain structure of aluminium-lithium sheet.

### Corrosion Resistance

The resistance of aluminium-lithium alloys to forms of general corrosion, such as pitting and dissolution, have been assessed by weight loss and microscopy for a wide range of alloys in different heat treatment conditions exposed to a natural situations that have included the rural, industrial, sea coast, tropical maritime and aircraft environments (76-79). In general terms, all the ingot metallurgy alloys have been found to pit, corrode intergranularly and exfoliate to some extent depending again on grain structure, heat treatment condition and alloy chemistry. 2090 and 8090 sheet alloys in the unrecrystallised condition tended to exhibit an exfoliation type of attack in the marine environment for example. For 8090 an ageing condition slightly below peak strength ( e.g. 16 hours ageing at 170°C ) conferred the highest susceptibility to the alloy, lighter ageing typical of an adhesive bonding cycle produced a highly resistant condition and overageing also produced good results. In slight contrast, the worst condition identified for 2090 appeared to be after a slack quench into boiling water whilst a high strength condition T8E41 gave good resistance to sea coast and tropical ocean exposure (80,81). Generally, 2091 performed well in comparison to the control alloys when exposed to natural environments (82). Again a naturally aged condition appeared to give good resistance to exfoliation and pitting. Some scatter reported in American tests was attributed to differences in grain structure (83).

The relative rates of attack and the nature of the attack in these natural environments have been compared to those obtained in accelerated media [ Table.9 ] and weight losses and corrosion susceptibilities have been explained to some extent (84,85) using electrochemical characteristics determined in the laboratory. For example, the current-potential diagrams for 8090 and 2091 in sheet forms reveal a performance typical of conventional aerospace aluminium alloys with cathodic corrosion with associated hydrogen evolution at low potential values, followed by passivity at intermediate levels up to the pitting potential with the onset of pitting or intergranular attack beyond the breakdown value according to the composition and heat treated condition (84). Artificially aging tended to promote a reduction in pitting potentials for the alloys studied in aerated 3.5% NaCl solution and was again associated with an increased tendency to promote grain boundary attack (85).

In accelerated laboratory testing environments increasing acidity in any corrosive agent increased the rate of attack and tended to encourage intergranular forms of attack. In freely corroding situations the composition of the matrix of the alloy selected tended to control the rate of attack, that is the rate of the cathodic reaction was controlling the corrosion rate and, was itself, strongly dependent upon the composition of the alloy. For example, those alloys rich in copper show a much more rapid rate of attack than aluminium-magnesium-lithium alloys under identical conditions. The relative cleanliness and dilute nature of many of the aluminium-lithium alloys tends to inhibit local pitting which may be encouraged by the presence of coarse intermetallic particles, whilst grain boundary attack was exacerbated by under-ageing conditions that produced near-continuous grain boundary precipitation. Again typical of most aerospace aluminium alloys, grain boundary microstructures that were very clean on a microscopic scale, e.g. as quenched conditions, tended to produce very high levels of corrosion resistance and thorough ageing of 2090 or 8090 to high strength levels and beyond restored relatively high levels of corrosion resistance associated, presumably, with grain boundary particle coarsening.

#### Exfoliation Attack

Considerable effort has been expended on the correlation of the results of accelerated media testing with those obtained in the natural environment such as the sea coast with particular respect to the prediction of sensitivity to exfoliation. Several researches have indicated concern over the value of the highly acidified EXCO test media and in general the MASTMAASIS test seems to give a more consistent correlation from alloy to alloy and temper to temper (83,86). However, exceptions can be found to this conclusion. Grain

boundary corrosion attack in the form of stress corrosion and exfoliation has been reported for most of the ingot metallurgy aluminium-lithium alloys in both sheet and plate forms and a reliable quick test would be of great value. Whilst, EXCO testing based on visual assessment or rating of exposed panels did not appear to be able to distinguish adequately the subtle nature of the response of the aluminium-lithium alloys in different ageing conditions, it has been claimed (87) that quantification of the degree of attack in the EXCO tests improves matters.

There is some evidence (88) that other production routes, that suppress or circumvent the formation of grain boundaries containing precipitates, such as mechanical alloying and possibly some of the rapid solidification techniques (89) can exhibit an inherently high resistance to these forms of grain boundary attack. For the bulk of the aluminium-lithium alloys however, it would appear that the conventional aluminium alloy scenario will be relevant with differing levels of performance being related to effects of composition, grain structure and heat treatment. In sampling the exfoliation resistance of plate materials, for example, the plane of the test sample in the plate is important. An attempt to compare the performances of the leading alloys in natural environments with those obtained in the laboratory is included [ Table.9 ].

It would appear that metallurgical conditions can be developed that will produce corrosion and exfoliation resistance in the aluminium-lithium alloys that at least matches that expected of conventional aerospace 2000 and 7000 series alloys. For example the high strength conditions developed for 2090 would appear to be capable of matching the performance of the incumbent 7075 in high strength tempers. A similar approximate comparison is achieved between damage tolerant 2091 and 8090 in comparison to 2024.

#### Stress Corrosion Cracking and Hydrogen Embrittlement

Stess corrosion cracking could also prove to be a problem with aluminium-lithium alloys. There is little doubt that the new alloys will stress corrode and, whilst intermediate levels of resistance to attack have been obtained by control of metallurgical variables, the levels of immunity associated with double aged aluminium-zinc alloys have so far not been achieved, with the possible exception of 905XL mechanically alloyed material. Comparisons of the stress corrosion cracking behaviour of different alloys and tempers is difficult to make unless all the results have been obtained in the same test house under identical conditions. This ideal situation has not yet been achieved for aluminium-lithium alloys, at least, as far as the author can ascertain. Comparisons made between test houses can reveal greater scatter for one material than is found for a whole range of alloys and conditions from a single test source.

Nevertheless, a comparison of the relative performances of selected plate alloys has been attempted in the form of threshold levels for cracking in standard alternate immersion testing to the appropriate ASTM standards [ Table.10 ] (90-92).

It would seem fairly clear that unrecrystallised sheet whether, 2090, 2091 or 8090, has a very high resistance to stress corrosion in the plane of the sheet ( exceeding 75% of the 0.2% PS ) even when the material is aged to very high levels of strength and in this respect is usually better than the incumbent alloy. The results for recrystallised sheet are much more confused with some sensitivity to stress corrosion cracking being demonstrated for both 2091 and 8090 in this damage tolerant form. However, once again, control of grain structure and precipitation appears to subtly affect the response at least as measured in accelerated testing (93). Extended ageing, for example, producing much improved stress corrosion resistance for 2091.

The short transverse threshold stresses for thicker gauges of plate, forgings and extrusions, tested by alternate immersion in 3.5% NaCl solution for example, would appear to approximate to a T76 temper when applied to 7075, and, consistent with this, stress corrosion cracking does occur in a variety of natural and marine environments. There appears to be evidence that, whilst full immersion testing produces little or no cracking in these aluminium-lithium alloys, alternate immersion is particularly damaging and that the role of atmospheric CO<sub>2</sub> is important (94,95). Some initial work has identified a contribution from hydrogen embrittlement in the stress corrosion process (96-99) and a sensitivity to pre-embrittlement. Extended ageing or double ageing appears to improve the stress corrosion resistance of 8090 plate significantly (87) as does the addition of some zinc to the alloy (100). Clearly further work on stress corrosion resistant tempers is required.

Stress corrosion crack growth rates have also been determined using double-cantilever-beam test pieces ( DCB ) for a limited range of alloys and conditions. Although somewhat discredited as a technique because of concerns over corrosion product wedging, the DCB technique can illustrate differences in the sensitivity of alloys to stress corrosion cracking once cracks have initiated. These preliminary results (76) [ Fig.28 ] appear to indicate that an intermediate level of resistance can be obtained, similar to the T76 level associated with aluminium-zinc alloys and consistent with the trend revealed by the stress corrosion tests for crack initiation. Differences in response have been recorded for selected corrodents and comparison between 8090-T651 plate and for example 7075-T651 or 2024-T351 showed the aluminium-lithium alloy to have a slight advantage making its resistance approximately equivalent to a 7075-T7651 condition, consistent with stressed beam and C-ring results.

## HIGH TEMPERATURE PROPERTIES

Some data has emerged (101-103) for the performance of the aluminium-lithium alloys at elevated temperature both in terms of tensile properties at elevated temperature and the "recovery" condition of room temperature performance after prior high temperature exposure. It would seem that, in the simple aspect of high temperature strength and recovery strengths, the new alloys are at least as good as the conventional Al-Cu alloys ( and Al-Zn ) they may well replace in high temperature applications [ Fig.29 ]. That is the high strength 2090 material outperforms 7075 and 8090 out performs the medium strength 2000 series. Indeed the level of improvement is such that a high temperature alloy can be envisaged to produce a consistent absolute improvement over 2618 or 2219 over the whole range of elevated temperature applications e.g. up to 200°C. However, some caution is required in that many of the alloys are offered in an underaged temper to maximise the relationship between fracture toughness and strength. Exposure at elevated temperatures can then be seen to produce an increase in strength both at temperature and on recovery, but there may well be an associated drop in fracture toughness. The copper-rich alloys such as 2090 and 2091 will be more prone to this especially at higher exposure temperatures of 170°C and above. Exposure of all the alloys at temperatures more typical of aircraft operation i.e. 70°C to 100°C has been found to produce smaller reductions in toughness and checks of recrystallised damage tolerant sheet alloys 2024, 8090 and 2091 after long periods of exposure to these more modest temperatures show only small toughness reductions (i.e. 10%).

Little creep data is available. However, what there is again seems to suggest that the alloys may have some benefits in this regard (104). On the other hand, there have been reports of a greater sensitivity of the aluminium-lithium alloys to creep cracking than for conventional materials, especially when they are stressed in the transverse directions (105,106). It has been claimed that this is an effect of the presence of low melting point impurity elements rather than an intrinsic susceptibility to creep cracking but, clearly, this issue requires further study.

## CRYOGENIC PROPERTIES

Considerable effort has been spent in investigating the low temperature behaviour of aluminium-lithium alloys because of their potential application in space structures and cryogenic tanking. Studies of 2090-T81 and 2091-T81 plate between ambient and 4°K show a consistently increasing strength, modulus and fracture toughness in the L-T and T-L directions (107). However, the toughness in the short transverse directions decreases slightly and more intergranular splitting is observed. Tests on 2090-T83 sheet show a slight reduction in

toughness with reducing temperature down to 77°K allowing a consistent argument to be raised that increased strength is achieved by restriction of slip systems and an increased strain hardening rate whilst plane strain toughness is improved by a mechanism of delamination and relaxation of the through thickness stresses towards a plane stress condition (108). Others, however, argue with this last hypothesis (109). Whilst 8090 was also found to show an increase in strength and elongation with reducing temperature, a minimum value in tensile strength coinciding with a maximum value in reduction of area was noted at 200°K associated with a minimum value in strain hardening exponent and a change in slip mode (110). Studies of the fracture toughness of 8090-T852 hand forgings showed strength and ductility to increase with reducing temperature but toughness to fall slightly and consistently in all three testing directions. A comparison of the strength-toughness relationship of superplastic sheet versions of 2090 and 8090 with 2219 showed the 2219 to maintain better properties at both 300°K and 77°K (111).

## MANUFACTURING TECHNOLOGIES

Sufficient work has now been conducted for a balanced appraisal of manufacturing aspects to be made. It has already been stated that the cost effectiveness of these new alloys depends, not only on their initial cost, but also on the ease of manufacture and finishing. Little can be said about proprietary practices in the aluminium factories except that it seems to be the case that all the conventional techniques of hot and cold rolling, forging, extrusion and drawing are being successfully applied to a range of aluminium-lithium alloys and that this, in itself, is a very good indication of their general acceptability as conventional aluminium alloys. Cold rolled sheet 2 metres wide has become available as have very large forgings. High levels of stretching are regularly applied to plate and extrusion again signifying a high level of conventional workability.

### Cold Forming

More specific studies of the formability of sheet, plate and extrusions have been undertaken. Generally it has been found that metallurgical conditions have been developed in which the aluminium-lithium alloys are at least as formable as their conventional counterparts. Problems of anisotropy have been identified, however, in trying to form unrecrystallised sheet variants and in the high strength and stiffness of some prestretched unrecrystallised products (112). In forming sheet both solution annealed and low temperature annealed conditions have been applied, although it would seem to be the case that the solution treated condition is the most formable.

Recrystallised versions of 2091 and 8090 sheet alloys prove to be highly formable with excellent retention of shape and relatively low rates of natural ageing. In this respect they appear to be a significant improvement over the incumbent 2000 series alloys (113).

Conventional workshop machining practices can all be applied without any extra difficulties, although it has been recommended that machining should be conducted using lubrication, especially when surfaces are heavily oxidised typically in the case of cast materials. This avoids the pollution of the workshops with alkaline oxides and hydroxides which are irritants. Similarly, it is recommended (114) by several manufacturers that material be pickled after high temperature treatments to remove surface oxides and carbonates.

Chemical treatments, such as chemical milling, de-oxidising, anodising and conversion coating have all been evaluated for 2090, 2091 and 8090 alloys and most results using conventional manufacturing processes appear favourable in comparison to conventional alloys. Corrosion protection afforded by conventional pretreatments and final painting appears to be at least as good as for the conventional alloys (115).

#### Superplastic Forming and Diffusion Bonding

Significant effort has been applied to the development of superplastic variants of the aluminium-lithium alloys, with the specific aim of further reducing structural weights and manufacturing costs in pieces of complex structure. It was discovered that not only were aluminium-lithium alloys superplastic but that they could be optimised to be more plastic than most conventional alloys. In the particular case of the dilute 8090 alloy, the benefit of low quench sensitivity is a further demonstrable advantage in that it allows the use of air cooling from the press after forming, rather than requiring a full reheat-treatment. A similar advantage could well be found for the aluminium-magnesium-lithium alloys. Should the effort in diffusion bonding currently being expended also come to fruition, then the ability to air-cool material will become a necessity to enable the heat-treatment of multi-leafed structures (116).

A significant data base has been developed for 2090 and 8090 material that has been superplastically formed and the slight deterioration in properties associated with the forming process has been quantified. Undoubtedly the proper control of lithium-loss from the surface of thin sheets and the suppression of internal cavitation are important features. Fatigue properties should be most sensitive to the internal and surface defects that can be produced by the superplastic technique yet an acceptable level of

performance has been established for several of the new alloys (117-119).

### Welding Technology

The three commercial ingot metallurgy alloys 2090, 2091 and 8090 have each been assessed fairly thoroughly for weldability. Gas metal arc, gas tungsten arc, electron beam and laser welding all seem viable for each of the alloys (120,121). Additionally techniques such as explosive bonding and solid state diffusion bonding are receiving increasing attention. Spot and seam electrical resistance techniques also seem viable. It would appear that the low thermal conductivity of aluminium-lithium alloys could prove a major advantage in producing high quality welds (122).

Consideration of the difficulties encountered during early welding trials all seem to indicate that porosity in the welds was a major concern. Appreciation of the chemistry and thickness of the surface films naturally encountered on heat treated aluminium-lithium alloys and a general improvement in the quality of cast metal in terms of gas content for example has improved the situation considerably. That is, it is recognised that the metal must have a low gas content and that the surfaces must be cleaned, chemically or mechanically, to remove oxides, nitrides and carbonates.

Filler materials seemingly preferred (123) for 2090 are based on 4000 series (Al-Si) and 2000 series (Al-Cu), whilst a clear preference for a variant of the Al-Mg system has developed for 8090. Autogeneous welding does not necessarily produce the best results.

Studies of the susceptibilities of the alloys to cracking in the fusion and heat affected zones revealed that both are possible, even likely, depending on the techniques applied (124), but this is a feature of the high strength aerospace aluminium alloys. The general perception appears to be that all three commercial aluminium-lithium alloys are more weldable than difficult alloys such as 2014 but slightly less weldable than 2219.

Benefit has been made of the low quench sensitivity of 8090 and of the natural ageing capability of 8090 and 2091 to produce welds in fully heat treated material using no post-weld heat treatments. It appears to be the case that with developments to the welding techniques these commercial aluminium-lithium alloys can produce acceptable welds even in comparison to the incumbent alloys such as 2219. The strengths of welded joints in these alloys can compare favourably in absolute terms with those of the best current high strength aluminium alloys with joint efficiencies in excess of 70% quite possible.

However, mention should be made of the Russian alloy 1420 and its variants in that this alloy has seemingly been extensively used in welded aircraft structures apparently with successful service applications and very significant weight savings (125).

A specialised development (126) of a new alloy or series of alloys coded "Weldalite" has continued with particular relevance to cryogenic welded tanks. This AL-Cu-Li-Ag-Mg-Zr alloy appears to be virtually as weldable as 2219 alloy and have the distinct benefit of a rapid natural ageing response. Unlike the higher lithium - lower copper alloys it does not require the application of deformation before ageing to achieve very high strengths and may well prove to be compatible with cryogenic requirements (127).

#### QUALIFICATION AND APPLICATION

The aluminium-lithium alloys considered in this paper are initially aimed at aerospace applications. Such applications require a long and careful process of testing and qualification before application is approved. Many such programmes are now underway. Part of the development process is the use in flight trials of demonstrator components. Early examples of these have been the upper wing panels in the McDonnell Douglas F15-SMTD variant (128), in the flying control surfaces of an experimental British Aerospace aircraft (129) and in the internal structure of the Dassault Rafale (130). Early civil demonstrator programmes include the use of aluminium-lithium forgings in a nose undercarriage by Boeing and in access panels on the Fokker F100 (131). 8090, 2090 and 2091 have all been used in one or other of these programmes.

The next steps involve the considerable undertaking of applying aluminium-lithium alloys to structures undergoing full-scale testing and in their embodiment in prototype or pre-production aircraft. Several manufacturers have reached this stage, with notable examples being the commitment (133) to test considerable quantities of aluminium-lithium alloys in the next generation of Airbus aircraft [ Fig.30 ], the completed testing by Dornier of a pressure cabin section (132) and the widespread application of aluminium-lithium alloys to the new Westland-Augusta EH101 helicopter (67). Potential European and North American applications to military aircraft can be found, and significant use has already been made in space structures.

#### CONCLUDING REMARKS

It would appear to be the case that the present casting capacity available in the Western World for aluminium-lithium alloys readily matches current levels of demand and has the capability to be stretched to the levels predicted

to be required during the next decade. Clearly, if aluminium-lithium alloys are to succeed, they must prove to be a cost effective route to significant weight savings. In this respect, it is most important that the early examples of application are brought to a thoroughly satisfactory conclusion. This being the case, then a very significant expansion in capacity will be sought in the next few years to match the increasing demands of the aerospace industry.

Whilst cost may dominate the arguments as to applicability of these developing alloys, some technical problems still require resolution by the aluminium-alloy industry. The relevance of individual technical issues depend critically on the application intended but, to the author, improved performance in high strength categories without benefit of cold work and a general improvement in short transverse behaviour of the thicker gauges of material remain the major issues.

#### ACKNOWLEDGEMENTS

The wealth of technical and scientific data now available for aluminium-lithium alloys is overwhelming. Whilst the opinions expressed in this paper are those of the Author alone, the very considerable contributions of his many colleagues is gratefully acknowledged.

C Copyright HMSO London 1990

#### REFERENCES

1. "Aluminium-lithium alloys" Proc 5th Int Conf Williamsburg March 1989 edited T H Sanders, E A Starke MCEP Birmingham 1989
2. P Assmann "Age hardened aluminium-lithium alloys" Z. Metallkunde Vol.18, p.51, 1926
3. O Reuleaux "Scleron Alloys" J Inst Met Vol.33, p.346, 1924
4. W R D Jones, P P Das "The mechanical properties of aluminium-lithium alloys" J Inst Met Vol.88, p435, 1959-1960
5. I N Fridlyander et al UK Patent No.1,172736, 1969
6. I M LeBaron US Patent No.2381219, 1945
7. H K Hardy, J M Silcock " The phase sections at 500°C and 350°C of aluminium-rich aluminium-copper-lithium alloys" J Inst Met Vol.84, p.423, 1955-1956

8. E S Balmuth, R Schmidt "A perspective on the development of aluminium-lithium alloys" Proc 1st Int Conf on aluminium-lithium alloys, Stone Mountain Georgia May 1980. Met Soc AIME 1981
9. J M Silcock "The structural ageing characteristics of aluminium-copper-lithium alloys" J Inst Met Vol.88, p.357, 1959-1960
10. J C Ekvall, J E Rhodes, G G Wald "Methodology for evaluating weight savings from basic material properties" ASTM STP 761 Design of fatigue and fracture resistant structure p.328, 1982
11. W E Quist, G H Narayanan, A L Wingert "Aluminium-lithium alloys for aircraft structure - An overview" Proc 2nd Int Ccnf aluminium-lithium alloys Monterey, 1983, Met Soc AIME
12. W R Wilson, J Worth, E P Short C F Pygall "Recycling of aluminium-lithium process scrap" Proc 4th Int Conf on Aluminium-lithium alloys Paris June 1987 Jnl de Physique, Vol.48, 1987
13. D Little "Overview" Proc 3rd Int Conf on aluminium-lithium alloys Oxford July 1985, p.15 Institute of Metals 1986
14. C J Peel "Current status of the application of aluminium-lithium alloys and the potentials for future development" AGARD Conf on New Light Alloys AGARD CP 444, 1989
15. F M Page, A T Chamberlain, R Grimes "The safety of molten aluminium-lithium alloys in the presence of coolants" as ref.12, p.C3-63
16. K A Kojima, R E Lewis, M J Kaufman "Microstructural characterisation and mechanical properties of a spray cast Al-Li-Cu-Mg-Zr alloy" as ref.1, p.85
17. N J Kim, R L Bye, S K Das "Recent developments in rapidly solidified aluminium-lithium alloys" Procs 1987 Symposium on Aluminium-lithium Alloys Design, development and application update, p.63, ASM INT 1988
18. R D Schelleng, A I Kemppinen, J H Weber "IncoMAP Alloy Al-905XL for aerospace forgings - Production Status" as ref.1, p.1577
19. W S Miller, L A Lenssen, F J Humphreys "The strength, toughness and fracture behaviour in aluminium-lithium based metal matrix composites" as ref.1, p. 931
20. J White, I R Hughes, T C Willis, R M Jordan "Metal matrix composites based on aluminium-lithium and silicon carbide" as ref.12, C3-347

21. R C Dickenson, K Wefers, K R Lawless "Internal hydride precipitation in Al-Li alloys" as ref.1, p.1337
22. S Fox, H M Flower, D S McDarmaid "Formation of solute-depleted surfaces in Al-Li-Cu-Mg-Zr alloys and their influence on mechanical properties" as ref.13, p.263
23. E R Clark, P Gillespie, F M Page "Heat treatment of Li/Al alloys in salt baths" ibid p.159
24. C J Peel, B Evans, C Baker, D A Bennet, P J Gregson and H M Flower "The development and application of improved aluminium-lithium alloys" as ref.11, p.363
25. B Noble, S J Harris, K Dinsdale "The elastic modulus of aluminium-lithium alloys" Jnl Mat Sci. Vol.17, p.461, 1982
26. G Lapasset, C Damerval, M Doudeau "Quench sensitivity of commercial Al-Li-Cu-Mg-Zr alloys" as ref.1, p.365
27. J T Staley, R D Doherty "Quench sensitivity of an Al-Cu-Li alloy plate" ibid p.345
28. R Grimes, K Gatenby, M A Reynolds, A Gray, I G Palmer "The evolution of damage tolerant aluminium-lithium alloys" Proc Int Conc on new aluminium and magnesium alloys, Amsterdam, June 1990 ASM
29. M Doudeau, P Meyer, D Constant "Al-Li alloys developed by Pechiney" as ref.14, p.2-1
30. C J Peel, D S McDarmaid, B Evans "Considerations of critical factors for the design of aerospace structures using current and future aluminium-lithium alloys" as ref.17, p.315
31. Y Barbaux "Proprietes des alliages Al-Li" as ref.14, p.8-1
32. N Ohrloff, A Gysler, G Lutjering "Fatigue crack propagation behaviour of 2091 T8 and 2024 T3 under constant and variable amplitude loading" as ref.12, p.C3-801
33. D S McDarmaid, C J Peel "Aspects of damage tolerance in 8090 sheet" as ref.1, p.993
34. W G J t'Hart, L Schra, D S McDarmaid, M Peters "Mechanical properties and fracture toughness of 8090-T651 plate and 2091 and 8090 sheet" as ref.14, p.5-1
35. S J Harris, B Noble, K Dinsdale " Fatigue crack growth characteristics of Al-Li based alloys" in Fatigue 84 EMAS, 1, p.361, 1984

36. M Peters, K Welpmann, D S McDarmaid, W G J t'Hart "Fatigue properties of Al-Li alloys" as ref.14, p.6-1
37. K T Venkateswara Rao, W Yu, R O Ritchie "Mechanisms of fatigue crack propagation in commercial aluminium-lithium alloys" as ref.17, p.173
38. L Farcy, C Carre, M Clavel, Y Barbaux, D Aliaga "Factors of crack initiation and microcrack propagation in aluminium-lithium 2091 and in aluminium 2024" as ref. 12, p.C3-769
39. K T Venkateswara Rao, R S Piascik, R P Gangloff, R O Ritchie "Fatigue crack propagation in aluminium-lithium alloys" as ref.1, p.955
40. D J Nicholls, J W Martin "Microstructural effects on small crack growth in aluminium-lithium alloys" as ref.1, p.1003
41. P S Pao, M A Imam, L A Cooley, G R Yoder "Corrosion fatigue crack growth in Al-Li alloy 2090" as ref.1, p.1125
42. J Petit, S Suresh, A K Vasudevan, R C Malcolm "Constant amplitude and post overload fatigue crack growth in Al-Li alloys" as ref.13, p.257
43. F L Haddleton, S Murphy, T J Griffin "Fatigue and corrosion fatigue of 8090 Al-Li-Cu-Mg alloy" as ref.12, p.C3-809
44. C Lespinasse, C Bathias "Fatigue crack growth of the 8090 alloy under overloading" as ref.43 p.C3-793
45. K T Venkateswara Rao, W Yu, R O Ritchie "Mechanisms of fatigue crack propagation in commercial aluminium-lithium alloys" as ref.17, p.173
46. C J Peel, D S McDarmaid "The present status of the development and application of 8090 and 8091 alloys" Aerospace
47. C J Peel, D S McDarmaid, B Evans "Considerations of critical factors for the design of aerospace structures using current and future aluminium-lithium alloys" as ref.17, p315
48. M Peters, K Welpmann, W Zink, T H Sanders "Fatigue behaviour of Al-Li-Cu-Mg alloy" as ref.13, p.239
49. V J Bolam, P J Gregson, A Gray "The influence of surface treatments on the fatigue performance of 8090" as ref.1, p.1097

50. P J Gregson, J Newman, A Gray "Effect of surface treatment on fatigue properties of Al-Li-Cu-Mg-Zr and Al-Zn-Mg-Cu-Zr plate" Mat Sci and Tech. 5, p.65, 1989
51. R Hermann, C N Reid "Enhancing the fatigue life of fastener holes in aluminium-lithium alloy 8090" as ref.1, p.1607
52. W Zink, J Weilke, L Schwarmann, K H Rendigs "Investigation on sheet material of 8090 and 2091 aluminium-lithium alloys" as ref.14, p.9
53. M Mohaghegh, F Zafari, C Spada, F Lin "Property trends for 2091 and 2090 sheet" as ref.17, p.237
54. S Fox, H M Flower, D S McDarmaid "Formation of solute depleted surfaces in Al-Li-Cu-Mg alloys and their influence on mechanical properties" as ref.13, p.263
55. J E Talia, P K Mazumdar "Detimental influence of oxide films on the fatigue behaviour of an aluminium-lithium alloy" as ref.1, p.1053
56. M Doudeau, P Meyer, D Constant "Al-Li alloys developed by Pechiney" as ref.14, p.2-1
57. R C Dorward "Al-Li development at Kaiser Aluminum" as ref.17, p.155
58. R Grimes, T Davis, H J Saxty, J E Fearon "Progress to aluminium-lithium semi-fabricated products" as ref.12, p.C3-11
59. W G J t'Hart, L Schra, D S McDarmaid, M Peters "Mechanical properties and fracture toughness of 8090-T651 plate and 2091 and 8090 sheet" as ref.14, p.5-1
60. P J Gregson, H M Flower  
Acta Metall, 33, p.527, 1985
61. S Fox, D S McDarmaid, H M Flower, "Anisotropy of mechanical properties of Al-Li based alloy plate"  
" Aluminium Technology" Inst of Metals London, March, 1986
62. C J Peel, B Evans, D S McDarmaid "Current status of UK lightweight lithium-containing aluminium alloys" as ref.13, p.26
63. S J Lynch to be published Jnl Mat Sci
64. D Webster "The effect of low melting point impurities on the properties of Al-Li alloys" as ref.12, p.C3-685

65. A K Vasudevan, A C Miller, M M Kersker "Contribution of Na-segregation to fracture behaviour of Al-11.4 at % Li alloys" as ref.11, p.181
66. C J Peel, B Evans, D S McDarmaid, as ref.17, p.315
67. A F Smith "Uses and properties of Al-Li on the new EH101 helicopter" as ref.14, p.19-1 and "A comparison of large AA8090, AA8091, and AA7010 die forgings for helicopter structural applications" as ref.1, p.1587
68. G R D Shrimpton, H C Angus "Forged components in aluminium-lithium alloys for aerospace applications" as ref.1, p.1565
69. N J Kim, D Raybould, R L Bye, S K Das "Microstructure and mechanical properties of rapidly solidified Al-Li-Cu-Mg-Zr die forgings" as ref.1, p.123
70. R E Lewis, E A Starke, W C Coons G J Shiflet, E Willner, J G Bjeletich, C H Mills, R M Harrington, D N Petrakis "Microstructure and properties of Al-Li-Cu-Mg-Zr (8090) heavy section forgings" as ref.12,p.C3-643
71. M D Goodyear "Alcoa alloy 2090" Alcoa green letter 2nd Edition ALCOA 1989
72. E A Starke, W E Quist "The microstructure and properties of aluminium-lithium alloys" as ref. 14, p.4-1
73. R Grimes, W S Miller, M A Reynolds "The status of Alcan's aluminium-lithium alloy programme" as ref. 17, p.17
74. K T Venkateswara Rao, R O Ritchie "Mechanisms influencing the cryogenic fracture toughness behaviour of aluminium-lithium alloys" Nov 1989, Submitted to Acta Metall 1990
75. P L Lane, J A Gray, C J E Smith "Comparison of corrosion behaviour of lithium-containing aluminium alloys and conventional aerospace alloys" as ref.13, p.273
76. C J E Smith, J A Gray, L Schra, J A M Boogers, R Braun, H Buhl, G Vaessen "Corrosion and stress corrosion of aluminium-lithium alloys" as ref.14, p.7-1
77. F S Lin, Y Moji, W E Quist, D V Badger "Corrosion resistance of aluminium-lithium alloys" as ref. 12, p.905
78. T S Srivatsan, G E BoBeck, T S Sudarshan, P A Molian "Environmental factors affecting the localised corrosion of Al-Li-Cu-Mg alloys as ref.1, p.1237

79. E L Colvin, B W Lifka "Accelerated and atmospheric exfoliation performance of Al-Li alloys" Proc Int Conf on "Localised Corrosion" NACE 1990
81. E W Lee, J Waldman "Aluminium-lithium alloys for navy aircraft" as ref.14, p.10-1
82. B Bavarian, J Becker, S N Parikh, M Zamanzadeh "Localised corrosion of 2090 and 2091 Al-Li alloys" as ref.1, p.1227
83. E L Colvin, S J Murtha "Exfoliation corrosion testing of Al-Li alloys 2090 and 2091" as ref.1, p.1251
84. A Roth, H Kaesche "Electrochemical investigation of technical aluminium-lithium alloys - Part 1: general aspects" as ref.1, p.1197
85. M Reboul, P Meyer "Intergranular and exfoliation corrosion of Al-Li-Cu-Mg-Zr alloys" as ref.12, p.C3-881
86. E L Colvin "Exfoliation and stress corrosion cracking performance of Al-Li alloys" as ref.17, p.273
87. A Gray "Factors influencing the environmental behaviour of aluminium-lithium alloys" as ref.12, p.C3-891
88. R D Schelleng, A I Kemppinen, J H Weber "IncoMAP alloy Al-905XL for aerospace forgings - production status" as ref.1, p.1577
89. W E Quist, C Y Bevers, G H Narayanan "Microstructure and engineering properties of alloy 644B" as ref.1, p.1695
90. M Ahmad "Correlation between ageing heat treatments, microstructure and stress corrosion properties of Al-Li-Cu-Mg alloys" as ref.12, p.C3-871
91. G Disson, M Reboul, C Fiaud "A stress corrosion cracking study of 2091 Al-Li alloy" as ref.1, p.1261
92. R Balasubramanian, D J Duquette "The stress corrosion cracking susceptibility of an aluminium-lithium-copper alloy" as ref.1, p.1271
93. as ref.52
94. J G Craig, R C Newman, M R Jarrett, N J H Holroyd "Local chemistry of stress corrosion cracking in Al-Li-Cu-Mg alloys" as ref.12, p. C3-825
95. J P Moran, G E Stoner "Solution chemistry effects on the stress corrosion cracking behaviour of alloy 2090 and alloy 2024" as ref.1, p. 1187

96. K S Shin, S S Kim, E W Lee "Hydrogen embrittlement of a 2090 Al-Li alloy" as ref.1, p.1319
97. E I Meletis, W Huang "Pre-exposure embrittlement in Al-Li-Cu alloys" as ref.1, p.1309
98. T Magnin, M Rebiere "The effect of hydrogen during stress corrosion cracking and corrosion fatigue of Al-Li-Cu alloys in 3.5% NaCl solutions" as ref.12, p.C3-835.
99. F C Rivet, R E Swanson "Influence of dissolved hydrogen on aluminium-lithium fracture behaviour" as ref.1, p.1329
100. A Gray, N J H Holroyd, J White "The influence of microstructure on the environmental cracking behaviour of Al-Li-Cu-Mg-Zr alloys" as ref.1, p.1175
101. C J Peel, D S McDarmaid, B Evans as ref.47
102. M Pridham, B Noble, S J Harris "Elevated temperature strength of Al-Li-Cu-Mg alloys" as ref.13, p.547
103. P S Gilman, J W Brooks, P J Bridges "High temperature tensile properties of mechanically alloyed Al-Mg-Li alloys" as ref.13, p.112
104. C C Wan, H Smallen, R V Carter "Tensile properties of 8090 Al-Li alloy at cryogenic and elevated temperatures" as ref.1, p.1553
105. K V Jata "Creep crack growth resistance of 2091 Al-Li alloy" as ref.1, p.1163
106. S J Lynch "Sustained load cracking in aluminium-lithium alloys" to be published Jnl Mat Sci
107. J Glazer, S L Verzasconi, R R Sawtell, J W Morris "Mechanical behaviour of aluminium-lithium alloys at cryogenic temperatures" Met Trans 18A, p1695, 1987
108. K T Venkateswara Rao, R O Ritchie "Mechanisms influencing the cryogenic fracture toughness behaviour of aluminium-lithium alloys" submitted to Acta Metall Nov 1989
109. J Glazer, J W Morris "The strength toughness relationship at cyogenic temperatures in aluminium-lithium alloy plate" as ref.1, p.1471
110. K Welpmann, Y T Lee, M Peters "Low temperature deformation behaviour of 8090" as ref.1, p. 1513
111. S L Verzasconi, J W Morris "Cryogenic mechanical properties of low density superplastically formable Al-Li alloys" as ref.1, p.1523

112. W E Quist, M Hyman D H Gane, D V Badger "Forming characteristics of Al-Li alloys" as ref.17, p.401
113. J Bevalot "Mise en oeuvre de l'alliage 2091" as ref.14, p.14-1
114. G LeRoy, P Meyer "Status of Al-Li development at Pechiney" as ref.17, p.77
115. F S Lin. Y Moji, W E Quist, D V Badger "Corrosion resistance of aluminium-lithium alloys" as ref.12, p.905
116. D S McDarmaid, A J Shakesheff "The effect of superplastic deformation on the tensile and fatigue properties of Al-Li (8090) alloy" as ref. 12, p.C3-257
117. R Grimes, W S Miller "Superplasticity in lithium-containing aluminium alloys" as ref. 11, p.153
118. A K Gosh, C Gandhi "Superplasticity in Al-Li alloys Procs. ICSMA-7, p.2065. Pergamon Oxford 1986
119. J Wadsworth, C A Henshall, T G Nieh "Superplastic aluminium-lithium alloys" as ref.13, p.199
120. M R Edwards, V E Stoneham "The fusion welding of Al-Li-Cu-Mg (8090) alloy" as ref. 12, p.C3-293
121. J C Lippold "Weldability of commercial aluminium-lithium alloys" as ref.1, p.1365
122. P A Molian, T S Srivatsan "Weldability of Al-Li-Cu alloy 2090 using laser welding" as ref.1, p.1435
123. C C Griffee, G A Jensen, T L Reinhart "Factors influencing the quality and properties of aluminium-lithium alloy welds" as ref.1, p.1425
124. T Zacharia, S A David, J M Vitek, R P Martukanitz "Weldability and microstructural characterisation of Al-Li alloys" as ref.1, p.1387
125. I N Fridlyander "Aluminium-lithium weldable alloy 1420 (Alloying system Al-Li-Mg-Zr)" as ref.1, p.1359
126. J R Pickens, F H Heubaum, T J Langan, L S Kramer "Al-Cu-Li-Ag-Mg-Zr alloy Weldalite 049" as ref.1, p.1397
127. A Cho, R F Ashton, G W Steele, J L Kirby "Status of weldable Al-Li alloy (Weldalite 049) development at Reynolds Metals Company" as ref.1, p.1377

128. P O Wakeling, S D Forness, E A W Heckman "The use of 8090 in the McDonnell-Douglas F15 SMTD aircraft" as ref.17, p.339
129. Metal Construction, Aug, 1987, p.444
130. G LeRoy, P Meyer "Status of Al-Li development at Pechiney" as ref.17, p.77
131. G J H Vaessen, C van Tilborgh, H W van Rocijen "Fabrication of test articles from Al-Li 2091 for Fokker 100" as ref. 14, p.13
132. I Gould, Flight Int. p.10, May 1988
133. J Koshorst "Point of view of a civil manufacturer on Al-Li alloy" as ref.14, p.18-1

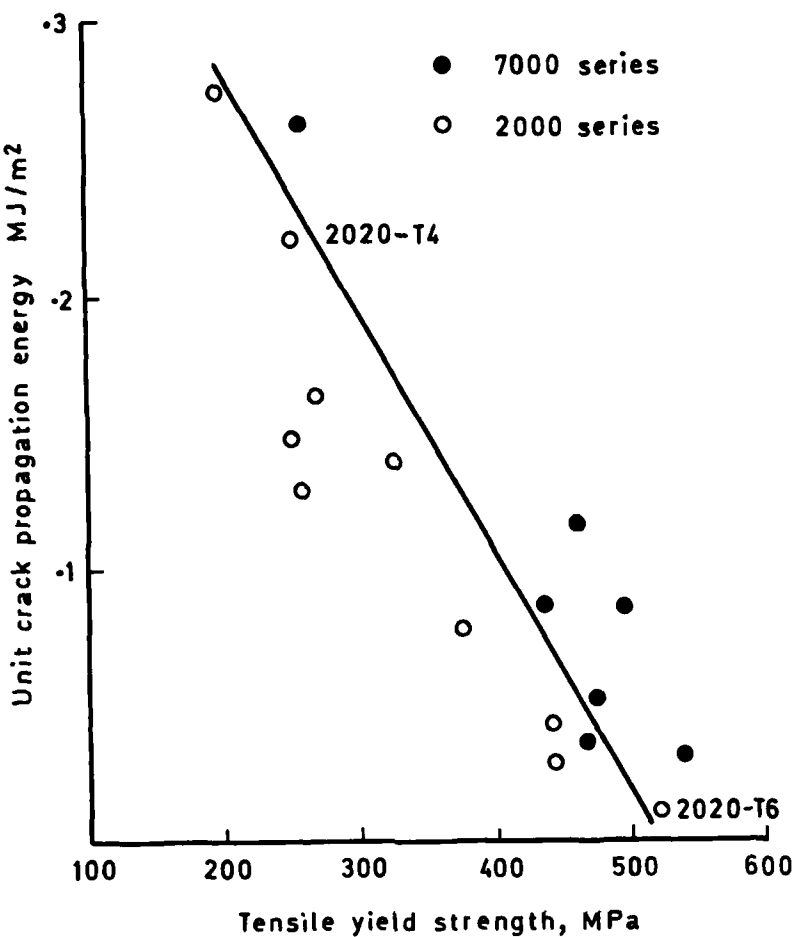


Fig.1 Toughness of 2020 alloy in T4 and T6 tempers in comparison to contemporary 1960's aerospace alloys

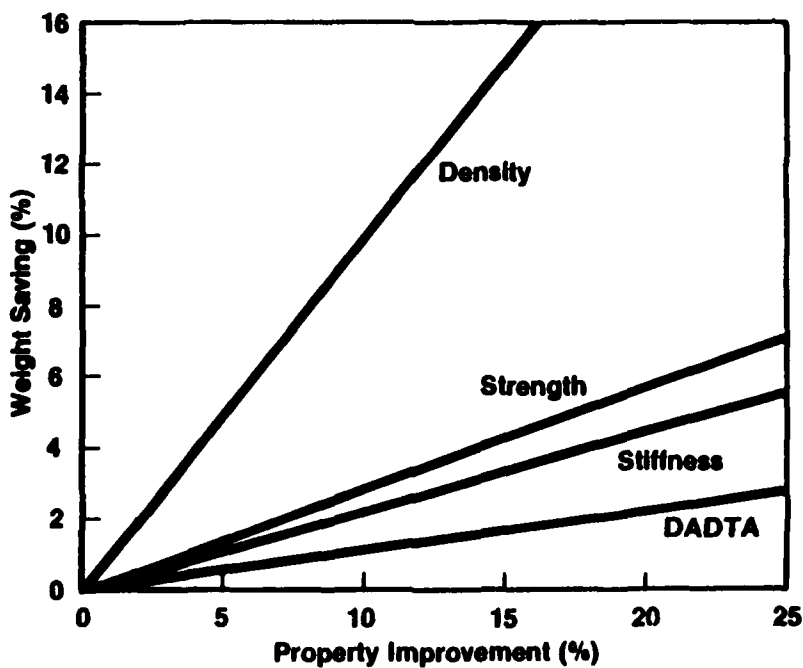


Fig.2 Mass savings as functions of property improvements after Ekvall et al ( Ref. 10 )

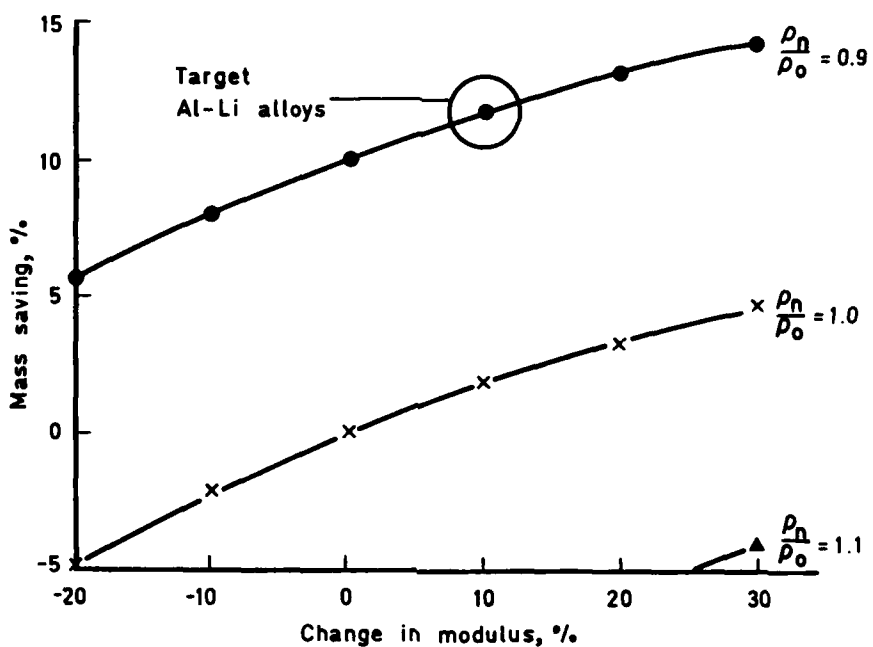


Fig.3 Mass savings predicted by the author for 8090 with a 10% density reduction and 10% stiffness increase compared with conventional alloy

<u>LONGITUDINAL DATA</u>						
	Damage tolerant	Medium strength	High strength			
Extrusions	[8090-T8151]	[8090-T851]	[8091-T851]			
Forgings	[8090-T6]	[8090-T652]	[8091-T6]			
Sheet	[8090-T81]	[8090-T6]	[8090-T8] [8091-T6] [8091-T8]			
Plate	[8090-T8151]	[8090-T8251]	[8090-T8771] [8091-T851]			
	300	350	400	450	500	550
	Current minimum values of 0.2% proof stress (MN/mm <sup>2</sup> )					

Fig.4 Schematic representation of the product forms and tempers required in the application of 8090

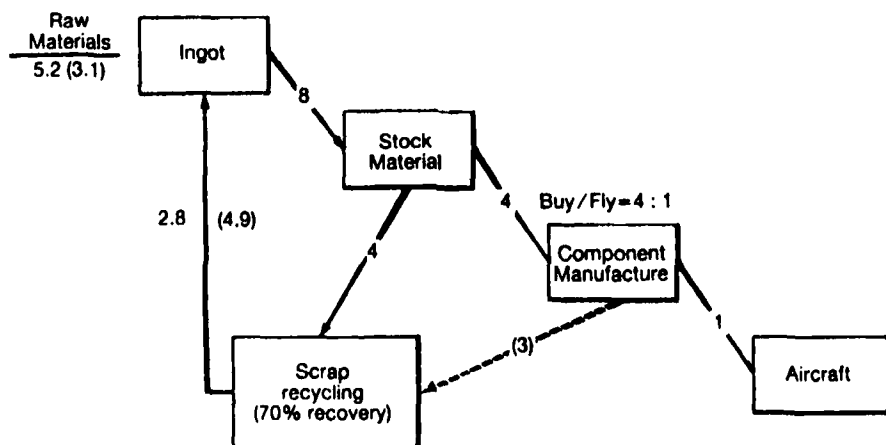


Fig.5 Primary and secondary scrap cycles after Little (Ref.13)



Fig.6 Samples of pure aluminium and aluminium-lithium poured molten into water and unsuccessfully detonated.

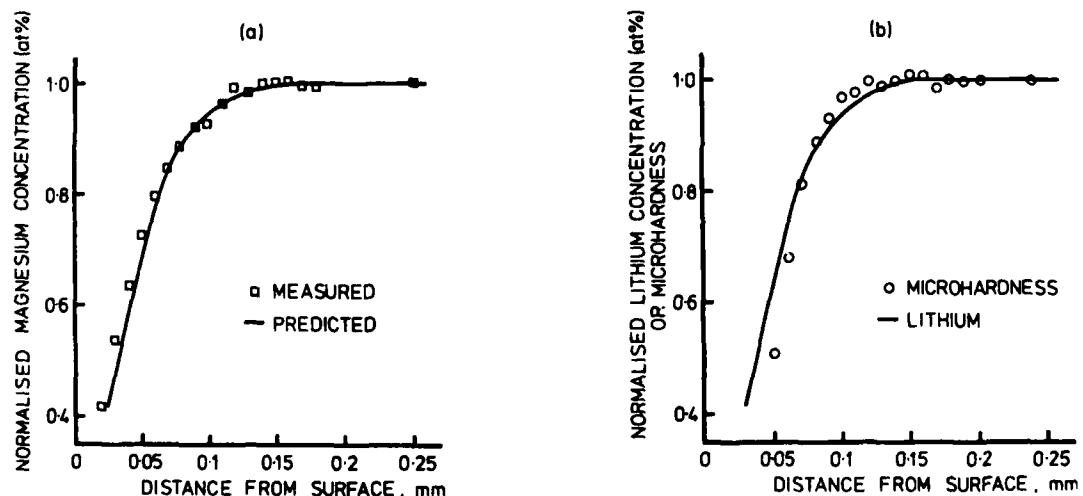


Fig.7 Predicted and measured magnesium (a), lithium (b) and microhardness gradients at the surface of 8090 solution heat treated at 530C for 1 hour after Fox et al ( Ref. 22 )

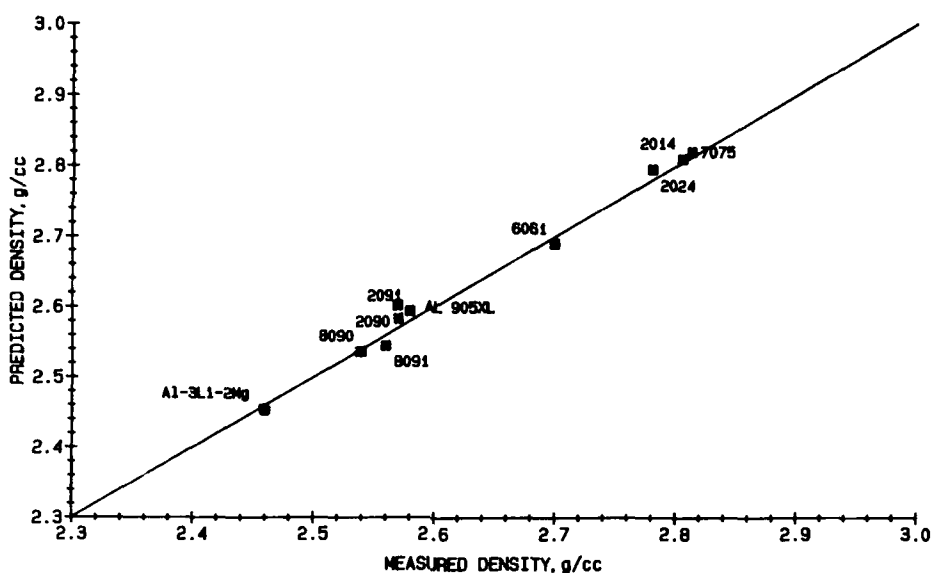


Fig.8 Predicted and measured densities for selected aluminium-lithium and conventional alloys ( Ref.24 )

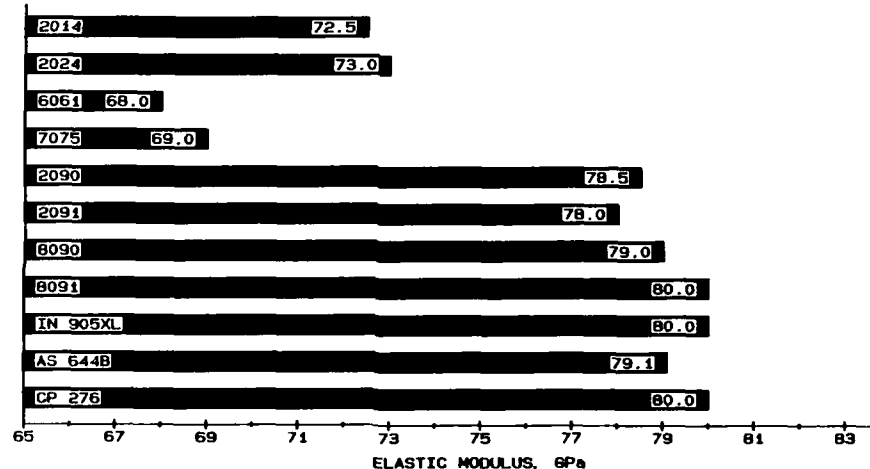


Fig.9 Elastic moduli of selected aluminium-lithium alloys

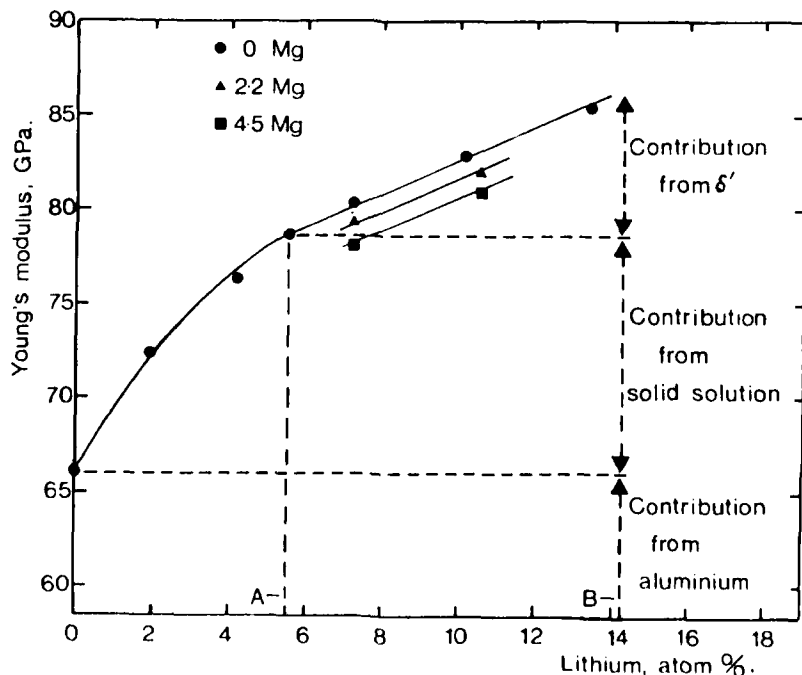


Fig.10 Relative contributions to the increase in elastic modulus achieved with lithium addition after Noble et al ( Ref.25 )

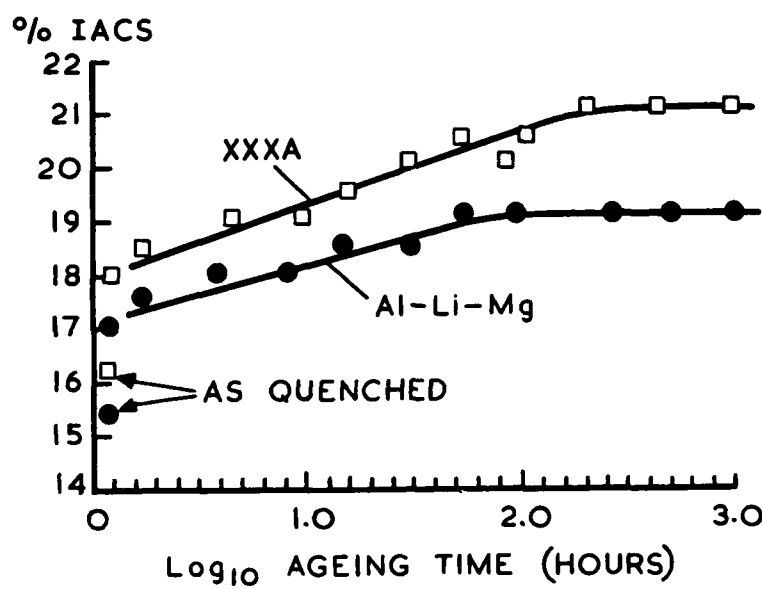


Fig.11 Electrical conductivities of unrecrystallised 8090 (XXXA) and 1420 alloy (Al-Li-Mg) developed during ageing at 170°C

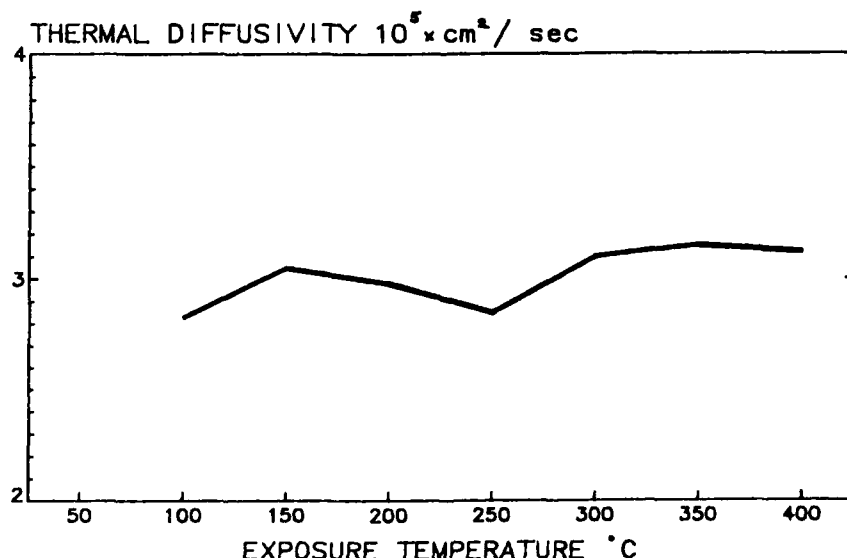
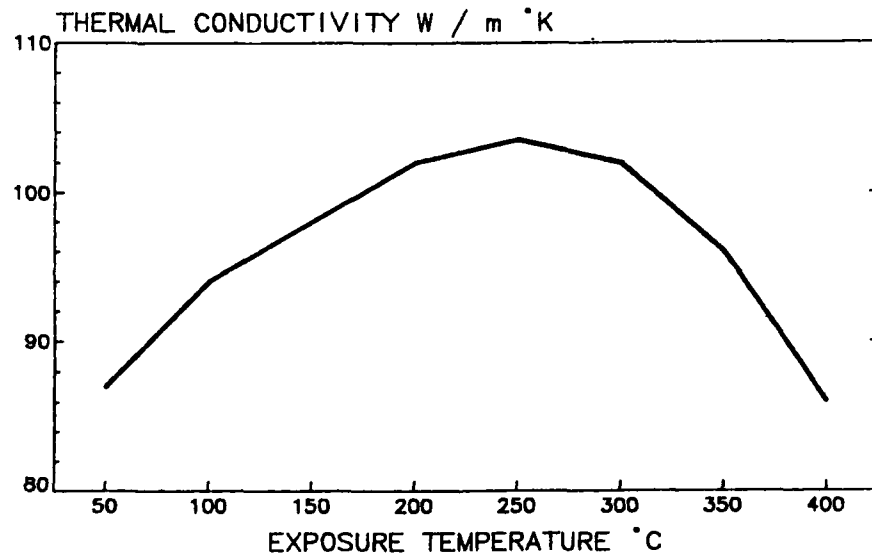


Fig.12 Thermal conductivity and thermal diffusivity of 8090 at selected exposure temperatures

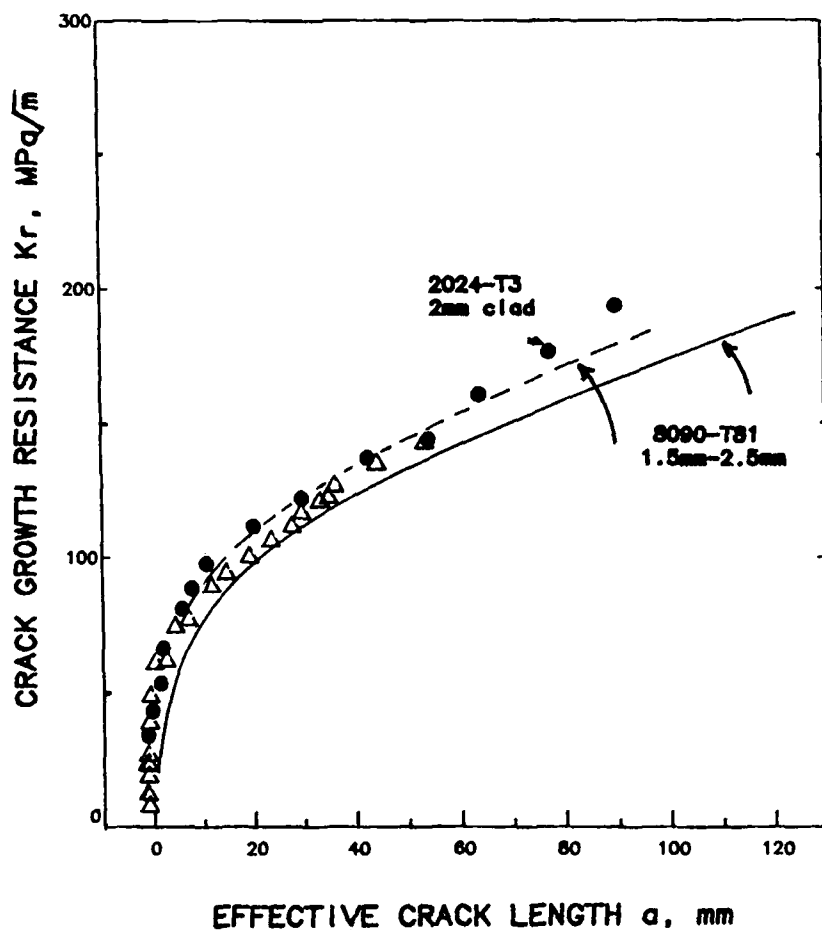


Fig.13 Fracture resistance  $K_r$  curves for damage tolerant 8090-T81 and clad 2024-T3 sheet after McDarmida et al ( Ref.30 )

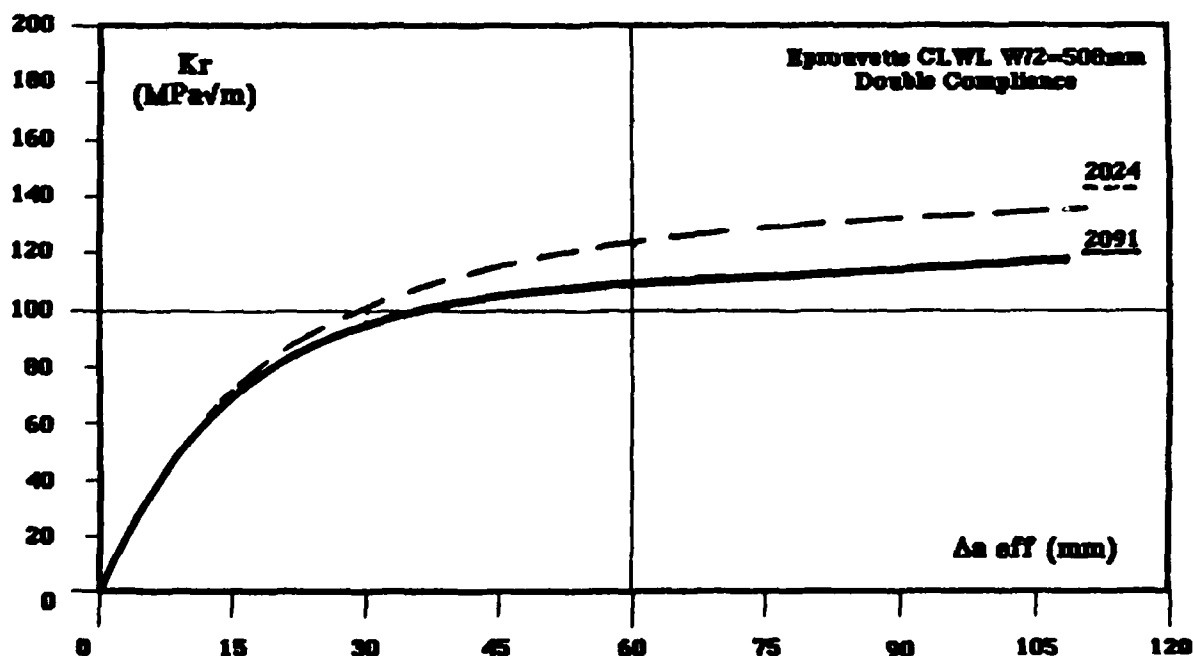


Fig.14 Fracture resistance curves for damage tolerant 2091-T81 and 2024-T3 sheet after Barbaux ( Ref.31 )

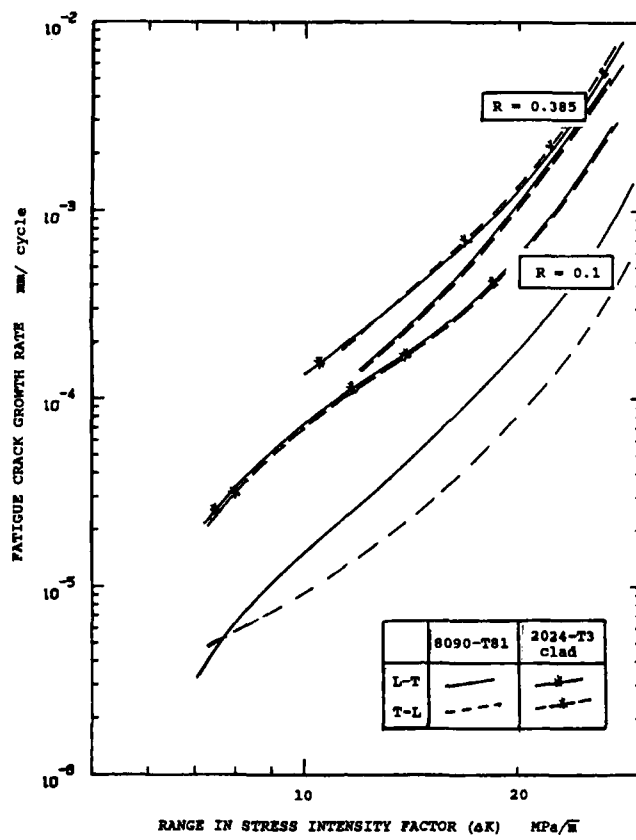


Fig.15 Fatigue crack growth resistance for damage tolerant 8090 under constant amplitude loading at two values of stress ratio. Wheeler, McDarmida et al

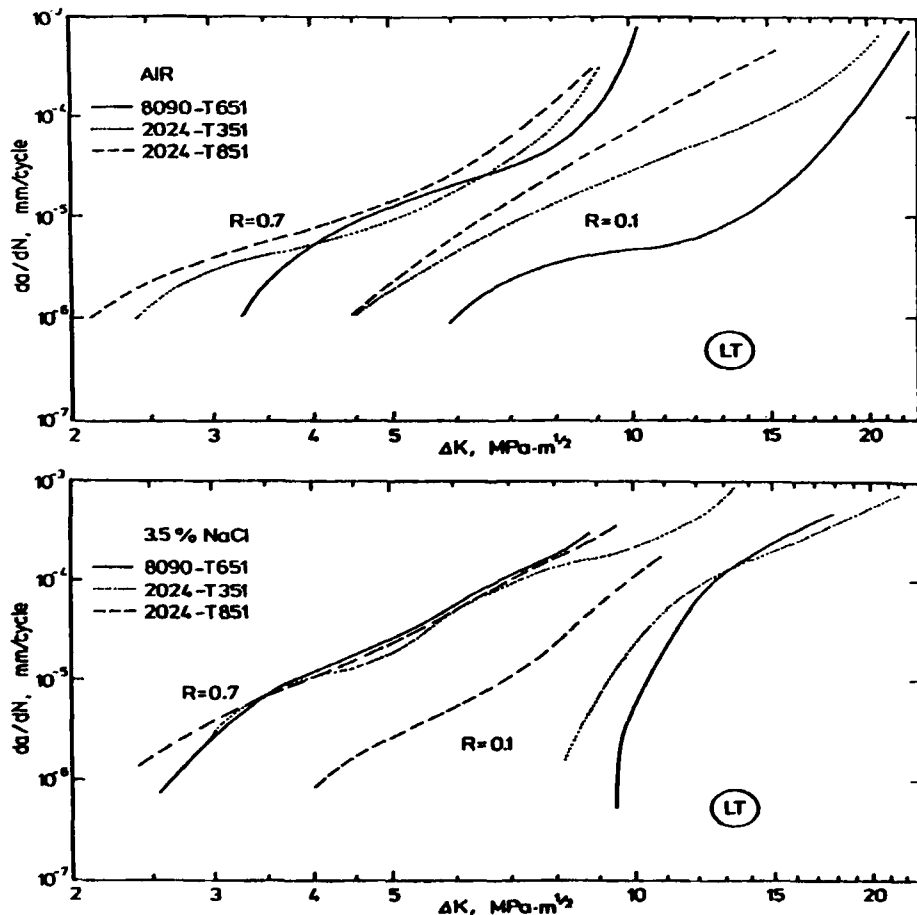


Fig.16a Fatigue crack growth resistance of 8090-T651 plate under constant amplitude loading in two environments at two levels of stress ratio, after Peters et al ( Ref.48 )

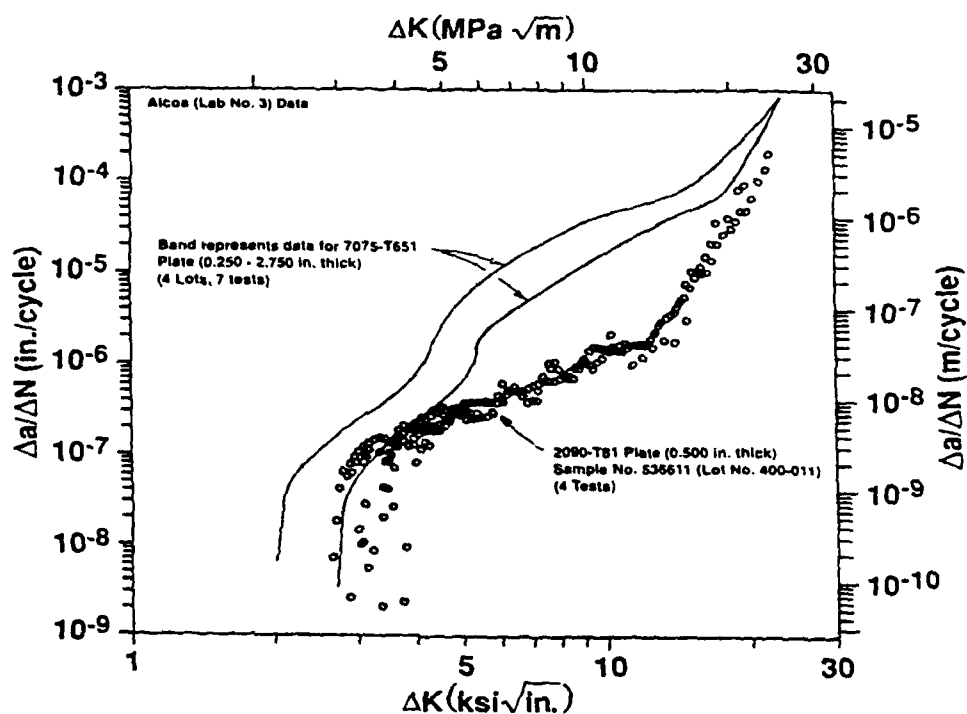


Fig.16b Fatigue crack growth resistance of high strength 2090-T81 plate compared with 7075-T651 tested under constant amplitude loading  $R=0.33$  in high humidity air ( rh=90% ) after Goodyear ( Ref.71 ).

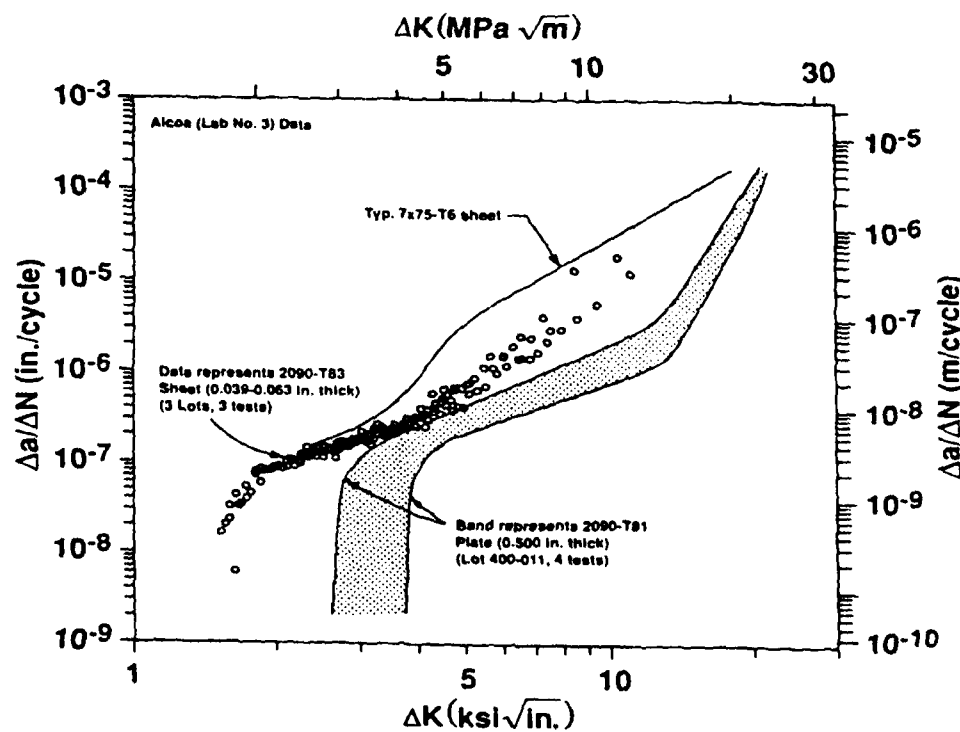


Fig.16c Fatigue crack growth resistance of high strength 2090-T83 sheet compared with 7X75-T6 sheet under constant amplitude loading,  $R=0.33$ , in high humidity air ( rh=90% ) after Goodyear ( Ref.71 )

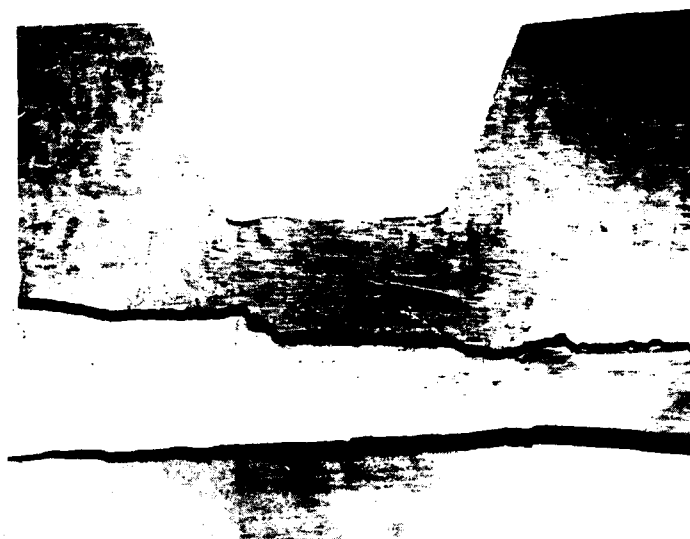


Fig.17 Macroscopic turning of fatigue cracks in damage tolerant 8090. Crystallographic texture in sheet [1] > sheet [2] > sheet [3].

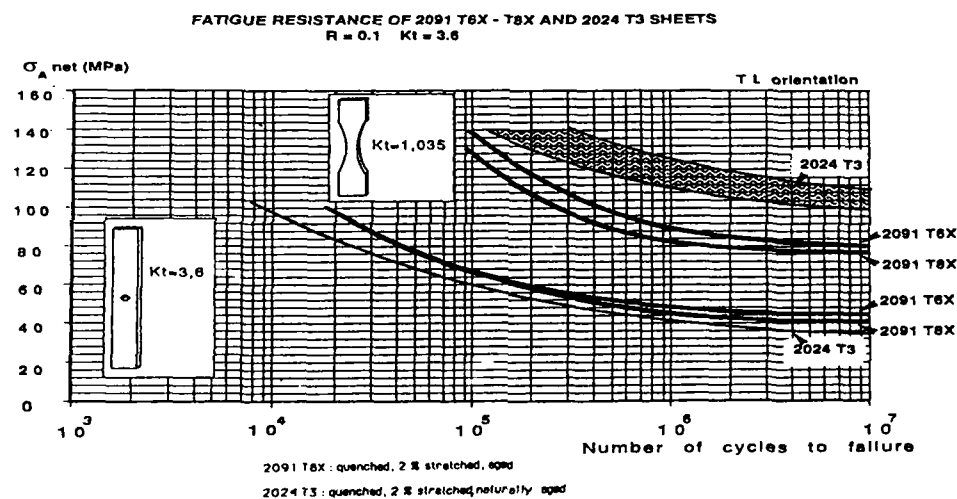


Fig.18a Fatigue strengths of damage tolerant 2091 sheet in two tempers for plain and notched test pieces after Doudeau et al ( Ref.29 ).

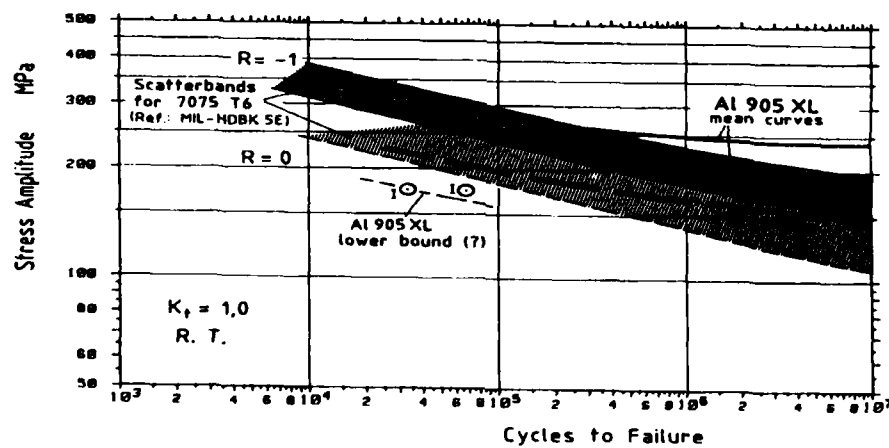


Fig.18b Fatigue strengths of Al905XL under constant amplitude loading after Schafer and Weiss ( as Ref.14 )

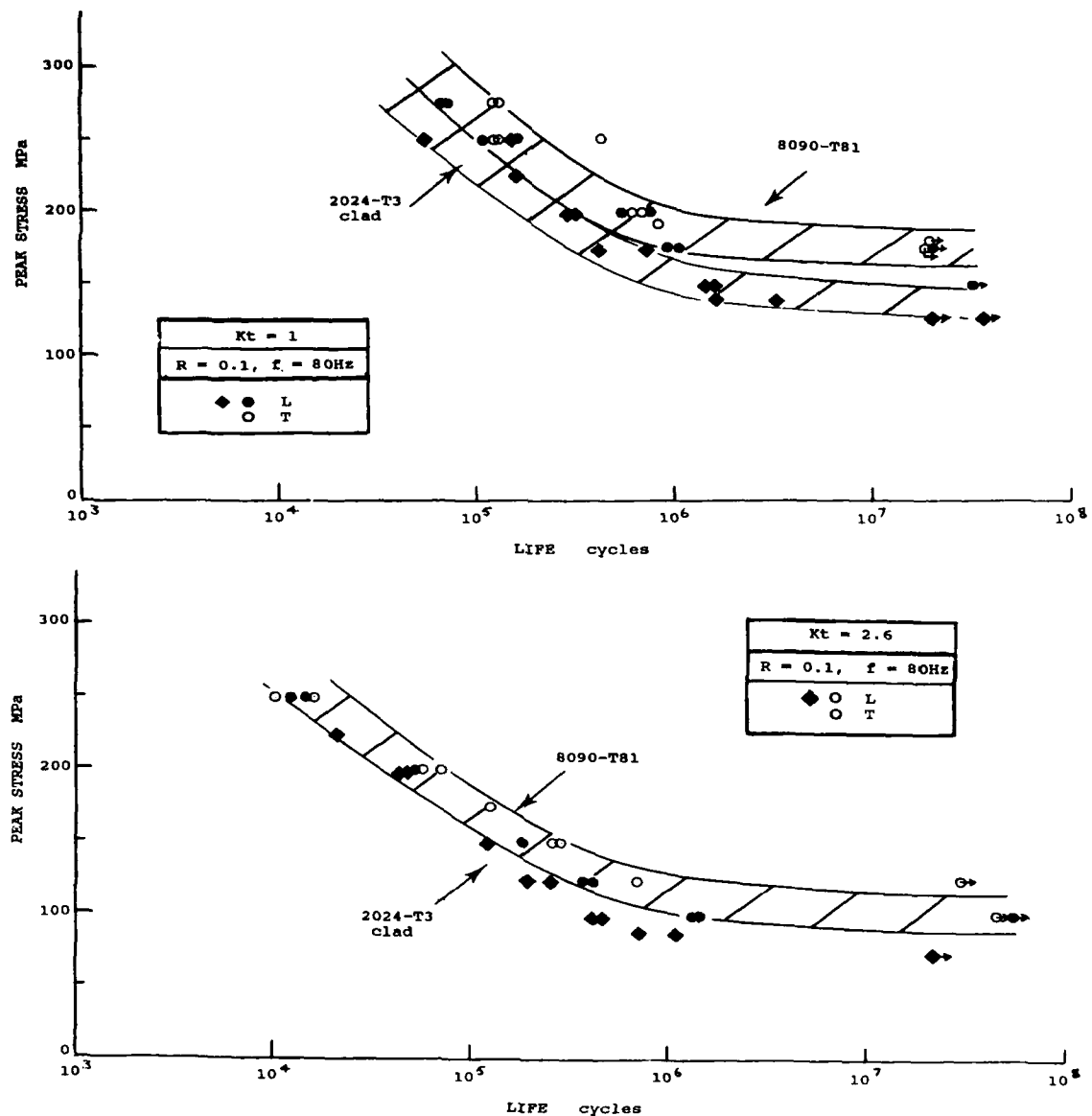


Fig.19 Fatigue strengths of damage tolerant 8090 sheet for plain and notched test pieces after McDarmaid

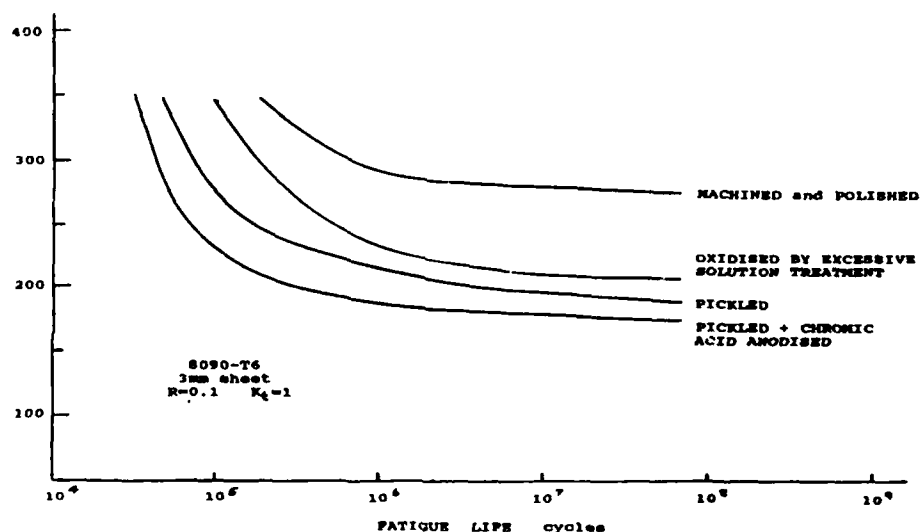


Fig.20 Showing the relative damage to fatigue strength associated with excessive oxidation of the surface in comparison with standard pickled surfaces ( Ref.30 ).

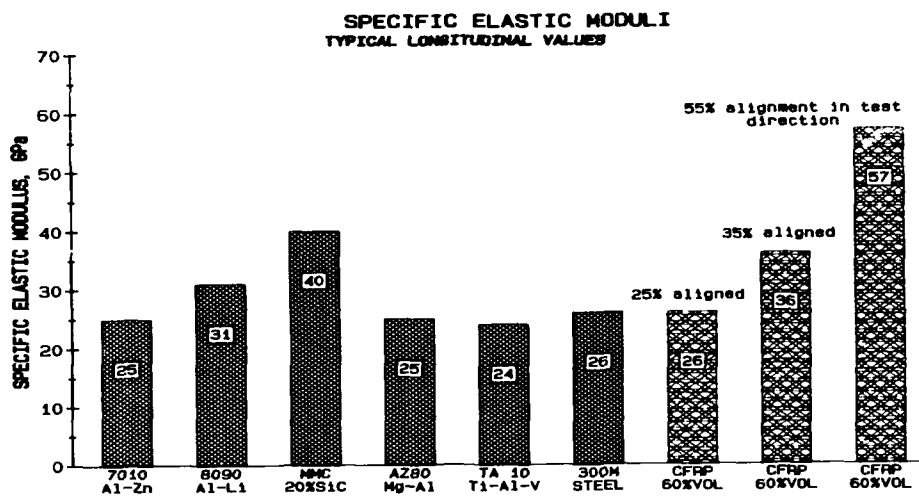


Fig.21a Specific elastic moduli of current monolithic and composite materials showing the relative performance of ingot 8090 alloy.



Fig.21b Specific buckling resistance of current monolithic and composite materials showing the relative performance of ingot 8090 alloy.

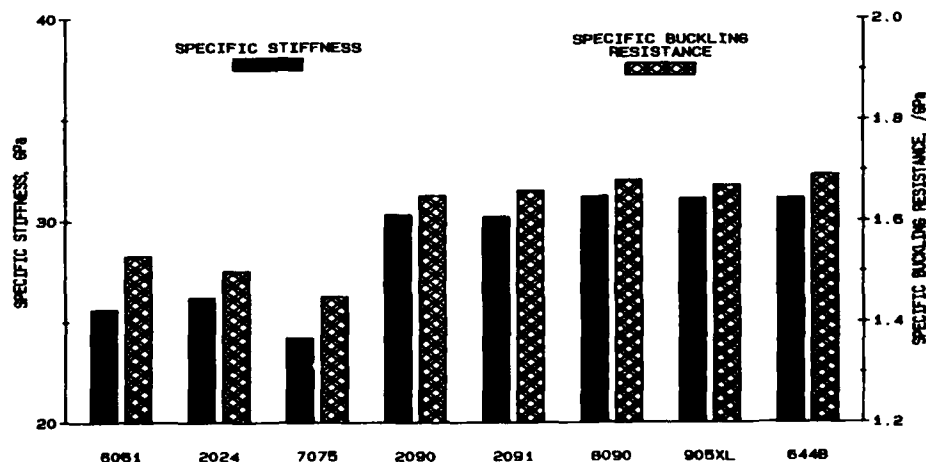


Fig.21c Specific stiffness and buckling resistance of selected aluminium-lithium alloys all showing similar performance.

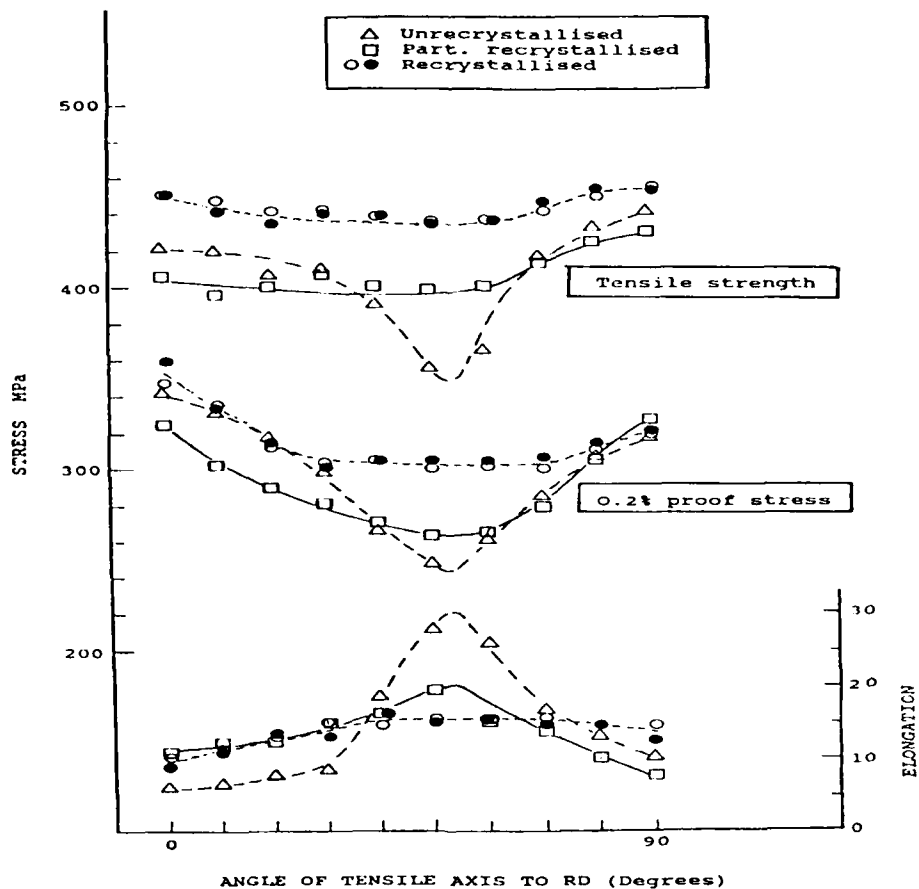


Fig.22 The effect of recrystallisation on the anisotropy in tensile properties of aluminium-lithium 8090 sheet ( Ref.30 ).

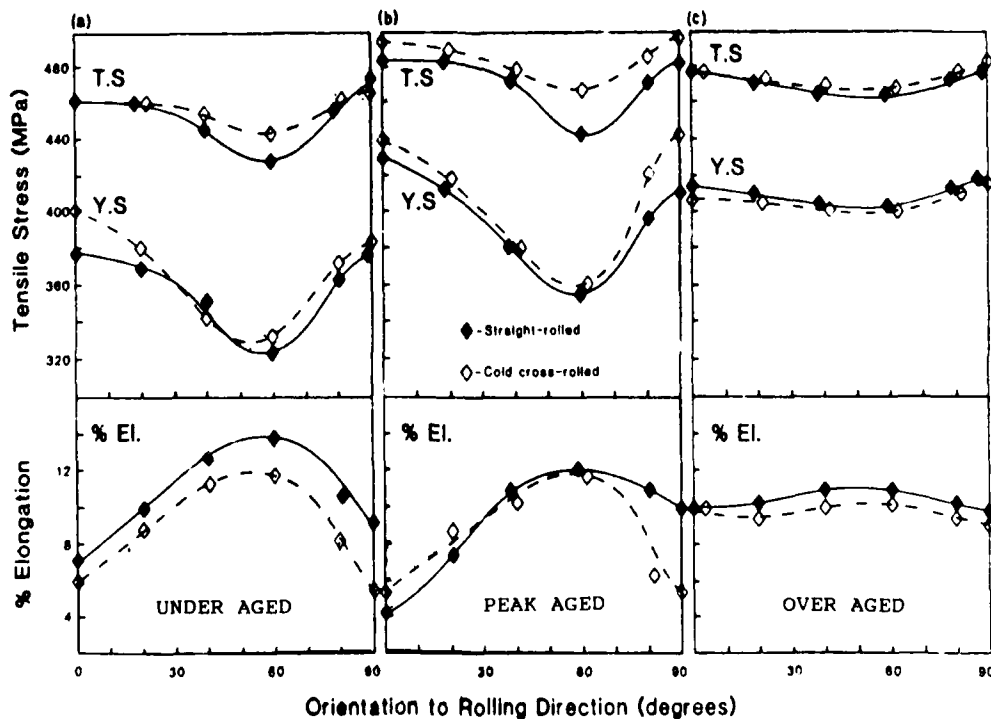


Fig.23 The effect of rolling direction and extended ageing after stretching on the anisotropy in unrecrystallised aluminium-lithium sheet after Gregson and Flower ( Ref.60 ).

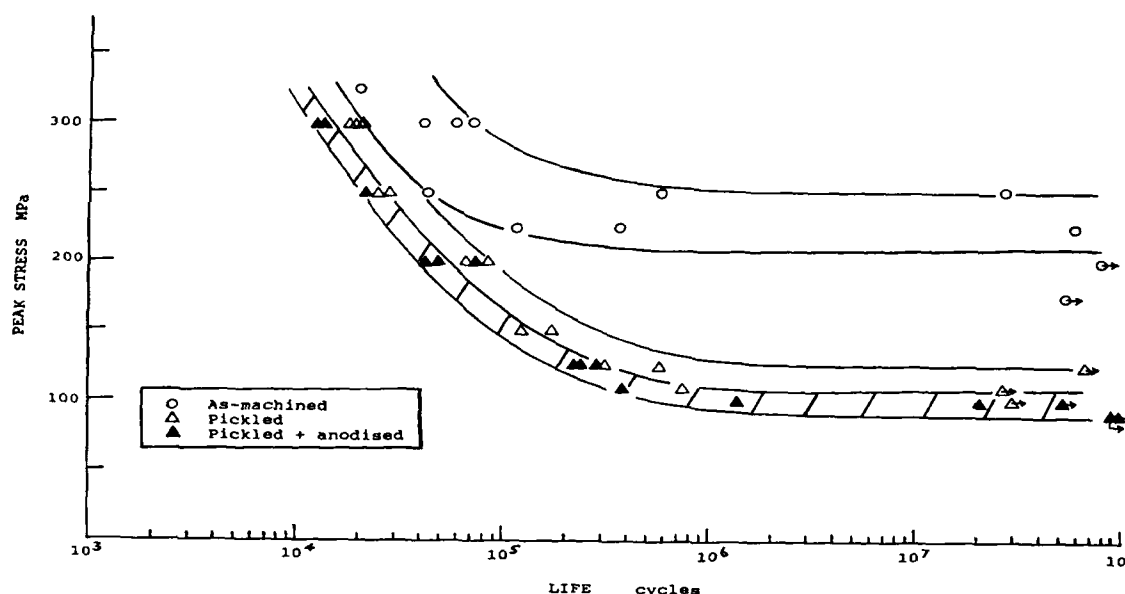


Fig.24a Short transverse fatigue strength of 90mm 7075-T7351 plate in the machined, pickled and anodised conditions ( CA R=0.1 ).

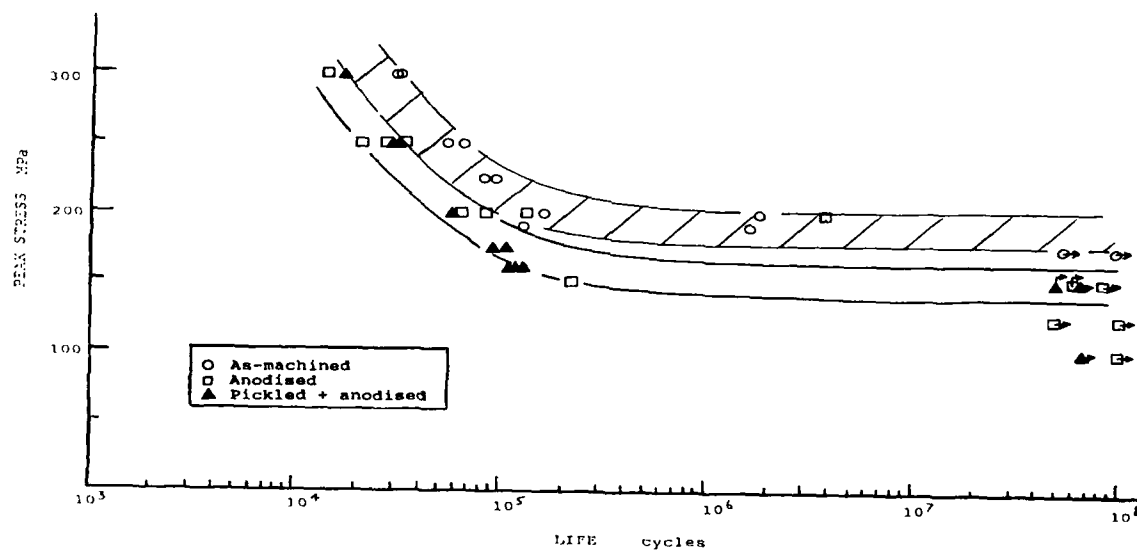


Fig.24b Short transverse fatigue strength of 90mm 8090-T8771 plate in the machined, pickled and anodised conditions, as 24a, after McDarmaid.

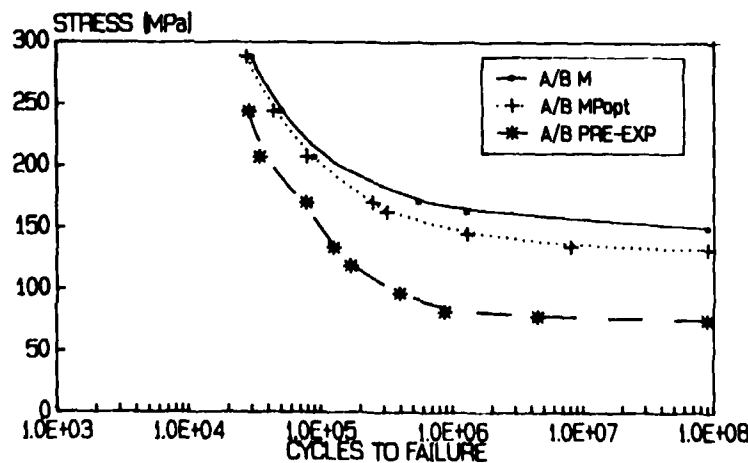


Fig.24c Short transverse fatigue strength of 60mm 8090-T851 plate after an optimised pickle and after 20 days prior alternate immersion in 3.5% NaCl ( CA R=-1.0 ) after Bolam et al ( Ref.49 ).

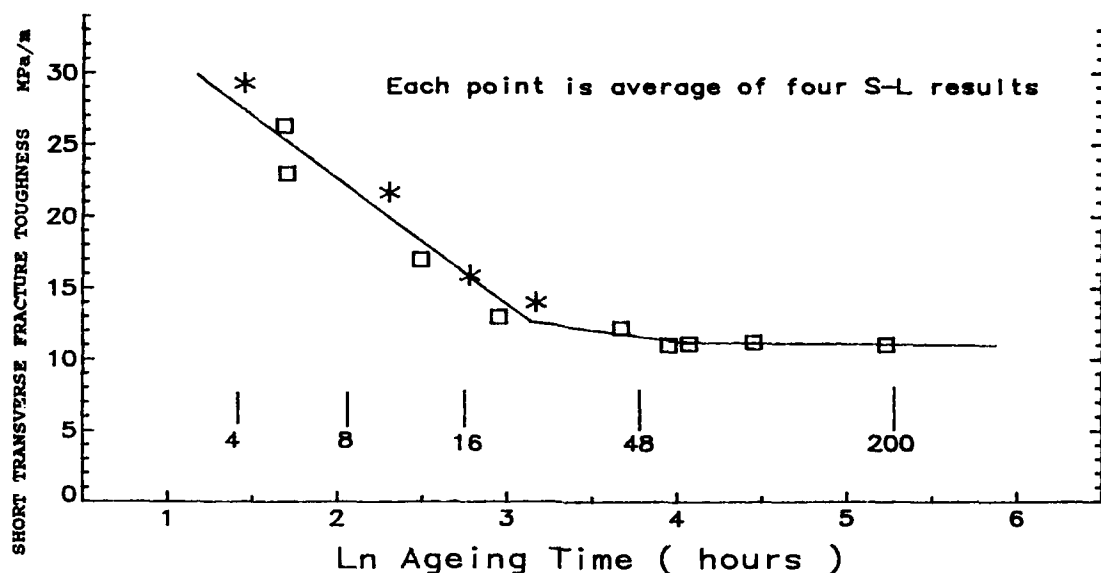


Fig.25 Decay in short transverse toughness of 8090-T651 plate with ageing at 190C after Peel et al ( as Ref.13 ).

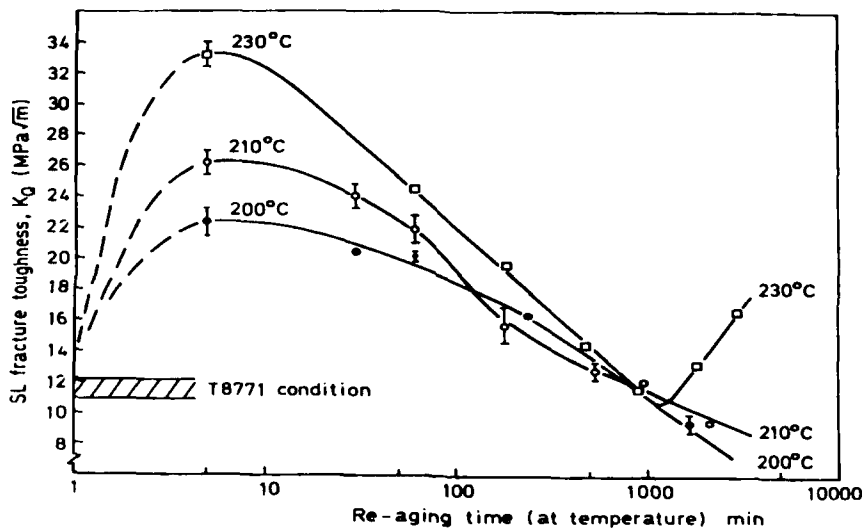


Fig.26 Reversion in short transverse fracture toughness with a short secondary ageing after Lynch ( Ref.106 ).

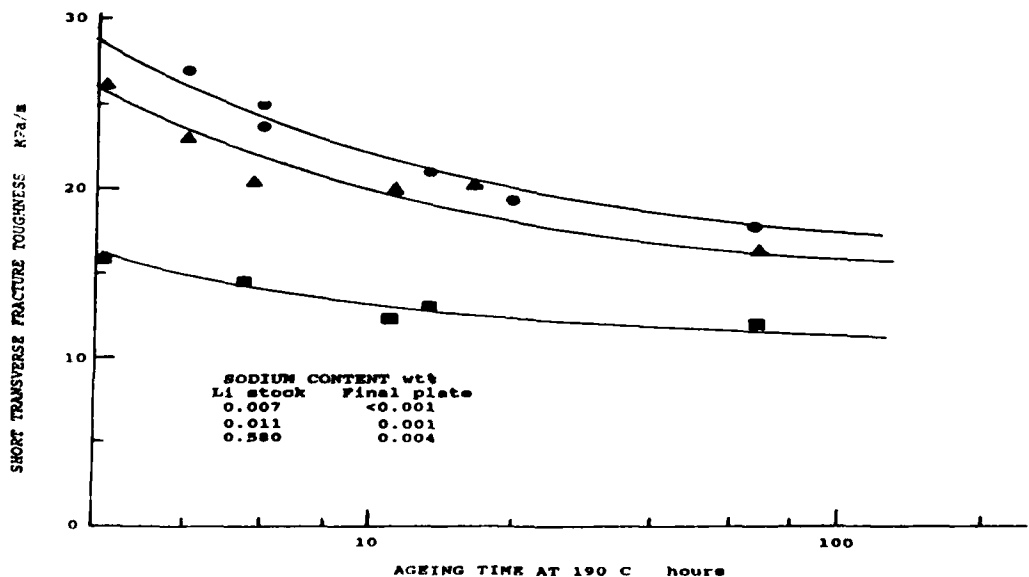


Fig.27 The effect of sodium contamination on the short transverse toughness of 8090 plate after Peel et al ( Ref.17 ).

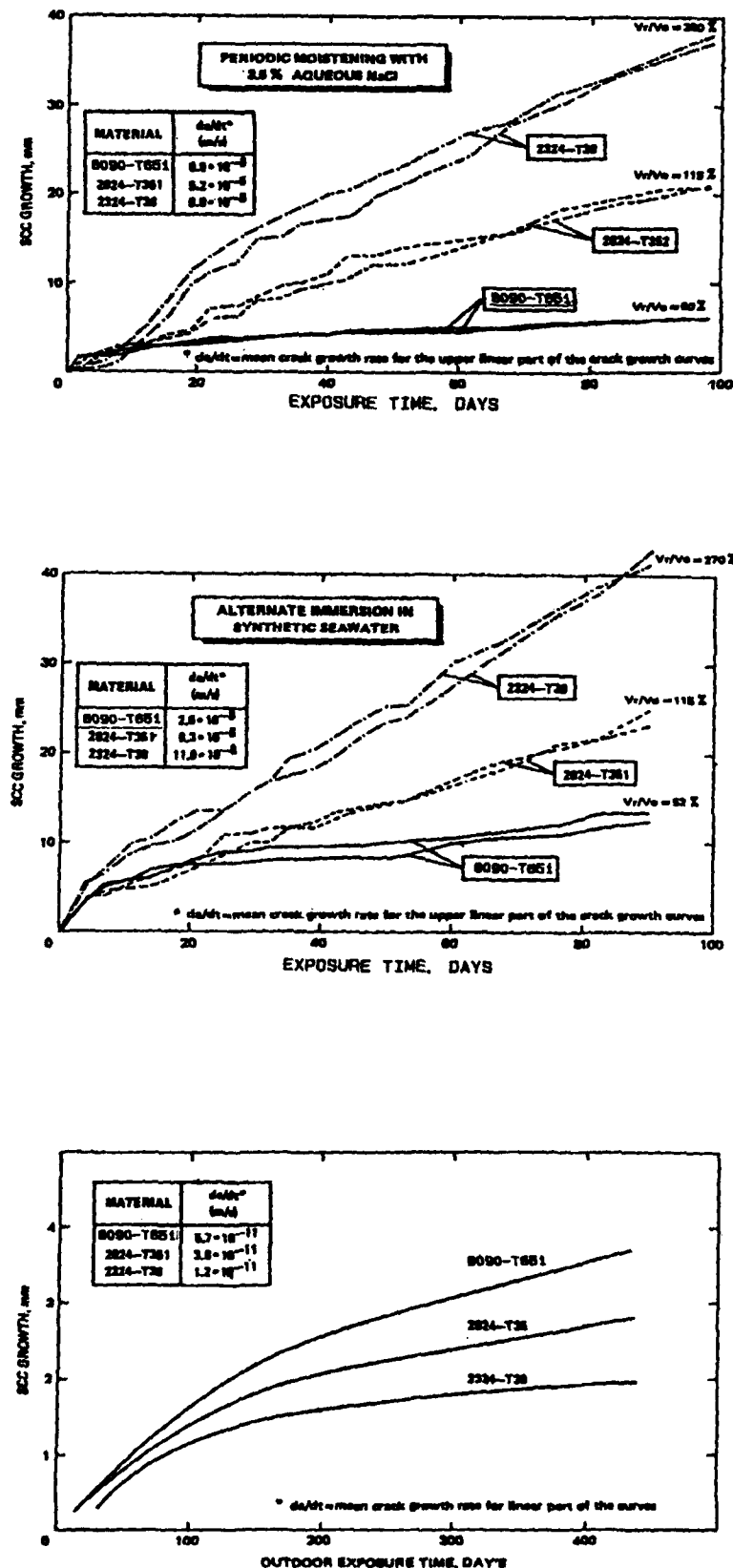


Fig. 28 Stress corrosion crack velocities in the S-L direction of 8090-T651, 2324-T39 and 2024-T351 plate showing the effect of environment after Smith et al (Ref. 76).

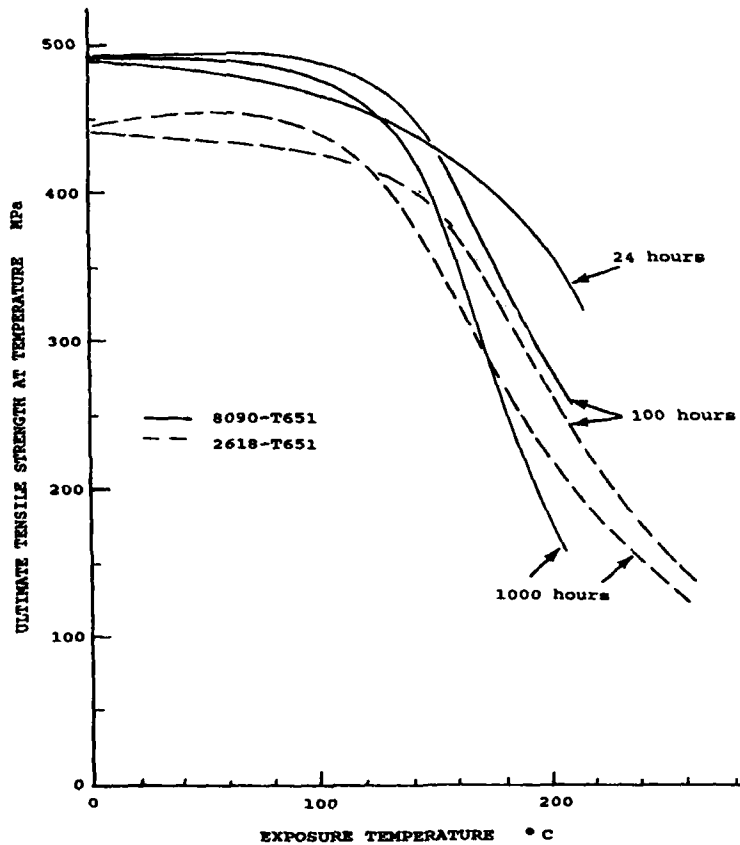


Fig.29 Tensile strengths of 8090-T651 plate tested at temperature after 24, 100, and 1000 hours prior exposure compared with 2618 aluminium alloy after Peel et al ( Ref.30 ).

### Full Scale Fatigue Test

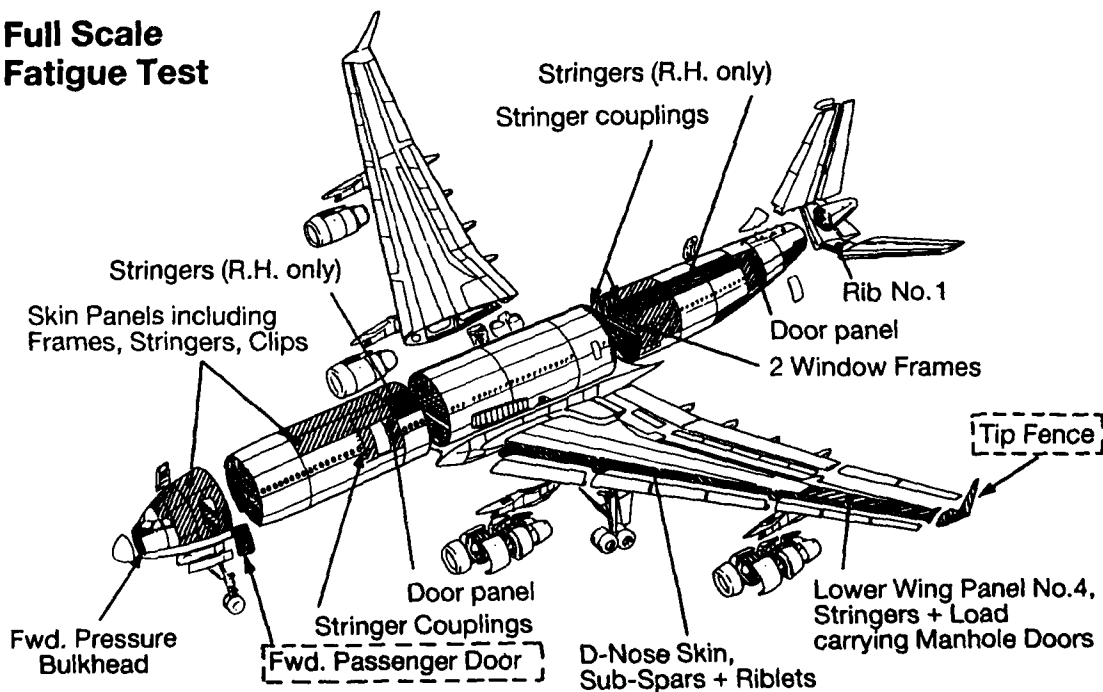


Fig.30 Schematical representation of declared full-scale testing programme for aluminium-lithium alloys on Airbus A330/340 after Koschorst ( Ref.133 ).

TABLE 1  
COMPOSITIONS OF SELECTED ALUMINIUM-LITHIUM ALLOYS

ALLOY	Li	Cu	Mg	Si	Fe	Zr	S.G.
1420	1.5-2.6	-	4.0-7.0	( Mn+Cr )	0.05-0.3	2.50	
2020	1.1	4.5	-	( Mn+Cd )	-	2.71	
2090	1.9-2.6	2.4-3.0	0.25	0.10	0.12	0.08-0.15	2.60
2091	1.7-2.3	1.8-2.5	1.1-1.9	0.20	0.30	0.04-0.10	2.58
8090	2.1-2.7	1.0-1.6	0.6-1.3	0.20	0.30	0.04-0.16	2.53
8091	2.4-2.8	1.8-2.2	0.5-1.2	0.30	0.50	0.08-0.16	2.54
8092	2.1-2.7	0.5-0.8	0.9-1.4	0.10	0.15	0.08-0.15	2.53
8192	2.3-2.9	0.4-0.7	0.9-1.4	0.10	0.15	0.08-0.15	2.51
905XL	1.5	-	4.0	( 1.1C + 0.80 )	-	2.57	
644B	2.55	1.0	0.5	0.03	0.03	0.50	2.52
WELD- ALITE	1.3	4.5-6.3	0.4	( 0.4Ag )	0.14	2.73	

TABLE 2  
CONTENDING ALLOYS FOR SELECTED POTENTIAL APPLICATIONS

POTENTIAL APPLICATIONS	PRODUCT FORMS	ALLOYS
DAMAGE TOLERANT STRUCTURE FUSELAGE SKIN AND WING SKIN FOR TRANSPORT AIRCRAFT AND HELICOPTERS	THIN PLATE, EXTRUSIONS RECRYSTALLISED SHEET	2091-TBX 2091-TBX51 8090-TB1 8090-TB151
MEDIUM STRENGTH AND STIFFNESS CRITICAL STRUCTURE DETAILED FORMED PARTS, SPF PARTS, WING AND FUSELAGE SKINNING, CONTROL SURFACES, EXTRUDED & FORMED STRINGERS, SEAT RAILS, FORGINGS FOR FUSELAGE FRAMES AND UNDERCARRIAGES. MAJOR SPACE STRUCTURAL APPLICATIONS	PLATE, EXTRUSIONS HAND AND DIE FORGINGS RECRYSTALLISED AND UNRECRYSTALLISED SHEET	2090-TB4 2091-T8/TBX 8090-T8/TB 2091-TB51(1) 8090-TB51(1) 8090-TB771 2090-T8E203 AL 905XL
HIGH STRENGTH APPLICATIONS FRAMES, RIBS, SPARS UNDERCARRIAGE PARTS FLOOR BEAMS UPPER WING SKINS	STRETCHED PLATE, EXTRUSIONS, FORGINGS STRETCHED SHEET	2090-TB1/B3 2090-T8E50 2090-T88 CP 276-TB51 8091-T8/TB 8090-TB771 8090-TB51

POTENTIAL APPLICATIONS ALSO EXIST FOR WELDALITE, 2090, 8090 ETC IN  
WELDED STRUCTURE SUCH AS CRYOGENIC STORAGE TANKS, SPACE STRUCTURE  
ETC AND FOR MINIMAL DENSITY CORROSION RESISTANT ALLOYS PERHAPS AS  
FORGINGS e.g. AL 905XL

TABLE 3  
TYPICAL PHYSICAL PROPERTIES OF ALUMINIUM-LITHIUM ALLOYS

PROPERTY		2090	2091	8090
DENSITY	g/cc	2.595	2.58	2.535
ELECTRICAL CONDUCTIVITY	%IACS	17-19	17-20	18-21
RESISTIVITY AT 20°C	u0cm	9.4	9.4	9.3
THERMAL CONDUCTIVITY AT 20°-100°C	W/m°C	70-80	76-88	80-90
SPECIFIC HEAT	J/Kg°C	1200	980	990
COEFFICIENT THERMAL EXPANSION AT 20°C-100°C	/°C × 10 <sup>-6</sup>	23.6	22	22

TABLE 4  
PROPERTIES OF DAMAGE TOLERANT VARIANTS

RECRYSTALLISED SHEET UP TO 3.5mm THICK

ALLOY	TEMPER	L	0.2% PS MPa	UTS MPa	EL %	Kapp MPa/m	Kc *
2091	T8X	L	348	440	18	100	150
		T	335	480	17	90	140
2091 CPHK	T8X	L	335	420	14	130	90
		T	325	435	13	125	85
8090	T81	L	340	435	11	100	150
		T	310	440	13	90	120
2024	T3	L	315	430	20	105	155
		T	285	425	18	95	145

\* 500mm OCT PANELS OF 1.6mm SHEET

RECRYSTALLISED AND PART RECRYSTALLISED THICK SHEET 3.5mm-7mm

2091	T8X51	L	410	490	13	-	-
		T	365	485	15	-	-

8090 T81 L 320 425 10 105 155 +

T 295 425 12 90 120

+ 400mm CCT PANELS 3-4mm THICK

UNRECRYSTALLISED STRETCHED PLATE UP TO 40mm THICK

2091	T8X51	L	410	490	13	Kq	45	MPa/m
		T	365	485	15		40	MPa/m

8090 T8151 L 380 450 10 >55 MPa/m

T 350 455 11 >55 MPa/m

TABLE 5  
MEDIUM STRENGTH AND HIGH STIFFNESS VARIANTS  
RECRYSTALLISED AND UNRECRYSTALLISED SHEET

ALLOY	TEMPER	0.2% PS			UTS			EI		Kapp	
		L	T	60°	L	T	60°	L	T	MPa/m	L-T
2091	T851	475	455	395	525	515	470	9	9	-	-
8090	UR T8/T82	395	380	345	465	470	455	5	8	80	50
	UR T8	455	405	365	515	520	500	6	8	55	-
	R T8	390	375	360	475	475	480	9	10	63	48
	R T82	360	325	320	450	455	455	10	11	-	-

## UNRECRYSTALLISED PLATE UP TO 100mm THICK

ALLOY	TEMPER	0.2% PS			UTS			EI		Kq/Kic	
		L	T	60°	L	T	60°	L	T	L-T	T-L
2091 *	T851	475	455	395	525	500	470	9	9	35	25
8090	T851	455	455	395	500	500	480	7	7	33	30
8090 *	T8771	475	465	425	515	500	475	6	6	37	33
8090	T8771	455	405	380	485	495	480	4	6	35	30

\* THIN GAUGE ONLY &lt; 25mm

## EXTRUDED SECTIONS

ALLOY	TEMPER	0.2% PS			UTS			EI		Kq	
		L	T	60°	L	T	60°	L	T	L-T	T-L
+ 8090 <8mm	T851	440	465	515	515	515	-	7	6	-	-
8090 <25mm	T851	505	425	550	495	495	-	5	5	33	17
8090 >75mm	T851	460	375	530	500	500	-	4	5	65	35

+ PECHINEY MATERIAL AS OPPOSED TO ALCAN

TABLE 6  
PROPERTIES OF ALUMINIUM LITHIUM ALLOY FORGINGS

## HAND FORGINGS

ALLOY	TEMPER	0.2% PS			UTS			EL		Kic	
		L	S	MPa	L	S	MPa	L	S	MPa/m	T-L
8090	T8	390	340	-	480	430	-	5	2	35	22
	T852	420	390	-	520	460	-	9	3	30	20
AL 905XL		450	440	-	515	490	-	11	-	-	35

## DIE FORGINGS

ALLOY	TEMPER	0.2% PS			UTS			EI		Kic	
		L	S	MPa	L	S	MPa	L	S	MPa/m	T-L
8090	T8	410	340	-	500	420	-	6	3	35	29
	T852	470	370	-	520	460	-	8	4	30	25
2090	T8E203	420	>345	-	495	455	-	6	4	25 - 18.5	*
AL 905XL		420	390	-	485	470	-	12	8	25 - 15	*

\* DEFINITION OF TEST DIRECTION IS DIFFICULT IN FORGINGS

TABLE 7  
PROPERTIES OF SELECTED HIGH STRENGTH ALLOYS  
UNRECRYSTALLISED SHEET

ALLOY	TEMPER	0.2% PS		UTS		EI		K <sub>c</sub>	
		MPa	MPa	L	T	L	T	MPa/m	L-T
2090	T83	510	490	565	540	5	7	65	55
2090	T84	470	460	525	520	-	-	90	80
<b>UNRECRYSTALLISED THIN PLATE</b>									
2090	T81	558	552	593	586	8	6	>27.5	>22
2090	T8E50	>435	>415	>490	>490	>5	>5	45	45
8091	T851	515	485	555	535	6	5	30	25
<b>THIN EXTRUDED SECTIONS</b>									
2090 +	T86	470	-	517	-	4	-	-	-
++	T86	510	-	545	-	4	-	-	-
+++	T86	517	485	550	-	5	-	-	-
8090	T851	440	465	515	515	7	6	-	-
CP 276 *	T851	550	450	640	550	7	7	40	35

+ 0 - 3.15 mm gauge  
++ 3.15 - 6.32 mm  
+++ 6.32 - 12.75 mm  
\* 8.0 - 30.0 mm

TABLE 8  
COMPARISON OF TENSION STRENGTHS WITH PRELIMINARY RESULTS FOR  
COMPRESSIVE STRENGTH FOR SELECTED HIGH STRENGTH ALLOYS

		8090 T8771	8091 T8771	2090 T83
Tension				
0.2% PS	L	450	515	545
	T	420	485	523
	45°	405	-	440
UTS	L	515	555	600
	T	500	535	565
	45°	465	-	503
Compression				
L P	L	345	400	-
	T	385	445	-
	45°	-	-	-
Y S (0.2%)	L	455	-	537
	T	450	-	565
	45°	-	-	482
UCS	L	655	750	-
	T	675	755	-
	45°	-	-	-

TABLE 9  
CORROSION AND EXFOLIATION RESISTANCE OF SELECTED ALLOYS  
RECRYSTALLISED AND UNRECRYSTALLISED SHEET

ALLOY	TEMPER	EXCO			MASTMAASIS			MARINE	
		1	2	4	1	2	4	1	2
2090	T83	-	-	EB	-	-	P	-	N
2091	T8X	N	-	EA	EA	EA/EB	-	-	EA/EB
2091 CPHK	T8X	P	-	EA	-	-	-	-	EA/EB
8090	T81	-	EA	EA	EA	EB	-	-	E
8090	T8	EB	EC	-	EA	EA	-	-	-
8090	T8	-	EA	ED	N	P	P/EA	EA	-

THIN PLATE	EXCO			MASTMAASIS			MARINE		
	1	2	4	1	2	4	1	2	
2090	T81	EA	ED	-	P	P	P	-	N
2091	T8X51	EA	EA	EB	-	-	P	-	-
8090	T851	EA	EC	ED	-	EB	-	-	E/EA
8090	T8151	E/EA	EA	EA	-	P	-	-	EA
8090	T8771	-	-	EA	-	-	-	-	-

+ TO ASTM G34-79 TIMES 1,2,4 DAYS

\* TO ASTM G85 TIMES 1,2,4 WEEKS

o DIFFERING MARINE ENVIRONMENTS TIMES 1,2 YEARS

TABLE 10  
TENTATIVE STRESS CORROSION THRESHOLDS FOR SELECTED  
ALUMINIUM-LITHIUM ALLOYS

SHEET

ALLOY	TEMPER	ALLOY CATEGORY	LT SCC THRESHOLD MPa
2090	T83	HIGH STRENGTH	-
2091	T8X	DAMAGE TOLERANT	75 < TH < 100
2091 CPHK	T8X	DAMAGE TOLERANT*	200 < TH < 250
8090	T81	DAMAGE TOLERANT	200
8090	T8/T8	MEDIUM STRENGTH	>350

\* WITH IMPROVED SCC RESISTANCE

THIN PLATE

ALLOY	TEMPER	ST THRESHOLD STRESS MPa 3.5%NaCl AI	ST THRESHOLD STRESS MPa MARINE EXPOSURE
2090	T81	172	172 < TH < 240
2091	T8X51	<6mm >200	-
2091	T8X51	<6mm >250	-
2091	T851	>200	-
8090	T851	50-75	125
8090	T8771	140	-

FORGED MATERIAL

ALLOY	TEMPER	THRESHOLD STRESS MPa
AL905XL	-	345
8090	T852	200

## THE MICROSTRUCTURE AND PROPERTIES OF ALUMINUM-LITHIUM ALLOYS

Edgar A. Starke, Jr.  
 School of Engineering and Applied Science  
 University of Virginia  
 Charlottesville, Virginia 22901

William E. Quist  
 Boeing Commercial Airplane Company  
 P.O. Box 3707, M/S 73-43  
 Seattle, Washington 98124

## ABSTRACT

The advantages to be gained by weight reduction of aerospace structures have encouraged the aluminum industry to develop a family of aluminum alloys which contain lithium as one of the alloying elements. When alloyed with aluminum, lithium can reduce the density by approximately three percent and increase the elastic modulus by six percent for every weight percent added. A new series of aluminum alloys, typified by 2090, 2091, 8090, and 8091, have been developed and are currently being produced in commercial quantities. These alloys have densities between 7% and 10% lower than the conventional alloy 7075 with correspondingly higher stiffness. Although a combined set of specific properties of the Al-Li-X alloys often exceeds those of the conventional aluminum materials used in aerospace, these properties seem to be much more sensitive to processing parameters. The strong processing-property relationship is associated with sharp crystallographic textures that are developed during primary processing and very complex precipitate microstructures whose distributions are sensitive to quench rates and degree of deformation prior to aging. This paper describes the processing-microstructure-property relationships of the new Al-Li-X alloys and focuses on strength, ductility, fracture toughness, fatigue and stress corrosion properties.

## INTRODUCTION

The development of Al-based alloys containing lithium began in Germany in the 1920's and was primarily concerned at first with additions of very small amounts of lithium to Al-Zn-Cu alloys to increase their strength (1,2). However, the development of modern aluminum-lithium alloys can be traced to the discovery by LeBaron in 1942 that lithium could be a major strengthening element in aluminum-copper alloys (3). Subsequent work by Hardy and Silcock (4,5) identified the lithium-containing strengthening phases in Al-Cu-Li alloys and contributed significantly to the scientific understanding of these complex materials. In the 1950's metallurgists at Alcoa recognized that lithium also increased the elastic modulus of aluminum and developed the high strength Al-Cu-Li alloy 2020. Later, metallurgists in Russia (6) developed the Al-Mg-Li alloy 01420 which had a considerable density advantage over other medium strength aluminum alloys. However, production problems combined with marginal engineering properties inhibited the widespread use of these lithium-containing aluminum alloys.

In the early 1970's escalating fuel costs and the desire to develop more fuel-efficient and high-performance aircraft generated a major interest in materials that would reduce weight and thereby increase structural efficiency. Reducing the density, without compromising strength, toughness, and corrosion resistance, has been shown to be the most efficient way to accomplish this goal (7). Although carbon fiber and boron fiber non-metallic composites offer a considerable density advantage over all other structural materials used in aircraft, improvements in the properties of aluminum alloys seemed desirable due to their relatively low acquisition cost and the aircraft community's extensive design and manufacturing experience with these materials. Aluminum-lithium alloys appeared attractive since lithium can reduce the density of aluminum by three percent and increase the elastic modulus by six percent for every weight percent added (8). These advantages have encouraged every major aluminum alloy producer in the U.S. and abroad to develop alloys containing lithium, usually at levels of 2.0 weight percent and higher. Both ingot metallurgy (I/M) and powder metallurgy (P/M) approaches were used during the alloy development programs; however, most major advances were made using the former technique.

Alloy designations and compositions of the new lithium-containing aluminum alloys are listed in Table 1. Many of these alloys possess good combinations of strength, damage tolerance and durability, in general are quite weldable, and several have demonstrated excellent cryogenic and elevated temperature properties. In addition, to those listed in Table 1, alloys are under development which show improved corrosion resistance and post-weld properties. One of these, a high strength, weldable Al-5.0Cu-1.3Li-0.4Mg-0.4Ag-0.1Zr alloy, Weldalite 049, was developed specifically for cryogenic tanks associated with launch vehicles (9). The properties of most of the new aluminum-lithium alloys appear particularly sensitive to small variations in composition and processing. This sensitivity seems to be associated with the difficulty in maintaining metal quality during casting, the presence of recrystallization inhibiting elements, and the complexity of the microstructure after primary processing and heat treatment. As with most aluminum alloys, microstructural features of importance for property control of Al-Li alloys include: (a) cast structure, (b) grain structure and crystallographic texture, (c) volume fraction, size and distribution of insoluble intermetallic particles and grain boundary precipitates and (d) coherency, volume fraction and distribution of strengthening precipitates.

TABLE 1. Current Al-Li Alloys and Compositions.

Alloy Element <sup>1</sup>	2090 Alcoa 8/6/84	2091 C Pechiney 4/8/85	8090 Alcan and C Pechiney May 1985	8090A Alcoa (Late 1985)	8091 Alcan 3/29/85	X8092 Alcoa May 1985	X8192 Alcoa Aug 1985
Si	0.10	0.20	0.20	0.10	0.30	0.10	0.10
Fe	0.12	0.30	0.30	0.15	0.50	0.15	0.15
Cu	2.4-3.0	1.8-2.5	1.0-1.6	1.1-1.6	1.8-2.2	0.5-0.8	0.4-0.7
Mn	0.05	0.10	0.10	0.05	0.10	0.05	0.05
Mg	0.25	1.1-1.9	0.6 to 1.3	0.8-1.4	0.5-1.2	0.9-1.4	0.9-1.4
Cr	0.05	0.10	0.10	0.05	0.10	0.05	0.05
Ni	—	—	—	—	—	—	—
Zn	0.10	0.25	0.25	0.10	0.25	0.10	0.10
Ti	0.15	0.10	0.10	0.15	0.10	0.15	0.15
Li	1.9-2.6	1.7-2.3	2.2-2.7	2.1-2.7	2.4-2.8	2.1-2.7	2.3-2.9
Zr	0.08-0.15	0.04-0.16	0.04-0.16	0.08-0.15	0.08-0.16	0.08-1.5	0.08-1.5
Other: Each	0.05	0.05	0.05	0.05	0.05	0.05	0.05
Total	0.15	0.15	0.15	0.15	0.15	0.15	0.15

\*Numbers Shown Are Either Maximums or Ranges

#### MICROSTRUCTURE AND DEFORMATION BEHAVIOR

##### Cast Structure:

Casting problems have been associated with the development of Al-Li alloys since Alcoa's entry with alloy 2020. Some of these are related to the reactivity of lithium-containing aluminum alloys and associated safety problems which have necessitated the use of modified refractories and degassing procedures, protective inert cover gases and/or surface fluxes during melting and casting, and special ingot cooling techniques (some employing organic coolants in place of water). These techniques have minimized the hazards of casting Al-Li alloys and current work is focusing on improving the quality of the as-cast product. The "as-cast quality" of ingot depends on both the surface quality, which determines the amount of scalping prior to further processing, and the internal structure which determines the processing steps necessary to produce the desired microstructure-property relationship. There can be, of course, some casting defects which are impossible to remove during subsequent processing. In addition to having a high surface quality and a crack-free ingot, the ingot should be free of spherical voids and blisters and have a medium-fine grain structure, a consistent composition throughout, a low inclusion and alkali impurity content, and a low gas content (10).

A fine cast grain structure reduces porosity and the tendency for ingot cracking. Aluminum-lithium alloys have been found to be more difficult to grain refine than conventional aluminum alloys (11). The difficulty has been partly associated with the presence of zirconium which is used to control the wrought grain structure, since zirconium enhances the formation of twinned columnar grains (TCG) (12). Zirconium has beneficial effects, of course, since it forms the coherent  $\text{Al}_3\text{Zr}$  during ingot preheat which is very efficient in inhibiting recrystallization without the adverse effects on fracture toughness that are sometimes associated with large  $\text{Al}_{12}(\text{Fe},\text{Mn})_3\text{Si}$ ,  $\text{Al}_9\text{Mn}_3\text{Si}$ , and  $\text{Al}_{20}\text{Cu}_2\text{Mn}_3$  particles present in many 2XXX alloys. During normal ingot breakdown, hot working and subsequent heat treatment, the  $\text{Al}_3\text{Zr}$  dispersoids inhibit recrystallization although the cast grains do elongate in the direction of metal flow. Consequently, in the final product most Al-Li alloys are unrecrystallized, and the cast grain structure relates directly to the grain structure.

Typical grain refining problems include a non-uniform grain size and the formation of twinned columnar grains (TCG) which not only result in increased cracking during processing but also reduce the elongation of the final product as shown in Figure 1. The as-cast grain size correlates well with both the toughness and the stress corrosion resistance of the final product. A fine as-cast grain size reduces fracture toughness, and fatigue crack growth resistance, since it minimizes the beneficial crack branching and the tortuous crack path often observed in larger-grained aluminum alloys. However, a fine as-cast grain size has been shown to have beneficial effects on the stress corrosion resistance of aluminum-lithium alloys, Figure 2. A reduction in grain size decreases the slip length and reduces the stress concentrations at grain boundaries thus reducing the mechanical component of stress corrosion cracking.

Inclusions may originate from the lining of the furnace, the flux, or from the presence of certain impurities, e.g., iron and silicon. The effect of iron content on the strength/toughness of alloy 2020 aged to the T8 temper (13) is shown in Figure 3. Molten metal filtering, fluxless or inert gas casting, and high purity starter materials are

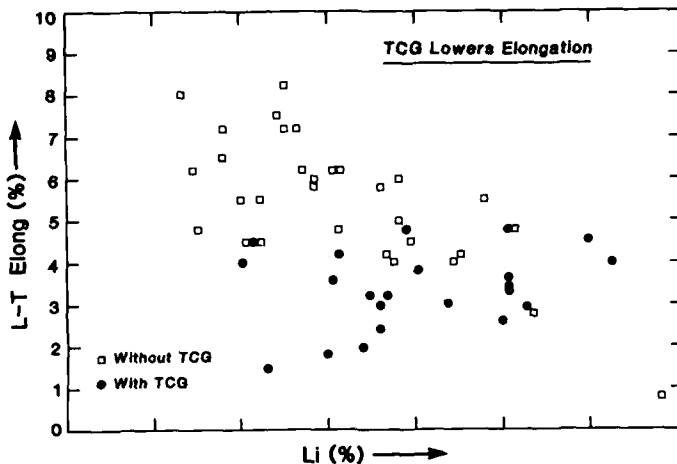


Figure 1. The effect of twin columnar grains and lithium content on the elongation of Al-Li alloys (From Labarre et al., reference 11).

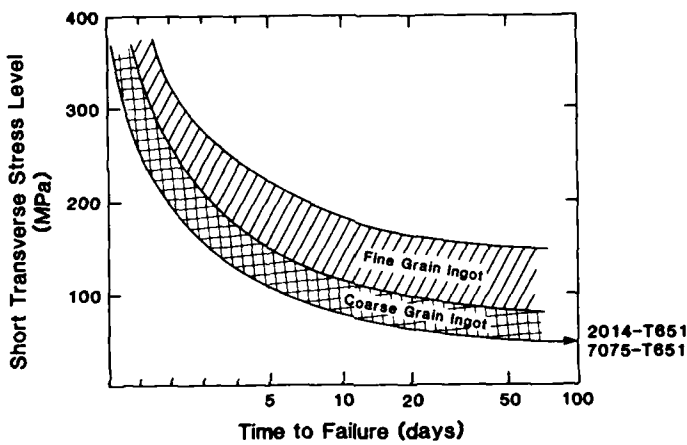


Figure 2. The effect of as-cast grain structure on the stress corrosion behavior of 8090-T851 plate. Base-line data of 2012-T651 and 7075-T651 is shown for comparison (Courtesy of A. Gray, Alcan International).

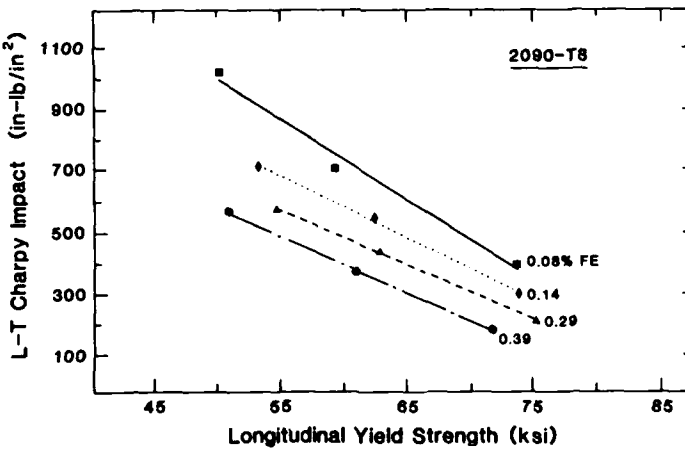


Figure 3. The effect of iron content on the strength/toughness relationship of 2090 (From Ashton et al., reference 13).

common methods used to minimize inclusion problems. Besides the well-known relationship between inclusion content and fracture toughness, a high silicon content is believed to have a detrimental effect on the corrosion properties of Al-Li alloys (14). For compositions containing greater than 0.08 wt.% Si, the equilibrium AlLiSi phase forms upon solidification and is retained through all subsequent thermal mechanical treatments. This phase serves as an active nucleation site for surface pitting upon exposure to salt water, and greatly diminishes the material's resistance to stress corrosion cracking.

#### Precipitate Structure, Deformation Behavior and Fracture:

**Al-Li:** When binary Al-Li alloys containing more than 1 wt.% lithium are quenched from the single-phase field and aged at a temperature below the solvus, homogeneous precipitation of the metastable ordered phase  $\delta'$  ( $\text{Al}_3\text{Li}$ ) occurs. For alloys containing more than 1.7 wt.% Li it may be impossible to suppress  $\delta'$  formation during quenching even when using ice water as the quenching medium (15). These precipitates have an  $\text{L}1_2$ -type superlattice structure, a spherical shape, and a cube/cube orientation with the aluminum matrix (16,17). High temperatures and/or long aging times at normal aging temperatures result in the heterogeneous precipitation of the equilibrium  $\delta$  ( $\text{AlLi}$ ) phase at grain boundaries and other planar interfaces. These precipitates consume lithium from the surrounding region and produce a lithium-depleted precipitate-free-zone (PFZ) adjacent to the grain boundary. The microstructural features just described are shown in the transmission electron micrographs (TEM's) of Figure 4a. In commercial Al-Li alloys that contain zirconium the small ( $\approx 50$  nm) coherent, ordered  $\text{Al}_3\text{Zr}$  dispersoids that form during the ingot preheat are isostructural with  $\text{Al}_3\text{Li}$  and can act as nucleation sites for these precipitates. These composite precipitates are often observed coexisting with the homogeneously nucleated  $\delta'$ . Although the  $\delta'$  precipitates can be sheared by moving dislocations, Figure 4b, they impede their motion and, consequently, greatly improve the strength over that of unalloyed aluminum. During artificial aging the  $\delta'$  precipitates coarsen but retain their coherency and spherical morphology to relatively large sizes ( $>50$  nm). A change in deformation mode from shearing to Orowan looping does not occur during practical heat-treatment times and temperatures.

When the  $\delta'$  precipitates are sheared by dislocations during deformation, their strengthening effect is reduced as both the degree of order and the precipitate size on the glide plane is reduced when the precipitate is sheared. Although dislocations move in pairs (superdislocations) in order to minimize the creation of antiphase domain boundaries in the  $\delta'$ , their shearing results successively in a local decrease in resistance to further dislocation motion, a concentration of slip into intense shear bands, Figure 5 (15), and a reduction in ductility and fracture toughness. Cassada et al. (18) have shown how the deformation can be homogenized and ductility improved by the addition of non-shearable precipitates. Since PFZ's are weaker than the precipitation-hardened matrix they can also lead to strain localization, thus further lowering the ductility and fracture toughness. This adverse effect is enhanced by the presence of the coarse grain boundary precipitates which may fracture or act as stress risers and preferential sites for microvoid nucleation and growth. Because of the severe strain localization effects associated with  $\delta'$  and PFZ's, all aluminum alloys containing lithium that are being developed for commercial use contain other alloying elements in order to modify the precipitate types and sequences and thereby develop acceptable combinations of strength and toughness.

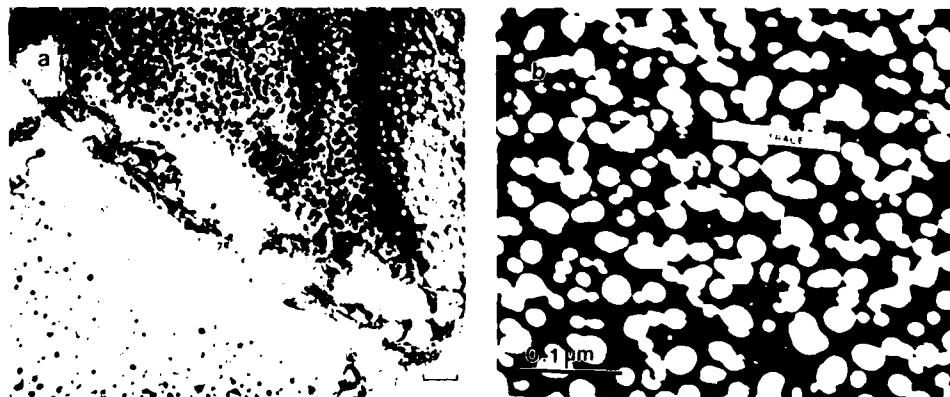
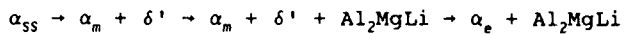


Figure 4. TEM's of an Al-Li alloy aged 24 h at 363K: (a) Bright-field image showing  $\text{Al}_3\text{Li}$  in the matrix,  $\text{AlLi}$  at grain boundaries and PFZ. (b) Dark field image showing the shearing of  $\text{Al}_3\text{Li}$  that occurs during deformation.



Figure 5. TEM showing intense shear bands in an Al-Li binary alloy.

**Al-Li-Mg:** The effect of magnesium additions on the phase equilibria of Al-Li alloys has been reported by a number of investigators (6,19,20). Magnesium decreases the solubility of lithium in aluminum at all temperatures below about 425°C (21). Similarly, the solubility of magnesium in aluminum is drastically reduced by the presence of lithium. Beyond the region of solid solution, in Al-Li-Mg ternary alloys with compositions close to the Al-Li binary, the decomposition of the supersaturated solid solution occurs via the  $\delta'$  to  $\delta$  precipitation sequence. However, as the composition of the ternary alloy is varied from the Al-Li binary towards the Al-Mg binary by increasing the magnesium to lithium ratio, the phase that is in equilibrium with the  $\alpha$  solid solution changes from  $\delta$  to  $\text{Al}_2\text{MgLi}$ . When supersaturated Al-Li-Mg alloys of practical interest are aged at temperatures below about 240°C, the precipitation sequence occurs as follows:



where  $\alpha_{ss}$ ,  $\alpha_m$ , and  $\alpha_e$ , refer to the supersaturated, the metastable and the equilibrium  $\alpha$  solid solutions, respectively.

The  $\delta'$  phase that forms in Al-Mg-Li alloys is similar to that which occurs in the Al-Li binary.  $\text{Al}_2\text{MgLi}$  has a cubic  $\alpha$ -Mn crystal structure and forms as rods along the <110> directions of the matrix (20). This phase is incoherent with the matrix, and nucleates predominately along the grain boundaries, dislocations and other structural inhomogeneities. Consequently, it does not contribute to precipitation hardening.  $\text{Al}_2\text{Li}$  is the only phase responsible for the strength of Al-Li-Mg alloys, with the magnesium contributing to some solid solution hardening (22). Therefore, the deformation behavior is coarse-planar, similar to that which occurs in Al-Li binary alloys, and the extensive strain localization that develops during deformation leads to premature failure. The lithium-rich  $\text{Al}_2\text{MgLi}$  phase that precipitates along grain and subgrain boundaries results in the formation of  $\delta'$  PFZ's during prolonged artificial aging. As discussed previously, these zones, and their associated coarse grain boundary precipitates, have deleterious effects on ductility, fracture toughness, and possibly corrosion resistance (19).

**Al-Li-Cu:** The addition of copper decreases the maximum solid solubility of lithium in aluminum at all temperatures (5). Copper in solid solution does not influence the basic character of the  $\delta'$  precipitation reaction (23), but it does introduce additional beneficial precipitation reactions that occur independent of the  $\delta'$  reaction. The natures of the metastable and equilibrium phases that form within this alloy system have been shown to be dependent on the Cu:Li ratio and the aging temperature (5). For example, during aging at temperatures typical of commercial aging practices (120° to 200°C) the decomposition of the solid solution in a 2090 type alloy (Al-2.2Li-2.7Cu-0.12Zr) results in the formation of the metastable  $\theta'$  ( $\text{Al}_2\text{Cu}$ -the primary strengthening phase in Al-Cu alloys) and the equilibrium  $T_1$  phase ( $\text{Al}_2\text{CuLi}$ ) (5,24,25).  $\text{Al}_2\text{Cu}$  has not been observed for Cu:Li ratios less than approximately 1.3.  $\text{Al}_2\text{Cu}$  has a tetragonal crystal structure and the precipitates form as platelets parallel to the {100} planes of the matrix.  $T_1$  has a hexagonal crystal structure with  $a = 0.497$  and  $c = 0.934$  nm and also forms as thin platelets but with a {111} habit plane. In commercial Al-Li-Cu alloys such as 2090,  $T_1$  is the predominant copper bearing strengthening phase present after artificial aging to the near peak strength condition, although  $\theta'$  may be present to a lesser degree. Figures 6a and 6b are TEM's of a 2090-type alloy showing the complex precipitate structure after aging to peak strength.

Both  $T_1$  and  $\theta'$  nucleate heterogeneously on dislocations and low angle grain boundaries, and other substructural features.  $\text{Al}_2\text{Li}$  normally is the first precipitate that forms during the aging of Al-Li-Cu alloys having compositions of commercial interest. Subsequent precipitation of  $T_1$  and  $\theta'$  may reduce the volume fraction and alter the distribution of  $\delta'$  since  $\delta'$  incorporates lithium and artificial aging may result in some

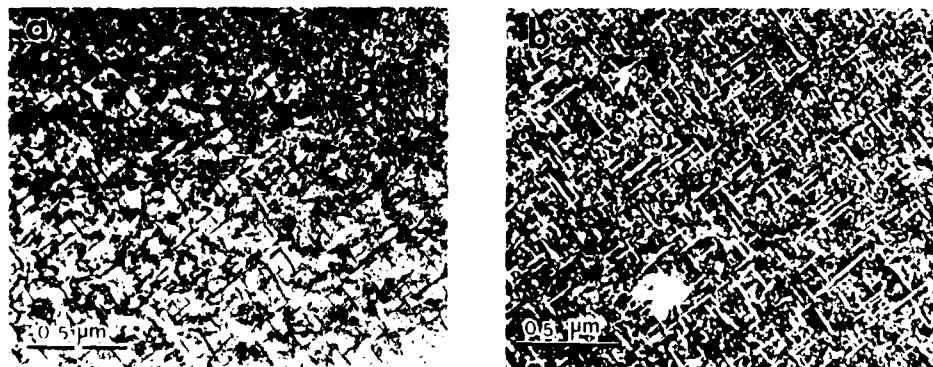


Figure 6. TEM's of the 2090 alloy solution heat treated showing a complex precipitate structure that includes  $\theta'$ ,  $T_1$ ,  $\delta'$ , and  $\text{Al}_2\text{Zr} (\beta')$ . (a) Bright field, (b) dark field.

reversion and reprecipitation of  $\delta'$ . Although Noble and Thompson (24) and Gregson and Flower (26) have suggested that growth of the  $T_1$  platelets is sustained by lithium from solid solution rather than dissolution of the  $\delta'$  particles, Sanders (27) has clearly shown that during growth the  $T_1$  precipitates cut through the  $\delta'$  precipitates and may consume them, Figure 7. Reducing the volume fraction of  $\delta'$  is beneficial in reducing the degree of strain localization (15).

Apart from the metastable  $\theta'$  and equilibrium  $T_1$  precipitates, the addition of copper also introduces another copper-containing phase,  $T_2$ , having the stoichiometry of  $Al_6CuLi$ , (5) which nucleates predominately on high angle boundaries. Electron (28-31) and x-ray diffraction (29) analyses of this phase provide strong evidence that  $T_2$  displays five fold icosahedral symmetry. The formation of the  $T_2$  phase particles (which are richer in lithium than  $\delta'$ ) along the grain boundaries lead to the development of  $\delta'$  PFZ's adjacent to these boundaries, Figure 8, with concomitant reduction in ductility and fracture toughness. Cassada et al. (30) have shown that in 2090-type Al-Li alloys the  $T_2$  phase is stable over the temperature range of 170°-520°C. Consequently, grain boundary precipitation of this phase should be anticipated in products that are slowly cooled or aged at temperatures above 170°C.

Early work by Price and Kelly (32) on Al-Cu single crystals aged to precipitate  $\theta'$  indicated that  $\theta'$  was not sheared but was looped and bypassed by moving dislocations in accordance with the Orowan model of strengthening. However, Starke and Lin (33) clearly showed that when the Al-Cu-Li alloy 2020 was aged to peak strength, where both  $\theta'$  and  $\delta'$  were present, deformation occurred by coarse planar slip. Huang and Ardell (34) obtained indirect evidence that  $T_1$  is looped and bypassed by glissile dislocations, confirming an earlier suggestion by Sainfort and Guyot (35). The former authors aged an Al-Li-Cu alloy to produce  $\delta'$  and  $T_1$ , and then applied a reversion treatment to eliminate  $\delta'$ . However, Jata and Starke (36) showed direct evidence of  $T_1$  shearing in an Al-Li-Cu alloy which also contained  $\theta'$  and  $\delta'$  precipitates. Howe et al. (37) used high resolution electron microscopy to study the structure and deformation behavior of  $T_1$  plates in an Al-2Li-1Cu alloy and showed conclusively that  $T_1$  plates are cut by dislocations during deformation and that such cutting leads to a disruption of nearest-neighbor bonding in the plates. Shearing of  $T_1$  and  $\theta'$  when  $\delta'$  is present may result from the superdislocations associated with  $\delta'$  having a pileup force sufficient to shear these partially coherent precipitates.

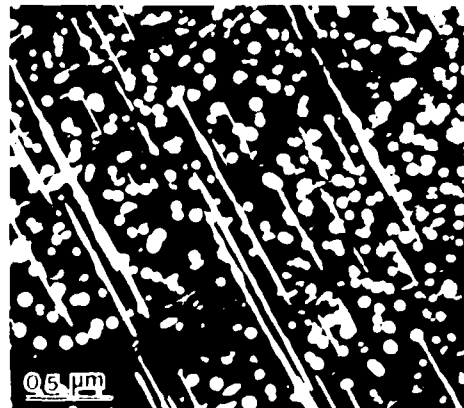


Figure 7. Dark-field micrograph showing  $T_1$  precipitates cutting through and consuming  $Al_3Li$  precipitates (Courtesy of T.H. Sanders, Jr.).



Figure 8. Micrographs illustrating grain boundary precipitates and associated PFZ: (a) Bright-field micrograph with  $T_2$  grain boundary precipitates with five-fold diffraction symmetry arrowed. (b)  $Al_3Li$  dark field showing the location of grain boundary and grain boundary precipitates (Courtesy of W.A. Cassada).

Although both  $\theta'$  and  $T_1$  may be sheared in the presence of  $\delta'$ , they do appear to decrease the extent of strain localization that occurs in binary Al-Li alloys. The resistance that a shearable strengthening precipitate offers to a glissile dislocation depends on a number of factors which include the coherency strain field, the interfacial energy, the internal structure of the precipitate, etc. For ordered precipitates, such as  $\delta'$ , the strengthening mechanism associated with the internal structure is reduced by shearing. The small lattice misfit (-0.18%) (16) and the small interfacial energy (180 ergs/cm<sup>2</sup>) (38) between  $\delta'$  and the matrix suggest that these strengthening mechanisms are not important for  $\delta'$ . However, the much larger misfits and interfacial energies between  $\theta'$ ,  $T_1$  and the matrix suggest that these strengthening mechanisms do operate when these precipitates are present. Neither strengthening mechanism is as effectively destroyed by particle shearing as is order strengthening and, therefore, the tendency for strain localization by work softening on the glide plane is reduced when  $\theta'$  and  $T_1$  are present. The alloy Weldalite may be used to illustrate the effect of  $\delta'$  and  $T_1$  on the deformation behavior of Al-Li-Cu alloys (39). Weldalite-T3 is characterized by fine GP zones and  $\delta'$  particles and deforms by intense localized planar slip, Figure 9a. When aged to the T8 temper,  $T_1$  is the only strengthening phase and deformation is more homogeneous, Figure 9b, indicating that there is no significant loss in strength on the slip plane during deformation (39) and supporting the contention that  $T_1$  is difficult to shear in the absence of  $\delta'$ .

**Al-Li-Cu-Mg:** When magnesium is added to Al-Li alloys containing copper, matrix precipitation of S' ( $\text{Al}_2\text{CuMg}$ ) occurs. The exact nature of the phase equilibria of the quaternary Al-Li-Cu-Mg alloys depends on the relative concentrations of all three alloying elements. For example, the addition of small amounts (0.5 to 1.0 wt.%) of magnesium to a high copper alloy such as 2090 suppresses the formation of  $\theta'$  and introduces the S' phase (40). Since S' contains no lithium,  $\delta'$  precipitation is not markedly influenced by the magnesium addition and  $T_1$  remains the dominant secondary phase in such an alloy. For alloys such as Al-3Cu-1.6Li-0.8Mg little or no  $\delta'$  forms and there appears to be equal amounts of  $T_1$  and S' (40). In higher lithium - lower copper alloys such as 8090, S', which precipitates with  $\delta'$  and a small amount of  $T_1$ , becomes the dominant Cu-bearing phase (26,41). As the magnesium to copper ratio is progressively increased, the precipitation of  $T_1$  is fully suppressed and S' becomes the primary Cu-bearing strengthening phase. This is the case for 2091 which has a nominal composition of Al-2Li-2.2Cu-1.5Mg-0.8Zr (42,43). When the concentration of magnesium exceeds that of copper the  $\text{Al}_2\text{MgLi}$  phase may precipitate in addition to S' (44).

The S' phase has an orthorhombic crystal structure ( $a = 0.405 \text{ nm}$ ;  $b = 0.905 \text{ nm}$ ;  $c = 0.72 \text{ nm}$ ) and forms initially as rods or needles aligned along the  $\langle 100 \rangle$  directions in the matrix. The precipitates are partially coherent with the matrix and show a strong tendency for heterogeneous nucleation along matrix dislocations, low angle grain boundaries and other structural inhomogeneities, Figure 10. However, unlike the case of  $T_1$  precipitation, the heterogeneous precipitation of S' does not result in PFZ's along either low or high angle grain boundaries. A  $T_2$ -type phase (possibly  $\text{Al}_6\text{Cu}(\text{LiMg})_3$ ) has been observed on grain boundaries of 8090-type alloys and, similar to such precipitation in Al-Li-Cu alloys, it does result in PFZ's. The combination of these microstructural features may lead to low ductility, fracture toughness, and corrosion resistance although the presence of S' in the matrix certainly minimizes these effects. Crooks et al. (45) and Crooks and Starke (40) have clearly shown that when S' is present in Al-Li-Cu-Mg alloys strain localization is suppressed indicating that the precipitate is not sheared by glissile dislocations. These observations were later confirmed by Gregson and Flower (26). The S' precipitates do not have densely packed slip planes parallel to the matrix slip planes and are, therefore, unlikely to be penetrated by dislocations (26).

A schematic representation of the various phases found in basic as well as the more complex Al-Li-X systems that encompass modern Al-Li alloys is shown in Figure 11.

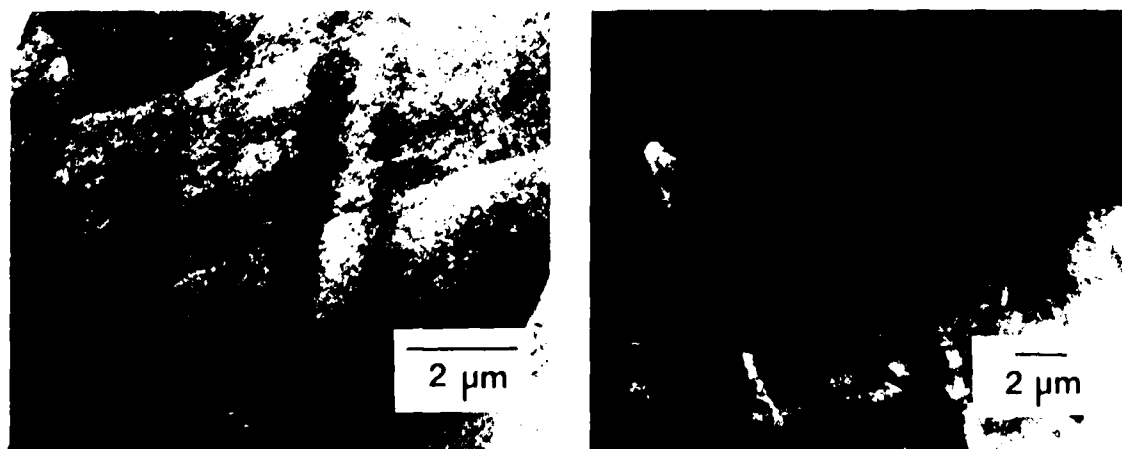


Figure 9. TEM showing deformation behavior in Weldalite (a) aged to the T3 temper, (b) aged to the T8 temper after 2% plastic strain.

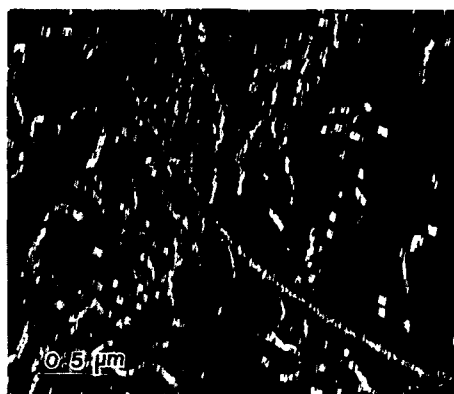


Figure 10. Dark field TEM showing  $\delta'$  precipitation on matrix dislocations and low angle boundaries in an Al-2.7Li-1.5Cu-1Mg-0.15Zr alloy.

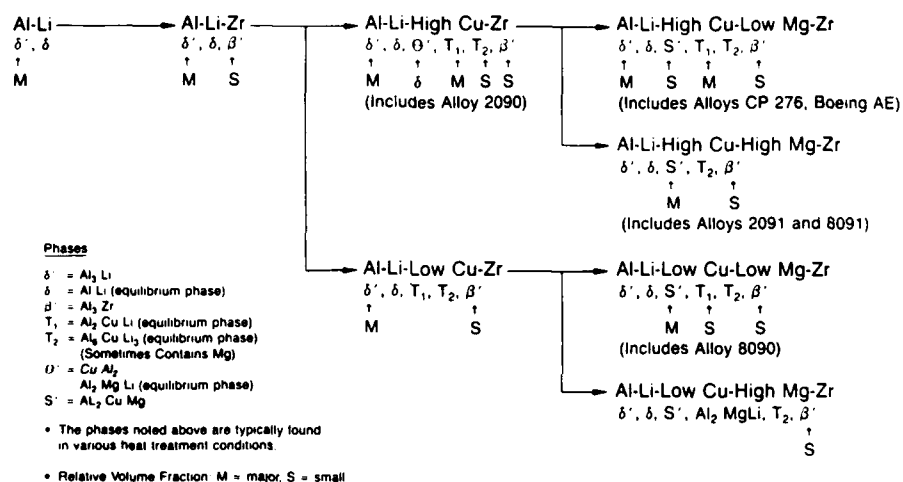


Figure 11. A schematic illustration of the precipitate phases that form in Al-Li-X alloys (from Narayanan and Quist).

#### EFFECT OF PROCESSING ON MICROSTRUCTURE DEVELOPMENT AND PROPERTIES

As mentioned previously, the first Al-Li-X alloys that were developed for commercialization suffered from low ductility and fracture toughness. These problems were primarily associated with strain localization and grain boundary precipitates, and alloying additions and processing methods were selected to minimize these problems. A variety of production methods, including rapid solidification and powder metallurgy consolidation, mechanical alloying, and ingot casting have been used for the development of the new Al-Li alloys. Rapid solidification and mechanical alloying were used as a means of reducing the grain size and extending solid solubility; however, ingot casting has proven to be the most feasible method for the production of large plate and extrusion products and is being used for the alloys that are currently in commercial production. However, powder metallurgy methods, including mechanical alloying, may offer advantages for certain product forms such as forgings.

Processing begins with homogenization to reduce segregation, remove the low-melting nonequilibrium phases, and thus improve workability. This thermal treatment also serves to precipitate the dispersoid-forming elements, such as those containing zirconium, so that they may perform their role of grain control during subsequent processing. One must be very careful in going to the final homogenization temperature to ensure that the low-melting phases are dissolved before their melting temperatures are reached. The atmosphere used in the homogenization treatment should be relatively dry in order to minimize oxidation and hydrogen pickup. One also needs to be concerned about lithium loss from the surface (46). The homogenization treatment is followed by hot working for ingot breakdown and shape change to the appropriate product form. The wrought product is then

solution heat treated, quenched, possibly worked, and aged to develop the desired microstructure. The temperature, amount of deformation prior to aging, etc., depend on the alloy composition and the final microstructure and properties that are desired.

#### Density and Elastic Modulus:

Lithium is the lightest metallic element and, with the exception of beryllium, is the only metal that both increases the modulus and reduces the density when alloyed with aluminum. Although the presence of heavier elements such as copper will somewhat offset the density advantage afforded by lithium, the overall reduction in density achieved will still be dominated by the amount of lithium added (47), Figure 12. Several investigators have developed empirical equations to predict alloy densities from known composition. One such formula by Peel et al. (41) is as follows:

$$\text{Density (g/cc)} = 2.71 + 0.024\% \text{Cu} + 0.018\% \text{Zn} + 0.022\% \text{Mn} - 0.079\% \text{Li} - 0.01\% \text{Mg} - 0.004\% \text{Si}.$$

In this equation the elemental concentrations are expressed in weight percent.

The modulus enhancement of aluminum by lithium additions is due to both solid solution effects as well as to the precipitation of lithium bearing compounds, and will change relative to both the amount of lithium added and the prior thermal treatment (48,49). Copper has a slight beneficial effect and magnesium a slightly negative effect on the modulus of aluminum (50,51). Recent studies by O'Dowd et al. (52) for 2090-type alloys and Broussaud and Thomas (53) for Al-Li binary alloys have shown that a maximum in modulus occurs just prior to the peak strength condition, Figure 13. Using the law of mixtures and a modulus for aluminum of 80.7 GPa O'Dowd et al. calculated a modulus for  $\delta'$  of 97 GPa and a modulus for  $T_1$  of approximately 350 GPa. They observed a sharp drop in modulus with the precipitation of the icosahedral  $T_2$  phase. Their data suggested that  $T_2$  has an extremely low intrinsic modulus and is very detrimental to the elastic properties of Al-Li-Cu alloys. Figure 14 shows a comparison of the modulus of elasticity of several Al-Li-X and baseline aluminum alloys (54).

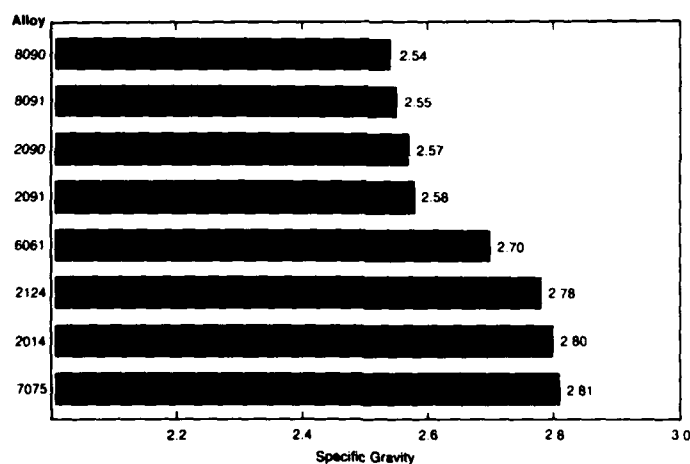


Figure 12. A comparison of densities for several Al-Li and conventional alloys (From Wakeling, reference 54).

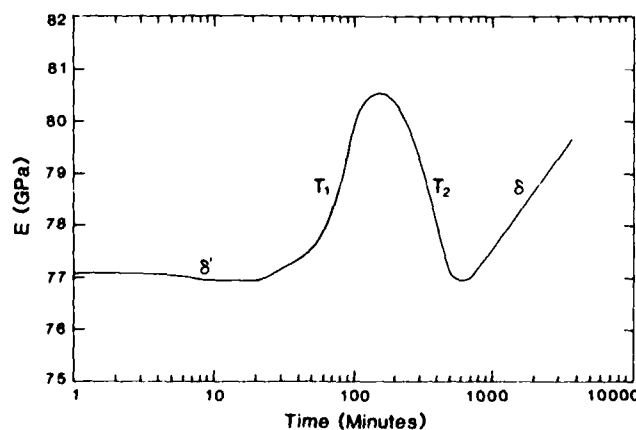


Figure 13. Young's modulus versus aging time at 190°C for an Al-2.31Li-2.24Cu-0.16Zr alloy. Precipitation occurs as indicated on the figure (From O'Dowd et al., reference 52).

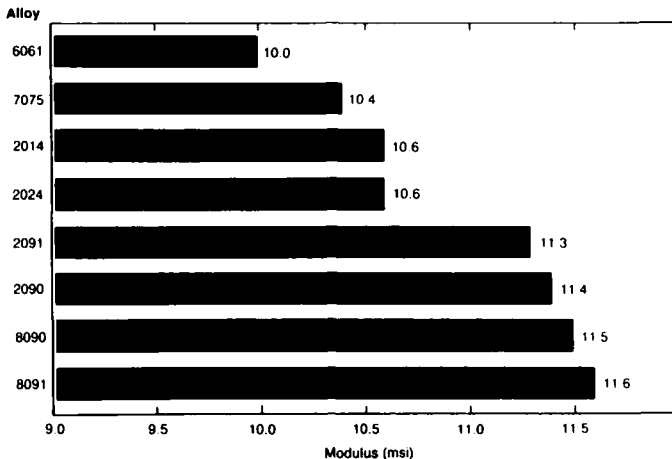


Figure 14. A comparison of Young's modulus for several Al-Li and conventional alloys (From Wakeling, reference 54).

#### Grain Structure and Crystallographic Texture:

Starke and Lin (33) showed that grain structure and texture can have a significant effect on the ductility of aluminum-lithium alloys. They related the poor ductility and fracture toughness of a 2020 alloy plate product to a partially recrystallized structure, very large recrystallized grains, and a high volume fraction of large inclusions. They were able to significantly improve the ductility of 2020 by thermomechanical treatments that produced either a completely recrystallized structure with small recrystallized grains or a completely unrecrystallized structure with a sharp deformation texture. Subsequently, Lin (55) showed that when PFZ's are present the grain aspect ratio of the recrystallized grains also has a major effect on the deformation behavior and fracture mode.

For alloys that deform by planar slip and/or have soft PFZ's, e.g., 2020, large recrystallized grains result in long slip lengths which produce large stress concentrations at grain boundaries and enhance low-energy intergranular fracture. Deformation is localized within the PFZ only when this region is favorably oriented for slip. This is always the case for equiaxed grains but occurs with less frequency for elongated grains when the stress axis is parallel to the long grain dimension. Grain boundary misorientation, i.e., texture, also plays a role in determining slip length and type of fracture. Grain boundaries can be a major barrier to slip if the misorientation is large, which is the usual case for recrystallized aluminum alloys. However, grain boundaries may not inhibit slip if the misorientation is small, e.g., for unrecrystallized materials with sharp deformation textures (56) (this is the situation for most Al-Li alloy products). The deformation process, i.e., the operative slip system(s), strongly depends on the crystal orientation. Shape accommodation, due to the constraint of material flow, varies with the crystal orientation and the misorientation between adjacent grains.

Small grains and large misorientations enhance multiple slip due to von Mises criterion, which may reduce stress concentrations at grain boundaries and the incidence of intergranular fracture. However, when the grain size is larger than some critical value, (which depends on the strength of the boundary, the degree of slip planarity, etc.) a large misorientation produces an effective barrier to slip, resulting in a stress concentration which may increase the incidence of intergranular fracture. A sharp deformation texture enhances slip continuity across grain boundaries and increases the probability of higher energy transgranular fracture. However, if slip is coarse-planar and strain localization extensive, the fracture toughness may be low even though the fracture mode is transgranular (27).

The desired grain structure may depend on the stress condition (57). Plane stress fracture toughness is believed to be controlled by the amount of plastic deformation occurring in a large plastic zone and a fine recrystallized grain structure aids in producing a maximum amount of plastic deformation. On the other hand, plane strain fracture toughness may be more influenced by grain boundary particles and increased toughness may result from a large grain boundary spacing. In Al-Li alloys these effects are particularly important, and it is found that sheet material with a recrystallized fine grain size often produces the highest plane stress toughness whereas unrecrystallized coarse grained thick section material is best for high plane strain fracture toughness (57).

Texture may have a significant effect on strength as predicted by the Taylor relationship:  $\sigma = M\gamma$ , where  $\sigma$  is the yield strength,  $\gamma$  the critical resolved shear strength on {111} planes and  $M$  an orientation factor which averages the distribution of grain orientations. When this distribution is isotropic,  $M = 3$ . The textures produced in aluminum alloys depend on a variety of parameters which include alloy content, precipitate structure and deformation mode, grain size and shape, starting texture, degree of recrystallization, directionality of deformation, and temperature of deformation. The crystallographic texture usually cannot be simply described since it may consist of a number of deformation and recrystallization components.

Commercial aluminum-lithium alloys normally have very strongly developed textures with resultant anisotropic properties (58-67). Both Al-Li-Cu-Zr and Al-Li-Cu-Mg-Zr alloys exhibit pronounced yield stress and ductility anisotropy in sheet, plate, and extruded products. In sheet products, mechanical properties vary with angle of the stress axis to the rolling direction (67), Figure 15. In thicker products, e.g., plate and extrusions, the texture may vary throughout the thickness resulting in an additional anisotropy, Figure 16 (65). Some of the through-thickness texture variation is usually associated with a limited amount of recrystallization that normally occurs near the surface. In addition to anisotropic effects due to crystallographic texture, variation in properties throughout a product may be due to variations in volume fraction and distribution of the strengthening and grain boundary precipitates (14). Rapid heat-up rates during solution heat treatment, e.g., associated with salt baths, may decrease the degree of anisotropy, Figure 15 (67).

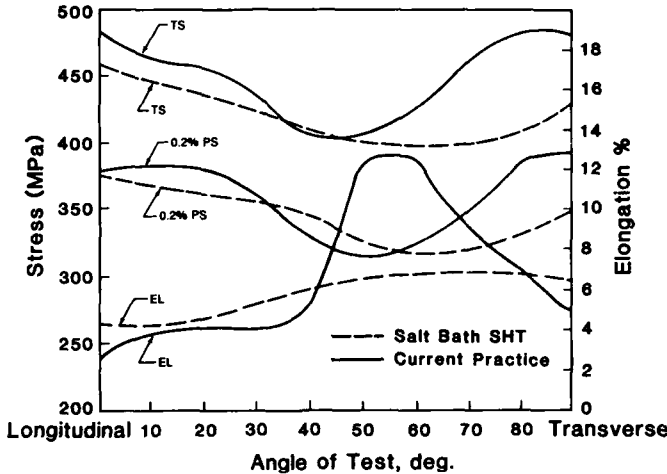


Figure 15. The mechanical properties of Al-Li alloy 8090 as a function of solution heat treatment practice and angle to the rolling direction (From Reynolds et al., reference 67).

The texture may also influence delamination cracks that are often observed in Al-Li alloys. Rolled plate and extrusions of 2090- and 8090-type Al-Li alloys may have a tendency to form delamination cracks extending in the processing direction during fracture (68-72). Some authors have suggested that the delamination phenomena increases the conventional fracture toughness due to "delamination toughening" (72), i.e., the L-T, L-S and T-S oriented specimens show higher fracture toughness than S-L and S-T specimens. Moreover, recent research indicates that the cryogenic fracture toughness in the L-T orientation is higher than at room temperature (68-71) and is accompanied by an increase in the yield strength, UTS, strain to fracture and the strain hardening exponent (68-70). Roven et al. (73) recently examined the influence of PFZ's and variations in the relative misorientations between grains in the S-direction on the delamination behavior of an 8090-type alloy at cryogenic and room temperature. Two conditions are investigated, i.e., one condition having a wide PFZ and the other condition with no PFZ. The recently developed (74) and modified EBSP technique in the SEM (75) was employed for micro-texture measurements. This technique is unique since it makes direct correlations between the microstructure and the crystallographic orientation possible on a macroscopic specimen (75).

Roven et al. (73) found that the delamination behavior could be characterized by (i) a "fine delamination" whose spacing was independent of both aging condition and test temperature, i.e., 77K and room temperature, and (ii) a "coarse delamination" whose spacing varied both with aging condition and test temperature (RT and 77 K). However, the coarse spacing was roughly equal for the two conditions at 77 K. The spacing of the "fine delaminations" correlated very closely to periodical events of high to low relative misorientations of grains in the S direction. The fracture processes of the PFZ-containing condition included slip localization both in slip bands and in the PFZs giving intergranular failure. In the PFZ-free condition the fracture process was dominated by slip localization in slip bands giving slip band decohesion. The latter condition had better cryogenic properties than the PFZ-containing microstructure.

The sharp textures that occur in Al-Li-X-Zr alloys are strongly associated with the use of zirconium as a grain refiner and recrystallization inhibitor. In addition, lithium probably has a contributory effect (76). Unless special procedures are applied no significant amount of recrystallization occurs in Al-Li-X-Zr alloys during ingot breakdown or subsequent thermomechanical processing, including intermediate anneals and solution heat treatments. This results in a very well defined deformation texture and the consequential effects mentioned previously. Cross rolling may spread the predominant poles and decrease the degree of anisotropy (13,61). As noted earlier, recrystallization textures normally lead to more isotropic properties and a very fine recrystallized grain size offers advantages under plane stress conditions (assuming grain boundary effects do not dominate). Sheet products of two alloys, 2091 and 8090, are being marketed in the recrystallized condition to optimize their plane stress fracture toughness.

Alloying additions and/or microstructural features that homogenize deformation normally reduce the effect that a sharp texture has on property variations. Although

Hirsch et al. (63) have shown that some control over texture may be obtained by controlling the initial texture, grain shape and aging, the anisotropy of properties associated with the texture of commercial Al-Li-X alloys is still a major problem and production methods need to be developed to produce the desired texture in all product forms.

#### Quench Sensitivity and Grain Boundary Precipitates:

The primary purpose of quenching age-hardenable aluminum alloys is to maintain a large degree of supersaturation of solute atoms homogeneously distributed in solid solution. This permits precipitation of an optimum concentration and distribution of hardening particles during the aging treatment. As quench rates decrease, more time is allowed for solute atoms to migrate to grain boundaries or precipitate as matrix phases. Grain boundaries act as heterogeneous nucleation sites by reducing the free energy barrier to nucleation (77). When thermodynamic and kinetic demands are satisfied, precipitation can occur along the grain boundary and enhance intergranular cracking, grain boundary decohesion and premature material failure (46).

Slow quench rates are unavoidable in very thick plate or heavy section forgings and under such conditions precipitation of grain boundary phases may occur. Lewis et al. (14) have shown that when 8090 is quenched from the solution treatment temperature at rates slower than 10°C/sec, precipitation of the icosahedral  $T_2$  phase occurs at high angle grain boundaries. These brittle precipitates can lead to low fracture toughness by acting as stress risers and preferential sites for microvoid nucleation and growth (78).

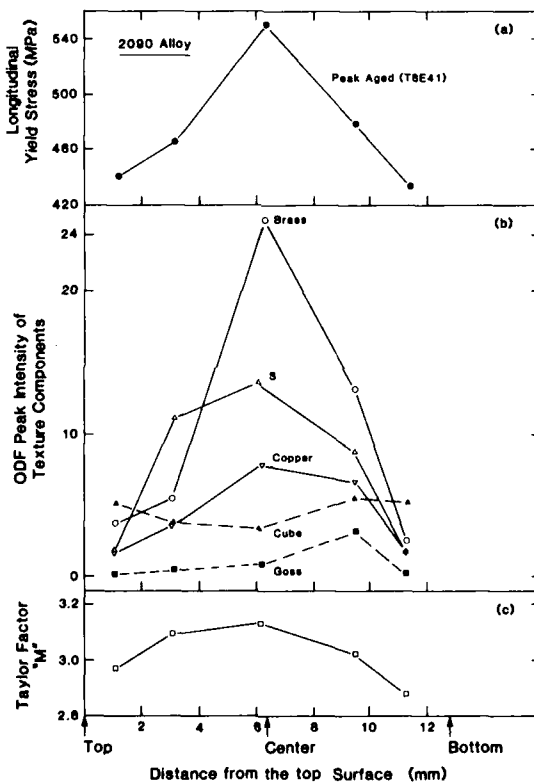


Figure 16. (a) Through thickness variation in longitudinal yield stress, (b) Through thickness variation in intensity of texture components, (c) Variation in the calculated Taylor factor ( $M$ ) through the thickness (From Vasudevan et al., reference 65).

Colvin and Starke (79) have determined time-temperature-transformation diagrams for the precipitation of both the  $T_2$  and S phases for two compositional variants of 8090, Figure 17. A solute-rich Al-2.58Li-1.36Cu-0.9Mg-0.13Zr alloy exhibited a greater sensitivity to quenching rates than did a solute-lean Al-2.28Li-0.86Cu-0.9Mg-0.13Zr alloy. Colvin and Starke related the precipitation of the  $T_2$  and S phases with the fracture toughness of the alloy, Figure 18, and concluded that  $T_2$  was the principal cause for the loss of mechanical properties in poorly quenched 8090. Staley (80) has recently determined TTT diagrams and related mechanical properties for 2090 and has found results similar to those obtained for 8090.

#### Strengthening Precipitates:

Engineering properties important in the design of Al-Li alloys for aerospace applications include a proper balance between strength, ductility, fracture toughness, fatigue resistance, formability, and corrosion resistance. The volume fraction, size, spacing, and distribution of the strengthening precipitates are important microstructural features that impact all of these properties. Processing of the wrought product to optimize the microstructure and properties begins with the proper selection of the solution heat-treatment temperature. This treatment should ensure that the maximum amount of solute

has been put in solid solution and that the rate of heat-up and maximum temperature does not result in nonequilibrium eutectic melting (81). The solution heat treatment is followed by a quench which should be sufficiently rapid to prevent deleterious precipitation of grain boundary phases, as discussed previously, without causing quench residual stresses that will produce warping. The warping issue is more serious than with normal aluminum alloys due to the relatively high solution treatment temperatures and low thermal conductivity associated with Al-Li alloys.

Quenching is often followed by some type of cold work in order to redistribute the quenched in residual stresses. However, for Al-Li-Cu and Al-Li-Cu-Mg alloys that contain  $\theta$ ,  $T_1$ , and  $S'$  strengthening precipitates, cold work prior to aging is used in conjunction with the aging temperature to control the distribution of the precipitates. Deformation prior to aging increases the dislocation density and thereby the number of nucleating sites for heterogeneous precipitation. Since the dislocations would also be in the vicinity of the grain boundary, precipitation of the strengthening precipitates would be encouraged in this region, thus minimizing the probability of PFZ formation. Dislocations are most effective as nucleation sites for those precipitates that have large interfacial energies and/or strains, e.g.,  $\theta'$ ,  $T_1$ , and  $S'$ , but have no significant effect on the nucleation of  $\delta'$ .

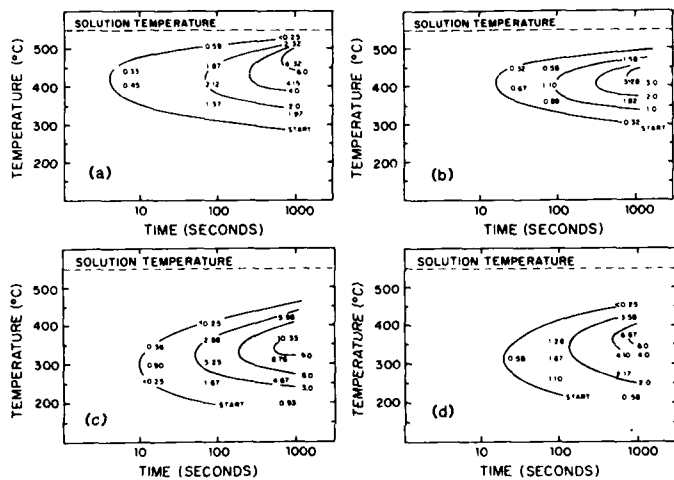


Figure 17. Time-temperature-transformation curves showing volume percents of  $T_2$  and  $S$  phases. (a)  $T_2$  for Al-2.58Li-1.36Cu-0.9Mg-0.13Zr (rich) alloy; (b)  $T_2$  for Al-2.28Li-0.86Cu-0.9Mg-0.13Zr (lean) alloy; (c)  $S$  for the rich alloy and (d)  $S$  for the lean alloy (From Colvin and Starke, reference 79).

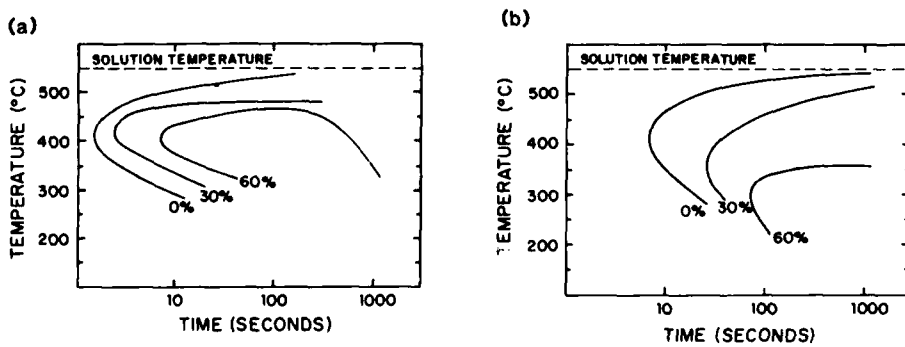


Figure 18. Iso mechanical lines showing the percent loss of Charpy energy values as a function of time at various temperatures (a) rich 8090 alloy and (b) lean 8090 alloy (From Colvin and Starke, reference 79).

Figure 19 shows the effects of different amounts of deformation prior to aging on the number density of the  $T_1$  precipitates formed during aging for various times at 190°C (82). Since strength is related to the precipitate structure, there is a corresponding effect on strength, as shown in Figure 19(b). The significance of this data relates to commercial processing and different product forms, since a nonuniform distribution of deformation prior to aging can result to wide variances in strength within a product. Some product forms, such as complex forgings and those formed by superplastic deformation, are

not easily conducive to cold deformation prior to aging. Consequently, there is interest in examining heat treatment procedures and/or alloying additions that may aid in the nucleation of the strengthening precipitates in a way that is similar to the effect of dislocations.

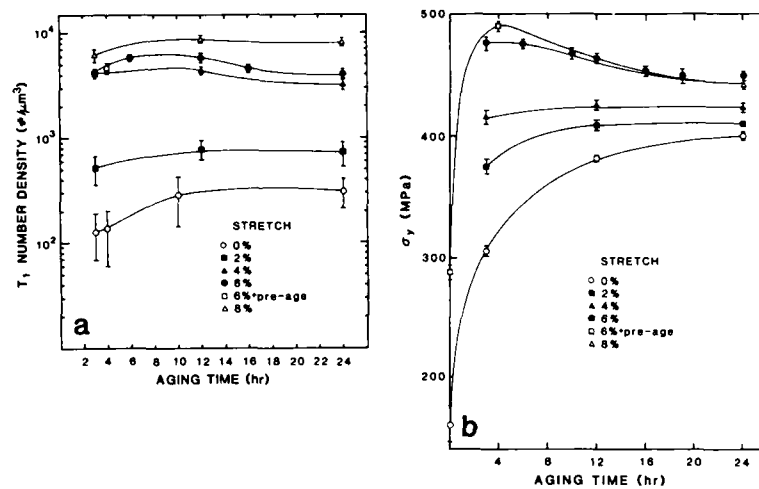


Figure 19. Effect of stretch on the precipitation and strength of an Al-2.4Li-2.4Cu-0.18Zr alloy. (a) Number density of  $T_1$  as a function of aging time at 463K for various degrees of stretch prior to aging and (b) corresponding yield strength vs. aging time (From Cassada, Shiflet and Starke, reference 82).

Lewis et al. (14) have improved the fracture toughness and stress corrosion resistance of 8090 by aging at 150°C instead of the commonly used 190°C. Pitcher (83) has recently shown that a slow heat-up rate to the aging temperature can lead to a better balance of tensile strength and toughness in 8091 than a rapid heat-up rate when deformation prior to aging is impossible. He relates the enhanced precipitation of  $S'$  to the release of vacancies, as the  $S'$  precipitates grow during the slow heat up. These vacancies assist the formation of homogeneous  $S'$ . A slow heat-up rate has the same effect as a duplex age, i.e., at a low temperature followed by aging at a high temperature. Both a slow heat-up rate to the aging temperature and a low  $\rightarrow$  high temperature duplex age are common practices for 7XXX alloys. Recent studies by Blackburn et al. (84) have demonstrated that small additions of indium to 2090 can aid in the nucleation of both  $T_1$  and  $\theta'$ . This has an effect similar to a 3 to 4% stretch, when compared with an indium-free alloy.

Ashton et al. (47) have established that a combination of cold work (up to 7%) prior to aging and a low aging temperature can significantly improve the strength-toughness relationship in both 2090 and 8091. As mentioned, deformation increases the number of nucleation sites for  $\theta'$ ,  $T_1$ , and  $S'$ . Lowering the aging temperature increases the degree of supersaturation and the driving force for nucleation of the strengthening precipitates. Consequently, higher strengths than realized at higher aging temperatures may be obtained. In addition, since diffusion rates are decreased, the size and volume fraction of the grain boundary precipitates are also decreased, which produces an improvement in the fracture toughness.

In general, for alloys that contain a low volume fraction of constituent phases and grain boundary precipitates, the fracture toughness is controlled by the deformation behavior, being maximized when deformation is homogeneous (36). Jata and Starke (36) showed that the fracture toughness variation with aging time can be quantitatively related to the changes in slip planarity, i.e., the fracture toughness decreases as the slip band width decreases and the slip band spacing increases. They also determined (85) that slip localization decreases with decreasing temperature, thus explaining the major reason for the large improvement in fracture toughness with decreasing temperature. The higher fracture toughness at cryogenic temperatures has also been attributed to: (a) low melting point grain boundary phases which solidify at low temperatures and remain liquid at room temperature (85,86), (b) a larger number of crack delaminations perpendicular to the short transverse direction or perpendicular to the fracture surface in an L-T oriented specimen (71,87) and in plane crack deflections (71) and (c) higher strain hardening capacity at low temperatures (88). The Jata and Starke model is consistent with the increase in strain hardening capacity at low temperatures.

The optimum microstructure for fatigue crack initiation resistance is consistent with that required for high fracture toughness (89). However, the situation is somewhat different for fatigue crack growth resistance (90). Lin and Starke (91) have shown that a tortuous crack path and crack branching, both of which are enhanced by coarse planar slip, are desirable for a high fatigue crack growth resistance in aluminum alloys. The tortuous crack path reduces the "crack driving force" due to extrinsic effects which include roughness-induced crack closure (92-94), Figure 20. The propensity of Al-Li

alloys to deform by coarse planar slip results in a significant improvement in fatigue crack growth resistance under both constant amplitude (57, 94-96) and variable amplitude loading (97) when compared with conventional high strength aluminum alloys. Figure 21, taken from the work of Ritchie and co-workers (98), compares the crack growth behavior of 2090-T8E41 (T-L orientation) with that for two different tempers of 2124 and 7150.

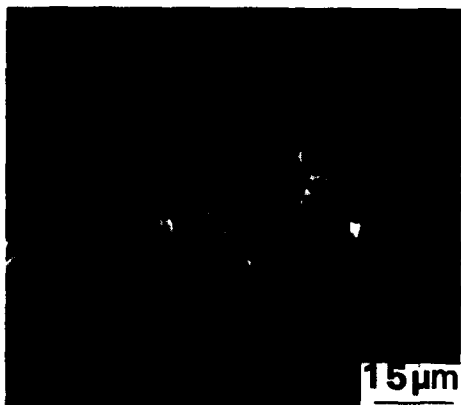


Figure 20. Scanning electron micrograph showing the fatigue crack profile and the presence of "roughness induced closure" in an Al-Li-Mg alloy.

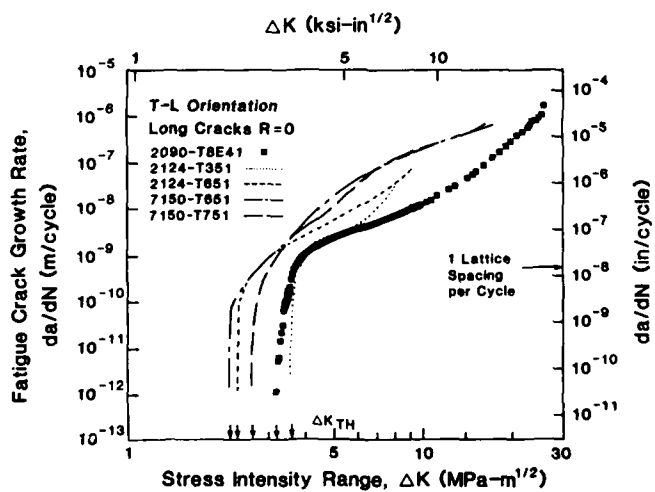


Figure 21. Crack propagation behavior of long fatigue cracks in 2090-T8E41 (T-L orientation), as a function of the nominal stress intensity range, compared to corresponding results in 2124 and 7150 alloys. Data for tests in moist air at  $R = 0.1$  (From Ritchie and coworkers, reference 98).

Aluminum-lithium alloys have not demonstrated the same significant advantages over baseline alloys for short crack growth resistance (99). This is partially the result of reduced crack tip shielding effects (94, 100). However, even in this regime Al-Li should show some improvement considering that they normally have a modulus of between 10 to 15 percent larger than conventional aluminum alloys. Although the fatigue crack initiation resistance of Al-Li alloys may be somewhat poorer than that of conventional alloys (101, 102) (most likely due to the extensive strain localization and sharp texture normally present) their overall fatigue performance under S-N type test conditions is generally equivalent to, or better than, that of standard aluminum alloys.

The precipitate structure also has a significant effect on the stress corrosion cracking behavior of Al-Li alloys (103). While Al-Li, Al-Li-Zr, and Al-Mg-Li-Zr alloy systems exhibit a high resistance to stress corrosion crack initiation (104, 105) the Al-Li-Cu-Zr and Al-Li-Cu-Mg-Zr systems do not (104, 106-110). This suggests that the presence of one of the copper containing precipitate phases, e.g.,  $T_1$ ,  $S'$ ,  $T_2$  or  $Al_6Cu(MgLi)_3$ , may be responsible for promoting crack initiation rather than  $AlLi$  or  $Al_2MgLi$  (103). Underaged tempers have been shown to be less susceptible than peak or overaged tempers to

SCC initiation for Al-Cu-Li-Zr alloys (103) but overaging has been shown to decrease the susceptibility of Al-Li-Cu-Mg-Zr alloys, Figure 22. Although underaged tempers appear to offer the highest resistance to SCC propagation for both alloy systems, Figure 23, the propagation behavior is relatively insensitive to temper as well as being insensitive to alloy chemistry and test environment (103).

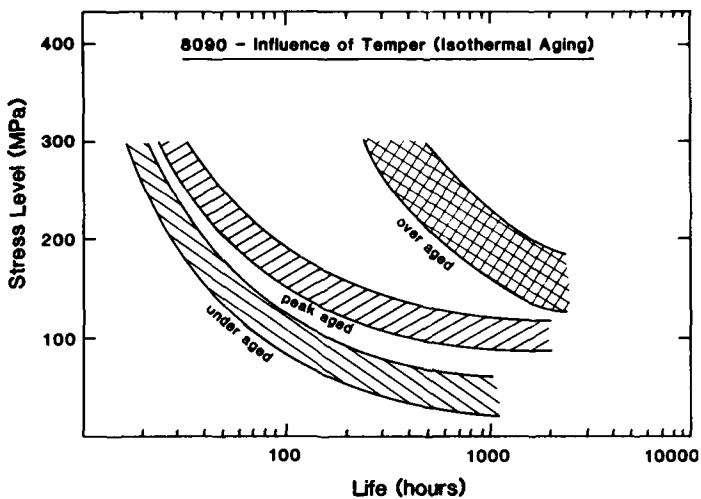


Figure 22. The influence of temper on the stress-life curve of 8090 plate (ST orientation). (From Gray et al., reference 103).

Aluminum-lithium alloys, particularly 2090, have surprisingly different forming characteristics than the industry standard aircraft aluminum alloys such as 2024 and 7075 (111). These differences in formability reflect the unique deformation behavior and grain structure exhibited by Al-Li alloys, in particular, their propensity for localized planar slip. The formability of Al-Li alloys has also been shown to be more sensitive to grain direction and prior cold work than the standard aircraft aluminum alloys. Maximum formability has been observed when Al-Li alloys are in the "as-quenched" condition and the bend axis is parallel to the long grain direction (111). It was previously shown that cold work prior to aging is necessary to develop the optimum strength-fracture toughness in Al-Li-Cu-X alloys. However, this step often reduces formability, forcing a compromise between the most desirable part shape and the resulting properties. This has necessitated the development of procedures which utilize the cold work imparted during forming to bring the final product to the required strength level.

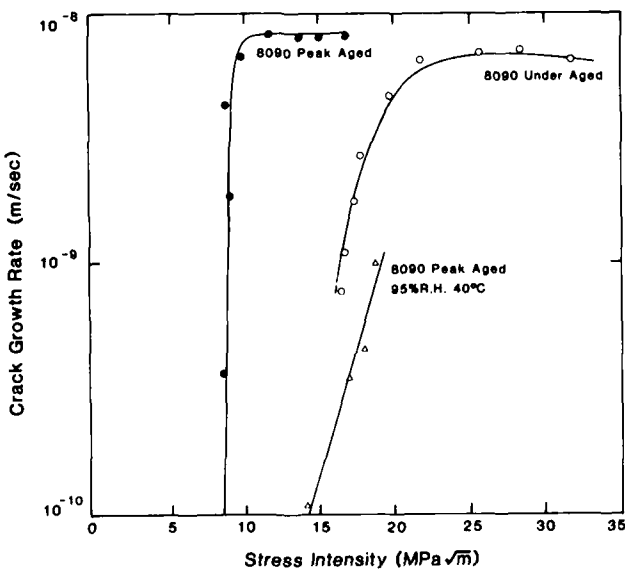


Figure 23. Crack growth velocity versus stress intensity curves for under- and peak-aged 8090 in artificial sea water and peak-aged 8090 in a 95 percent relative humidity atmosphere at 40°C (From Gray et al., reference 103).

## OTHER ENGINEERING PROPERTIES

In addition to those properties discussed above, there are certain other engineering properties of Al-Li alloys that are attractive in comparison to conventional baseline aluminum alloys. For example, most Al-Li alloys are amenable to superplastic forming (112,113), display moderate to good weldability (114,115), can be chemically milled, bonded, anodized, alclad, and painted. On the debit side, as noted previously, Al-Li alloys often display considerable anisotropy in strength and ductility. They are somewhat more susceptible to surface oxidation at moderate temperatures, and are prone to warping during quenching (mostly attributable to the relatively high quenching temperature). Diffusion of lithium can occur out to the surface during high temperature heat treatments which may lead to a lithium-depleted layer, and for sheet products a reduction in strength (116). In addition, all Al-Li-X alloys suffer from low ductility and fracture toughness in the short transverse direction. These problems are due to a combination of grain structure and segregation effects and should be minimized by improved processing. Most problems associated with Al-Li-X alloys appear to be solvable by the development of intelligent processing methods and the advantages in density and modulus that they offer over conventional aluminum alloys have already led to their usage in a number of aerospace systems.

## ACKNOWLEDGEMENTS

One author, Edgar A. Starke, Jr., would like to gratefully acknowledge support from the following: U.S. Army Research Office, under grant #DAAL03-86-K0128, Dr. Andrew Crowson, Program Monitor; U.S. Air Force Office of Scientific Research, under grant #AFOSR-87-0082, Dr. Alan Rosenstein, Program Monitor; and U.S. Office of Naval Research, under grant #N00014-85-0526, Dr. George Yoder, Program Monitor.

## REFERENCES

1. Reuleaux, O., J. Inst. Met., 33, 1925, p. 346.
2. Scheuer, E., Z. Metallkunde, 19, p. 16.
3. LeBaron, I. M., U.S. Patent No. 2,381,219, Application date 1942, Granted 1945.
4. Hardy, H.K. and J.M. Silcock, J. Inst. Met., 84, 1955-56, p. 423.
5. Silcock, J.M., J. Inst. Met., 88, 1959-60, p. 357.
6. Fridlyander, I.N., V.F. Shamray and N.V. Shirayera, Russian Metallurgy, No. 2, 1965, p. 83, Translated from Izvestiya Akademii nauk SSSR Metally, No. 2, p. 153.
7. Ekwall, J.S., J.E. Rhodes and G.G. Wald in Design of Fatigue and Fracture Resistant Structures, ASTM STP 671, 1982, p. 328.
8. Sankaran, K.K. and J.J. Grant, Aluminum-Lithium Alloys, ed. T.H. Sanders, Jr. and E.A. Starke, Jr., The Metall. Soc. AIME, 1981, p. 205.
9. Pickens, J.R., Heubaum, F.H., Langan, T.J., and Kramer, L.S., in Aluminum-Lithium Alloys V, ed. T.H. Sanders, Jr., and E.A. Starke, Jr., MCE Publications Ltd., Birmingham, U.K., 1989, Vol. III, p. 1397.
10. Bretz, P.E., Aluminum-Lithium Alloys; Design, Development and Application Update, ed. Ramesh J. Kar, Suphal P. Agrawal and William E. Quist, ASM International, 1988, p. 1.
11. Labarre, L.C., R.S. James, J.J. Witters, R.J. O'Malley and M.R. Emptage, 4th International Aluminum Lithium Conference, ed. by G. Champier, B. Dubost, D. Miannay and L. Sabetay, J. de Physique, Colloque C3, 1987, p. C3-93.
12. Last, H.R., T.H. Sanders, Jr. and J. G. Gonsalves, "Stability of Twinned Columnar Grain Structures in Aluminum Alloy Castings," submitted to Metall. Trans. A.
13. Ashton, R.F., D. S. Thompson and F.W. Gayle, Aluminum Alloys - Physical and Mechanical Properties, ed. E.A. Starke, Jr. and T.H. Sanders, Jr., EMAS, Warley, West Midlands, U.K., 1986, p. 403.
14. Lewis, R.E., E.A. Starke, Jr., W.C. Coons, G.J. Shiflet, E. Willner, J.G. Bjeletich, C.H. Mills, R.M. Harrington, and D.N. Petrakis, 4th International Aluminum Lithium Conference, ed. by G. Champier, B. Dubost, D. Miannay, and L. Sabetay, J. de Physique, Colloque C3, 1987, p. C3-643.
15. Sanders, T.H., Jr., and E.A. Starke, Jr., Acta Met., 36, 1982, p. 927.
16. Noble, B., and G.E. Thompson, Met. Sci. J., 5, 1971, p. 114.
17. Williams, D.B., and J.W. Edington, Met. Sci., 2, 1975, p. 529.
18. Cassada, W.A., G.J. Shiflet and E.A. Starke, Jr., Acta Met., 34, 1986, p. 367.

19. Sanders, T.H., Jr., "Development of an Al-Mg-Li Alloy", Final Report, Naval Air Developmental Center Contract No. N622269-74-C-0328, 1976.
20. Thompson, G.E., and B. Noble, J. Inst. of Met., 101, 1973, p. 111.
21. Mondolfo, L.F., "Aluminum Alloys - Structure and Properties", Butterworths, London, 1976, p. 554.
22. Sanders, T.H., Jr., H.R. Last and S.C. Jha, "Microstructure and Properties of Al-Li-Mg Alloys," Proceedings of the International SAMPE Metals Conference, Cherry Hill, N.J., August 18-20, 1987, in press.
23. Bauman, S.F., and D.B. Williams, in Aluminum-Lithium Alloys II, ed. E.A. Starke, Jr. and T.H. Sanders, Jr., The Metallurgical Society of AIME, Warrendale, PA., 1983, p. 17.
24. Nobel, B., and G.E. Thompson, Met. Sci. J., 6, 1972, p. 167.
25. Rioja, R.J., and E.A. Ludwiczak, in Aluminum-Lithium Alloys III, ed. C. Baker, P.J. Gregson, S.J. Harris, and C.J. Peel, The Institute of Metals, London, 1985, p. 471.
26. Gregson, P.J. and H. M. Flower, Acta Met., 33, 1985, p. 527.
27. Sanders, T.H., Jr., Unpublished Research Presented at "Aluminum-Lithium II", Monterey, CA, April 12-14, 1983.
28. Cassada, W.A., G.J. Shiflet, and E.A. Starke, Jr., Scripta Met., 20, 1986, p. 751.
29. Cassada, W.A., G.J. Shiflet, and S.J. Poon, Phys. Rev. Lett., 56, 1986, p. 2276.
30. Cassada, W.A., G.J. Shiflet and E.A. Starke, Jr., in Aluminum Alloys, Their Physical and Mechanical Properties, Vol. II., ed. E. A. Starke, Jr. and T.H. Sanders, Jr., EMAS, 1986, p. 695.
31. Barges, C., M.H. Tosten, P.R. Howell and E.R. Ryba, J. Mat. Sci., 22, 1987, p. 1663.
32. Price, R.J., and A. Kelly, Acta Met., 12, 1964, p. 159.
33. Starke, E.A., Jr., and F.S. Lin, Metall. Trans. A., 13A, 1982, p. 2259.
34. Huang, J.C., and A.J. Ardell, 4th International Aluminum Lithium Conference, ed. G. Champier, B. Dubost, D. Miannay, and L. Sabetay, J. de. Physique, Colloque C3, 1987, p. C3-373.
35. Sainfort, P. and P. Guyot, in Aluminum-Lithium Alloys III, ed. by C. Baker, P.J. Gregson, S. J. Harris and C.J. Peel, Inst. of Metals, London, 1986, p. 420.
36. Jata, K.V., and E. A. Starke, Jr., Metall. Trans. A., 17A, 1986, p. 1011.
37. Howe, J.M., Lee, J. and Vasudevan, A.K., Metall. Trans. A, 19A, 1988, p. 2911.
38. Tomura, M., T. Mori and T. Nakamura, J. Japan Inst. Metals, 34, 1970, p. 919.
39. Blankenship, C.P., Jr., and Starke, E.A., Jr., "The Fatigue Crack Growth Behavior of the Al-Cu-Li Alloy Weldalite 049," submitted to the Journal of Engineering Materials and Structures.
40. Crooks, R.E., and E.A. Starke, Jr., Metall. Trans. A., 15A, 1984, p. 1367.
41. Peel, C.J., B. Evans, C.A. Baker, D.A. Bennett, P.J. Gregson and H.M. Flower, in Aluminum-Lithium II, ed. E.A. Starke, Jr. and T.H. Sanders, Jr., The Metall. Society AIME, Warrendale, PA, 1984, p. 363.
42. Sainfort, P., and B. Dubost, in 4th International Aluminum-Lithium Conference, ed. G. Champier, B. Dubost, D. Mainnay, L. Sahetay, Journal De Physique, Colloque C3, 1987, p. 407.
43. Hautefeuille, I., R. Rahouadj, Y. Barbaux and M. Clavel, ibid, p. 669.
44. Narayanan, G.H., B.L. Wilson, W.E. Quist, and A.L. Wingert, "Low Density Aluminum Alloy Development", Third Interim Technical Report; 1983, AFWAL Contract No. F33615-81-5053.
45. Crooks, R.E., E.A. Kenik and E.A. Starke, Jr., Scripta Met., 17, 1983, p. 643.
46. Ashton, R.F., D.S. Thompson, E.A. Starke, Jr., and F.S. Lin, in Aluminum-Lithium Alloys III, ed. by. C. Baker, P.J. Gregson, S.J. Harris and C.J. Peel, The Institute of Metals, London, 1986, p. 66.
47. Dean, W.A., in Aluminum-Properties and Physical Metallurgy, ed. J.L. Hatch, ASM, Metals Park, OH, 1984, p. 200.

48. Muller, W., E. Bubeck and V. Gerold, in Aluminum-Lithium Alloys, III, ed. by C. Baker, P.J. Gregson, S.J. Harris, and C. Peel, The Institute of Metals, London, 1986, p. 435.
49. Agyekum, E., W. Ruch, E.A. Starke, Jr., S.C. Jha, and T.H. Sanders, Jr., *ibid*, p. 4 .
50. Narayanan, G.H., W.E. Quist, B.L. Wilson, and A.L. Wingert, "Low Density Aluminum Alloy Development", First Interim Tech. Report, 1982, AFWAL Contract No. F33615-81-C-5053, p. 95.
51. Dudzinski, N., *J. Inst Met.*, 81, 1952-53, p. 49.
52. O'Dowd, M.E., W. Ruch and E.A. Starke, Jr., in 4th International Aluminum-Lithium Conference, ed. G. Champier, B. Dubost, D. Miannay, L. Sabetay, *J. de Physique, Colloque C3*, 1987, p. 565.
53. Broussaud, F., and M. Thomas, in Aluminum-Lithium Alloys, III, C. Baker, P.J. Gregson, S.J. Harris, and C.J. Peel, The Institute of Metals, London, 1986, p. 442.
54. Wakeling, P.O., "ALCAN Developments in Al-Li Technology," NASA Workshop, Langley, VA, 1987.
55. Lin, F.S., *Scripta Met.*, 16, 1982, p. 1295.
56. Kuo, Victor W.C., and E.A. Starke, Jr., *Metall. Trans. A*, 16A, 1985, p. 1089.
57. Peel, C.J., D. McDarmad, and B. Evans, "Considerations of Critical Factors for the Design of Aerospace Structures Using Current and Future Aluminum-Lithium Alloys", in Aluminum-Lithium Alloys: Design, Development and Application Update, ed. R.J. Kar, S.P. Agrawal, and W.E. Quist, ASM International, Metals Park, Ohio, 1987, p. 315.
58. Peters, M., K. Welpmann, and T.H. Sanders, Jr., Advanced Materials Research and Developments for Transport Light Metals, RVII, Les Editions, Les Ulis, France, 1985, p. 63.
59. Peters, M., J. Eschweiler and K. Welpmann, *Scripta Met.*, 20, 1986, p. 259.
60. Fox, S., H.M. Flower and D.S. McDarmad, Aluminum Alloys - Physical an' Mechanical Properties, ed. E.A. Starke, Jr., and T.H. Sanders, EMAS, West Midlands, United Kingdom, 1986, p. 939.
61. Bull, M.J. and D.J. Lloyd, Aluminum Lithium Alloys III, ed. C. Baker, P.J. Gregson, S.J. Harris and C.J. Peel, The Institute of Metals, London, 1986, p. 402.
62. Broussaud F. and C. Diot, 4th International Aluminum Lithium Conference, ed. G. Champier, B. Dubost, D. Miannay and L. Sabetay, *J. de Physique, Colloque C3*, 48, 1987, p. C3-597.
63. Hirsch, J., O. Engler, K. Lucke, M. Peters and K. Welpmann, 4th International Aluminum Lithium Conference, ed. G. Champier, B. Dubost, D. Miannay and L. Sabetay, *J. de Physique, Colloque C3*, 48, 1987, p. C3-605.
64. Lipinski, P., M. Berveiller, A. Hihi, P. Sainfort and P. Meyer, 4th International Aluminum Lithium Conference, ed. G. Champier, B. Dubost, D. Miannay and L. Sabetay, *J. de Physique, Colloque C3*, 48, 1987, p. C3-613.
65. Vasudevan, A.K., W.G. Fricke, Jr., R.C. Malcolm, R.J. Bucci, M.A. Pivystupa and F. Barlat, *Metall. Trans. A*, 19A, 1988, p. 731.
66. Sadananda, K., and K.V. Jata, *Metall. Trans. A*, 19A, 1988, p. 847.
67. Reynolds, M.A., A. Gray, E. Creed, R.M. Jordan and A.P. Titchener, in Aluminum-Lithium Alloys III, ed. by C. Baker, P.J. Gregson, S.J. Harris and C.J. Peel, The Institute of Metals, London, 1986, p. 57.
68. Jata, K.V., and Starke, E.A., Jr., *Scripta Met.*, 22, 1988, p. 1553.
69. Morris, J.W., Jr., and J. Glazer, Lecture at the 1988 Int. Cryogenic Mater. Conf., Shenyang, China (1988).
70. Glazer, J., Ph.D. Thesis, Lawrence Berkeley Lab., Univ. of California, July 1989.
71. Rao, K.T.V., H.F. Hayashigatani, W. Yu and R.O. Ritchie, *Scripta Met.*, 22, 1988, p. 93.
72. Rao, K.T.V., W. Yu, and R.O. Ritchie, *Metall. Trans. A*, 20A, 1989, p. 485.

73. Roven, H.J., E.A. Starke, Jr., O. Sodahl, and J. Hjelen, *Scripta Met.*, 1990, in press.
74. Dingley, D.J., *Scanning El. Micro.* 2, 1984, p. 569.
75. Hjelen, J., and Nes, E., Proc. 3th Int. Conf. on Textures of Materials, AIME, Warrendale, PA, 1988, p. 597.
76. Makin, P.L. and W.M. Stobbs, *ibid*, 1986, p. 392.
77. Christian, J.W., The Theory of Transformations in Metals and Alloys, First Edition, Pergamon Press, Oxford, England (1965).
78. Starke, E.A., Jr., in Strength of Metals and Alloys, ICSMA 6, ed. by R.C. Gifkins, Vol. 3, Pergamon Press, 1982, p. 1025.
79. Colvin, G.N., and E.A. Starke, Jr., *SAMPE Quarterly*, 19, 1988, p. 10.
80. Staley, J.T., Alcoa Research Laboratory, Alcoa Center, PA, unpublished research, 1988.
81. Bourgassier, P., J.A. Wert and E.A. Starke, Jr., "Intergranular Fracture of an Al-Li-Cu-Mg Alloy as a Result of Non-equilibrium Eutectic Melting During Solution Treatment", *Materials Science and Technology*, in press.
82. Cassada, W.A., G.J. Shiflet and E.A. Starke, Jr., in 4th International Aluminum Lithium Conference, ed. by G. Champier, B. Dubost, D. Miannay, and L. Sabetay, *J. de Physique, Colloque C3*, 1987, p. C3-397.
83. Pitcher, P.D., "Ageing of Forged Aluminum-Lithium 8091 Alloy", *Scripta Met.*, in press.
84. Blackburn, L., W. Casada, G. Colvin, G. Shiflet, and E.A. Starke, Jr., Aluminum-Lithium Alloys: Design, Development and Application Update, ed. Ramesh J. Kar, Suphal P. Agrawal, and William E. Quist, ASM International, Metals Park, Ohio, 1987, p. 187.
85. Webster, D., Aluminum Lithium Alloys III, ed. by C. Baker, P.J. Gregson, S.J. Harris and C.J. Peel, Institute of Metals, London, 1986, p. 602.
86. Webster, D., *Met. Trans. A*, 18A, 1987, p. 2181.
87. Dorward, R.C., *Scripta Met.*, 20, 1986, p. 1379.
88. Glazer, J., S.L. Verzasconi, R.R. Sawtell and J.W. Morris, *Met. Trans. A*, 18A, 1987, p. 1695.
89. Starke, Edgar A., Jr., and Gerd Luetjering, "Cyclic Plastic Deformation and Microstructure", in Fatigue and Microstructure, ed. M. Meshii, ASM, Metals Park, Ohio, 1979, p. 205.
90. Starke, E.A., Jr., and J. C. Williams, "Microstructure and the Fracture Mechanics of Fatigue Crack Propagation", Fracture Mechanics: Perspectives and Directions, STP 1020, ed. R.P. Wei and R.P. Gangloff, ASTM, Philadelphia, PA, 1989, p. 184.
91. Lin, F.S., and E.A. Starke, Jr., *Mater. Sci. and Engr.*, 43, 1980, p. 65.
92. Jata, K.V., and E.A. Starke, Jr., in Aluminum-Lithium Alloys III, ed. by C. Baker, P.J. Gregson, S.J. Harris and C.J. Peel, The Institute of Metals, London, 1986, p. 247.
93. Petit, J., S. Suresh, A.K. Vasudevan and R.C. Malcolm, *ibid*, 1986, p. 257.
94. Venkateswara Rao, K.T., W. Yu and R.O. Ritchie, *Scripta Met.*, 20, 1986, p. 1459.
95. Coyne, E.J., Jr., T.H. Sanders, Jr., and E.A. Starke, Jr., in Aluminum-Lithium Alloys, ed. T.H. Sanders, Jr., and E.A. Starke, Jr., AIME, Warrendale, PA, 1981, p. 293.
96. Vasudevan, A.K., P.E. Bretz, A.C. Miller and S. Suresh, *Mat. Sci. and Engr.*, 64, 1984, p. 113.
97. Scarich, G.V., K.M. Bresnahan, and P.E. Bretz, in "Fatigue Crack Growth Resistance of Aluminum Alloys Under Spectrum Loading", Vol. II, Aluminum-Lithium Alloys, Tech. Rep. No. NOR-85-141, NASC, Northrop Corporation, Hawthorne, CA.
98. Venkateswara Rao, K.T., W. Yu and R.O. Ritchie, *Met. Trans. A*, 19A, 1988, p. 549.
99. Venkateswara Rao, K.T., W. Yu and R.O. Ritchie, *ibid*, 1988, p. 563.
100. James, M.R., *Scripta Met.*, 21, 1987, p. 783.

101. Peters, M., K. Welpmann, W. Zink and T.H. Sanders, Jr., in Aluminum-Lithium Alloys III, ed. C. Baker, P.J. Gregson, S.J. Harris and C.J. Peel, The Institute of Metals, London, 1986, p. 239.
102. Farcy, L., C. Carre, M. Clavel, Y. Barbaux and D. Aliaga, in 4th International Aluminum-Lithium Conference, ed. by G. Champier, B. Dubost, D. Miannay and L. Sabetay, J. de Physique, Colloque C3, 1987, p. 565.
103. Gray, A., N.J.H. Holroyd and W.S. Miller, "The Environmental Cracking Behaviour of Aluminum-Lithium Based Alloys", Proceedings of the International SAMPE Metals Conference, Cherry Hill, N.J., August 18-20, 1987, in press.
104. Holroyd, N.J.H., A. Gray, G.M. Scamans and R. Hermann, in Aluminum-Lithium Alloys III, ed. C. Baker, P.J. Gregson, S.J. Harris and C.J. Peel, Institute of Metals, London, 1986, p. 310.
105. Christodoulou, L., L. Struble and J.R. Pickens, in Aluminum-Lithium Alloys II, ed. by E.A. Starke, Jr., and T.H. Sanders, Jr., The Met. Soc. AIME, 1984, p. 561.
106. Meletis, E.I., "Stress Corrosion Cracking Properties of 2090 Al-Li Alloy", Proceedings International Conference on Fatigue Corrosion Cracking, Salt Lake City, UT, 1985.
107. Rinker, J.G., M. Marek and T.H. Sanders, Jr., Mat. Sci. Eng., 64, 1984, p. 203.
108. Vasudevan, A.K., P.R. Ziman, S.C. Jha and T.H. Sanders, Jr., in Aluminum-Lithium Alloys III, ed. by C. Baker, P.J. Gregson, S.J. Harris and C.J. Peel, Institute of Metals, London, 1986, p. 303.
109. Colvin, E.L., S.J. Murtha and R.K. Wyss, in Aluminum Alloys: Physical and Mechanical Properties, ed. by E.A. Starke, Jr., and T.H. Sanders, Jr., EMAS, 1986, p. 1853.
110. Meletis, E.I., J.M. Sater and T.H. Sanders, Jr., ibid, 1986, p. 1157.
111. Yavari, P., D. Ward and J.J. Christiana, "Forming and Post-Formed Properties of 2090", presented at the Al-Li Conference, WESTEC, Los Angeles, CA, March, 1988, to be published in the Proceedings.
112. Agrawal, S.P. and R.J. Kar, eds., "Aluminum-Lithium Development, Application and Superplastic Forming", Proceedings, WESTEC '86, ASM, Metals Park, Ohio, 1986.
113. Wadsworth, J., C.A. Hensahall and T.E. Nieh, in Aluminum-Lithium III, ed. by C. Baker, P.J. Gregson, S.J. Harris and C.J. Peel, The Institute of Metals, London, 1986, p. 199.
114. Pickens, J.R., "A Review of the Weldability of Lithium-Containing Aluminum Alloys", Martin-Marietta Report MML TR 84-22.
115. Edwards, M.R. and V.E. Stoneham, in 4th International Aluminum-Lithium Conference, ed. G. Champier, B. Dubost, D. Miannay and L. Sabetay, J. de Physique, Colloque C3, 1987, p. C3-293.
116. Papazian, J.M., G.G. Bott, and P. Shaw, in Proceedings of the 17th National SAMPE Conference, 1985, p. 688.

## LES COMPOSITES A MATRICE METALLIQUE A FIBRES LONGUES

par

J.F. STOHR

ONERA, Direction des Matériaux  
B.P. 72, F-92322 Châtillon Cedex, France

### Résumé

**Le renforcement des matrices métalliques par des fibres longues de céramique comme l'alumine, le carbone, le carbure de silicium, conduit à des caractéristiques spécifiques en rigidité et résistance très élevées, tant à température ambiante qu'à haute température.** Les progrès enregistrés dans le développement de nouvelles fibres plus performantes a redonné un nouveau souffle aux études sur les composites à matrice métallique. Après un rappel des lois élémentaires de la mécanique linéaire des composites unidirectionnels et la mise en évidence du rôle fondamental joué par l'interface fibre-matrice dans la micromécanique et le comportement de ces matériaux, l'article traite de la mise en oeuvre et des caractéristiques des composites à matrice métallique. On montre ainsi que les nouvelles générations de composites doivent beaucoup non seulement au traitement de surface des fibres, mais également aux technologies dérivées de la fonderie pour l'élaboration par voie liquide, et aux techniques de dépôt par voie physique ou issues de la solidification rapide depuis l'état liquide pour l'élaboration par densification en phase solide.

Des caractéristiques concernant les composites à matrice d'alliages légers, de composés intermétalliques et de superalliages sont présentées. Enfin, les problèmes spécifiques de tenue au cyclage thermique et de corrosion sont abordés pour quelques composites.

### Abstract

The reinforcement of metal matrices by long ceramic fibres such as alumina, carbon, silicon carbide, leads to very high specific characteristics such as stiffness and strength at both room and high temperature. Progress achieved in the development of new fibres more performing has revived the interest for metal matrix composites development. After having briefly reviewed the basic laws of unidirectional composites linear mechanics and shed some light on the major role played by fibre-matrix interface in the micromechanics and behaviour of these materials, the article deals with their processing techniques and characteristics.

The improvement of the mechanical characteristics of the new generation of composites arises not only from the fibre surface treatment leading to a control of fibre matrix bond strength, but also to the processing techniques derived either from casting or rapid solidification rate techniques.

Mechanical characteristics of the most relevant MMC are presented for both metallic and intermetallic matrices. Attention is drawn to particular behaviours such as thermal expansion, thermal cycling and corrosion resistance.

### INTRODUCTION

Les composites à matrice métallique renforcée par des fibres longues présentent, comme les composites à matrice organique, des caractéristiques spécifiques élevées (fig. 1) [1] et une faible masse volumique, caractéristique essentielle aujourd'hui dans l'industrie aéronautique et spatiale où la réduction de la masse des structures est primordiale. Par rapport aux matrices organiques, et en dépit des gains en température obtenus avec les matrices polyimides, les matrices métalliques présentent les avantages :

- d'une tenue en température supérieure,
- d'un allongement à rupture plus élevé que celui des fibres et d'une ténacité élevée,
- d'une bonne stabilité à l'environnement, rayonnement et humidité,
- d'une bonne conductibilité thermique et électrique.

Le développement de ces matériaux avait jusqu'alors été freiné à la fois par des problèmes de mise en oeuvre et par la faiblesse de certaines propriétés intrinsèques, comme la tenue au cyclage thermique et la stabilité thermique.

Aujourd'hui, le besoin en nouveaux matériaux associé aux projets spatiaux - satellites et lanceurs - ou aéronautiques - nouvelles cellules - a relancé l'intérêt pour ces composites, intérêt qui était tombé après les travaux importants des années 70.

Le développement, d'une part de nouvelles fibres, carbure de silicium en mèche, carbone à allongement accru et à fort module, monofilament de carbure de silicium ou de diborure de titane, d'autre part de nouveaux traitements de surface permettant d'assurer une double compatibilité chimique et mécanique avec la matrice, a donné un nouvel essor aux études conduites sur ces matériaux. Ainsi, à côté des composites à matrice d'alliage léger aluminium ou et magnésium, trouve-t-on des composites à matrice de titane dont certaines nuances pourraient travailler à 950°C et, bien sûr, à matrice superalliage pour les températures atteignant 1100°C.

Parallèlement à ces travaux sur les composants, les retombées des résultats acquis dans la compréhension du comportement mécanique des composites à matrice organique se sont traduites par un choix plus judicieux des systèmes fibres/revêtement/matrice. C'est à partir de cette réflexion que nombre de travaux ont pu déboucher aujourd'hui sur des composites performants et réalisables industriellement.

## 1 - MECANIQUE ELEMENTAIRE DES COMPOSITES UNIDIRECTIONNELS

Le souhait de tout concepteur de composites serait d'en prévoir les caractéristiques mécaniques (rigidité, résistance à la rupture) à partir de celles des deux constituants, sans avoir à faire intervenir les notions de régularité d'alignement ou d'hétérogénéité de distribution des fibres. Ce chapitre traitera principalement de la résistance à la rupture d'un composite unidirectionnel sollicité parallèlement à la direction des fibres.

### 1.1 - Rigidité

Dans le cas le plus général d'un composite orthotrope qui comprend trois plans de symétrie orthogonaux entre eux, le tenseur d'élasticité est défini par neuf constantes indépendantes ; si, de plus, le matériau est isotrope dans le plan normal aux fibres, le nombre de constantes se réduit à cinq. Le calcul rigoureux de ces constantes conduit aux expressions suivantes [2] :

$$E = E_f V_f + E_m V_m + 4V_f V_m (\nu_m - \nu_f)^2 / \left( \frac{V_m}{K_{pf}} + \frac{V_f}{K_{pm}} + \frac{1}{G_m} \right) \quad (1.1)$$

$$\nu = \nu_f V_f + \nu_m V_m + V_f V_m (\nu_f - \nu_m) \left( \frac{1}{K_{pm}} - \frac{1}{K_{pf}} \right) / \left( \frac{V_m}{K_{pf}} + \frac{V_f}{K_{pm}} + \frac{1}{G_m} \right) \quad (1.2)$$

$$\frac{1}{K_{xy}} = \frac{V_f}{K_{pf}} + \frac{V_m}{K_{pm}} - V_f V_m \left( \frac{1}{K_{pf}} - \frac{1}{K_{pm}} \right)^2 / \left( \frac{V_m}{K_{pf}} + \frac{V_f}{K_{pm}} + \frac{1}{G_m} \right) \quad (1.3)$$

$$\frac{1}{G_{xz}} = \frac{1}{G_{yz}} = \frac{1}{G} = \frac{V_f}{G_f} + \frac{V_m}{G_m} - V_f V_m (G_f - G_m)^2 / [G_f G_m (G_f (1 + \nu_f) + G_m \nu_m)] \quad (1.4)$$

$$\frac{1}{G_{xy}} = \frac{V_f}{G_f} + \frac{V_m}{G_m} - V_f V_m (G_f - G_m)^2 / (G_f^2 G_m^2) \left( \frac{V_m}{G_f} + \frac{V_f}{G_m} + \frac{1}{G_m} + \frac{2}{K_{pm}} \right) \quad (1.5)$$

où les lettres E, G, V, K, et  $\nu$  désignent respectivement le module d'Young, le module de cisaillement, la fraction volumique de chaque constituant, le module de compressibilité en déformation plane et le coefficient de Poisson, les indices f et m désignant chacun des deux constituants, les fibres et la matrice.

Pour la majorité des composites, du fait que l'écart à la loi des mélanges est proportionnel à  $(\nu_f - \nu_m)^2$ , quantité dont la valeur est très faible, l'équation (1.1) conduit à la forme usuelle du module d'Young donnée par la loi des mélanges :

$$E = E_f V_f + E_m V_m \quad (1.6)$$

Dans la plupart des cas, l'écart entre la valeur exacte du module donnée par (1.1) et celle résultant de l'application de la loi des mélanges reste inférieur à 2 %.

Pour le coefficient de Poisson, du fait que  $\nu_f$  est plus petit que  $\nu_m$  et que  $K_{xy}$  est plus grand que  $K_{pm}$ , la valeur de  $\nu$  est inférieure à celle prédicta par la loi des mélanges.

### 1.2 - Résistance à rupture du composite

#### 1.2.1 - Courbe de traction du composite unidirectionnel

Dans le cas général, où à la fois fibres et matrice ont un comportement plastique, la courbe contrainte-déformation du composite présente quatre stades :

- 1 - Fibres et matrice se déforment élastiquement
- 2 - La matrice se déforme plastiquement et les fibres élastiquement
- 3 - Les deux constituants sont plastiques
- 4 - La rupture de l'un des constituants se produit

Dans le stade 1, le module d'Young du composite est donné par la loi des mélanges, tandis que dans le stade 2 il prend la forme :

$$E_c = E_f V_f + V_m \left( \frac{d\sigma_m}{d\epsilon_m} \right) \epsilon_c \quad (1.7)$$

le terme  $(d\sigma_m/d\epsilon_m)\epsilon_c$  représentant la consolidation de la matrice dans le composite.

Si la déformation à rupture des fibres reste supérieure à la déformation de la matrice pour sa limite d'élasticité.

Pour des métaux purs, et si la distance entre fibres reste suffisamment grande ( $\geq 10 \mu\text{m}$ ), la contribution de la consolidation de la matrice au module tangent, très faible (de l'ordre de  $E_m/100$ ), peut être négligée. Le module du composite dans le stade 2 est alors égal à la contribution pondérée des fibres  $E_f V_f$ .

### 1.2.2 - Contrainte à rupture en mécanique linéaire (cas déterministe) [3]

Lorsque fibres et matrice se déforment plastiquement, la rupture du composite est régie, comme dans le cas des matériaux monolithiques métalliques, par l'apparition de la striction. Pour un composite unidirectionnel soumis à une charge  $F_c = \sigma_f A_f + \sigma_m A_m$ , où  $A_f$  et  $A_m$  désignent les fractions surfaciques de fibres et de matrice dans une section droite, la condition de stabilité du matériau avant la striction spécifie que pour tout incrément de déformation  $d\epsilon$ , l'incrément de charge reste positif :

$$dF_c = \sigma_f dA_f + A_f d\sigma_f + \sigma_m dA_m + A_m d\sigma_m \geq 0 \quad (1.8)$$

l'incrément d'allongement étant le même pour les deux constituants :

$$d\epsilon = - dA_f / A_f = - dA_m / A_m$$

Il vient :

$$V_f \left( \frac{d\sigma_f}{d\epsilon} - \sigma_f \right) + V_m \left( \frac{d\sigma_m}{d\epsilon} - \sigma_m \right) \geq 0 \quad (1.9)$$

En admettant que les relations contrainte-déformation des fibres et de la matrice suivent une loi puissance, Mileiko [4] a démontré que la contrainte à rupture du composite prend la forme :

$$\sigma_{cu} = \lambda_f \sigma_f V_f + \lambda_m \sigma_m V_m \quad (1.10)$$

où  $\lambda_f$  et  $\lambda_m$  sont des expressions complexes qui ne dépendent que des paramètres des lois puissances reliant contrainte et déformation des deux constituants. Si, de plus, les élongations à rupture des fibres et de la matrice sont les mêmes (modèle déterministe admettant l'unicité de ces valeurs), alors les facteurs  $\lambda_f$  et  $\lambda_m$  sont tous deux égaux à l'unité et l'on retrouve la loi des mélanges :

$$\sigma_{cu} = \sigma_{fu} V_f + \sigma_{mu} V_m \quad (1.11)$$

où  $\sigma_{fu}$ ,  $\sigma_{mu}$  et  $\sigma_{mu}$  désignent les contraintes à rupture du composite, des fibres et de la matrice respectivement. La relation (1.11) constitue une limite supérieure de la contrainte à rupture du composite.

Si maintenant l'allongement à rupture des fibres est très inférieur à celui de la matrice, et que parallèlement la contrainte à rupture des fibres est très supérieure à celle de la matrice - ce qui est généralement le cas dans les CMM -,  $\sigma_{fu} V_f$  est beaucoup plus grand que  $\sigma_{mu} V_m$ , et l'application de la loi des mélanges à l'allongement à rupture des fibres conduit alors à une limite inférieure de la contrainte à rupture du composite :

$$\sigma_{cu} = \sigma_m' V_m + \sigma_{fu} V_f \quad (1.12)$$

où  $\sigma_m'$  désigne la contrainte dans la matrice pour la déformation à rupture des fibres. Il s'ensuit que la contrainte à rupture du composite va se trouver à l'intérieur du triangle ABC (fig. 2).

Il importe de mentionner ici que pour un composite renforcé par des fibres à haute résistance, la déformation à rupture du composite, généralement égale à celle des fibres pour des fractions volumiques du renfort pas trop faibles, reste très petite, de sorte que  $\sigma_m'$  sera très petit devant  $\sigma_{fu}$ . Pour ces composites à fibres fragiles, la rupture d'une fibre entraînera celle des autres dans la même section droite et, partant, celle du composite, sauf si la fraction volumique de fibres reste suffisamment faible pour que la matrice, du fait de sa consolidation, puisse soutenir la charge une fois les fibres rompues. La contrainte à rupture du composite ne sera alors donnée par (1.12) que si :

$$\sigma_{cu} \geq \sigma_{mu} (1 - V_f) \quad (1.13)$$

de sorte que la relation (1.12) ne s'appliquera que pour les fractions volumiques supérieures à  $V_{min}$  tel que :

$$V_{min} = \frac{\sigma_{mu} - \sigma_m'}{\sigma_{fu} + (\sigma_{mu} - \sigma_m')} \quad (1.14)$$

Pour les faibles fractions volumiques de fibres, inférieures à  $V_{min}$  :

$$\sigma_{cu} = \sigma_{mu} (1 - V_f) \quad (1.15)$$

De plus, dans cette région de faible fraction volumique de fibres, le renforcement de la matrice par les fibres ne se fera sentir que pour les fractions volumiques de fibres supérieures à  $V_{crit}$  tel que :

$$\sigma_{fu} V_f + \sigma_m' (1 - V_f) \geq \sigma_{mu} \quad (1.16)$$

$$V_{crit} = \frac{\sigma_{mu} - \sigma_m'}{\sigma_{fu} - \sigma_m'} \quad (1.17)$$

Pour des fractions volumiques de fibres inférieures à  $V_{\min}$ , le composite peut être déformé sans rupture à des allongements bien plus élevés que l'allongement à rupture des fibres : c'est le domaine de la rupture multiple des fibres, où les fibres rompent en segments dont la longueur tend vers une limite avec la déformation du composite. Cette limite de la longueur des segments de fibres résulte de la déformation plastique de la matrice, qui induit une contrainte de cisaillement  $\tau$  à l'interface fibre-matrice, près d'une extrémité de fibre ; c'est cette contrainte de cisaillement qui conduit au recharge ment linéaire de la fibre à partir de son extrémité (fig. 3). La limite supérieure de  $\tau$  est la contrainte de rupture en cisaillement de l'interface ou de la matrice. Pour une fibre de rayon  $r$ , la longueur des segments sera comprise entre  $l_c$  et  $2l_c$ , avec  $l_c = \sigma_h r / \tau$ .

L'approche précédente, due essentiellement à Kelly [5], ne s'applique que dans certaines limites pour les fractions volumiques de fibres supérieures à  $V_{\min}$  ; en effet dans la mesure où le matériau présente un comportement fragile, toute rupture de fibre entraînant celle du composite, deux correctifs sont à apporter :

- 1 - Les fibres ne possèdent pas une contrainte de rupture unique, mais une distribution de contrainte à rupture bien décrite par la loi de Weibull ;
- 2 - La rupture du matériau interviendra donc lorsqu'un défaut de taille critique, au sens de la mécanique de la rupture, se sera développé dans une section du composite. L'approche de la rupture du composite, soit par une analyse statistique, soit en mécanique de la rupture à partir de la notion de défaut critique, repose sur la micromécanique à l'échelle de la fibre, indispensable pour évaluer l'état des contraintes dans les fibres rompues et leur redistribution.

### 1.3 - Le transfert de charge entre fibres et matrice

La description et la compréhension du mécanisme de renforcement par des fibres discontinues, de même que celle des phénomènes qui interviennent lors de la rupture de fibres dans un composite à fibres continues, requièrent que soit connue la manière dont la contrainte est transférée de la matrice aux fibres. Lorsqu'un composite contenant des fibres alignées uniaxiallement est soumis à une contrainte parallèle à la direction des fibres, les déplacements de points courants situés en vis-à-vis, mais à une certaine distance l'un de l'autre, dans les fibres et la matrice ne seront pas identiques, en raison de la différence des modules d'élasticité des deux phases. Il en résultera des déformations en cisaillement sur les plans parallèles aux fibres. Les champs de déformation en cisaillement et les contraintes afférentes sont les processus par lesquels les charges supportées par les fibres et la matrice se distribuent entre les deux constituants.

#### 1.3.1 - Rechargement élastique

La manière dont une fibre se recharge à partir d'une extrémité peut être calculée simplement, dans le cas d'un composite monofilamentaire (fig. 4). Suivant Cox [6], la variation de la charge  $P$  à une distance  $x$  de son extrémité peut s'exprimer de deux manières, d'une part en fonction de la différence des déplacements  $u$  de la fibre et  $v$  de la matrice :

$$\frac{dp}{dx} = H(u - v) \quad (1.18)$$

où  $H$  est une constante,

d'autre part en fonction des constantes élastiques  $E_f$  de la fibre et de sa déformation  $du/dx$  :

$$P = E_f A_f \frac{du}{dx} \quad (1.19)$$

où  $A_f$  est la fraction volumique de fibres.

De plus, pour ce matériau modèle à faible fraction volumique de fibres, la déformation globale à l'écart de la fibre est homogène et égale à  $dv/dx$ . En regroupant (1.18) et (1.19), il vient :

$$\frac{d^2P}{dx^2} = H \left[ \frac{P}{E_f A_f} - e \right] \quad (1.20)$$

Cette équation différentielle conduit à une contrainte dans la fibre en forme de sinus hyperbolique :

$$\sigma = E_f e \left[ 1 - \frac{\cosh \beta (1/2 - x)}{\cosh \beta 1/2} \right] \quad (1.21)$$

$$\text{avec } \beta = \left( \frac{H}{E_f A_f} \right)^{1/2}$$

Aucune charge n'étant transmise à la fibre par sa section à ses extrémités, la contrainte dans la fibre croît à partir de ses extrémités, ce qui implique que seules les fibres de longueur infinie peuvent atteindre la déformation du composite.

Une valeur approchée de  $H$  peut être obtenue dans le cas des composites où les fibres sont régulièrement disposées, en remarquant qu'au voisinage des fibres, et en admettant que la fibre ne glisse pas par rapport à la matrice, le déplacement

dans la différentiel fibre-matrice  $W$  est égal à celui de la fibre  $u$ ; en revanche, à mi-distance  $R$  entre deux fibres, ce déplacement sera celui de la matrice  $v$ . L'équilibre en cisaillement de la matrice impose alors :

$$2\pi r \tau = 2\pi (r + dr)(\tau + d\tau) \quad (1.22)$$

$$\text{soit } \tau(r) = \tau_i \frac{r_f}{r}$$

où  $r_f$  est le rayon de la fibre et  $\tau_i$  la contrainte de cisaillement à l'interface fibre-matrice, parallèlement à l'axe des  $x$ .

En remarquant que la contrainte de cisaillement dans la matrice  $\tau(r)$  s'exprime en fonction du déplacement radial suivant :

$$\text{il s'ensuit : } \tau(r) = G_m \frac{du}{dr}$$

où  $G_m$  est le module de cisaillement de la matrice, il vient :

$$\begin{aligned} u(r_f) &= u(R) + \frac{\tau_i r_f}{G_m} \ln \frac{R}{r_f} \\ \text{alors } H &= \frac{2\pi G_m}{\ln R/r_f} \end{aligned} \quad (1.23)$$

La distribution des contraintes en extrémité de fibre prend alors la forme suivante :

$$\sigma = E_f e \left[ 1 - \frac{\cosh B(1/2 - x)}{\sinh B 1/2} \right] \quad (1.24)$$

$$\tau = E_f e \left( \frac{G_m}{2 E_f \log R/r_f} \right)^{1/2} \frac{\sinh B(1/2 - x)}{\cosh B 1/2} \quad (1.25)$$

où  $\sigma$  est la contrainte longitudinale dans la fibre, et  $\tau$  la contrainte de cisaillement à l'interface fibre-matrice (fig. 5).

L'évolution des contraintes de cisaillement à l'interface fibre-matrice peut conduire soit à une déformation plastique de la matrice, soit à une décohésion fibre-matrice, la continuité du déplacement élastique n'étant alors plus assurée. Une fois la décohésion fibre-matrice intervenue, la contrainte de cisaillement à l'interface fibre-matrice en extrémité de fibre restera limitée. Suivant Ochiai [7] et Jacques [8], le profil des contraintes prend alors la forme illustrée sur la figure 6. La fibre est décollée de sa gaine de matrice sur une longueur  $l_c$ , sur laquelle la contrainte de cisaillement à l'interface fibre-matrice est purement frictionnelle et supposée constante et égale à  $\tau_i$ . La contrainte de cisaillement remonte alors jusqu'à la contrainte ultime de cohésion fibre-matrice  $\tau_u$ , puis décroît suivant le profil élastique du modèle de Cox. Ce schéma n'est bien évidemment valable que si la contrainte ultime de décohésion fibre-matrice reste inférieure à la contrainte d'écoulement plastique de la matrice  $\tau_p$ . Dans le cas contraire, le transfert de charge de la matrice à la fibre sera régi par la contrainte d'écoulement de la matrice  $\tau_p$ .

Sur le plan expérimental, dans les composites à matrice métallique, on peut avoir accès à la valeur de la contrainte moyenne maximale de transfert de charge à l'interface fibre-matrice  $\tau_m$  en effectuant un essai de traction sur composite monofilamentaire.

### 1.3.2 - Approche expérimentale de la contrainte de transfert de charge par cisaillement à l'interface fibre-matrice

Dans l'essai de fragmentation sur éprouvette monofilamentaire (fig. 7), la traction est poursuivie jusqu'à saturation, c'est-à-dire jusqu'à ce que les segments de fibres ne puissent plus rompre\*, la contrainte maximum atteinte dans chaque segment restant inférieure à sa contrainte à rupture.

La contrainte de cisaillement maximale moyenne à l'interface fibre-matrice est alors donnée par :

$$\tau_m = \frac{3}{8} \frac{r_f \sigma_{f_u}}{1} \quad (1.26)$$

A titre d'illustration, le cas des composites à matrice TA6V (Ti-6-4) ou d'aluminium (A9, 5083) renforcés par des fibres de carbure de silicium de fort diamètre est brièvement décrit ci-dessous.

Pour les composites à matrice d'aluminium renforcés par des fibres de carbure de silicium AVCO [9], et quel que soit l'alliage d'aluminium utilisé comme matrice, la contrainte maximale moyenne de transfert de charge est toujours égale

\* Dans les composites à matrice métallique, la détection des ruptures de fibres se fait par émission acoustique, la saturation est alors atteinte lorsque les signaux d'émission acoustique provenant de la fibre cessent.

à la contrainte d'écoulement plastique de la matrice en cisaillement [9]. Pour ces matériaux, c'est toujours la matrice qui sera limitante sauf si, dans le composite à forte fraction volumique de fibres, la consolidation de la matrice devenait importante du fait de la limitation du libre parcours moyen des dislocations résultant de la faible distance interfibre.

Pour les composites à matrice d'alliage de titane TA6V (Ti-6-4) renforcés par des fibres SCS6 d'AVCO, en revanche, la contrainte maximale moyenne de cisaillement à l'interface fibre-matrice reste, pour toute température comprise entre 20 et 900°C, inférieure à la contrainte limite d'écoulement en cisaillement de la matrice [10]. Cette résistance modérée de l'interface fibre-matrice est corroborée par les déchaussements de fibres observés à la surface de rupture du composite ; la décohésion fibre-matrice se produit à l'interface fibre SiC-revêtement, ce dernier jouant le rôle de fusible mécanique<sup>1</sup>. De ce fait, dans ce composite, la contrainte de cisaillement à l'interface fibre-matrice aura une forte composante de friction ; en conséquence, la contrainte de cisaillement à l'interface fibre-matrice évoluera de manière importante avec la température, du fait de la diminution des contraintes de frettage de la fibre par la matrice lorsque la température augmente. Le transfert de charge de la matrice à la fibre perdra donc de son efficacité lorsque la température d'essai s'élève. Cette perte d'efficacité du transfert de charge lorsque la température croît est sans aucun doute un des paramètres qui permet d'expliquer la baisse des caractéristiques des composites SiC(AVCO)-TA6V avec la température.

Pour bien comprendre le rôle des divers paramètres, il est indispensable d'avoir une approche de la rupture des composites qui dépasse la modélisation déterministe d'Aveston, Cooper et Kelly, et prenne en compte le caractère aléatoire de la rupture des fibres lié à la présence de défauts distribués au hasard dans leur volume.

#### 1.4 - Résistance à la rupture dans le sens long

##### 1.4.1 - Distribution statistique des contraintes à rupture dans les fibres et modèles statistiques

Toutes les fibres utilisées pour la réalisation des composites à matrice métallique ont une contrainte de rupture qui peut être décrite par une statistique de Weibull, dans laquelle la probabilité pour une fibre de rompre entre les contraintes  $\sigma$  et  $\sigma + d\sigma$  est donnée par la fonction densité de probabilité  $f(\sigma)$  :

$$f(\sigma) = L \alpha^{-m} \sigma^{m-1} \exp(-L \alpha \sigma^m) \quad (1.27)$$

où  $L$  est la longueur de la fibre,  $\alpha$  et  $m$  deux paramètres. Avec cette formulation, Coleman [11] a montré que la valeur moyenne de la contrainte à rupture et l'écart type sont reliés aux paramètres  $\alpha$  et  $m$  par les relations :

$$\bar{\sigma} = (\alpha L)^{-1/m} \Gamma(1 + 1/m) \quad (1.28)$$

$$s = (\alpha L)^{-1/m} \{ \Gamma(1 + 2/m) - \Gamma^2(1 + 1/m) \}^{1/2} \quad (1.29)$$

Le coefficient de variation  $cv$ , quotient de l'écart type par la valeur moyenne de la contrainte à rupture, ne dépend que de  $m$  :

$$cv = \frac{s}{\bar{\sigma}} = \frac{\{ \Gamma(1 + 2/m) - \Gamma^2(1 + 1/m) \}}{\Gamma(1 + 1/m)} \quad (1.30)$$

Rosen [12,13] a alors montré que pour les valeurs du  $cv$  faibles, comprises entre 0,05 et 0,5, le module de Weibull  $m$  restait proche de l'unité ( $m = 0,92$ ), de sorte que l'inverse de  $m$  est une mesure du coefficient de variation et que, pour les fibres usuelles,  $m$  sera largement supérieur à l'unité. Ainsi, pour un module de Weibull de 10, un changement de la longueur de fibre d'un facteur 10 n'entraînera qu'une diminution de 25 % de sa contrainte à rupture. Pour les fibres de verre, le module de Weibull est de 11 environ alors qu'il se situe entre 3 et 6 pour les fibres de bore. La contrainte de rupture la plus probable des fibres de longueur  $L$ , obtenue en écrivant que la dérivée de (1.27) est nulle, s'écrit :

$$\sigma^* = [(m - 1) / m]^{1/m} (\alpha L)^{-1/m} \quad (1.31)$$

ce qui, dans le cas des modules de Weibull élevés, conduit à :

$$\sigma^* = (L \alpha)^{-1/m} \quad (1.32)$$

la quantité  $(L \alpha)^{-1/m}$  pouvant être considérée comme une référence pour le niveau de la contrainte à rupture des fibres.

Le cas des torons de fibres a été traité par Daniels [14], qui a montré que pour des nombres de fibres  $N$  élevés dans les torons, la distribution de la contrainte moyenne de rupture des fibres approche une loi normale à la contrainte de rupture du toron, qui s'écrit :

$$\sigma_T = \sigma_{f_{max}} [1 - F(\sigma_{f_{max}})] \quad (1.33)$$

où  $F(\sigma)$  est la loi cumulée de distribution des contraintes à rupture donnée par :

$$F(\sigma) = \int_0^\sigma f(u) du$$

<sup>1</sup> Les revêtements effectués sur les fibres jouent plusieurs rôles dans les CMM, à savoir : barrière de diffusion, mais également contrôle de l'adhésion fibre-matrice, voire diminution du nombre de défauts de surface.

Daniels a ainsi montré que pour des fibres dont la contrainte de rupture obéit à une statistique de Weibull, la valeur maximale et la valeur moyenne de la contrainte à rupture d'un toron s'écrivent respectivement :

$$\begin{aligned}\sigma_T^{\max} &= (L \alpha m)^{-1/m} \\ \sigma_T &= (L \alpha m e)^{-1/m}\end{aligned}\quad (1.34)$$

#### 1.4.2 - Approche d'un critère de rupture

Ce sont Rosen [12,13] et Zweben [15] qui les premiers ont proposé des modèles qui permettent de prévoir la contrainte à rupture de composites à fibres fragiles dont la matrice présente une rigidité bien plus faible que celle du renfort. Dans son modèle, Rosen [12] suppose que la rupture du composite résulte du cumul de ruptures élémentaires de fibres, séparées par des barrières à la propagation des fissures qui ne sont rien d'autre que la matrice, supposée tenace, c'est-à-dire ne permettant pas à une fissure lenticulaire de se développer. Pour ce faire, le composite unidirectionnel (pli élémentaire) est supposé constitué de N fibres de longueur  $l_c$  juxtaposées parallèlement les unes aux autres (fig. 8). Pour une contrainte appliquée  $\sigma$ , certaines des fibres rompent tandis que les autres demeurent intactes. La rupture d'une fibre individuelle ne la rend pas incapable de supporter la charge sur toute sa longueur, mais seulement au voisinage de la rupture sur une longueur  $l_c$  appelée distance d'inefficacité, sur laquelle la charge supportée par la fibre est alors nulle. Rosen passe alors de ce modèle dit "parallèle" à un modèle dit "série", dans lequel le composite est constitué d'un empilement de P couches d'épaisseur  $l_c$ , chaque couche étant constituée d'un toron contenant N fibres. En conséquence, si une fibre rompt dans une couche, la totalité de la longueur de fibre sera inefficace, et la charge supportée avant rupture par cette fibre sera redistribuée après rupture sur toutes les autres fibres du toron, ce qui exclut la notion de concentration locale de contraintes. La contrainte de rupture est atteinte lorsqu'un élément de hauteur égale à  $l_c$  se trouve dans l'incapacité de supporter une augmentation de contrainte du fait du cumul de rupture de fibres individuelles. Ce modèle dépend bien évidemment fortement de la distance d'inefficacité  $l_c$  que Rosen avait considéré être égale à la distance sur laquelle la contrainte dans la fibre retrouvait, par recharge ment élastique, 90 % de sa valeur avant rupture<sup>1</sup>.

La contrainte à rupture du composite est alors donnée par la contrainte à rupture du toron, pondérée par la fraction volumique de fibres, soit :

$$\sigma_{cu} = V_f \sigma_T = V_f (l_c \alpha m e)^{-1/m} \quad (1.35)$$

Dans son modèle série, Rosen ne prenait pas en compte les effets de report local de la charge sur les plus proches voisines, lors de la rupture d'une fibre. Zweben [15] les a effectivement pris en considération dans le sien, en admettant que le composite était constitué de  $N \times P$  éléments. Ainsi, lors de la rupture d'un élément, la charge qu'il supportait avant rupture est reportée sur les éléments proches voisins par le biais d'un facteur multiplicatif K. Toutefois, ce mode opératoire conduit à des durées de calcul prohibitives, de sorte que l'on préfère généralement considérer seulement le cas du modèle série en ne prenant en compte qu'une tranche d'épaisseur  $l_c$ , dont l'épaisseur peut évoluer avec le chargement [10].

Les améliorations à ce modèle de cumul de dommages proposées depuis par divers auteurs ont essentiellement porté sur les points suivants :

- le cas de composites hybrides, en considérant la rupture soit de deux fibres contiguës, soit de deux fibres séparées par une fibre intacte [16] ;
- la prise en compte des effets dynamiques qui accompagnent la rupture d'une fibre [17] ;
- enfin, l'intégration aux modèles de Zweben et Rosen d'interfaces plus réalistes, prenant en compte une décohésion fibre-matrice [18].

Néanmoins, l'intégration dans ces modèles de mesures expérimentales de la cohésion fibre-matrice, ou encore de la contrainte moyenne de cisaillement à l'interface fibre-matrice, n'a pas encore été réalisée ; c'est l'objet de ce qui suit.

#### 1.4.3 - Modélisation de la rupture de composites unidirectionnels : influence de la contrainte de transfert de charge à l'interface fibre-matrice [8]

Les composites unidirectionnels à matrice d'aluminium (6061) ou de titane (Ti-6-4) renforcée par des fibres de carbure de silicium de fort diamètre sont de bons candidats pour l'évaluation de modèles de rupture. En effet, il est possible de mesurer dans ces deux systèmes la contrainte moyenne maximum de transfert de charge à l'interface fibre-matrice par un essai de fragmentation sur composite monofilamentaire d'une part, et d'en déduire la contrainte de transfert de charge à l'interface dans les unidirectionnels, du fait de leur fraction volumique de fibres relativement faible, 30 à 45 %, d'autre part.

La simulation de la rupture s'effectue en utilisant un modèle de type série. Dans ce modèle, on considère une tranche de composite d'épaisseur L à laquelle va être appliqué le chargement ; la contrainte dans chaque fibre supposée identique est obtenue par la loi des mélanges. Chaque fibre se voit attribuer une contrainte à rupture déterminée à l'aide de la statistique de Weibull. La rupture de la première fibre intervient lorsque la contrainte qu'elle supporte  $\sigma_i$  est supérieure à sa contrainte de rupture  $\sigma_n$  ; la charge supportée par cette fibre, avant rupture, est reportée après rupture sur les plus

<sup>1</sup> Le fait de considérer des fibres de longueur  $l_c$  dans l'équation (2.36) conduira à un accroissement de la contrainte à rupture par rapport à celle que l'on obtiendrait à partir de la contrainte à rupture de torons de longueur  $l > > l_c$ . Cet effet avait été prévu par Rosen.

proximes voisines (six dans le cas d'un arrangement hexagonal). Ce report de charge s'effectue, comme dans le modèle de Rosen, par une longueur dite d'inefficacité  $L_i$ , calculée à l'aide de la contrainte de transfert de charge mesurée par la relation :

$$L_i = \frac{\sigma_{fu} r}{\tau_m} \quad (1.36)$$

Lors de la poursuite du chargement de la tranche de composite, le nombre de zones endommagées à fibres rompues croît jusqu'à ce que l'augmentation du nombre de ruptures de fibres devienne catastrophique, pour une valeur de la contrainte appliquée égale à la contrainte à rupture du composite. Les résultats d'une simulation effectuée sur un composite représentatif renfermant 400 fibres ( $20 \times 20$ ) a permis de dégager les conclusions suivantes :

- une augmentation du module de Weibull des fibres se traduit par une forte augmentation de la contrainte à rupture du composite (fig. 9a). En effet, pour une même contrainte moyenne à rupture des fibres, de 4000 MPa pour une longueur de jauge de 5 mm, le fait de passer d'un module de Weibull de 4 à un module de Weibull de 24 conduit à une augmentation de la contrainte à rupture de plus de 55 %. En revanche, un faible module de Weibull permet une accumulation plus grande de l'endommagement avant rupture du composite (fig. 9a,b,c) ;
- l'effet du transfert de charge matrice → fibre est d'autant plus sensible que le module de Weibull des fibres est faible (fig. 10). Cette influence s'estompe pour les modules de Weibull élevés ( $m \geq 20$ ) ;
- la localisation de la surcontrainte locale lors de la rupture d'une fibre sur une faible longueur (longueur d'inefficacité  $L_i$  petite) est favorable ;
- la concentration de contrainte locale résultant d'une rupture de fibre est d'autant moins nocive que le nombre de fibres affectées par le report est important ;
- enfin, en ce qui concerne les dimensions de la fibre, un petit diamètre de fibre est favorable, d'autant qu'il minimise les effets dynamiques de transfert d'énergie qui accompagnent toute rupture de fibre.

En ce qui concerne la comparaison simulation-expérience, les résultats obtenus sur les composites à matrice d'aluminium (SCS2) et de titane (SCS6 ; Ti-6-4) ont permis de dégager les points suivants :

- le facteur limitant le transfert de charge de la matrice à la fibre est la contrainte d'écoulement plastique de la matrice pour les composites base aluminium, et la décohésion fibre-revêtement pour les composites à matrice titane (cf § 1.3) ;
- pour les composites à matrice d'aluminium, dans lesquels la seule diminution des caractéristiques mécaniques de la matrice avec la température ne permettait pas de rendre compte de la baisse de résistance observée avec la température par le biais de la loi des mélanges, la forte chute de la capacité de la matrice à transférer la charge lorsque la température augmente permet de rendre compte de la diminution de résistance du composite SCS2-6061 à partir de 350°C (fig. 11a) ;
- pour les composites à matrice de titane, dans lesquels une décohésion fibre-revêtement se produit, la contrainte de transfert de charge par cisaillement à l'interface fibre-matrice comprend une forte composante de friction provenant de la zone décollée de la fibre. Cette composante de friction est proportionnelle à la contrainte de frettage de la fibre par la matrice, qui décroît fortement avec la température. La simulation effectuée en tenant compte de ce paramètre conduit à une reproduction correcte de la courbe expérimentale (fig. 11b).

En conclusion, les modèles de prévision de la rupture des composites unidirectionnels qui se fondent sur le caractère aléatoire de la rupture des fibres commencent à conduire à des résultats encourageants. Toutefois, une connaissance correcte des mécanismes de transfert de charge à l'interface fibre-matrice semblable à celle acquise pour les composites à matrice organique [8] est indispensable.

### 1.5 - Résistance en traction dans le sens travers

Il est généralement bien admis que la contrainte à rupture dans le sens travers des composites à matrice métallique dépend essentiellement de la résistance de l'interface fibre-matrice, mais également de la fraction volumique de fibres. La résistance dans le sens travers des CMM est très faible par rapport à celle dans le sens long (fig. 12). Pour les composites fibres de bore/matrice alliage d'aluminium 6061, une étude assez complète effectuée par Prewo & Kreider [19] montre l'influence de l'état de la matrice brute de fabrication (F) ou traitée thermiquement au pic de revenu (T6) sur la contrainte à rupture dans le sens travers. Ainsi le composite à l'état T6 présente-t-il une contrainte de rupture de 140 MPa et un allongement à rupture faible ( $\approx 8.10^4$ ), tandis qu'à l'état brut de fabrication la contrainte à rupture est plus faible (90 MPa) et l'allongement plus élevé, indiquant l'existence d'une liaison fibre-matrice plus faible à l'état F qu'à l'état T6.

Pour les composites carbone-aluminium, Islam & Wallace [20] montrent, dans leur revue effectuée sur les composites de première génération, que la résistance en traction dans le sens travers reste très faible, comprise entre 10 et 50 MPa, alors que les caractéristiques dans le sens long dépassent 1100 MPa. Pour la grande majorité des composites à matrice métallique il en est de même, avec des contraintes à rupture dans le sens travers très inférieures à la limite de rupture de la matrice seule, ce qui montre la forte contribution de la décohésion fibre-matrice. Ce rôle dominant de la liaison fibre-matrice est confirmé par la décroissance de la contrainte à rupture observée lorsque la fraction volumique de fibres augmente [19].

Là encore, un contrôle des caractéristiques de l'interface fibre-matrice apparaît indispensable.

- Une augmentation de la taille du composite (nombre de fibres très élevé) ne modifie pas les conclusions, mais entraîne des temps de calcul prohibitifs.

## 1.6 - Ténacité des composites à matrice métalliques

L'application stricte de la mécanique linéaire de la rupture, développée pour des matériaux homogènes et isotropes, aux composites à matrice métallique n'a bien évidemment pas permis d'obtenir des caractéristiques - facteur d'intensité des contraintes K ou taux d'énergie libérée en fond de fissure G - intrinsèques pour un matériau donné. Dans un matériau composite, il faut prendre en compte les effets locaux, arrachement des fibres de la matrice et plasticité de la matrice induite à fond de fissure par l'effort de fermeture des fibres non rompues, qui agissent alors comme des raidisseurs. Pour un composite à fibres continues, l'énergie libérée à fond de fissure peut alors s'écrire comme la somme de trois termes [21] :

$$G_{IC} = G_I + W_{ext} + W_p \quad (1.37)$$

où

- G, est l'énergie libérée à fond de fissure par un matériau biphasé dans lequel les deux phases sont supposées se déformer identiquement ;
- $W_{ext}$  est le travail nécessaire pour extraire les fibres de leur gaine de matrice sur la longueur décohérée ;
- $W_p$  est le travail de déformation plastique de la matrice résultant du pontage des lèvres de la fissure par les fibres.

Cette formulation se comprend sur la base du cumul d'une approche macroscopique de la ténacité, représentée par le premier terme, et d'une approche locale [21], décrite par les deux autres ; l'énergie de fracture macroscopique  $G_{IM}$  peut être estimée à l'aide de la mécanique linéaire de la rupture, dans le cas d'une isodéformation des deux phases [22], en considérant un matériau homogène équivalent (fig. 13). Le terme s'écrit alors :

$$G_{IM} = \lim_{\delta a \rightarrow 0} \frac{1}{\delta a} \int_0^{\delta a} \sigma_y^c u_y^c dx \quad (1.38)$$

où a est la longueur de fissure,  $\sigma_y^c$  et  $u_y^c$  les contrainte et déplacement dans le matériau homogène équivalent parallèlement à la direction des efforts ;

$$G_{IM} = [V_m (E_m G_{Im}/E_c)^{1/2} + (E_f G_{If}/E_c)^{1/2}]^2 \quad (1.39)$$

où  $G_i$  est le taux d'énergie restituée en fond de fissure dans un solide infini de la phase i ( $i = m, f$ ) défini par une équation identique à (1.38). Dans le cas où  $v_c = v_m = v_f$  (1.39) se simplifie et l'on a alors :

$$G_{IM} = \pi (1 - v_c^2) \sigma_c^2 a / E_c \quad (1.40)$$

La contribution de l'extraction des fibres au taux de restitution d'énergie à fond de fissure a été calculée dans le cas de composites à fibres longues possédant des points faibles par Cooper [23], et celle résultant de la déformation plastique de la matrice par Pigott [24] ou Ishikawa & Taya [22] à l'aide de la méthode de l'ouverture critique (COD).

L'énergie totale de rupture d'un composite unidirectionnel  $W_R$  peut être représentée par l'aire sous-tendue par la courbe force-déplacement. L'énergie de rupture par unité de surface est alors le quotient du travail de rupture  $W_R$  par le double de l'aire du ligament. Cette quantité a été estimée par Taya & al [25 à 27] en intégrant l'équation (1.37) entre les dimensions initiale  $a_0$  et finale  $a_n$  conduisant à la rupture du composite, d'une fissure lenticulaire préexistante. Les valeurs de l'énergie de rupture obtenues par cette méthode recoupent les valeurs expérimentales mesurées dans les composites C/6061 et B/Al 1100.

## 2 - LES CONSTITUANTS ELEMENTAIRES : FIBRES ET MATRICES

### 2.1 - Les fibres utilisables pour les composites à matrice métallique

Les caractéristiques essentielles recherchées pour les composites à matrice métallique étant la résistance et la rigidité spécifiques, les fibres candidates au renforcement des CMM devront posséder à la fois des propriétés mécaniques élevées et une faible densité. De plus, elles devront être le plus inertes chimiquement vis-à-vis de la matrice, afin de conserver leurs caractéristiques tant pendant la phase d'élaboration du matériau que pendant celle de son utilisation, dans le cas des composites destinés à travailler à haute température. A côté des fibres longues utilisées dans les composites élaborés par synthèse, il faut mentionner les trichites de carbure de métal de transition, qui constituent le renfort des composites de solidification obtenus par réaction eutectique, dont le domaine d'utilisation est celui des hautes températures. Les fibres de renfort peuvent ainsi être classées en deux groupes suivant le domaine de température d'utilisation des composites.

#### 2.1.1 - Composite dont la température d'utilisation ne dépasse pas 400°C

Une grande variété de fibres peuvent être utilisées pour ces matériaux, que l'on peut ramener à quatre composés principaux : le bore, le carbone, le carbure de silicium et les alumino-silicates (tableau 1).

Les fibres de bore ou de carbure de silicium de fort diamètre (100 à 140  $\mu\text{m}$ ) sont toutes deux obtenues par dépôt chimique en phase vapeur sur un filament préchauffé de tungstène pour le bore, de tungstène ou de carbone pour le carbure de silicium. Malgré leurs caractéristiques spécifiques très élevées, ces fibres demeurent peu utilisées en raison de leur coût élevé et de leur manque de souplesse, ce qui rend leur mise en œuvre difficile (ces fibres ne sont par exemple pas tissables).

Les fibres de carbure de silicium obtenues sous forme de torons de filaments de faible diamètre, par pyrolyse d'un précurseur organométallique, contiennent généralement des impuretés en teneur très élevée - oxygène pour les fibres

d'origine japonaise Nicalon ou Tyranno, azote pour les fibres françaises de Rhône-Poulenc. Cette teneur élevée en oxygène est une des raisons de la thermostabilité limitée à très haute température ( $\approx 1200^{\circ}\text{C}$ ) pour les fibres japonaises, avec un avantage pour la fibre Tyranno ; quant aux fibres Rhône-Poulenc, leur thermostabilité a été largement accrue par rapport à la fibre Nicalon. Les caractéristiques mécaniques de ces fibres sont donc plus limitées que celles des fibres obtenues par dépôt chimique en phase vapeur (tableau 1) ; en revanche, elles possèdent une grande souplesse et une excellente inertie chimique vis-à-vis des matrices aluminium ou magnésium, sauf lorsqu'elles contiennent de la silice (surtout en surface) qui réagit violemment avec le magnésium liquide.

Les fibres d'alumino-silicates ( $x\text{Al}_2\text{O}_3, (1-x)\text{SiO}_2$ ) sont produites soit sous forme de torons de filaments continus de 10 à 20  $\mu\text{m}$  de diamètre, soit sous forme de fibrilles discontinues de 1 à 7  $\mu\text{m}$  de diamètre (tableau 1). La forte réactivité des fibres contenant de la silice avec le magnésium à l'état liquide conduit à leur dégradation ; en revanche, la relative inertie de ces fibres vis-à-vis de l'aluminium liquide se traduit par une adhésion fibre-matrice faible, qu'il est possible d'augmenter par l'emploi d'alliages aluminium-lithium.

Les fibres de carbone sont de divers types selon le précurseur utilisé et les caractéristiques mécaniques recherchées (tableau 1). Il existe essentiellement deux types de précurseurs utilisés pour la fabrication des fibres de carbone : le polyacrylonitrile (PAN) et le brai.

Les fibres issues du précurseur PAN peuvent être classées en deux grandes familles selon la température de pyrolyse :

- une pyrolyse à basse température de l'ordre de  $1500^{\circ}\text{C}$  conduit aux fibres à haute résistance, supérieure à 3500 MPa ; les fabricants de fibres ont fait évoluer les caractéristiques des fibres en affinant le précurseur et en augmentant le taux d'étrage des fibres PAN, ce qui s'est traduit par une augmentation de l'allongement à rupture, voisin de 1 % pour les fibres dites de première génération, caractérisées par la fibre T300 de Toray, à près de 2 % pour les dernières fibres apparues sur le marché, caractérisées par la fibre T800H ;
- une pyrolyse effectuée à très haute température conduit aux fibres à haute module en raison d'un taux de graphitisation élevé, caractérisées par la fibre GY70 de Celion.

Les fibres issues de précurseur brai sont toutes des fibres à haut module, dont l'allongement à rupture a suivi une évolution parallèle tout en restant à des niveaux nettement plus modestes que celle des fibres à haute résistance ; les dernières-nées possèdent des modules très élevés (840 MPa) proches du module théorique du graphite.

L'ensemble des fibres de carbone ou de carbure de silicium utilisables dans l'industrie aérospatiale sont regroupés sur la figure 14 dans un diagramme module-résistance à rupture qui permet de séparer le domaine des matériaux pour structures spatiales, essentiellement dimensionnés en module, de celui des matériaux pour structure aéronautique, où la résistance reste un critère de dimensionnement important.

Le coût de ces diverses fibres dépend à la fois de leur nature et du volume produit annuellement (fig. 15) [28]. Les fibres monofilamentaires obtenues par dépôt chimique en phase vapeur restent très onéreuses (plus de 1500 \$/kg), suivies de près par les fibres de carbure de silicium élaborées par pyrolyse d'un précurseur organométallique (700 \$/kg pour les fibres Nicalon) ; à l'opposé les fibres d'alumino-silicates sont produites à des coûts très faibles, de 2 à 40 \$/kg. Pour les fibres de carbone, les coûts varient largement, de 50 à 100 \$/kg pour les fibres haute résistance courantes, à près de 4000 \$/kg pour les fibres haut module expérimentales.

### 2.1.2 - Composites pour application à haute température ( $> 400^{\circ}\text{C}$ )

La nature des fibres pour des composites utilisables à haute température est beaucoup plus restreinte, dans la mesure où les fibres doivent à la fois :

- conserver leurs caractéristiques en température ;
- être inertes vis-à-vis de la matrice, tant dans la phase d'élaboration que dans celle de l'utilisation.

De ce fait, la nature des fibres retenues pour un composite est fortement liée à celle de la matrice, constituée essentiellement à l'heure actuelle d'alliage de titane ou de superalliage.

Pour les alliages de titane, les fibres utilisables sont nécessairement des monofilaments de fort diamètre, en raison de la très forte réactivité du titane avec le bore ou le carbure de silicium (cf. § 3.1.2). Pour ces matériaux, le développement de fibres de diborure de titane est engagé aux Etats-Unis, compte tenu de la bonne stabilité de ce composé.

Les fibres utilisables avec des matrices superalliages sont soit des monofilaments de tungstène, soit des trichites de carbure de métaux de transition obtenus directement par croissance dans les composites de solidification (tableau 2).

### 2.2 - Les matrices utilisables pour les CMM

Dans les matériaux composites de façon générale - et les CMM n'échappent pas à la règle -, les rôles essentiels de la matrice sont, d'une part d'assurer la cohésion entre les fibres et d'assurer le transfert de charge, d'autre part d'éviter les agressions de l'environnement. Diverses matrices métalliques peuvent être employées en fonction de la température de fonctionnement des composites ; on trouvera ainsi par température d'utilisation croissante les alliages légers d'aluminium ou de magnésium (utilisables jusqu'à  $400^{\circ}\text{C}$  au plus), puis les alliages de titane (jusqu'à  $550$  ou  $650^{\circ}\text{C}$ ), les composés intermétalliques de titane (dont certains peuvent atteindre  $950^{\circ}\text{C}$ ), les superalliages de nickel (pour des températures de  $1100^{\circ}\text{C}$ ), et enfin, mais il s'agit là de prospective, les alliages de niobium (utilisables jusqu'à  $1300^{\circ}\text{C}$ ).

### 2.2.1 - Les matrices basse température, d'aluminium ou de magnésium

Pour ce qui est des alliages d'aluminium, nombre de matrices ont été utilisées pour la réalisation de composites à matrice métallique. On trouve ainsi :

- les matrices d'aluminium pur de la série 1100 ;
- les alliages aluminium-magnésium de la série 5000, qui ont été très largement employés pour les composites de la première génération élaborés dans les années 70 : il s'agit essentiellement des nuances 5056, 5154, Al-5Mg, Al-10Mg. Toutefois, il faut remarquer que tous les alliages aluminium-magnésium sont des alliages de corroyage dans lesquels le contrôle de la microstructure et, partant, les propriétés mécaniques, résultent de traitements thermomécaniques mettant en jeu des taux de déformation élevés qu'il est bien évidemment impossible de réaliser dans des composites à fibres longues ;
- les alliages aluminium-silicium de la série 6000, soit faiblement alliés comme le 6061, soit très riches en silicium comme les alliages Al-13Si ;
- les alliages aluminium-cuivre de la série 2000, comme l'alliage 2024.

Il convient de remarquer que les alliages aluminium-zinc très haute résistance de la série 7000, comme le 7075, ont été très peu utilisés comme matrice de composites à fibres longues.

Pour les matrices base magnésium, les alliages les plus employés sont :

- d'une part le magnésium pur,
- d'autre part les alliages magnésium-aluminium, tels les alliages AZ61 et AZ91.

### 2.2.2 - Les matrices moyenne température de titane ou de composés de titane

La forte réactivité des matrices à base de titane imposant une mise en oeuvre à l'état solide, les alliages les plus utilisés sont ceux que l'on peut trouver sous forme de feuillards de faible épaisseur, de l'ordre de 100 µm, qui de plus possèdent un domaine contrainte-température dans lequel ils sont superplastiques.

Pour les alliages de titane, le plus utilisé est le TA6V (Ti-6-4), alliage  $\alpha$ - $\beta$  laminable qui présente un domaine de superplasticité au-delà de 900°C. On trouve également des composites réalisés avec l'alliage 15-3-3-3 (15-3) de TIMET, alliage  $\beta$  métastable, facilement laminable et disponible sous forme de feuillards de faible épaisseur.

Pour les composés intermétalliques de titane, les seuls composés envisagés à ce jour sont les composés base Ti<sub>x</sub>Al, soit l'alliage de base Ti-14Al-25Nb<sup>\*</sup> [29], soit encore le composé super- $\alpha$ , Ti-14Al-20Nb-3V-2Mo\* [30], tous deux développés aux Etats-Unis par TIMET, et que l'on peut obtenir sous forme de feuillards de faible épaisseur [31]. Ces matériaux, utilisables jusqu'à une température maximale de 650°C, font l'objet d'une évaluation comme matrice de matériaux composites [32].

Les aluminures de titane dérivés du composé TiAl, dont la tenue à l'oxydation est supérieure, devraient, eux, être utilisables à des températures voisines de 950°C ; toutefois, actuellement les nuances d'alliages ne sont pas encore complètement figées. De ce fait, la réalisation de composites avec ces matrices en est encore au stade des études.

### 2.2.3 - Les matrices superalliages pour emploi jusqu'à 1200°C

Les superalliages de nickel sont actuellement utilisés sous forme d'aubes monocristallines jusqu'à des températures de l'ordre de 1050°C [33]. Il faut cependant noter que les autres catégories de superalliages ont des températures d'emploi limitées à 980°C.

Deux types de composites à matrice superalliages sont susceptibles d'être utilisés :

- les composites de synthèse, renforcés par des fibres longues de tungstène ;
- les composites de solidification, renforcés par des trichites de carbure.

Dans le premier cas, de nombreuses matrices sont utilisables, les seules limitations étant liées d'une part au procédé de fabrication - les matériaux devant être disponibles soit sous forme de feuillards, soit sous forme de poudres préalliées - , d'autre part aux réactions fibre-matrice. Ainsi, pour ces composites de synthèse, nombre de matrices en superalliages (Hastelloy X, 713C, ...) [34], en alliage à forte résistance à l'oxydation (FeCrAlY) ou en composé intermétallique (dérivé des systèmes NiAl, FeAl, Fe<sub>3</sub>Al) sont des candidates sérieuses.

Dans le second cas, la composition des matrices est limitée par les diagrammes d'équilibre des phases, tant lors de la solidification dirigée que lors de l'utilisation, du fait des réactions en phase solide.

### 2.2.4 - Les matrices pour très haute température

Au-delà de 1200°C, les seules matrices utilisables actuellement sont des alliages base niobium durcies seulement en solution solide, comme les alliages Nb-1%Zr utilisables à condition d'être protégés contre l'oxydation au-delà de 1300°C.

\* Pourcentages pondéraux

### 2.3 - La compatibilité fibre-matrice

Dans les composites à matrice métallique, la compatibilité entre fibre et matrice se pose à deux niveaux, chimique et mécanique.

#### 2.3.1 - Compatibilité chimique

La compatibilité chimique est à considérer lorsque des réactions peuvent se produire entre les fibres et la matrice, à l'interface, tant lors de la mise en oeuvre du matériau que lors de son utilisation à haute température. Les problèmes qui se posent et les remèdes qui peuvent être apportés sont spécifiques à chaque couple fibre-matrice.

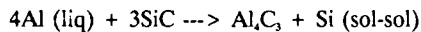
Dans les composites à matrice d'aluminium, les fibres dont la compatibilité avec la matrice mérite une attention particulière sont les fibres de carbone et celles de carbure de silicium ou de bore :

- les fibres de carbone réagissent avec l'aluminium pour former du carbure d'aluminium  $\text{Al}_3\text{C}_2$ , qui croît à l'interface fibre-matrice sous forme de particules anguleuses [35]. La présence de cette phase à l'interface induit au niveau du composite plusieurs effets délétères [36] :

- . une baisse de résistance de la résistance intrinsèque des fibres ;
- . une augmentation du nombre des sites d'amorçage de fissures en raison de leur forme et de leur dureté ;
- . une détérioration des caractéristiques de corrosion, déjà très médiocres dans les composites C-Al.

De ce fait, les composites C-Al requièrent pour leur mise en oeuvre que la protection des fibres de carbone soit assurée à l'aide d'un revêtement ; celui-ci devra en outre assurer le mouillage des fibres par l'aluminium liquide, les fibres de carbone n'étant pas naturellement mouillées par l'aluminium liquide.

- le carbure de silicium réagit avec l'aluminium, pour les températures supérieures à 557°C [37], suivant la réaction :



Pour les températures inférieures, le carbure de silicium et l'aluminium sont en équilibre. A haute température, la réaction entre l'aluminium liquide et le carbure de silicium s'arrête lorsque la teneur en silicium dans l'aluminium correspond à l'équilibre entre le métal liquide et la phase SiC (figure 16).

En ce qui concerne le mouillage du carbure de silicium par l'aluminium, il est possible d'affirmer aujourd'hui que celui-ci ne résulte pas de la formation du carbure d'aluminium ; le mouillage est obtenu naturellement pour des durées de contact de l'ordre de 60 minutes [38]. De ce point de vue, le carbure de silicium apparaît être un matériau de protection des fibres de carbone bien adapté.

- pour les composites à matrice d'alliage de titane, les fortes réactions observées tant avec les fibres de bore [39] qu'avec celles de carbure de silicium n'ont pas permis d'utiliser ces fibres sans protection de surface. En effet, l'importance des zones de diffusion à l'interface fibre-matrice (plusieurs micromètres de largeur) et la présence dans ces zones de composés intermétalliques fragiles ( $\text{TiB}_2$ ,  $\text{Ti}_3\text{Si}_5$ ,...) conduisaient à des matériaux très médiocres sur le plan mécanique [40].

#### 2.3.2 - Compatibilité thermique

La compatibilité thermique, et par conséquent mécanique, se pose en raison de la grande différence des valeurs des coefficients de dilatation thermique entre les fibres céramiques et la matrice métallique, qui peut atteindre  $24,7 \cdot 10^{-6}/^\circ\text{C}$  dans les composites carbone-aluminium. Cette forte différence des valeurs des coefficients de dilatation entre fibres et matrice va se traduire par l'existence dans les CMM de contraintes internes élevées, qui peuvent induire une plastification généralisée de la matrice.

Pour répondre aux problèmes liés à la compatibilité fibre-matrice, il est nécessaire de pouvoir contrôler les caractéristiques de l'interface fibre-matrice, par le biais de revêtements de surface des fibres notamment.

### 3 - L'INTERFACE FIBRE-MATRICE : TRAITEMENTS DE SURFACE ET REVÊTEMENTS PROTECTEURS

Comme dans tout composite, les caractéristiques de l'interface fibre-matrice jouent un rôle fondamental dans l'élaboration, les caractéristiques mécaniques et la stabilité thermique des CMM.

Pour ce qui est de l'élaboration, les propriétés recherchées sont à la fois une bonne mouillabilité de la fibre par le métal liquide dans le cas d'une mise en oeuvre par des procédés dérivés de la fonderie, et une inertie chimique relative de la fibre vis-à-vis du métal liquide afin d'éviter sa dégradation et la formation de phases indésirables à l'interface.

Pour ce qui est des caractéristiques mécaniques, le but visé est le contrôle de l'adhésion fibre-matrice par le biais des réactions à l'interface lors de l'élaboration.

Enfin, pour la stabilité thermique, l'objectif est la limitation des réactions fibre-matrice en phase solide.

L'objectif à atteindre est donc double : il faut mettre en place une barrière de diffusion qui présente toutefois une réactivité non totalement nulle avec la matrice, afin de permettre un réglage de l'adhésion fibre-matrice.

Les moyens d'action du concepteur procèdent d'une part du contrôle des conditions d'élaboration, traité dans le chapitre suivant, d'autre part du traitement de surface des fibres.

Les traitements de surface diffèrent selon le procédé de mise en oeuvre et les objectifs recherchés. Deux exemples concernant les fibres de carbone et de carbure de silicium de fort diamètre seront traités plus en détail ; les autres traitements de surface, en cours de développement, seront seulement mentionnés.

### 3.1. - Le traitement des fibres de carbone dans les composites C-Al

De tout temps, les fibres de carbone utilisées pour le renfort des composites à matrice d'aluminium et, dans une moindre mesure, de ceux à matrice de magnésium, ont nécessité un revêtement de surface à la fois pour les rendre mouillables par l'aluminium liquide et pour éviter leur attaque et la formation de carbure d'aluminium  $\text{Al}_3\text{C}_2$ .

#### 3.1.1 - Traitement d'imprégnation des torons par voie liquide

Pour les composites de première génération, élaborés au début des années 1970, l'essentiel des traitements étaient destinés à améliorer la mouillabilité des fibres ; leur intérêt, surtout historique jusqu'à un passé récent, renaît en raison de la meilleure homogénéité de la distribution des fibres au sein du composite que l'on obtient lorsqu'elles sont mouillées par l'aluminium liquide.

Il est ainsi utile de mentionner :

- l'imprégnation aux métaux alcalins (sodium, potassium) [41], effectuée sur les torons, traitement dans lequel le mouillage résulterait de l'intercalation d'atomes alcalins dans les plans graphitiques du carbone. Dans ce procédé, onéreux mais conduisant à des caractéristiques mécaniques proches de la limite donnée par la loi des mélanges, la protection des fibres contre l'attaque de l'aluminium liquide est assurée par un film d'alliage Sn-2%Mg, probablement par la formation d'un composé intermétallique  $\text{Mg}_3\text{Sn}$  ;
- l'imprégnation par des solutions colloïdales d'argent, qui permet, grâce à l'enrobage de chaque filament par un dépôt fin et homogène, un excellent mouillage des mèches [42] ;
- le dépôt électrolytique de cuivre ou de nickel conduit également à un bon mouillage ; toutefois, la nécessité de revêtir de manière homogène chaque fibre conduit dans le composite à des alliages chargés en cuivre ou en nickel, ce qui nuit à la fois aux caractéristiques de la matrice et à sa densité.

Néanmoins, tous ces dépôts métalliques ne permettent pas d'assurer lors de l'imprégnation des mèches par le métal liquide une bonne protection des fibres de carbone contre l'attaque par l'aluminium liquide ; c'est l'une des raisons qui leur fait préférer les revêtements céramiques, utilisés à la fois comme barrière de diffusion, donc justifiables de mises en oeuvre en phase solide comme en phase liquide, et pour assurer le mouillage des fibres par l'aluminium liquide.

#### 3.1.2 - Dépôts de céramiques

Divers revêtements de céramiques ont été utilisés, tant pour protéger les fibres elles-mêmes que pour assurer leur mouillabilité, bien que les céramiques soient généralement mal mouillées par l'aluminium [43]. Les céramiques les plus utilisées sont soit des carbures de titane ou de silicium, soit des composés de bore et de titane  $\text{Ti}_3\text{B}_4$ , soit encore de la silice  $\text{SiO}_2$ . Tous ces revêtements sont réalisés par Dépôt Chimique en Phase Vapeur (DCPV) [43 à 45], procédé dans lequel on décompose par voie thermique (figure 17) un composé contenant les éléments chimiques du composé que l'on souhaite déposer. Il est également possible de n'apporter que l'un des deux constituants du composé, l'autre étant alors fourni par le substrat lui-même ; dans ce dernier cas, on parle de dépôt chimique en phase vapeur réactif.

Le non-mouillage des céramiques par l'aluminium liquide au voisinage de son point de fusion est vraisemblablement lié à la présence d'une fine pellicule d'alumine à la surface du métal liquide [46].

Dans le cas de dépôts effectués de manière non réactive, il est en général nécessaire d'opérer sous pression réduite, inférieure à la pression atmosphérique, et avec des débits d'espèces réactives faibles afin d'obtenir un revêtement homogène des fibres au sein du toron. En effet, la cinétique de dépôt comporte deux régimes en fonction de la température (figure 18) :

- un régime dit de surface, observé à basse température, dans lequel ce sont les phénomènes de surface (adsorption puis réaction dans la phase adsorbée) qui contrôlent la vitesse de dépôt, toujours lente ;
- un régime dit diffusionnel, observé à plus haute température, dans lequel la vitesse de dépôt est régie par l'accès des espèces réactives à la surface du substrat. Ce régime est bien évidemment à proscrire, car il ne conduit pas à une concentration en espèces réactives identique à cœur et en surface du toron ; le dépôt est alors limité aux fibres externes.

La faible vitesse de dépôt en régime de surface observée sous pression atmosphérique peut être améliorée en diminuant la pression de travail ; la transition régime de surface/régime diffusionnel se trouve en effet repoussée vers les hautes températures lorsque la pression dans le réacteur est abaissée (figure 18). Dans ces conditions, les dépôts obtenus par germination et croissance présentent généralement une structure équiaxe, ou à grains colonnaires pour les dépôts plus épais. Les vitesses de dépôt, de quelques micromètres à l'heure, restent acceptables dans le cadre d'un traitement industriel, dans la mesure où les épaisseurs des revêtements nécessaires à la protection des fibres de carbone demeurent faibles, généralement de l'ordre de quelques dizaines à quelques centaines de nanomètres. Un grand nombre de composés peuvent ainsi être obtenus sous forme de revêtement protecteur des fibres, de carbone notamment (tableau 3).

Actuellement, sur le plan industriel et en ce qui concerne les fibres de carbone, seul le co-dépôt de titane et de bore ( $\text{Ti}_3\text{B}_4$ ) a fait l'objet d'une industrialisation aux Etats-Unis par la société Materials Concept Inc. Les dépôts réalisés, très fins (20 nm), sont utilisés pour l'obtention de préimprégnés filamentaires.

Pour ce qui est des dépôts chimiques en phase vapeur réactifs, la variété des espèces qu'il est possible de déposer est bien évidemment plus réduite et serait, dans le cas des fibres de carbone, limitée aux carbures. Ce procédé présente toutefois l'avantage théorique de donner sur des torons des revêtements d'épaisseur très homogène du fait de son autorégulation. En effet, le revêtement s'effectuant en empruntant l'un des éléments, ici le carbone, à la fibre, la cinétique de croissance du revêtement sera notablement plus faible pour les fibres déjà revêtues (en raison de la nécessité pour l'élément métallique de diffuser à travers le dépôt pour réagir ensuite avec la fibre) que pour les fibres nues. Cette technique a été appliquée avec succès au revêtement de fibres de carbone, essentiellement haute résistance, par l'équipe du Professeur Bouix [47]. Les revêtements obtenus sont minces (quelques dizaines à quelques centaines de nanomètres), continus et protègent efficacement les fibres de carbone contre l'oxydation [48]. Son efficacité en tant que barrière de diffusion pour l'élaboration de composites carbone-aluminium est en cours d'évaluation.

### 3.2 - La protection de surface des fibres de bore et de carbure de silicium

Les fibres de bore ou de carbure de silicium utilisées pour le renforcement des composites à matrice titane demandent la mise en place d'une barrière de diffusion.

Pour les fibres de bore, la meilleure barrière de diffusion est le carbure de bore B<sub>4</sub>C, et des fibres B/B<sub>4</sub>C ont été produites industriellement par la société AVCO (filiale de TEXTRON) sous licence SNPE dans les années 70.

En ce qui concerne les fibres de carbure de silicium, le seul producteur industriel actuel est la société AVCO, qui a développé deux types de finition de surface des fibres selon la nature de la matrice, aluminium ou titane. Ces revêtements, généralement complexes, jouent plusieurs rôles, barrière de diffusion et adaptateur mécanique, qui seront détaillés dans le cas de la fibre dénommée SCS6, destinée aux composites à matrice titane. La fibre SCS6 est obtenue par dépôt chimique en phase vapeur sur un filament chaud de carbone, ce qui autorise de très fortes vitesses de croissance, et le traitement de surface est réalisé en ligne dans le réacteur qui sert à élaborer la fibre. Une fibre SCS6 (figure 19) est donc constituée [40] :

- d'un cœur de carbone de 33 µm de diamètre ;
- d'une couronne de carbure de silicium (B) de 100 µm d'épaisseur environ ;
- d'un revêtement protecteur constitué de plusieurs couches, riche en carbure de silicium vers l'intérieur et en carbone vers l'extérieur.

La complexité du revêtement, qui comprend six à sept couches, ainsi que la finesse des microstructures à l'intérieur de chaque couche, n'ont pu être élucidées qu'en faisant appel aux techniques de microscopie électronique à haute résolution [49]. La couche interne est constituée de microcristallites de SiC noyés dans une gangue de carbone turbostratique (figure 20a), tandis que la couche externe est presque uniquement constituée de carbone turbostratique (figure 20b).

Le fonctionnement de ce revêtement peut se comprendre comme suit : lors de la mise en œuvre du composite, le carbone présent à la surface de la fibre réagit avec le titane de la matrice pour former une couche plus ou moins continue de carbure de titane Ti<sub>3</sub>C<sub>4</sub>, qui va jouer le rôle de barrière de diffusion [50]. Toutefois, il n'est pas possible d'obtenir ce résultat en effectuant un simple dépôt de carbone sur la fibre de carbure de silicium obtenue par DCVP ; en effet, la forte différence des coefficients de dilatation du carbone et du carbure de silicium conduit, pour des dépôts de carbone de 3 à 4 µm d'épaisseur, à un décollement du dépôt de carbone de la fibre. Afin d'obtenir un dépôt adhérent, il est donc nécessaire de passer graduellement des caractéristiques du carbure de silicium à celles du carbone turbostratique de surface, ce que réalise le revêtement de la fibre SCS6.

La fibre SCS6 représente donc un excellent exemple de la réalisation d'un revêtement évolutif, capable d'assurer l'adaptation mécanique de la barrière de diffusion à la fibre.

### 3.3 - Les autres revêtements protecteurs de fibres

Des revêtements protecteurs peuvent être nécessaires pour assurer la compatibilité de fibres avec des matrices différentes de celles déjà mentionnées, aluminium, magnésium ou titane. Parmi les matrices utilisables à haute température, les superalliages et les composés intermétalliques, essentiellement de titane [51], ont déjà été cités. Pour ces derniers, un double effet peut être avancé, d'une part une élévation des températures de mise en œuvre et de fonctionnement, qui peut nécessiter de nouveaux revêtements, d'autre part (et cela vaut essentiellement pour les aluminures de titane) une stabilité accrue du carbure de silicium dans certains composés du titane, comme le Ti<sub>3</sub>Al [52]. Si une nouvelle protection des fibres de carbure de silicium s'avère nécessaire, il sera possible de faire appel à des composés très stables vis-à-vis du titane, comme les oxydes de terres rares.

Pour effectuer le revêtement des fibres, diverses techniques peuvent être utilisées [45] : il s'agit essentiellement des techniques de dépôt physique en phase vapeur (figure 21), de dépôt chimique en phase vapeur assisté par plasma (figure 22) ou par laser, ce qui permet d'abaisser les températures de dépôt, et enfin des techniques sol-gel.

#### 3.3.1 - Dépôt physique en phase vapeur (DPPV)

Dans le cas des céramiques, les vitesses de dépôt obtenues en pulvérisation cathodique restaient trop faibles pour espérer effectuer des revêtements en des temps compatibles avec un procédé industriel. Toutefois, l'adjonction d'un champ magnétique a permis d'augmenter la densité du plasma au voisinage de la cible et, partant, la vitesse de pulvérisation. Les céramiques sont généralement produites en utilisant des atmosphères réactives d'oxygène pour les oxydes, d'azote pour les nitrides et de méthane pour les carbures. Les vitesses de dépôt peuvent être élevées, de l'ordre de quelques µm/min [52]. Toutefois, les techniques de DPPV restent très directive, et demandent que les torons soient étalés afin d'éviter les effets d'ombrage, particulièrement marqués.

### 3.3.2 - Dépôt chimique en phase vapeur assisté par plasma ou laser

L'utilisation d'un plasma, développé jusqu'ici essentiellement pour les dépôts dans l'industrie de la microélectronique, permet un abaissement substantiel des températures de réaction. De nombreux composés : carbures, nitrures, borures, ont ainsi été déposés [43,45]. L'utilisation de cette technique pour le revêtement des fibres présente tous les avantages du DPPV, sans l'inconvénient d'une forte directivité. La réalisation de revêtements d'oxydes par décomposition de chlorures en présence de méthane rend ainsi possible le revêtement de fibres en dessous de 1000°C. Cet abaissement de la température de dépôt présente également l'avantage de conduire à une taille de grain plus petite dans le revêtement.

### 3.3.3 - Revêtement par voie sol-gel

L'utilisation de techniques sol-gel pour l'élaboration de films minces de céramiques fait aujourd'hui l'objet d'études de développement [53 à 58]. Les gels, composés généralement amorphes, présentent l'avantage de pouvoir être synthétisés à température ambiante soit à partir de suspensions colloïdales d'oxydes ou d'hydroxydes métalliques, soit à partir de polymères inorganiques, comme les alkoxydes M(OR)<sub>n</sub>, qui peuvent être obtenus avec une grande pureté. Il est ainsi possible d'obtenir des gels d'une grande variété d'oxydes métalliques (SiO<sub>2</sub>, TiO<sub>2</sub>, ZrO<sub>2</sub>...).

Les gels ont reçu un grand nombre d'applications dans la réalisation de films minces [53] ; cette technique serait bien adaptée à la protection des fibres, dans la mesure où elle n'exige pas l'emploi de températures élevées.

## 4 - LES PROCÉDÉS D'ELABORATION DES COMPOSITES A MATRICE METALLIQUE

Les procédés d'élaboration des composites à matrice métallique peuvent être classés en deux grandes familles selon que l'on opère en phase solide ou en phase liquide [59]. La mise en oeuvre en phase solide implique généralement, et c'est toujours le cas pour les matrices à bas point de fusion, d'avoir recours à des préimprégnés, matériaux intermédiaires unidirectionnels dans lesquels les fibres sont recouvertes d'une fine couche de métal. Par ailleurs, et cela vaut pour les deux types de mise en oeuvre, il est également possible d'opérer à partir d'empilements de couches de fibres et de feuillards métalliques minces que les procédés conventionnels de la métallurgie - coulée + transformation thermomécanique - ne permettent d'obtenir que pour les nuances d'alliage corroyables. De ce point de vue, les techniques du refroidissement rapide depuis l'état liquide s'avèrent prometteuses [60].

### 4.1 - Les procédés par voie liquide

Les procédés par voie liquide sont utilisés dans le cas des alliages d'aluminium et de magnésium, soit pour réaliser directement des pièces de forme simple, plaques, tubes, raidisseurs, soit - et cela a constitué les premières élaborations de CMM - la fabrication de préimprégnés filamentaires.

#### 4.1.1 - Préimprégnés filamentaires

Ce type de demi-produit présente un intérêt limité dans la mesure où il se présente sous forme d'une baguette rigide qui n'accepte pas de faible rayon de courbure, du fait de sa raideur. Le procédé, généralement adapté pour la réalisation de fils, consiste à faire passer une mèche de fibres de carbone dans un bain d'aluminium liquide. Le mouillage des fibres doit être quasi instantané, ce qui implique un traitement adéquat préalable du toron. De bons résultats ont été obtenus pour les fibres de carbone avec un revêtement de titane et de bore [61].

#### 4.1.2 - Procédés dérivés des techniques de fonderie

Ces procédés apparaissent aujourd'hui comme les plus intéressants du fait de leur capacité à permettre la fabrication de pièces finies à des prix de revient acceptables. Pour ces techniques, de nombreux problèmes ont dû être résolus ; ils concernent :

- les préformes fibreuses,
- les outillages et conditions d'élaboration.

L'intérêt essentiel des préformes fibreuses réside dans la diversité des architectures réalisables, adaptée à chaque pièce ; les fibres qu'il est possible d'employer doivent être de ce fait tissables, ce qui exclut les monofilaments de fort diamètre en bore ou en carbure de silicium, trop rigides, et les fibres d'alumine FP, trop fragiles.

Les technologies de mise en oeuvre doivent à la fois assurer une bonne infiltration de la préforme fibreuse et permettre un contrôle précis des durées de cycles, qui sont déterminantes tant sur le plan de la productivité que sur celui de la qualité du composite obtenu. Des études récentes [62,63] montrent qu'à une vitesse d'infiltration donnée, l'anisotropie de l'architecture fibreuse joue peu mais, en revanche, que sa température et celle du métal liquide ont un rôle prépondérant (fig. 25). Sur le plan de la santé du matériau, les deux paramètres microstructuraux qu'il importe de contrôler sont d'une part l'intégrité des fibres et leur liaison avec la matrice, d'autre part leur séparation, qui toutes trois conditionnent pour une grande part les caractéristiques mécaniques du composite [64].

Les procédés issus de la fonderie et ayant déjà donné lieu à des fabrications industrielles de petites pré-séries de faisabilité et de démonstration, tant aux Etats-Unis qu'au Japon ou en Europe, vont de la coulée par gravité à la coulée sous forte pression. Parmi ces procédés, il convient de mentionner :

- le procédé de coulée sous pression modérée développé par la société Craycir [65], dénommé "Liquid pressure forming", qui permet la réalisation de pièces de forme ;
- le procédé de forgeage liquide, ou coulée sous haute pression, qui met en jeu des pressions plus élevées, de l'ordre de 1000 bar.

Dans le procédé LPF (fig. 24), l'élaboration se fait en quatre étapes successives :

- introduction de la préforme et fermeture du moule,
- mise sous vide du moule,
- coulée du métal liquide dans le moule par mise sous pression du bain,
- solidification du composite et éjection.

Les principaux avantages du procédé, selon Craycir, résultent d'une part de la mise sous vide du moule, qui évite toute présence de porosité, d'autre part du prélèvement de métal liquide au cœur du bain, ce qui évite toute pollution par le film d'oxyde superficiel.

Dans le procédé de forgeage liquide, les très fortes pressions utilisées ( $\approx 1000$  bar) permettent à la fois de s'affranchir des difficultés d'imprégnation liées à la mouillabilité médiocre des fibres de carbone ou de carbure de silicium par l'aluminium (ou le magnésium) liquide, et de réduire la porosité finale du composite. L'inconvénient principal provient de la détérioration possible du renfort lors de l'application de la pression, surtout pour les préformes très rigides.

#### **4.2 - Les procédés par voie solide**

La mise en œuvre des composites à matrice métallique s'effectue :

- soit directement à partir d'empilements alternés de couches d'architecture fibreuse et de feuillards ou de feuilles métalliques ;
- soit à partir de préimprégnés.

##### **4.2.1 - Les techniques de réalisation des préimprégnés drapables**

L'utilisation de préimprégnés en forme de nappes procède d'une part de l'idée générale de transposer aux CMM les techniques de mise en œuvre des composites à matrice organique, et ceci vaut pour les matrices aluminium et magnésium, d'autre part de disposer de produits intermédiaires manipulables.

###### **4.2.1.1 - Les préimprégnés à matrice aluminium ou magnésium**

Deux procédés peuvent être utilisés pour réaliser des préimprégnés en nappes carbone-aluminium ou carbone-magnésium<sup>1</sup>, l'évaporation thermique ou la pulvérisation cathodique. Une caractéristique commune à ces deux techniques est leur forte directivité, qui impose une mise à plat des torons de fibres de manière à les disposer parallèlement dans un même plan, afin d'éviter les effets d'ombrage d'une fibre sur l'autre.

L'évaporation thermique présente l'avantage de vitesses de dépôt plus élevées ; en revanche, elle ne permet ni le dépôt d'alliages - sauf si les tensions de vapeur des métaux à déposer ne sont pas trop différentes - ni le revêtement simultané des deux faces de la nappe. Des nappes sont réalisées sur un plan semi-industriel [66].

La pulvérisation cathodique permet le dépôt d'alliage et le traitement des nappes de fibres en une seule opération, et une excellente adhésion fibre-matrice ; c'est pourquoi, en dépit de vitesses de dépôt plus lentes qu'avec l'évaporation, cette dernière technique est actuellement préférée.

###### **4.2.1.2 - Les préimprégnés à matrice de titane ou de composés de titane**

A l'heure actuelle, les composites ayant une matrice à base de titane sont exclusivement renforcés par des fibres de carbure de silicium. Les feuillards de composites comprennent une couche unidirectionnelle de fibres noyées dans une matrice d'alliage ; ces composites monocouches ont une épaisseur égale au diamètre des fibres,  $140 \mu\text{m}$ . Ils sont réalisés en faisant appel aux propriétés de superplasticité de la matrice.

La réalisation d'un feuillard de composite monocouche comprend les étapes suivantes (fig. 25) :

- 1) Réalisation d'une nappe unidirectionnelle de fibres rendues solidaires par un liant fugace. Cette nappe est généralement obtenue par bobinage sur un cylindre suivi d'imprégnation par le liant fugace ; l'obtention de la nappe plane résulte du découpage des fibres le long d'une génératrice du cylindre
- 2) Empilement de la nappe de fibres entre deux feuillards de  $75 \mu\text{m}$  d'épaisseur
- 3) Pressage sous vide à  $925^\circ\text{C}$  de l'ensemble précédent, en utilisant des feuillards de molybdène revêtus de démolant

Une alternative à cette méthode est d'effectuer directement le dépôt de métal liquide sur le mandrin tournant, après disposition des fibres parallèlement à la génératrice du cylindre<sup>2</sup>. Dans le cas des alliages de titane, ceci impose de travailler sous pression réduite de gaz neutre afin d'éviter toute pollution de l'alliage de titane par les interstitiels azote et oxygène.

###### **4.2.2 - Procédés d'élaboration de feuillards métalliques dérivés des technologies de la solidification rapide**

Les technologies de la solidification rapide permettent d'obtenir sous forme de produits minces - rubans, feuillards - ou divisés - poudres, fibrilles - des alliages que leur composition rend intransformables par les méthodes usuelles de la

<sup>1</sup> Compte tenu des applications visées, aéronautiques et spatiales, ce sont les renforts de carbone qui sont les plus intéressants.

<sup>2</sup> Cette technique a été employée avec succès par la société AVCO pour la réalisation de composites SiC-Al.

métallurgie. Ces nuances d'alliages présentent un grand intérêt en tant que matrices de composites, en raison de leurs caractéristiques - tenue à l'oxydation par exemple - et de la finesse de leur microstructure, qui facilite la mise en oeuvre à l'état solide.

Parmi les techniques d'élaboration des alliages par solidification rapide, les plus pertinentes pour les CMM sont [60] :

- les procédés dérivés de la trempe sur rouleau, comme la coulée pelliculaire<sup>”</sup> qui permet d'obtenir en grande largeur et faible épaisseur - quelques centaines de micromètres - des feuillards d'alliages difficilement laminables comme ceux de magnésium, ou non transformables comme les MCrAlY, où M désigne l'un des éléments Fe, Co ou Ni ;
- les méthodes de pulvérisation, qui conduisent à des poudres fines, de 70 à 150 µm en moyenne pour les alliages de titane, à quelques dizaines de micromètres pour les alliages légers. L'obtention de films métalliques de faible épaisseur facilement manipulables à partir de ces poudres fait appel, comme pour les nappes unidirectionnelles de fibres, à un liant organique fugace ; les produits correspondants sont dénommés chiffons métalliques<sup>”</sup>.

#### 4.3 - Fabrication de composites

Diverses variantes de mise en oeuvre peuvent être utilisées pour la réalisation des composites ; elles relèvent néanmoins toutes du pressage à chaud, technique dans laquelle des empilements de préimprégnés ou de couches alternées de fibres et de feuillards de matrice sont comprimés entre deux plateaux ou dans un moule porté en température. La densification du matériau s'effectue grâce aux mécanismes de diffusion à l'état solide et d'écoulement plastique de la matrice, prépondérant dans le cas de certaines matrices titane en raison de leur comportement superplastique. Par cette méthode, les composites peuvent être directement mis en forme en utilisant des procédés dérivés de ceux utilisés pour les composites à matrice organique.

Un autre procédé de densification, direct, est l'utilisation de la projection de métal fondu à l'aide d'un chalumeau plasma [21]. Par cette technique, on peut facilement réaliser des corps creux résistant à la pression.

### 5 - APPLICATIONS ET POTENTIEL DES COMPOSITES A MATRICE METALLIQUE A FIBRES LONGUES

Les composites à matrice métallique à fibres longues se caractérisent à la fois par des caractéristiques mécaniques et un prix de revient élevés, associés pour la majorité d'entre eux à une densité faible.

De ce fait, ils sont essentiellement destinés à des pièces de structure aéronautiques, spatiales, ou encore de systèmes de propulsion pour lesquels des valeurs élevées des caractéristiques spécifiques sont requises (fig. 26) [67]. A côté de ces applications structurales, les caractéristiques de conductibilité thermique et de stabilité dimensionnelle les rendent attrayants pour l'industrie électronique.

Les composites à matrice métallique à fibres longues peuvent être classés en deux groupes relativement distincts, les composites pour basse température - utilisables jusqu'à 400°C -, dont la matrice est un alliage d'aluminium ou de magnésium (tableau 4a), et les composites moyenne et haute température - utilisables jusqu'à 1100°C - à matrice superalliage (tableau 4b).

#### 5.1 - Composites basse température

##### 5.1.1 - Composites pour applications structurales

Les caractéristiques en traction de quelques composites unidirectionnels sont rassemblées dans le tableau 5. S'il est possible d'atteindre des caractéristiques très élevées dans le sens longitudinal pour les composites à renfort carbone, les caractéristiques travers restent extrêmement faibles, surtout pour des fractions volumiques de fibres aussi élevées que 70 %, qui ne permettent pas d'assurer la santé métallurgique du matériau. De ce point de vue, des résultats récents obtenus en France sur des composites à matrice d'aluminium-10 % de silicium renforcée par des fibres Nicalon, ou de magnésium renforcée par des fibres de carbone M40, élaborés en phase liquide, ont montré que :

- les composites unidirectionnels Al-10Si renforcés par 45 % de fibres présentaient une contrainte à rupture de 450 MPa, de 20 à 350°C [68] ;
- les composites unidirectionnels AZ61 renforcés par 40 % environ de fibres présentaient à 20°C une contrainte à rupture de l'ordre de 1000 MPa [69].

Le niveau et la reproductibilité des caractéristiques sont obtenus par une maîtrise des conditions d'élaboration par infiltration, qui permet de contrôler le temps de contact entre la fibre et le métal liquide, paramètre dont l'importance est unanimement reconnue aujourd'hui [68 à 70] pour tous les CMM. Un autre intérêt des CMM à matrice d'alliage léger est un maintien des caractéristiques à des niveaux de température où la matrice ne présente plus aucune caractéristique (fig. 27). Ainsi un composite unidirectionnel (SiC/6061) conserve-t-il ses caractéristiques dans le sens long jusqu'à plus de 200°C, tandis qu'un quasi-isotope 0/90/90/0 conserve les siennes jusqu'à 400°C.

<sup>”</sup> Les vocables anglais pour ce procédé, plus connus, sont "melt drag" ou "melt overflow".

<sup>””</sup> La dénomination anglo-saxonne est "powder cloth".

Une autre caractéristique importante pour ces matériaux est leur coefficient de dilatation et, partant, leur stabilité dimensionnelle. En appliquant la loi des mélanges, le coefficient de dilatation thermique s'écrit :

$$\alpha_c = \frac{\alpha_f V_f E_f + \alpha_m V_m E_m}{E_f V_f + E_m V_m} \quad (5.1)$$

Pour que  $\alpha_c$  soit le plus faible possible, il est nécessaire que le dénominateur soit le plus élevé possible, et donc de réaliser les composites avec des fibres à haut module. La figure 28 donne les variations des coefficients de dilatation avec la température pour quelques composites à matrice métallique comparés avec le composite organique C-GY70/matrice époxyde. C'est le composite C-P100/Mg qui présente le coefficient de dilatation le plus faible dans la plage 0-70°C, avec une valeur de moins de 10<sup>-6</sup>C. C'est la raison qui rend ce matériau attrayant pour la réalisation de structures spatiales, du fait de son excellente stabilité dimensionnelle.

La stabilité dimensionnelle se caractérise par le coefficient  $k_t/\alpha_t$ , quotient de la conductibilité thermique dans le sens travers par le coefficient de dilatation dans le sens long ; elle représente la capacité d'un matériau à rester indéformable en présence d'une irradiation thermique asymétrique, comme l'éclairement par le soleil d'une tour d'antenne de satellite ; plus ce coefficient est élevé, meilleure est la stabilité dimensionnelle. Le composite C-P100/Mg est de de point très supérieur à tous les autres composites (fig. 29).

### 5.1.2 - Composites pour l'industrie électronique

Les matériaux support de circuit doivent posséder à la fois une bonne conductibilité thermique, un faible coefficient de dilatation thermique et, pour les applications embarquées, une faible densité.

Les composites aluminium-fibres de carbone haut module réalisés en utilisant un empilement quasi-isotrope (fig. 30) répondent au cahier des charges, avec une conductibilité proche de celle de l'aluminium et un coefficient de dilatation thermique proche de celui de l'alumine [72]. Ces produits proposés par la société DWA sont en concurrence avec les composites STALAB de Péchiney à matrice d'aluminium renforcée par des fibres SiC Nicalon [73]. Les caractéristiques de ces deux composites sont comparées dans un diagramme conductibilité thermique-coefficient de dilatation thermique (fig. 30) avec d'autres matériaux utilisables pour cette application.

### 5.2 - Les composites à moyenne et haute température

Deux types de composites appartiennent à cette classe de matériaux : ceux à matrice titane, et ceux à matrice superalliage.

#### 5.2.1 - Les composites à matrice titane

Actuellement, seuls les composites à matrice d'alliage de titane Ti-6-4 (TA6V) ou Ti-15-3 ont fait l'objet de travaux poussés jusqu'à une pré-série industrielle. Les caractéristiques du composite SiC-SCS6/TA6V sont très élevées (tableau 5). Malheureusement, la température d'emploi de ce matériau restera limitée par la tenue à l'oxydation de la matrice à 500, voire 550°C.

Les composites à matrice TiAl pourront atteindre des températures de 650°C, et ceux à base de TiAl 950°C. Les données concernant ces matériaux à matrice intermétallique restent très limitées, mais leurs caractéristiques de traction se situent vers 1500 MPa à température ambiante, et décroissent lentement jusqu'à 650°C (fig. 31) [74]. Pour ces composites, la forte zone de réaction fibre-matrice peut expliquer l'écart à la loi des mélanges, notamment à haute température. De plus, leurs caractéristiques en sens travers restent très faibles.

#### 5.2.2 - Les composites à matrice superalliage

Les composites à matrice superalliage à base de nickel doivent permettre, grâce au renforcement fibreux, d'augmenter la température de fonctionnement du métal des aubes de turbine. Ils peuvent être renforcés soit par des fibres de tungstène, s'il s'agit de composites de synthèse élaborés par pressage en phase solide à chaud [75], soit par des trichites de carbure de métaux de transition, niobium et tantale essentiellement, qui sont obtenus comme les superalliages à grains colonnaires par solidification dirigée [76]. La caractéristique dimensionnante des aubes de turbine étant la tenue en fluage, les températures potentielles d'emploi pour une durée de vie en fluage de 1000 heures sous une contrainte de 150 MPa de divers alliages sont comparées (fig. 32) avec l'un des composites de solidification les plus performants.

Toutefois, les composites de synthèse, comme les composites de solidification, souffriront d'un handicap de coût par rapport aux alliages monocristallins, lié à la mise en oeuvre pour les composites de synthèse, à la faiblesse de la vitesse de solidification (2 cm/h au lieu de 30 à 40 cm pour les aubes monocristallines) pour les composites de solidification.

Les composites de synthèse, qui peuvent être associés à de nombreuses matrices, pourront toutefois présenter un avantage pour la propulsion à l'hydrogène, dans la mesure où ils pourront renforcer des matrices insensibles à la fragilisation par l'hydrogène et donner naissance à des matériaux sans concurrence.

<sup>1</sup> En fait, Levin [71] a montré que le coefficient de dilatation dans le sens long d'un composite unidirectionnel  $\alpha$  était encadré par deux valeurs  $\alpha^{\min}$  et  $\alpha^{\max}$  telles que :

$$\alpha^{\min} = E\alpha/E < \alpha < K\alpha/K < \alpha^{\max} \quad (5.2)$$

où  $E\alpha$  et  $E$  sont données dans (5.1),  $K\alpha$  et  $K$  étant des expressions similaires avec le module de compressibilité, relié à  $E$  par  $K = E/3(1-2\nu)$  où  $\nu$  désigne le coefficient de Poisson.

### 5.3 - Quelques problèmes spécifiques des CMM

Deux caractéristiques mécaniques sont à considérer avec une attention particulière dans les CMM, la tenue en cyclage thermique et la tenue en fatigue.

#### 5.3.1 - Tenue en cyclage thermique

Le cyclage thermique est pour les CMM la sollicitation thermique la plus sévère. L'endommagement du composite en cyclage thermique résulte de la forte différence des coefficients de dilatation des deux constituants, qui peut atteindre  $24,7 \cdot 10^{-6}/^{\circ}\text{C}$  dans le cas du composite fibres de carbone haut module-matrice d'aluminium. Pour une amplitude de variation en température de  $200^{\circ}\text{C}$ , la déformation d'origine thermique dans la matrice sera de  $5 \cdot 10^{-3}$ , c'est-à-dire bien supérieure à la déformation à la limite élastique de la matrice.

La plasticité induite dans la matrice conduira à un endommagement de même nature que celui observé en fatigue oligocyclique. Dans les composites à fibres longues de toute nature [77], l'endommagement est souvent localisé à l'interface fibre-matrice, où il se manifeste sous forme de décohésion résultant de la coalescence de pores ou de la propagation de fissures. Cet endommagement est décelable par les variations dimensionnelles auxquelles il conduit, aussi bien en sens long qu'en sens travers. L'endommagement en cyclage thermique conduit à une baisse des caractéristiques mécaniques ; ainsi, dans le composite B-Al (6061), un cyclage thermique avec une amplitude de  $320^{\circ}\text{C}$  ne conduit à aucune baisse de caractéristiques en 2000 cycles, tandis qu'une amplitude de  $420^{\circ}\text{C}$  conduit à une baisse de 40 % de la contrainte à rupture [78].

C'est là l'un des principaux handicaps des CMM pour des applications imposant de fortes variations thermiques. Sur le plan de la stabilité dimensionnelle, un moyen de pallier les variations dimensionnelles du matériau est de jouer sur les séquences d'empilement des plis [79].

Enfin, un important travail de base reste à faire pour comprendre et modéliser l'endommagement, notamment dans les composites à forte fraction volumique de fibres, dans lesquels le comportement de la matrice dans le composite diffère certainement notablement de celui de la matrice prise isolément [80].

#### 5.3.1 - Comportement en fatigue

La tenue en fatigue des composites, et surtout des unidirectionnels, est bien plus élevée que celle de la matrice seule. Toutefois, les composites s'endommagent en fatigue par fissuration de la matrice et décohésion fibre-matrice [77]. Dans les composites B-Al, cet endommagement conduit à une forte réduction du module du composite, comme l'ont montré Dvorak et Johnson [81] dans le cas d'un composite à empilement symétrique  $[0, (\pm 45), 90, 0, (\pm 45), 90]$ , où un essai effectué avec une contrainte maximum de 350 MPa conduit à une baisse du module de 40 % après  $2,5 \cdot 10^3$  cycles, et de près de 50 % après  $10^6$  cycles. Cette forte influence de la contrainte maximale sur la limite d'endurance a donné lieu au développement d'un modèle simple par Gouda et ses collaborateurs [82]. Dans leur modèle, ils séparent les deux types de défauts, la propagation de fissure conduisant à une courbe d'endurance en forme de sigmoïde, semblable à celle résultant de la propagation des fissures dans une matrice monolithique. En revanche, et dans le cas de fibres parfaites ne présentant pas de maillons faibles, la décohésion fibre-matrice conduit à une courbe d'endurance plate, la limite d'endurance étant alors égale à la contrainte à rupture en traction monotone. Les fibres n'étant pas parfaites, la courbe réelle se situe généralement entre les deux formes ci-dessus (fig. 33). Ces formes de courbes ont été observées dans le cas de composites Al<sub>2</sub>O<sub>3</sub>, FP/AZ41 [83], une liaison fibre-matrice forte conduisant à une forme sigmoïdale de la courbe d'endurance et une liaison fibre-matrice faible à une courbe contrainte-nombre de cycles à rupture très plate.

Au-delà de ces études macroscopiques, des travaux visant à comprendre la phase d'amorçage et portant sur le mécanisme du transfert de charge fibre-matrice [84] et sur le comportement plastique de la matrice dans le composite sont indispensables au développement de ces matériaux.

### 5.4 - Tenue à la corrosion des composites à matrice d'alliage léger [85]

L'essentiel des travaux publiés concernent les composites à matrice d'aluminium [86,87], probablement en raison du développement plus récent de ces matériaux et de leur domaine d'application potentiel spatial. Toutefois, pour les composites à matrice de magnésium, la corrosion peut se produire lors des périodes de stockage au sol.

La corrosion des composites à matrice métallique peut avoir plusieurs origines [87] :

- la corrosion galvanique entre fibre et matrice ;
- la corrosion galvanique entre des phases intermétalliques et la matrice ;
- l'attaque préférentielle sur le carbone ayant diffusé des fibres vers la matrice ;
- l'accroissement du nombre de sites anodiques du fait de la présence des interfaces.

#### 5.4.1 - Les composites à matrice d'aluminium

Dans le cas des composites bore-aluminium, Pohlman [87] a montré que la corrosion galvanique provient non pas du couple bore-aluminium, mais du couple aluminium-borure d'aluminium formé lors de l'élaboration par pressage à chaud du matériau ou de traitements thermiques.

Dans des composites à matrice d'aluminium commerciaux, ou l'alliage Al-Si-Mg 357, renforcés par des whiskers d'alumine SAFFIL ou des fibres Nicalon, Otani et al. [88] concluent que la corrosion n'est pas directement liée au renfort mais aux modifications microstructurales de la matrice liées au procédé d'élaboration du composite par coulée. Par exemple, la présence de seconde phase comme Al<sub>2</sub>Fe, dont le potentiel de corrosion est plus élevé que celui de l'aluminium, risque

d'avoir un effet de pile. Il faut alors modifier la composition de l'alliage en améliorant sa pureté et/ou, lorsque cela est possible, homogénéiser le matériau par un traitement thermique. Cette influence des phases intermétalliques a été confirmée par McIntyre et al. [89] dans des composites SiC/2124.

Pour les composites carbone-aluminium, le mécanisme avancé pour leur corrosion en brouillard salin comprend les étapes suivantes [90] :

- pénétration de l'agent corrodant dans le matériau par piqûration, au droit d'un défaut, par capillarité le long des fibres ;
- corrosion galvanique de l'aluminium à l'interface C/Al, régie par réduction de l'oxygène sur les fibres de carbone ;
- dégradation mécanique par un effet de coin des produits de réaction formés au cours de la deuxième étape.

La réduction de l'oxygène à la surface des fibres de carbone a été particulièrement étudiée par Jagannathan [91], qui a montré que la cinétique de cette réaction est plus rapide sur les fibres de bas module.

Il est important de mentionner que si un revêtement de silice ou la présence de couches enrichies en silicium diminuent la cinétique de réduction de l'oxygène à la surface des fibres et, partant, la corrosion galvanique [90], la présence de cuivre ou de nickel a un effet opposé.

Enfin, il convient de mentionner le rôle néfaste que peut jouer la présence dans le composite de traces de produits issus du traitement de mouillage des fibres. Hihara et al ont ainsi mis en évidence dans un composite P100/6061 une corrosion accélérée dans les régions du composite qui contenaient du chlore ; ce dernier provenait du revêtement à base de Ti-B réalisé en atmosphère gazeuse de  $TiCl_4$ ,  $BCl_3$  et Zn.

#### 5.4.2 - Composites carbone-magnésium

Quelques observations ont été rapportées par Hall [90] sur un composite T300/Mg-1%Al élaboré par coulée sous pression par Honda au Japon, à l'état brut de fabrication et après un maintien de 72 h à 500°C destiné à favoriser la formation du carbure  $Al_xC$ , à l'interface fibre-matrice. L'exposition à l'air ambiant conduit à l'hydrolyse des carbures, avec formation d'acétylène, et à une corrosion galvanique entre fibre et matrice avec une vitesse de pénétration voisine de 100  $\mu\text{m/an}$ . Suivant Hall, les carbures n'affectent pas de façon significative le comportement en corrosion des composites C-Mg.

En conclusion sur la corrosion des composites à matrice d'alliage léger, il faut surtout retenir :

- l'importance possible de l'effet de pile entre les phases intermétalliques et la matrice environnante ;
- l'effet bénéfique sur la corrosion galvanique du couple C/Al de revêtements contenant du silicium.

### CONCLUSION

Les composites à matrice métallique renforcée par des fibres longues possèdent aujourd'hui un ensemble de caractéristiques qui doit leur permettre à terme de répondre aux besoins des industries aérospatiales. Quelques problèmes sont encore non résolus et des travaux complémentaires restent à accomplir avant que leur introduction au niveau des structures froides ou chaudes ne devienne une réalité.

#### 1. En ce qui concerne l'élaboration des composites, les avancées concernent :

- les traitements de surface des fibres réalisés essentiellement par dépôt chimique en phase vapeur, maîtrisés et contrôlés pour les fibres de gros diamètre et en cours d'évaluation pour les fibres de carbone ;
- l'élaboration des composites à matrice d'alliage léger aluminium ou magnésium, pour lesquels la maîtrise du procédé permet d'obtenir des produits sains à petite échelle en milieu industriel. Si les matériaux apparaissent en catalogue, pour l'industrie électronique notamment, les prix de revient restent élevés, faute d'un volume de production suffisant ;
- l'élaboration en phase solide, qui restera vraisemblablement encore longtemps la seule méthode pour les composites à matrice d'alliage ou de composé intermétallique de titane, devrait bénéficier des acquis des technologies du refroidissement rapide, grâce à la métallurgie des poudres et aux techniques de projection.

#### 2. Les caractéristiques mécaniques des composites à matrice d'aluminium ou de magnésium approchent maintenant celles correspondant à l'application de la loi des mélanges grâce à un strict contrôle des réactions interfaciales, et donc de l'adhésion fibre-matrice.

Des travaux sont encore nécessaires afin de répondre aux questions suivantes :

- la liaison fibre-matrice doit-elle être forte ou faible ; comment l'ajuster au bon niveau dans chaque système ;
- l'endommagement en cyclage thermique inhérent à certains matériaux les condamne-t-il à une plage réduite d'utilisation en température ? Convient-il de développer des fibres stables thermodynamiquement et mécaniquement ;
- 3. la modélisation du comportement des CMM doit être développée, afin d'affiner les modèles de prévision de la rupture :
  - modélisation réaliste du transfert de charge et prévision des contraintes à rupture ;
  - comportement plastique de la matrice dans le composite, en second lieu l'établissement de lois de comportement permettant un dimensionnement des pièces.

La réponse aux questions qui se posent encore, la poursuite de l'étude du comportement mécanique et le développement de l'industrialisation des composites permettant d'abaisser leur coût de manière à en augmenter la diffusion font qu'aujourd'hui encore le succès de ces matériaux appartient toujours un peu au futur.

### REMERCIEMENTS

- Ce texte a été écrit en faisant largement appel :
- . pour la partie concernant la mécanique des composites unidirectionnels :
    - à des ouvrages spécialisés dont les principaux sont :
      - Strong Solids (réf. [2])
      - Metal Matrix Composites Thermomechanical Behaviour (réf. [20])
      - Handbook of Composites (réf. [74])
    - à des articles généraux ou faisant autorité, tels que ceux de Aveston Cooper et Kelly (réf. [5]), Rosen (réf. [12,13]), Zweben (réf. [14]), Ochiai et al. (réf. [7]), Islam et Wallace (réf. [20,36]), Quenisset (réf. [59]) ;
    - enfin, à des résultats récents obtenus à l'ONERA sur la micromécanique des composites organiques (Jacques, réf. [7]) ou métalliques (Molliex, réf. [9]) ;
  - . pour les autres parties, à la compilation de la documentation.

Enfin, l'auteur tient à remercier tout particulièrement M. Molliex pour de fructueuses discussions sur la modélisation de la rupture des composites unidirectionnels, et M. Mévrel pour la partie concernant la corrosion, qui est totalement empruntée à une synthèse bibliographique en cours d'achèvement : "La corrosion des composites à matrice métallique".

### REFERENCES BIBLIOGRAPHIQUES

- [1] K. SCHULTE, W. BUNK, Metal matrix composites: A promising alternative to conventional alloys?, AGARD Conf. Proc. 444, New Light Alloys, Mierlo (Pays Bas), 3-5 octobre 1988
- [2] Z. HASHIN, J. Mech. Phys. Solids 13, 119 (1965)
- [3] A. KELLY, Strong Solids, Clarendon Press, Oxford (1973) p. 166
- [4] S.T. MILEIKO, J. Mat. Sci. 4, 974 (1969)
- [5] J. AVESTON, G.A. COOPER and A. KELLY, Single and multiple fracture. Properties of fibre composites, Conf. Proc. NPL, IPC Sci. & Techniques, Guilford (1971)
- [6] H.L. COX, Br. J. Appl. Phys. 3, 72 (1952)
- [7] S. OCHIAI and K. OSAMURA, Zeitung für Metallkunde 76, 7 (1985) p. 485-491
- [8] D. JACQUES, Thèse de Doctorat "Transfert de charge entre fibre et matrice dans les composites résines : comportement en traction d'un modèle monofilamentaire", INPL, Nancy, mai 1989
- [9] Documentation AVCO - Fibres et Composites -, Specialty materials Division, 2 Industrial Av., Lowell, Mass. 01851, USA
- [10] L. MOLLIEX, Thèse de Doctorat, Université d'Orsay, à paraître
- [11] B.D. COLEMAN, J. Mech. Phys. Solids 7, 60 (1958)
- [12] B.W. ROSEN, Fibre Composite Materials, Am. Soc. Metals (1965) p. 37
- [13] B.W. ROSEN, Proc. Roy. Soc. A319, 69 (1970)
- [14] H.E. DANIELS, Proc. Roy. Soc. A183, 405 (1945)
- [15] C. ZWEBEN and B. ROSEN, J. Mech. Phys. Solids 18, 189 (1970)
- [16] H. FUKUDA, Recent advances in composites in the United States and in Japan, K. Kawata ed., ASTM, Philadelphia (1985) p. 5-15
- [17] I. KIMPARA and T. OZAKI, Composites 86: Recent advances in Japan and the United States, K. Kawata ed., Jap. Soc. Comp. Mat. (1986) p. 93-100
- [18] S. OCHIAI and K. OSAMURA, ibid, p. 751-759

- [19] K.M. PREWO and K.G. KREIDER, Met. Trans. 3 (1972) p. 2201, 2211
- [20] M.U. ISLAM and W. WALLACE, Carbon fibre reinforced aluminium matrix composites: a critical review, Rapport de la Division du Génie Mécanique, Conseil National de Recherches du Canada (1984)
- [21] M. TAYA and R.J. ARSENAULT, Metal matrix composites thermomechanical behaviour, Pergamon Press (1989)
- [22] H. ISHIKAWA and M. TAYA, Progress in science and engineering of composites, T. Hayashi et al eds., Jap. Soc. Comp. Mat. (1982) p. 676-680
- [23] G.A. COOPER, J. Mat. Sci. 5 (1970) p. 645-654
- [24] M.R. PIGOTT, J. Mat. Sci. 5 (1970) p. 669-675
- [25] M. TAYA and A.J. DAIMARU, J. Mat. Sci. 18 (1983) p. 3105-3116
- [26] A. DAIMARU, T. HATA and M. TAYA, Recent advances in composites in the United States and Japan, ASTM STP 864, J.R. Vinson and M. Taya eds., Philadelphia (1985) p. 505, 521
- [27] T. KYONO, I.W. HALL and M. TAYA, J. Mat. Sci. 21 (1986) p. 1879-1888
- [28] M.H. STACEY, Mat. Sci. Tech. 4 (1988) p. 227-230
- [29] US patent nr 4,292,077, 29 septembre 1981
- [30] US patent nr 4,716,020, 29 décembre 1987
- [31] A. BASSI, J.A. PETERS, J. WITTENAUER, J. of Metals (septembre 1989) p. 18-20
- [32] D.R. TENNEY, W.B. LISAGOR, S.C. DIXON, J. Aircraft 26, 11 (1989)
- [33] M.A. HICKS, New metallic materials for gas turbines, AGARD/NATO Conf. Propulsion Energetic Panel, Bath (UK), October 3-5, 1988
- [34] D.W. PETRASEK, J.R. STEPHENS, NASA Tech. Mem. 100880, AGARD/NATO Conf. Propulsion Energetic Panel, Bath (UK), October 3-5, 1988
- [35] H.L. MARCUS, Interface character of an aluminium-graphite MMC, University of Texas, Office of Naval Research Contract N 00014-78-C-0094 (1982)
- [36] ISLAM, WALLACE, Adv. Mat. and Manufact. Processes 3 (1) (1988) p. 1-35
- [37] P. FORTIER, Interaction chimique dans les composites à matrice métallique : systèmes Mg-C ; Al-C-Si ; Al-C-O-Si, Thèse de doctorat, Université Lyon I (UCB), 20 mai 1988
- [38] V. LAURANT, D. CHATAIN, X. DUMANT, N. EUSTATHOPOULOS, The wetting kinetics of aluminium and its alloys in single crystal SiC, World Materials Congress, Symposium on Advances in Cast-reinforced Metal Composites, Chicago (USA), septembre 1988
- [39] R. PAILLER, P. MARTINEAU, M. LAHAYE, R. NASLAIN, Rev. Chim. Min. 18 (1981) p. 520-543
- [40] Y. LEPEITTCORPS, Caractérisation physico-chimique et mécanique de filaments CVD de carbure de silicium ou de bore - Application aux matériaux composites 1D SiC-TA6V, Thèse de doctorat, Université de Bordeaux, 18 décembre 1985
- [41] R.T. PEPPER et al., US patent nr 3,770,488, 6 novembre 1973
- [42] R. LIGNON, Brevet français n° 2.081.237, mars 1970
- [43] D.R. BISWAS, J. Mat. Sci. 21 (1986) p. 2217-2223
- [44] P. FAUCHAIS, J. DEMAISON, J. MACHET, L'industrie Céramique (1987) p. 812
- [45] D.S. RICKERY, Br. Ceram. Trans. J. 87 (1988) p. 176-180
- [46] L. COUDURIER, J. ADRIAN, D. PIQUE, N. EUSTATHOPOULOS, Rev. Int. des Hautes Températures et Réfractaires, 21 (1984) p. 81-93
- [47] J. BOUIX, J. DAZORD, J.L. PONTHENIER, J.C. VIALE, C. VINCENT, H. VINCENT, Brevet français n° 8.617.157, 4 décembre 1986
- [48] J. BOUIX et al, J. Physique, Colloque C5, supplément au n° 5

- [49] M. LANCIN, J. THIBAUT-DESSAUX, J.S. BOUR, J. Micr. Spectr. El. 13 (1988) p. 503-517
- [50] J.S. BOUR, Caractérisation microstructurale et chimique d'interfaces dans des composites à fibres longues, Thèse de doctorat, Université Paris XI, 22 décembre 1988
- [51] T. RONALD, Materials challenge for NASP, AIAA 1<sup>er</sup> Aero-Space Plane Conf., 20-21 July 1989, Dayton, OH (USA)
- [52] W.D. BREWER, J. UNNAM, NASA Tech. Paper 2066, août 1982
- [53] J. PHALIPPOU, L'industrie Céramique 813 (1987) p. 131
- [54] C. GUIZARD, A. LARBOT, L. COT, Le Vide, Les Couches Minces 40, 227 (1985) p. 277
- [55] Ph. COLOMBAN, ibid., p. 269
- [56] R. MORINEAU, ibid., p. 281
- [57] H. DISLICH, ibid., p. 261
- [58] N. TOHGE, A. MATSUDA, T. MINAMI, J. Am. Ceram. Soc., 70, 1 (1987)
- [59] J.P. ROCHER, F. GIROT, J.M. QUENISSET, R. PAILLER, R. NASLAIN, Mem. Sci. Rev. Met., p. 69-85 (1986)
- [60] I.E. LOCCI, R.D. NOEBE, The role of rapid solidification processing in the fabrication of fibre-reinforced metal matrix composites, NASA Tech. Mem. 101450 (janvier 1989)
- [61] E.G. KENDALL, R.T. PEPPER, Brevet américain 4,082,864 (4 avril 1978)
- [62] J.A. CORNIE, Y.M. CHIANG, D.R. UHLMANN, A. MORTENSEN, J.M. COLLINS, Ceramic Bulletin, 65, 2 (1986)
- [63] J.M. QUENISSET, Effect of the squeeze casting conditions on the infiltration of ceramic preforms, World Materials Congress: Symposium on Advances in Cast-reinforced Metal Composites, 25-30 septembre 1988
- [64] A. MORTENSEN, J.A. CORNIE, M.C. FLEMINGS, J. of Metals, 2 (1988) p. 12-19
- [65] Documentation CRAYCIR Advanced Technology SA, rue Jambe du Commun, CH-24000 Le Locle
- [66] TOHO BELSON Co. Ltd., Japan Kokkai Tokkyo Koho, JP 58, 120, 876, July 18 (1983)
- [67] Y. BARBAUX, J.P. HEBERT, H. ABIVEN, Mem. Et. Sci. Rev. Met., 4 (1989)
- [68] S. DERMARDJIAN, Entretiens technico-économiques, Paris La Défense, 19 octobre 1989
- [69] M. RABINOVITCH, M.H. VIDAL-SETIF, R. MEVREL, Travaux non publiés
- [70] J.R. STEPHENS, High temperature metal matrix composites for future aerospace systems, AIAA 24<sup>th</sup> Joint Propulsion Conference, Boston (Mass.) USA, July 11-13, 1988
- [71] V.M. LEVIN, Meckanika Tverdogo Tela 2 (1967) p. 88-94
- [72] Documentation commerciale DWA, DWA Composites Specialties, Inc., 21119 Superior Street, Chatsworth (CA) USA
- [73] Documentation commerciale Péchiney
- [74] P.K. BRINDLEY, P.A. BARTOLETTA, Investigation of a SiC/Ti-24Al-11Nb composite, NASA Tech. Mem. 100956, NASA Lewis Research Center, Cleveland (OH) USA
- [75] D.W. PETRASEK, J.R. STEPHENS, NASA Tech. Mem. 100880, AGARD/NATO Conf. Propulsion Energetic Panel, Bath (UK), October 3-5, 1988
- [76] M. RABINOVITCH, J.F. STOHR, T. KHAN, H. BIBRING, Directionally solidified composites for application at high temperature, Handbook of Composites, A. Kelly and Yu.N. Rabotnov eds., vol. 4, p. 295-372, Elsevier Science Publishers, P.O. Box 1991, 1000 BZ Amsterdam (Holland)
- [77] Ibid [20] p. 135-149
- [78] H.H. GRIMES, R.A. LAD, J.E. MAISEL, Met. Trans. 8A (1977) p. 1999-2005
- [79] B.K. MIN, Advances in composite materials and structures, ASME Bound Volume, edited by S.S. Wang and Y. Rajapakse, en impression
- [80] H. LILJOLM, The strength of MMC under mechanical and thermal loading, Actes du Colloque ICSMA8, Tampere (Finlande), août 1988, p. 61-79
- [81] G.J. DVORAK, W.S. JOHNSON, Int. J. Fract. 16 (1980) p. 582-602

- [82] M. GOUDA, K.M. PREWO, A.J. McEVILY, Fatigue of fibrous composite materials, ASTM STP 723 (1981) p. 101-115
- [83] J. NUNES, E.S.C. CHIN, J.M. SLEPETZ, N. TSANGARAKIS, Proc. ICCM5, W.C. Harrigan Jr et al. eds, TMS of AIME (1985) p. 723-745
- [84] P. BONIFACE, P. FLEISHMAN, R. FOUGERES, P.F. GOBIN, D. ROUBY, F. LONCA-HUGNOT, M. BOIVIN, Modélisation statistique du processus de fragmentation dans les composites modèles à monofilaments, JNC6, Paris, J.P. Favre ed. (1988)
- [85] R. MEVREL, La corrosion des composites à matrice métallique, Rapport Technique ONERA, à paraître
- [86] S.L. POHLMAN, Corrosion and electrochemical behaviour of boron-aluminium composites, Corrosion-NACE 34 (5) (1978) p. 157-159
- [87] R.C. PACIEJ, V.S. AGARWALA, Corrosion 44 (1) (1988) p. 680-684
- [88] T. OTANI, B. McENAMEY, D.V. SCOTT, Corrosion of metal matrix composites, in Cast Reinforced Metal Composites, S.G. Fishman, A.G. Dhingra eds., ASM (1988) p. 383-389
- [89] J.F. McINTYRE, H. LEA, S. GOLLEDGE, R. CONRAD, Corrosion behaviour of SiC reinforced aluminium alloys, NSWC-TR-87 (1987) p. 326
- [90] L.C. DASH, The mechanism of corrosion and corrosion control of aluminium/graphite MMC, The Ohio State University (1988), Résumé dans Dissert. Abstract Int. 49 (8) (février 1989) p. 229
- [91] V. JAGANNATHAN, The influence of interphase structure on the kinetics of oxygen reduction on graphite used in aluminium-graphite MMC - Dissertation, The Ohio State University (1988), Résumé dans Dissert. Abstract Int. 49 (8) (février 1989) p. 174
- [92] I.H. IHARA, R.M. LATANISION, Localized corrosion of graphite fiber/6061-T6 aluminium alloy MMC in aerated and deaerated sodium sulphate solutions, Second Int. SAMPE Metals Conf., Dayton (USA), 2-4 août 1988
- [93] I.W. HALL, Corrosion of C-Al MMC, Scripta Met. 21 (1987) p. 1717-1721

Tableau 1

Fibres utilisables pour les composites à matrice métallique  
pour emploi à température basse ou moyenne

Fibre	Fabricant	Diamètre ( $\mu\text{m}$ )	Masse volumique ( $\text{Mg/m}^3$ )	Module (GPa)	Résistance (MPa)	Allongement (%)
B (C)	AVCO	100	2,2	365	3 280	-
B/B <sub>4</sub> C (W)	AVCO/SNPE	140	2,5	405	4 075	-
SiC (C) (SCS6)	AVCO	140	3,05	420	4 000	0,8
SiC	Nicalon	10-15	2,6	220	2 700	1,5
SiC	Tyranno	10-13	2,4	220	> 2 500	-
SiC	Rhône P.					
Al <sub>2</sub> O <sub>3</sub> Saffil RF	ICI	1-5	3,3	300	2 000	0,67
Al <sub>2</sub> O <sub>3</sub> FP	du Pont	20	3,9	380	> 1 400	0,36
Carbone	T300	Toray	7	1,75	230	3 500
	T800	Toray	5,5	1,80	294	5 590
	GY70	Celion	8,4	1,96	690	1 860
	P55	UC	10	2,25	517	2 070
	P100	UC	10	2,25	690	2 240

Fibre	Fabricant	Diamètre ( $\mu\text{m}$ )	Masse volumique ( $\text{Mg/m}^3$ )	Module (GPa)	Résistance (MPa)	Allongement (%)
SiC	AVCO	140	-	-	-	-
W	-	25-150	19,3	340 410	2 900 3 700	$\approx 1$
Trichites (TaC)	-	0,5-1	40	500	25 000	-
B <sub>4</sub> C (W)	-	-	2,36	483	2 280	-
TiB <sub>2</sub> (W)	-	-	4,48	510	100	-

Tableau 2 - Fibres utilisables pour les composites à matrice métallique pour emploi à haute température.

Composé déposé	Précureur	Température (°C)	Processus réactionnel
SiC	CH <sub>3</sub> SiCl <sub>3</sub>	1400	Réduction par H <sub>2</sub>
TiC	SiCl <sub>4</sub> , CH <sub>4</sub>	1000	
SiO <sub>2</sub>	SiCl <sub>4</sub> , CO <sub>2</sub>	800	
B <sub>4</sub> C	BCl <sub>3</sub> , CH <sub>4</sub>	1300	
Si	SiH <sub>2</sub> Cl <sub>2</sub>	1050-1150	
C	CH <sub>4</sub>	> 1000	Pyrolyse
TiB	TiCl <sub>4</sub> , BC <sub>1</sub> <sub>3</sub>	> 800	Réduction par H <sub>2</sub> ou Zn
SiC*	SiCl <sub>4</sub>	$\approx 1100$	Réduction par H <sub>2</sub>

Tableau 3 - Revêtements obtenus par dépôt chimique en phase vapeur.

\* Dépôt chimique en phase vapeur réactif

Fibre	Matrice	Procédé de fabrication	Domaine d'application
B revêtu SiC	Al	Métallurgie des poudres	Aérospatial
C revêtu (Ti, B), SiC	Al	Type fonderie	Aéronautique
C	Mg et ses alliages	Type fonderie	Spatial
C	Mg et ses alliages	Consolidation par pressage en phase solide à chaud	Spatial
SiC toron	Al et ses alliages	Type fonderie	Aéronautique Electronique
SiC monofilament	Al et ses alliages	Projection plasma + consolidation en phase solide à chaud	Aéronautique Corps pressurisés
SiC monofilament	Alliages de Ti	Consolidation à chaud en phase solide	Applications multiples
Al <sub>2</sub> O <sub>3</sub>	Al-Li	Type fonderie	Aéronautique Propulsion

Tableau 4a - Composites à matrice d'alliage léger.

Tableau 5

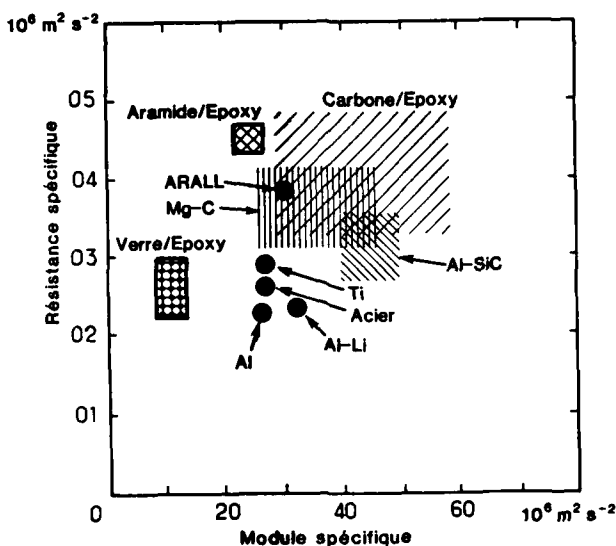
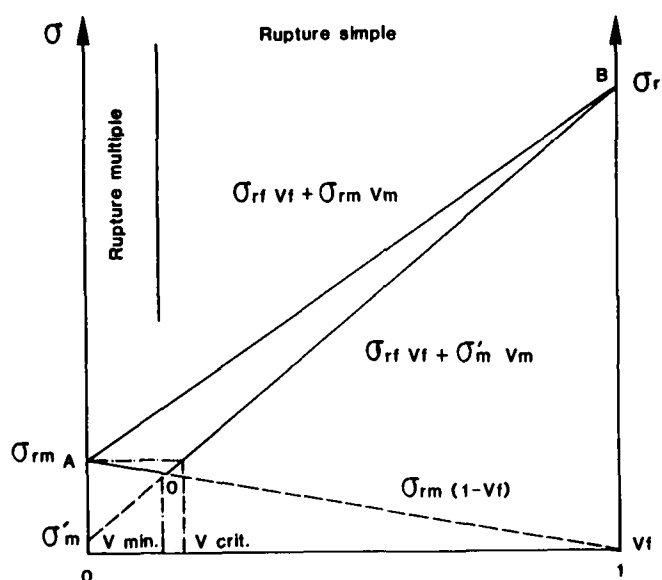
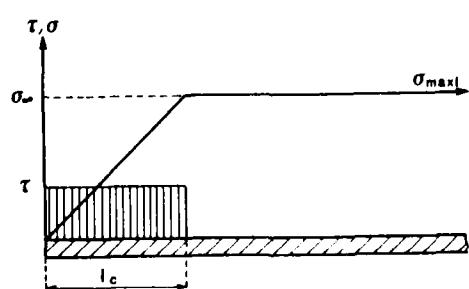
Caractéristiques de traction à température ambiante  
de quelques composites unidirectionnels

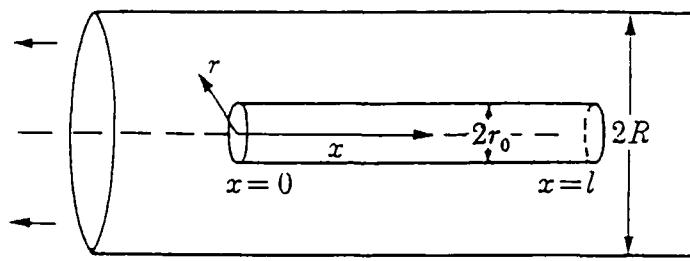
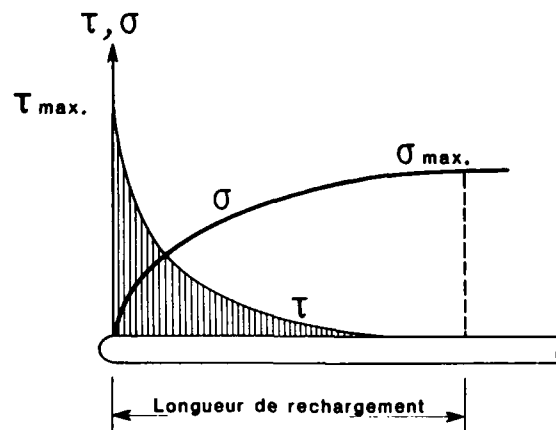
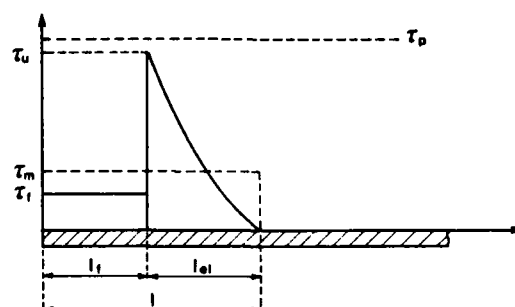
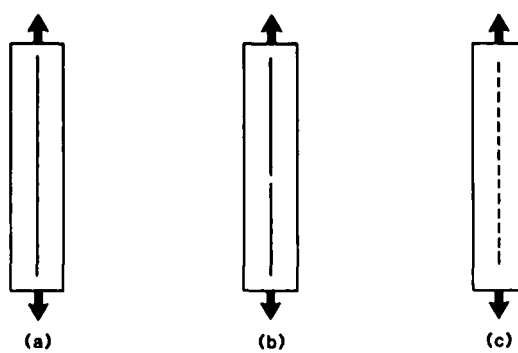
CMM	Densité (g/cm <sup>3</sup> )	Fraction vol. de fibres (%)	Contrainte à rupture (MPa)	Module élastique (GPa)	Allongement à rupture (%)
<b>a) Sens long</b>					
B/A1	2,5	48	1220	247	0,5
C/A1	2,1	70	1250	250	0,5
C/Mg	1,7	70	1350	150	0,9
FP/A1	3,2	50	570	200	-
FP/Mg	2,8	50	520	200	0,3
B/Ti	3,5	50	962	210	-
SiC/Ti	4,05	35	1470	240	-
<b>b) Sens travers</b>					
B/A1	2,5	48	150	-	-
FP/A1	3,2	50	140	150	-
FP/Mg	2,8	50	70	100	0,24
B/Ti	3,5	50	408	195	-

Tableau 4b

Composites pour application haute température

Fibre	Matrice	Procédé de fabrication	Domaine d'application
SiC	Inter métallique "Ti <sub>3</sub> Al"	Type métallurgie des poudres	Propulsion Structures aéronautiques chaudes (650°C)
SiC	Inter métallique "TiAl"	"	" (950°C)
TiB <sub>2</sub>	Inter métallique de titane	"	" (?)
W	Superalliage	"	Propulsion
W	Inter métallique base Fe, Ni	"	" (1100°C)
Trichites de métaux de transition Nb, Ta, Cr	Superalliage	Solidification dirigée	" (1100°C)

**Figure 1****Figure 2****Figure 3**

**Figure 4****Figure 5****Figure 6****Figure 7**

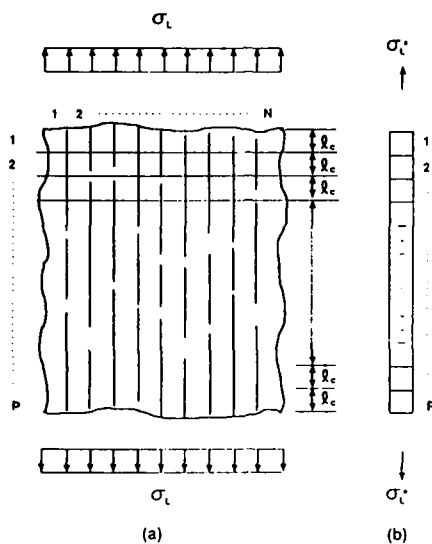


**Figure 8**

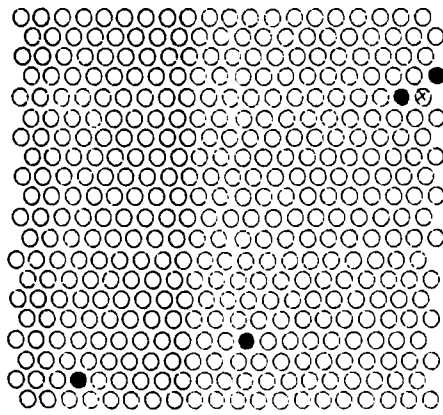
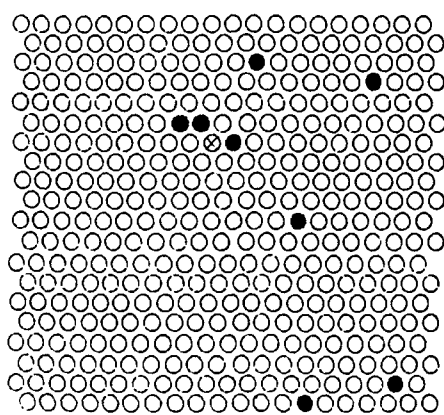
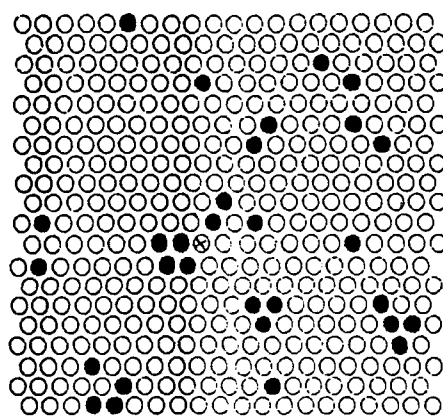
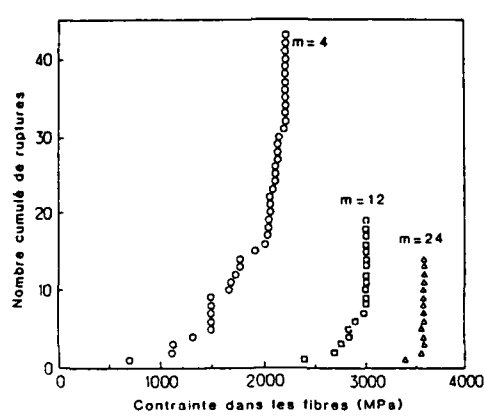
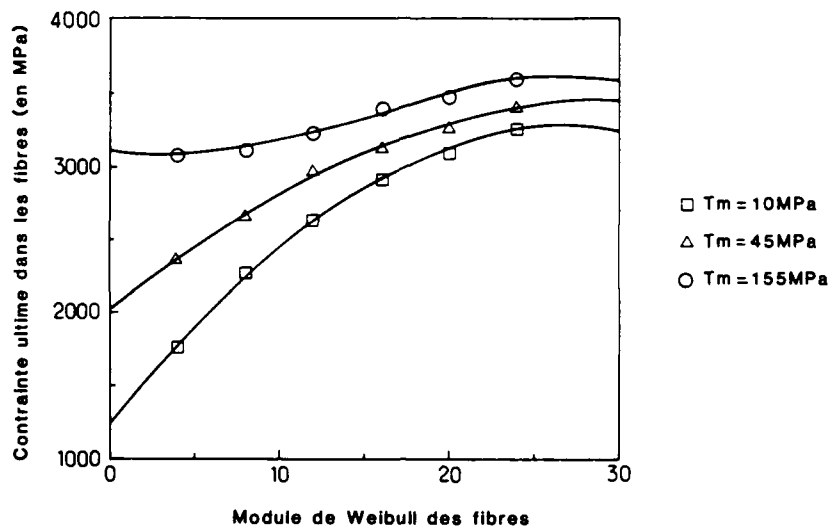
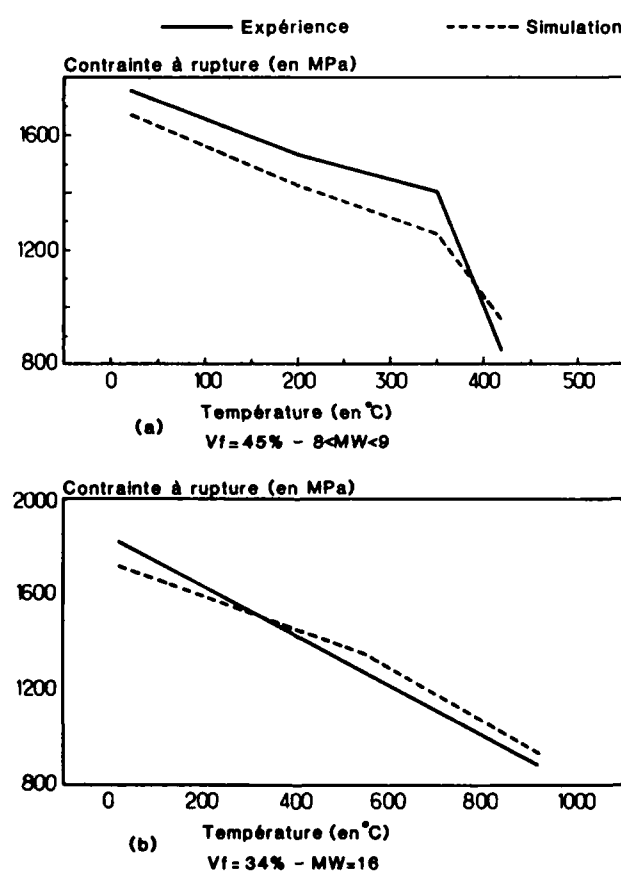


Figure 9

Figure 10Figure 11

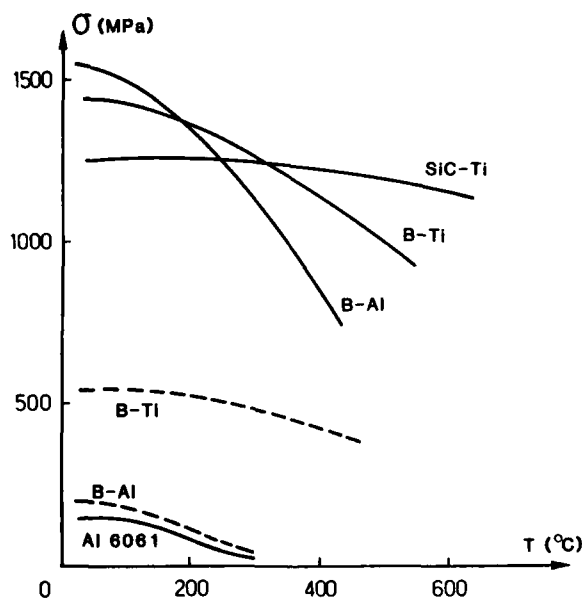


Figure 12

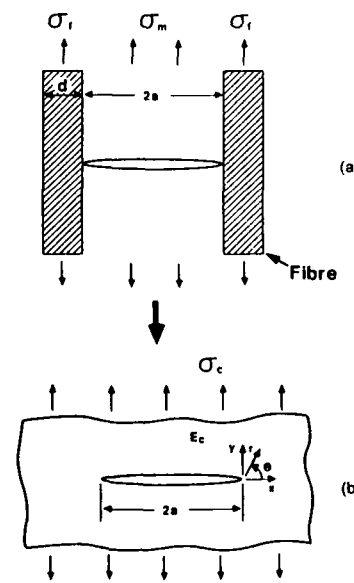


Figure 13

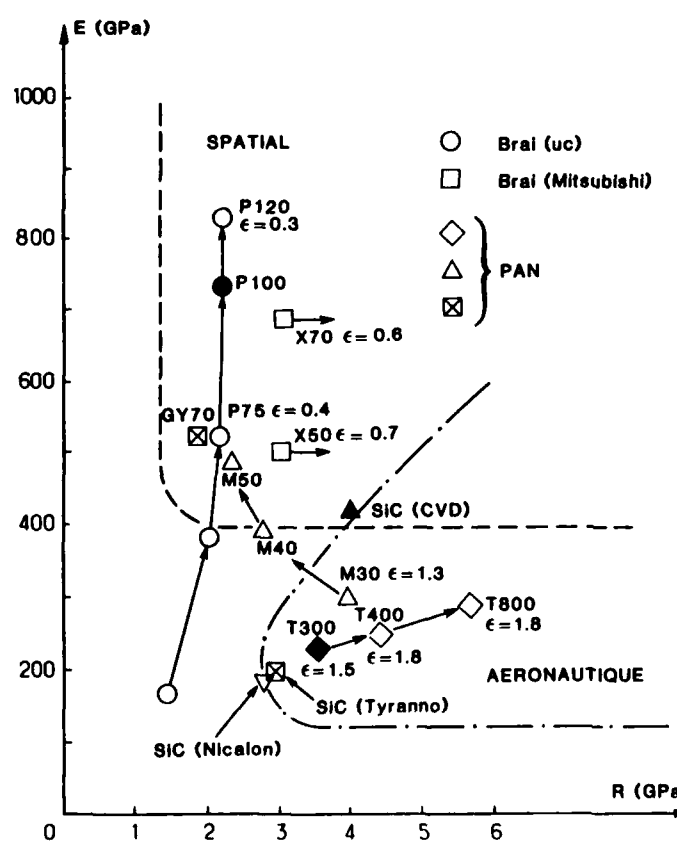
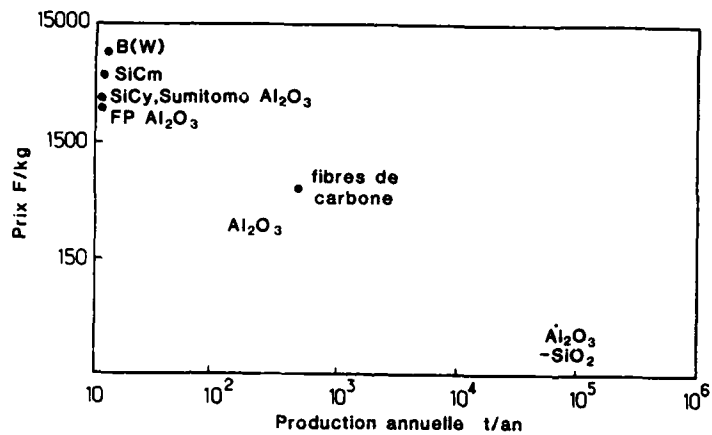
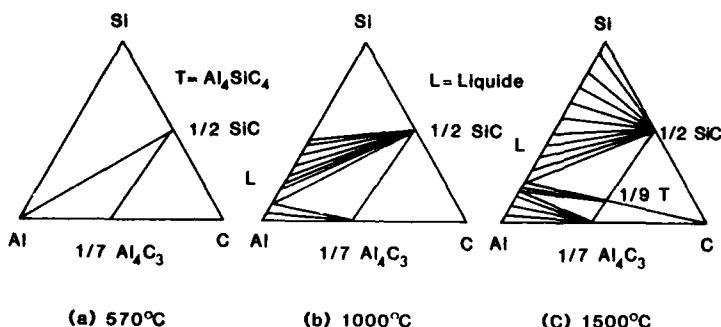
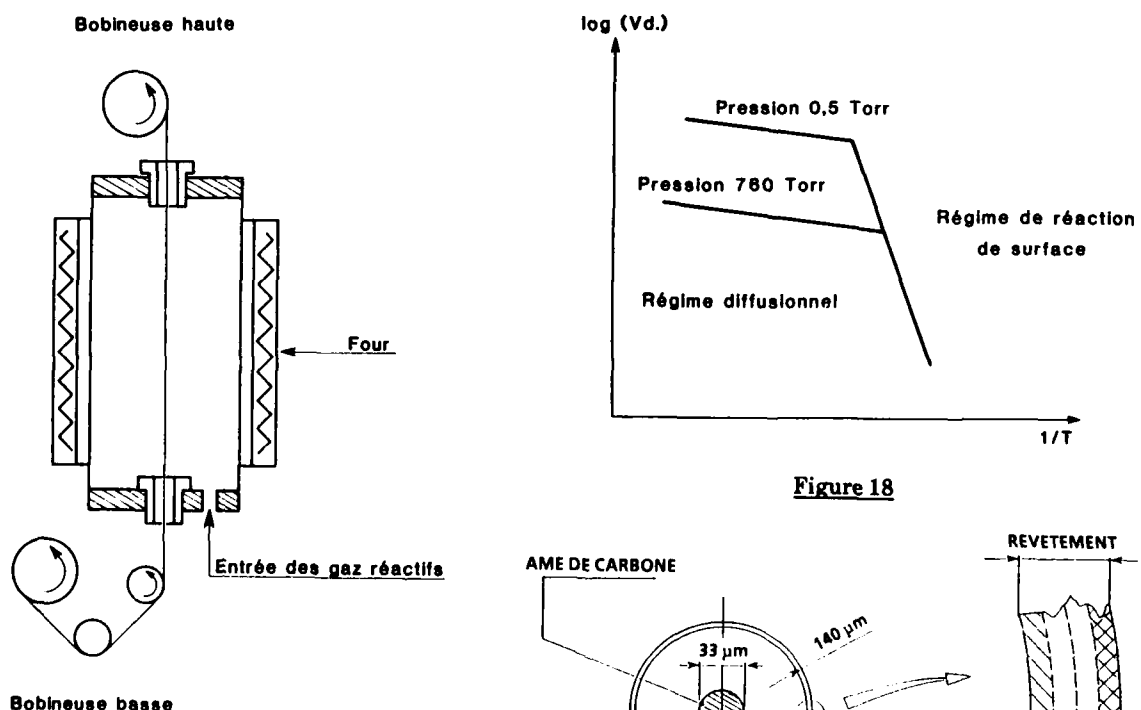
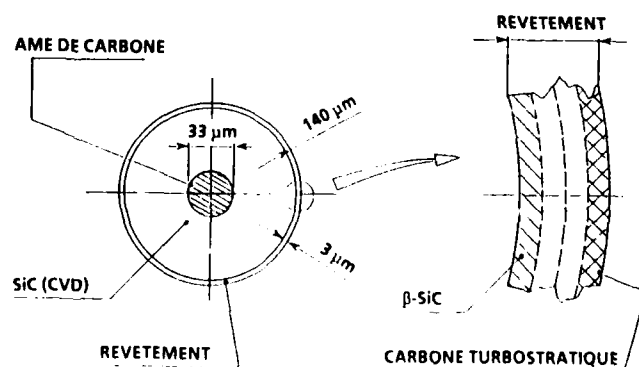


Figure 14

Figure 15Figure 16Figure 17Figure 19

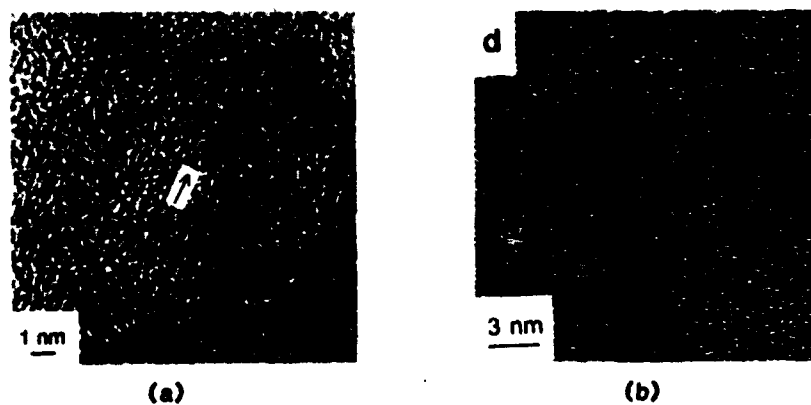


Figure 20

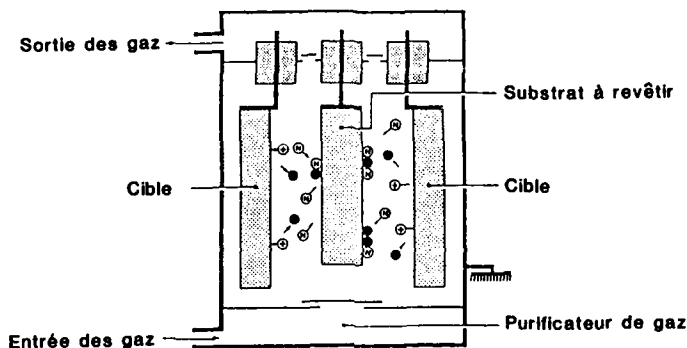


Figure 21

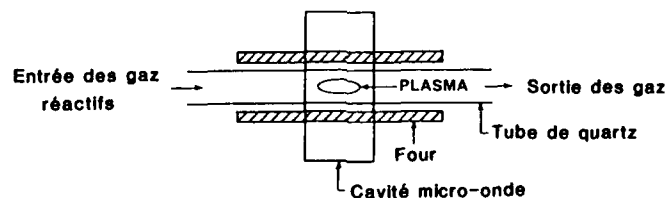


Figure 22

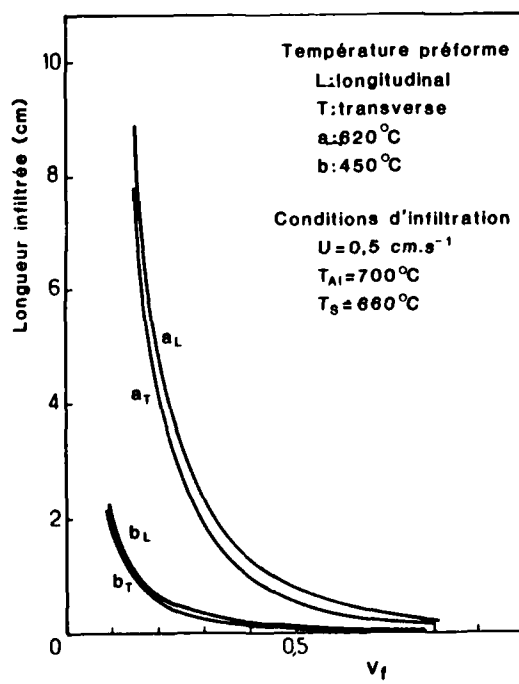


Figure 23

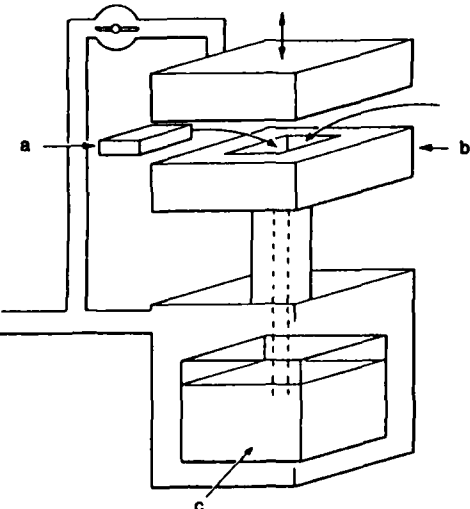


Figure 24

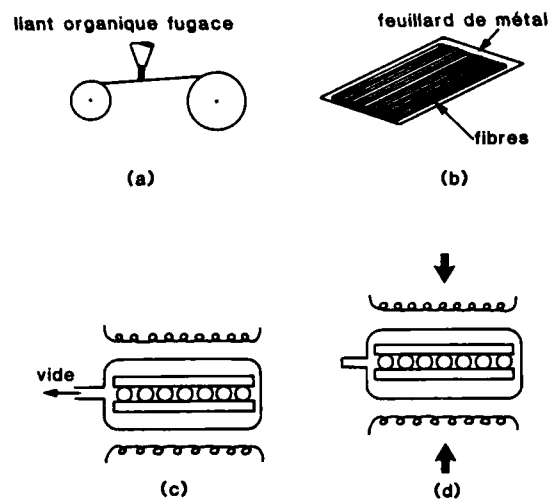


Figure 25

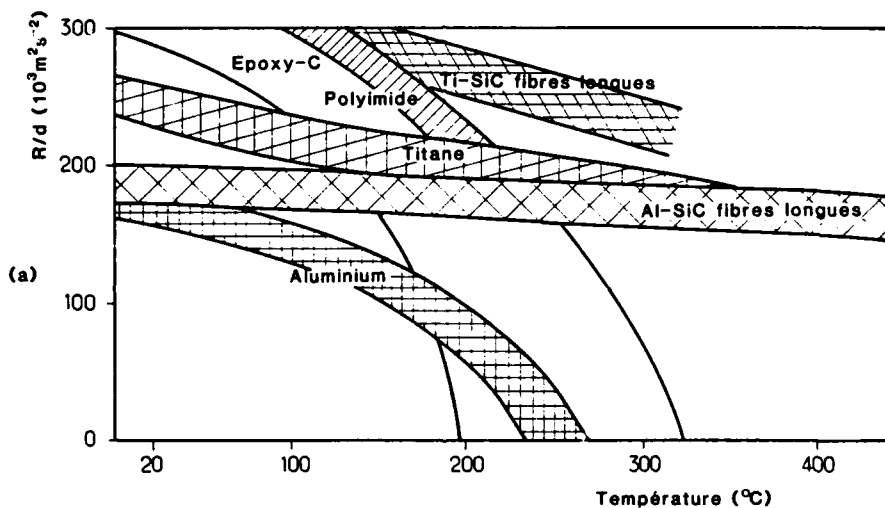


Figure 26a

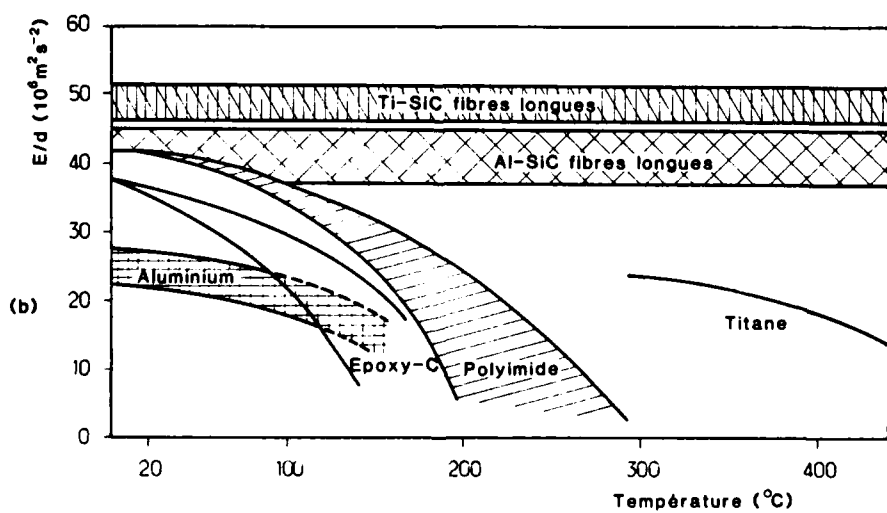
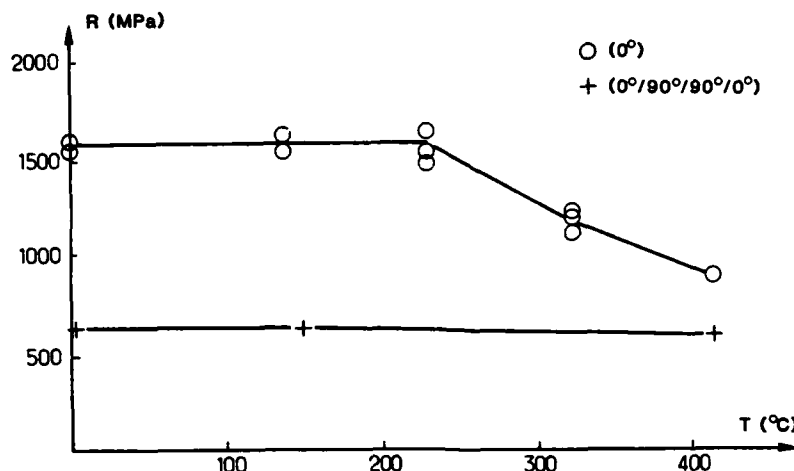
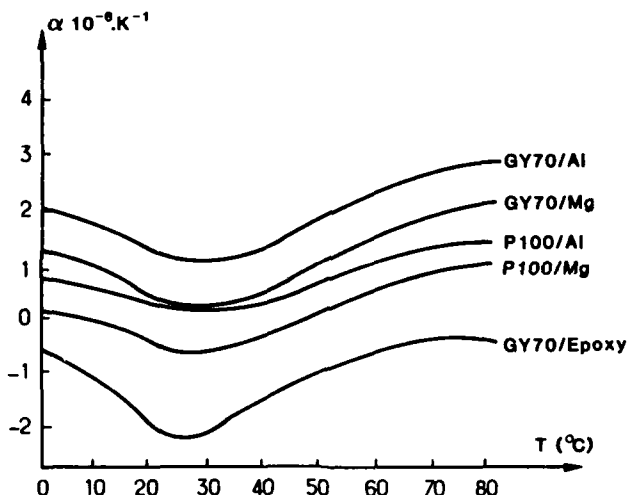
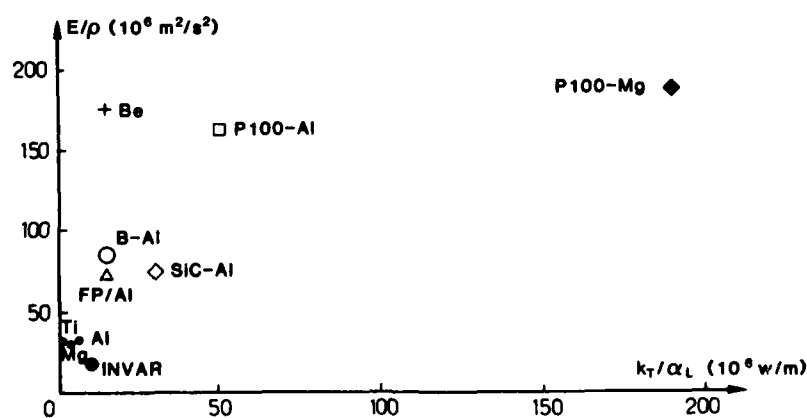


Figure 26b

Figure 27Figure 28Figure 29

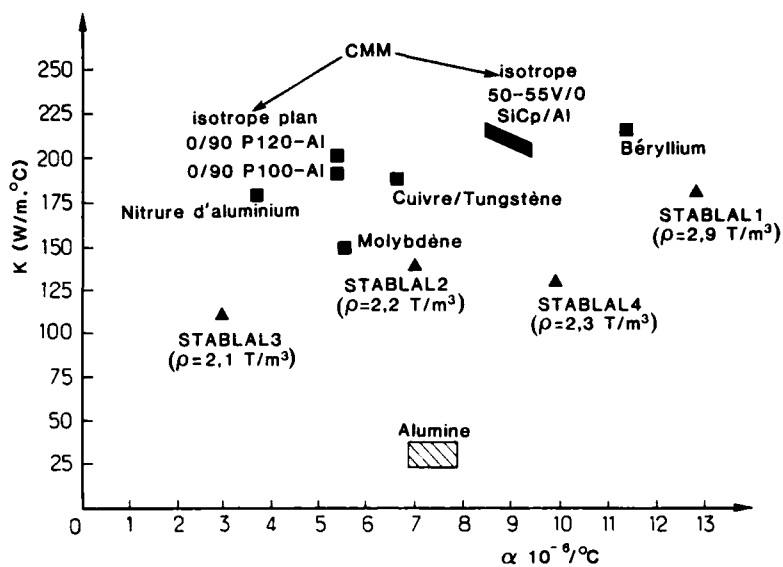


Figure 30

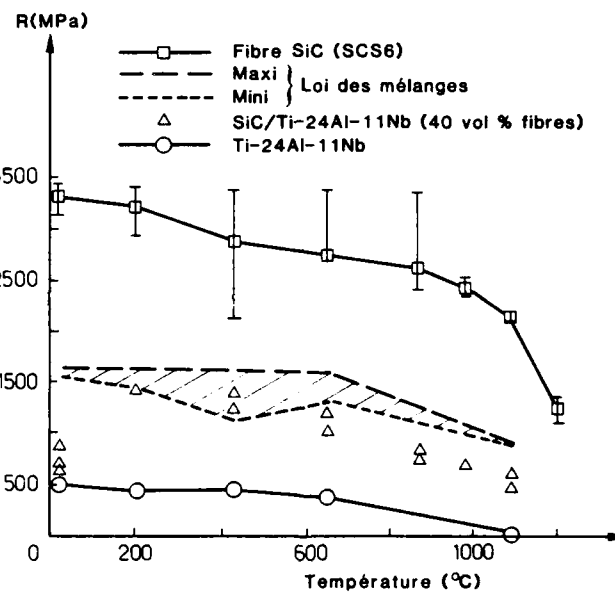


Figure 31

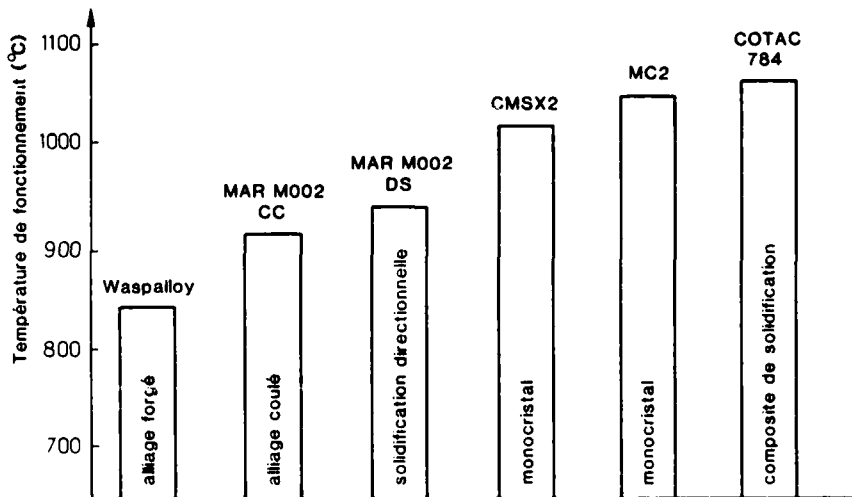


Figure 32

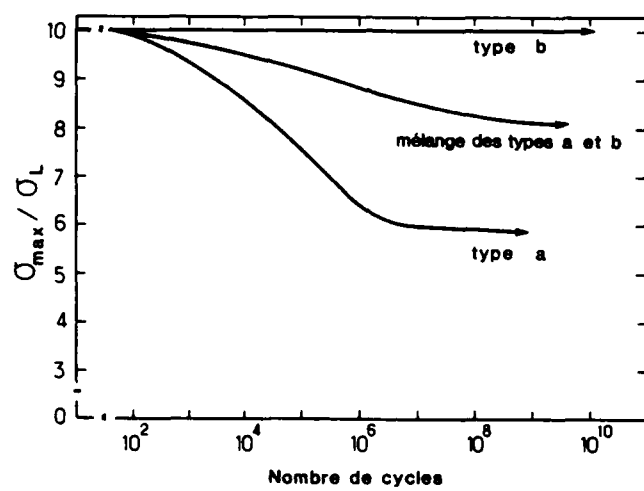


Figure 33

## LISTE DES FIGURES

- Figure 1 :** Caractéristiques spécifiques de composites quasi-isotropes comparées à celles d'alliages métalliques (d'après [1])
- Figure 2 :** Diagramme contrainte de rupture-fraction volumique de fibres : domaines de rupture multiple et de rupture simple
- Figure 3 :** Rechargement linéaire d'une fibre à partir de son extrémité
- Figure 4 :** Composite monofilamentaire : géométrie du modèle de Cox
- Figure 5 :** Rechargement élastique d'une fibre dans un composite : distribution des contraintes dans la fibre et la matrice
- Figure 6 :** Contraintes de cisaillement à l'interface fibre-matrice à l'extrémité d'une fibre ; cas du décollement fibre-matrice sur une longueur  $l_c$
- Figure 7 :** Essai de fragmentation sur éprouvette monofilamentaire  
 a) Eprouvette vierge  
 b) Premières ruptures de la fibre  
 c) Saturation de la fragmentation
- Figure 8 :** Modèle de Rosen : schéma parallèle et schéma série (d'après [12])
- Figure 9 :** Simulation de la rupture dans un composite unidirectionnel  
 a) Influence du module de Weibull des fibres sur la contrainte à rupture du composite  
 b,c,d) Influence du module de Weibull des fibres sur le nombre et la distribution des ruptures de fibres lors de celle du composite
- Figure 10 :** Influence de la contrainte de transfert de charge par cisaillement à l'interface fibre-matrice sur la contrainte à rupture du composite en fonction du module de Weibull des fibres
- Figure 11 :** Comparaison simulation-expérience de l'évolution avec la température de la contrainte à rupture (d'après [9])  
 a) Composite SiC (SCS2)/Al-6061  
 b) Composite SiC (SCS6)/Ti-6-4
- Figure 12 :** Caractéristiques de traction sens long et sens travers de quelques composites à matrice métallique en fonction de la température
- Figure 13 :** Transformation d'un composite unidirectionnel en un matériau homogène équivalent (d'après [21])
- Figure 14 :** Fibres longues utilisables pour les structures aéronautiques et spatiales
- Figure 15 :** Coût de quelques fibres de renfort en fonction du volume produit annuellement (d'après [28])
- Figure 16 :** Coupes du diagramme d'équilibre Al-Si-C à trois températures : nature des phases liquides en équilibre avec SiC et  $\text{Al}_2\text{C}_3$
- Figure 17 :** Schéma d'appareil de dépôt chimique en phase vapeur pour traitement en continu de fibres (d'après [45])
- Figure 18 :** Vitesse de dépôt en fonction de l'inverse de la température : régime de surface et régime diffusionnel
- Figure 19 :** Coupe d'une fibre SiC SCS6 d'AVCO montrant la nature des diverses strates
- Figure 20 :** Microstructure du revêtement de la courbe SCS6 en microscopie électronique à haute résolution  
 a) Microcristallite de  $\beta$ -SiC (zone interne)  
 b) Carbone turbostratique (zone externe)
- Figure 21 :** Schéma d'une installation de pulvérisation cathodique (d'après [45])
- Figure 22 :** Schéma d'une installation de dépôt chimique en phase vapeur assisté par plasma (d'après [45])
- Figure 23 :** Influence des paramètres d'élaboration sur la distance infiltrée (d'après [63])
- Figure 24 :** Schéma de principe du procédé LPF de Craycir SA (d'après [65])  
 a) Préforme fibreuse  
 b) Moule  
 c) Réserve de métal liquide
- Figure 25 :** Réalisation de feuilards monocouches SiC-alliage de titane par formage superplastique
- Figure 26 :** a) Résistance spécifique en fonction de la température pour quelques composites unidirectionnels  
 b) Module spécifique en fonction de la température pour quelques composites unidirectionnels (d'après [67])

Figure 27 : Evolution avec la température des caractéristiques de traction de composites SiC/6061 (d'après [9])

Figure 28 : Variation avec la température des coefficients de dilatation sens long de quelques composites unidirectionnels.

Figure 29 : Stabilité dimensionnelle et module spécifique de quelques composites

Figure 30 : Caractéristiques thermiques et dilatométriques comparées de quelques matériaux potentiels de support de circuits électroniques

Figure 31 : Evolution avec la température de la contrainte à rupture d'un composite SiC-SCS6/(Ti<sub>x</sub>Al-Nb) et comparaison avec la loi des mélanges

Figure 32 : Températures potentielles d'emploi de composites à matrice superalliage et de superalliages usuels pour une durée de vie en fluage de 1000 h sous une contrainte de 150 MPa

Figure 33 : Diverses formes de courbes d'endurance pour les composites unidirectionnels (d'après [82])

- a) Fissuration de la matrice seule
- b) Décohésion fibre-matrice seule
- c) Endommagement mixte (a+b)

## DEVELOPMENTS IN PARTICULATE AND SHORT FIBRE COMPOSITES

by

S.J. Harris

Department of Materials Engineering and Materials Design  
University of Nottingham  
Nottingham NG7 2RD, UK

### **ABSTRACT**

Major programmes exist in the USA and Europe to produce lightweight, stiff and strong metallic materials with the aid of discontinuous reinforcement. These efforts relate to light metal matrix alloys (aluminium, magnesium and titanium) and the use of short fibres, whiskers and particles of ceramic to provide the necessary reinforcement. Major interest has recently been centred on the development of particulate reinforcement of aluminium alloys. This paper reviews the various methods of producing these metal matrix composites. Then the influences of reinforcement size, shape and volume fraction, matrix alloy selection, processing route and heat-treatment on the mechanical properties, e.g. stiffness, strength and toughness of the composites, are discussed. Microstructural evidence is used to interpret property data where possible. Elevated temperature and creep properties are described, as well as the ability of these composites to handle thermal cycling. Other properties, e.g. fatigue and corrosion, which influence the life of components fabricated from these materials also come under review.

### **1. INTRODUCTION**

To provide competition to the increasing use of polymer-based composites in airframe parts (1), the development of lightweight metallic materials has been continued vigorously. The availability of metallic matrix composites (MMCs) with attractive physical and mechanical properties at reasonable cost would become a significant part of the competition. Two distinct forms of reinforcement for these composites are under consideration, i.e. continuous fibres which are ceramic monofilaments or discontinuous reinforcements which may be short fibres, whiskers or particles, again of ceramics. The use of discontinuous reinforcement, which is the subject of this paper, provides opportunities for smaller gains in mechanical properties, such as stiffness or strength, than would be the case with continuous fibres. Whilst the gains are modest, the ability to provide more or less isotropic behaviour from these materials is a major advantage in many potential applications.

In the past decade, major efforts have been made to develop production methods for MMCs with discontinuous reinforcements. These efforts have involved techniques of allowing metal to infiltrate preprepared fibre arrangements or preforms, blending and consolidation of powdered metals and ceramic reinforcement, and the cospray of liquid metal and solid ceramic particles. Many of these developments were laboratory-based five years ago and have, within the past year, become pilot scale, and this has meant that materials are now coming forward in greater quantities and with better levels of consistency. Although net shape components are of interest to the aerospace industry, the majority of the effort has been in the production of rolled sheet and plate and also of extruded forms. Machining of such materials has begun to be studied (2) so that production routines and costs of expensive diamond tooling can be optimised. Problems in joining these materials do exist in a number of instances but there are indications that processes such as friction welding may come to the fabricators' assistance.

Within the discontinuous reinforced MMC, greater attention has been focused on particle-reinforced alloys. This move away from short fibres and whiskers has been influenced by the availability of relatively cheap  $\alpha$ -silicon carbide particles or grit, the abilities to handle such particles in a composite fabrication operation, and finally to produce properties which are not judged to be inferior to those produced from other reinforcements.

Aluminium alloys still predominate as the matrix materials and a range of 2000, 6000 and 7000 series alloys have been used. The prime requirement for reduced weight in these MMCs has allowed aluminium-lithium alloys, e.g. 8090 Al-Li-Cu-Mg to be used. This has been necessary as the addition of silicon carbide to aluminium alloys does raise the density. The lithium addition to the matrix is more than capable of balancing that increase. Suitable reinforcement particles or fibres with densities less than that of aluminium are difficult to find, one attempt (3) has been made with boron carbide (B<sub>4</sub>C). Other matrix alloys, i.e. titanium, magnesium, and intermetallics, such as aluminides, are also of significant interest. Magnesium, with its very low density, has great attractions but until solutions are found to its corrosion problems, which already limit the application of these alloys in the unreinforced state, then efforts to reinforce them will be low key. The reinforcement of titanium by suitable ceramic particles would be a great attraction. Unfortunately, chemical or metallurgical interaction at the reinforcement-titanium alloy interface during fabrication or in elevated temperature service do provide a major problem. This manifests itself by causing embrittlement and by the inability to deliver satisfactory strength properties. The nature and properties of interfaces in titanium and aluminium alloy MMCs is considered in more detail later. Intermetallic matrices are under active development for elevated temperature applications. Possibilities do exist for improving the ductilities of these materials but a need for reinforcement is necessary. This reinforcement is most likely to be continuous fibres.

This paper attempts to display the range of properties achieved in light metal alloy reinforced with discontinuous reinforcements. It represents an update on the paper presented at the AGARD meeting on New Light Alloys at Mierlo in the Autumn of 1988 (4). Besides dealing with short term and long term mechanical properties, thermal behaviour, etc. the paper attempts to provide information on the current understanding of reinforcement-matrix interfaces and matrix microstructures and to show how they may influence yield, fracture and fatigue processes.

## 2. FABRICATION OF SHORT FIBRE AND PARTICULATE COMPOSITES

Initially, major efforts were made to produce composites with short fibre and whisker reinforcement. This made use of short fibre preforms which were infiltrated with liquid metal either under vacuum or by the application of pressure as in squeeze casting (5,6), or by the mixing of powders and reinforcing whiskers followed by consolidation by pressing and heating (7). A greater emphasis has now been placed upon particulate reinforcement whereby three methods of manufacture have gained much attention:

- (a) stirring reinforcing ceramic particles into a melt
- (b) spray deposition of solid ceramic particles with atomised droplets of liquid metal
- (c) mixing and blending of metal powders with reinforcing particles in a related fashion to that mentioned above with whisker reinforcement.

Whilst methods (a) and (b) use the metal in the liquid state to promote effective mixing and dispersion of the particles, the powder based system may promote the liquid phase in small amounts during the consolidation and not in the mixing stage.

Melt stirring represents the simplest form of production for particle reinforced MMCs (8). The particles, usually  $\alpha$ -SiCp ( $\approx 10\mu\text{m}$  in size) are surface treated prior to being stirred into the molten alloy. Surface treatment of the particles is necessary to obtain particle wetting and thereby achieve even distribution in the melt. Excessive reaction between particles and melt has to be guarded against by selecting the alloy matrix and controlling the level of superheat and time of mixing prior to solidification. Increasing levels of superheat promotes a reaction at the matrix-particle interface.



which allows crystals of aluminium carbide to grow, see fig. 1. The presence of silicon in the original alloy does slow down the reaction and prevent the deterioration of properties in the resultant composite. Solidification of the casting results in the silicon carbide particles occupying the intercellular regions which have grown from the melt and pushed the SiCp ahead of the liquid-solid interface. The cell sizes, as in the unreinforced alloys, can be modified by cooling rate, see fig. 2, and this may influence the distribution of particles. At faster cooling rates the cell size approaches that of the SiCp and this promotes interdendritic trapping of the particles, and a better distribution of the reinforcement than is the case with more slowly cooled composites, see fig. 3. Variations in particle distribution do occur through the casting section as cooling rates change from the surface to the centre.

A variant on stir casting is Rheocasting or Compocasting (9), where the metal is held in the semi-solid or 'mushy' condition when particle mixing takes place. Thixotropic conditions occur, provided that adequate control is maintained over the volume fraction of solid particles (dendrites and SiCp). The products from the melt stirring and Compocasting operations may be cast to shape or be subjected to a working operation in the solid state or with a proportion of liquid present, where it may be referred to as thixoforging.

Spray deposition has developed as a feasible technique for producing unreinforced and reinforced alloys (10,11). Here metal is melted in a crucible usually by induction heating and under pressure of a suitable gas, e.g. nitrogen, see fig. 4. The metal is passed from crucible through a nozzle into an atomizer. The resultant atomized stream of metal is then collected on a substrate placed in the line of flight. Final product shape depends on the atomizing conditions and the shape and motion of the collector, e.g. extrusion ingots, forging stock or hollow tubes can be produced. Metal flow rates can exceed 6 kg/min and typical recovery efficiencies are in the range 50-85% depending upon the product form. Fine as-cast grain sizes can be produced of approximately  $15\mu\text{m}$  with minimum segregation thus minimising times for homogenisation. Metal matrix composite ingots can be obtained by introducing ceramic particles, e.g.  $13\mu\text{m}$  diameter  $\alpha$ -SiCp, into the metal spray stream. Good control over the atomising process and the particle feed can promote more even distribution of the reinforcement in a matrix which is 95-98% dense. Ingots of 100 kg are currently being produced and possibilities exist for doubling this weight. A wide range of alloys (2000, 6000, 7000, 8000 and Al-Si casting alloys) have been sprayed to form composites with 10-15 vol.% of SiCp. Sprayed MMC ingots have been fabricated by extrusion, rolling, forging and remelting. Prior to working, the ingots are machined. Conventional extrusion procedures are adopted but some increases in applied forces as well as significant wear on extrusion dies has been noted. Some alignment of the SiCp takes place, the degree depends on the extrusion ratio employed. Minimal particle breakdown and decohesion at particle-matrix interfaces have been observed in the composite. Hot rolling characteristics of the MMC are similar to those of conventional alloys. The higher elastic modulus and work hardening rates do influence cold working response; despite this, MMCs have been rolled down to  $100\mu\text{m}$  foil.

As already indicated, a solid state consolidation route has been in use for some time for the production of whisker and particulate based MMCs (7). The processing involves the preparation of suitable pre-alloyed powders to which SiC in whatever form is added, see fig. 5.. This allows SiC particles to be added over a wide size range, i.e. 3-40 $\mu$ m. Particular care is taken over the blending operation to ensure effective distribution of the reinforcing particles (11). The blended powders are canned and vacuum degassed prior to hot pressing in order to minimise surface oxidation and contamination. An alternative to conventional hot pressing is the use of hot isostatic pressing (HIPping) in order to provide more homogeneous consolidation. Secondary processing such as extrusion, forging or rolling is necessary to break up remaining interparticle films. Although this form of processing can lead to net-shaped parts, the major efforts have been concentrated on sheet, plate and extruded sections. A variant of the powder based route, which is termed 'Mechanical Alloying', subjects a mixture of metal powders, oxides and carbides to a ball-milling treatment in order to achieve the necessary blending of constituents (12).

### 3. INTERFACES IN AS-FORMED COMPOSITES

The interface produced between the reinforcing particle or fibre and the matrix does have a major effect on the subsequent performance of the composite in service. The fabrication stage has a major influence on the interfacial condition which exist within any given MMC but other opportunities do exist to modify the interface, e.g. during heat-treatment or service particularly at elevated temperatures. An interfacial reaction involving the formation of Al<sub>4</sub>C<sub>3</sub> has already been referred to in the melt stirring process with aluminium and silicon carbide. The availability of oxygen on metal or reinforcement interfaces has been shown to be important in controlling reactions between the carbides, or boron and the aluminium alloy matrix. Electron microscope observations on SiC whisker-aluminium alloy (Al-Cu-Mg) produced by a solid state fabrication route have shown small crystalline precipitates at the interface, see fig. 6; the EELS technique was able to demonstrate that they contained oxygen; EDS gave evidence of magnesium; and diffraction patterns revealed a structure corresponding to MgO. More recently Warner and Stobbs (13) have compared chemically cleaned SiC (F-600 grit) with oxidised SiC in an Al-1.9%Mg alloy matrix. The materials were prepared by the spray route and had subsequently been extruded. Samples were examined in the TEM before and after heat-treatment for 20h at 625°C. With the clean SiCp particles no reaction products were seen before heat-treatment but after the treatment Al<sub>4</sub>C<sub>3</sub> existed for distances up to 300nm from the interface on the alloy matrix side. Evidence also existed of stressing of the SiCp below the reaction products and of a heavily dislocated matrix. The oxidised SiCp had an irregular zone (10-30nm thick) of mixed microcrystalline and amorphous material existed at the interface in the pre-heat-treated MMC. Heat-treatment changed matters with small precipitates appearing at the interface and an amorphous layer of uniform thickness (2nm) forming continuously around the SiCp MgO reflections were observed from the small precipitates. It would appear that the amorphous layer is oxygen-containing and this seems to inhibit Al<sub>4</sub>C<sub>3</sub> formation.

Reinforcement of titanium and its alloys by particulates is strongly influenced by the conditions which are generated during fabrication or whilst they operate at elevated temperatures. SiCp reacts with titanium at temperatures in excess of 650°C particularly if they are maintained at this temperature level for periods up to 1000h. A multi-layered interface product forms involving titanium carbide (TiC) and titanium silicides such as Ti<sub>5</sub>S<sub>3</sub> together with a solution of carbon in titanium and titanium taken up in the SiCp (14). Within the silicide layer precipitation of titanium carbide occurs. Parabolic growth laws apply to the formation of the interface layer. Increased volume fractions of SiCp reduces the rate of growth of the interfacial layers as the carbon content of the matrix saturates at an early stage. These reactions are capable of significantly reducing the volume fraction of SiC in the composite and promoting weak and brittle interfaces. Since titanium and its alloys are significantly stronger alloys than aluminium there is a requirement for higher integrity interfaces in these materials. Possibilities do exist for either putting a coating on the SiCp in order to prevent or limit reaction or the introduction of a different type of particulate. Observations on TiC particles in a Ti6Al4V alloy matrix have shown that carbon diffusion from fibre to matrix occurs at elevated temperatures. This reverses with decreasing temperature if the cooling rate is slow. Changing the alloy to Ti24Al11Nb prevents the carbon from diffusing back as a stable precipitate. Ti<sub>3</sub>(AlNb)C forms in the alloy close to the interface (15).

### 4. INFLUENCE OF REINFORCEMENT ON MICROSTRUCTURE

In aluminium alloys it has been demonstrated that the following variables influence the microstructure of the alloy:

- (a) the size and shape of the reinforcement
- (b) the volume fraction of the reinforcement
- (c) the processing route for the composite
- (d) the relative coefficient of expansion of reinforcement and matrix
- (e) the type of alloy.

Composites have been produced with  $\beta$ -silicon carbide whiskers (diameter <1 $\mu$ m and aspect ratio 50:1),  $\alpha$ -silicon carbide particles (size 3-40 $\mu$ m irregular in shape with an aspect ratio of 2:1 and  $\delta$ -alumina fibres (diameter 3 $\mu$ m, aspect ratio 50:1). The volume fraction of reinforcement varies from 5 to 40 vol.%, but the majority of investigations have concentrated in the 10 to 20 vol.% range. The differing processing routes can interact with the differing reinforcement size, shape and amount. As described already

in the stir cast route, the processing conditions, e.g. cooling rate, can influence particle distribution (8). A significant amount of particulate and whisker reinforced composite has been hot or cold worked either during or after consolidation. Interactions between forming temperature, particle size, volume fraction and deformation rate all influence the subsequent microstructure of the matrix (16). The major influence relates to the processes of recovery and recrystallisation and the resultant grain sizes, substructures and textures which remain in the composite after processing (17). The grain size does reduce with particle diameter and with increasing volume fraction, see fig. 7. It is possible to prevent recrystallisation at small particle diameters <5 $\mu\text{m}$  and at higher volume fractions, e.g. 30 vol.% of 3 $\mu\text{m}$  particles. Textures in the matrix alloy can be influenced by the reinforcement, e.g. use of SiCp in an 8090 alloy has been shown to remove the strong crystallographic textures which are produced in the unreinforced versions of this alloy (18).

Forming processes, e.g. extrusion, can have a major influence on the form and orientation of the reinforcement which has a significant aspect ratio, e.g. as whiskers or short fibres. During such a hot working process, significant levels of whisker or fibre fracture can take place which can reduce aspect ratio down to 2 or 3. The high temperature deformation of MMCs depends upon the kinetics of dislocation motion and the diffusive mass transport in the matrix. If both of these are inadequate to allow matrix strain around the hard reinforcing fibres then a sharp rise in matrix flow occurs and microstructural and particularly fibre damage will take place (19). Consequently, strain rate has a strong effect on flow stress and the only the use of high extrusion temperatures permits high rates of deformation. The presence of a compressive hydrostatic stress component during extrusion may also have a beneficial effect by reducing fibre failure and it most certainly does limit cavitation at the interface, particularly at fibre ends. Small diameter fibres of high strength, e.g. whiskers, are more capable of resisting damage because the critical bend radius is reduced and for a given aspect ratio the relaxation kinetics are enhanced as they depend on fibre length.

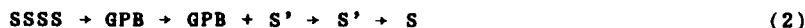
In both the  $\alpha$ -SiC-aluminium alloy and  $\delta$ -Al<sub>2</sub>O<sub>3</sub> aluminium alloy systems there is a significant difference in the coefficient of thermal expansion,  $\alpha$ , between fibre and matrix, e.g.  $\delta$ -Al<sub>2</sub>O<sub>3</sub>  $\alpha = 6 \times 10^{-6} \text{ K}^{-1}$  and Al,  $\alpha = 23 \times 10^{-6} \text{ K}^{-1}$ . After casting, hot working or heat-treatment, the cooling process down to ambient promotes internal stresses in the composite. At temperatures in excess of 200°C these are, in part, relaxed by matrix plastic deformation which can promote increased dislocation densities. Humphreys (17) has demonstrated that in SiCp reinforced aluminium composites a dislocation cell structure is formed during a fast cool or quench from 500°C. Under similar cooling conditions an Al-Cu-Mg (2014) alloy also reinforced with SiC particles was found to have dislocation loops and helices. Nardone and Prewo (20) and Taya and Arsenault (21) have demonstrated that such dislocations do form inhomogeneously in the matrix, i.e. close to the reinforcement. It is suggested by Humphreys (17) that such dislocations are more likely in an alloy matrix where higher friction stress would be found. Cooling below 200°C may promote further plastic deformation but now as the matrix flow stress rises with decreasing temperature the ability to retain elastic stresses increases. This leads to a situation where the reinforcement goes into compression and the matrix remains in tension. The residual misfit can be calculated in small volume fractions using Eshelby's theory. Many workers, Mori and Tanaka (22), Taya and Arsenault (21) have sought to apply this theory to large volume fractions of particles or whiskers. Withers et al (23) have demonstrated the existence of these stresses in short SiC fibre reinforced aluminium composites using a neutron diffraction technique to measure lattice parameters of matrix and fibre during a heating and cooling cycle, see fig. 8. Differences may be expected between the mechanical behaviour of a whisker or short fibre composite at ambient and that of a composite containing more equiaxed particles. For equiaxed particles, the residual stress is hydrostatic whilst the pattern of such stresses in the whisker or short fibre composite has an anisotropic shear component. In addition, large diameter short fibre composites may have greater residual stresses when comparison is made with composites containing whiskers of similar aspect ratios as the relaxation processes will be more difficult to operate in cooling. This will produce a higher compressive stress in the as-quenched composite, see fig. 9.

A prime requirement for obtaining reasonable strength levels in discontinuous reinforced MMCs is the use of a matrix with the ability to be heat-treated. The heat-treatment procedure usually requires the alloy to be quenched from a solution treatment temperature close to 500°C. Such a quench will significantly increase the dislocation density of the matrix, probably in an inhomogeneous fashion. Two distinct and different patterns of age hardening kinetics results in Al-Si-Mg (6061), Al-4%Cu, Al-Cu-Mg (2014 and 2124) as a result of the presence of the reinforcement, these are:-

- (i) natural and low temperature artificial ageing
- (ii) higher temperature artificial ageing.

Natural and low temperature ageing usually requires the assistance of quenched-in vacancies in order to assist with the formation of GP zones or intermediate precipitates such as O'-CuAl<sub>2</sub> in Al-Cu alloys. The retardation of such precipitation in alloys reinforced with both particles or whiskers (see fig. 10b) can be explained in terms of the reduction of the available vacancy concentration produced by the presence of the reinforcement (24). Nucleation problems at lower ageing temperatures can cause problems for certain forms of precipitation usually produced at higher temperatures, as transition precipitates can assist with the in-situ nucleation of higher temperature precipitates in unreinforced alloys. The twin influences of enhanced dislocation densities and reduced vacancy concentration promoted by the presence of SiCp or  $\delta$ -Al<sub>2</sub>O<sub>3</sub> short fibres accelerates the kinetics of formation of higher temperature precipitates, e.g. O'-CuAl<sub>2</sub>

in Al-4%Cu, see fig. 10a. Measurements made by DSC, dilatometer and observations by TEM have shown the early onset of  $\theta'$  precipitation in this alloy system (24,25). Since the enhanced dislocation density plays a key role in assisting with the nucleation of  $\theta'$  (see fig. 11), the uneven distribution of dislocation in the matrix region can have a major effect. Higher particle volume fractions, finer particle sizes and good particle distributions do improve the distribution and fineness of precipitation. Adding magnesium to Al-Cu so that copper-magnesium ratios approach 2.2:1 promotes the following ageing sequence of 2124 alloy with increasing temperature of ageing:-



The  $\text{S}'(\text{Al}_2\text{MgCu})$  phase also nucleates on dislocations after ageing for short periods at 177°C. The higher dislocations found in the composite are punched from threads of the SiC whisker during cooling in order to reduce thermal induced residual stress (26). A number of helical dislocation loops which possibly arise from quenched-in vacancies also promote further precipitation. The punching of dislocations at whisker ends does appear to promote even dislocation and  $\text{S}'$  phase distribution in the matrix. Similar enhanced ageing patterns were also obtained with SiCp reinforced 2124 alloys, see fig. 12.

With 7000 series (Al-Zn-Mg-Cu) alloys difficulties are experienced in gaining maximum hardening from these alloys (27). Homogeneous precipitation of  $\eta'(\text{Mg}_2\text{Zn})$  precipitation does occur in association with equilibrium  $\eta(\text{Mg}_2\text{Zn})$  at SiCp/matrix interfaces (28). It is probably that the maximum volume fraction of  $\eta'$  is not forming in the matrix as a possible reduced vacancy concentration inhibits the intermediate reaction and allows precipitation on the grain boundaries instead.

Work on lithium-containing alloys, e.g. 8090 (Al-Li-Mg-Cu) with fine SiCp has shown that the kinetics of natural and artificial ageing are accelerated by the presence of this kind of reinforcement. Reasons for hardness plots rising to a plateau after 10h natural ageing may suggest that GPB is forming more quickly in the composite than in the unreinforced alloy where 50-100h is required. This explanation does appear to be contrary to that given earlier for Al-Cu and other alloys where reduced vacancy concentrations are held responsible for sluggish GP zone formation and metastable precipitation. At elevated temperatures, e.g. 170 and 190°C ageing is also quicker than in the unreinforced alloy (29). Explanations of this are again difficult as the only change appears to be a finer distribution of  $\delta'(\text{Al}_3\text{Li})$  precipitate which does not usually depend upon dislocations to assist nucleation. The  $\text{S}'(\text{Al}_2\text{CuMg})$  phase which does require additional dislocations to allow nucleation was not discovered in significant amounts until the reinforced alloy had been overaged, e.g. at 190°C.

Evidence has also been found of precipitation at reinforcement-matrix interface of equilibrium phases under conditions of overageing, i.e.  $\theta(\text{CuAl}_2)$  in Al-4%Cu and  $\text{T}_2$  phase in 8090 (Al-Li-Cu-Mg) alloy (24). Here the interface is acting as a high angle grain boundary. Precipitate-free zones can also result in certain circumstances when reaction takes place between reinforcement and matrix. An example of this has been found where magnesium from an Al-Cu-Mg (2618) alloy reacted with the silica-rich surface of  $\delta\text{-Al}_2\text{O}_3$  short fibres. The local removal of the magnesium from the matrix prevents the formation of the  $\text{S}(\text{Al}_2\text{CuMg})$  phase even though dislocations were available to assist with its nucleation.

## 5. MECHANICAL BEHAVIOUR AT ROOM TEMPERATURE

### Young's Modulus

Short fibres, whiskers and particles of high modulus ceramics produce improvements in the stiffness when added to metallic matrices. Whiskers and short fibres when preferentially oriented within the composite can promote enhanced stiffness in the direction of alignment. The modulus does not increase in a linear fashion with increasing volume fraction of discontinuous reinforcement as is the case with uniaxially aligned continuous fibres in a metallic or polymeric matrix, see fig. 13. This is influenced to some degree by the fibre aspect ratio and the orientation of each fibre relative to the test direction. Warner and Stobbs (30) have measured the modulus of SiC particle and whisker reinforced 2000 series alloy produced by extrusion from blended powder. The degree of alignment and aspect ratios were measured and tests carried out on samples taken at a number of orientations with respect to the alignment of the reinforcement. Predictions of modulus were also made from calculations of mean strain values associated with reinforcement and matrix using methods devised by Eshelby (31) for high volume fractions of elliptical inclusion in a metal matrix. Results and predictions are in good agreement for aspect ratios between 1 and 5 and for volume fractions up to 30%, see fig. 14.

The moduli achieved in all the aluminium matrix composites referred to in Table I exceed those of recently developed aluminium-lithium alloys (8090, 2090 etc.). However, additions of silicon carbide or alumina to aluminium alloys usually produce a small increase in density. Values of specific modulus of 33 GPa  $\text{m Mg}^{-1}$  are obtained with reinforced composites prepared from 2000, 6000 or 7000 series matrix alloys and these offer a small improvement over values for aluminium-lithium alloys ( $\approx 31.5$  GPa  $\text{m Mg}^{-1}$ ). It has been demonstrated that silicon carbide particles can be introduced into lithium-containing alloys such as 8090 and this produces specific modulus values closer to 40 GPa  $\text{m Mg}^{-1}$  which represents a 50% improvement over unreinforced 2000 series alloys.

### Yield Behaviour

Proof stress values are increased by the addition of 5% or more whiskers, short fibres and particles to a variety of matrix alloys, see Table I. There are instances where this property has shown small improvements with a variety of reinforcements, e.g.  $\delta$ - $\text{Al}_2\text{O}_3$  short fibres in Al-Mg or Al-Mg-Cu alloys and SiC particles in certain Al-Zn-Mg alloys. It is usual that an increase in proof stress takes place as the volume fraction increases from 5 to 20% whilst increases beyond 25% reinforcement are more marginal. Larger improvements in strength are usually encouraged by smaller particles and by lower strength alloy matrices. Work by Miller et al (11) has demonstrated that  $3\mu\text{m}$  particles can increase the 0.2% proof stress of an alloy by 60-70 MPa over a composite with  $23\mu\text{m}$  diameter particles, see fig. 15. Data in Table I also demonstrates that 10% particles of intermediate size ( $\approx 10\mu\text{m}$ ) are capable of improving a lower strength 6061 alloy by 60 MPa whilst 20% of fine particles ( $3\mu\text{m}$ ) only promote 80 MPa improvement in a higher strength 2124 alloy. Reasons for these changes in yield or proof stress are complex and relate to processing route, differential contraction between reinforcement and matrix, interfacial conditions as well as particle and matrix alloy characteristics. Such a situation can be simplified by considering two major contributions to the yield stress:-

- (a) residual thermal stresses, and
- (b) matrix strengthening effects.

The residual thermal stresses arise from the differential contraction and these can leave the matrix in tension prior to applying external load, thereby reducing the effective yield stress. A number of processes can relax the magnitude of the thermal stresses in the matrix, e.g. recovery. This ability diminishes as the temperature falls, particularly in higher strength alloys. Formation of certain types of matrix precipitation, e.g.  $\Theta$ -CuAl, in Al-Cu alloys can promote volume changes which may offset residual tensile stresses (25). Matrix strengthening processes rely on refinement of grain structures, increased dislocation densities, particularly if they are evenly distributed between the particles and fibres, and fine precipitation which may take place on dislocations or homogeneously within the matrix. All of these processes depend upon the manufacture route and the choice of particle size and volume fraction. As shown earlier, the grain size and dislocation contents are extremely dependent on these factors (17). The influence of fibre or particle aspect ratio and fibre orientation on yield stress is complex and attempts by Warner and Stobbs (30) to resolve this situation using the Eshelby model has proved to be only partially successful. Interfacial bonding between reinforcement and matrix might also be considered as being critical in this area in order to ensure effective load transfer. Results obtained by Warner and Stobbs (13), with clean and oxidised SiCp in an Al-Mg matrix, show differences in elastic modulus which can be explained in terms of enhanced bonding but this does not appear to influence the yield stress.

### Work Hardening

High rates of work hardening has been found to take place in all particle, whisker and short fibre reinforced MMCs immediately after yield. Contributions do arise from load transfer to the reinforcement most probably via Orowan dislocation loops. Humphreys (16) has calculated the work hardening rate for the particle case using the Brown and Stobbs equation (ref)

$$\tau = G' T V_f \epsilon \quad (3)$$

(where  $\tau$  is the matrix mean stress,  $G'$  the effective composite shear modulus,  $T$  is the Eshelby accommodation factor,  $V_f$  the particle volume fraction and  $\epsilon$  the strain on the composite). This calculation indicates a work hardening rate which is close to that measured immediately after yield. At higher strain rates where the work hardening rates in most composites begin to fall other mechanisms may become involved, these may include relaxation of Orowan loops and the generation of more dislocations. Gao and Harris (32) have compared the stress-strain plots (see fig. 16) and the work hardening rate in a short fibre and a particle-reinforced Al-4%Cu alloy matrix and this indicates a somewhat higher and sustained rate of work hardening with the fibres which have a larger aspect ratio. This would imply that more effective stress transfer to the reinforcement takes place and that relaxation does not take place until higher stresses are achieved.

### Tensile Strength

The breaking strength of discontinuous systems is dependent upon the type, aspect ratio, volume fraction and distribution of the reinforcement, the alloy and its heat treatment and the fibre or particulate-matrix bond. If short fibres or whiskers are aligned parallel to the loading direction, then their strength levels can be represented in terms of a modified rule of mixtures equation:-

$$\sigma_c^F = \sigma_f^F (1 - l_c/2l) V_f + \sigma_m^F V_m \quad (4)$$

where  $\sigma_m^F$  is the stress carried by the matrix at failure,  $l$  is the half length of the fibre, and  $l_c$  is the minimum fibre length that will be capable of carrying the fracture stress of the fibres,  $\sigma_f^F$  in the composite, it is given by:-

$$l_c = \frac{\sigma_f^F d}{T} \quad (5)$$

where  $d$  is the fibre diameter and  $\tau$  is the shear stress acting parallel to the fibre axis. When the lengths of fibres or whiskers are 10 times  $d$ , then the strength of the composite is over 90% of that of a continuous fibre-reinforced material assuming similar fibre strengths, etc. (33). Attempts have been made to align whiskers and short fibres without causing damage during the fabrication stage. This has been of limited success with short fibres which remain random in the plane of sheet or bar material, whilst more alignment has been achieved with whiskers in extrusion processes. Consequently with random reinforcement it is to be expected that strength levels will be reduced below those given by equation 4.

Strength values obtained with SiC whisker reinforced alloys has usually been superior to those achieved with  $\delta\text{-Al}_2\text{O}_3$  short fibre composites. Comparison between data obtained on the two forms of reinforcement when fabricated within a 6061 alloy matrix (T6 condition) reveals a 60% improvement in tensile strength for the whisker reinforcement above that achieved in the short fibre composite (34,35). SiC whiskers produce significant improvement in tensile strength in virtually all aluminium alloys and in many cases this can almost double the values achieved on the corresponding wrought matrix alloy. With extruded whisker materials differences in strengths are measured between samples tested longitudinal and transverse to the extrusion direction, e.g. 584 MPa compared with 480 MPa for a 20 vol.% SiC-6061 (T6) alloy. Particulate reinforced alloys again show improvement in tensile strengths over the unreinforced alloys. Strength increases tend not to be as high as whisker reinforcement particularly if there is some whisker alignment through extrusion processing. With the stronger 2000 series alloys in peak aged condition the improvement in strength is close to 25% as a result of adding 15-20% of reinforcing particles. Greater improvements in strength are achieved by reducing particle size and here strength increases approaching 10% can be achieved by using 3 $\mu\text{m}$  rather than 23 $\mu\text{m}$  particles (11), see fig. 15. It should be noted that some improvement in specific strength does take place when SiC whiskers or particles are added to aluminium alloys, these improvements are quite modest as the SiC raises the density of the composite.

Elongation to failure values are reduced quite markedly by the introduction of whiskers or fibres and values below 3% have been measured when the reinforcement levels exceed 10% by volume (27). Composites with short fibres show lower degrees of ductility than those with whisker reinforcement. Significant improvement in this property does take place when the aspect ratio and also the size of the reinforcement reduces. Elongation values approaching 10% are achieved with composites using 3 $\mu\text{m}$  diameter particles at a volume fraction approaching 20% provided the matrix is subjected to a T4 treatment rather than a peak age (11,29). This produces a composite with a higher tensile strength and elongation, i.e. ~600 MPa and 8.0% but with a comparatively low 0.2% proof stress of ~400 MPa. Use of a lower density lithium-containing matrix alloy (8090) has obvious attractions but problems still exist with the ductility levels when particles are added, even when the alloy is underaged (11,29).

#### Fracture

Fracture strain in discontinuous MMCs of all types varies between 0.7 and 10%. The lower values result from higher volume fractions of reinforcement with large aspect ratios, strong reinforcement-matrix interfacial bond strengths, strong matrix alloys and reinforcement with small failure strains. Examination of fracture surfaces reveals evidence of ductile failure of the matrix, failure at fibre-matrix interfaces and brittle fracture of the reinforcement.

Low strain to failure values have always been found where greater than 10 vol.% of short fibres have been introduced into low and high strength matrix alloys. In higher strength alloys (2618 Al-Cu-Mg) where a strong interfacial bond resulted from interaction between the magnesium in the alloy and the silica near the surface of  $\delta\text{-Al}_2\text{O}_3$  fibres the strains to failure were less than 1% and no effective strengthening of the alloy was obtained (36,37). Use of lower strength matrices, e.g. Al-4%Cu and reduced fibre-matrix bond strengths did promote higher strains to failure (2.2%) and thereby effective strengthening, see Table I. With the stronger bond, the associated larger aspect ratios of the fibres, and the problems of achieving stress relaxation in the matrix, the applied stresses are more efficiently transferred from matrix to the fibres and opportunities increase for the fibre to reach its breaking stress. If this takes place at numerous positions in the cross-section, e.g. in the fibre-rich area, the composite is weakened and the cracks propagate from the fibres across the strongly bonded interface into the matrix. In the more weakly bonded systems, e.g. Al-4%Cu, load is not as effectively transferred to the fibres and eventually, with increasing stress, the fibre-matrix bond breaks down at the ends of fibres aligned in the loading direction or at other positions around the fibre periphery when they are transverse to that direction.

Use of whisker reinforcement has produced a number of improvements in toughness when comparison is made with the short fibre systems referred to above. Nevertheless, Nieh et al (38) and Hesson et al (39) have shown that whisker materials are still notch sensitive. Extruded composites prepared from 20% by volume SiC in a 6061 (T6) alloy matrix give  $K_{IC}$  values of ~23 MPa $\sqrt{\text{m}}$  in the L-T direction whilst a similar system in the form of rolled plate gives values of 6-7 MPa $\sqrt{\text{m}}$  (40). The higher toughness found in the extruded material was explained in terms of the larger effective mean path between the whiskers due to the alignment. Changes in the root radius of the notch in the test samples also produced significant changes in  $K_{IC}$  values. The linear relationship between crack opening displacement at crack initiation and the root radius indicated that initiation was a strain-controlled process.

The role of the whisker-matrix interface has been shown to be crucial to the toughness of the material. It has already been demonstrated that the SiC-Al interfaces contain small oxide precipitates. These precipitates were found to be MgO in 6061 (Al-Si-Mg) alloy, see fig. 6. Nutt (41) was able to show that interfacial decohesion can take place at fibre ends or sides where a continuous oxide layer was present, initial fracture taking place within the oxide layer. However, examination of fracture surfaces in a variety of whisker reinforced alloys showed only minor evidence of oxide induced failure and a greater predominance of failure involving void nucleation and coalescence. It has also been demonstrated that whisker ends are sites of intense plastic flow at relatively low macroscopic strains. TEM examination showed that whiskers with flat ends caused more intense plastic straining in the matrix adjacent to 90° corners and this leads to void initiation in that region, see fig. 17. Growth of the voids involves the emission of matrix dislocations from the fibre ends (42). As soon as the voids nucleate at the corners they tend to grow inwards towards the centre of the whisker end. Voids approaching the whisker diameter (0.5μm) are formed and these are surrounded by large plastic zones which extend for several whisker diameters. As the number of voids build up at a number of whisker ends then the possibility of fracture initiation within the composite becomes greater.

With particle reinforcement the controlling factors in fracture are more complex. It is clear that fracture toughness decreases with increase in volume fraction of particles (43), as with whiskers, etc, see fig. 18. Particle size is also considered to be a major variable. Differences have been found on composite fracture surfaces where small particles (3-10μm) are not fractured whilst larger particles 20μm show significant numbers of particle fractures, see fig. 19. Experiments by Flom and Arsenault (43) on components with mean SiC particle sizes in the range 2-20μm in an 1100 series alloy have confirmed this situation and have shown two dimple populations; one associated with the SiC particles and the other small dimples situated between. A section through a sample with a partially propagated crack gives evidence of a series of short cracks ahead of the main crack, see fig. 20. These short microcracks appear to be associated with clusters of SiCp. Here, in these matrix regions, it is maintained that a high density of dislocations and a tensile triaxial state exist which encourages a plastic constraint. A measure was also made on crack initiation fracture toughness and crack growth fracture toughness. It was demonstrated that initiation toughness was independent of particle size at constant volume fractions up to 20μm diameter, but at 250μm diameter a reduction in toughness was measured, see fig. 21a. This was explained in terms of the high probability of flaws existing in the larger brittle particles which then permitted fracture at a lower stress intensity. Crack growth fracture toughness came from the tearing modulus of a J-integral versus average size of SiCp plot, see fig. 21b. An increase in this tearing modulus occurred with increasing particle size. Analysis of the many factors, e.g. crack deflection, plastic zone size, void formation, failed to show any dominant effect on crack initiation which is the case until particle fracture becomes more dominant at sizes >20μm. The increase in crack growth toughness with particle size is explained in terms of increase in plastic deformation as inter-particle spacings increase. Crack propagation, it is claimed, follows a pattern of microcrack formation ahead of the main crack. The main crack propagates when the microcracks are joined together by micro-void coalescence; this explains the dimpled pattern on the fracture surface. The crack front deviates around the small SiC particles. Miller et al (11) have demonstrated that there are benefits to the ductility and toughness of SiC particle reinforced 2124 alloys by the use of fine 3μm particle sizes provided care is taken to obtain good particle distributions in the matrix. Experiments by Hunt et al (28) on a 7000 series alloy with SiC particles of 16μm mean size showed that particle clustering helped to generate damage ahead of a blunt notch. These workers (28) also demonstrated that an underaged treatment given to the alloy did promote fractures in larger SiC particles ahead of the crack tip; this was not the case with the overaged matrix alloy. There is no definite evidence of SiC-matrix cracking in well produced particulate composites which does represent a different pattern to that found with fracture in whisker systems. The major problem with fine particle systems is the need for controlling the manufacturing systems so that good particle distribution can be guaranteed, thus preventing particle cluster and sites for lower stress intensity crack initiation.

## 6. MECHANICAL PROPERTIES AT ELEVATED TEMPERATURES

It has been demonstrated that MMCs containing particles, whiskers and short fibres do show improvements in modulus and strength at elevated temperature over unreinforced alloys (34,44). In the case of aluminium alloy matrices, composite strengths in excess of 200 MPa can be achieved at 300°C during short periods of exposure at this temperature, see Fig. 22. Comparative data for continuous fibre reinforced systems is also given on Fig. 22. Investigations have been made on more extended times at temperature and during thermal cycling and this has revealed certain dimensional instabilities. As the temperature rises, the internal stresses within the composites begin to relax. At temperatures above 250°C processes of recovery take place more quickly and have been shown up by techniques such as neutron diffraction analysis (23).

Humphreys (17) has suggested that a transition in mechanical behaviour takes place in the discontinuous composites when tested at temperatures in the range 200-300°C. Below the transition, high work hardening rates, high flow stresses and low ductilities are found. Above the transition, the work hardening rate reduces and increased ductilities become apparent. Thermally controlled diffusional relaxation of stresses around particles have been put forward as the reason for this transition. Dislocations associated with the particles begin to climb at the elevated temperature, so that they do not accumulate around the particles as deformation takes place.

Silicon carbide whisker ( $V_f = 20\%$ ) reinforced 2024 alloys have been stress rupture tested at 200°C and 300°C. At the higher temperatures these materials show that they can carry the same applied stress for a hundred times longer than the unreinforced 2024 alloy (45). Creep tests were also carried out on a similar type of composite material with the exception that the matrix alloy was 6061. The creep curves determined on specimens held at temperatures in the range 232-371°C had short primary, long steady state and negligible tertiary stages (46). The steady state creep rate with the composite is significantly lower than that found in the unreinforced alloy and the activation energy obtained from the data is three times greater than the activation energy for diffusion of aluminium. Lilholt and Taya (47) have confirmed that the stress sensitivity of such composites are larger than those associated with the matrix. Creep failure occurs in a ductile manner with no evidence of fibre failure.

At temperatures in excess of 500°C particulate composites begin to show evidence of grain boundary sliding. Under certain conditions, i.e. composites with small particles, 5 $\mu\text{m}$  in size and a fine matrix grain size  $<10\mu\text{m}$ , superplastic deformation of MMCs becomes possible (48). In the presence of large particles, coarse grains and higher strain rates (48), lower ductilities can result.

## 7. FATIGUE

Improvements in fatigue properties have been shown (7,49-51) to take place in a number of particle, whisker and short fibre composites. Where the reinforcement produces an increase in tensile strength it is usually that the fatigue strength, as indicated by stress amplitude versus number of cycle plots (S-N) will also be improved, particularly under low cycle conditions. Where tensile strengthening does not take place, as with certain short fibre 6-Al<sub>2</sub>O<sub>3</sub> composites, then the fatigue performance is below that of the unreinforced alloy under low cycle conditions, but begins to approach it at high cycle lives. With large monotonic strength improvements associated with whisker reinforced alloys, then greater improvement in fatigue has been found. Work has shown only a small increase in S-N curve behaviour if 10% by volume of 10 $\mu\text{m}$  SiC particles are added to 6061 and 2024 alloys, see fig. 23. Much greater improvements are found with 17 vol.% of 3 $\mu\text{m}$  SiC particles in a 2124 matrix (T4 condition), see fig. 24; this shows an improvement of  $\approx 140$  MPa over the unreinforced material when tested in a similar condition at 10<sup>6</sup> cycles. The tensile strength is raised by  $\approx 200$  MPa as a result of making this kind of particle addition.

From observations made on fracture surfaces and on samples subjected to cyclic loading in a four point bend test rig, it appears that in weakly bonded short fibre systems, cracks initiate at either fibre-matrix interfaces or at interfaces involving larger (25 $\mu\text{m}$ ) ceramic particles (shot) which are included on a random basis from the fibre production route. The multiple cracks grow into the matrix and then coalesce as the number of cycles increases. In the more strongly bonded systems, the large shot particles crack and initiate fatigue cracks in the matrix at relatively low cyclic plastic strains. The cracks then continue to grow through fibre and matrix at crack growth rates which exceed those determined on the unreinforced matrix at all values of  $\Delta K$ .

Williams and Fine (52) have carried out a study of microcrack initiation and growth on silicon carbide-whisker-reinforced 2124 alloy under cyclic loading conditions. Crack initiation occurred at the poles of the SiC whiskers after a certain number of cycles. Propagation then proceeded down the fibre-matrix interface provided that it was favourably oriented to the stress direction. These observations correspond to those made on static fracture test specimens. The density of cracks increased quite rapidly (to 10<sup>9</sup>/m<sup>2</sup>) after a few hundred stress cycles in appropriate stress-cycle ranges. Crack lengths then increased with the number of cycles while the number of cracks decreased. Comparisons of whisker reinforced 2124 alloy with the unreinforced material revealed that the composite had crack growth rates that were slower than those observed in the alloy. It was noted that the unreinforced material was able to sustain cracks which were 500 $\mu\text{m}$  long at peak cycle stress close to its yield stress whilst the composite could only maintain a crack of 30 $\mu\text{m}$  length at a stress which was 60% of its yield stress. Improvement in long crack growth resistance occurred at low  $\Delta K$  values and when the crack was propagating normal to the fibres aligned by the extrusion process during fabrication. At high  $\Delta K$  values, the crack growth rates in the composite exceeded those in the matrix, thus supporting the fracture-toughness observations.

Crack initiation studies on fine SiCp (3 $\mu\text{m}$ ) reinforced alloys have been carried out (53). It has been observed that cracks did not begin to propagate until after the specimen had received a large number of cycles at high stress levels. The cracks were found to initiate in very discrete regions where particle clustering was found, see fig. 25. Within the particle clusters evidence of matrix voidage was found and it was from such a region that a crack began eventually to grow into the matrix. Shang and Ritchie (54) have determined fatigue crack growth rates on a composite containing 15 vol.% of 16 $\mu\text{m}$  SiCp. This showed poorer crack growth resistance at low  $\Delta K$  values than the unreinforced alloy, improvement at intermediate  $\Delta K$  and, at high  $\Delta K$ , the pattern reverted back in favour of the unreinforced alloy. Evidence was found of SiC particle cracking ahead of the main crack growth front when high  $\Delta K$  values were imposed. The particles which had cracked were not aligned with the main crack and therefore crack ligaments were formed which required linking for further propagation of the main crack. This promoted slower effective crack growth rates at given  $\Delta K$ . Further work (55) on the effect of particle size on crack propagation rates has shown that fine particles (5 $\mu\text{m}$ ) give an inferior performance closer to threshold than coarse particles (16 $\mu\text{m}$ ) when the load ratio  $R = K_{min}/K_{max}$  is 0.1. At intermediate and high  $\Delta K$  values there is little difference between

coarse and fine particle reinforced 7000 series alloys. Raising  $R$  to 0.75 does promote a significant change in the order of these plots near threshold. Now the fine particle composites have the superior results and are more able to resist crack growth propagation at low  $\Delta K$  values. This is explained in terms of crack closure effects whereby the coarse particles become exposed on the fracture surface and thereby produce changes in  $K_{min}$ . In these circumstances the crack tip is shielded from the full range of  $\Delta K$  and crack growth slows down. Fine particles do not promote the same levels of closure and the cracks continue to grow more quickly. At higher values of  $R$  closure is not influential and therefore crack propagation with the coarse particle system is faster.

Overall fatigue behaviour of MMCs appears to be controlled by particle sizes. The presence of larger  $25\mu m$  particles in the  $\delta\text{-Al}_2\text{O}_3$  composites was a key feature in initiating cracks either by particle cracking with a strong interfacial bond or by interface debonding with a weak bond. In coarse particulate composites the possibility of particle cracking remains, particularly if the particle sizes are  $>20\mu m$ . With fine particles clustering becomes more of a problem and initiation takes place within such arrangements. Crack propagation is also influenced by particle size but in this case coarse particles may be more influential in that they cause closure problems and consequentially greater crack propagation resistance results, particularly at low  $\Delta K$  values. At intermediate and high  $\Delta K$  values particle sizes do not influence crack growth. The presence of the particles at high  $\Delta K$  values does reduce crack growth resistance when  $da/dN$  vs.  $\Delta K$  plots are compared with the unreinforced alloy equivalents. This might be expected with the kind of fracture toughness behaviour of these composites which has been described earlier.

## 8. THERMAL PROPERTIES

With the majority of ceramic fibre or particle reinforced materials there is a significant difference in thermal expansion coefficient between reinforcement and aluminium alloys. It has already been indicated earlier that  $\delta\text{-Al}_2\text{O}_3$  short fibres have one quarter of the expansion coefficient of aluminium whilst the difference is greater in the case of  $\alpha\text{-SiC}$  ( $3.8 \times 10^{-6}/K$ ) and aluminium ( $23 \times 10^{-6}/K$ ). The resultant coefficient for the composite depends upon the volume fraction of the reinforcement and in the case of short fibres or whiskers any alignment patterns will also influence the values. Fig. 28 demonstrates the change in the value of the coefficient in the temperature range 0-170°C which has taken place by the addition of 20%  $\delta\text{-Al}_2\text{O}_3$  short fibres to an Al-4%Cu alloy. The fibres here are arranged randomly in the plane and measurements were made parallel to that plane. Dinwoodie et al (34) have demonstrated in a similar system that the value of the coefficient begins to change in a linear manner with increasing fibre volume fraction but as  $V_f$  increases above 12% the change occurs at a slower rate. It is also to be noted that processes such as precipitation of a second phase, recovery or other stress relieving processes in the matrix may influence the expansion characteristics of the composite. Several workers (56,57) have noted a large enhanced creep deformation during thermal cycling SiC particulate and whisker reinforced aluminium under load. This cycle behaviour occurs without early void nucleation and fracture and also without changing the dislocation substructure from cycle to cycle. It is concluded by Pickard and Derby (57) that a mechanism must exist which allows recovery of the dislocations which have been generated during straining.

The introduction of discontinuous ceramic reinforcement into metal matrix reduced its thermal conductivity. The amount of the reduction depends on the volume fraction shape and distribution of the reinforcement. Taya (58) has attempted to model this and other physical properties associated with short fibres with some success. The model is based upon Eshelby's model for elastic behaviour.

## 9. CORROSION BEHAVIOUR

A limited number of corrosion studies (59-61) have been carried out on fibre and particulate-reinforced aluminium alloys. The level and type of corrosion attack in chloride solutions depends on type of reinforcement, the presence of reinforcement-matrix interfaces and the type of alloy and its heat-treated condition when the reinforcement is a noble phase, e.g. SiC, then the level of attack is increased (59). Regions where SiC particles are clustered do enhance the level of attack and there is also evidence of attack at particle-matrix interfaces in certain alloy systems. Much remains to be done before an accurate assessment can be made of the influences of alloy type, processing and heat-treatment on corrosion properties.

## 10. SUMMARY

Although work has been carried out on discontinuous metal matrix composites for the past ten years or more, effective understanding of their behaviour has become apparent only in the past two to three years. In reviewing the work which has been carried out on a range of reinforcements (short fibres, whiskers and particles), it is now possible to show some of the influences of reinforcement size and shape on a range of mechanical properties. Because a degree of randomness is introduced into short fibre and whisker reinforced materials then enhanced directional mechanical properties are difficult to realise. Such reinforcements also can initiate fracture at lower strains and smaller levels of ductility than is the case with more equiaxed particles. This deleterious behaviour is controlled in part by the nature of the interfaces between reinforcement and matrix. Recent work with small particle reinforcements ( $\sim 3\mu m$  diameter) has provided some encouraging results; this does depend on their effective dispersion in the matrix. When more even distribution does occur then higher ductility levels, better toughness and improved resistance to fatigue crack initiation may result.

Much of the effort on these MMCs has turned around a range of aluminium alloys. Frequent use has been made of 2000, 6000 and 7000 alloy matrices to produce higher modulus and strength results. Unfortunately, the use of SiC particles or whiskers in these alloys does increase the density of the resultant composites. Attempts to use a lithium-containing alloy are considered to be important from a weight reduction viewpoint. It is then possible to produce significant improvements in the specific properties of MMCs if these alloys are employed. Magnesium and titanium matrix alloys could benefit from the introduction of a suitable form of reinforcement. However, significant progress in these areas is being held up by the need for a more corrosion-resistant magnesium alloy and the development of an effective way of preventing damaging reactions between titanium and most forms of reinforcement.

#### ACKNOWLEDGEMENTS

The author is indebted to his colleagues, Dr. B. Noble, Mr. K. Dinsdale, Mr. Y. Gao, Mr. P. Weatherburn and Mr. J. Williams, for providing data for this paper. He would also like to thank Dr. J. White of Alcan International, Banbury, and Dr. W.S. Miller of BP Research Ltd., Sunbury-on-Thames, for provision of materials and general support.

#### REFERENCES

1. C.A. Stubbington, "Materials trends in military airframes", *Metals and Materials*, 4, 1988, pp. 424-431.
2. G.A. Chadwick and P.J. Heath, "Machining metal matrix composites", *Metals and Materials*, 6, 1990, pp. 73-77.
3. J. White, I.G. Palmer, I.R. Hughes and S.A. Court, "Development of metal matrix composite systems based on aluminium-lithium", in *Aluminium-Lithium V* edited by E.A. Starke, Jr. and T.H. Sanders, Jr., 1989, M.C.E.P. Ltd., Birmingham, pp. 1635-1646
4. S.J. Harris, "Short fibre and particulate metal matrix composites", in 'New Light Alloys', Conference Proceedings No. 444, AGARD, Mierlo, 1988, paper 25, pp. 1-13.
5. Y. Abe, S. Horikiri, K. Fujimura and E. Ichiki, in Proc. Fourth Int. Conf. on 'Composite Materials', ICCMIV (ed. T. Hayashi et al), 1982, Japanese Society for Composite Materials, Tokyo, pp. 1315-1322.
6. T.W. Clyne and M.G. Bader, in Proc. Fifth Int. Conf. on 'Composite Materials', ICCMV (ed. W.C. Harrigan, Jr. et al), 1985, AIME, Philadelphia, PA, pp. 755-771.
7. S.V. Nair, J.K. Tien and R.C. Bates, "SiC reinforced aluminium metal matrix composites", *Int. Met. Rev.*, 30, 1985, pp. 275-290.
8. D.J. Lloyd, "The solidification microstructure of particulate reinforced aluminium-SiC composites", *Composite Science and Technology*, 35, 1989, pp. 159-179.
9. G.G. Levi, C.J. Abbashchian and R. Mehrabian, in Proc. Workshop on 'Rheocasting', 1978, Battelle, Columbus, OH, pp. 41-54.
10. T.C. Willis, J. White, R.M. Jordan and I.R. Hughes in Third Int. Solidification Processing Conference, 1987, University of Sheffield, pp. 21-24.
11. W.S. Miller, L.A. Lenssen and F.J. Humphreys, "The strength, toughness and fracture behaviour in aluminium-lithium based metal matrix composites", in *Aluminium-Lithium V*, ed. by E.A. Starke, Jr. and T.H. Sanders, Jr., 1989, M.C.E.P. Ltd., Birmingham, pp. 931-941.
12. P.J. Bridges, J.W. Brooks and P.S. Gilman, Proc. Conf. on Advanced Materials Research and Development for Transport, 1985, Strasbourg, p. 85.
13. T.J. Warner and W.M. Stobbs, "Clean or dirty interfaces? The influence of interfacial morphology on the mechanical properties of MMCs", in *ICCMVII*, vol. 1, ed. by Wu Yunshu et al, Pergamon Press, Beijing, 1989, pp. 503-508.
14. H.J. Dudek, R. Leucht and G. Ziegler, Proc. Fifth Int. Conf. on Titanium, Munich, vol. 4, 1984, p. 1773.
15. D.G. Konitzer and M.H. Loretto, "Interfacial interactions in titanium-based metal matrix composites", *Materials Science and Engineering*, A107, 1989, pp. 217-223.
16. C.A. Stanford-Beale and T.W. Clyne, "Deformation of fibrous metal matrix composites at temperatures close to the matrix solidus", in 9th Riso Int. Symposium on Metallic and Ceramic Composites (ed. S.I. Andersen et al), 1988, Riso National Laboratory, pp. 479-484.
17. F.J. Humphreys, "Deformation and annealing mechanisms in discontinuously reinforced metal matrix composites", *ibid*, pp. 51-74.
18. A.W. Bowen and F.J. Humphreys, "Texture development in aluminium alloy-SiCp metal matrix composites", Conf. on MMC: Property Optimisation and Applications, Institute of Metals, 1989, paper 22.

19. C.A. Stanford-Beale and T.W. Clyne, "Extrusion and high temperature deformation of fibre reinforced aluminium", *Composite Science and Technology*, 35, 1989, pp. 121-157.
20. V.C. Nardone and K.M. Prewo, "On the strength of discontinuously reinforced aluminium composites", *Scripta Met.*, 20, 1986, pp. 43-48.
21. M. Taya and R.J. Arsenault, "Comparison between shear lag model and Eshelby model in predicting mechanical properties of short fibre composites", *Scripta Met.*, 21, 1987, pp. 349-354.
22. T. Mori and K. Tanaka, "Average stresses in matrix and elastic energy of materials with misfitting inclusions", *Acta Met.*, 21, 1973, pp. 571-574.
23. P.J. Withers, D. Juul Jenson, H. Lilholt and W.M. Stobbs, "Evaluation of internal stress in short fibre reinforced MMC by neutron diffraction", in Proc. Sixth Int. Conf. on 'Composite Materials', ICCMVI (ed. by F.L. Matthews et al), vol. 2, 1987, Elsevier, London, pp. 255-263.
24. P.B. Prangnell and W.M. Stobbs, "The effect of SiC particulate reinforcement on the ageing behaviour of aluminium based matrix alloys", in ICCM VII, vol. 1, ed. by Wu Yunshu et al, Pergamon Press, Beijing, 1989, pp. 573-578.
25. S.J. Harris, S.F. Moustafa and T.E. Wilks, presented at Conf. on 'Metal Matrix Composites: Structures and Property Assessment', 1987, Institute of Metals, London.
26. T. Christmas and S. Suresh, "Microstructural development in an aluminium alloy-SiC whisker composite", *Acta Met.*, 36, 1988, 1691-1704.
27. D.L. McDanel, "Mechanical behaviour of aluminium matrix composites containing SiC reinforcement", *Metall. Trans. A*, 16, 1985, pp. 1105-1115.
28. J.J. Lewandowski, C. Lui and W.H. Hunt, Jr., "Effects of matrix microstructure and particle distribution on fracture of an aluminium metal matrix composite", *Materials Science and Engineering*, A107, 1989, pp. 241-255.
29. C.J. Peel, R. Moreton and S.M. Flitcroft, "The optimisation of isotropic metal matrix composites for aerospace use", to be published.
30. T.J. Warner and W.M. Stobbs, "Modulus and yield stress anisotropy of short fibre metal matrix composites", *Acta Met.*, 37, 1989, pp. 2873-2882.
31. J.D. Eshelby, *Proc. R. Soc.*, 252A, 1959, p. 561.
32. Y. Gao and S.J. Harris, to be published.
33. A. Kelly and W.R. Tyson, in 'High Strength Materials', ed. by V.F. Zackay, John Wiley and Sons, New York, 1965, p. 578.
34. J. Dinwoodie, B. Moore, C.A.J. Lanigan and W.R. Symes in Proc. Fifth Int. Conf. on 'Composite Materials', ICCMV (ed. W.C. Harrigan et al), 1985, AIME, Philadelphia, PA, pp. 671-685.
35. R.J. Arsenault and M. Taya, in Fifth Int. Conf. on 'Composite Materials', ed. by W.C. Harrigan et al, AIME, Philadelphia, 1985, pp. 21-36.
36. S.J. Harris, 'Cast Metal Matrix Composites', *Materials Science and Technology*, 4, 1988, pp. 231-239.
37. S.J. Harris, 'Fibre Reinforced Aluminium Alloys', Chap. 9 in *Aluminium Alloys - Contemporary Research and Applications*, ed. by A.K. Vasudevan and R.D. Doherty, Academic Press, San Diego, 1989, pp. 256-294.
38. T.G. Nieh, R.A. Rainen and D.J. Chellman, in Fifth Int. Conf. on 'Composite Materials', ed. by W.C. Harrigan et al, AIME, Philadelphia, 1985, pp. 825-842.
39. D.F. Hasson, S.M. Hoover and C.R. Crowe, *J. Mater. Sci.*, 20, 1985, p. 4147.
40. C.R. Crowe, R.A. Grey and D.F. Hasson, in Fifth Int. Conf. on 'Composite Materials', ed. by W.C. Harrigan et al, AIME, Philadelphia, 1985, pp. 843-866.
41. S.R. Nutt, "TEM characterisation of aluminium-based composites", Chapter 13 in *Aluminium Alloys - Contemporary Research and Applications*, ed. by A.K. Vasudevan and R.D. Doherty, Academic Press, San Diego, 1989, pp. 389-409.
42. T. Christmas, A. Needleman, S. Nutt and S. Suresh, "On microstructural evolution and micromechanical modelling of deformation of a whisker reinforced metal matrix composite", *Materials Science and Engineering*, A107, 1989, pp. 49-61.
43. Y. Flom and R.J. Arsenault, "Effects of particle size on fracture toughness of SiC/Al composite materials", *Acta Met.*, 37, 1989, pp. 2413-2423.
44. W.H. Hunt, O. Richmond and R.D. Young, "Fracture in particle hardened materials with

- high volume fractions", in Proc. Sixth Int. Conf. on 'Composite Materials', ICCMVI (ed. F.L. Matthews et al), vol. 2, 1987, Elsevier, London, pp. 209-233.
45. H.J. Rack, T.R. Baruch and J.L. Cook, in Proc. Fourth Int. Conf. on 'Composite Materials', ICCMIV, (ed. T. Hayashi et al), 1982, Japanese Society for Composite Materials, Tokyo, pp. 1471-1485.
46. T.G. Nieh, "Creep rupture of a silicon carbide reinforced aluminium composite", Met. Trans., 15A, 1984, pp. 139-146.
47. H. Lilholt and M. Taya, "Creep behaviour of the metal matrix composite Al2124 with SiC fibres", in Proc. Sixth Int. Conf. on 'Composite Materials', ICCMVI (ed. F.L. Matthews et al), vol. 2, 1987, Elsevier, London, pp. 234-244.
48. M.W. Mahoney and A.K. Ghosh, "Superplasticity in high strength powder alloys with and without SiC reinforcement", Met. Trans. 18A, 1987, 1987, pp. 653-661.
49. S.J. Harris and T.E. Wilks, "Tensile and fatigue behaviour of alumina-reinforced Al alloys at ambient and elevated temperatures", in Fibre Reinforced Composites, 1986, Institute of Mechanical Engineers, London, pp. 19-28.
50. S.J. Harris and T.E. Wilks, "Fatigue crack growth in discontinuous fibre reinforced aluminium alloys", in Proc. Sixth Int. Conf. on 'Composite Materials', ICCMVI, vol. 2, Elsevier, London, pp. 113-126.
51. S.J. Harris, K. Dinsdale, Y. Gao and B. Noble, "Influence of heat-treatment on the monotonic and fatigue properties of aluminium alloy composites", in 9th Riso Int. Symposium on Metallic and Ceramic Composites (ed. S.I. Andersen et al), 1988, Riso National Laboratory, pp. 373-382.
52. D.R. Williams and M.E. Fine, in Fifth Int. Conf. on 'Composite Materials', ed. by W.C. Harrigan Jr. et al, AIME, Philadelphia, 1985, pp. 639-670.
53. Y. Gao and S.J. Harris, to be published.
54. J.K. Shang and R.O. Ritchie, "Crack bridging by uncracked ligaments during fatigue-crack growth in SiC-reinforced Al alloy composites", Met. Trans. A, 20A, 1989, p. 897.
55. J.K. Shang and R.O. Ritchie, "On the particle size dependence of fatigue crack propagation thresholds in SiC-particulate-reinforced aluminium alloy composites: role of crack closure and crack trapping", Acta Met., 37, 1989, pp. 2267-2278.
56. M.Y. Wu and O.D. Sherby, "Superplasticity in a silicon carbide whisker reinforced aluminium alloy", Scripta Met., 18, 1984, pp. 773-776.
57. S.M. Pickard and B. Derby, "Thermal cycle creep of Al/SiC particulate composite", in 9th Riso Int. Symposium on Metallic and Ceramic Composites (ed. S.I. Andersen et al), 1988, Riso National Laboratory, pp. 447-452.
58. M. Taya, "Modelling of physical properties of metallic and ceramic composites: generalised Eshelby model", ibid, pp. 201-231.
59. R.C. Paciej and V.S. Agarwala, "Influence of process variables on the corrosion susceptibility of metal matrix composites", Corrosion, 44, 1988, pp. 680-684.
60. P.P. Trzaskoma and E. McCafferty, "Corrosion behaviour of SiC/Al matrix composites", J. Electrochem. Soc., 130, 1984, pp. 1804-1809.
61. D.M. Aylor and P.J. Moran, "Effect of reinforcement on the pitting behaviour of aluminium based MMC", 132, 1986, pp. 1277-1281.

**TABLE I**  
**Tensile Properties of Metal Matrix Composites**

Material	Fabrication Method & Form	Young's Modulus (GPa)	0.2%PS (MPa)	U T S (MPa)	Elongation (%)	Fracture Toughness (MPa <sup>1/2</sup> )
Al-Cu	squeeze cast	70.5	174	261	14.0	-
Al-Cu+Al <sub>2</sub> O <sub>3</sub> (V <sub>f</sub> =0.2 fibre)	squeeze cast	95.4	238	374	2.2	-
Al-Cu-Mg (T6) (2014)	spray formed sheet	73.8	432	482	10.2	-
Al-Cu-Mg+SiC (T6) (V <sub>f</sub> = 0.1, 10μm particle)	spray formed sheet	93.8	437	484	6.9	-
Al-Cu-Mg (T4) (2124)	powder rolled plate	72.4	360	525	11.0	-
Al-Cu-Mg+SiC (T4) (V <sub>f</sub> = 0.17, 3μm particle)	powder rolled plate	99.3	420	610	8.0	18
Al-Cu-Mg (T6) (2124)	powder rolled plate	73.1	425	474	8.0	26
Al-Cu-Mg+SiC (T6) (V <sub>f</sub> = 0.17, 3μm particle)	powder rolled plate	99.6	510	590	4.0	17
Al-Si-Mg (T6) (6061)	spray rolled sheet	69.0	240	264	12.3	-
Al-Si-Mg+SiC (T6) (V <sub>f</sub> = 0.1, 10μm particle)	spray rolled sheet	91.9	321	343	3.8	-
Al-Zn-Mg-Cu (T6) (7075)	spray formed extrusion	71.1	617	659	11.3	-
Al-Zn-Mg-Cu+SiC (T6) (V <sub>f</sub> =0.12, 10μm particle)	spray formed extrusion	92.2	597	646	2.6	-
Al-Li-Cu-Mg (T6) (8090)	spray formed plate	79.5	420	505	6.5	38
Al-Li-Cu-Mg+SiC (T6) (V <sub>f</sub> =0.17, 3μm particle)	spray formed plate	104.5	510	550	2.0	-

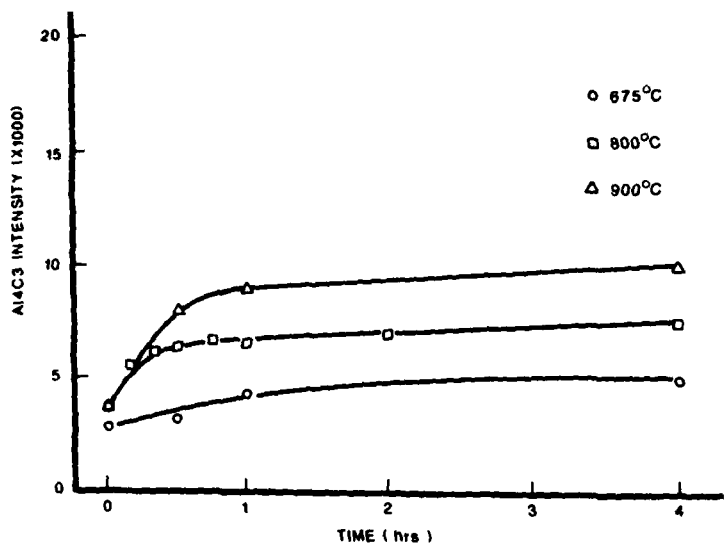


Fig. 1. Variation in Al<sub>4</sub>C<sub>3</sub> X-ray peak intensity with time at different levels of superheat for a stir cast 2014-20 vol. % SiCp composite (after Ref. 8).

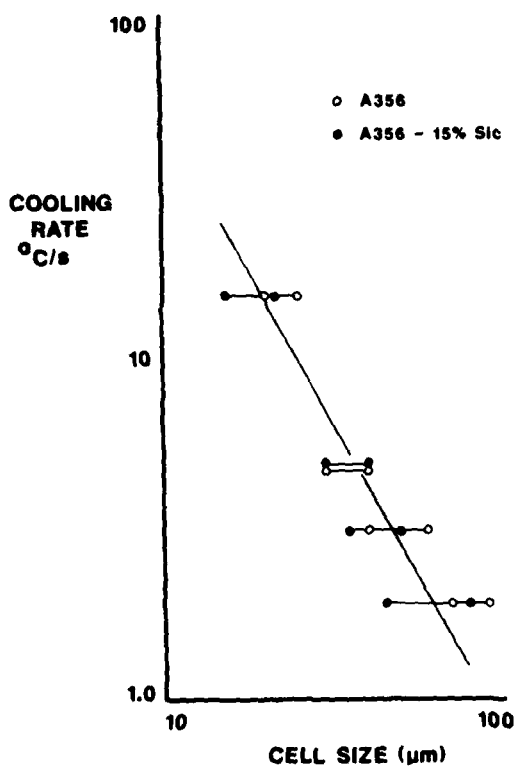


Fig. 2. Relationship between as-solidified cell size for a stir cast A356 alloy with and without the addition of 15% SiC particles and the cooling rate applied to the casting (after Ref. 8).

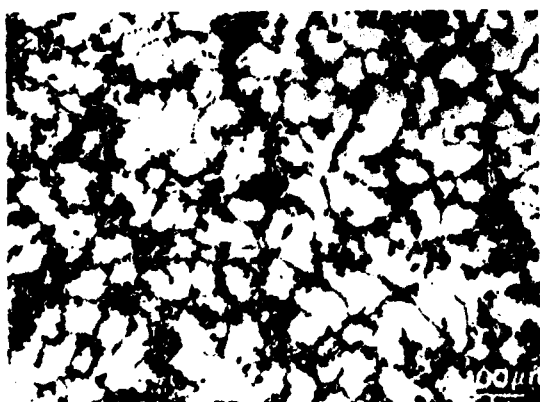


Fig. 3. Microstructure of an A356 alloy with 15 vol. % SiCp produced by stir casting and subsequently cooled at a rate of 1°C/s. Note the uneven dispersion of SiCp (after Ref. 8).

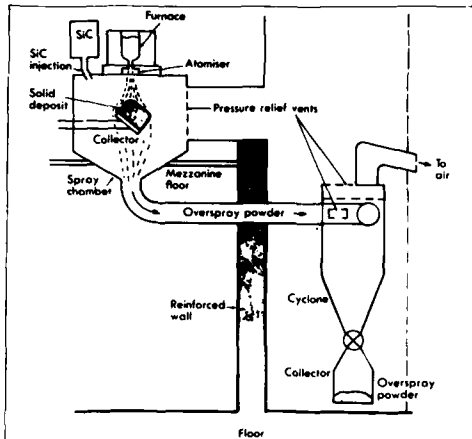


Fig. 4. Spray forming of metal matrix composite (after Ref. 3).



Fig. 6. End-on view of SiC whiskers in 2124 Al alloy showing oxide particles clustering along the interface (after Ref. 41).

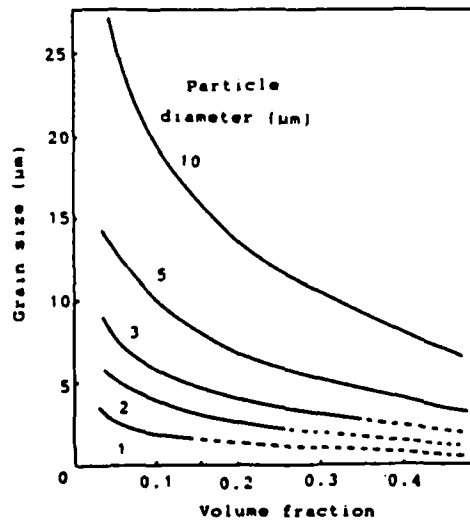


Fig. 7. Predicted recrystallised grain size as a function of particle size and volume fraction. Recrystallisation will not probably occur in the dotted regions (after Ref. 17).

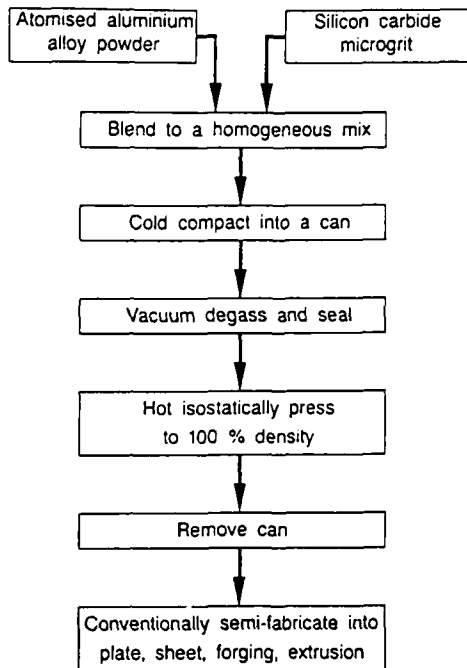


Fig. 5. Processing route for metal matrix composite using powder metallurgy technology (after Ref. 11).

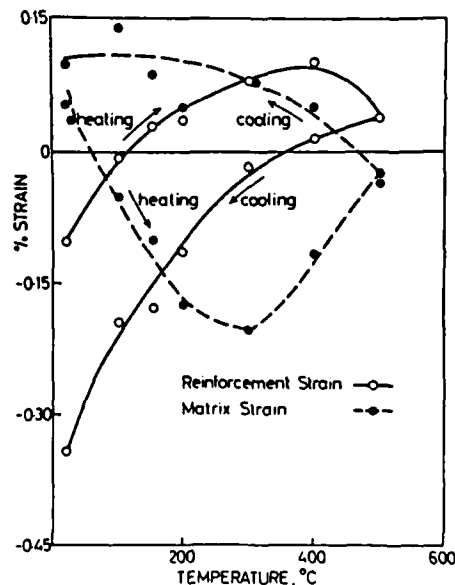


Fig. 8. Mean longitudinal strain values obtained on an (a) aluminium matrix, and (b) silicon carbide whisker reinforcement during a heating and cooling cycle (after Ref. 23).

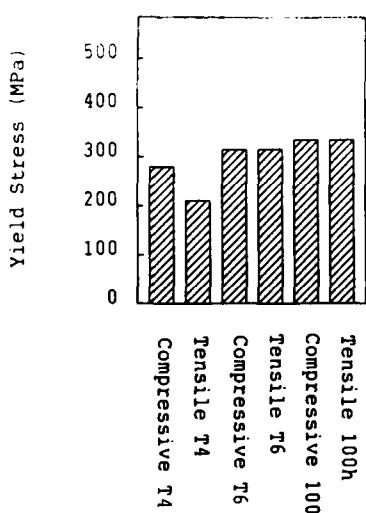


Fig. 9. Compressive and tensile yield stress in an  $\delta\text{-Al}_2\text{O}_3$  reinforced Al-4%Cu alloy after natural (T<sub>4</sub>) and artificial ageing (T<sub>6</sub>).

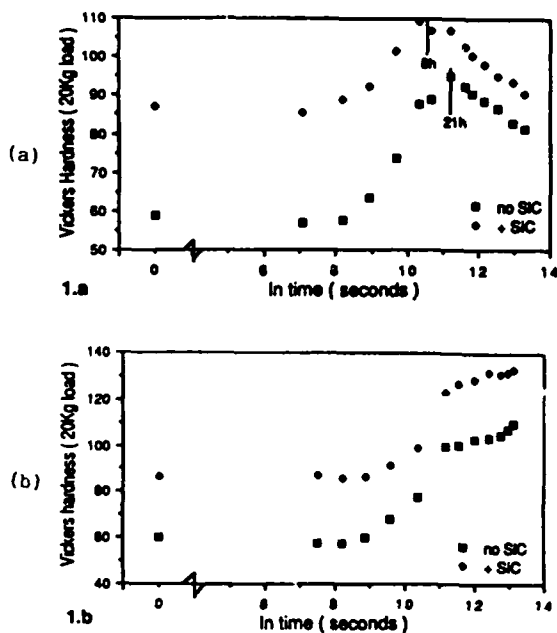


Fig. 10. Ageing curves for a 10%SiCp reinforced Al-4.3%Cu alloy and the same alloy without reinforcement (a) aged at 195°C and (b) aged at 135°C (after Ref. 24).

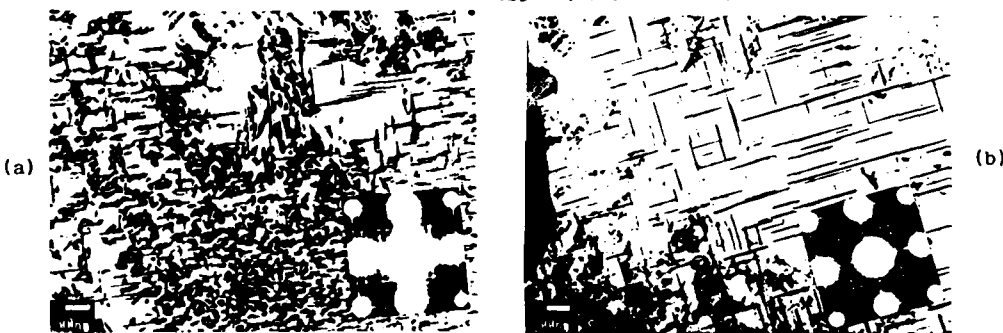


Fig. 11. TEM micrographs of an Al-4.3% matrix alloy (a) without reinforcement and (b) reinforced with 10% SiCp. Sample (a) has mainly  $\theta''$  precipitation and sample (b)  $\theta'$  precipitation although both samples were aged for 19h at 195°C (after Ref. 24).

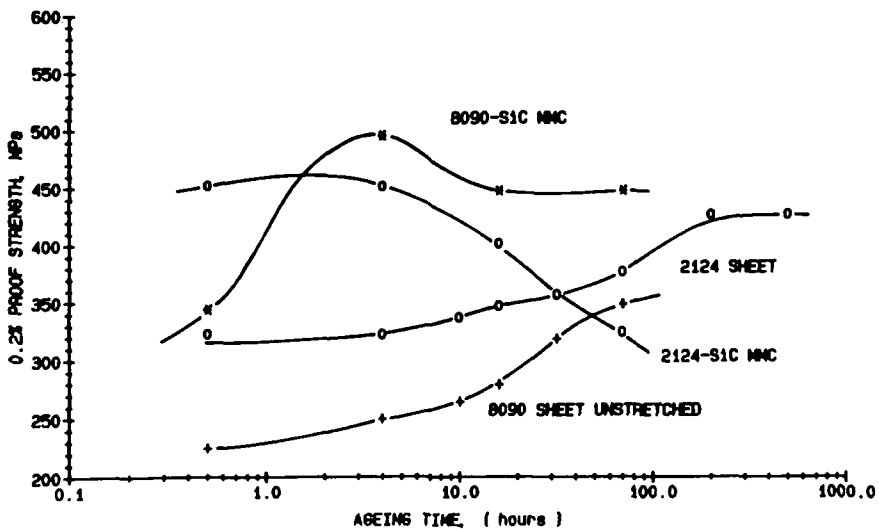


Fig. 12. 0.2% proof stress values obtained on 2124 (Al-Cu-Mg) and 8090 (Al-Li-Cu-Mg) alloy in sheet form both with and without 20% SiCp reinforcement (after Ref. 29).

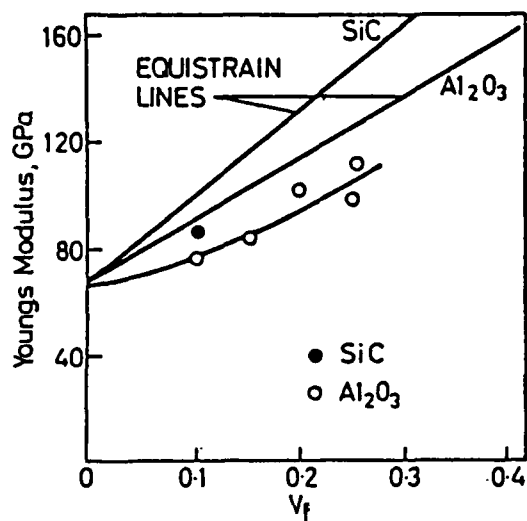


Fig. 13. Young's modulus values,  $E$ , determined on aluminium alloys reinforced with  $\delta\text{-Al}_2\text{O}_3$  and  $\alpha\text{-SiCp}$ ; comparisons are made with plots obtained from Rule of Mixtures equation which assume equal strain in matrix and reinforcement (after Ref. 36).

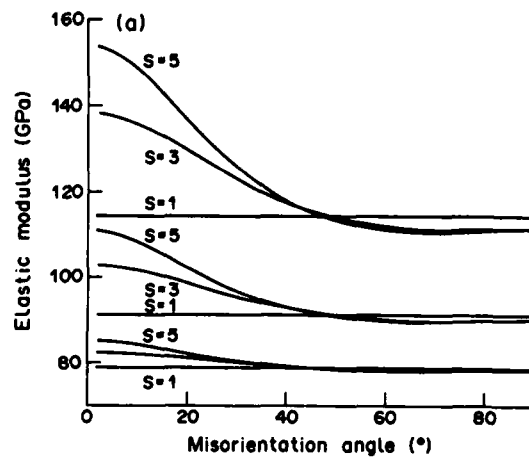


Fig. 14. Elastic modulus values predicted for different aspect ratios of 1, 3 and 5 for volume fractions of 30% (highest plot), 15% (middle plot) and 5% (lowest plot) of SiC reinforcements at different misorientation angles (after Ref. 30).

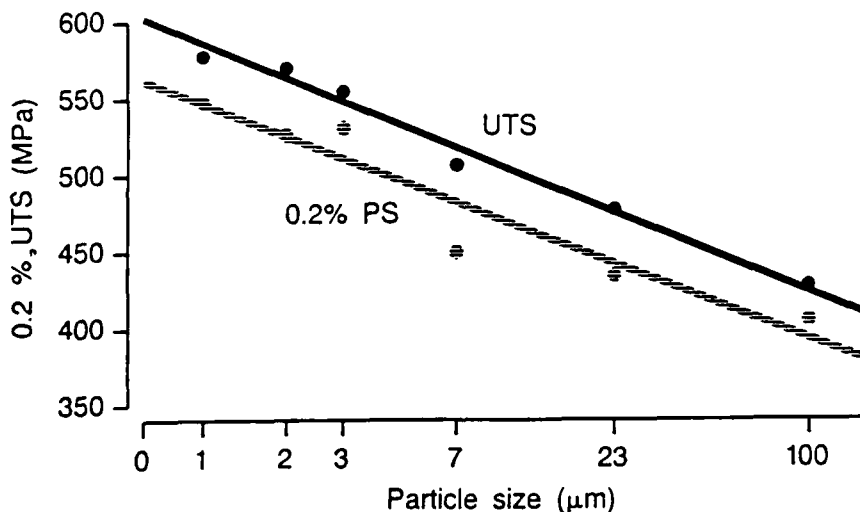


Fig. 15. The effect of SiCp size on the proof stress and tensile strength of a series of composites each containing 20% by volume of reinforcement (after Ref. 11).

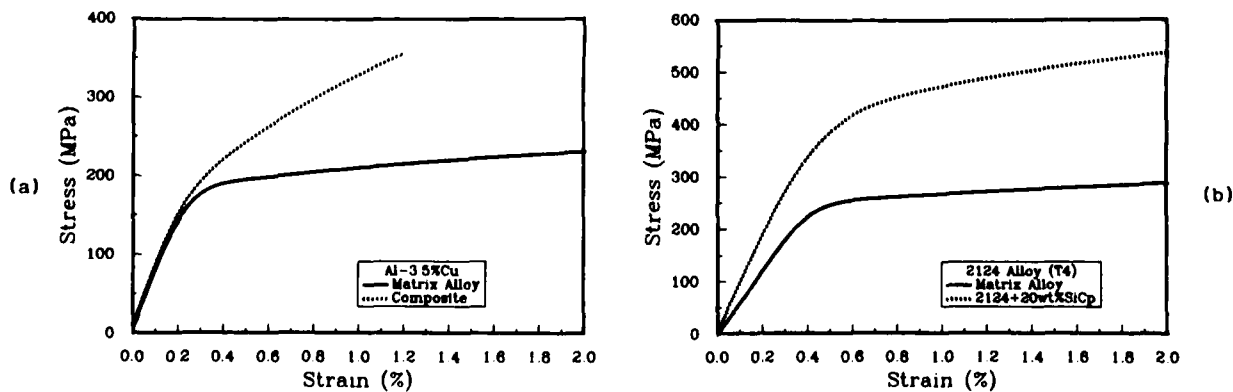


Fig. 16. The shape of stress-strain plots for (a) an Al-3.5%Cu alloy with and without 20% by vol. of  $\delta\text{-Al}_2\text{O}_3$  short fibres and (b) 2124 alloy with and without 20 wt.% SiC (=17 vol.%) particles.



Fig. 17. Void nucleation at whisker end near fracture surface in tensile fracture specimen of an artificially aged 6061 Al-Si Cw composite (after Ref. 41).

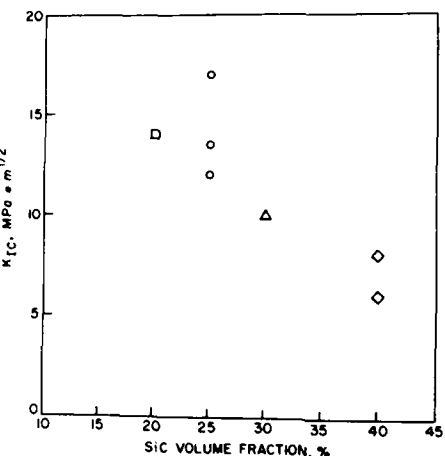


Fig. 18. Fracture toughness as a function of SiC volume fraction for a SiCp/Al composite (after Ref. 43).

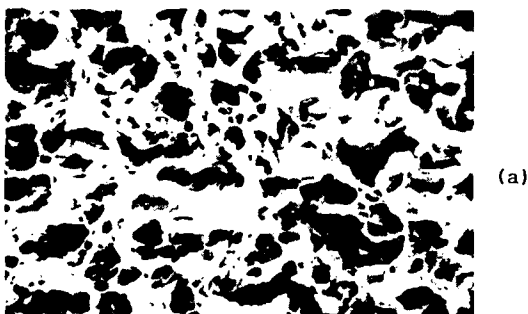


Fig. 19. Fracture surface of (a) 3.2  $\mu\text{m}$  and (b) 20  $\mu\text{m}$  average particle size SiC/Al composite (after Ref. 43).

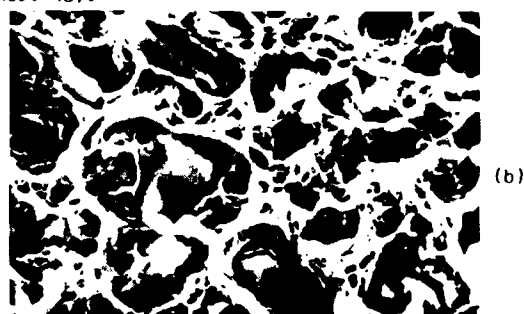
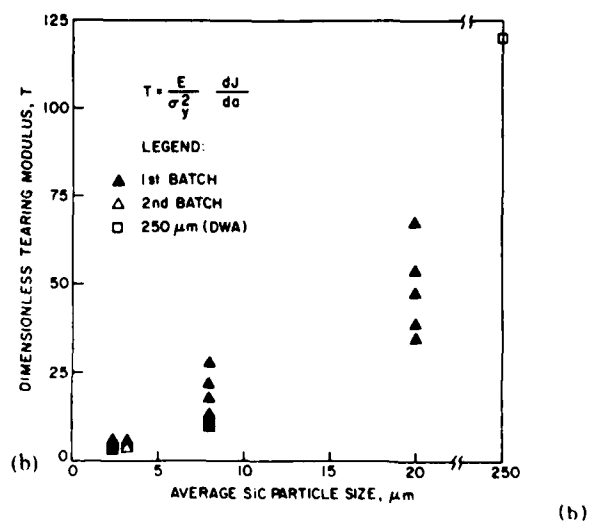
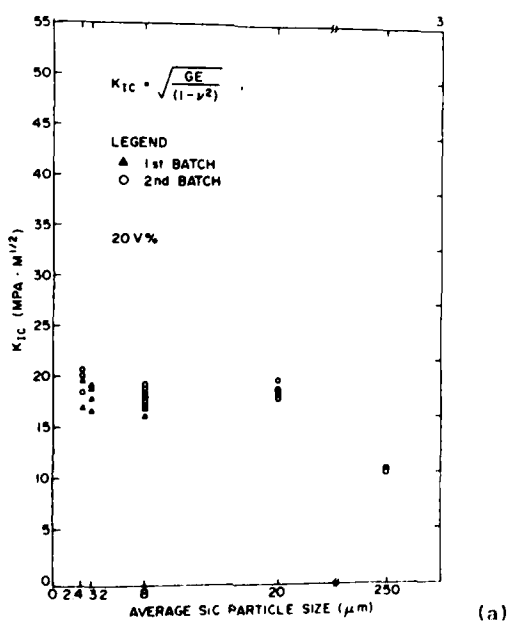


Fig. 20. Cross-section showing crack tip region in a 20  $\mu\text{m}$  SiCp/Al composite (after Ref. 43).



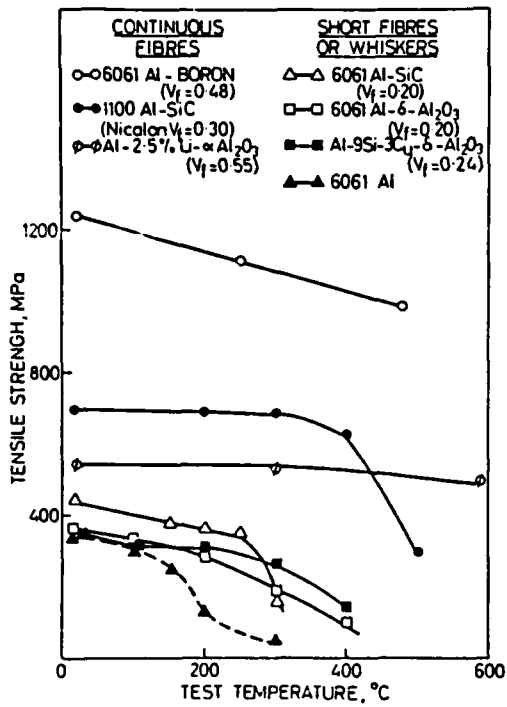


Fig. 22. Tensile strength values for continuous fibre, whisker and short fibre reinforced alloys plotted against test temperature.

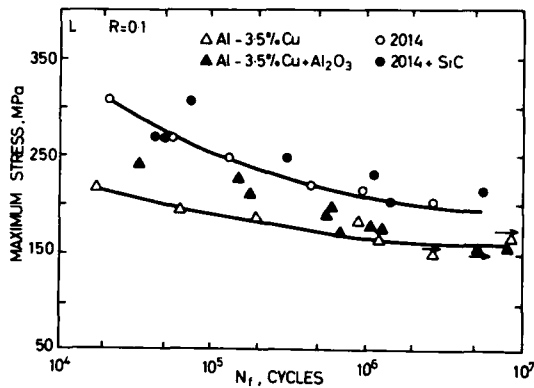


Fig. 23. S-N plots for Al-3.5%Cu alloy with and without  $\delta$ -Al<sub>2</sub>O<sub>3</sub> fibres and 2014 with and without  $\alpha$ -SiCp. The alloys are in the T6 condition with the exception of reinforced 2014 where a T8 treatment was applied.

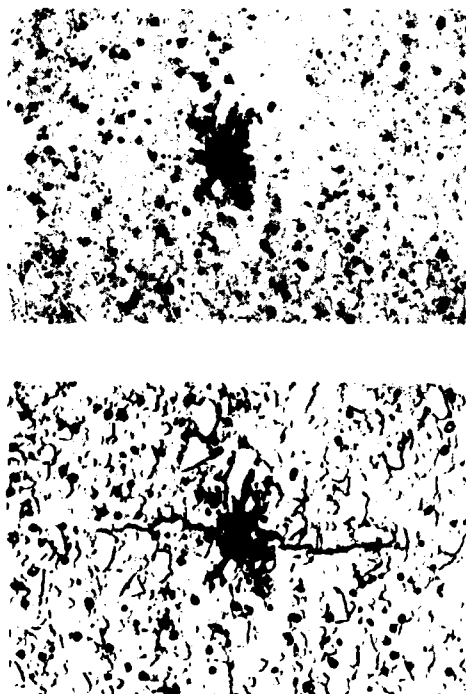


Fig. 25. Crack initiation and propagation in a 2124 alloy with 17 vol.% SiCp (T4 condition). The average particle size is 3 $\mu$ m diameter.

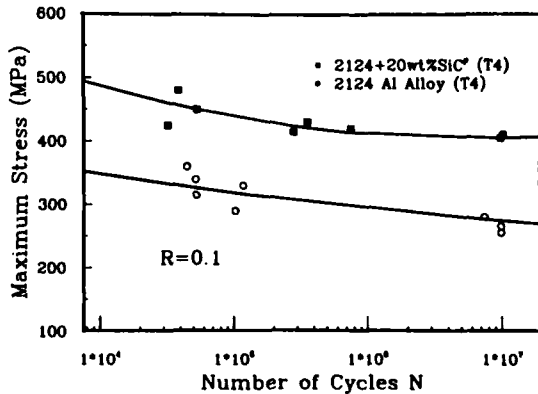


Fig. 24. S-N plots for 2124 alloy with and without 20 wt.% (17 vol.%) SiCp in the T4 condition. The average particle size is 3 $\mu$ m diameter.

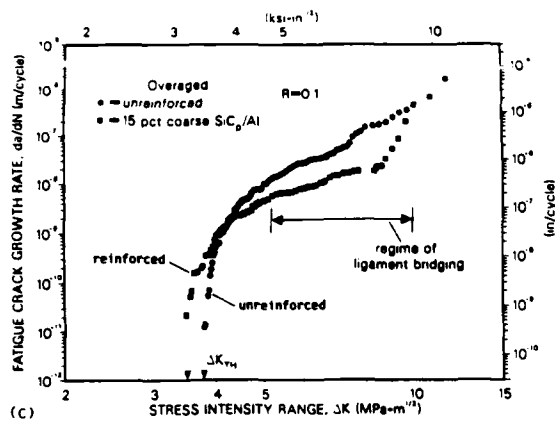


Fig. 26. Fatigue crack growth rates  $\frac{da}{dN}$  plotted against  $\Delta K$  for 15% by vol. SiCp/7000 series Al alloy. The particle average size is  $16\mu\text{m}$  (after Ref. 54).

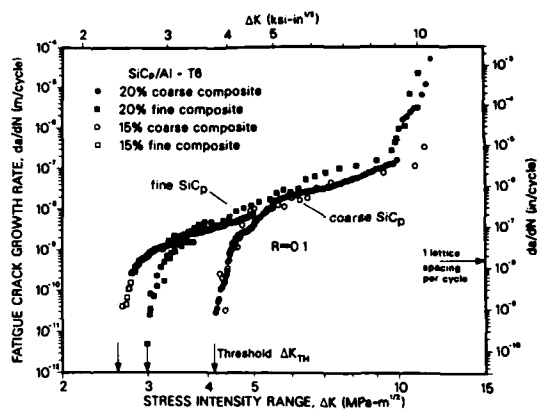


Fig. 27. Fatigue crack growth rates  $\frac{da}{dN}$  plotted against  $\Delta K$  for SiCp/7000 series alloys. Fine and coarse SiCp have an average diameter of  $5\mu\text{m}$  and  $16\mu\text{m}$  respectively (after Ref. 55).

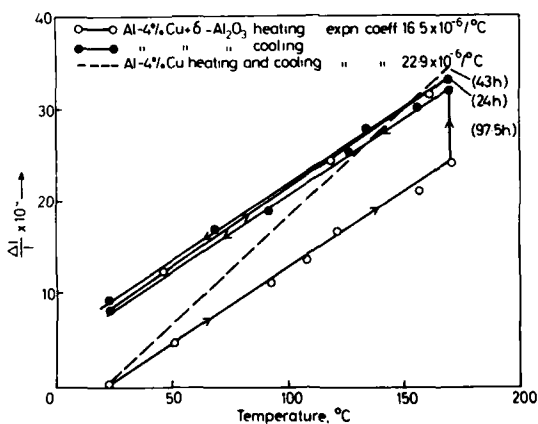


Fig. 28. Volume changes which take place in an Al-4%Cu alloy with and without  $\delta\text{-Al}_2\text{O}_3$  short fibre reinforcement. The alloy and composite have been heated to  $170^\circ\text{C}$  and allowed to age for 100h and then they are cooled.

## Aluminum Powder Alloys - An Overview

Gregory J. Hildenman  
Alcoa Technical Center  
Alcoa Center, Pennsylvania

and

Michael J. Koczak  
Department of Materials Engineering  
Drexel University  
Philadelphia, PA 19104

### **Abstract**

The historic development of aluminum powder metallurgy dates back to the early 1900's with initial flake powder production and has matured to the present day production of viable aerospace alloys. Primary powder production and processing techniques, such as atomization and mechanical alloying are reviewed. Processing-microstructure-property relationships in four classes of high performance powder metallurgy (PM) aluminum alloys are considered. These are (i) high strength alloys (Al-Zn-Mg-Cu-Co); (ii) high specific modulus alloys (Al-Li-Cu); (iii) high temperature alloys (Al-Fe-Co, Al-Fe-Ni); (iv) mechanically alloyed material (Al-Mg) and composite alloys. Direct property comparisons with counterpart ingot metallurgy alloys are presented where ever appropriate. Aluminum powder metallurgy alloy development is now at a mature stage of growth where commercial and aerospace application are being sought and developed in competition with traditional aluminum ingot metallurgy, titanium, and composite structures. The future growth and development of these alloy systems is vested in reliable economic processing and design reliability.

### **I. Introduction**

#### **A. Historic Development of Aluminum Powder-Metallurgy Alloys**

Over one hundred years ago, Hall and Heroult independently discovered a process to produce aluminum by electrolysis. This refining technology opened the door for economical production of the light metal and initiated a search for new applications. Use of aluminum as powders began when flake-type aluminum powder was manufactured in the early 1900s by milling or attriting thin sheets into tiny flakes used as an additive pigment in paint formulations. Introduction of the atomization process in the 1920s provided for a more efficient production process and marked a new era in aluminum-powder production. This process, coupled with the beginning of World War II and the development of aluminized explosives, created a major market for atomized aluminum powder. Subsequently, atomized aluminum powder has found commercial applications in diverse commercial and defense-related areas of technology. A partial listing includes pigments for paints and roofing, commercial blasting materials, reducing agents for the manufacture of metals and alloys, pharmaceuticals, alumiweld conductors, cellular concrete, pyrotechnics, chemicals, and rocket propellants. Furthermore, the commercial viability of low-cost pressed and sintered aluminum powder-metallurgy parts emerged in the 1960s, resulting in a further expansion of the powder-metal market into near-net shape components. The chronological development of dispersion and precipitation powder-metallurgy alloys is charted in Tables I and II. Table I can be divided into three classes: high temperature, low density, and high modulus alloys, which can include powder-metallurgy aluminum metal matrix composites. In contrast, the precipitation-strengthened PM alloys (Table II) can be conveniently categorized by conventional wrought-alloy designations; e.g., 2000, 7000 series. Exception however, is noted for the pressed and sintered alloys, which are designated by 201, 601, and so on.

Considering dispersion alloys during the 1940s and 1950s, aluminum powders were investigated for use in high-temperature applications. Sintered aluminum products (SAP) or (XAP) utilized  $\text{Al}_2\text{O}_3$  dispersions to improve the high-temperature strength and creep response of parts consolidated from milled aluminum powder [1-4]. Shortly after this period, experimental work [5-7] on atomized aluminum powders containing high-solute contents was initiated and provided the genesis of research which has evolved into development of the current aluminum PM alloys. These alloys utilized the benefits derived from rapid solidification, which include alloying flexibility, increased solid-solubility limits, fine-scale microstructures, and composition-al homogeneity.

From early research efforts emerged several types of alloy systems which can be classified into dispersion-strengthened alloys, precipitation-strengthened alloys, and hybrid systems; e.g., mechanically alloyed or composite-reinforced systems. The dispersion-strengthened aluminum PM alloys contain fine dispersions of relatively insoluble intermetallic phases. These alloys have good elevated-temperature strength, thermal stability, wear resistance, and they exhibit a high elastic modulus. An example of this type of alloy system is the Al-Fe-X alloys where X represents a variety of elements which form a high volume fraction (typically ranging from 5 to 40% of intermetallic aluminide phases in an aluminum matrix). In addition, Al-Li and Al-Li-Be alloys for lower-density and blended powder-metallurgy composites; e.g., 2000 series with SiC whiskers and particulate reinforcement, for greater stiffness are currently being explored as of the later 1980's. Given the advantages of rapid solidification and the flexibility inherent in blending different powders, an opportunity exists to develop novel alloys with tailored or designed physical and mechanical properties for a wide variety of high-performance applications.

A second major alloy class (see Table II) developed along the lines of traditional heat-treatable 2XXX and 7XXX ingot-metallurgy compositions. In this sector, rapid solidification resulted in the ability to produce a fine grain size and refined constituent microstructure in powders. After consolidation, subsequent PM alloys have demonstrated combinations of strength, fracture toughness, fatigue resistance, and corrosion resistance superior to ingot alloys. Alloys 7064, 7090, and 7091 have been introduced in the 1980s and are examples of advanced PM materials which are developed for commercial aerospace applications.

Techniques for processing powder metallurgy alloys have also evolved. Rapidly solidified particulate, in the form of powder, ribbon, or attrited flake, must be consolidated to full density to maximize mechanical properties. Processing procedures must, therefore, be carefully designed to maintain the refined structure and to obtain the benefits inherent in powder alloys. Advances in powder processing such as vacuum degassing, consolidation, hot isostatic pressing, direct spray deposition, extrusion, forging, and rolling have aided the development of aluminum powder-metallurgy alloys for structural applications. To this end, rapidly solidified particulate produced by atomization, mechanical alloying, or attriting melt spun ribbon has been consolidated to full density with excellent mechanical properties. Additional information on the development of aluminum powder metallurgy alloys and processing techniques is contained in reviews by Jones [8], Pickens [9], Palmer and Tietz [10], Singer [11], and Froes et al., [12].

#### B. Development of Rapid-Solidification Concepts

Since the 1950s, rapid solidification of aluminum alloys was based on gas-atomization techniques. This processing technique allowed researchers to explore formation of aluminum-base alloys containing high nonequilibrium levels of a wide variety of solute elements. Since the early work of Roberts [7], Towner [5], and Towner and Lyle [6], greater understanding of the effect of cooling rate on refinement of dendrite arm spacing (DAS) has evolved.

Based on the work of Spear and Gardner [13], Dean and Spear [14], and Flemings [15], a linear relationship between dendrite arm spacing and cooling rate was established from measurements on Al-Cu alloy castings, atomized powder, and a splat-cooled sample. Subsequent research by Matyja et al., [16] confirmed extrapolation between DAS and cooling rate to cooling rates of over  $10^8$  K/sec. Using Al-Fe and Al-Si splat-quenching techniques pioneered by Pol Duwez [17]. The general relationship between cell size and cooling rate is illustrated in Figure 1. The graph shows that rapid solidification inherent in atomization and melt spinning can refine the cell size by over two orders of magnitude compared to direct-chill (DC) cast ingot. Today, we know from the work of many researchers, which has been summarized by Mehrabian [18], that a microstructural characteristic such as dendrite arm spacing is a function of the liquid-solid interface velocity, which is controlled by variables; e.g., the amount of undercooling developed before nucleation, the rate of heat flow, as well as thermodynamic and kinetic factors which are dependent upon the alloy system considered. Figure 1 is, however, useful in that it provides a perspective on the ability of rapid-solidification process such as atomization, melt spinning, planar flow casting, and splat quenching to refine the microstructure of an alloy. A wide variety of rapid-solidification processes have been applied to aluminum alloys [19]. These include gas atomization, centrifugal atomization, rotating cup, rotating electrode process, plasma rotating electrode process, single and double roll quenching, ultrasonic gas atomization, the Osprey process, and soluble gas atomization process.

In addition to refinement of the dendrite arm spacing, extension of solid solubility is of importance in maximizing the volume fraction of second phases which can be precipitated from an extended solid solution. Table III lists the maximum extended solid solubility reported by various investigators. Following production of alloy powders, secondary processes; i.e., mechanical alloying combining carbide or oxide reinforcement, provide opportunities for high temperature strength and modulus improvements. The refinement of microstructure via rapid solidification and the extension of solid solubility are important physical features of the process. The resulting benefits; i.e., the mechanical-property improvement versus weight saving, demonstrate the future utility of aluminum powder-metallurgy alloys in aerospace applications, Figure 2. For example, a 30% increase in strength or a 50% increase in elastic modulus in a PM alloy or composite can translate into a 10% savings in weight in aerospace applications. This goal for weight savings is equivalent to that of Al-Li ingot alloys.

### C. Advantages and Barriers to Aluminum Powder-Metallurgy Alloys

The ability to achieve a refined microstructure combined with economical powder-processing techniques creates the potential for aluminum PM alloys to be applied where high strength and stiffness, elevated-temperature performance, corrosion, or wear resistance are required. In addition, powder metallurgy alloys can offer combinations of mechanical (strength, modulus, fracture toughness) and physical properties; e.g., thermal and electrical conductivity, tailored coefficients of thermal expansion, density, which are superior to cast alloys'. The benefits of rapid solidification are highlighted in Table IV. Advances in PM aluminum have been achieved in the areas of alloy design, atomization, and consolidation processes. The future challenges involve the development of even greater levels of properties coupled with reliability and reproducibility in powder properties and processing, so that design confidence and cost-effective applications can be developed in commercial and defense sectors. Significant achievements in weight savings are possible as illustrated in Figure 2, when strength, modulus, and fatigue improvements are developed in aluminum powder-metallurgy alloys. Barriers to the future development of aluminum PM alloys include the necessary processing quality control and reliability of design properties required for structural applications coupled with a required cost reduction necessary for wider acceptance in commercial automotive and aerospace applications. Initial commercial applications in four areas include: (1) high strength alloys for aircraft structural components, (2) wear resistant alloys and composites for automotive engines and appliances, (3) high modulus composite alloys for stiffness, and (4) high temperature alloys for airframe and engine applications.

Although aluminum PM alloys offer significant potential in terms of mechanical properties, there are several barriers which limit their application and acceptance in the marketplace. These are listed as barriers to growth in Table IV. As with most new materials, the cost of substitution is usually a major hurdle. In addition, the cost effectiveness must be clearly established in the total product life

cycle. Excluding pressed and sintered parts, the cost of wrought PM aluminum alloys are greater than alloys produced from ingot metallurgy because of the additional processing steps as shown in Figure 3. As of the late 1980s, estimates indicate that PM alloys will cost 1.5-5 times as much as ingot alloys. Therefore, applications for PM alloys will initially be limited to components where superior performance and effective materials utilization justifies their use. It is expected, however, that the cost of PM alloys should be reduced as the volume of powder-metallurgy components increases. This is because the capital cost in terms of equipment will be spread over a larger quantity of material produced. In addition, producers of rapidly solidified components will seek more efficient methods to produce atomized powders and attrited melt spun ribbons for consolidated components.

The growth of PM alloys has also been constrained by the size and availability of billets which can be processed into wrought products. In the 1970s and 1980s, applications were limited to forgings, extruded shapes and sheet products which could be fabricated from billets of less than 160 kg. As of the late 1980s, a number of material producers (including Alcoa, Allied, Kaiser, Novamet, and Pratt & Whitney) are in the process of increasing the size of the consolidated billet up to 550 kg [20-21], which will also be a step to reduce the cost as well as increase the availability of advanced powder-metallurgy materials.

Quality is another issue which must be addressed. Mechanical properties such as fracture toughness and fatigue are extremely sensitive to the size, number, and distribution of inclusions. At least part of the improvement of PM alloys in these areas can be attributed to a refined microstructure which results in intrinsic metallurgical benefits compared to ingot-metallurgy alloys. However, care must be taken during processing of the powders to avoid contamination by particles which could degrade inclusion-sensitive mechanical properties.

Another factor that may be important to the growth of higher-cost materials is a greater attention to the life-cycle cost of a component. For example, over the 20-year life of an aerospace component, the cost of a PM part may be lower due to savings in fuel because of lower weight. Reduced frequency of inspection as well as fewer maintenance or part-replacement requirements for fatigue or corrosion damage are also factors in evaluating life-cycle costs. Consideration of these factors will aid acceptance of wrought powder metallurgy as cost effective structural materials. There is, therefore a need for joint effort combining the skills of design and materials engineers to clearly assess performance-cost-life cycle trade-offs and to determine future directions of powder processed aluminum alloys for commercial, defense, and aerospace markets.

## II. Precipitation- and Solid-Strengthened Powder-Metallurgy Alloys

### A. 7000 Series PM Alloys

#### 1. Exploratory Investigations

High-strength 7XXX PM alloys are strengthened by precipitates; e.g., Guinier-Preston Zones, composed of elements such as Zn, Mg, and Cu which are soluble in aluminum. These alloys offer combinations of strength and damage tolerance as determined by fracture-toughness, fatigue, crack propagation, and corrosion-resistance evaluations, which are superior to their ingot-metallurgy counterparts. Atomized powder compositions in the 7XXX series (Al-Zn-Mg-Cu) were among the earliest systems to be explored. In the 1950s and 1960s, a number of researchers were active in investigating combinations of Zn, Mg, and Cu for high strength with a variety of dispersoid forming elements to control recrystallization and maintain a fine grain size. Initial efforts were directed at achieving high strength levels. For example, Roberts [22] obtained yield strengths as high as 810 MPa. Towner and Lyle [23] and Haar and Lyle [24] produced Al-Zn-Mg-Cu extrusions with yield strengths of 858 MPa. Unfortunately, the ductility of extrusions at these strength levels was low, typically less than 1% elongation. From this early work, there were indications that high-strength alloys made by powder metallurgy had corrosion-resistance and fatigue-endurance limits which were superior to ingot-metallurgy alloys'. Subsequent work by Cebulak and Truax [25] demonstrated that good combinations of strength (654 MPa), elongation (8%), exfoliation resistance (immune), fatigue limit (207 MPa), and fracture toughness (21 MPa $\cdot$ m $^{1/2}$ ) were obtainable in 7XXX PM alloys.

#### 2. Process Development of Al-Zn-Mg-Cu Alloys

During the 1960s and 1970s, processing of powder-metallurgy alloys advanced specifically in the understanding of powder handling prior to consolidation. Cebulak [26] and Roberts [27] independently reported that vacuum degassing greatly improves toughness in high-strength PM alloys. Figure 4 from Lyle and Cebulak [28] illustrates improvements in the ratio of notch tensile strength to yield strength for a die-forged Al-8.0% Zn-2.5% Mg-1.0% Cu-1.5% Co alloy obtained by vacuum degassing compared to forgings fabricated from billets which were heated in argon. Discovery of the benefit of vacuum degassing was a significant step following a series of powder-metallurgy processing patents [29] discussing the importance of heating the powder in a flowing protective atmosphere in order to degas the powders. Later in the 1970s and 1980s, degassing procedures became more sophisticated by incorporating a deputative gas treatment [30] progressive evacuation cycles [31], and vacuum hot compaction without a canister [32,33]. The nature of complex decomposition processes of the aluminum hydroxides during degassing has also been investigated [34-36].

In addition, effort has been directed at scaling up the powder billet size to allow fabrication of plate and sheet products combined with cost reduction. One of the first efforts to scale up billet size was conducted by Cebulak [37]. In that program, billets weighing 1500 kg composed of a high-strength Al-Zn-Mg-Cu PM alloy were produced which were subsequently rolled into plate. More recently, Billman and Jatkar [21] developed processing techniques to produce 550 kg billets for both heat-treatable and dispersion-strengthened PM alloys. In

addition to producing large billets which could be rolled to sheet gauge, alternative powder-to-sheet techniques have been examined. For example, Daugherty [38] discussed a method where plus 200 mesh aluminum powders are fed continuously into a hot rolling mill to yield sheet. More recently, Ro [39] examined the concept of blending Al-Zn-Mg-Cu alloy powders with Al powders to develop a low-cost method to produce high-strength 7XXX sheet.

### 3. Commercial and Second Generation 7XXX Alloys

The decade of the 1980s has been a milestone in the development of commercial high-strength alloys. In 1980, the Aluminum Company of America (Alcoa) registered powder-metallurgy alloys 7090 and 7091 and Kaiser Aluminum and Chemical Corporation (Kaiser) registered X7064 in 1985. The compositions of these alloys are listed in Table V. Comparison of the compositions between 7091 and X7064 shows these alloys contain similar amounts of Zn, Mg, and Cu but have different dispersoid-forming elements. As shown in Table VI, properties of X7064-TX73 and 7091-T7E69 are similar and offer higher strength, fracture toughness, and resistance to stress corrosion cracking compared to ingot-metallurgy 7075-T73.

The compositions of two other 7XXX alloys, CW67 (developed by Alcoa) and PM61 (a Kaiser developed composition), are also listed in Table V. Ping [40] reported that PM61 was developed for peak-strength T6 applications with yield strengths of 752 MPa and has been evaluated for seat tracks in aircraft. Research at Alcoa by Hildeman et al., [41], was directed at achieving high strengths similar to 7090's and a fracture toughness equivalent to 7091's in the T7 stress-corrosion-resistant temper. Figures 5 and 6 illustrate that the second-generation alloys; i.e., CW67, X7090, and X7091 has met the desired goals by demonstrating the highest combination of strength and toughness in a commercial die forging.

Fatigue properties are vital to many aerospace applications. Alcoa studies reported by Hart [42] demonstrated that S-N fatigue resistance of powder-metallurgy alloys 7090 and 7091 was superior to that of 7075 and 2024. Evaluation of fatigue response addressed three major areas: S-N fatigue resistance, fatigue crack growth ( $da/dN$ ) versus  $K$ , and spectrum fatigue response. Early studies in the 1970's showed constant amplitude fatigue crack growth (FCG) rates of the PM alloys were greater than conventional alloys'. Subsequent studies [43-45] have shown that although constant-amplitude FCG rates of PM alloys may be higher than those of ingot alloys, under spectrum fatigue conditions simulating actual load conditions, crack growth rates of powder-metallurgy alloys can be lower than growth rates of ingot alloys. It is, therefore important to conduct screening tests for fatigue which simulate the load and notch-stress fatigue conditions that are expected in the actual application.

### B. 2000 Series PM Alloys

Powder metallurgy alloys containing Cu and Mg as the major alloy additions fall into the 2XXX alloy-composition classification. As in the case of 7000 series compositions, 2000 series PM alloys exhibit improved combinations of strength and toughness compared to ingot metallurgy alloys which have moderately high strengths (typically 300 to 450 MPa yield strength) with good damage tolerant properties, including fatigue and corrosion resistance.

While most of the effort since the 1950s in heat-treatable alloys has been directed at 7XXX compositions, a number of investigators have examined application of powder metallurgy processing to Al-Cu-Mg compositions. Roberts [22], and later Lebo and Towner and Lyle [6], Grant [47] and Voss [31] examined alloy 2024. Compared to alloy 2024, a gain in tensile strength and fatigue life of PM 2024 fabricated from the splat quenched droplets was obtained by Lebo and Grant. However, to maximize the benefit that powder-metallurgy processing can provide, alternative compositions and process techniques appear to be necessary.

Addition of Zr in order to form stable dispersoids was one route pursued by Kaiser and Alcoa/Lockheed. Table VII includes two 2024 powder-metallurgy alloys: PM63 under development by Kaiser [48] and PM042 developed by Alcoa [49,50]. Both of these alloys contain levels of Zr which are close to or exceed the solid-state solubility limit of 0.28% Zr in aluminum. These additions of Zr exceed that which is possible for ingot metallurgy and results in a fine grain size PM alloy with excellent combinations of strength and toughness. Figure 7 demonstrates that powder-metallurgy variations of 2000 series alloys containing Zr as a dispersoid result in superior combinations of strength and fracture toughness compared to conventional 2XXX alloys.

Another route to improve 2000 series alloys by powder metallurgy processing is by mechanical alloying. Using the process technology developed by Benjamin and Bamford [51] for Al-Al<sub>2</sub>O<sub>3</sub>, Novamet has developed alloy IN9021, which has a composition listed in Table VII to be similar to 2024 except for the oxygen and carbon contents, which are a result of the process. These alloys are produced by attriting mixtures of Al, Cu, and Mg powders with organic additives which control welding and fracturing during milling. During this process, fine dispersions of oxides and carbides are formed from the reaction of the organic additives with the milled powder. After consolidation and heat treatment, the alloy is strengthened by precipitates and a fine grain size typically less than 0.5 um. As shown in Table VIII, IN9021-T4 forgings [20,52] exhibit greater strength, toughness, and stress corrosion cracking resistance compared to 2024-T4's.

#### C. Pressed and Sintered PM

An economical processing method to produce aluminum PM parts is by pressing loose powders in a die and sintering the compact in a low dew point atmosphere. Early research [53,54] demonstrated the feasibility of producing specimens with tensile strengths of 275 MPa for Al-Cu sintered compacts. Subsequent work by Storchheim [55] and Dudas and Dean [56] have made pressed and sintered aluminum PM a commercial success. There are primarily two types of alloys which are extensively utilized for pressed and sintered PM. Alloy 201AB contains 4.4% Cu, 0.8% Si, and 0.4% Mg, while 601AB contains 0.25% Cu, 0.0% Si, and 1.0% Mg. Both alloys offer combinations of strength, ductility, and finishing characteristics to provide a low-cost alternative for replacement of die-cast or machined parts.

#### D. 5000 Series PM Alloys

In the 1960s, only a limited amount of research on Al-Mg alloys was reported. Towner and Lyle [6] explored aluminum atomized Al-Mg powder alloys in extruded form. Roberts [46] evaluated the mechanical properties of cast and powder extrusions of alloy 5083. A twofold increase in yield strength was obtained for the PM alloy compared to the cast alloy. In a comparison of 5005 sheet with roll-compacted 5005 particles, Daugherty [38] also demonstrated increases in strength for the powder-metallurgy alloy, which was considerably more resistant than conventional alloys to recrystallization.

In the early 1980s, International Nickel Company (INCO) developed a mechanically alloyed Al-4% Mg designated IN9051 [57]. This alloy utilized a combination of strengthening mechanisms including solid-solution strengthening from Mg, substructure strengthening from a fine grain size of less than 0.5 um and dispersion strengthening from oxides and carbides. Alloy IN9051 was subsequently replaced by IN9052 (Table VII), which has an equivalent level of Mg but contains a higher dispersoid content. As shown in Table VIII, IN9052 alloy forgings [52] (1984) exhibit excellent combinations of strength, toughness, and SCC resistance compared to ingot-metallurgy alloy 5083.

#### E. Low Density Aluminum Alloys

Based upon a calculated rule of mixtures [58,59] additions of Li, Mg, or Be to aluminum have a significant effect on reducing density. Lithium is the most potent since every 1 wt % addition reduces the density of aluminum by 3% coupled with a modulus improvement. Additions of almost 6 and 7 wt % of Mg and Be, respectively, are required to reach equivalent density reductions. Since the maximum solid-solubility limits of Li, Mg, and Be are 4.0, 18.9, and 0.063 wt %, respectively, density reductions are limited to approximately 12% for Li, 8% for Mg, and 0.03% for Be solely based upon solid solubility considerations. It is, therefore, clear that powder metallurgy processing offers alternatives in providing the ability to reduce density through supersaturation of alloy additions beyond the equilibrium solid solubility limits and increase strength via dispersion strengthening from fine second phase particles produced by rapid solidifications.

In the 1950s and early 1960s, Lyle et al., [40] and Towner and Lyle [6,46] explored Al-Li and Al-Be atomized powder alloys. Since these elements simultaneously increase the elastic modulus while decreasing density, they are attractive additions for alloys which require high stiffness which is controlled by the ratio of modulus to density. Unfortunately, the reactivity of Li and Be as well as the toxicity of Be have hindered development of low-density alloys containing these elements.

Driven by the economics of aircraft operational costs (such as the increases in the cost of fuel in the late 1970s and early 1980s [62]), development of aluminum alloys containing lithium was initiated. While most of the efforts by the major aluminum companies focused on Al-Li compositions such as 2090, 2091, and 8091 (Table IX), which could be formed into cast and wrought products a number of studies utilized the potential powder metallurgy advantages of a fine homogeneous microstructure to improve the low ductility and fracture toughness associated with alloy 2020, an Al-Cu-Li alloy developed by Alcoa in the 1950s. Initial research on PM Al-Li alloys investigated compositions similar to 2024 with additions of Li. Sankaran and Grant [63] showed that additions of 1 to 3% Li increased the specific strength of 2024.

Additional studies by Gysler et al., [64] compared the properties of PM and IM versions of 2020. In 1981, Palmer and Tietz [10] reviewed the properties of PM and IM alloys which were being investigated at that time. They concluded that powder-metallurgy Al-Li alloys exhibited better combinations of specific strength and elongation compared to ingot metallurgy alloys. Subsequent studies [65] have shown that similar combinations of strength and elongation were obtained for PM and IM Al-3% Li-1.5% Cu-1.0% Mg-0.15% to 0.2% Zr alloys.

It is, therefore, apparent that if the mechanical properties of low-density PM alloys are to greatly exceed those of ingot metallurgy compositions, alloy developers will need to focus on chemistries which provide weight savings greater than the 8-10% offered by IM alloys such as 2090, 2091, or 8091 (Table IX). A comparison of a spray-deposited Al-Li alloy; e.g., 8090, versus the cast and wrought counterparts, Table X depicts the improvement in strength and ductility. A number of companies are exploring Al-Li PM alloys in order to take advantage of higher specific modulus; e.g., Allied, Alcan, Lockheed, and INCO (Novamet), Table X.

### III. Dispersion Strengthened Powder Metallurgy Alloys

#### A. Elevated Temperature Alloys--Pioneering Studies

The concept of using aluminum alloys for elevated-temperature applications dates back to the late 1940s, when oxide-dispersion-strengthened aluminum was developed. At that time in Switzerland, Irmann discovered that sintered aluminum had mechanical properties similar to those of aluminum alloys; he attributed this enhancement in strength to the presence of oxide films surrounding the individual powder particles in the sintered matrix. On subsequent cold compaction and hot-working, the oxide was broken up and distributed as small dispersoids, thereby giving rise to strengthening of the aluminum matrix. These materials are known as the sintered aluminum products (SAP).

Subsequently in the United States, Alcoa developed a range of oxide dispersion-strengthened aluminum materials similar to SAP or XAP. The first detailed study of these SAP-type materials in the United States was conducted by Lyle [3], who investigated SAP-type alloys containing 7.8-16.5% oxide by weight. It was found that these materials had moderate room-temperature strength, compared to 2000 series aluminum alloys. However, SAP alloys were stronger than ingot-metallurgy alloys at temperatures above 200°C and had the ability to retain strength after prolonged exposure at temperatures as high as 482°C. Moreover, strength decreased with increasing temperature at a lower rate than for conventional aluminum alloys with comparable room temperature strength.

The pioneering work on SAP-type alloys lead to the development of other types of dispersion strengthened aluminum alloys based on rapid solidification in which intermetallic compounds generally 5-40% by volume constituted the dispersed phase. These fine dispersoid reinforcements, typically less than 0.5 microns, are formed in situ during atomization of the alloy melt. Such powders are termed prealloyed powders and are subsequently compacted and hot consolidated to produce a wrought alloy.

Roberts [7] and Towner and Lyle [5,6] independently studied several alloys in which the dispersoid was an intermetallic. The rationale for selecting the alloying elements was to achieve a fine dispersion of an insoluble constituent in the aluminum matrix. Hence, alloying elements such as Fe, Cr, and other transition elements having low solid solubilities, high liquid solubilities, and low diffusion rates in solid aluminum. In addition, many of the transition elements form thermally stable intermetallic compounds of relatively low density, so that appreciable amounts of alloying elements may be added without a prohibitive increase in the density of the final alloy.

Towner and Lyle [6,23] found that binary Al-Fe alloys containing 7.5 wt %, 10 wt %, and 12.8 wt % Fe gave the highest tensile strengths at 315°C and 427°C. More complex alloys of composition 7.8 wt % Fe and 0.2 wt % each of Cr, Ti, V, and Zr, and a quaternary alloy of aluminum with 2.5 wt % Fe, 0.4 wt % Cr, and 3.4 wt % V also gave excellent high-temperature strength up to temperatures of 427°C. The complex alloy of aluminum containing 7.8 wt % Fe and 0.2 wt % each of Cr, Ti, V, and Zr had the best stress rupture properties.

These alloys exhibited high-temperature strength due to microstructural stability at elevated temperatures relative to precipitation thermodynamically stable and resistant to coarsening which is a strengthened alloys. This is because aluminides are relatively thermodynamically stable and resistant to coarsening, which is a consequence of the extremely low equilibrium solid solubilities and small diffusion rates of the alloying elements in the aluminum matrix. To achieve sufficient strength at ambient and elevated temperatures, it is necessary to have a high volume fraction of the dispersoids on a fine scale that are uniformly distributed throughout the matrix. This can only be achieved by resorting to rapid solidification and PM processing. It is impossible to produce these alloys by conventional ingot solidification since attendant slower cooling rates result in considerable macrosegregation. In addition, the intermetallic dispersoids formed at cooling rates of one degree per second in ingots are relatively coarse and would not make a significant strength contribution.

In addition to research directed at exploring alloy compositions, Microstructural transitions in rapidly solidified binary alloys of Al with Fe, Ni, Cr, Mn, Co, Ti, and V were studied by Jones [66] among others. It was observed that metallographically, two types of distinct zones were present, they were designated zone A and zone B. Zone A consisted of a very fine dendritic or cellular aluminum structure and was optically featureless. The microhardness of this zone was approximately twice that of zone B and did not change significantly with annealing up to temperatures of 200°C, after which it decreased. Zone B consisted of a much coarser structure. The transition from the zone-A to the zone-B structure was explained in terms of the cooling rates experienced by the two regions.

The microstructural stability of strengthening dispersoids is a very important criterion in the selection of a new class of aluminum alloys for high-temperature applications. Pontikakos and Jones [67] studied the coarsening behavior of intermetallics in several Al-transition metal alloys produced by rapid solidification. Al-Fe, Al-Ni, and Al-Cr alloys were heat treated at 500°C to 625°C for time periods up to 1,000 hrs and the size and distribution of the corresponding dispersoids were analyzed with respect to current particle-coarsening theories. At lower temperatures, coarsening was enhanced due to residence of the dispersoids on the grain boundaries. The observed increases in the average particle size of FeAl, were found to be in good agreement with predictions based on grain boundary diffusion control at 500°C, and lattice diffusion control at 600°C. The highest resistance to coarsening was exhibited by CrAl, at 500°C while FeAl, was more resistant than NiAl, for all conditions.

As a result of these preliminary investigations, Al-8 wt % Fe was considered an excellent host binary candidate system. There were further developments during the late 1970s. In that time period, significant research efforts sponsored by the Air Force as well as companies; e.g., Alcoa, Alcan, Allied, Sumitomo Light Metals, Pechiney, Pratt & Whitney, Lockheed, and Kaiser, spawned the development of alloy systems such as in Al-Fe-Ci, Al-Fe-V, Al-Fe-Ni, and Al-Fe-Mo ternaries as well as quaternary variants of these systems which exceeded the mechanical properties of 2000 series ingot alloys. The objective of these programs was to determine optimum production processes and alloy compositions for dispersion-strengthened alloys. Major factors include powder-solidification rate, powder cleanliness, oxygen content, outgassing conditions, (time, temperature), and powder-consolidation conditions; e.g., extrusion temperature and reduction ratio. Each of these factors can contribute or detract from mechanical properties by altering the second-phase aluminide size, effecting bonding between powder particles and modification of microstructural texture.

An example of the advantage of a dispersion-strengthened alloy which evolved from these studies is shown in Figure 7. The yield strength of Al-Fe-Ce PM alloy [68] is plotted against typical properties of 2219, 2024, and 7178. It is apparent that at temperatures above 150°C, the dispersion-strengthened PM alloy exhibits better strength. In addition, the room-temperature properties of the dispersion-strengthened Al-Fe-Ce alloy are retained after exposure to elevated temperatures whereas conventional precipitation strengthened alloys will lose much of their strength after exposure to elevated temperatures. In addition to the Al-Fe-Ce alloy by Alcoa, several other alloys were under development; e.g., Al-Fe-Mo by Pratt & Whitney, Al-Fe-V-Si by Allied Signal, and Al-Cr-Mn-Zr by Alcan.

### Volume fraction

Fig. 7. Predicted recrystallised grain size as a function of particle size and volume fraction. Recrystallisation will not probably occur in the dotted regions (after Ref. 17).

Fig. 8. Mean longit...

on an (a) aluminium matrix, and (b) silicon carbide whisker reinforcement during a heating and cooling cycle (after Ref. 23).

5-9

## B. Elevated-Temperature Alloys---Development Efforts

Based on the earlier composition and powder processing studies, the development of high temperature aluminum alloys narrowed and matured to a number of candidate alloy systems: Al-Fe-Ce, Al-Fe-Mo-V, Al-Fe-Zr-V, Al-Fe-V-Si, and Al-Cr-Zr-Mn. Table X compares strength elongation and modulus for the Al-8Fe, Al-8Fe-4Ce, Al-8Fe-2Mo, and two Allied alloys and an Alcan high-temperature alloy. Alternative approaches for production of rapidly solidified alloys consider atomization, splat quench and rotating disc techniques. The eventual successful alloy system must combine high performance with cost-effective processing. In each of these alloy systems, the ability of the dispersoids and intermetallic compounds to achieve a uniform and fine intermetallic particle distribution is essential for the high temperature strength of the candidate systems. Consequently, the development of a low angle grain boundary structure that is pinned by fine dispersions can provide enhanced elevated temperature stability. As of the late 1980s, dispersion strengthened aluminum PM alloys are being examined for use in aircraft and jet engines as a replacement for 2000 series aluminum or titanium alloys. Rainen and Ekwall [70] determined that Al-Fe-Ce and Al-Fe-V-Si sheet show potential for significant weight and cost savings. Figure 9 plots the mechanical properties of Al-7.1Fe-6.0Ce (Alcoa designation C242) and Allied's Al-8Fe-1V-2Si; e.g., FVS0812, on a specific property basis as a function of test temperature and exposure. In addition, if a comparison is made of retained strength of the aforementioned alloys, the stability of FVS0812 and C242 are shown to be superior to that of 2090, 2024, and 2219 ingot-metallurgy alloys, Figure 10. Furthermore, the dispersion-strengthened PM alloys exhibit secondary properties; e.g., fracture toughness and crack propagation rates, which are equivalent to those of 7075-T6 as shown in Figures 11 and 12.

In an evaluation of aluminum PM alloys, it is useful to compare the performance with not only ingot metallurgy alloys but with other isotropic metals, metal and polymer matrix composites. On this basis, Allied's FVS1212 (Al-12.4 wt % Fe-1.2 wt % V and 2.3 wt % Si) is compared against a particulate SiC-aluminum metal-matrix composite, 2618-T61 and a graphite-polyamide-resin-matrix composite. The ultimate tensile strength and specific modulus versus temperature are shown in Figures 13 and 14, respectively. Unidirectional polymer-matrix composites and some quasi-isotropic composites generally excel with regard to specific strength and specific modulus. However the properties must be considered on a cost-effective basis and in terms of the life-cycle cost of the product.

In summary, the elevated-temperature aluminum alloys utilize a dispersion of aluminides and silicides ranging in volume fraction from 5 to 40% in an aluminum matrix for strengthening. The size, distribution, and coarsening response for the intermetallic phases provide for excellent elevated-temperature strength with a significant increase in modulus. Important issues to resolve are the processing and mechanical property reliability, economy of scale of billet production coupled with the ability to produce complex structural shapes via forging, extrusion, or rolling superplastic forming or forging approaches. Issues that also pose challenges to these high temperature structural alloy systems are the elevated-temperature coarsening response, fatigue crack initiation, and propagation response coupled with the oxidation and stress corrosion performance.

## IV. Hybrid Powder-Metallurgy Alloy Systems

### A. Mechanically Alloyed Aluminum Powder Alloys

With the development of high-strength 7000 series alloys and dispersion-strengthened elevated-temperature alloys, it would be desirable to further strengthen these alloys by superimposing an additional constituent; e.g., an oxide or carbide dispersoid, to improve elevated-temperature response, or a high-volume fraction of a whisker or particulate to increase the strength and modulus. To this end, several hybrid aluminum powder-metallurgy alloys have been developed. These include mechanically alloyed elemental and pre-alloyed aluminum alloy powder systems; the mechanical alloying of aluminum powders and carbides; aluminum metal-matrix composites developed by mixing and consolidation aluminum powder and high-modulus, low-density micron- and submicron-sized carbides (e.g., SiC, TiC, B<sub>4</sub>C); and direct-spray deposition of aluminum powders with refractory reinforcements (e.g. Osprey). In each of these processes, the additional constituents provide for desirable and detrimental changes to the alloy's mechanical and physical properties. With the addition of refractory SiC particulates and/or whiskers, the strength, modulus, and wear resistance increase with a reduction of

### B. Elevated-Temperature Alloys---Development Efforts

Based on the earlier composition and powder processing studies, the development of high temperature aluminum alloys narrowed and matured to a number of candidate alloy systems: Al-Fe-Ce, Al-Fe-Mo-V, Al-Fe-Zr-V, Al-Fe-V-Si, and Al-Cr-Zr-Mn. Table XI compares strength elongation and modulus for the Al-8Fe, Al-8Fe-4Ce, Al-8Fe-2Mo, and two Allied alloys and an Alcan high-temperature alloy. Alternative approaches for production of rapidly solidified alloys consider atomization, splat quench and rotating disc techniques. The eventual successful alloy system must combine high performance with cost-effective processing. In each of these alloy systems, the ability of the dispersoids and intermetallic compounds to achieve a uniform and fine intermetallic particle distribution is essential for the high temperature strength of the candidate systems. Consequently, the development of a low angle grain boundary structure that is pinned by fine dispersions can provide enhanced elevated temperature stability. As of the late 1980s, dispersion strengthened aluminum PM alloys are being examined for use in aircraft and jet engines as a replacement for 2000 series aluminum or titanium alloys. Rainen and Ekwall [70] determined that Al-Fe-Ce and Al-Fe-V-Si sheet show potential for significant weight and cost savings. Figure 9 plots the mechanical properties of Al-7.1Fe-6.0Ce (Alcoa designation CZ42) and Allied's Al-8Fe-1V-2Si; e.g., FVS0812, on a specific property basis as a function of test temperature and exposure. In addition, if a comparison is made of retained strength of the aforementioned alloys, the stability of FVS0812 and CZ42 are shown to be superior to that of 2090, 2024, and 2219 ingot-metallurgy alloys, Figure 10. Furthermore, the dispersion-strengthened PM alloys exhibit secondary properties; e.g., fracture toughness and crack propagation rates, which are equivalent to those of 7075-T6 as shown in Figures 11 and 12.

In an evaluation of aluminum PM alloys, it is useful to compare the performance with not only ingot metallurgy alloys but with other isotropic metals, metal and polymer matrix composites. On this basis, Allied's FVS1212 (Al-12.4 wt % Fe-1.2 wt % V and 2.3 wt % Si) is compared against a particulate SiC-aluminum metal-matrix composite, 2618-T61 and a graphite-polyamide-resin-matrix composite. The ultimate tensile strength and specific modulus versus temperature are shown in Figures 13 and 14, respectively. Unidirectional polymer-matrix composites and some quasi-isotropic composites generally excel with regard to specific strength and specific modulus. However the properties must be considered on a cost-effective basis and in terms of the life-cycle cost of the product.

In summary, the elevated-temperature aluminum alloys utilize a dispersion of aluminides and silicides ranging in volume fraction from 5 to 40% in an aluminum matrix for strengthening. The size, distribution, and coarsening response for the intermetallic phases provide for excellent elevated-temperature strength with a significant increase in modulus. Important issues to resolve are the processing and mechanical property reliability, economy of scale of billet production coupled with the ability to produce complex structural shapes via forging, extrusion, or rolling superplastic forming or forging approaches. Issues that also pose challenges to these high temperature structural alloy systems are the elevated-temperature coarsening response, fatigue crack initiation, and propagation response coupled with the oxidation and stress corrosion performance.

### IV. Hybrid Powder-Metallurgy Alloy Systems

#### A. Mechanically Alloyed Aluminum Powder Alloys

With the development of high-strength 7000 series alloys and dispersion-strengthened elevated-temperature alloys, it would be desirable to further strengthen these alloys by superimposing an additional constituent; e.g., an oxide or carbide dispersoid, to improve elevated-temperature response, or a high-volume fraction of a whisker or particulate to increase the strength and modulus. To this end, several hybrid aluminum powder-metallurgy alloys have been developed. These include mechanically alloyed elemental and pre-alloyed aluminum alloy powder systems; the mechanical alloying of aluminum powders and carbides; aluminum metal-matrix composites developed by mixing and consolidation aluminum powder and high-modulus, low-density micron- and submicron-sized carbides (e.g., SiC, TiC, B<sub>4</sub>C); and direct-spray deposition of aluminum powders with refractory reinforcements (e.g. Osprey). In each of these processes, the additional constituents provide for desirable and detrimental changes to the alloy's mechanical and physical properties. With the addition of refractory SiC particulates and/or whiskers, the strength, modulus, and wear resistance increase with a reduction of

Advances in fiber, whisker, and particulate chemistry and processing have led to programs to reinforce aluminum-base materials. Specifically, the addition of fiber, whiskers, or particulate SiC produces a composite material with excellent specific mechanical properties. Techniques can include mechanical alloying, powder blending, and consolidation or spray deposition, Figures 21, 22, and 23. The strength of fiber, whisker, and particulate reinforced aluminum clearly depends upon the fiber and matrix properties, whisker volume fraction, interface, aspect ratio, and orientation. In addition, the excellent fiber or whisker reinforcement properties must be maintained during the consolidation and extrusion process in order to achieve the full potential of metal matrix composites. If a reduction of fiber length or surface damage occurs, the subsequent metal-matrix composite will suffer a natural strength reduction. These factors have been examined analytically and experimentally to define structurally competitive properties of reinforced aluminum-base material systems. A balance of properties must be achieved in these reinforced alloys. Specifically, reinforcements; e.g., SiC, will enhance modulus, strength, and creep resistance while reducing ductility, fracture toughness, and notched tensile properties. A compromise in the volume fraction, size, and distribution of the reinforcement phase is required in order to achieve a useful structural alloy. Figure 24 compares of 8090 alloys and 8090 with SiC additions formed by spray deposition. In general, increases in the modulus and yield strength occur with a marked reduction in failure strain. Furthermore, when carbide or oxide additions are combined by mechanical alloying, similar increases in strength and a reduction in ductility are noted, Figures 17 and 18. The application of aluminum-metal matrix composite via the powder-metallurgy route or combined by mechanical alloying or spray deposition offers a high-modulus, high-temperature material. However, it is not clear whether the addition processing costs will limit acceptance in the commercial marketplace.

#### V. Summary

Aluminum powder metallurgy offers a processing technology with great potential. Progress to date includes the development of dispersion-strengthened, precipitation-hardened and metal-matrix composite PM alloys. These alloys have been shown to exhibit superior combinations of mechanical properties (such as strength, fracture toughness, elastic modulus, fatigue, and corrosion resistance) compared to ingot-metallurgy alloys. As of the late 1980s, the high cost of wrought PM components appears to be the major barrier hindering acceptance and growth of aluminum powder-metallurgy alloys as a structural materials. Nevertheless, the technology has developed new alloys and processing concepts for aluminum alloys with superior ambient- and elevated-temperature, which can be utilized in future structural applications to take advantage of their higher performance.

#### References

1. Irmann, R. (1949). "Technische Rudnschan," 41, 36, p. 19.
2. Irmann, R. (1952). "Metallurgia," 46, p. 125.
3. Lyle, J.P. Jr. (1952 December). "Metal Progress," p. 109.
4. Gregory, E., and Grant, N.J. (1954). "Trans. AIME," 200, p. 247.
5. Towner, R.J. (1958). "Metal Progress," 73, p. 70.
6. Towner, R.J., and Lyle, J.F. Jr. (1960). Alcoa Internal Report.
7. Roberts, S.G. (1957) WADC Report no. 56-481.
8. Jones, H. (1978). "Aluminum," 54, pp. 274.
9. Pickens, J.R. (1981). "J. Mater. Sci.," 16, 1437.
10. Palmer, I.G., and Tietz, T.E. (1981). In "Advances in Powder Technology," ed. G.Y. Chin. American Society for Metals, Metals Park, Ohio, pp. 189-224.
11. Singer, R.F. (1986). "Powder Met. Intl.," 18, no. 2, pp 79-83.
12. Froes, F.H., Kim, Y.W., and Hehmann, F. (1987). "J. of Metals," 39, no. 8, pp. 14-21.
13. Spear, R.E., and Gardner, E.R. (1963). "Trans. Am. Foundrymens Soc.," 71, pp 209-215.
14. Dean, W.A., and Spear, R.E. (1966). "Proceedings of the 12th Army Materials Research Conference," Syracuse University Press, Syracuse, N.Y., p. 268.
15. Flemings, M.C. (1966). "Proceedings of the 12th Army Materials Research Conference," Syracuse University Press, Syracuse, N.Y., p. 268.
16. Matzja, H., Giessen, B.G., and Grant, N.J. (1968). "Journal Institute of Metals," 96, pp. 30-32.
17. Duweg, P. (1967). "Trans. ASM," 60, pp 607-633.

18. Mehrabian, R. (1982). "International Metals Reviews," 27, no. 4, pp. 185-208.
19. Grant, N.J., (1982). In "High Strength Powder Metallurgy Aluminum Alloys," eds., M.J. Koczak and G.J. Hildeman. TMS-AIME, Warrendale, Penn., p. 3.
20. Schelling, R.D., and Donachie, S.J. (1983). "Metal Powder Report," 38, no. 10.
21. Billman, F.R., and Jatkar, A.D. (1986). AFWAL Contract F33615-82-C-5063.
22. Roberts, S.G. (1961A). In "Powder Metallurgy," ed. W. Leszynski, Interscience, p.799.
23. Towner, R.J., and Lyle, J.P. Jr. (1962). ASTIA Report AD 289526.
24. Haar, A.P., and Lyle, J.P. Jr. (1966). Contract no. DA-36-034-ORD-3559RD. Report no. AD 487,764.
25. Cebulak, W.S., and Traux, D.J. (1971). Contract DAAA 25-70-C-0358.
26. Cebulak, W.S. (1973). Contract DAAA 25-72-C-0593.
27. Roberts, S.G. (1973). Contract DAAG 46-73-C-0040.
28. Lyle, J.P. Jr., and Cebulak, W.S. (1975). "Met. Trans.," 6A, p. 685.
- 29.
30. Roberts, S.G. (1978). U.S. Patent 4,104,061.
31. Voss, D.P. (1979). AFOSR Grant 77-3440, Report no. DFVLR-FB79-34.
32. Kulic, J.C., and Billman, F.R. (1982). AFWAL TR-82-4071.
33. Singleton, O.R. (1984). AFWAL TR-83-4142.
34. Morgan, J.T., Gegel, H.L., Doraivelu, S.M., Matson, L.E., Martorell, I.A., and Thomas, J.F. Jr. (1982). In "High Strength Powder Metallurgy Aluminum Alloys," eds. M.J. Koczak and G.J. Hildeman, AIME, pp. 193-206.
35. Kim, Y-W., Griffith, W.M., and Froes, F.H. (1983). "ASM Metals/ Materials Technology Series," no. 8305-048, American Society for Metals, Metals Park, Ohio.
36. Ackerman, L., Guillemin, I., Lalauze, R., and Pijolat, C. (1985). In "High Strength Powder Metallurgy Aluminum Alloys II," eds. G.J. Hildeman and M.J. Koczak, AIME, pp. 175-191.
37. Cebulak, W.S. (1977). Contract DAA 25-72-C-0593, Report FA-TR-76067.
38. Daugherty, T.S. (1964). "Journal of Metals," 16, pp. 827-830.
39. Ro, D.H., (1981). AFWAL Contract No. F-33615-80-C-5161.
40. Ping, S.W. (1986). In "Rapidly Solidified Powder Aluminum Alloys," eds. M.E. Fine and E.A. Starke, Jr., ASTM STP890, ASTM, Philadelphia, pp.369-380.
41. Hildeman, G.J., Labarre, L.C., Hafeez, A., and Angers, L.M. (1985). In "High Strength Powder Metallurgy Aluminum Alloys II," TMS-AIME, Warrendale, Penn., pp. 25-43.
42. Hart, R.M. (1981). Alcoa Green Letter.
43. Bretz, P.E. (1984). Alcoa Technical Brief.
44. Langenbeck, S.L. (1982). In "High Strength Powder Metallurgy Aluminum Alloys," eds. M.J. Koczak and G.J. Hildeman, TMS-AIME, Warrendale, Penn., pp. 87-105.
45. Scarich, G.V. (1984). IRAD Spectrum Fatigue Data. Northrop Corporation, Hawthorne, California.
46. Lyle, J.P. Jr., and Towner, R.J. (1970). U.S. Patent 3,544,392.
47. Lebo, N., and Grant, N.J. (1974). "Met. Trans.," 5, p. 1547.
48. Ping, S.W. (April 1985). Kaiser Aluminum and Chemical Corporation Data Sheet.
49. Paris, H.G. (1986). U.S. Patent 4,629,505.
50. Paris, H.G., and Chellman, D.J. (1986). In "Rapidly Solidified Powder Aluminum Alloys, ASTM STP890," eds. M.E. Fine and E.A. Starke, Jr., ASTM, Philadelphia, pp. 527-544.
51. Bomford, M.J., and Benjamin, J.S. (1974). U.S. Patent 3,816,080.
52. Novamet Aluminum (1984). Data Sheet.
53. Hardy, J. (1940). Unpublished Alcoa Research Laboratory Data.
54. Cremer, G.D., and Cordiano, J.J. (1943). "Trans. AIME," 152, pp. 152-1162.
55. Storchheim, S. (1962). "Progress in Powder Metallurgy," 18, pp. 124-130.
56. Dudas, J.H., and Dean, W.A. (April 1969). "International Journal of Powder Metallurgy," 5.
57. Pickens, J.R., Schelleng, R.D., Donachie, S.J., and Nichol, T.J. (1981). U.S. Patent 4,292,079.
58. Dudzinski, N., Murray, J.R., Mott, B.W., and Chalmers, B. (1947). "Journal Inst. of Metals," 74, pp. 291-314.
59. Dean, W.A. (1967). In "Aluminum Vol. I Properties, Physical Metallurgy and Phase Diagrams," ed. K.R. Van Horn, American Society for Metals, Metals Park, Ohio, p. 168.
60. Towner, R.J., and Lyle, J.P. Jr., (1960). Alcoa Internal Report.
61. Towner, R.J., and Lyle, J.P. (1961) U.S. Patent 3,004,331.
62. Quist, W.E., and Lewis, R.E. (1986). In "Rapidly Solidified Powder Metal Aluminum Alloys," eds. M.E. Fine and E.A. Starke, Jr. ASTM STP890, ASTM, Philadelphia, pp. 7-38.

63. Sankaran, K.K., and Grant, N.J. (1981). In "Aluminum-Lithium Alloys," eds., T.H. Sanders, Jr. and E.A. Starke, Jr., TMS-AIME, Warrendale, Penn. p. 101.
64. Gysler, A., Crooks, R., and Starke, Jr., E.A. (1981). In "Aluminum-Lithium Alloys," eds. T.H. Sanders, Jr. and E.A. Starke, Jr., TMS-AIME, Warrendale, Penn. p. 263.
65. Palmer, I.G., Lewis, R.E., Crooks, D.D., Starke, Jr., E.A., and Crooks, R.E. In "Aluminum-Lithium Alloys II," eds. T.H. Sanders, Jr., and E.A. Starke, Jr. TMS-AIME, Warrendale, Penn. p. 91.
66. Jones, H., (1969). "Mater. Sci. Eng.", 5, p. 1.
67. Pontikakas, I., and H. Jones, (1982). "Metal Science," 16, 27.
68. Sanders, R.E. Jr., and Hildeman, G.J. (1981). AFWAL-TR-81-4076.
69. Hildeman, G.J., and Sanders, Jr., R.E. (1983). U.S. Patent 4,379,719.
70. Rainen, R.A., and Ekvall, J.C. (1988). "J. of Metals," 40, no. 5, p. 18.
71. Roberts, S.G. (1969). U.S. Patent 3,462,248.
72. Gilman, P.S., Brooks, J.W., and Bridges, P.J. (1985). In "Proceedings of the Third International Conference on Aluminum Lithium," Oxford, England.
73. Allied Technical Data Sheet, Allied Signal Corporation (1988). Morristown, N.J.
74. Lyle, J.R., Jr., and Granger, D.A. (1985). "Ullman's Encyclopedia of Industrial Chemistry," vol. 1A, VCH Publishers, pp. 481-528.

#### Acknowledgement

The author would like to acknowledge program support from the Air Force Office of Scientific Research and the Naval Air Development Command in the development of powder metallurgy aluminum alloys.

**TABLE I**  
DEVELOPMENT OF ALUMINUM POWDER-METALLURGY ALLOYS—DISPERSION ALLOYS

Alloy type	1950	1960	1970	1980	Reference <sup>a</sup>
<i>Elevated Temperature:</i>					
(SAP)-XAP-Ae					
Al-Al <sub>2</sub> O <sub>3</sub>					
Al-X*					1-3
Al-Fe, Al-X					7
Al-Si					5.6
Al-Al <sub>2</sub> O <sub>3</sub> (MA) <sup>b</sup>					(Dixon and Skelly, 1965)
Al-Mn-Si <sup>c</sup>					51
Al-X <sup>d</sup>					37
					(Read et al., 1975)
					(Erich, 1980)
Al-X'(MA)					68.69
Al-Fe-Ce					73
Al-Fe-Mo					(Miller, 1984)
Al-Cr-Zr					(Skinner et al., 1984)
Al-Fe-V-Si					
<i>High modulus:</i> <sup>e</sup>					
Al-TiC, Al-Mn, Al-Fe <sup>f</sup>					(MacDonald and Ransley, 1954)
Al-Mn, Fe, Cr					5
					(Vidov, Lewis et al., 1986)
					(Divecha et al., 1981)
Al-SiC (MA)					(Donachie and Gilman, 1983)
					(Meschter et al., 1986)
<i>Low Density</i>					
Al-Li, Al-Be					(Lyle and Towner, 1960)
					2024 + Li
					63
					Al-Li-Cu-Mg
					(Palmer et al., 1982)
					Al-Mg-Li(MA)
					(Donachie and Gilman, 1983)
					Al-Li-Be
					(Lewis and Starke, 1986)

## Notes:

<sup>a</sup> Reference numbers in right-hand column refer to references at end of chapter.<sup>b</sup> X = Mn, Ni, Co, Cr, Ti, Zr, V.<sup>c</sup> MA = mechanically alloyed.<sup>d</sup> Also has low thermal expansion.<sup>e</sup> X = Ti, V, Cr, Mn, Fe, Co, Ni, Zr, Nb, Mo, Si.<sup>f</sup> X = Fe, Co, Ti, Mg, Mn, Zn, Ni, Cr, Cu.<sup>g</sup> A number of elevated temperature alloys also have a high elastic modulus.<sup>h</sup> Blended Al and elemental Mn, Ni, Fe powders.

**TABLE II**  
DEVELOPMENT OF ALUMINUM POWDER-METALLURGY ALLOYS PRECIPITATION STRENGTHENED

Alloy type	1950	1960	1970	1980	Reference <sup>i</sup>
<i>Pressed and sintered</i> (Al-Cu-Mg-Si):					
Al-Cu					53
Al-Cu-Mg-Mn					54
					55
Al-Cu					56
201AB, 601AB					
<i>Prealloyed/wrought</i> 2XXX (Al-Cu):					
Al-Mn-Cu					61
2024					22
					47
2124					(Erich and Donachie, 1982)
IN9021					50
					2024, 2024 + Zr
					40
<i>Corrosion-resistant</i> 5XXX (Al-Mg): <sup>j</sup>					
					IN9051, IN9052
					57
					6
<i>High-strength</i> 7XXX (Al-Zn-Mg-Cu):					
7XXX <sup>k</sup>					22, (Lyle and Towner, 1962)
					24
7XXX + Co, Fe + Ni					19.28 (Grant, 1982)
7XXX + (Co, Zr, Cr)					30
					(Alcan, 1980)
7000/7091					(Kaiser, 1985)
7064					7XXX + Zr + Ni (Hildeman et al., 1985)
					7XXX + Mn (Kozak, 1982)
					7XXX + Cr, Zr (Alcan, 1986)

## Notes:

<sup>i</sup> Reference numbers in right-hand column refer to references at end of chapter.<sup>j</sup> Al-Mg alloys exhibit excellent corrosion resistance.<sup>k</sup> Investigated elemental additions up to 15% Zr, 15% Mg, 20% Cu plus transition elements (Mn, Fe, Ni, Cr, Ti, V, Zr, Co, Mo, W) additions up to 4%

**TABLE III**  
EXTENSION OF SOLID SOLUBILITY FOR BINARY ALUMINUM ALLOYS

Elements	At % equilibrium	At % reported maximum
Ce	0.01	1.9
Co	0.01	0.5-5
Cr	0.44	5-6
Cu	2.5	17-8
Fe	0.025	4-6
Mg	18.9	37-40
Mn	0.7	6-9
Mo	0.07	>1.0
Ni	0.023	1.2-7.7
Si	1.59	10-16
Ti	0.15	.22-2
V	0.2	1.4-2
Zn	66.5	38
Zr	0.083	1.15-1.5

Source: After Jones [8].

**TABLE IV**  
ADVANTAGES AND BARRIERS TO GROWTH OF WROUGHT ALUMINUM PM ALLOYS

<i>Advantages:</i>
Unique compositions
Fine-grain, constituent, and disperoid sizes
Homogeneous distribution of alloy elements
Superior combinations of strength, toughness, and resistance to corrosion and fatigue
Potential for improved modulus, thermal stability, and low density
<i>Barriers:</i>
High cost
Product availability and size limitation
Quality-control issues

**TABLE V**  
NOMINAL COMPOSITIONS OF 7XXX ALUMINUM PM ALLOYS

Alloy	Zn	Mg	Cu	Co	Cr	Zr	Ni	O	Al
7064	7.1	2.3	2.0	0.2	0.1	0.2	—	.2	Bal.
PM61	8.5	2.5	1.5	0.6	—	0.2	—	.2	Bal.
7090	8.0	2.5	1.0	1.5	—	—	—	.35	Bal.
7091	6.5	2.5	1.5	0.4	—	—	—	.35	Bal.
CW67	9.0	2.5	1.5	—	—	0.14	0.1	.35	Bal.

Source: For 7064 and PM61, Kaiser Aluminum and Chemical Corp., Data Sheet, April 1985. For 7091 and 7092, Aluminum Company of America, Technical Brief, March 1985. For CW67, Alcoa Internal Research and Development (IRAD), April 1983.

Note: Elements in wt %.

**TABLE VI**  
TYPICAL PROPERTIES OF 7XXX-T7 ALUMINUM PM ALLOY DIE FORGINGS

Alloy temper	Test direction	YS (MPa)	UTS (MPa)	Elong. (%)	K <sub>IC</sub> <sup>a</sup> (MPa · m <sup>1/2</sup> )	SCC (MPa)
X7064-TX76	L	572	607	15	30	—
	LT	551	600	12	—	—
	ST	545	593	6	—	241
X7064-TX73	L	517	572	15	33	—
	LT	503	551	12	—	—
	ST	496	551	9	—	310
7090-T7E71	L	550	600	13	22	—
	T	540	574	7	23	241
7091-T7E69	L	514	566	14	30	—
	T	496	549	9	28	290
7075-T73	L	467	525	12	22	—
	(IM)	414	474	7	20	290

Source: Kaiser Aluminum and Chemical Corp., Data Sheet, April 1985, for X7064-TX76, X7064-TX73, and 7075-T73. Aluminum Company of America, November 1984, for 7090-T7E71 and 7091-T7E69.

Notes:

<sup>a</sup>L-T orientation per ASTM E399.

L = Parallel to grain flow.

T = Nonparallel to grain flow.

ST = Short transverse

LT = Long transverse

**TABLE VII**  
NOMINAL COMPOSITIONS OF 2XXX AND 5XXX PM ALLOYS

Alloy	Cu	Mg	Mn	Zr	Cr	O	C	A
PM63	4.5	1.8	0.8	0.25	—	N.D.	—	Bal.
PM042	3.7	1.8	0.2	0.6	—	N.D.	—	Bal.
IN9021	4.0	1.5	—	—	—	0.8	1.1	Bal.
2024 IM	4.4	1.5	0.4	—	—	—	—	Bal.
IN9051	—	4.0	—	—	—	0.6	0.75	Bal.
IN9052	—	4.0	—	—	—	0.8	1.1	Bal.
5083 IM	—	4.4	0.7	—	0.15	—	—	Bal.

Source: Kaiser Aluminum and Chemical Corp., April 1985, for PM63. Alcoa/Lockheed California, August 1981, for PM042. Novamet Aluminum, Data Sheet, August 1984, for IN9021, IN9051, and IN9052.

Note: Elements in wt %.

N.D. = not determined.

**TABLE VIII**  
**TYPICAL PROPERTIES OF IN-9021 AND IN-9052 FORGINGS**

	IN-9021-T4	2024-T4	IN-9052	5086-H34
Ultimate tensile strength, MPa (-Ksi)	538 (78)	469 (68)	448 (65)	324 (47)
Yield strength 0.2% MPa (-Ksi)	469 (68)	324 (47)	379 (55)	255 (37)
Elongation, %	13	19	13	10
Fracture toughness.				
K <sub>IC</sub> MPa $\sqrt{\text{m}}$ (-Ksi $\sqrt{\text{in.}}$ )	40 (36)	29 (26)	44 (40)	—
Elastic modulus, GPa (-Msi)	74.4 (10.8)	(10.6)	71.0 (10.3)	71.0 (10.3)
Density, g/cm <sup>3</sup> (-lb/in. <sup>3</sup> )	2.80 (0.101)	2.80 (0.101)	2.66 (0.096)	2.66 (0.096)
Threshold for SCC, <sup>a</sup> MPa (-Ksi)	>413 (>60) <sup>b</sup>	296 (43) <sup>b</sup>	>379 (>55) <sup>c</sup>	Susceptible if heated at 150° for long times <sup>c</sup>

Source: 2024-T4 and 5086-H34 data from *Aluminum Standards and Data* (Al. Assoc. Inc.) and *Military Standardization Handbook-5C* (U.S. Department of Defense).

<sup>a</sup> 90-day alternate immersion on 3% NaCl.

<sup>b</sup> Long transverse.

<sup>c</sup> Sensitized at 200°F for 7 days; short transverse.

**TABLE IX**  
**COMPOSITION OF LOW-DENSITY ALUMINUM ALLOYS**

	Li	Cu	Mg	Zr	O	C	Mn	Cd
2020	1.0	4.5	—	—	—	—	0.8	0.15
2024	—	4.4	1.5	—	—	—	0.6	—
01420 (USSR)	2.2	2.7	—	0.12	—	—	—	—
Alcoa (CW56)	2.2	2.7	—	0.12	—	—	—	—
Lockheed Alloy 1	3.0	1.5	1.0	0.2	—	—	—	—
Lockheed Alloy 2	2.0	3.0	1.0	0.2	—	—	—	—
Novamet (INCO) Alloy	1.4	—	3.8	—	—	—	—	—
Allied 643	34.-3.6	0.8-0.1	0.4-0.6	0.4-0.6	0.6	1.1	—	—
Allied 644	3.0-3.2	0.8-1.1	0.4-0.6	0.4-0.6	—	—	—	—
Alcan	2.5-1.9	1.2	0.7	—	—	—	—	—
2090	1.9-2.6	2.4-3.0	0.25	0.10	—	—	0.05	—
2091	1.7-2.3	1.8-2.5	1.1-1.9	0.25	—	—	0.10	—
8090	2.2-2.7	1.0-1.6	0.6-1.3	0.25	—	—	0.10	—
8091	2.4-2.8	1.8-2.2	0.5-1.2	0.25	—	—	0.10	—

**TABLE X**  
**COMPARISON OF MECHANICAL PROPERTIES OF 8090 ALUMINUM ALLOYS**

		Conventional direct chill cast and forged	Spray-cast and hot isostatic pressed
<sup>a</sup> y	Yield strength MPa (ksi)	310 (45)	310 (45)
<sup>a</sup> UTS	Ultimate strength MPa (ksi)	345-380 (50-55)	449 (65)
<sup>a</sup> f		0.25-0.55	9-10
K <sub>ISB</sub>	MPa(m) <sup>1/2</sup> [ksi(m) <sup>1/2</sup> ]	11-20 (10-17)	31-35 (28-32)
As-cast grain size	(microns)	200-500	15-30
Grain-boundary film thickness	(microns)	2-3	0.1-0.2

Source: Lewis, R.E. [Private Communication]

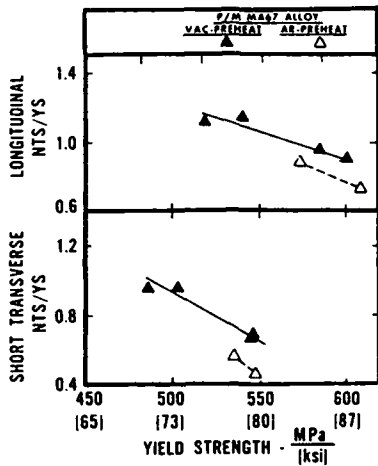


FIG. 4. Effects of preheat method on toughness and strength of PM MA 67 die forgings.

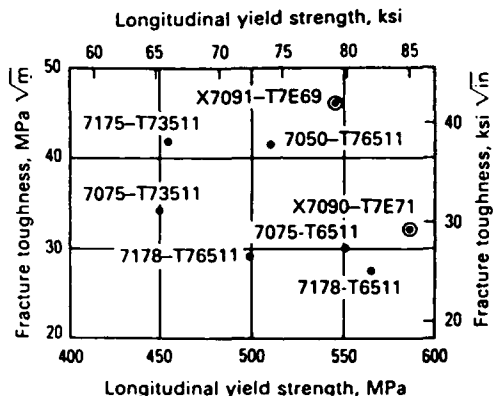


FIG. 5. Typical fracture toughness versus yield strength for high-strength aluminum extruded shapes. Specimens were 6.4–38 mm (0.25–1.5 in.) thick.

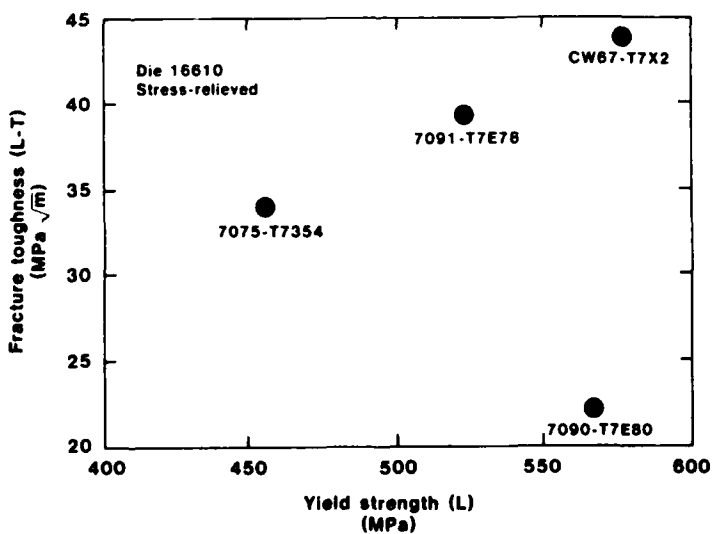


FIG. 6. Fracture toughness and yield strength for 7XXX PM versus 7075 IM forgings.

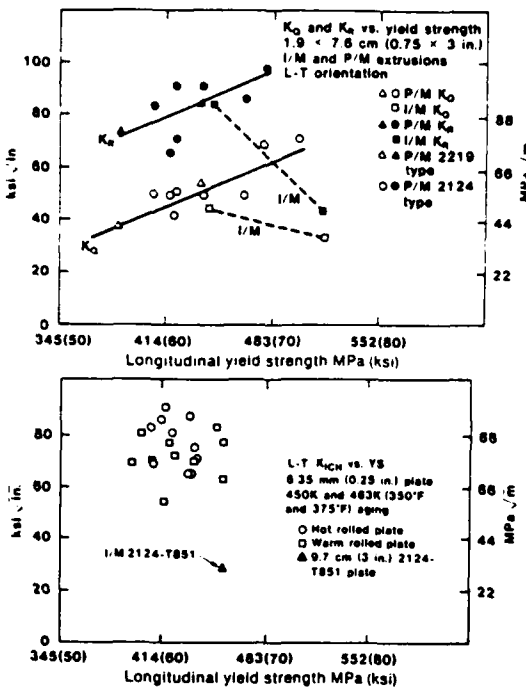


FIG. 7. Toughness versus yield-strength relationships in extrusion and plate. Top: Dependency of  $K_0$  and  $K_r$  on the yield strength of the extrusions. Bottom: Dependency of charpy toughness on the yield strength of the 6.35-mm plate.

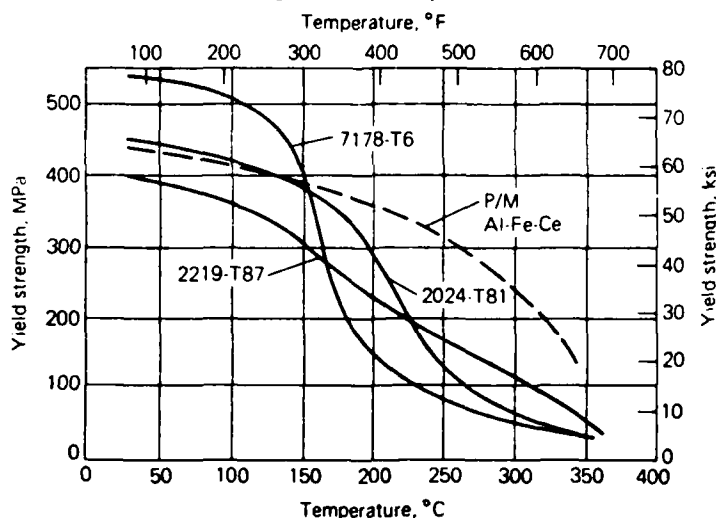


FIG. 8. Yield strength versus temperature for PM Al-Fe-Ce compared to ingot-metallurgy alloys 2219-T87, 2024-T81, and 7178-T6 following 100 hours exposure at the temperature indicated.

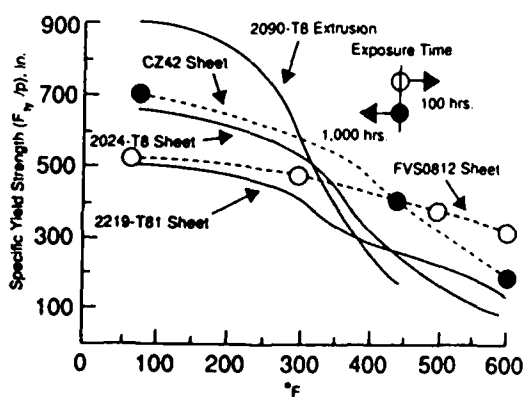


FIG. 9 Comparison of elevated-temperature PM aluminum alloy (FVS0812 and CZ42 and 2090-T8) as a function of thermal exposure test temperature.

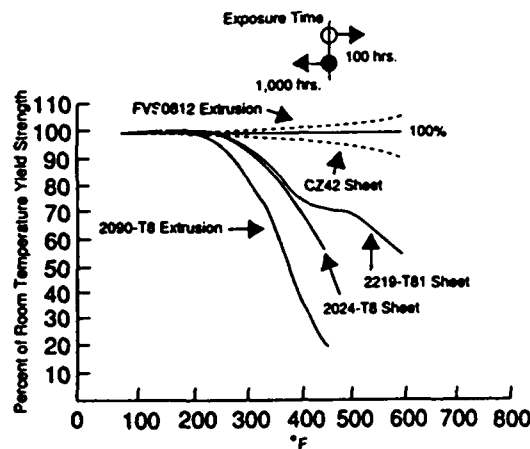


FIG. 10. Elevated-temperature stability of CZ42 and FVS0812 as a percentage of room-temperature strength.

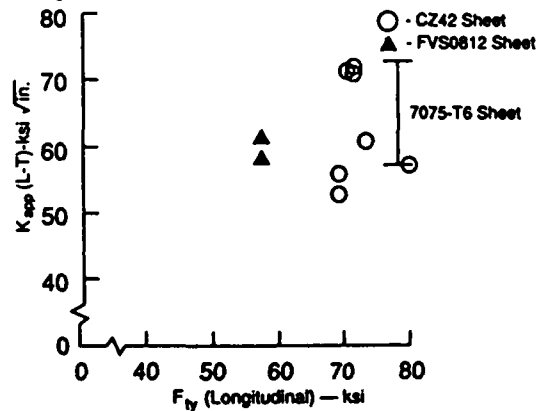


FIG. 11. A comparison of fracture toughness versus longitudinal yield strength for FVS0812, CZ42, and 7075 sheet. [73]

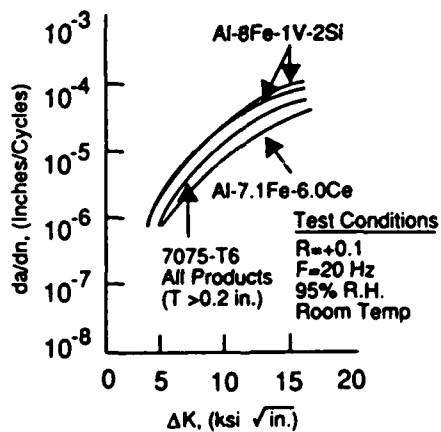


FIG. 12. Fatigue crack propagation  $da/dN$  versus  $\Delta K$  of thin extrusions. [73]

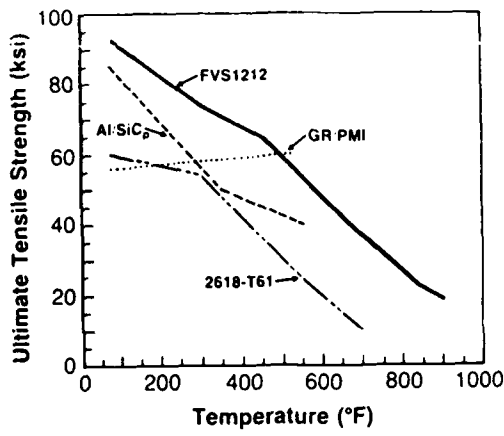


FIG. 13. Ultimate tensile strength of Allied FVS1212 compared to ingot-metallurgy (2618-T61) polymer (GR-PMI) and metal-matrix (Al-SiC<sub>p</sub>) composites. [73]

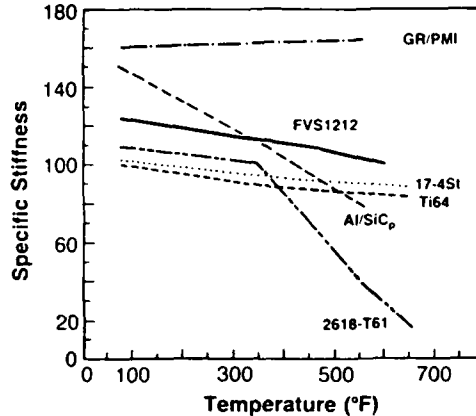


FIG. 14. Specific stiffness versus temperature of Allied FVS1212 compared to ingot metallurgy (2618-T61), polymer (GR-PMI), and metal-matrix composites (Al-SiC<sub>p</sub>). [73]

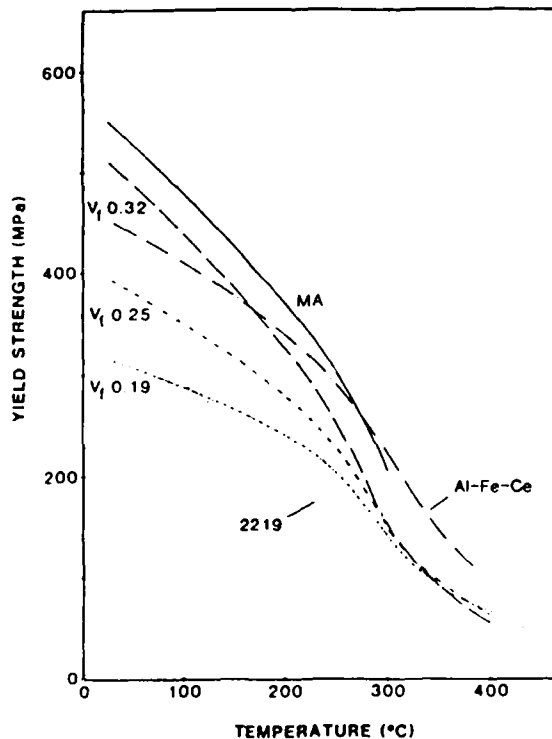


FIG. 15. Elevated-temperature yield-strength response for Al-Fe-Ni ( $\alpha$ ,  $V_f = 0.19, 0.25,$  and  $0.32$  of FeNiAl), 2219, Al-Fe-Ce and Al-Fe-Ni ( $\alpha$ ,  $V_f = 0.19$  which has been mechanically alloyed (MA). From (Ezz et al. 1986).

**TABLE XI**  
**PROPERTIES OF DISPERSION-STRENGTHENED PM ALLOYS**

Alloy	Temp. °C	YS		UTS		E	
		MPa (ksi)	MPa (ksi)	EL %	GPa	(msi)	
Al-8Fe	RT	504 (73.1)	572 (83.0)	5.0	81.4	(11.8)	
	232	260 (37.7)	280 (40.6)	9.6	55.2	(8.0)	
	343	148 (21.4)	172 (24.9)	12.3	40.0	(5.8)	
Al-8Fe-4Ce	RT	445 (64.5)	550 (79.8)	9.0	78.1	(11.3)	
	232	367 (53.3)	395 (57.3)	6.0	—	—	
	343	152 (22.0)	176 (25.5)	7.0	—	—	
Al-8Fe-2Mo	RT	472 (68.4)	492 (71.3)	6.7	86.2	(12.5)	
	204	427 (62.0)	452 (65.5)	7.0	79.3	(11.5)	
	343	200 (29.0)	222 (32.2)	10.0	75.9	(11.0)	
Allied 1	RT	596 (86.4)	621 (88.9)	6.3	—	—	
	232	425 (61.6)	433 (62.8)	6.8	—	—	
	343	253 (36.7)	270 (39.2)	11.4	—	—	
Allied 2	RT	632 (91.7)	645 (93.6)	8.7	—	—	
	232	414 (60.0)	420 (60.9)	7.3	—	—	
	343	240 (34.8)	252 (36.6)	10.2	—	—	
Alcan	RT	540 (78.3)	580 (84.1)	12	82	(11.9)	
	250	415 (60.2)	437 (63.4)	14	—	—	
	300	270 (39.2)	300 (43.5)	15	—	—	

Note: RT = Room Temperature (20°C)

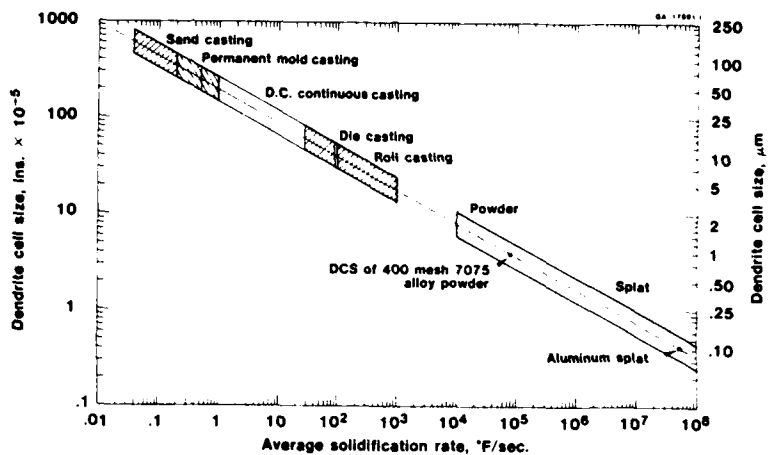


FIG. 1. Cooling rate and cell packings of various casting processes.

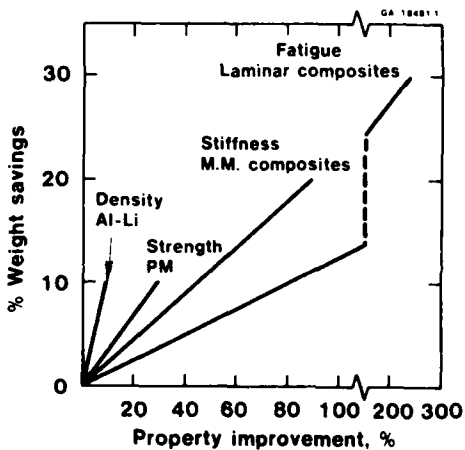


FIG. 2. The relationship between weight savings and property improvements

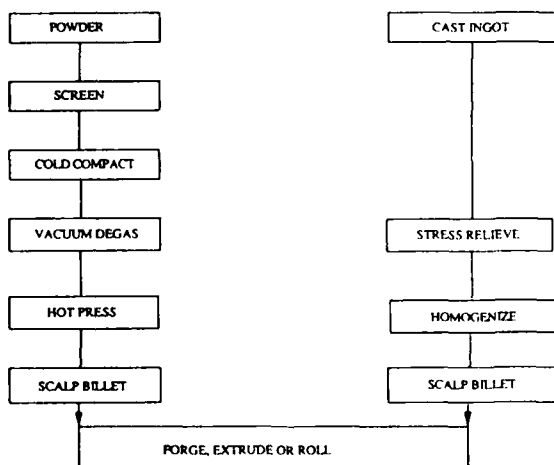


FIG. 3. Comparison of powder-metallurgy and ingot-metallurgy processing steps

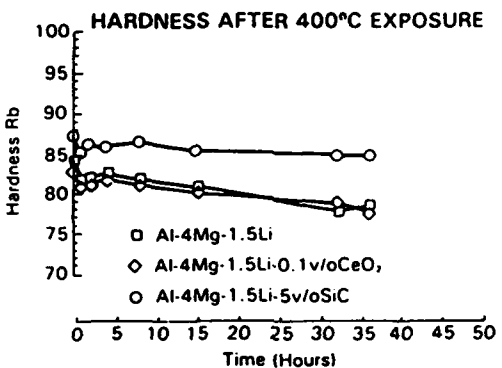


FIG. 16. Hardness of various Al-Mg alloys following exposures at 400°C. [72,73]

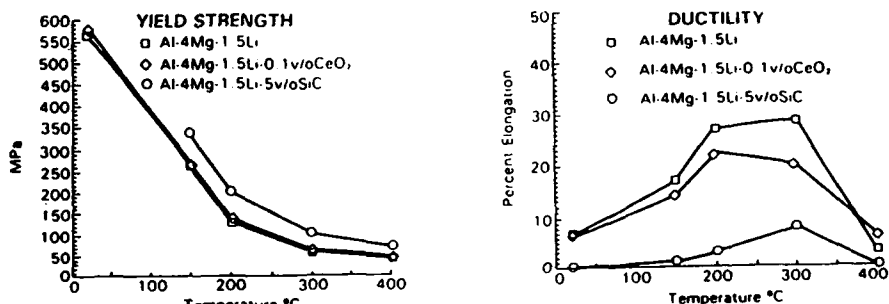


FIG. 17. Yield strength and ductility response versus test temperature for various mechanically alloyed Al-Mg alloys. [72,73]

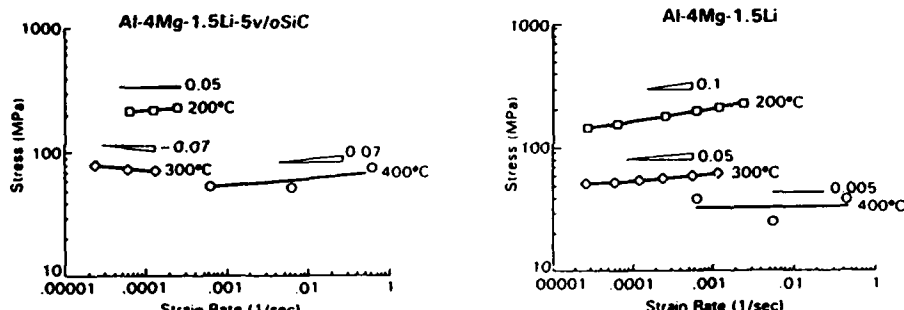


FIG. 18. Creep response at various temperatures for SiC-reinforced and unreinforced mechanically alloyed Al-Mg-Li Alloys. [72,73]

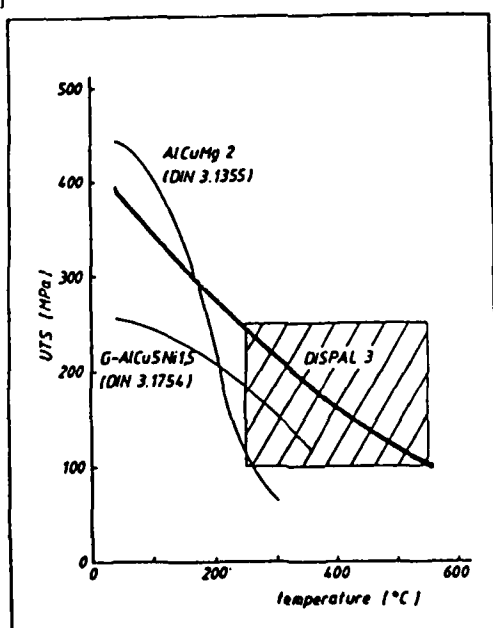


FIG. 19. Elevated-temperature response of Al-Cu alloys versus Dispal 3.

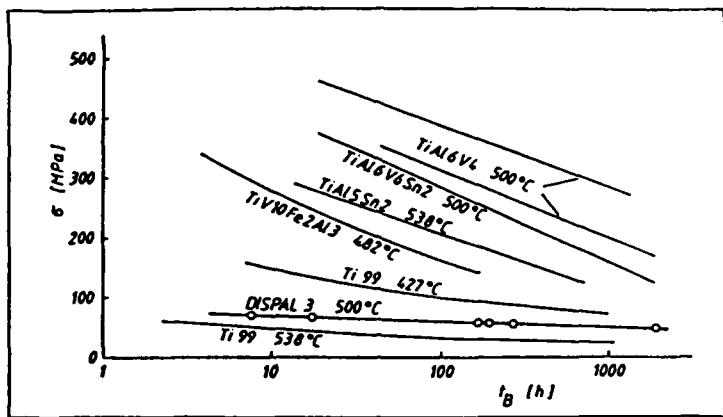


FIG. 20. Elevated-temperature stress-rupture response for various alloys.

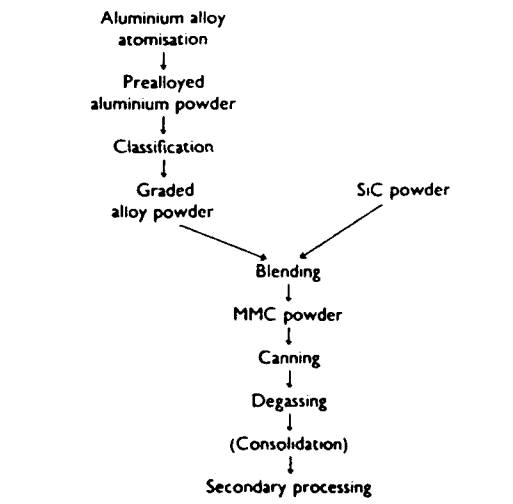


FIG. 21. Powder-blending route for metal-matrix composites.

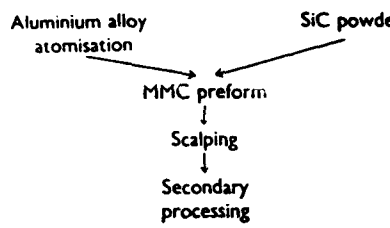


FIG. 22. Spray-deposition route for metal-matrix composites.

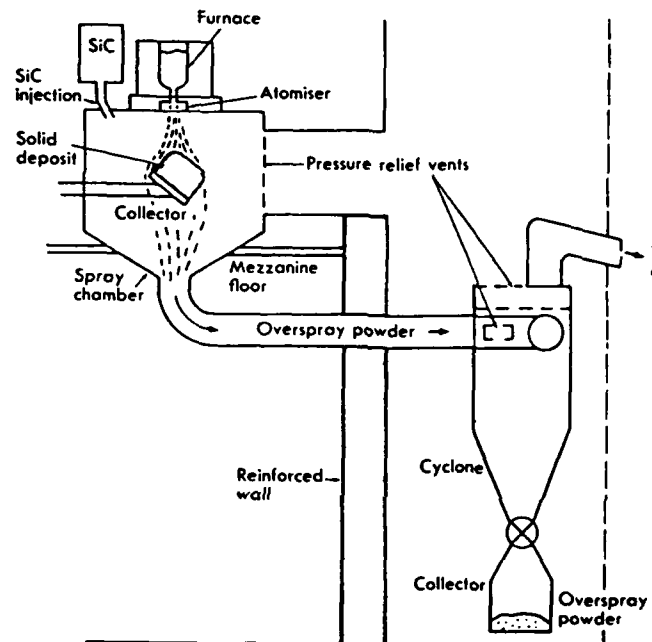


FIG. 23. Schematic diagram of Osprey fabrication of metal-matrix composites.

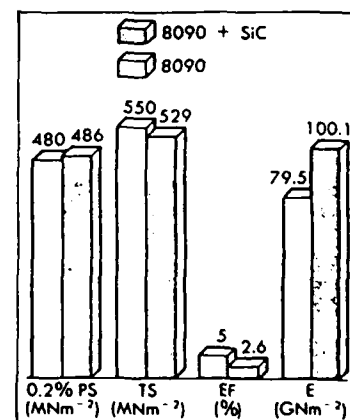


FIG. 24. Longitudinal yield strength, tensile strength, percent elongation, and modulus for Al-Li (8090) alloy and Al-Li (8090) with SiC additions.

After the exposure at 425°C the size of the precipitates  $\text{Al}_{13}\text{Fe}_4$  and  $\text{Al}_{13}\text{Fe}_3\text{Ce}$  is between 0.3 and 0.4  $\mu\text{m}$ ; the first ones contain often plane faults [23]. The precipitate size versus the isothermal exposure time increases regularly, that results from the ripening controlled by the diffusion of the solute atoms, Fe and Ce, along the grain boundaries [24]. When a tensile stress is applied during the exposure at high temperature the ripening is faster and the precipitates are larger (fig. 5). The size of the matrix grain increases slightly at the beginning of the exposure, from 0.7 to 0.9  $\mu\text{m}$  for about ten hours, and then it remains nearly constant.

Room temperature mechanical properties of these alloys were determined by hardness measurements [25,26], tensile [21,27] and compression tests [28]. The thermal stability of these properties after an exposure at high temperature was explored using the same tests. After an exposure for one hour the hardness decreases slightly at a temperature not exceeding 350°C and beyond its decrease is more marked [25] (fig. 6a). After an exposure at 300°C it remains unchanged until 1050 hours [26] (fig. 6b). The tensile and compression yield stress decrease after an exposure at 149 and 232°C for 1000 hours and at 316°C for 100 hours [27,28] (fig. 7). The comparison with the conventional 2219 alloy shows the advantage of the Al-Fe-Ce alloys in the hardness [26] and also in the yield stress [21]: for the 2219 alloy, the hardness decreases by 37.5% after an exposure at 300°C for 100 hours (fig. 6b); its yield stress starts decreasing after an exposure at 95°C for 1000 hours and at 315°C its diminution reaches 50%; it is only 10% in the alloys Al-Fe-Ce for the same tests (fig.8).

The elevated temperature tensile properties, up to 316°C, were measured for several compositions [21]. The corresponding results are summarized below:

Alloy	Temp. °C	Yield stress Mpa	Tensile strength Mpa	Elonga- tion %	Toughness Mpa/m	Density g/cm <sup>3</sup>	Young's modulus GPa
A17.1Fe6.1Ce (extruded)	25	387	493	11.7	12.2	2.957	78.9
	149	362	425	6.0			
	232	332	367	4.7			
	316	212	237	10.4			
A17.1Fe6.1Ce (extruded and forged)	25	524	567	5.7	26	2.957	78.9
	149	403	427	5.0			
	232	278	304	5.0			
	316	150	176	6.5			
A18.1Fe6.8Ce (extruded)	25	440	525	9.0	6.2	3.00	85.6
	149	364	433	4.0			71.8
	232	297	351	6.0			70.4
	316	211	246	9.0			63.5
A18.4Fe7.2Ce (extruded)	25	458	563	8.0	6.4	3.01	80.1
	149	448	484	4.0			
	232	391	424	4.0			
	316	225	271	7.3			
A19.8Fe7.8Ce	25	490	613	5.0		3.06	83.8
	149	492	525	2.6			
	232	410	450	2.6			
	316	255	295	5.3			

The yield stress and the tensile strength decrease versus the temperature while the elongation passes through a maximum at about 200-250°C. Elevated temperature mechanical properties of these alloys are superior to that of the conventional 2618 alloy and hopeful when compared to the Ti6Al4V alloy (fig.9).

It is worthwhile noticing that the high temperature properties are very sensitive to processing conditions: atomization, degassing and consolidation. The influence of the extrusion ratio and the residual hydrogen content is reported in the figure 10 [21]: an increase from 5.6 to 14 ppm in the hydrogen content does not modify the yield stress and the tensile strength, in return the minimum of the elongation disappears. An increase from 4:1 to 20:1 of the extrusion ratio diminishes the yield stress and the tensile strength but does not influence the elongation.

The compression tests performed between 250 and 550°C [23] indicate that the ripening cannot account for the degradation of the mechanical properties. It is suggested that at least one of the precipitated phases undergoes a plastic deformation beyond 450°C.

Creep experiments performed at a temperature between 250 and 350°C under stress from 20 to 115 MPa [30] underline a change in the deformation mechanism when the stress overcomes a threshold value. No explanation is available so far.

The fatigue crack growth is easier in the Al-Fe-Ce alloys compared to the conventional 2219 alloy [26]: at 25 and 300°C the crack growth rate is respectively 2 and 3 times larger (fig. 11).

The corrosion resistance, as measured by the weight loss, is higher for the Al-Fe-Ce alloys when compared to the conventional 2024-T3 and 7075-T6 alloys: in a 3.5% sodium chloride solution, corrosion rates from 7 to 15 times lower were reported during a 16 days exposure for Al-Fe-Ce alloys. The stress corrosion is also improved: the threshold value for fracture, 240 MPa, after a 30 days exposure is close to that of 7050-T7451 and 2219-T87 alloys and higher than that of 7075 alloy [29].

The mechanical properties of the Al-Fe-Ce alloys, at temperature higher than 250°C, is improved by the dispersion of fine  $\text{Al}_2\text{O}_3$  oxide and/or  $\text{Al}_4\text{C}_3$  carbide particles, from 10 to 40 nm in size, added by mechanical alloying. Besides the process was used with rapidly solidified powder [31,32,33].

The microstructure of the rapidly solidified and mechanically alloyed (R.S.M.A.) alloys with compositions close to Al-8Fe-4Ce depends on the extrusion conditions. At 245°C with an extrusion ratio of 16:1 [31], the resulting grain size is of the order of  $0.3 \pm 0.1 \mu\text{m}$  for the rapidly solidified (R.S.) and the R.S.M.A. alloys, the distribution of the precipitates is more homogeneous in the latter. After an exposure at 610°C for 1 hour dispersoid sizes in the R.S.M.A. alloy remain small while the grain size increases moderately from 0.25 to  $0.70 \mu\text{m}$ . At 550°C with an extrusion ratio 10:1 [32], small grain sizes are measured, about  $1 \mu\text{m}$ , in R.S. alloys while elongated grains along the extrusion direction, up to  $30 \mu\text{m}$ , are observed in R.S.M.A. alloys. The microstructure differences after consolidation are attributed to the differences in the stored energy, which is higher in R.S.M.A. alloys because of the larger value of the extrusion strain and the hardening of the grains due to the dispersoids. This excess of free enthalpy favours the recrystallization in the R.S.M.A. alloys.

The thermal stability was investigated for 245°C-extruded alloys [31]. The change in the hardness versus the exposure time at 450°C and versus the exposure temperature for 1 hour is reported in the figure 12. The hardness of the R.S.M.A. alloy, 24% higher than that of the R.S. alloy before exposure, remains constant after an exposure at 450°C for 300 hours while that of the R.S. alloy drops away. After an exposure for 1 hour the hardness of the R.S.M.A. alloy is preserved up to 500°C, only 300°C for the R.S. alloy: it appears that the lower quality of the R.S. alloy results from the ripening of the  $\text{Al}_{13}\text{Fe}_4$  and  $\text{Al}_{13}\text{Fe}_3\text{Ce}$  precipitates by diffusion of Fe and Ce atoms along the grain boundaries. In R.S.M.A. alloys the dispersoids, essentially located on the grain boundaries, first act as vacancy sinks lowering the diffusion process therefore the ripening mechanism and second prevent from a later recrystallization. After an exposure at 540°C for 288 hours the R.S. alloy has a  $1 \mu\text{m}$  grain size, to compare to the  $0.25 \mu\text{m}$  as measured in the R.S.M.A. alloy.

Whatever the temperature the ductility of the R.S.M.A. alloys is nearly to zero [31] while it reaches 10% for the R.S. alloy (fig. 13): cleavages are observed on the fracture surface of the former, dimples for the latter.

The compression tests performed at different temperatures with different strain rates on the alloys extruded at 550°C underline the advantage of the mechanical alloying [32,33]. For a fixed temperature the change in the ratio of the strain rate to the self-diffusion coefficient of aluminium versus the ratio of the maximum stress, from 3 to 5% in strain, to the Young's modulus is plotted in the figure 14: continuous curves are related to the R.S. alloy [23] and the points to the R.S.M.A. alloy. At 250°C the same behaviour is observed for both alloys: the small grained R.S. alloy is hardened by the high dislocation density tangles left by the extrusion process and the large grained R.S.M.A. alloy is hardened by precipitates and dispersoids. At higher temperature, the recovery releases the dislocation configurations, the ripening of the precipitates and the slip at the grain boundaries and/or the deformation of at least one precipitated phase deteriorate the mechanical behaviour of R.S. alloys. In the R.S.M.A. alloys, at the same temperature, the dispersoids delay the ripening and contribute to the hardening.

Furthermore, tensile creep resistance behaviour of R.S.M.A. alloys is clearly higher than that of R.S. alloys: at 380°C and under a 103 MPa loading, the creep strain rate of the R.S.M.A. alloy is  $3.5 \times 10^{-4}$  times lower than that of R.S. alloy [31].

### 3.2 - Al-Fe-V-Si ALLOYS

The alloys Al-Fe-Si rapidly solidified contain the metastable phase  $\text{Al}_{13}\text{Fe}_3\text{Si}$  which crystallizes in the bcc,  $\text{Im}3$ , structure and whose precipitate shape is almost spherical. Unfortunately this phase is metastable and it was not possible to benefit from its characteristics in order to maintain the good level of mechanical properties at high temperature; it transforms into the stable monoclinic  $\text{Al}_{13}\text{Fe}_4$  and hexagonal  $\text{Al}_8\text{Fe}_7\text{Si}$  phases, the morphology of their precipitates does not favour a good ductility. However it was shown that it is possible to stabilize the metastable phase by the addition of a fourth element (V, Mn, Cr, Mo) which substitutes for iron [34]. Vanadium was found as

the most promising element [35]. In order to precipitate only the  $\text{Al}_{12}(\text{Fe},\text{V})_3\text{Si}$  phase, adjusted compositions and high cooling rates are required. Melt-spinning technique was used and then the ribbon was ground and the powder was consolidated by the conventional techniques.

The microstructure of melt-spun ribbons of Al-Fe-V-Si alloys is made up wholly of the so-called "A" zone, i.e. featureless at a magnification up to 1000 [36]. Examinations at higher magnification show a cellular-dendritic microstructure with fine intermetallic compound  $\text{Al}_{12}(\text{Fe},\text{V})_3\text{Si}$  precipitates whose size ranges from 10 to 30 nm. However a too low quenching rate produces a quasicrystalline phase. Consolidation does not induce any modification of  $\text{Al}_{12}(\text{Fe},\text{V})_3\text{Si}$  precipitates, only a very small ripening is eventually observed. The distribution of these precipitates is uniform, they are located at the grain and sub-grain boundaries and also inside the grains with a size ranging from 40 to 80 nm [37].

The crystalline structure of the  $\text{Al}_{12}(\text{Fe},\text{V})_3\text{Si}$  is described by empty icosahedra (Fe+V) located at the sites of the bcc lattice; they are parallel and each of them is connected to eight neighbours along its threefold axes through a slightly contracted octahedron. Each icosahedron (Fe+V) contains an empty (Al+Si) icosahedron with the same orientation. These last icosahedra are connected through chains of three distorted octahedra [38]. This phase exists for a range of composition according to  $\text{Al}_{12-14}(\text{Fe},\text{V})_3\text{Si}_{0.9-1.29}$ , with a Fe:V ratio from 5:1 to 11.5:1. The lattice parameter varies with composition from 1.2587 to 1.2620 nm [37].

A volume fraction up to 42% of these precipitates can be obtained in the Al-Fe-V-Si alloys. Their ripening rate, depending on the Fe:V ratio value, is very low, from  $8.4 \cdot 10^{-27}$  to  $2.9^{-26} \text{ m}^3/\text{h}$ , when compared to the intermetallic compounds obtained in Al-Fe base alloys and the  $\text{Al}_3\text{Zr}$ ,  $\text{L1}_2$ -structure and coherent with the matrix, precipitates. This small ripening rate is explained by the formation of interface steps increasing the number of coincidence sites and thus decreasing the interfacial energy, rather than putting forward some coherency arguments [37].

The room temperature mechanical properties achieve a good standard: the highest the volume fraction of precipitates, the highest the standard [36, 37, 39, 40]. The thermal stability studies confirm the small ripening rate of the  $\text{Al}_{12}(\text{Fe},\text{V})_3\text{Si}$  precipitates: after an exposure at 524°C for 1000 hours, no change in the yield stress or the elongation is observed (fig. 16). After an exposure for 100 hours at a temperature less than 540°C, the yield stress remains constant in Al-Fe-V-Si alloys and it starts decreasing at higher temperature. This limit temperature is only 300°C in other Al-Fe-X alloys (fig. 17). After an exposure at a temperature higher than 500°C [41] the tensile decreases even for a comparatively short time (fig. 18). At 500°C the microstructure is stable after an exposure until 100 hours with a 0.47μm grain size and 160nm precipitate size. At 550°C the ripening of the precipitates is marked and a continuous distribution of precipitates appears along the grain boundaries; at the same time the recrystallization of the matrix starts and thus the grain size is equal to 0.9μm. This evolution is faster at 600°C with a 1.2μm grain size and 260nm precipitate size.

The elevated temperature mechanical properties were measured on extruded, forged and rolled alloys. The results obtained for the two most investigated compositions are reported in the table in the next page [36, 40].

When the temperature rises, the yield stress and the tensile strength decrease while the elongation passes through a minimum. When compared to other P/M Al-Fe-X alloys, the tensile strength of the FVS1212 alloy is larger in the full range of temperature and that of the FVS0812 alloy is larger at a temperature higher than 350°C (fig. 19). The behaviour of the first alloy is close to that of a to be discovered aluminium alloy with the same specific tensile strength as the Ti-6Al-4V alloy. Up to about 220°C the tensile strength is mainly controlled by the interaction between the mobile dislocations and the precipitates. For higher temperature it is controlled by the diffusion of the solute atoms and the precipitate size does not really matter [34, 37].

The testing temperature at which the minimum elongation is observed depends on the strain rate [42, 43]. For a fixed strain rate a plateau is noticed at this temperature (fig. 20) on the tensile strength versus the testing temperature curve. This is due to a particular hardening mechanism for this temperature-strain rate combination. The proposed explanation [41] assumes that the solute atoms, mainly iron atoms, of the supersaturated solid solution form atmospheres around the forest dislocations. When the mobile dislocations come close to the trees of the forest, the solute atoms have enough time to diffuse to their cores and consequently to lock them, producing a decrease in the ductility and an increase in the tensile strength.

The Al-Fe-V-Si alloys exhibit a good creep behaviour under compression [44] because of a high volume fraction of thermally stable precipitates.

## FVS0812 : Al-8.5Fe-1.3V-1.7Si and FVS1212 : Al-11.7Fe-1.15V-2.4Si

Alloy		Temp. °C	Yield stress Mpa	Tensile strength Mpa	Elonga- tion %	Toughness Mpa/m	Density g/cm <sup>3</sup>	Young's modulus GPa
FVS0812	L	24	390	437	10	31	2.957	88.4
Extruded	T		387	440	10			
Rolled	L	150	340	372	7			83.2
	T		335	372	5			
	L	204	312	341	8			
	T		307	344	7			
	L	260	280	308	9			
	T		279	312	9			
	L	315	244	261	9			73.1
	T		244	280	11			
FVS0812	L	24	434	462	12			
Forged	L	150	345	372	6			
	L	204	303	338	6			
	L	260	276	290	8			
	L	315	241	248	9			
FVS1212	L	24	605	636	8.7	11	3.02	95.5
Extruded	L	150	486	505	3.5			86.2
Plate	L	230	432	443	3.3			82.8
	L	345	276	286	6.7			78.6
	L	450	133	147	8.9			
	L	480	103	126	10.8			

Nevertheless the n exponent of the creep law,  $\dot{\epsilon} = k \cdot \sigma^n$ , is somewhat higher than usual, from 13 to 32 instead of from 3 to 6 (fig. 21). This particular behaviour is likely due to the enhancement of the ripening under stress: during an exposure at 400°C the precipitate size remains constant without applied load, it grows up one hundred times under a 158 MPa stress (fig. 22).

The Al-Fe-V-Si alloys compare quite well with the conventional alloy when one deals with the corrosion resistance, as measured by the weight loss techniques: in a 3.5% sodium chloride solution the loss is six times less than that measured in the 2014-T6 alloy.

### 3.3 - Al-Cr-Zr ALLOYS.

Among the R.S. Al-Cr-X and Al-Cr-Zr-X alloys, the Al-Cr-Zr and Al-Cr-Zr-Mn alloys were the most likely to lead to an industrial development [46,47]. Nevertheless in order to achieve the optimum properties, a thermal treatment is required after the rapid solidification. The ageing phenomena is due to zirconium: the hardness of Al-3Cr-xZr and Al-yCr-1Zr alloys, as-quenched and peak aged, versus respectively x and y is very sensitive to the value of x as peak aged and no sensitive to the value of y (fig. 23). The higher the Zr content, the larger the ageing effect [48,49]. This result is confirmed by the hardness change versus ageing time in the (1) Al-1.8Cr, Al-1.7Zr and Al-1.8Cr-1.7Zr alloys at 400°C (fig. 24) [50] and (2) Al-4.5Cr-1.7Zr alloy at 350, 400 and 450°C (fig. 25) [49,51,52]. In any case the optimum mechanical properties are reached after an ageing treatment.

The requirement of a thermal treatment for the Al-Cr-Zr can be an advantage compared to the rapidly solidified Al-Fe-X alloys. As a high temperature is needed during the consolidation, a degradation of the properties is expected in the Al-Fe-X alloys, in return this heating can be a part of the ageing treatment for the Al-Cr-Zr alloys. The properties of the as-quenched Al-Cr-Zr alloys are lower than that of the Al-Fe-X alloys, but after consolidation they will be equivalent if not improved (fig. 26) [48,52].

The microstructure of the powder particles is made of a solid solution and intermetallic Al<sub>1.3</sub>Cr<sub>2</sub> precipitates, from 0.5 to 2 μm in size. This compound has a monoclinic, C2/m, crystalline structure and it is non coherent with the matrix. During the ageing new Al<sub>1.3</sub>Cr<sub>2</sub> precipitates appear and the previous ones coarsen and also very fine Al<sub>1.3</sub>Zr precipitates are observed. This last compound has a cubic L1<sub>2</sub> crystalline structure and it is coherent with the matrix. The ageing effect is due mainly to the precipitation of the Al<sub>1.3</sub>Zr phase inside the grain as well in the neighbourhood of the boundaries giving a discontinuous precipitation [53]. The differential scanning calorimetry pattern reveals two peaks: between 270 and 400°C in connection with the Al<sub>1.3</sub>Zr precipitation and close to 475°C in relation to the ripening of Al<sub>1.3</sub>Cr<sub>2</sub> precipitates (fig.27) [49,51].

initiation is delayed. For the conventional alloys the crack grows along the smooth elongated grain boundaries as obtained after rolling while for R.S. alloys the small grain size (from 1 to 3  $\mu\text{m}$ ) imposes a wavy path to the crack propagation, i.e. an increase in the fracture energy. The crack growth rate is 3.7 times higher in 7075 T73 alloy than in 7091 T7E69 alloy, in salted solutions [8,9].

## 2.2 - MECHANICAL ALLOYING (M.A. ALLOYS)

Carbon and oxygen are mainly introduced in these M.A. alloys in order to precipitate  $\text{Al}_2\text{O}_3$  and/or  $\text{Al}_4\text{C}_3$  dispersoids. If necessary Si or Mg can be added. Some of the compositions reported in the litterature are listed below [10,11,12]:

Alloy	O	C	Mg	Si	$f_v$ (%)
DISPAL 0	2.5	-	-	-	4
DISPAL 2	1	2	-	-	10-12
DISPAL 3	0.8	3	-	-	
DISPAL 1Si12	1	1	-	12	6-10
IN9052	0.6	1.1	4	-	6

$f_v$  represents the volume fraction; 1wt% C corresponds to  $f_v = 4.5\%$  of aluminium carbide and 1wt% O to  $f_v = 1.6\%$  of oxide.

The existence of amorphous compounds with C and/or O is proved by the rings observed on the electron diffraction patterns obtained after grinding. Crystallized compounds only appear during the consolidation process [13] as very fine dispersoids, from 30 to 40 nm in size for the oxide and from 20 to 100 nm for the carbide; they are usually located at the grain boundaries, isolated or gathered together. The grain size lies between 0.2 and 0.5  $\mu\text{m}$ . Some intermetallic precipitates  $\text{Al}_3\text{Mg}_2$  were also reported.

Room temperature tensile properties of these alloys are summarized below:

Alloy	Yield stress Mpa	Tensile strength Mpa	Elongation %	Toughness Mpa/m	Density g/cm <sup>3</sup>	Young's modulus GPa
DISPAL 2	300-340	340-380	8-12		2.70	80
DISPAL 1Si12	300-340	340-380	4-8		2.66	85
IN9052	380	450	13	44	2.68	76

These properties depend on the oxygen or carbon content, i.e. on the volume fraction of dispersoids. Results obtained with a pure Al matrix are given in the figure 2 [10]: a linear increase of the yield stress and the tensile strength versus the volume fraction is noticed. When compared to SAP an advantage of 100-150 MPa is measured. In both the cases the ductility is a decreasing function of the volume fraction.

Most of the dispersoids are located on the grain boundaries, i.e. they do not contribute to the intragranular hardening mechanism. Thus the grain size is likely to provide the main contribution to the yield stress. However the Hall-Petch relation was not checked because of the limited range of grain size resulting from mechanical alloying. For the IN9052 alloy a solid solution hardening due to Mg is expected.

The thermal stability of Al-C-O alloys is noteworthy: their microstructure, therefore their mechanical properties remain nearly unchanged after an exposure at 510°C for 100 hours, no evolution of grain and dispersoid size [14], or at 500°C for 250 hours, constant tensile strength and elongation [12,15,16,17] (fig. 3). Lower performances were measured on IN9052 alloys: the decrease of the tensile strength, about 14%, after an exposure at 510°C for 100 hours is explained by the ripening of the  $\text{Mg}_2\text{Al}_3$  compound [14].

However for the elevated temperature loading a fast deterioration of the mechanical properties is observed: at 300°C, for DISPAL 2, the tensile strength is only one half of that measured at 20 °C, and only 40% for DISPAL 1Si12 (fig. 4a) [12], while the ductility is lowered. The same behaviour is observed on all the Al-C-O alloys [17]. For the IN9052 alloy, the ductility goes through a maximum but the degradation is more important (fig. 4b) [18].

Mechanical alloying improves the corrosion resistance of the sensitive Al-Mg alloys. Conversely to the equivalent compositions processed by the conventional route, not exfoliation nor stress corrosion are observed. During periodic immersion in a 3.5% sodium chloride solution at 30°C, the corrosion rate reduces to 4  $\mu\text{m}$  per year for the IN9052 and 5083-H112 alloys whereas it goes up to 227  $\mu\text{m}$  per year for the conventional 7075-T73 alloy. The threshold value for stress corrosion under the same conditions is 380 MPa for the IN9052 alloy [18].

The mechanical alloying applied to conventional alloys can be detrimental: for instance for 7075 alloy

	7075-T6	As M.A.	M.A + T6
Yield stress (MPa)	503	550	595
Tensile strength (MPa)	572	615	645
Elongation (%)	10	2	3.5

The mechanical alloying of 7075 alloy leads to a marked increase in the yield stress and the tensile strength unfortunately counterbalanced by a strong loss of ductility [10].

### 3. ALLOYS FOR ELEVATED TEMPERATURE APPLICATIONS

The high temperature deformation is controlled by diffusion mechanisms: vacancies for the dislocation climbing, solute atoms diffusion along the dislocation cores and the grain boundaries, matter transportation through the matrix. The degradation of the mechanical properties at high temperature can be related to the recrystallization, the precipitate ripening due to a high solubility and a large diffusivity of some alloying elements and also other deformation mechanisms related to the dislocation climbing and the grain boundary sliding.

The remedy for the aluminium alloys is to pin the grain boudaries by dispersoids and to harden the matrix by fine, thermally stable precipitates with low interfacial energy, made up of low diffusivity and low solubility alloying elements. Transition metals and rare earths fulfil most of these requirements.

The first studies reported on the binary Al-Fe alloy rapidly solidified by splat cooling [19]. Metallographic observations show two zones: one featureless, called "A", and an other one with thin metastable  $\text{Al}_6\text{Fe}$  precipitates within a columnar eutectic structure, called "B". As the temperature is raised, a degradation of the mechanical properties is noticed while the microstructure tends toward the equilibrium phases  $\alpha\text{-Al} + \text{Al}_{13}\text{Fe}_4$ , step by step. Further studies were developed on ternary and quaternary alloys leading to precipitates which met the previous requirements on the thermal stability: some of them will be presented further, Al-Fe-Ce and Al-Fe-V-Si; the case of the Al-Cr alloys will be also reported, mainly the alloy Al-Cr-Zr; more specific cases will be discussed: low interfacial energy precipitates in Al-Zr-V and high volume fraction of precipitates in Al-Mn-Si and Al-Cr-Y.

#### 3.1 - Al-Fe-Ce ALLOYS

Preliminary studies [20] of aluminium alloys with transition metals (Mn, Co, Fe, Ni, Cr) and rare earth metals (Ce, La) showed an interesting behaviour of Al-Fe-Ce alloy rapidly solidified by gas atomization and compacted by forging. Numerous studies are on the way to make clear the properties of this alloy in order to foresee the possible developments.

The sum of the concentrations of the alloying elements, Fe and Ce, lies between 5 and 7 at% with a concentration ratio from 3 to 5 [21]. The microstructure of the powder particles depends on their size and on the solidification conditions. Generally an evolution from a plane solidification front towards a coarse dentritic structure, through a cellular one, is observed. The intercellular or interdendritic zones contain intermetallic precipitates, from 10 to 100 nm in size, nucleated during the solidification. Larger precipitates are mentioned after consolidation. In the alloy Al-8.8Fe-3.7Ce (wt%) the volume fraction of precipitates just after extrusion is 20% [22], mainly made up of a quasicrystalline metastable phase  $\text{Al}_{20}\text{Fe}_5\text{Ce}$ , other metastable intermetallic compounds,  $\text{Al}_6\text{Fe}$  and  $\text{Al}_{10}\text{Fe}_2\text{Ce}$ , are detected; the stable phases,  $\text{Al}_{13}\text{Fe}_4$  and  $\text{Al}_{13}\text{Fe}_3\text{Ce}$ , are also present but in small quantity. The  $\text{Al}_6\text{Fe}$  precipitates are globular in shape and about 0.1  $\mu\text{m}$  in size; the quasicristal precipitates are rod-like with a length, 0.1  $\mu\text{m}$ , about three times their diameter and parallel to the extrusion direction; the precipitates  $\text{Al}_{10}\text{Fe}_2\text{Ce}$  are equiaxed with a size of about 0.3  $\mu\text{m}$ , they often contain plane faults.

An exposure of the alloy at 316°C for 2160 hours produces the transformation of the metastable phase  $\text{Al}_6\text{Fe}$  into the stable one  $\text{Al}_{13}\text{Fe}_4$ . At higher temperature, 425°C for 240 hours, the ternary metastable phases transform into the stable phase  $\text{Al}_{13}\text{Fe}_3\text{Ce}$ . The composition and the crystalline structure of each phase are indicated [22]:

$\text{Al}_6\text{Fe}$	orthorhombic	$a=0.645$	$b=0.744$	$c=0.878 \text{ nm}$	Cmcm
$\text{Al}_{13}\text{Fe}_4$	monoclinic	$a=1.549$	$b=0.808$	$c=1.248 \text{ nm}$	$\beta=107^\circ 43' \text{ C2/m}$
$\text{Al}_{20}\text{Fe}_5\text{Ce}$	quasicrystal				
$\text{Al}_{10}\text{Fe}_2\text{Ce}$	orthorhombic	$a=1.02$	$b=1.62$	$c=0.42 \text{ nm}$	Cmm2 or C222
$\text{Al}_{13}\text{Fe}_3\text{Ce}$	orthorhombic	$a=0.89$	$b=1.02$	$c=0.91 \text{ nm}$	Cmcm or Cmc2

The mechanical properties of the Al-Cr-Zr alloys depend on the consolidation temperature: the yield stress and the tensile strength strongly decrease if the extrusion temperature is higher than 450°C in alloys as-extruded and exposed for 1000 hours at 300°C (fig.28) [52].

The mechanical properties for different compositions and extrusion parameters are reported below [51,52]:

(1) Extrusion at 400°C

Alloy	Yield stress Mpa	Tensile strength Mpa	Elonga- tion %	Toughness Mpa/m	Density g/cm³	Young's modulus GPa
<hr/>						
Al-5Cr-2.2Zr						
Diam. 7.8mm as-ext.	440	455	20		2.82	80.8
Diam.19.1mm as-ext.	478	498	10.5			
76.2×15.9mm as-ext. + 10 h at 350°C	342 358	362 376	16.8 10.9	11.3 10.9		
<hr/>						
Al-3Cr-3Zr						
Diam.19.1mm	468	487	5.8			
<hr/>						
Al-5.2Cr-1.9Zr-1Mn						
Diam.19.1mm as-ext. +10 h at 350°C	426 453	460 474	14.2 14.0		2.86	86.5

The ageing at 350°C for 10 hours increases the yield stress and the tensile strength and it decreases the elongation, nevertheless the reached value is acceptable [52].

(2) Rolling at 250 and 350°C, Al-5.2Cr-1.89Zr-.96Mn alloy [51]

Tempera- ture of rolling		Yield stress Mpa	Tensile strength Mpa	Elonga- tion %
250°C	As-rolled	569	591	1.8
	+100 h at 300°C	471	539	7.1
	+ 1 h at 350°C	458	514	8.1
	+ 1 h at 450°C	435	486	5.4
350°C	As-rolled	480	504	6.6
	+100 h at 300°C	458	509	8.9
	+ 1 h at 350°C	445	487	7.2
	+ 1 h at 450°C	413	464	8.5

The highest properties are obtained at the lowest rolling temperature. After exposure at high temperature or ageing, the observed evolution is due to a change in the distribution of the precipitates. During the exposure at 300°C the very fine metastable Al<sub>3</sub>Zr precipitates form. During the exposure at 450°C the Al<sub>13</sub>Cr<sub>2</sub> and Al<sub>3</sub>Zr precipitates ripen [51].

(3) Two powder particle sizes, Al-5.2Cr-1.9Zr-1Mn alloy [51]

Powder particle size		Yield stress Mpa	Tensile strength Mpa	Elonga- tion %
< 38 µm	As-extruded	523	539	2.5
	+ 100 h at 300°C	486	536	7.7
	+ 1 h at 350°C	465	508	6.6
	+ 1 h at 450°C	433	481	8.1
< 65 µm	As-extruded	506	532	3.6
	+ 100 h at 300°C	432	491	6.2
	+ 1 h at 350°C	425	479	8.1

The finest the powder particle, the highest the mechanical properties, this is due to a larger homogeneity of the microstructure [51].

The change in the yield stress of the Al-Cr-Zr alloys versus the temperature, shown in the figure 29, is compared to that of the conventional 2219 alloy: an improvement of 140 MPa is observed with the Al-Cr-Zr alloys in all the temperature range.

### 3.4 - ALLOYS WITH A LOW ENERGY OF THE MATRIX-PRECIPITATES INTERFACE

The precipitate ripening is controlled mainly by the solute atoms diffusion throughout the crystal lattice or along the grain boundaries, according to the following law:

$$\bar{d}^n - \bar{d}_0^n = K_n \cdot (t - t_0)$$

$\bar{d}_0$  and  $\bar{d}$  are the values of the mean diameter of the precipitates at  $t_0$  and  $t$ . The  $n$  exponent equals 3 for the lattice diffusion and 4 for the grain boundary diffusion.  $K_n$  is a parameter characteristic of the couple

matrix-precipitate. For  $n=3$ ,  $K_n$  is proportional to the interfacial energy, for  $n=4$  this is only approximate if the interfacial energy differs from the grain boundary energy. Thus the lowest the interfacial energy, the lowest the ripening rate. Furthermore this energy depends on the coherency level of the interface: the highest the coherency, the lowest the interfacial energy and so the ripening rate. The understanding of these mechanisms is one of the basis of the superalloy development for elevated temperature applications.

Systematic undergoing studies of intermetallic compounds  $\text{Al}_3\text{X}$ ,  $\text{X}=\text{Ti}, \text{V}, \text{Zr}, \text{Hf}$  [54] report quadratic structures  $\text{DO}_{22}$  for  $\text{X}=\text{Ti}, \text{V}$  and  $\text{DO}_{23}$  for  $\text{X}=\text{Zr}, \text{Hf}$  with cell parameters  $a$  and  $c$  directly related to the aluminium parameter  $a_0$ :  $a/a_0\sqrt{2}=0.9505$  and  $0.9333$ ,  $c/2a_0=1.0631$  and  $1.0275$  respectively for Ti and V;  $a/a_0=0.9910$  and  $0.9851$ ,  $c/4a_0=1.0693$  and  $1.0591$  respectively for Zr and Hf. All these ratios are close to unit. The idea is then to combine different X elements within the compound in order to get closer to unit [55,56,57]. Furthermore Zr or Hf additions to  $\text{Al}_3\text{Ti}$  or  $\text{Al}_3\text{V}$  compounds transform the  $\text{DO}_{22}$  structure into a  $\text{DO}_{23}$  one whose the stability range is larger. A mismatch parameter is defined by:  $\delta=(2/3) \cdot |1-a/a_0| + (1/3) \cdot |1-c/4a_0|$

The values of this parameter for different compounds are listed below:

$\text{Al}_3\text{Zr}$	$\delta = 0.0288$
$\text{Al}_3(\text{V}_{0.875} \text{Zr}_{0.125})$	$\delta = 0.0239$
$\text{Al}_3(\text{V}_{0.875} \text{Hf}_{0.125})$	$\delta = 0.0269$
$\text{Al}_3(\text{Ti}_{0.875} \text{Zr}_{0.109} \text{Hf}_{0.016})$	$\delta = 0.0270$

The  $\text{Al}-\text{Zr}-\text{V}$  alloy related to the lowest  $\delta$  value was extensively studied: in a first step, a dilute alloy, 1% volume fraction of precipitates, was prepared by rapid solidification. The resulting solid solution breaks up giving rise to metastable, sphere- and rod-like, precipitates of the  $\text{Ll}_2$  structure. The parameter difference with that of the matrix is  $-0.1 \pm 0.2\%$ : there is a nearly coherency, a low interfacial energy is expected, a low ripening rate also. The  $\text{Al}_3\text{Zr}$  compound has also a structure  $\text{Ll}_2$  but the parameter difference is higher, about  $1 \pm 0.2\%$ . So the  $\text{Al}_3\text{V}_{0.875}\text{Zr}_{0.125}$  alloy seems very promising. Indeed, the ripening rate is very low for  $\text{Ll}_2$  compounds and particularly for this alloy (fig. 30) [55].

During a further ageing, the metastable phase transforms into the stable  $\text{DO}_{23}$  phase with plate-like precipitates. The ripening rate of the  $\text{DO}_{23}$  structure is eight times higher than that of the  $\text{Ll}_2$  one for the same composition.

For higher Zr and V contents, 5 % volume fraction of the precipitates, melt spinning or splat cooling always leads to a supersaturated solid solution [56,57]. During annealing, on the one hand, an intragranular precipitation of the metastable  $\text{Ll}_2$ ,  $\text{Al}_3(\text{Zr},\text{V})$  phase, 5 nm in precipitate size, and on the other hand, an intergranular one of the stable phases  $\text{DO}_{23}$ ,  $\text{Al}_3(\text{Zr},\text{V})$  and  $\text{Al}_{10}\text{V}$  are observed. The ripening rate of the metastable phase is still lowered compared to the dilute alloy,  $4.7 \cdot 10^{-28}$  instead of  $1.6 \cdot 10^{-26} \text{ cm}^3/\text{h}$ . This result was unexpected because the  $K_n$  parameter is proportional to the squared volume fraction of precipitates. In order to explain this phenomena it was suggested either that the solute segregation at the matrix-precipitate interface could noticeably decrease the interfacial energy or that the  $\text{Al}_{10}\text{V}$  precipitates could trap the solute atoms and so limit their diffusion towards the  $\text{Ll}_2$ ,  $\text{Al}_3(\text{Zr},\text{V})$  precipitates. The creep behaviour of these alloys is good and it compares quite well with that of  $\text{Al}-\text{Fe}-\text{Ce}$  alloys (fig. 31) [58].

When the Zr and V contents increase, up to 8 % in volume fraction of the precipitates, a very high cooling rate,  $10^7^\circ\text{C/s}$ , is required in order to reduce the precipitation of the  $\text{Al}_{10}\text{V}$  phase. Moreover the highest solute concentrations, the highest critical cooling rate: it is difficult to get a high volume fraction of coherent precipitates by the usual rapid solidification techniques.

### 3.5 - ALLOYS WITH A HIGH VOLUME FRACTION OF THE PRECIPITATES

In the Orowan mechanism, related to the by-passing of the obstacles by the mobile dislocations, the hardening is proportional to the cube root of the volume fraction of the dispersoids. As this quantity is less than unit, it should be interesting to increase it; its augmentation is obtained either by increasing the content of alloying elements or by choosing intermetallic compounds whose the composition requires a high number of Al atoms per alloying element atom, for instance  $\text{Al}_{10}\text{V}$ ,  $\text{Al}_{12}\text{Mo}$ ,  $\text{Al}_{20}\text{Cr}_2\text{Y}$  [60],  $\text{Al}_{20}\text{Cr}_2\text{Ce}$  [61],  $\text{Al}_{12}(\text{Cr},\text{Mn})$  [62],  $\text{Al}_{15}\text{Mn}_3\text{Si}_2$ ....

The volume fraction of  $\text{Al}_{16}\text{Mn}_3\text{Si}_2$  can reach the value of 34.7% in the Al-4.8Si-12.6Mn alloy. This compound is cubic, space group Pm3, with a cell parameter of 1.265 nm. The extruded alloy exhibits a good stability up to 400°C after an exposure for 100 hours (fig. 32) [60]. At higher temperature the tensile strength decreases slightly and the elongation is strongly reduced. In the as extruded alloy the matrix grain size equals 1-3  $\mu\text{m}$  and the precipitates, from 100 to 500 nm in size, are placed in the grain boundaries. After an exposure at 490°C for 100 hours the grain size increases up to 3-5  $\mu\text{m}$ , new precipitates, from 50 to 200 nm in size, appear inside the grains and the previous precipitates placed in the grain boundaries grow up to 250-1000 nm forming a continuous structure. Up to about 250°C this alloy behaves like the Al-Fe-Ce alloys with a reasonable ductility; at higher temperature the tensile strength decreases and the elongation strongly increases; this behaviour is explained by a marked growth of the grains and the precipitates (fig. 33). [60].

The volume fraction of  $\text{Al}_{20}\text{Cr}_2\text{Ce}$  can increase up to 37.6% in the alloy Al-6.8Cr-5.7Y. This intermetallic compound is cubic, space group Fd3m, and its cell parameter equals 1.437nm; the precipitates often contain plane faults [60]. The thermal stability of this alloy is comparable with that of the previous alloy but its ductility is nearly zero (fig. 32); it has a smaller grain size, about 1  $\mu\text{m}$  and a slightly higher tensile strength, the precipitates have about the same size. For high temperature tests, the tensile strength behaves like that of the Al-Mn-Si alloy and, as previously, a strong increase in the ductility is noticed beyond 250°C (fig. 33).

#### 4 - CONCLUSION

The alloying of aluminium with transition metals, rare earth metals, carbon and/or oxygen opens new application fields for the aluminium alloys, particularly by an improvement of the room temperature strength and the high temperature behaviour. The elaboration of such alloys requires the use of the powder metallurgy techniques and consequently encounters their inherent difficulties in the transfer of the results from the laboratory scale to the industrial one. The full development of such alloys requires a careful handling of the powders in order to reduce the number of defects in the final product and the introduction of control methods at the different steps of the process. Furthermore economical factors have to be taken into account in order to check that the cost increase for the alloy development remains reasonable.

#### References

1. QUIST W.E. and LEWIS R.E., The Need for Rapidly Solidified Powder Metallurgy Aluminum Alloys for Aerospace Applications, *Rapidly Solidified Powder Aluminum Alloys*, ASTM STP 890, Fine M.E. and Starke Jr E.A., Eds., American Society for Testing and Materials, Philadelphia, 1986, 7.
2. FRAZIER W.E., PM Al Alloys: Hot Prospects for Aerospace Applications, *Advanced Materials and Processes*, 133, (1988), 42.
3. FROES F.H., KIM Y-W. and KRISHNAMURTHY S., Rapid Solidification of Lightweight Metal Alloys, *Mat. Sci. Eng.*, A117, (1989), 19.
4. FROES F.H. and PICKENS J.R., Powder Metallurgy of Light Metal Alloys for Demanding Applications, *J. Metals*, 36, (January 1984), 14.
5. HILDEMAN G.J., LABARRE L.C., HAFEEZ A. and ANGERS L.M., Microstructural, Mechanical Property and Corrosion Evaluations of 7xxx P/M alloy CW67, *High Strength Powder Aluminum Alloys II*, Hildeman G.J. and Koczak M.J., Eds., The Metallurgical Society of AIME, Toronto, 1986, 25.
6. BOHLEN J.W., KAR R.J. and CHANANI G.R., A Comparative Evaluation of Aluminum Alloy Powders Used for Fabricating High-Strength Powder Metallurgy Extrusions, *Rapidly Solidified Powder Aluminum Alloys*, ASTM STP 890, M.E. Fine and Starke Jr E.A., Eds., American Society for Testing and Materials, Philadelphia, 1986, 166.
7. PEASE L.F. and POTTER V.C., Mechanical Properties of P/M Materials, *Powder Metallurgy*, Metals Hanbook, Vol. 7, American Society for Metals, 1984, 463.
8. PICKENS J.R., GORDON J.R. and CHRISTOLOUDOU L., Stress-Corrosion Cracking and Hydrogen Embrittlement in P/M X7091 and I/M 7075, *High-Strength Powder Metallurgy Aluminum Alloys*, M.J. Koczak and G.J. Hildeman, Eds., The Metallurgical Society of AIME, Dallas, 1982, 177.
9. SUMMERSON T.J. and SPROWLS D.O., Corrosion Behavior of Aluminum Alloys, *Aluminum Alloys - Physical and Mechanical Properties*, E.A. Starke Jr and T.H. Sanders Jr, Eds., Emas, Charlottesville, 1986, 1576.
10. WEBER J.H. and SCHELLENG R.D., Mechanical Alloying of Dispersion Strengthened Aluminum: A Retrospective Review, *Dispersion Strengthened Aluminum Alloys*, Kim Y-W. and Griffith W.M., Eds., The Minerals, Metals & Materials Society, 1988, 467.

11. BENN R.C. and MIRCHANDANI P.K., Dispersion Strengthening by Mechanical Alloying, *New Materials by Mechanical Alloying*, Arzt E. and Schultz L., Eds., Deutsche Gesellschaft für Metallkunde, 1989, 19.
12. ARNHOLD V. and HUMMERT K., Properties and Applications of Dispersion Strengthened Aluminum Alloys, *New Materials by Mechanical Alloying*, Arzt E. and Schultz L., Eds., Deutsche Gesellschaft für Metallkunde, 1989, 263.
13. SINGER R.F., OLIVER W.C. and NIX W.D., Identification of Dispersoid Phases Created in Aluminum During Mechanical Alloying, *Metall. Trans.*, 11A, (1980), 1895.
14. HAWK J.A., RUCH W. and WILSDORF H.G.F., Microstructure and Fracture Analysis of Oxide and Carbide Strengthened Mechanically Alloyed Aluminum Alloys, *Dispersion Strengthened Aluminum Alloys*, Kim Y-W. and Griffith W.M., Eds., The Minerals, Metals & Materials Society, 1988, 603.
15. HAWK J.A., MIRCHANDANI P.K., BENN R.C. and WILSDORF H.G.F., Evaluation of the Elevated Temperature Strength and Microstructural Stability of Dispersion Strengthened MA Aluminum Alloys, *Dispersion Strengthened Aluminum Alloys*, Kim Y-W. and Griffith W.M., Eds., The Minerals, Metals & Materials Society, 1988, 517.
16. HAWK J.A. and WILSDORF H.G.F., Tensile Strength of MA Aluminum Alloys After Prolonged Elevated Temperature Exposure, *Scripta Metall.*, 22, (1988), 561.
17. BROCKMANN G.J. und BAUMGARTEN J., Pulvermetallurgische Herstellung von hochtemperaturfesten Aluminiumwerkstoffen, *Aluminium*, 65, (1989), 393.
18. INCO ALLOYS INTERNATIONAL, IncoMAP alloy Al-9052, *Publication No IAI-34*, 1987.
19. JONES H., Observations on a Structural Transition in Aluminium Alloys Hardened by Rapid Solidification, *Mat. Sci. Eng.*, 5, (1969/70), 1.
20. GRIFFITH W.M., SANDERS, Jr R.E. and HILDEMAN G.J., Elevated Temperature Aluminum Alloys for Aerospace, *High-Strength Powder Metallurgy Aluminum Alloys*, M.J. Koczak and G.J. Hildeman, Eds., The Metallurgical Society of AIME, Dallas, 1982, 209.
21. KIM Y-W., Processing/Microstructure/Properties of Al-Fe-Ce Powder Alloys, *Dispersion Strengthened Aluminum Alloys*, Kim Y-W. and Griffith W.M., Eds., The Minerals, Metals & Materials Society, 1988, 517.
22. RAGHAVAN AYER, ANGERS L.M., MUELLER R.R., SCANLON J.C. and KLEIN C.F., Microstructural Characterization of the Dispersed Phases in Al-Fe-Ce System, *Metall. Trans.*, 19A, (1988), 1645.
23. YANEY D.L. and NIX W.D., Elevated Temperature Deformation Behavior of an Al-8.4wtPctFe-3.6wtPctCe Alloy, *Metall. Trans.*, 18A, (1987), 893.
24. ANGERS L., FINE M.Z. and WEERTMAN J.R., Effect of Plastic Deformation on the Coarsening of Dispersoids in a Rapidly Solidified Al-Fe-Ce Alloy, *Metall. Trans.*, 18A, (1987), 555.
25. KIM Y-W. and GRIFFITH W.M., Annealing Behavior and Tensile Properties of Elevated-Temperature PM Aluminum Alloys, *Rapidly Solidified Powder Aluminum Alloys*, ASTM STP 890, Fine M.E. and Starke Jr E.A., Eds., American Society for Testing and Materials, Philadelphia, 1986, 435.
26. SMITH H.H., MICHEL D.J. and REED J.R., Fatigue Crack Growth in Rapidly Solidified Aluminum alloys at 25 and 300°C, *Metall. Trans.*, 20A, (1989), 2425.
27. LANGENBECK S.L., GRIFFITH W.M., HILDEMAN G.J. and SIMON J.M., Development of Dispersion-Strengthened Aluminum Alloys, *Rapidly Solidified Powder Aluminum Alloys*, ASTM STP 890, Fine M.E. and Starke Jr E.A., Eds., American Society for Testing and Materials, Philadelphia, 1986, 410.
28. LANGENBECK S.L., COX J.M. and SIMENZ R.F., Characterization of Al-Fe-Ce Alloys, *Rapidly Solidified Powder Aluminum Alloys*, ASTM STP 890, Fine M.E. and Starke Jr E.A., Eds., American Society for Testing and Materials, Philadelphia, 1986, 450.
29. RAINEN R.A. and EKVALL J.C., Elevated Temperature Al Alloys for Aircraft Structure, *J.O.M.*, 40, (May 1988), 16.
30. LEGZDINA D. and PARTHASARATHY T.A., Deformation Mechanismn of Rapidly Solidified Al-8.8Fe-3.7Ce Alloy, *Metall. Trans.*, 18A, (1987), 1713.
31. EZZ S.S., LAWLEY A. and KOCZAK M.J., Dispersion Strengthened Al-Fe-Ce: a Dual Rapid Solidification/Mechanical Alloying Approach, *Dispersion Strengthened Aluminum Alloys*, Kim Y-W. and Griffith W.M., Eds., The Minerals, Metals & Materials Society, 1988, 243.
32. YANEY D.L., OVECOGLU M.L. and NIX W.D., The Effect of Mechanical Alloying on the Deformation Behavior of a Rapidly Solidified Al-Fe-Ce Alloy, *Dispersion Strengthened Aluminum Alloys*, Kim Y-W. and Griffith W.M., Eds., The Minerals, Metals & Materials Society, 1988, 619.

**PHYSICAL METALLURGY  
OF ALUMINIUM POWDER ALLOYS**

Georges CHAMPIER  
UA-CNRS 155, Ecoles des Mines  
Institut National Polytechnique de Lorraine  
Parc de Saurupt, 54042 NANCY Cedex, France

**Abstract**

The discovery of new alloy compositions and new processes increases the application field of aluminium alloys. In particular the powder metallurgy route allows alloying with transition and rare earth metals, oxygen and carbon usually forbidden by the classical ingot metallurgy route. Further improvements can be obtained by rapid solidification and/or mechanical alloying by modifying the microstructures. This paper will deal with the relation between microstructure and mechanical properties of (1) High strength alloys for room temperature applications (7090, 7091, CW67 and Al-C-O), (2) alloys for high temperature applications (Al-Fe-Ce, Al-Fe-V-Si, Al-Cr-Zr, Al-Zr-V, Al-Cr-Y and some other under studies).

**1 - INTRODUCTION**

The ability of Al alloys to conquer new markets depends on the improvement of their properties: some of them must undergo a substantial progress but without any deterioration of the others. One can deal with physical properties (density for instance), mechanical properties (yield stress ...) as well as chemical properties (corrosion resistance ...).

The quality of Al alloys obtained by the classic ingot route was optimized by an appropriate choice of alloying elements, compositions, engineering processes, thermal and thermomechanical treatments. Therefore better performances can be achieved either with alloying compositions forbidden by the classic route or with new processing techniques, or both. The common objective is to obtain refined microstructures (small grain size, fine dispersoids, ...) and better thermal stability.

Because such refined microstructures cannot be achieved in bulk material, as obtained in the ingot route, production of Al alloys by the P/M technique was developed. Two different processes can be used: (1) for alloying elements with a high solubility in the liquid bath, the homogeneity of the alloy is maintained by rapid solidification of a liquid stream, either continuously (melt spinning process) or discontinuously (powder, splats and flakes); (2) for alloying elements with a poor solubility in molten aluminium, mixture in solid phase was preferred: grinding of thin particles allows incorporation of such elements on the fracture surface and then in the bulk by friction welding, this technique is called mechanical alloying.

Among the possible application fields, three kinds of alloys are developed [1,2] :

(1) low density alloys for aeronautical industry (in replacement of conventional 2024-T3, 7075-T6 and 7075-T3 alloys), the decrease in density is mainly obtained by lithium addition.

(2) high strength alloys for room temperature applications (in replacement of 7075-T6 alloy) obtained either by rapid solidification of 7xxx alloys enriched with transition elements or by mechanical alloying of aluminium or aluminium-magnesium alloy hardened by aluminium carbide and aluminium oxide.

(3) alloys for high temperature applications, 350 °C, (in replacement of titanium alloys and steels) mainly obtained by rapid solidification of rare earth and transition metals-aluminium alloys; studies on the influence of a further mechanical alloying treatment are also on the way.

The first alloy category (low density alloys) will be ignored in the following of this paper because this topic is extensively discussed elsewhere in this series. The two remaining categories will be now presented in detail.

**2 - HIGH STRENGTH ALLOYS FOR ROOM TEMPERATURE APPLICATIONS**

Plastic deformation of Al alloys at 20°C is controlled by dislocation gliding through the matrix. Hardening results from their interaction with dislocations of the different slip systems (forest dislocations), with solute atoms and precipitates. The precipitates can be either sheared or bypassed by the dislocations. This latter interaction, called Orowan mechanism, can be expressed according to the following relation:

$$\sigma_{ok} = \alpha \cdot G \cdot b / D_p = \alpha \cdot G \cdot b \cdot f_v^{1/2} / d_p$$

$\alpha$  is a coefficient close to unity, G the shear modulus of the matrix, b the Burgers vector of the dislocation,  $D_p$  the mean distance between precipitates.

$d_p$ , their mean size and  $f_v$ , the volume fraction: for a constant  $f_v$  value, the smallest  $d_p$ , the highest the Orowan hardening. The last parameters to be taken care of are the grain size and the texture resulting from the consolidation process: the contribution of grain boundaries is given by:

$$\sigma_{GB} = k \cdot D^{-1/2}$$

$k$  is a coefficient depending on the matrix properties and  $D$  the grain size. The contribution of the texture, if any, can be evaluated through the Taylor factor. For a given volume fraction of precipitates the highest yield stress will be achieved with the smallest particle and grain size. Results obtained by the two previously mentioned techniques are presented below.

### 2.1 - RAPIDLY SOLIDIFIED ALLOYS (R.S. ALLOYS)

The chemical compositions of 7xxx alloys is modified by additions of transition elements like Co, Zr or Ni in order to precipitate very thin intermetallic phases. The table below compares the composition of four of such alloys to that of the conventional 7050 and 7075 series [3] (wt%):

Alloy	Zn	Mg	Cu	Co	Zr	Ni
7090	8	2.5	1	1.5	-	-
7091	6.5	2.5	1.5	0.4	-	-
CW67	9	2.5	1.5	-	0.14	0.1
PM64	7.4	2.4	2.1	0.3	-	0.2
7050	6.2	2.2	2.3	-	0.12	-
7075	5.6	2.5	1.6	-	-	-

Rapid solidification leads to the formation of  $MgZn_2$  precipitates which characterize the 7xxx series, but the Co addition gives rise to  $Al_xCo_2$  precipitation which contributes to the hardening, prevents from recrystallization, refines the grain size and trap the impurities, for instance iron form the ternary  $Al_x(Co,Fe)_2$  compound [4]. Nickel addition leads to the formation of  $Al_x(Ni,Fe)_2$ , probably during the consolidation step [5]. Concerning zirconium, the litterature seems to indicate a limited  $Al_xZr$  precipitation.

The mechanical properties of the R.S. alloys, as summarized in the following table, can be compared with those of the 7075 alloy:

Alloy	Yield stress Mpa	Tensile strength Mpa	Elonga- tion %	Toughness Mpa/m	Density g/cm <sup>3</sup>	Young's modulus GPa
7090 T6E192 L	641	676	10		2.850	73.8
Extruded LT	600	648	10			
T7E71 L	579	621	9	31		
ST	490	558	8	20		
Forged T7E71	579	613	10			
7091 T6E192 L	558	614	11		2.823	72.4
Extruded LT	538	586	13			
T7E69 L	545	593	11	46		
LT	496	545	9	33		
ST	455	524	9	26		
Forged T7E69	530	579	13			
CW 67 L	579	614	12	47	2.88	
Extruded LT	528	570	10	26		
ST	499	560	9	24		
Forged T7X2 L	579	602	14	44		
LT	572	606	15			
ST	531	572	9	34		
PM 64 TX7	540	585	10	34		
7075 L	456	530	13	34	2.796	71.7
LT	447	520	12			
ST	441	510	8	28		

The line segments plotted in the figure 1 [5] show the evolution of the material toughness versus its yield stress, after appropriate thermal treatments. The CW67 alloy exhibits the best performances concerning the yield stress (from 586 to 660 MPa) as well as the toughness (from 38 to 53 MPa/m).

The R.S. 7xxx alloys exhibit a better corrosion and stress corrosion resistance than the 7xxx alloys obtained by ingot solidification. The oxide film is about 7 nm thick for all the alloys. Stress corrosion in the conventional 7xxx alloys increases with the iron content and with the precipitate size. Because the R.S. technique leads to trapping of iron impurities in small precipitates ( $Al_x(Co,Fe)_2$ ,  $Al_x(Ni,Fe)_2$ , ...) the crack

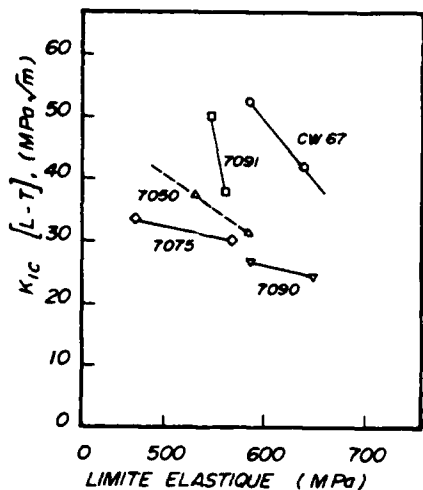


Fig. 1. The toughness vs the yield stress in the rapidly solidified (7090, 7091 and CW67) and conventional (7050 and 7075) alloys [5].

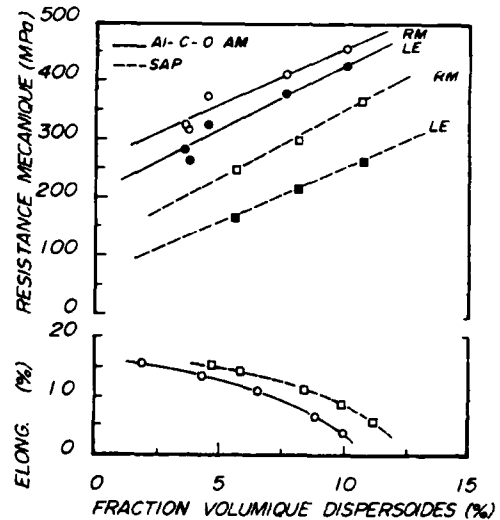


Fig. 2. The yield stress (LE), tensile strength (RM) and elongation vs the volume fraction of the dispersoids in the mechanically alloyed Al-C-O alloys; comparison with the SAP alloy [10].

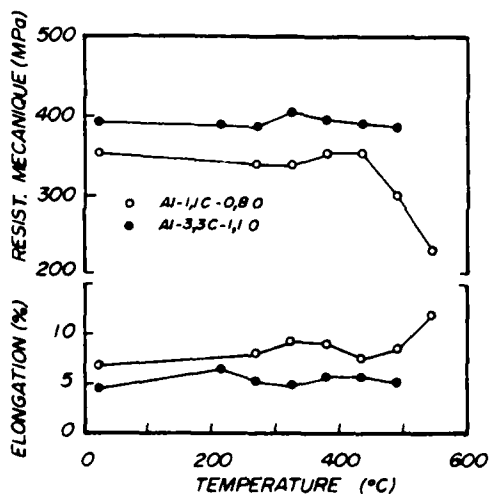


Fig. 3. Change in the tensile strength and elongation measured at room temperature in the Al-1.1C-0.8O and Al-3.3C-1.1O alloys vs the exposure temperature for 100 hours [15].

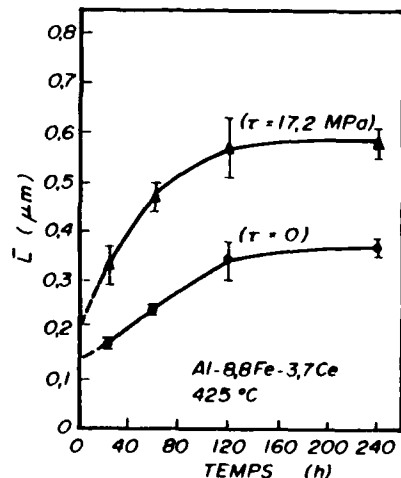


Fig. 6. Change in the precipitate size vs the time at 425°C in Al-8.8Fe-3.7Ce alloy; effect of an applied stress [24].

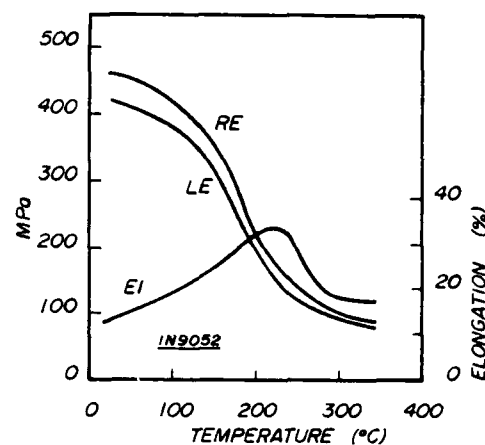
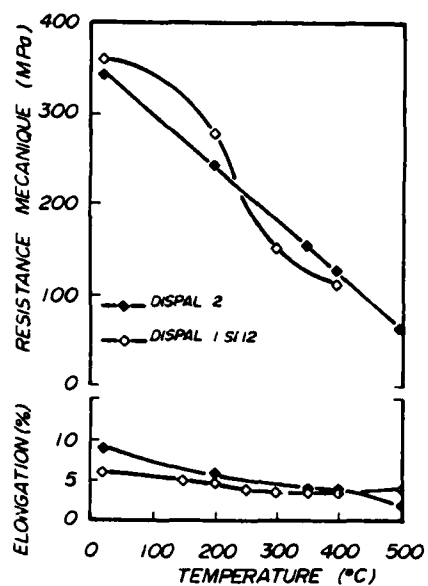


Fig. 4. Change in the yield stress (LE), tensile strength (RM) and elongation vs the temperature in (a) DISPAL 2 and DISPAL 1Si12 alloys [12] and (b) IN9052 alloy [18].

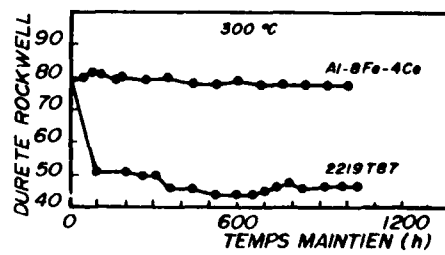
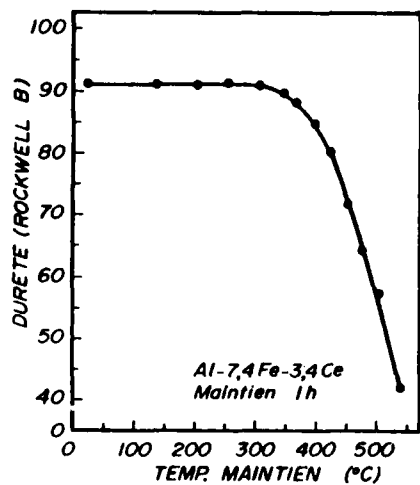


Fig. 6. Change in the hardness measured at room temperature vs (a) the exposure temperature for 1 hour in the Al-7.4Fe-3.4Ce alloy [25] and (b) the time exposure at 300°C in the Al-8Fe-4Ce alloy; comparison with the conventional 2219-T87 alloy [26].

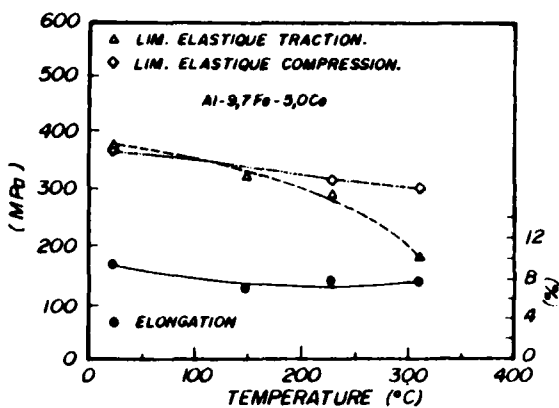


Fig. 7. Change in the tensile and compression yield stresses measured at room temperature vs the exposure temperature for 1000 hours in Al-9.7Fe-5.0Ce alloy. [27,28].

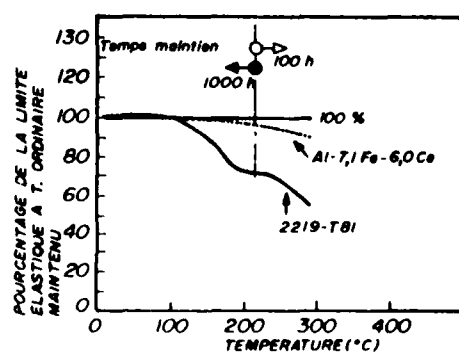


Fig. 8. Effect of an exposure at high temperature upon the yield stress measured at room temperature in the Al-7.1Fe-6.0Ce and the conventional 2219-T81 alloys [29].

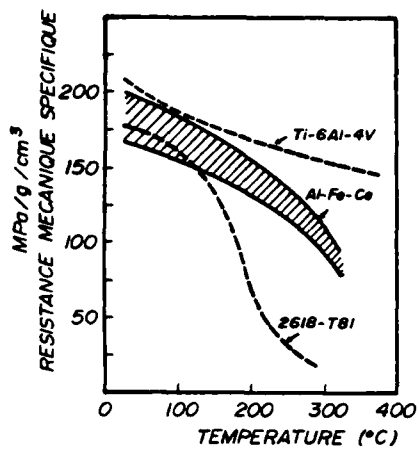


Fig. 9. Change in the specific tensile strength vs the temperature in the rapidly solidified Al-Fe-Ce alloys and conventional 2518-T81 and Ti-6Al-4V alloys [21].

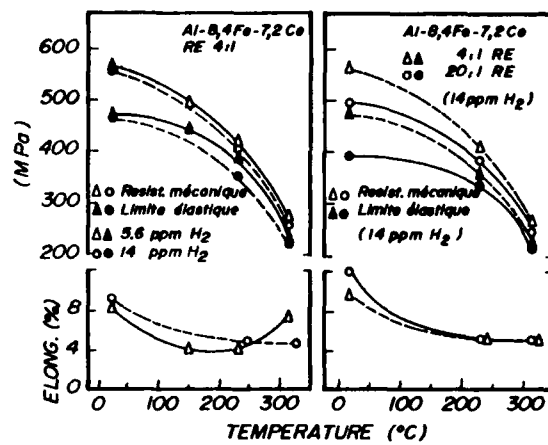


Fig. 10. Change in the yield stress, tensile strength and elongation vs the temperature in the Al-8.4Fe-7.2Ce alloy; (a) effect of the hydrogen content; (b) effect of the extrusion ratio [21].

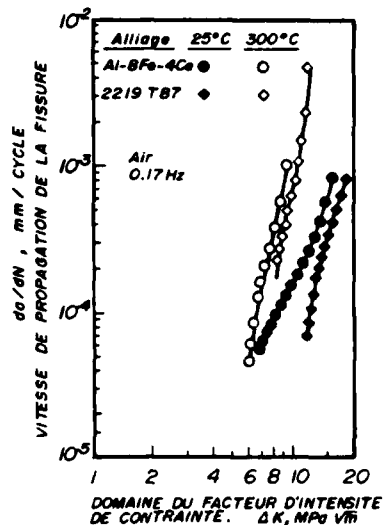


Fig. 11. Fatigue crack growth rate in the rapidly solidified Al-8Fe-4Ce and conventional 2219-T87 alloys at 25 and 300 °C [26].

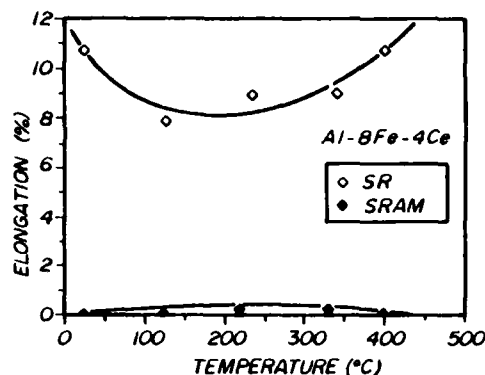


Fig. 13. Change in the elongation vs the temperature in the rapidly solidified (SR) and then mechanically alloyed (SRAM) Al-8Fe-4Ce alloy [31].

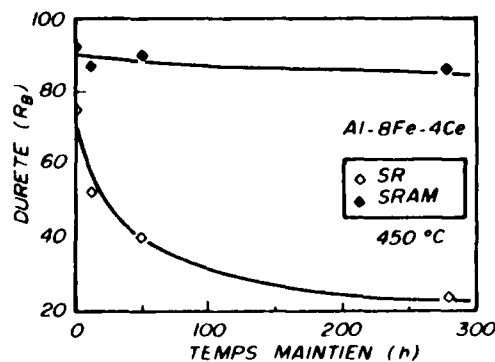
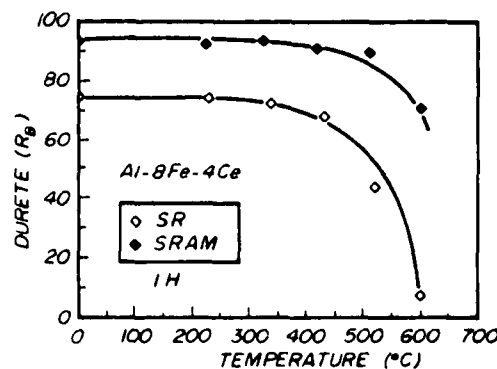


Fig. 12. Change in the hardness measured at room temperature vs (a) the exposure time at 450 °C and (b) the exposure temperature for 1h in the rapidly solidified (SR) and then mechanically alloyed (SRAM) Al-8Fe-4Ce alloy [31].



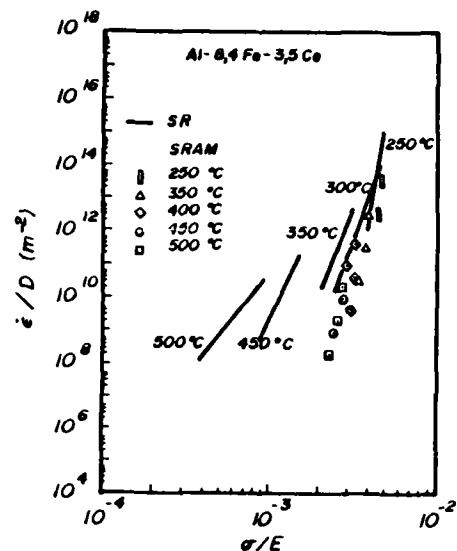


Fig. 14. Compression test at high temperature in rapidly solidified (SR) and then mechanically alloyed (SRAM) Al8.4Fe3.5Ce alloy: strain rate / self-diffusion coefficient of Al vs applied stress / Young's modulus [36].

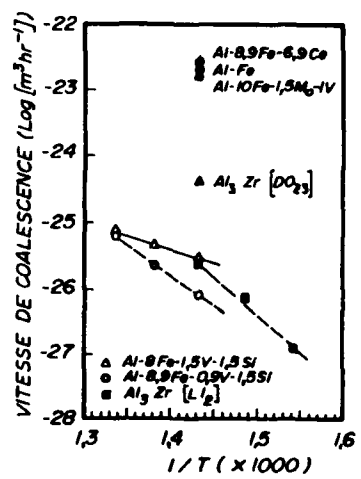


Fig. 15. Change in the ripening rate of the precipitates vs the temperature in the Al-Fe-V-Si alloys, comparison with that of the precipitates in Al-Fe-X alloys and Al<sub>3</sub>Zr (DO<sub>23</sub> and L<sub>1</sub><sub>2</sub> structure) [37].

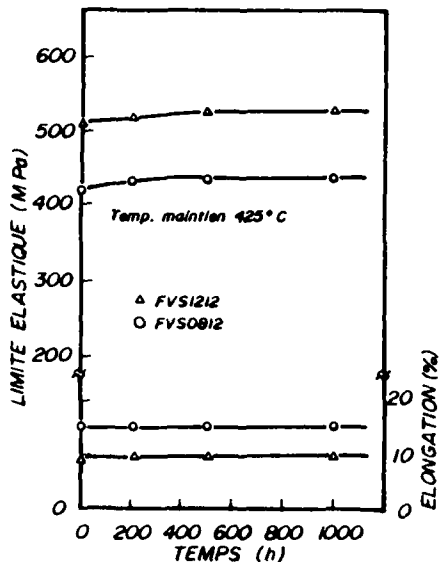


Fig. 16. Change in the yield stress and elongation measured at room temperature vs the exposure time at 425 °C in Al-Fe-V-Si alloys [36].

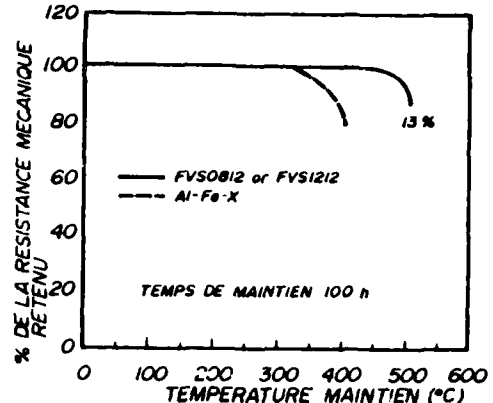


Fig. 17. Change in the tensile strength measured at room temperature vs the exposure temperature for 100 hours in the Al-Fe-V-Si alloys and comparison with the Al-Fe-X alloys [36].

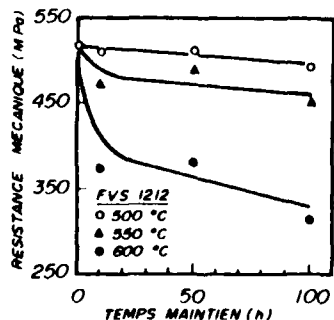
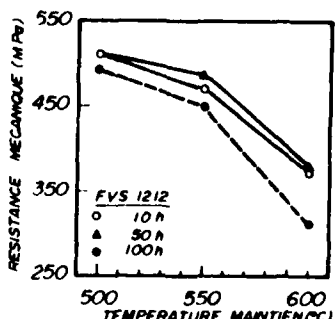


Fig. 18. Change in the tensile strength measured at room temperature vs (a) the exposure time at 600, 650 and 600 °C and (b) the exposure temperature for 10, 50 and 100 h in the FVS 1212 alloy [41].



33. OVECOGLU M.L. and NIX W.D., Elevated Temperature Characterization and Deformation of Mechanically Alloyed Rapidly Solidified Al-8.4wt%Fe-3.5wt%Ce Alloy, *New Materials by Mechanical Alloying*, Arzt E. and Schultz L., Eds., Deutsche Gesellschaft für Metallkunde, 1989, 287.
34. SKINNER D.J., BYE R.L., RAYBOULD D., BROWN A.M. and ZEDALIS M.S., Dispersion Strengthened Al-Fe-Si Alloys Containing V, Mn, Cr or Mo, *Processing of Structural Metals by Rapid Solidification*, Froes F.H. and Savage S.J., Eds., ASM International, Orlando, 1986, 291.
35. SKINNER D.J., BYE R.L., RAYBOULD and BROWN A.M., Dispersion Strengthened Al-Fe-V-Si Alloys, *Scripta Metall.* 20, (1986), 867.
36. GILMAN P.S. and DAS S.K., Rapidly Solidified Aluminum Alloys for High Temperature/High Stiffness Applications, *Int. Conf. PM Aerospace Materials*, Metal Powder Report, (1897), p 27-1.
37. SKINNER D.J., The Physical Metallurgy of Dispersion Strengthened Al-Fe-V-Si alloys, *Dispersion Strengthened Aluminum Alloys*, Kim Y-W. and Griffith W.M., Eds., The Minerals, Metals & Materials Society, 1988, 181.
38. GUYOT P. and AUDIER M., A quasicrystal Structure Model for Al-Mn, *Phil. Mag.*, 52B, (1985), L15.
39. ZEDALIS M., RAYBOULD D., SKINNER D.J. and DAS S.K., Microstructure/Tensile Property Relationship in Elevated Temperature RS Al-Fe-V-Si Rolled Sheet, *Processing of Structural Metals by Rapid Solidification*, Froes F.H. and Savage S.J., Eds., ASM International, Orlando, 1986, 347.
40. DAS S.K., Rapid Solidification and Powder Metallurgy at Allied Signal Inc., *Int. J. Powder Metallurgy*, 24, (1988), 175.
41. FRANCK R.E. and HAWK J.A., Effect of Very High Temperatures on the Mechanical Properties of Al-Fe-V-Si alloy, *Scripta Metall.*, 23, (1989), 113.
42. SKINNER D.J., ZEDALIS M.S. and PELTIER J., Anomalous Ductility Variation at Intermediate Temperatures in Rapidly Solidified Al-Base Alloys, *Dispersion Strengthened Aluminum Alloys*, Kim Y-W. and Griffith W.M., Eds., The Minerals, Metals & Materials Society, 1988, 71.
43. SKINNER D.J., ZEDALIS M.S. and GILMAN P.S., Effect of Strain Rate on Tensile Ductility for a Series of Dispersion-Strengthened Aluminum-Based Alloys, *Mat. Sci. Eng.*, A119, (1989), 81.
44. PHARR G.M., ZEDALIS M.S., SKINNER D.J. and GILMAN P.S., High Temperature Creep Deformation of a Rapid Solidified Al-Fe-V-Si Alloy, *Dispersion Strengthened Aluminum Alloys*, Kim Y-W. and Griffith W.M., Eds., The Minerals, Metals & Materials Society, 1988, 309.
45. BROWN A.M., SKINNER D.J., RAYBOULD D., DAS S.K., BYE R.L. and ADAM C.M., Crack Growth and Fracture Properties of Rapidly Solidified Al-Fe-V-Si Alloys, *Aluminum Alloys - Physical and Mechanical Properties*, E.A. Starke Jr and T.H. Sanders Jr, Eds., Emas, Charlottesville, 1986, 1029.
46. MIDSON S.P., BUCKLEY R.A. and JONES H., Aging Behaviour of Aluminium-Rich Al-Cr-Zr Alloy Solid Solutions Extended by Rapid Solidification, *Rapidly Quenched Metals*, Steeb S. and Warlimont H., Eds., Elsevier Science Publishers, Würzburg, 1985, 923.
47. TSAKIROPOULOS P., PRATT R.C., JONES H., RESTALL J.E. and GARDINER R.W., Development of Al-Cr-X and Al-Cr-Zr-X Alloys Rapidly Solidified from the Melt, *Sixth Int. Conf. Rapidly Quenched Metals*, *Mat. Sci. Eng.*, 98, (1988), 143.
48. HUGHES I.R., MARSHALL G.J. and MILLER W.S., Production and Processing of Rapidly Solidified Aluminium Alloys, *Rapidly Quenched Metals*, Steeb S. and Warlimont H., Eds., Elsevier Science Publishers, Würzburg, 1985, 1743.
49. MARSHALL G.J., HUGUES I.R. and MILLER, Effect of Consolidation Route on Structure and Property Control in Rapidly Solidified Al-Cr-Zr-Mn Powder Alloy for High Temperature Service, *Mat. Sci. Tech.*, 2, (1986), 394.
50. TANAGUCHI Y., FURUSHIRO N., TAI H. and HORI S., Precipitation Behavior During Aging in a Rapidly Solidified Al-1.8Cr-1.7Zr Alloy, *J. Japan Inst. Light Metals*, 37, (1987), 300.
51. MILLER W.S., HUGUES I.R., PALMER I.G., THOMAS M.P., SAINI T.S. and WHITE J., Production and Properties of Rapidly Solidified Aluminium-Chromium-Zirconium Alloys, *High Strength Powder Aluminum Alloys II*, Hildeman G.J. and Koczak M.J., Eds., The Metallurgical Society of AIME, Toronto, 1986, 311.
52. PALMER I.G., THOMAS M.P. and MARSHALL G.J., Development of Thermally Stable Al-Cr-Zr Alloys Using Rapid Solidification Technology, *Dispersion Strengthened Aluminum Alloys*, Kim Y-W. and Griffith W.M., Eds., The Minerals, Metals & Materials Society, 1988, 217.

53. OCTOR H. and NAKA S., Early Stage of Al Zr Precipitation in a Rapidly Solidified Al-Cr-Zr Alloy, *Phil. Mag.* **59**, (1989), 229.
54. ZEDALIS M. and FINE M.E., Lattice Parameter Variation of Al (Ti,V,Zr,Hf) in Al-2at% (Ti,V,Zr,Hf) alloys, *Scripta Metall.*, **17**, (1983), 1251.
55. ANGERS L., CHEN Y., FINE M.E., WEERTMAN J.R. and ZEDALIS M.S., Rational Design of High Temperature Alloys, *Aluminum Alloys - Physical and Mechanical Properties*, E.A. Starke Jr and T.H. Sanders Jr, Eds., Emas, Charlottesville, 1986, 321.
56. ZEDALIS M.S. and FINE M.E., Precipitation and Ostwald Ripening in Dilute Al Base-Zr-V Alloys, *Metall. Trans.*, **17A**, (1986), 2187.
57. FINE M.E., Stability and Coarsening of Dispersoids in Aluminum Alloys, *Dispersion Strengthened Aluminum Alloys*, Kim Y-W. and Griffith W.M., Eds., The Minerals, Metals & Materials Society, 1988, 103.
58. CHEN Y.C., FINE M.E., WEERTMAN J.R. and LEWIS R.E., Coarsening behavior of  $L1_2$  Structured  $Al_3(Zr_xV_{1-x})$  Precipitates in Rapidly Solidified Al-Zr-V Alloy, *Scripta Metall.*, **21**, (1987), 1003.
59. YANEY D.L., LEWIS R.E. and NIEH T.G., Microstructural Characterization of Rapidly Solidified Al-Zr-V Alloys, *Dispersion Strengthened Aluminum Alloys*, Kim Y-W. and Griffith W.M., Eds., The Minerals, Metals & Materials Society, 1988, 59.
60. HAWK J.A., ANGERS L.M. and WILSDORF H.G.F., High Volume Fraction P/M Aluminum Alloys - Stability and Strength at Elevated Temperatures, *Dispersion Strengthened Aluminum Alloys*, Kim Y-W. and Griffith W.M., Eds., The Minerals, Metals & Materials Society, 1988, 339.
61. FERNANDEZ RIVERA C., ARCADE P. and CHAMPIER G., Microstructure and Mechanical Properties of Al-3Cr-1Ce (at%) Alloy, *Int. Conf. Advanced Aluminium and Magnesium Alloys*, ASM Europe, Amsterdam, 20-22 june 1990, (sous presse).
62. ZAIDI A., ARCADE P. and CHAMPIER G., Mechanical Behaviour of Rapidly Solidified Al-3Cr-xMn (at%) Alloys, *Int. Conf. Advanced Aluminium and Magnesium Alloys*, ASM Europe, Amsterdam, 20-22 june 1990, (sous presse).

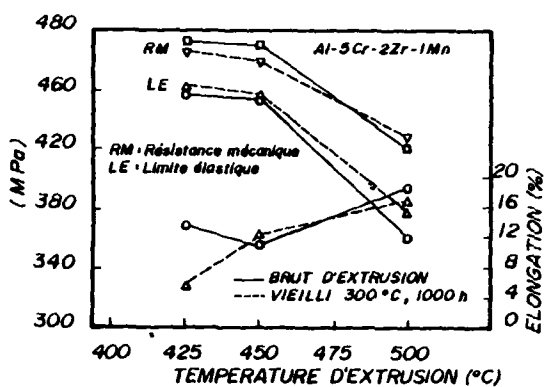


Fig. 28. Change in the yield stress (LE), tensile strength (RM) and elongation vs the extrusion temperature in the, pre-heated for 45 min, as-extruded and aged for 1000 hours at 300°C Al5Cr2Zr1Mn alloy [52].

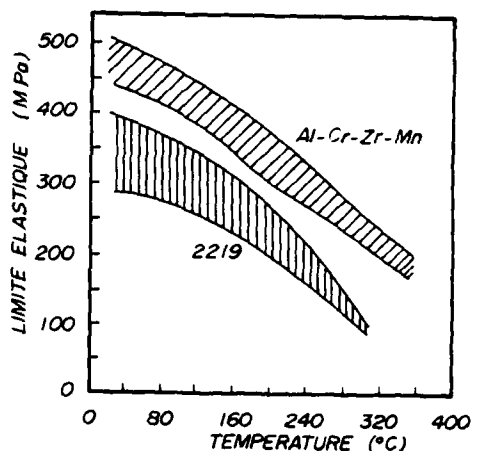


Fig. 29. Change in the yield stress vs the temperature in the Al-Cr-Zr-Mn and 2219 alloys [52].

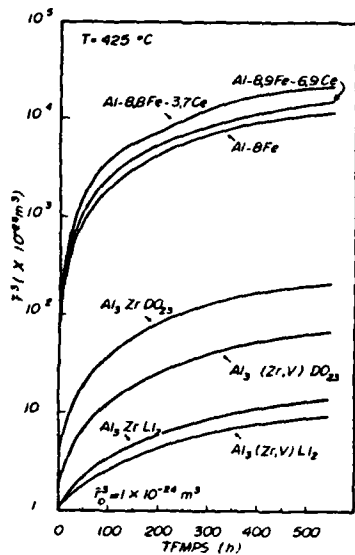


Fig. 30. Comparison of the precipitate coarsening rates for different alloys at 425°C, all the curves are shifted so  $r_0$  is  $1 \times 10^{-24} m$  [55].

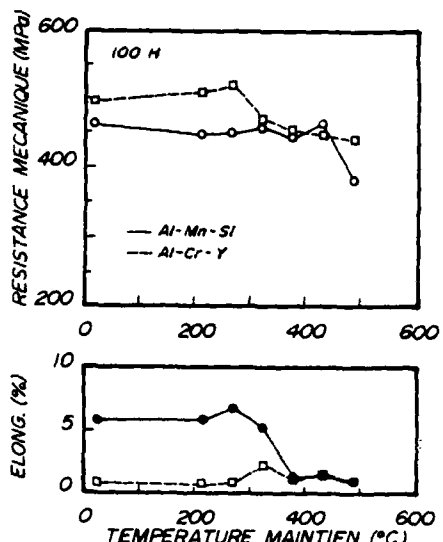


Fig. 32. Change in the tensile strength and elongation measured at room temperature vs the exposure temperature for 100 hours in the Al-4.8Si-12.6Mn and Al-6.8Cr-5.1Y alloys [60].

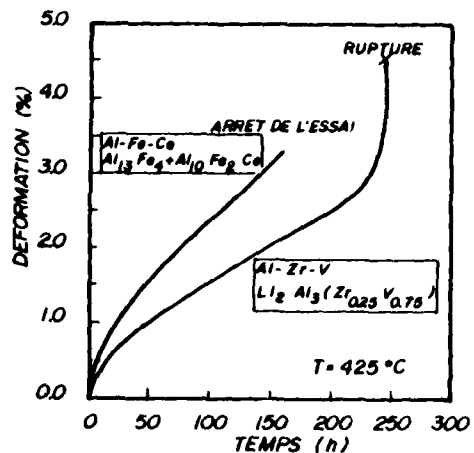


Fig. 31. Creep strain curves in the Al-Fe-Ce and Al-V-Zr alloys [67].

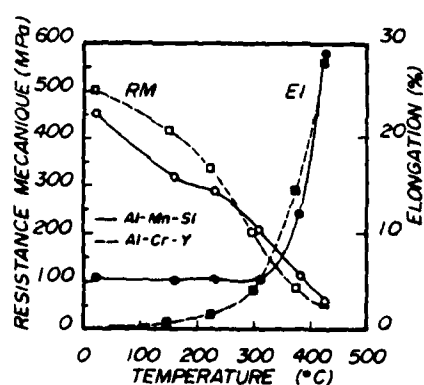
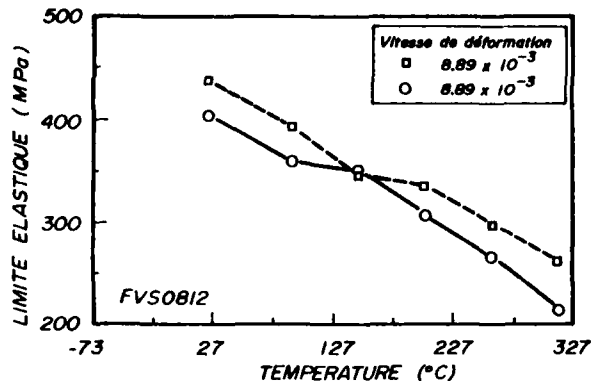
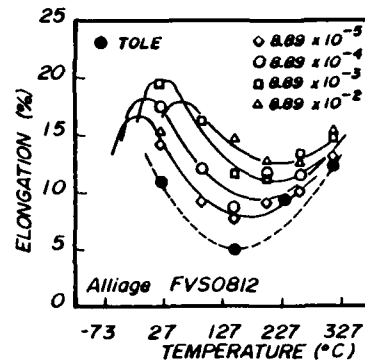


Fig. 33. Change in the tensile strength (RM) and elongation (EI) vs the temperature in the Al-4.8Si-12.6Mn and Al-6.8Cr-5.1Y alloys [60].



(a)



(b)

Fig. 20 Change in (a) the yield stress and (b) the elongation vs the temperature in the FVS 1212 alloy at different strain rates [42,43]

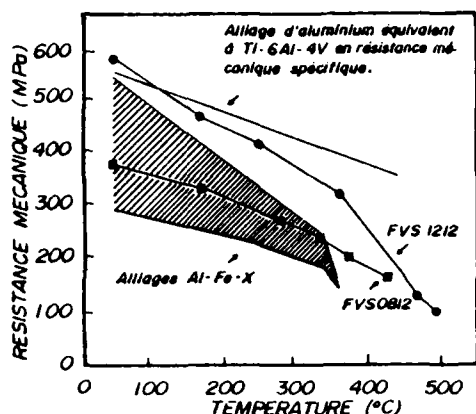


Fig. 19. Change in the yield stress vs the temperature in the AlFeVSi alloys, comparison with the AlFeX alloys and AlX alloy with the same specific yield stress as the Ti6Al4V alloy [36].

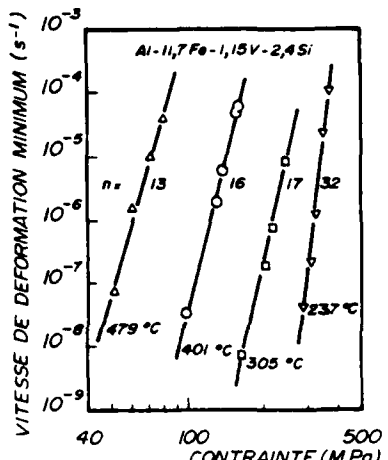


Fig. 21. Change in the creep strain rate vs the applied stress at different temperatures in the Al11.7Fe1.15V2.4Si alloy [44].

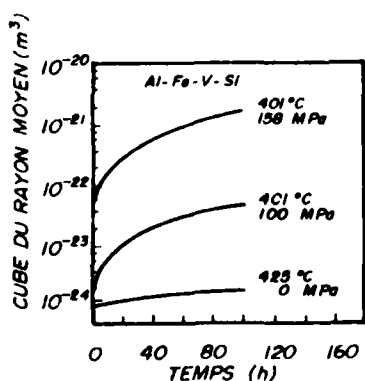
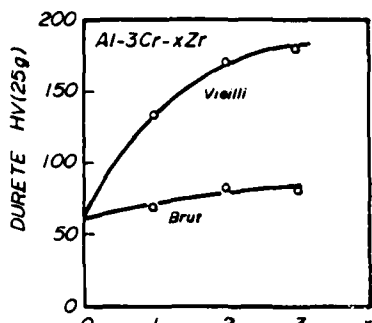
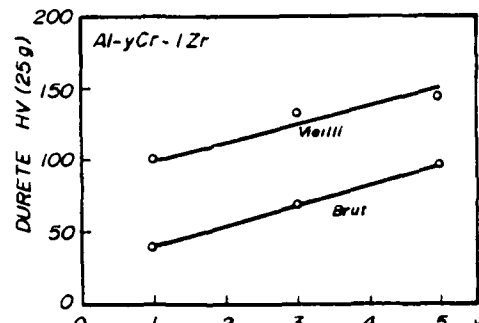


Fig. 22. Change in the average radius cubed of the precipitates vs the time in AlFeVSi alloys; effect of an applied stress [44].



(a)



(b)

Fig. 23. Change in the hardness of (a) the  $\text{Al}-3\text{Cr}-x\text{Zr}$  alloy vs  $x$  and (b) the  $\text{Al}-y\text{Cr}-1\text{Zr}$  alloy vs  $y$  as rapidly solidified and peak aged [48,49].

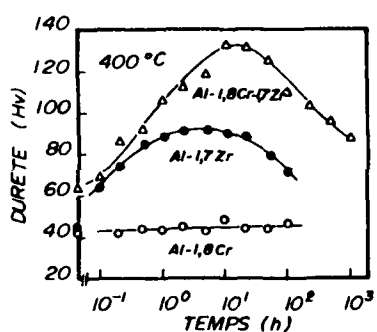


Fig. 24. Change in the hardness of the  $\text{Al}1.8\text{Cr}$ ,  $\text{Al}1.7\text{Zr}$  and  $\text{Al}1.8\text{Cr}1.7\text{Zr}$  alloys during aging at  $400^\circ\text{C}$  [50].

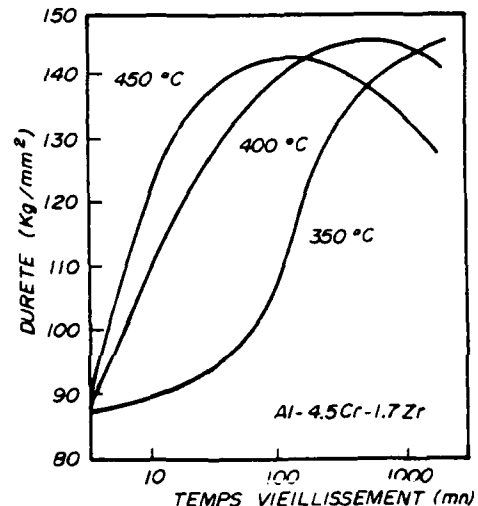


Fig. 25. Change in the hardness of the  $\text{Al}4.5\text{Cr}1.7\text{Zr}$  alloy during aging at 350, 400 and  $450^\circ\text{C}$  [49,51,52].

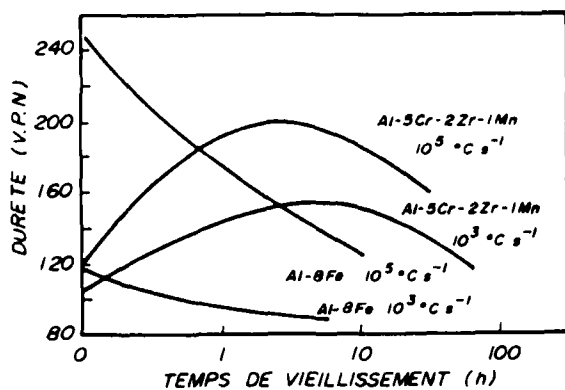


Fig. 26. Change in the hardness of the rapidly solidified  $\text{Al}8\text{Fe}$  and  $\text{Al}5\text{Cr}2\text{Zr}1\text{Mn}$  alloys during aging: effect of the solidification rate [62].

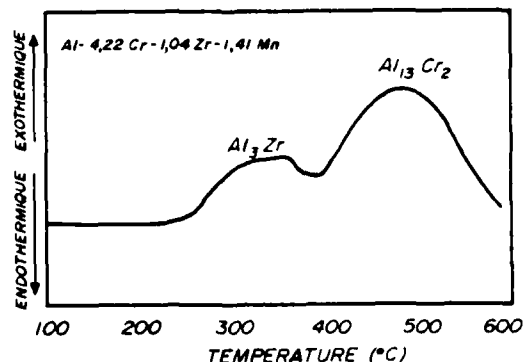


Fig. 27. DSC chart showing the decomposition of the rapidly solidified solid solution in the powder of  $\text{Al}-4.28\text{Cr}-1.04\text{Zr}-1.41\text{Mn}$  alloy [49].

## METALLURGIE PHYSIQUE DES ALLIAGES MP D'ALUMINIUM

Georges CHAMPIER  
UA-CNRS 155, Ecoles des Mines  
Institut National Polytechnique de Lorraine  
Parc de Saurupt, 54042 NANCY Cedex, France

### Résumé

L'extension des domaines d'applications des alliages d'aluminium requiert de nouvelles compositions et la mise en oeuvre de nouveaux procédés. La métallurgie des poudres offre la possibilité d'utiliser des compositions comportant des éléments proscrits dans les alliages conventionnels: métaux de transition, terres rares, oxygène, carbone par exemple. Les méthodes relevant de la solidification rapide et de l'alliage mécanique permettent d'éliminer ou de corriger les éléments de la microstructure qui limitaient fortement l'utilisation de tels alliages obtenus par les procédés classiques. Les microstructures et les propriétés mécaniques des alliages à forte résistance mécanique à la température ordinaire, 7090, 7091, CW67 et Al-C-O seront présentées. Les différents types d'alliages pour applications à haute température seront également revus: Al-Fe-Ce, Al-Fe-V-Si, Al-Cr-Zr, Al-Zr-V, Al-Cr-Y et d'autres dont l'étude est en cours.

### 1 - INTRODUCTION

L'utilisation d'alliages d'aluminium dans de nouveaux domaines d'application requiert l'amélioration d'au moins une ou deux propriétés sans pour autant qu'il y ait dégradation des autres propriétés. Il peut s'agir d'une propriété physique, la densité par exemple, d'une propriété mécanique, la résistance mécanique par exemple, ou encore d'une propriété chimique, la résistance à la corrosion par exemple.

Pour les alliages conventionnels, l'optimum a été atteint tant au niveau de la composition, choix et concentration des éléments d'addition, qu'au niveau des procédés, en particulier les traitements thermiques et thermomécaniques. Pour améliorer les performances on doit avoir recours soit à de nouvelles compositions, mais alors les procédés conventionnels ne conviennent pas, soit à de nouveaux procédés avec les compositions conventionnelles ou avec des compositions nouvelles. On doit alors viser à obtenir des microstructures ayant certaines caractéristiques comme par exemple des grains plus petits, des dispersoïdes plus fins, plus stables thermiquement,...

Ces nouvelles microstructures sont obtenues par des procédés au cours desquels l'alliage se trouve divisé en particules de poudre plus ou moins fines. Pour les éléments d'addition solubles dans l'aluminium liquide, la division est réalisée dans l'état liquide et chaque goutte se solidifie rapidement; une autre possibilité est de projeter un jet d'alliage fondu sur un support tournant et de récupérer soit des paillettes, soit un ruban très mince; ces procédés relèvent des techniques de la solidification rapide. Pour les éléments d'addition peu solubles dans l'aluminium liquide, on procède par broyage des particules dans un milieu contrôlé: les phénomènes de rupture et de soudure qui se succèdent permettent d'incorporer dans l'alliage soit mécaniquement, soit par réaction chimique sur la surface fraîche de rupture, des éléments contenus dans le milieu environnant (gaz, liquide ou solide); ces procédés relèvent des techniques de l'alliage mécanique.

Trois domaines d'applications sont envisagés pour le développement de ces nouveaux alliages d'aluminium [1,2]:

(1) alliages à faible densité en vue de remplacer les alliages 2024-T3, 7075-T6 et 7075-T3 dans la construction aéronautique; la réduction de la densité est obtenue par addition de lithium. Ce sujet faisant l'objet de deux conférences particulières dans cette Série, il ne sera pas abordé par la suite.

(2) alliages à forte résistance mécanique à la température ordinaire en vue de remplacer l'alliage 7075-T6; ce renforcement de la résistance mécanique est obtenu soit par solidification rapide d'alliages 7xxx auxquels on ajoute des éléments des métaux de transition, soit par alliage mécanique d'aluminium ou d'alliage aluminium-magnésium dans lesquels on incorpore de l'oxyde et du carbure d'aluminium.

(3) alliages pour applications à température élevée ( $350^{\circ}\text{C}$ ) en vue de remplacer les alliages de titane et les aciers; la faible densité des alliages d'aluminium et la facilité de leur usinage constituent des avantages; ces alliages sont obtenus par solidification rapide d'alliages d'aluminium avec des éléments des métaux de transition et des terres rares; des essais sont faits pour bénéficier e.i. outre des potentialités de l'alliage mécanique.

### 2 - ALLIAGES A FORTE RESISTANCE MECANIQUE A LA TEMPERATURE ORDINAIRE

La déformation plastique des alliages d'aluminium à la température ordinaire est associée au glissement des dislocations à travers le réseau de la matrice. Le durcissement de l'alliage est dû à l'interaction des dislocations mobiles avec les atomes des solutés, les précipités et les dislocations de la forêt; deux autres paramètres contrôlent le durcissement: la texture et la taille des grains [2]. L'interaction des dislocations mobiles avec les précipités peut se produire soit par cisaillement du précipité, soit par son contournement suivant le mécanisme d'Orowan; dans le cas des alliages à

forte résistance mécanique ayant à subir des expositions à haute température, le mécanisme d'Orowan est prépondérant car il s'agit de précipités durs et incohérents avec la matrice. La contribution de cette interaction à la limite élastique s'exprime en première approximation par:

$$\sigma_{OR} = \alpha \cdot G \cdot b / D_p = \alpha \cdot G \cdot b \cdot f_v^{1/3} / d_p$$

$\alpha$  est un coefficient dont la valeur est voisine de l'unité,  $G$  le module de cisaillement de la matrice,  $b$  le vecteur de Burgers des dislocations mobiles,  $D_p$  la distance moyenne entre précipités,  $d_p$  leur taille et  $f_v$  leur fraction volumique. La contribution  $\sigma_{OR}$  sera d'autant plus forte que  $D_p$  sera plus petit ou encore, à fraction volumique constante, que  $d_p$  sera plus petit. La contribution de la taille des grains à la limite élastique s'exprime par:

$$\sigma_G = k \cdot D^{-1/2}$$

$k$  est un coefficient qui dépend de la nature de la matrice et  $D$  la taille moyenne des grains. Enfin la contribution de la texture, si elle existe, s'exprime à travers le facteur de Taylor. La limite élastique et la résistance mécanique seront d'autant plus élevées que les précipités seront plus petits, leur fraction volumique plus grande et la taille des grains de la matrice plus petite. La texture introduit une anisotropie de l'alliage.

Les alliages d'aluminium à forte résistance mécanique sont obtenus par les deux méthodes indiquées dans l'introduction: soit par solidification rapide, soit par alliage mécanique.

## 2.1 - ALLIAGES OBTENUS PAR SOLIDIFICATION RAPIDE

Ces alliages sont considérés comme des alliages de la série 7xxx auxquels on ajoute des éléments des métaux de transition en vue d'obtenir des précipités finement dispersés. Quatre alliages ont été plus particulièrement étudiés, leur compositions sont indiquées ci-après [3] (pds%):

Alliage	Zn	Mg	Cu	Co	Zr	Ni
7090	8,0	2,5	1	1,5		
7091	6,5	2,5	1,5	0,4		
CW67	9,0	2,5	1,5		0,14	0,1
PM64	7,4	2,4	2,1	0,3		0,2
7050	6,2	2,2	2,3		0,12	
7075	5,6	2,5	1,6			

Par rapport aux alliages conventionnels 7050 et 7075, la concentration en zinc est plus forte et les éléments Co, Zr+Ni et Co+Ni sont ajoutés. L'addition de cobalt conduit après la solidification rapide à une dispersion fine de précipités  $Al_3Co_2$  qui apportent une contribution supplémentaire à la résistance mécanique, en plus des précipités  $MgZn_2$  caractéristiques des alliages de la série 7xxx. En outre les précipités  $Al_3Co_2$  bloquent la recristallisation, affine la taille du grain de la matrice et piège les impuretés comme le fer en donnant des composés du type  $Al_3(Co,Fe)_2$  [4]. L'addition de nickel produit les précipités  $Al_3(Ni,Fe)_2$ , ceux-ci se formeraient par une réaction à l'état solide durant la consolidation de la poudre d'alliage [5]. Les précipités  $Al_3Zr$  n'apparaissent qu'en très petit nombre.

Les propriétés mécaniques en traction des alliages solidifiés rapidement, à la température ordinaire, sont indiquées ci-après, elles sont comparées à celles des alliages conventionnels [4,5,6,7]:

Alliage	Limite élast.	Resist. mécan.	Elongat. rupture	Ténacité	Densité g/cm <sup>3</sup>	Module d'Young; GPa
				MPa		
7090 T6E192 Extrudé	L	641	676	10	2,850	73,8
	LT	600	648	10		
	L	579	621	9		
	ST	490	558	8		
Forgé T7E71					20	31
7091 T6E192 Extrudé	L	558	614	11	2,823	72,4
	LT	538	586	13		
	L	545	593	11		
	LT	496	545	9		
Forgé T7E69	ST	455	524	9	26	33
CW67 Extrudé	L	579	614	12	47	2,88
	LT	528	570	10		
	ST	499	560	9		
	Forgé T7X2	L	579	602		
					44	

	LT	572	606	15		
	ST	531	572	9	34	
PM64 TX7		540	585	10	34	
7075	L	456	530	13	34	2,796
	LT	447	520	12		71,7
	ST	441	510	8	28	

La comparaison des propriétés des alliages extrudés 7090, 7091 et CW67 avec les autres alliages de la série 7xxx est faite sur un diagramme limite élastique-ténacité: chaque alliage est représenté par un segment de droite correspondant aux différentes combinaisons de la limite élastique et de la ténacité qu'il est possible d'obtenir avec un traitement thermique approprié (fig. 1) [5]. On note clairement les avantages de l'alliage CW67 sur tous les autres alliages: il présente la meilleure combinaison de la limite élastique (de 586 à 660 MPa) et de la ténacité (de 38 à 53 MPa/m).

Les alliages 7xxx + métal de transition présentent une meilleure résistance à la corrosion et à la corrosion sous contrainte que les alliages 7xxx associés conventionnels. L'épaisseur du film d'oxyde est pratiquement la même pour tous ces alliages, de l'ordre de 7 nm. La corrosion sous contrainte est très sensible à la microstructure: la fissure de corrosion s'amorce d'autant plus facilement que celle-ci comporte de gros précipités contenant en général le fer qui reste toujours en impureté dans l'aluminium, c'est le cas des alliages classiques de la série 7xxx. La solidification rapide a pour effet d'éliminer les gros précipités, de produire des précipités fins qui piègent le fer: l'amorçage de la fissure de corrosion sous contrainte n'intervient qu'au bout d'un temps plus long. Par ailleurs dans les alliages conventionnels, les joints de grains sont relativement longs et plats et la fissure peut s'y propager sur des distances de plusieurs dizaines de microns sans rencontrer d'obstacle. Dans les alliages solidifiés rapidement les grains ont une taille de 1 à 3 microns, le tracé des joints y est irrégulier et tourmenté, ce qui entraîne un fort ralentissement de la propagation de la fissure; la vitesse de propagation dans l'alliage 7075-T73 est 3,7 fois plus forte que dans l'alliage 7091-T7E69 en solution à 3,5% de chlorure de sodium [8,9].

## 2.2 - ALLIAGES OBTENUS PAR ALLIAGE MECANIQUE

Ces alliages contiennent tous de l'oxygène sous forme d'oxyde  $\text{Al}_2\text{O}_3$  et du carbone sous forme de carbure  $\text{Al}_4\text{C}_3$ . Ils peuvent contenir en outre du silicium et du magnésium. Quelquesunes des compositions citées dans la littérature sont indiquées ci-après [10,11,12]:

Alliage	O	C	Mg	Si	$f_v(\%)$
DISPAL 0	2,5	-	-	-	
DISPAL 2	1	2	-	-	10-12
DISPAL 3	0,8	3	-	-	
DISPAL 1Si12	1	1	-	12	6-10
IN9052	0,6	1,1	4	-	6

$f_v$  désigne la fraction volumique des dispersoïdes; 1% en poids de carbone produit 4,5% en volume de carbure et 1% en poids d'oxygène produit 1,6% en volume d'oxyde.

Dans la poudre brute de broyage, l'oxygène et le carbone sont impliqués dans des composés amorphes qui produisent des anneaux sur les clichés de diffraction des électrons. Les composés cristallisés n'apparaissent qu'après les différentes phases du traitement de consolidation [13]. Ils forment des dispersoïdes très fins dont les tailles sont de 30-40 nm pour l'oxyde et de 20-100 nm pour le carbure; ils sont placés sur les joints de grains, isolés ou regroupés; quelques uns sont à l'intérieur des grains. La taille des grains de la matrice est égale à 0,2-0,5  $\mu\text{m}$ . Dans l'alliage IN9052 il peut apparaître également des précipités du composé intermétallique  $\text{Al}_3\text{Mg}_2$ .

Les propriétés mécaniques en traction de ces alliages à la température ordinaire sont indiquées ci-après:

Alliage	Limite élast.	Resist. mécan.	Elongat. rupture	Ténacité	Densité	Module d'Young
	MPa	MPa	%	MPa/m	g/cm <sup>3</sup>	GPa
DISPAL 2	300-340	340-380	8-12		2,70	80
DISPAL 1Si12	300-340	340-380	4-8		2,66	85
IN9052	380	450	13	44	2,68	76

Ces propriétés ont également été mesurées en faisant varier la concentration en oxygène et en carbone et par voie de conséquence la fraction volumique des dispersoïdes; le résultat obtenu avec une matrice l'aluminium pur est indiqué à la figure 2 [10], la limite élastique et la résistance mécanique croissent linéairement avec la fraction volumique; la comparaison sur la même figure avec l'alliage SAP montre nettement l'avantage de l'alliage mécanique: il y a un gain de 100 à 150 MPa. Dans les deux cas l'élongation à la rupture décroît quand la fraction volumique augmente.

Seuls les dispersoïdes placés à l'intérieur des grains constituent des obstacles au

déplacement des dislocations; comme ils sont relativement peu nombreux, leur contribution à la limite élastique n'est pas prépondérante. Il est probable que la contribution la plus importante est celle de la taille des grains D; cependant la loi en  $D^{-1/2}$  ne peut pas être vérifiée car l'alliage mécanique ne produit qu'un domaine restreint de taille de grain. Dans le cas de l'alliage IN9052, le magnésium peut également apporter une contribution en tant que soluté.

La stabilité thermique des alliages Al-C-O est remarquable: leur microstructure est maintenue et leurs propriétés mécaniques mesurées à la température ordinaire sont conservées après un maintien à haute température. Un maintien de 100 heures à 510°C ne modifie ni la taille des grains de la matrice, ni la taille des dispersoïdes [14]. Un maintien allant jusqu'à 250 heures à une température de 500°C n'entraîne aucune variation de la résistance mécanique, ni de l'élongation à la rupture [12,15,16,17] (fig. 3). L'alliage IN9052 n'est pas aussi thermiquement stable: sa résistance mécanique mesurée à la température ordinaire diminue de 14% environ après un maintien de 100 heures à 510°C [14]; cette diminution est probablement due à la coalescence des précipité du composé  $\text{Al}_3\text{Mg}_2$ .

Dès que la température s'élève, les propriétés mécaniques de ces alliages se dégradent. À 300°C la résistance mécanique de l'alliage DISPAL 2 ne représente plus que 52% de celle mesurée à la température ordinaire; cette proportion est encore plus faible, 40%, pour l'alliage DISPAL 1S112 (fig. 4a) [12]. On remarque que l'élongation à la rupture diminue régulièrement. Tous les alliages Al-C-O ont un comportement du même type [17]. Pour l'alliage IN9052 la dégradation est encore plus marquée (fig. 4b) [18]; on note que l'élongation à la rupture passe par un maximum.

L'alliage mécanique améliore aussi la résistance à la corrosion qui est caractéristique des alliages Al-Mg. Cependant à l'inverse des alliages conventionnels de même composition de base, l'alliage IN9052 est résistant à la corrosion par exfoliation et à la corrosion sous contrainte. Par immersion alternée dans une solution à 3,5% de chlorure de sodium à 30°C, l'attaque n'est que de 4  $\mu\text{m}$  par an pour les alliages IN9052 et 5083-H112 alors qu'elle est de 227  $\mu\text{m}$  par an pour l'alliage 7075-T73. Le seuil de contrainte pour la corrosion sous contrainte dans les mêmes conditions est de 380 MPa pour l'alliage IN9052 [18].

L'application de la méthode de l'alliage mécanique aux alliages conventionnels ne conduit pas toujours à des résultats satisfaisants; c'est le cas par exemple de l'alliage 7075:

	7075-T6	Brut d'AM	AM + T6
Limite élastique (MPa)	503	550	595
Résistance mécanique (MPa)	572	615	645
Elong. à la rupture (%)	10	2	3,5

On note bien une augmentation importante de la limite élastique et de la résistance mécanique, mais au détriment de la ductilité [10].

### 3 - ALLIAGES POUR APPLICATIONS A HAUTE TEMPERATURE

La déformation plastique à haute température est contrôlée essentiellement par les phénomènes de diffusion: diffusion des lacunes nécessaires à la montée des dislocations, diffusion des solutés le long des dislocations et le long des joints de grains pouvant entraîner des modifications de la microstructure, diffusion à travers le réseau correspondant à un transport de matière. La dégradation des propriétés mécaniques des alliages quand la température augmente peut être attribuée à la recristallisation de la matrice, si les joints de grains peuvent se déplacer aisément, au grossissement par coalescence des précipités, si les éléments constitutifs sont solubles et diffusent facilement à travers la matrice, enfin à de nouveaux mécanismes de déformation liés à la diffusion, montée des dislocations et glissement aux joints de grains par exemple.

Dans le cas des alliages d'aluminium, pour limiter la dégradation des propriétés mécaniques quand la température augmente, on cherchera donc à bloquer le déplacement des joints de grains de la matrice par des dispersoïdes placés sur eux et à réaliser le durcissement de l'alliage par des précipités durs, thermiquement stables et qui ne coalescent que très lentement, c'est-à-dire, d'une part, qui comportent des éléments d'addition ayant une faible solubilité et une faible diffusivité et, d'autre part, qui ont une faible énergie d'interface avec la matrice. Les éléments des métaux de transition et des terres rares répondent bien à la plupart de ces exigences.

Les premières études ont porté sur l'alliage binaire aluminium-fer solidifié rapidement [19] sous forme de paillettes. Par observation au microscope métallographique au grandissement 1000 deux types de microstructure ont été mis en évidence: une zone "A" sans détails visibles et une zone "B" qui contenait des précipités très fins de la phase métastable  $\text{Al}_6\text{Fe}$  associés à une structure colonnaire eutectique. Quand la température augmente, cette microstructure tend vers la microstructure d'équilibre,  $\alpha\text{-Al} + \text{Al}_3\text{Fe}_4$  par étapes successives et on note simultanément une dégradation importante des propriétés mécaniques. Les études se sont alors poursuivies par la recherche d'alliages ternaires ou quaternaires conduisant à de nouveaux précipités répondant mieux aux exigences de stabilité thermique. Les cas des alliages Al-Fe-Ce et Al-Fe-V-Si seront traités dans les paragraphes suivants. Les alliages à base aluminium-chrome, et plus spécialement l'alliage Al-Cr-Zr, seront aussi présentés; les résultats se rapportant à des alliages

plus particuliers dont les précipités ont été choisis pour avoir soit une faible énergie d'interface avec la matrice, Al-Zr-V, soit une forte fraction volumique, Al-Mn-Si et Al-Cr-Y, seront discutés.

### 3.1 - ALLIAGES Al-Fe-Ce

Une étude exploratoire [20] sur les alliages d'aluminium avec des métaux de transition (Mn, Co, Fe, Ni, Cr) et des métaux des terres rares (Ce, La) a montré que les alliages Al-Fe-Ce solidifiés rapidement par pulvérisation par gaz puis compactés et consolidés par forgeage présentaient des propriétés intéressantes. De nombreux travaux ont été effectués sur ces alliages pour préciser leurs performances et en déduire leurs possibilités de développement.

Les concentrations de ces alliages sont variables : de 5 à 7 at% pour la somme des concentrations atomiques en fer et en céryum et de 3 à 5 pour le rapport des concentrations [21]. La microstructure des particules de poudre dépend de leur taille et des conditions de solidification ; d'une façon générale le front plan de solidification s'altère au cours de sa progression, il y a formation d'une microstructure cellulaire qui se transforme progressivement en microstructure dendritique plus ou moins grossière. Les zones intercellulaires ou interdendritiques contiennent des précipités intermétalliques dont la taille varie de 10 à 100 nm et qui se sont développées pendant la solidification. Dans l'alliage consolidé des précipités plus gros sont observés. Dans l'alliage Al-8,8Fe-3,7Ce (pdts%) brut d'extrusion l'ensemble des phases précipitées correspond à une fraction volumique de 20% [22] : la phase la plus abondante est la phase quasicristalline métastable  $\text{Al}_{20}\text{Fe}_5\text{Ce}$ , d'autres composés intermétalliques métastables ont été détectés,  $\text{Al}_6\text{Fe}$  et  $\text{Al}_{10}\text{Fe}_2\text{Ce}$ ; les phases stables,  $\text{Al}_{13}\text{Fe}_4$  et  $\text{Al}_{13}\text{Fe}_3\text{Ce}$ , sont aussi présentes mais en très petite quantité. Les précipités  $\text{Al}_6\text{Fe}$  sont globulaires avec une taille de l'ordre de 0,1  $\mu\text{m}$ ; les quasicristaux  $\text{Al}_{20}\text{Fe}_5\text{Ce}$  se présentent sous la forme de bâtonnets avec une longueur (environ 0,1  $\mu\text{m}$ ) égale à trois fois le diamètre, les axes des bâtonnets sont parallèles à la direction de l'extrusion; les précipités  $\text{Al}_{10}\text{Fe}_2\text{Ce}$  sont équiaxes avec une taille de l'ordre de 0,3  $\mu\text{m}$ , ils contiennent souvent des fautes planes.

Un maintien de l'alliage à 316°C pendant 2160 heures entraîne la transformation de la phase métastable  $\text{Al}_6\text{Fe}$  en la phase stable  $\text{Al}_{13}\text{Fe}_4$ . Au cours d'un maintien à plus haute température, 425°C, pendant 240 heures les phases métastables ternaires se transforment en la phase stable  $\text{Al}_{13}\text{Fe}_3\text{Ce}$ . La composition et la structure cristalline de chacune de ces phases sont indiquées ci-après [22] :

$\text{Al}_6\text{Fe}$	orthorhombique	a=0,645	b=0,744	c=0,878 nm	Cmcm
$\text{Al}_{13}\text{Fe}_4$	monoclinique	a=1,549	b=0,808	c=1,248 nm    b=107°43'	C2/m
$\text{Al}_{20}\text{Fe}_5\text{Ce}$	quasicristal				
$\text{Al}_{10}\text{Fe}_2\text{Ce}$	orthorhombique	a=1,02	b=1,62	c=0,42 nm	Cmm2 ou C222
$\text{Al}_{13}\text{Fe}_3\text{Ce}$	orthorhombique	a=0,89	b=1,02	c=0,91 nm	Cmcm ou Cmc2

Après le maintien à 425°C les précipités  $\text{Al}_{13}\text{Fe}_4$  et  $\text{Al}_{13}\text{Fe}_3\text{Ce}$  peuvent atteindre des tailles de l'ordre de 0,3 à 0,4  $\mu\text{m}$ ; les premiers contiennent souvent des fautes [23]. L'étude de la variation de la taille des précipités en fonction du temps de maintien isotherme montre une croissance régulière qui résulte d'une coalescence contrôlée par la diffusion des atomes solutés, Fe et Ce, le long des joints de grains [24]; l'application d'une contrainte de traction pendant le maintien à haute température produit une accélération de la coalescence et conduit à des précipités plus gros (fig. 5). La taille du grain de la matrice croît très légèrement au début du maintien, de 0,7 à 0,9  $\mu\text{m}$  en une dizaine d'heures, puis elle reste pratiquement constante.

Les propriétés mécaniques des alliages Al-Fe-Ce à la température ordinaire ont été mesurées par des essais de dureté [25,26], de traction [21,27] et de compression [28]. La stabilité thermique de ces propriétés après un maintien à haute température a été explorée par les mêmes essais. Pour un maintien de une heure, la dureté diminue très faiblement jusqu'à 350°C et au-delà sa décroissance est très marquée [25] (fig. 6a); pour un maintien à 300°C, elle reste pratiquement constante jusqu'à 1050 heures [26] (fig. 6b). La limite élastique tant en traction qu'en compression diminue pour des maintiens de 1000 heures à 149, et 232°C et de 100 heures à 316°C [27,28] (fig. 7). La comparaison avec l'alliage conventionnel 2219 montre bien l'intérêt de alliages Al-Fe-Ce tant pour la dureté [26] que pour la limite élastique [21]: pour l'alliage 2219, la dureté décroît de 37,5% après un maintien de 100 heures à 300°C (fig. 6b); sa limite élastique commence à décroître après un maintien de 1000 heures à 95°C et pour une température plus élevée, 315°C, la décroissance atteint 50%; elle n'est que de 10% pour les alliages Al-Fe-Ce dans les mêmes conditions (fig. 8).

Les propriétés mécaniques en traction à haute température, jusqu'à 316°C, ont été mesurées pour différentes compositions [21]; les résultats obtenus sont indiqués ci-après en même temps que la ténacité, la densité et le module d'Young:

Alliage	Temp. °C élast.	Limite élast. MPa	Resist. mécan. MPa	Elongat. rupture %	Ténacité Densité MPa/m g/cm <sup>3</sup>	Module d'Young GPa
Al7,1Fe6,1Ce (extrudé)	25 149	387 362	493 475	11,7 6,0	12,2 2,957	78,9

	232 316	332 212	367 237	4,7 10,7			
A17,1Fe6,1Ce (extrudé et laminé)	25 149	524 403	567 427	5,7 5,0	26,0	2,957	78,9
	232	278	304	5,0			
	316	150	176	6,5			
A18,1Fe6,8Ce (extrudé)	25 149	440 364	525 433	9,0 4,0	6,2	3,00	85,6 71,8
	232	297	351	6,0			70,4
	316	211	246	9,0			63,5
A18,4Fe7,2Ce (extrudé)	25 149	458 448	563 484	8,0 4,0	6,4	3,01	80,1
	232	391	424	4,0			
	316	225	271	7,3			
A19,8Fe7,8Ce	25 149	490 492	613 525	5,0 2,6	3,06		83,8
	232	410	450	2,6			
	316	255	295	5,3			

On note une décroissance de la limite élastique et de la résistance mécanique quand la température augmente alors que l'elongation à la rupture passe par un minimum vers 200-250°C. La comparaison de la variation de la résistance mécanique spécifique des alliages Al-Fe-Ce par rapport à celle de l'alliage conventionnel 2618, en fonction de la température est nettement en faveur des nouveaux alliages [21]; la comparaison avec l'alliage de titane Ti-6Al-4V montre que les résultats obtenus à ce jour sont encourageants (fig.9) .

Il est à noter que les propriétés mécaniques et leurs variations en fonction de la température sont sensibles aux conditions de préparation des alliages: pulvérisation, pressage, dégazage, consolidation. Sur la figure 10 [21] on observe à titre d'exemple l'effet de la concentration d'hydrogène résiduel ou encore celle de la valeur du rapport d'extrusion. Une augmentation de la teneur en hydrogène, de 5,6 à 14 ppm, n'affecte pratiquement pas la limite élastique ni la résistance mécanique, en revanche l'elongation à la rupture est supérieure dans tout le domaine de température exploré et le minimum a disparu. Une augmentation de la valeur du rapport d'extrusion, de 4:1 à 20:1, diminue à la fois les valeurs de la limite élastique et de la résistance mécanique mais n'affecte pratiquement pas celle de l'elongation à la rupture.

L'étude de la déformation en compression à plus haute température [23], dans le domaine de 250 à 550°C, a montré que la coalescence des précipités ne peut pas expliquer la dégradation observée des propriétés mécaniques et une analyse des résultats obtenus suggère que, au moins, une des deux phases présentes dans les précipités est susceptible de se déformer au-dessus de 450°C.

L'étude du fluage en traction dans le domaine de température de 250 à 350°C pour des contraintes variant de 20 à 115 MPa [30] montre l'existence de deux régimes de fluage, séparés par une valeur seuil de la contrainte. L'origine de ces deux régimes est encore mal expliquée.

La propagation des fissures en fatigue est plus rapide dans le cas des alliages Al-Fe-Ce par comparaison à l'alliage conventionnel 2219 [26] à 25 et 300°C; la vitesse de propagation est respectivement 2 et 3 fois plus grande (fig 11).

La résistance à la corrosion mesurée en terme de perte de poids révèle un avantage pour les alliages Al-Fe-Ce par rapport aux alliages classiques 2024-T3 et 7075-T6; la vitesse de corrosion pour une exposition de 16 jours dans une solution à 3,5% de chlorure de sodium est de 7 à 15 fois plus faible pour les alliages Al-Fe-Ce. La résistance à la corrosion sous contrainte est également améliorée: la valeur de la contrainte seuil pour la rupture au bout de 30 jours est égale à 240 MPa pour les alliages Al-Fe-Ce; c'est une valeur comparable à celle des alliages 7050-T7451 et 2219-T87 mais plus élevée que celle de l'alliage 7075 [29].

L'amélioration des propriétés mécaniques des alliages Al-Fe-Ce à des températures supérieures à 250°C peut être obtenue par l'introduction de dispersoïdes réfractaires finement dispersés, du type oxyde ou carbure. La technique de l'alliage mécanique permet effectivement de renforcer le matériau par des dispersoïdes de  $\text{Al}_2\text{O}_3$  et  $\text{Al}_4\text{C}_3$ , dont la taille varie de 10 à 40 nm; par ailleurs pour bénéficier des avantages de la solidification rapide, la technique a été utilisée avec de la poudre solidifiée rapidement [31,32,33].

Pour des alliages de composition voisine de Al-8Fe-4Ce , la microstructure de l'alliage solidifié rapidement et allié mécaniquement (SRAM) dépend des conditions de consolidation par extrusion. Pour une température d'extrusion de 245°C et un rapport de 16:1 [31], la taille du grain est de l'ordre de 0,2 à 0,4  $\mu\text{m}$  pour l'alliage solidifié rapidement (SR) et l'alliage SRAM; la distribution des précipités est plus uniforme dans le second. Après maintien d'une heure à 610°C, les dispersoïdes de l'alliage SRAM sont

encore fins et la taille des grains n'a que très légèrement augmenté, de 0,25 à 0,7 µm. Pour une température d'extrusion de 550°C et un rapport de 10:1 [32], les grains de l'alliage SR gardent une taille petite, de l'ordre du micron, alors que ceux de l'alliage SRAM sont légèrement allongés dans la direction de l'extrusion avec une taille de 30 µm environ; à cause de la forte déformation imposée lors de l'extrusion et du durcissement important des grains dû à la présence des dispersoïdes  $\text{Al}_2\text{O}_3$  et  $\text{Al}_4\text{C}_3$ , il y a eu recristallisation avec grossissement de la taille des grains.

L'étude de la stabilité thermique a été conduite sur les alliages extrudés à 245°C [31]. Les variations de la dureté mesurée à la température ordinaire après un maintien à 450°C en fonction du temps de maintien d'une part et après maintien d'une heure en fonction de la température de maintien d'autre part sont représentées à la figure 12. On note une augmentation d'environ 24% de la dureté à la température ordinaire quand on passe de l'alliage SR à l'alliage SRAM; en outre, au bout de 300 heures à 450°C, la diminution de la dureté de l'alliage SRAM est très faible alors que celle de l'alliage SR est très importante. Pour un maintien d'une heure, la dureté de l'alliage SRAM est pratiquement conservée jusqu'à 500°C alors que pour l'alliage SR cette température n'est que de 300°C. La dégradation de la dureté de l'alliage SR est produite par la coalescence des précipités  $\text{Al}_{13}\text{Fe}_4$  et  $\text{Al}_{13}\text{Fe}_4\text{Ce}$  par diffusion des atomes de fer et de cérium le long des joints de grains. Dans l'alliage SRAM les dispersoïdes réfractaires sont placés sur les joints de grains, ils jouent le rôle de puits de lacunes et ralentissent d'autant la diffusion des solutés et par voie de conséquence la coalescence des phases précipitées; en outre ils peuvent aussi bloquer la recristallisation: après un maintien de 288 heures à 450°C la taille du grain de l'alliage SR est de 1 µm alors que celle de l'alliage SRAM n'est que de 0,25 µm. Tous ces effets contribuent à déplacer le début de la dégradation de la dureté vers une température plus élevée.

L'essai de traction effectué à différentes températures [31] a révélé une ductilité pratiquement nulle pour l'alliage SRAM alors que l'élongation à la rupture de l'alliage SR est de l'ordre de 10% (fig. 13). La surface de rupture de l'alliage SR présente des cupules à toute température alors que pour l'alliage SRAM de petites surfaces de clivage sont observées.

L'essai de compression appliquée à l'alliage extrudé à 550°C pour différentes valeurs de la vitesse de déformation et pour différentes températures [32,33] met en évidence l'avantage tiré de l'alliage mécanique. Les courbes de la figure 14 représentent les variations à température constante de la vitesse de déformation rapportée au coefficient d'autodiffusion de l'aluminium en fonction de la contrainte maximale relevée sur la courbe de déformation (pour une déformation de 3 à 5%) rapportée au module d'Young. Les courbes en trait continu correspondent à l'alliage SR [23] et les données ponctuelles à l'alliage SRAM. A 250°C les deux alliages ont pratiquement le même comportement: l'alliage SR, à petits grains, est durci par les configurations de dislocations à forte densité laissées par l'extrusion et l'alliage SRAM, à gros grains, est durci par les précipités et les dispersoïdes. A plus haute température, le phénomène de restauration relâche les configurations des dislocations de l'alliage SR, la coalescence des précipités, le glissement aux joints et/ou la déformation d'au moins l'une des phases contribuent à la dégradation des propriétés mécaniques. Pour l'alliage SRAM, les dispersoïdes réfractaires retardent la coalescence des précipités et contribuent au durcissement.

La résistance au flUAGE en traction de l'alliage SRAM est nettement plus grande que celle de l'alliage SR. Pour un contrainte appliquée de 103 MPa, à une température de 380°C, la vitesse de déformation de l'alliage SRAM est  $3,5 \times 10^4$  fois plus petite que celle de l'alliage SR [31].

### 3.2 - ALLIAGES Al-Fe-V-Si

Les alliages Al-Fe-Si solidifiés rapidement contiennent la phase métastable  $\text{Al}_{12}\text{Fe}_3\text{Si}$  qui cristallise dans le système cubique à maille centrée, groupe d'espace Im3, et dont la forme des précipités est presque sphérique. Malheureusement cette phase est métastable et l'on ne peut pas tirer un bénéfice de ses caractéristiques pour maintenir des propriétés mécaniques intéressantes quand la température augmente: elle se transforme en donnant les phases stables  $\text{Al}_{13}\text{Fe}_4$ , monoclinique, et  $\text{Al}_8\text{Fe}_2\text{Si}$ , hexagonale, dont les morphologies ne favorisent pas une ductilité acceptable. Cependant il a été montré [34] qu'il était possible de stabiliser la phase métastable en ajoutant un quatrième élément X (V, Mn, Cr, Mo) susceptible de se substituer au fer. Le vanadium s'est révélé le plus intéressant [35]. Pour éviter toute présence autre que  $\text{Al}_{12}(\text{Fe},\text{V})_3\text{Si}$  il est nécessaire d'ajuster la composition de l'alliage et d'opérer avec une très grande vitesse de solidification. C'est la technique de la trempe sur roue qui s'impose; le ruban est ensuite broyé et la poudre obtenue est compactée suivant les méthodes classiques.

La microstructure des rubans d'alliage Al-Fe-V-Si trempés sur roue est constituée entièrement de zone dite "A", c'est-à-dire sans détail visible au microscope optique avec un grossissement de 1000 [36]. Un examen à plus fort grossissement montre l'existence d'une microstructure cellulaire-dendritique avec des précipités très fins du composé intermétallique  $\text{Al}_{12}(\text{Fe},\text{V})_3\text{Si}$  avec une taille de 10 à 30 nm. Si la trempe sur roue n'a pas été effectuée dans des conditions correctes, des précipités de phase quasi-cristallines peuvent être observés. Au cours des opérations de consolidation, la phase  $\text{Al}_{12}(\text{Fe},\text{V})_3\text{Si}$  ne se transforme pas, au pire elle coalesce un peu; ce comportement assure une grande uniformité de la distribution des précipités dans l'alliage; ceux-ci sont

placés aux joints des grains et des sous-grains ainsi qu'à l'intérieur, leur taille varie de 40 à 80 nm [37].

La structure cristalline du composé  $\text{Al}_{12}(\text{Fe},\text{V})_3\text{Si}$  peut être décrite par des icosaèdres vides de ( $\text{Fe}+\text{V}$ ) placés aux sommets et au centre de la maille cubique; ils sont parallèles entre eux et ils sont reliés suivant les directions  $<111>$  par six atomes qui forment un octaèdre légèrement contracté dans la direction des liaisons. Chaque icosaèdre de ( $\text{Fe}+\text{V}$ ) contient un icosaèdre vide de ( $\text{Al}+\text{Si}$ ) de même orientation; ces icosaèdres sont interconnectés par des chaînes de trois octaèdres distordus partageant des faces triangulaires [38]. Cette phase existe dans un certain domaine de composition suivant la formule  $\text{Al}_{12,0-14,0}(\text{Fe},\text{V})_3\text{Si}_{0,9-1,29}$  avec un rapport Fe:V pouvant varier de 5:1 à 11,5:1. La longueur du paramètre de la maille cubique est fonction de la composition, elle varie de 1,2587 à 1,2620 nm [37].

Les alliages Al-Fe-V-Si peuvent être obtenus pour différentes valeurs de la fraction volumique du composé  $\text{Al}_{12}(\text{Fe},\text{V})_3\text{Si}$ , jusqu'à 42%. La vitesse de coalescence de cet intermétallique est très faible, de  $8,4 \times 10^{-27}$  à  $2,9 \times 10^{-26}$  m/h en fonction de la valeur du rapport Fe:V. On note sur la figure 15 qu'elle se situe bien au-dessous de celle des autres intermétalliques qui apparaissent dans les alliages à base Al-Fe et pratiquement au niveau du composé  $\text{Al}_3\text{Zr}$  de structure cubique L12 qui est cohérent avec la matrice d'aluminium. La faible valeur de la vitesse de coalescence du composé  $\text{Al}_{12}(\text{Fe},\text{V})_3\text{Si}$  n'est pas attribuée à une certaine cohérence avec le réseau de la matrice; elle serait due à la formation à l'interface de marches qui favoriseraient la coïncidence de sites atomiques et du même coup diminuerait l'énergie d'interface précipité-matrice [37].

Les propriétés mécaniques à la température ordinaire sont d'un très bon niveau, elles sont d'autant plus élevées que la fraction volumique de précipités est plus forte [36, 37, 39, 40]. La stabilité thermique de ces propriétés mesurées à la température ordinaire après un maintien à haute température confirme la stabilité thermique du composé  $\text{Al}_{12}(\text{Fe},\text{V})_3\text{Si}$  due à sa faible vitesse de coalescence. Après un maintien de 1000 heures à 425°C aucune modification n'est décelée tant sur la limite élastique que sur l'elongation à la rupture (fig. 16). Après un maintien de 100 heures la limite élastique des alliages Al-Fe-V-Si ne décroît qu'à partir de 450°C alors que pour les autres alliages Al-Fe-X cette température se situe vers 300°C (fig. 17). Pour une température de maintien supérieure à 500°C [41], la résistance mécanique diminue, même au bout d'un temps relativement court (fig. 18). A 500°C la microstructure est stable jusqu'à 100 heures avec une taille de grain de 0,47 μm et une taille de précipité de 160 nm. A 550°C la coalescence des précipités est marquée et il se forme un réseau continu de précipités le long des joints de grains; en même temps la recristallisation de la matrice commence et la taille des grains est alors de 0,9 μm. Cette évolution est encore plus rapide à 600°C: les grains ont une taille de 1,2 μm et les précipités de 260 nm.

Les propriétés mécaniques à haute température ont été mesurées sur des alliages extrudés, forgés et laminés. Les résultats obtenus sont reportés ci-après pour les deux compositions qui ont été le plus étudiées [36, 40]:

FVS0812 : Al-8,5Fe-1,3V-1,7Si et FVS1212 : Al-11,7Fe-1,15V-2,4Si

Alliage		Temp. °C	Limite élast. MPa	Resist. mécan. MPa	Elongat. rupture %	Ténacité MPa/m	Densité g/cm <sup>3</sup>	Module d'Young GPa
FVS0812	L	24	390	437	10	31	2,957	88,4
Extrudé	T		387	440	10			
Laminé	L	150	340	372	7			83,2
	T		335	372	5			
	L	204	312	341	8			
	T		307	344	7			
	L	260	280	308	9			
	T		279	312	9			
	L	315	244	261	9			73,1
	T		244	280	11			
FVS0812	L	24	434	462	12			
Forgé	L	150	345	372	6			
	L	204	303	338	6			
	L	260	276	290	8			
	L	315	241	248	9			
FVS1212	L	24	605	636	8,7	11	3,02	95,5
Extrudé	L	150	486	505	3,5			86,2
Tole	L	230	432	443	3,3			82,8
	L	345	276	286	6,7			78,6
	L	450	133	147	8,9			
	L	480	103	126	10,8			

On note une décroissance de la limite élastique et de la résistance mécanique quand la

température augmente. Dans tous les cas l'elongation à la rupture passe par un minimum. La comparaison de la variation de la résistance mécanique de ces alliages avec celle des autres alliages Al-Fe-X préparés par la métallurgie des poudres montre la supériorité de l'alliage FVS1212 dans tout le domaine des températures et celle de l'alliage FVS0812 au delà de 350°C (fig. 19). Cette variation se rapproche de celle d'un alliage d'aluminium qui reste à trouver et dont la résistance mécanique spécifique serait égale à celle de l'alliage de titane Ti-6Al-4V. Jusqu'à 220°C environ, la résistance mécanique est contrôlée essentiellement par l'interaction des dislocations mobiles avec les précipités; au-delà de cette température, la taille des précipités l'a plus d'influence et le mécanisme qui contrôle la déformation est en relation avec la diffusion [34, 37].

La température pour laquelle se produit le minimum de l'elongation à la rupture est fonction de la vitesse de déformation [42, 43]; il lui correspond un palier sur la courbe qui représente les variations de la résistance mécanique en fonction de la température (fig. 20); ce palier peut être interprété comme un renforcement de la résistance mécanique pour cette combinaison des valeurs de la température et de la vitesse de déformation. L'explication proposée [41] suppose que les atomes de solutés restant en sursaturation, essentiellement du fer, se regroupent en atmosphères autour des dislocations arbres de la forêt; quand les dislocations mobiles viennent au contact des dislocations arbres et y restent pendant un certain intervalle de temps, les atomes solutés de l'atmosphère peuvent avoir le temps de diffuser vers le cœur des dislocations mobiles et ainsi les bloquer, d'où l'augmentation de la résistance mécanique et la diminution de la ductilité observées. Dans le plan température-vitesse de déformation, l'expérience montre que le réseau des lignes à elongation à la rupture constante et celui des lignes qui limitent les différents domaines de formabilité sont très voisins [42].

Les alliages Al-Fe-V-Si ont une bonne résistance au fluage en compression [44]. Ce résultat est dû à la valeur importante de la fraction volumique des précipités  $Al_{12}(Fe,V)_3Si$  qu'il est possible d'introduire et à leur grande stabilité thermique. L'étude de la variation de la vitesse de fluage en fonction de la contrainte appliquée ( $\dot{\epsilon} = k \cdot \sigma^n$ ) a montré que l'exposant  $n$  avait des valeurs nettement supérieures aux valeurs mesurées habituellement, de 13 à 32 au lieu de 3 à 6 (fig. 21). Ce comportement particulier peut être dû à une coalescence accélérée des précipités sous l'effet de la contrainte appliquée; on note sur la figure 22 que le volume d'un précipité est multiplié par 100 environ quand une contrainte de 158 MPa est appliquée pendant le maintien à 400°C; sans contrainte le volume du précipité ne varie pas.

La résistance à la corrosion mesurée en terme de perte de poids montre la supériorité des alliages Al-Fe-V-Si par comparaison avec les alliages conventionnels : par rapport à l'alliage 2014-T6 par exemple, la perte de poids est six fois plus petite pour l'alliage Al-Fe-V-Si pour une immersion dans une solution de chlorure de sodium à 3,5% [45].

### 3.3 - ALLIAGES Al-Cr-Zr

Parmi les alliages Al-Cr-X et Al-Cr-Zr-X rapidement solidifiés étudiés [46, 47], il est apparu que les alliages Al-Cr-Zr et Al-Cr-Zr-Mn étaient susceptibles de donner lieu à un développement. Cependant pour obtenir l'optimum des propriétés de ces alliages il faut les traiter thermiquement après la solidification rapide. Les courbes de la figure 23 représentent la variation de la dureté d'une part de l'alliage Al-3Cr-xZr et d'autre part de l'alliage Al-yCr-1Zr quand  $x$  et  $y$  varient dans l'état brut de trempe et après vieillissement au maximum de la dureté. On note que le phénomène de vieillissement est dû à la présence du zirconium et que son effet est d'autant plus marqué que sa concentration est plus grande [48, 49]. Ce résultat est confirmé par les courbes de la figure 24 qui représentent les variations de la dureté pendant le vieillissement à 400°C des alliages Al-1,8Cr, Al-1,7Zr et Al-1,8Cr-1,7Zr [50]. Les courbes de la figure 25 représentent la variation de la dureté de l'alliage Al-4,5Cr-1,7Zr au cours du vieillissement à 350, 400 et 450°C [49, 51, 52]. Dans tous les cas on note bien que l'alliage atteindra l'optimum de ses propriétés mécaniques après un traitement de vieillissement.

La nécessité d'un traitement de vieillissement pour les alliages Al-Cr-X peut constituer un avantage par rapport aux alliages Al-Fe-X solidifiés rapidement; en effet le fait d'avoir à travailler à une température plus ou moins élevée pendant les différentes phases de la consolidation peut entraîner une dégradation des propriétés des alliages Al-Fe-X alors que ce passage à température élevée peut s'inscrire dans le procédé de vieillissement des alliages Al-Cr-X (fig. 26) [48, 52]. Même si dans l'état brut de solidification rapide les propriétés des alliages Al-Cr-X sont moins bonnes que celles des alliages Al-Fe-X, après consolidation et vieillissement on peut s'attendre à des propriétés au moins aussi bonnes, si ce n'est meilleures.

La microstructure des particules de poudre brutes de solidification est constituée d'une matrice, solution solide de chrome et de zirconium dans l'aluminium, et de petits précipités du composé  $Al_{13}Cr_2$  dont les tailles varient de 0,5 à 2  $\mu m$ . Ce composé a une structure cristalline monoclinique,  $C2/m$ , et il est incohérent avec la matrice. Après un maintien à haute température, par consolidation ou/et par vieillissement, le Cr et le Zr en sursaturation précipitent: d'une part il peut apparaître de nouveaux précipités du composé  $Al_{13}Cr_2$  ou les précipités initiaux grossissent, d'autre part il apparaît des précipités très fins du composé métastable  $Al_3Zr$  de structure cristalline cubique,  $L1_2$ , et parfaitement cohérent avec la matrice. L'effet du vieillissement est dû essentiellement à la précipitation du composé  $Al_3Zr$ ; celle-ci se produit tant à l'intérieur des grains qu'au voisinage des joints où elle donne lieu à une précipitation discontinue [53]. La

calorimétrie différentielle met en évidence deux pics: le premier , entre 270 et 400°C, correspond à la précipitation de l'intermétallique  $\text{Al}_3\text{Zr}$  et le second, au voisinage de 475°C, à la coalescence de l'intermétallique  $\text{Al}_{13}\text{Cr}_2$  (fig 27) [49,51].

Les propriétés mécaniques des alliages Al-Cr-Zr sont sensibles aux conditions de température au cours de la consolidation. Les courbes de la figure 28 représentent les variations de la limite élastique, de la résistance mécanique et de l'élongation à la rupture en fonction de la température d'extrusion, d'une part dans l'état brut d'extrusion et d'autre part après un maintien de 1000 h à 300°C [52]. On note une diminution de la limite élastique et de la résistance mécanique pour une température d'extrusion supérieure à 450°C.

Les propriétés mécaniques pour différentes compositions et pour différentes conditions de consolidation sont reportées ci-après [51,52]:

(1) Extrusion à 400°C, [52]

Alliage	Limite élast. MPa	Resist. mécan. MPa	Elongat. rupture %	Ténacité MPa/m	Densité g/cm <sup>3</sup>	Module d'Young GPa
Al-5Cr-2,2Zr						
Diam. 7,8mm brut	440	455	20,0		2,82	80,8
Diam. 19,1mm brut	478	498	10,5			
76,2x15,9mm brut	342	362	16,8	11,3		
76,2x15,9mm +10 h à 350°C	358	376	10,9	10,9		
Al-3Cr-3Zr						
Diam.19,1mm	468	487	5,8			
Al-5,2Cr-1,9Zr-1Mn						
Diam. 19,1mm brut	426	460	14,2		2,86	86,5
+10 h à 350°C	453	474	14,0			

Le vieillissement de 10 heures à 350°C augmente les valeurs de la limite élastique et de la résistance mécanique mais il diminue celle de l'élongation à la rupture, tout en conservant cependant une valeur acceptable [52].

(2) Laminage à 250 et 350°C, Al-5,2Cr-1,89Zr-0,96Mn, [51]

T lam.	Etat	Limite élast. MPa	Resist. mécan. MPa	Elongat. rupture %
250°C	Brut	569	591	1,8
	+100 h à 300°C	471	539	7,1
	+ 1 h à 350°C	458	514	8,1
	+ 1 h à 450°C	435	486	5,4
350°C	Brut	480	504	6,6
	+100 h à 300°C	458	509	8,9
	+ 1 h à 350°C	445	487	7,2
	+ 1 h à 450°C	413	464	8,5

Les propriétés les plus élevées sont obtenus pour la température de laminage la plus basse. Dans l'état maintenu ou vieilli, les différences observées sont dues à une modification de la distribution des précipités. Pendant le maintien à 300°C, les précipités très fins métastables  $\text{Al}_3\text{Zr}$  se forment; pendant le maintien à 450°C, les précipités des composés  $\text{Al}_3\text{Zr}$  et  $\text{Al}_{13}\text{Cr}_2$  coalescent [51].

(3) Pour deux tailles de particules de poudre, Al-5,2Cr-1,9Zr-1Mn, [51]

Taille poudre	Etat	Limite élast. MPa	Resist. mécan. MPa	Elongat. rupture %
Poudre<38μm	Brut	523	539	2,5
	+100 h à 300°C	486	536	7,7
	+ 1 h à 350°C	465	508	6,6
	+ 1 h à 450°C	433	481	8,1
Poudre<65μm	Brut	506	532	3,6
	+100 h à 300°C	432	491	6,2
	+ 1 h à 350°C	425	479	8,1

Plus la poudre est fine, plus les propriétés mécaniques sont élevées; ceci est dû à une homogénéité plus grande de la microstructure [51].

La variation de la limite élastique à haute température des alliages Al-Cr-Zr est représentée à la figure 29 et elle est comparée à celle de l'alliage 2219. On note un excès d'environ 140 MPa pour les alliages Al-Cr-Zr dans tout le domaine de température étudié [52].

### 3.4 - ALLIAGES A FAIBLE ENERGIE D'INTERFACE MATRICE-PRECIPITE

Le phénomène de coalescence des précipités est contrôlé en général par la diffusion des atomes de solutés, soit à travers le réseau cristallin de la matrice, soit le long de ses joints de grains. L'accroissement de la taille des précipités obéit à une loi du type:

$$\bar{d}^n \cdot \bar{d}_0^n = K_n \cdot (t - t_0)$$

où  $\bar{d}_0$  et  $\bar{d}$  désignent les valeurs du diamètre moyen des précipités aux instants  $t_0$  et  $t$ ;  $n=3$  pour la diffusion à travers le réseau et  $n=4$  pour la diffusion le long des joints de grains;  $K_n$  est un paramètre caractéristique de la matrice, du soluté et de la nature du précipité. En particulier, pour  $n=3$ ,  $K_n$  est proportionnel à l'énergie d'interface matrice-précipité et, pour  $n=4$ , cette proportionnalité n'est qu'approchée si l'énergie d'interface diffère de celle des joints de grains de la matrice. La coalescence sera donc d'autant plus lente que l'énergie d'interface sera plus faible. En outre cette énergie dépend du degré de cohérence entre le réseau de la matrice et celui du précipité, elle est d'autant plus faible que ce degré est élevé. C'est cette relation de cohérence qui est utilisée dans les superalliages à base nickel pour obtenir un bon comportement mécanique à haute température.

Une étude systématique des composés intermétalliques  $Al_3X$  ( $X=Ti,V,Zr,Hf$ ) a été entreprise [54]. Leur structure cristalline est quadratique  $DO_{22}$  pour les deux premiers et  $DO_{23}$  pour les deux derniers et il existe des relations métriques simples entre les paramètres de ces réseaux quadratiques,  $a$  et  $c$ , et le paramètre du réseau cubique,  $a_0$ , de l'aluminium. Pour les composés de structure  $DO_{22}$  on trouve  $a / (\sqrt{2} \cdot a_0) = 0,9505$  et  $0,9333$  et  $c / (2 \cdot a_0) = 1,0631$  et  $1,0275$ . De même pour les composés de structure  $DO_{23}$  on obtient  $a/a_0 = 0,9910$  et  $0,9851$  et  $c / (4 \cdot a_0) = 1,0693$  et  $1,0591$ . On remarque que tous ces rapports ont des valeurs voisines de l'unité; l'idée de base est alors de combiner les éléments  $X$  dans le même composé et de suivre la variation des longueurs des paramètres  $a$  et  $c$  de façon que les valeurs des rapports définis précédemment se rapprochent de l'unité [55,56,57]. En outre l'addition de zirconium ou de hafnium aux composés  $Al_3Ti$  et  $Al_3V$  fait passer la structure de  $DO_{22}$  à  $DO_{23}$ , cette dernière a un domaine de stabilité beaucoup plus large; on définit alors un paramètre d'écart par:

$$\delta = (2/3) \cdot |1 - a/a_0| + (1/3) \cdot |1 - c/(4 \cdot a_0)|$$

A titre d'exemple on trouve pour ces composés mixtes:

$Al_3Zr$	$\delta = 0,0288$
$Al_3(V_{0,875} Zr_{0,125})$	$\delta = 0,0239$
$Al_3(V_{0,875} Hf_{0,125})$	$\delta = 0,0269$
$Al_3(Ti_{0,875} Zr_{0,109} Hf_{0,016})$	$\delta = 0,0270$

L'alliage  $Al-Zr-V$  correspondant à la plus faible valeur du paramètre d'écart a donné lieu à une étude systématique. Dans une première étape, l'alliage dilué (fraction volumique de précipité égale à 1%) a conduit par solidification rapide à une solution solide sursaturée. Par recuit cette solution solide se décompose en donnant des précipités en forme de sphères et de bâtonnets; en fait cette phase est métastable, elle a une structure cristalline cubique du type L12 et son paramètre diffère de celui de la matrice de  $-0,1 \pm 0,2\%$ ; il y a donc pratiquement cohérence et l'on peut s'attendre à une énergie d'interface faible et par voie de conséquence à une vitesse de coalescence très petite. Le composé intermétallique  $Al_3Zr$  possède également une structure cubique métastable du même type mais avec un paramètre qui diffère de  $1 \pm 0,2\%$ . Le composé  $Al_3(V_{0,875} Zr_{0,125})$  est le plus favorable. Les courbes de la figure 30 montrent la variation du cube du rayon moyen des précipités de différents composés intermétalliques à  $425^\circ C$  en fonction du temps; on note en accord avec les considérations structurales précédentes une très faible vitesse de coalescence pour les composés de structure L12 et plus particulièrement pour  $Al_3(V_{0,875} Zr_{0,125})$  [55].

Si le recuit se poursuit, la phase métastable se transforme en phase stable de structure cristalline quadratique  $DO_{23}$  et les précipités ont la forme de platelets. La vitesse de coalescence de la structure  $DO_{23}$  est 8 fois plus grande que celle de la structure L12 pour la même composition  $Al_3(V_{0,875} Zr_{0,125})$ .

Pour les alliages  $Al-Zr-V$  plus concentrés (fraction volumique de précipités égale à 5%) solidifiés rapidement en rubans ou en paillettes [56,57], on obtient toujours dans l'état brut de trempe une solution solide sursaturée. Au cours du recuit on observe bien la précipitation très fine de la phase métastable L12  $Al_3(Zr,V)$  à l'intérieur des

grains, avec une taille de 5 nm environ, mais on détecte aussi la précipitation de la phase  $\text{DO}_{23}$   $\text{Al}_3(\text{Zr},\text{V})$  et du composé intermétallique  $\text{Al}_{10}\text{V}$  sur les joints de grains. On note par ailleurs une vitesse de coalescence de la phase métastable encore plus faible que dans l'alliage dilué,  $4,7 \cdot 10^{-28} \text{ cm}^3/\text{h}$ , au lieu de  $1,6 \cdot 10^{-26} \text{ cm}^3/\text{h}$ . Ce résultat est inattendu dans la mesure où le coefficient  $K_n$  est proportionnel au carré de la fraction volumique. Il a été suggéré pour expliquer cette anomalie qu'une ségrégation importante de solutés à l'interface matrice-précipité pourrait réduire l'énergie interfaciale et du même coup la vitesse de coalescence, ou encore, que les précipités  $\text{Al}_{10}\text{V}$  placés sur les joints de grains pourraient jouer le rôle de puits pour les solutés et limiter ainsi leur diffusion vers les précipités  $\text{L12}$   $\text{Al}_3(\text{Zr},\text{V})$ . Ces alliages ont une bonne tenue en fluage et ils supportent bien la comparaison avec les alliages Al-Fe-Ce (fig. 31) [58].

Quand on cherche à augmenter la fraction volumique des précipités, jusqu'à 8 %, en utilisant les méthodes classiques de pulvérisation et de trempe sur roue, on ne peut pas éviter la formation des précipités  $\text{Al}_{10}\text{V}$ , à moins d'utiliser des vitesses de solidification très élevées, de  $10^6$  à  $10^7^\circ\text{C/s}$ . Par ailleurs cette vitesse de solidification critique est d'autant plus élevée que la concentration en soluté est plus grande [59]. Il est difficile dans ces conditions d'introduire des fractions volumiques de précipités cohérents aussi importantes que dans le cas des superalliages à base nickel. Des investigations complémentaires sont encore nécessaires pour pousser plus loin l'analogie.

### 3.5 - ALLIAGES A FORTE FRACTION VOLUMIQUE DE PRECIPITES

Quand l'interaction des dislocations mobiles et des dispersoïdes est contrôlée par le mécanisme de contournement d'Orowan, sa contribution à la limite élastique est proportionnelle à la racine cubique de la fraction volumique de ces dispersoïdes; comme ce paramètre est inférieur à l'unité, il peut être effectivement intéressant de chercher à l'augmenter. Pour obtenir une forte fraction volumique il faudra soit augmenter les concentrations des éléments d'alliage, soit retenir des composés intermétalliques dont la composition comporte le plus grand nombre d'atomes d'aluminium par atome d'élément d'addition, par exemple  $\text{Al}_{10}\text{V}$ ,  $\text{Al}_{12}\text{Mo}$ ,  $\text{Al}_{20}\text{Cr}_2\text{Y}$  [60],  $\text{Al}_{20}\text{Cr}_2\text{Ce}$  [61],  $\text{Al}_{12}(\text{Cr},\text{Mn})$  [62],  $\text{Al}_{15}\text{Mn}_3\text{Si}_2$  [60]...

L'étude de l'alliage Al-4,8Si-12,6Mn a montré que la fraction volumique du composé  $\text{Al}_{15}\text{Mn}_3\text{Si}_2$  pouvait aller jusqu'à 34,7%; ce composé est cubique avec un paramètre du réseau égal à 1,265 nm et il appartient au groupe d'espace  $\text{Pm}3$ . L'alliage extrudé a une bonne stabilité thermique jusqu'à  $400^\circ\text{C}$  environ après un maintien de 100 heures (fig. 32) [60]; au delà on note une légère décroissance de la résistance mécanique et surtout une perte presque totale de ductilité. A l'état brut d'extrusion les grains de la matrice ont une taille de l'ordre de 1 à 3  $\mu\text{m}$  et les précipités, de taille de 100 à 500 nm, sont placés sur les joints de grains. Après un maintien de 100 heures à  $490^\circ\text{C}$ , la taille des grains augmente jusqu'à 3-5  $\mu\text{m}$ , de nouveaux précipités, de 50 à 200 nm, apparaissent à l'intérieur des grains et les précipités placés sur les joints grossissent, de 250 à 1000 nm, et forment une structure continue. Jusqu'à  $250^\circ\text{C}$  environ cet alliage a une résistance mécanique comparable à celle des alliages Al-Fe-Ce avec une ductilité raisonnable; à plus forte température la résistance mécanique décroît et l'elongation à la rupture croît fortement; ce comportement est expliqué par une croissance marquée de la taille des grains et de celle des précipités (fig. 33) [60].

La fraction volumique du composé  $\text{Al}_{20}\text{Cr}_2\text{Y}$  dans l'alliage Al-6,8Cr-5,1Y peut atteindre 37,6%. Cet intermétallique est cubique, le paramètre de sa maille est égal à 1,437 nm et il appartient au groupe d'espace  $\text{Fd}3\text{m}$ . Il apparaît souvent avec des fautes planes [60]. Sa stabilité thermique est comparable à celle de l'alliage précédent mais il n'est pratiquement pas ductile (fig. 32). Son grain est un peu plus petit, 1 micron environ, et sa résistance mécanique est légèrement plus élevée; les précipités ont des tailles comparables. La variation de la résistance mécanique en fonction de la température a la même allure et on note à nouveau une forte croissance de l'elongation à la rupture à partir de  $250^\circ\text{C}$  environ (fig. 33).

### 4 - CONCLUSION

L'addition d'éléments des métaux de transition, des terres rares, d'oxygène ou de carbone ouvre de nouveaux domaines d'applications pour les alliages d'aluminium, plus particulièrement par un renforcement de la résistance mécanique à la température ordinaire et par une meilleure tenue à haute température. Cependant ces compositions nécessitent l'utilisation des techniques de la métallurgie des poudres et connaissent de ce fait les difficultés qui leur sont propres quand il faut passer des résultats obtenus en laboratoire à une mise en oeuvre à l'échelle industrielle. Le plein développement de ces alliages nécessite, d'une part, une manipulation très soignée pour que les défauts dans le produit final soient ramenés à un niveau acceptable et, d'autre part, des méthodes de contrôle fiables aux différentes étapes de la production. Il faut aussi considérer le facteur économique et s'assurer que le coût supplémentaire pour améliorer telle ou telle propriété ne conduise pas à un prix prohibitif.

## Références

1. QUIST W.E. and LEWIS R.E., The Need for Rapidly Solidified Powder Metallurgy Aluminum Alloys for Aerospace Applications, *Rapidly Solidified Powder Aluminum Alloys*, ASTM STP 890 Fine M.E. and Starke Jr E.A., Eds., American Society for Testing and Materials, Philadelphia, 1986, 7.
2. FRAZIER W.E., PM Al Alloys: Hot Prospects for Aerospace Applications, *Advanced Materials and Processes*, 133, (1988), 42.
3. FROES F.H., KIM Y-W. and KRISHNAMURTHY S., Rapid Solidification of Lightweight Metal Alloys, *Mat. Sci. Eng.*, A117, (1989), 19.
4. FROES F.H. and PICKENS J.R., Powder Metallurgy of Light Metal Alloys for Demanding applications, *J. Metals*, 36, (January 1984), 14.
5. HILDEMAN G.J., LABARRE L.C., HAFEEZ A. and ANGERS L.M., Microstructural, Mechanical Property and Corrosion Evaluations of 7xxx P/M alloy CW67, *High Strength Powder Aluminum Alloys II*, Hildeman G.J. and Koczak M.J., Eds., The Metallurgical Society of AIME, Toronto, 1986, 25.
6. BOHLEN J.W., KAR R.J. and CHANANI G.R., A Comparative Evaluation of Aluminum Alloy Powders Used for Fabricating High-Strength Powder Metallurgy Extrusions, *Rapidly Solidified Powder Aluminum Alloys*, ASTM STP 890, M.E. Fine and Starke Jr E.A., Eds., American Society for Testing and Materials, Philadelphia, 1986, 166.
7. PEASE L.F. and POTTER V.C., Mechanical Properties of P/M Materials, *Powder Metallurgy, Metals Handbook*, Vol. 7, American Society for Metals, 1984, 463.
8. PICKENS J.R., GORDON J.R. and CHRISTOLOUDOU L., Stress-Corrosion Cracking and Hydrogen Embrittlement in P/M X7091 and I/M 7075, *High-Strength Powder Metallurgy Aluminum Alloys*, M.J. Koczak and G.J. Hildeman, Eds., The Metallurgical Society of AIME, Dallas, 1982, 177.
9. SUMMERSON T.J. and SPROWLS D.O., Corrosion Behavior of Aluminum Alloys, *Aluminum Alloys - Physical and Mechanical Properties*, E.A. Starke Jr and T.H. Sanders Jr, Eds., Emas, Charlottesville, 1986, 1576.
10. WEBER J.H. and SCHELLENG R.D., Mechanical Alloying of Dispersion Strengthened Aluminum: A Retrospective Review, *Dispersion Strengthened Aluminum Alloys*, Kim Y-W. and Griffith W.M., Eds., The Minerals, Metals & Materials Society, 1988, 467.
11. BENN R.C. and MIRCHANDANI P.K., Dispersion Strengthening by Mechanical Alloying, *New Materials by Mechanical Alloying*, Arzt E. and Schultz L., Eds., Deutsche Gesellschaft für Metallkunde, 1989, 19.
12. ARNHOLD V. and HUMMERT K., Properties and Applications of Dispersion Strengthened Aluminum Alloys, *New Materials by Mechanical Alloying*, Arzt E. and Schultz L., Eds., Deutsche Gesellschaft für Metallkunde, 1989, 263.
13. SINGER R.F., OLIVER W.C. and NIX W.D., Identification of Dispersoid Phases Created in Aluminum During Mechanical Alloying, *Metall. Trans.*, 11A, (1980), 1895.
14. HAWK J.A., RUCH W. and WILSDORF H.G.F., Microstructure and Fracture Analysis of Oxide and Carbide Strengthened Mechanically Alloyed Aluminum Alloys, *Dispersion Strengthened Aluminum Alloys*, Kim Y-W. and Griffith W.M., Eds., The Minerals, Metals & Materials Society, 1988, 603.
15. HAWK J.A., MIRCHANDANI P.K., BENN R.C. and WILSDORF H.G.F., Evaluation of the Elevated Temperature Strength and Microstructural Stability of Dispersion Strengthened MA Aluminum Alloys, *Dispersion Strengthened Aluminum Alloys*, Kim Y-W. and Griffith W.M., Eds., The Minerals, Metals & Materials Society, 1988, 517.
16. HAWK J.A. and WILSDORF H.G.F., Tensile Strength of MA Aluminum Alloys After Prolonged Elevated Temperature Exposure, *Scripta Metall.*, 22, (1988), 561.
17. BROCKMANN G.J. und BAUMGARTEN J., Pulvermetallurgische Herstellung von hochtemperaturfesten Aluminiumwerkstoffen, *Aluminium*, 65, (1989), 393.
18. INCO ALLOYS INTERNATIONAL, IncoMAP alloy Al-9052, Publication No IAI-34, 1987.
19. JONES H., Observations on a Structural Transition in Aluminum Alloys Hardened by Rapid Solidification, *Mat. Sci. Eng.*, 5, (1969/70), 1.
20. GRIFFITH W.M., SANDERS, Jr R.E. and HILDEMAN G.J., Elevated Temperature Aluminum Alloys for Aerospace, *High-Strength Powder Metallurgy Aluminum Alloys*, M.J. Koczak and G.J. Hildeman, Eds., The Metallurgical Society of AIME, Dallas, 1982, 209.
21. KIM Y-W., Processing/Microstructure/Properties of Al-Fe-Ge Powder Alloys, *Dispersion Strengthened Aluminum Alloys*, Kim Y-W. and Griffith W.M., Eds., The Minerals, Metals & Materials Society, 1988, 517.

22. RAGHAVAN AYER, ANGERS L.M., MUELLER R.R., SCANLON J.C. and KLEIN C.F., Microstructural Characterization of the Dispersed Phases in Al-Fe-Ce System, *Metall. Trans.*, 19A, (1988), 1645.
23. YANEY D.L. and NIX W.D., Elevated Temperature Deformation Behavior of an Al-8.4wtPctFe-3.6wtPctCe Alloy, *Metall. Trans.*, 18A, (1987), 893.
24. ANGERS L., FINE M.E. and WEERTMAN J.R., Effect of Plastic Deformation on the Coarsening of Dispersoids in a Rapidly Solidified Al-Fe-Ce Alloy, *Metall. Trans.*, 18A, (1987), 555.
25. KIM Y-W. and GRIFFITH W.M., Annealing Behavior and Tensile Properties of Elevated-Temperature PM Aluminum Alloys, *Rapidly Solidified Powder Aluminum Alloys*, ASTM STP 890, Fine M.E. and Starke Jr E.A. Eds., American Society for Testing and Materials, Philadelphia, 1986, 485.
26. SMITH H.H., MICHEL D.J. and REED J.R., Fatigue Crack Growth in Rapidly Solidified Aluminum alloys at 25 and 300°C, *Metall. Trans.*, 20A, (1989), 2425.
27. LANGENBECK S.L., GRIFFITH W.M., HILDEMAN G.J. and SIMON J.M., Development of Dispersion-Strengthened Aluminum Alloys, *Rapidly Solidified Powder Aluminum Alloys*, ASTM STP 890, Fine M.E. and Starke Jr E.A., Fds., American Society for Testing and Materials, Philadelphia, 1986, 410.
28. LANGENBECK S.L., COX J.M. and SIMENZ R.F., Characterization of Al-Fe-Ce Alloys, *Rapidly Solidified Powder Aluminum Alloys*, ASTM STP 890, Fine M.E. and Starke Jr E.A., Eds., American Society for Testing and Materials, Philadelphia, 1986, 450.
29. RAINEN R.A. and EKVALL J.C., Elevated Temperature Al Alloys for Aircraft Structure, *J. Metals.*, 40, (May 1988), 16.
30. LEGZDINA D. and PARTHASARATHY T.A., Deformation Mechanism of Rapidly Solidified Al-8.8Fe-3.7Ce Alloy, *Metall. Trans.*, 18A, (1987), 1713.
31. EZZ S.S., LAWLEY A. and KOCZAK M.J., Dispersion Strengthened Al-Fe-Ce: a Dual Rapid Solidification/Mechanical Alloying Approach, *Dispersion Strengthened Aluminum Alloys*, Kim Y-W. and Griffith W.M., Eds., The Minerals, Metals & Materials Society, 1988, 243.
32. YANEY D.L., OVECOGLU M.L. and NIX W.D., The Effect of Mechanical Alloying on the Deformation Behavior of a Rapidly Solidified Al-Fe-Ce Alloy, *Dispersion Strengthened Aluminum Alloys*, Kim Y-W. and Griffith W.M., Eds., The Minerals, Metals & Materials Society, 1988, 619.
33. OVECOGLU M.L. and NIX W.D., Elevated Temperature Characterization and Deformation of Mechanically Alloyed Rapidly Solidified Al-8.4wt%Fe-3.5wt%Ce Alloy, *New Materials by Mechanical Alloying*, Arzt E. and Schultz L., Eds., Deutsche Gesellschaft für Metallkunde, 1989, 287.
34. SKINNER D.J., BYE R.L., RAYBOULD D., BROWN A.M. and ZEDALIS M.S., Dispersion Strengthened Al-Fe-Si Alloys Containing V, Mn, Cr or Mo, *Processing of Structural Metals by Rapid Solidification*, Froes F.H. and Savage S.J., Eds., ASM International, Orlando, 1986, 291.
35. SKINNER D.J., BYE R.L., RAYBOULD D. and BROWN A.M., Dispersion Strengthened Al-Fe-V-Si Alloys, *Scripta Metall.* 20, (1986), 867.
36. GILMAN P.S. and DAS S.K., Rapidly Solidified Aluminum Alloys for High Temperature/High Stiffness Applications, *Int. Conf. PM Aerospace Materials*, Metal Powder Report, (1897), p 27-1.
37. SKINNER D.J., The Physical Metallurgy of Dispersion Strengthened Al-Fe-V-Si alloys, *Dispersion Strengthened Aluminum Alloys*, Kim Y-W. and Griffith W.M., Eds., The Minerals, Metals & Materials Society, 1988, 181.
38. GUYOT P. and AUDIER M., A quasicrystal Structure Model for Al-Mn, *Phil. Mag.*, 52B, (1985), L15.
39. ZEDALIS M., RAYBOULD D., SKINNER D.J. and DAS S.K., Microstructure/Tensile Property Relationship in Elevated Temperature RS Al-Fe-V-Si Rolled Sheet, *Processing of Structural Metals by Rapid Solidification*, Froes F.H. and Savage S.J., Eds., ASM International, Orlando, 1986, 347.
40. DAS S.K., Rapid Solidification and Powder Metallurgy at Allied Signal Inc. *Int. J. powder Metallurgy*, 24, (1988), 175.
41. FRANCK R.E. and HAWK J.A., Effect of Very High Temperatures on the Mechanical Properties of Al-Fe-V-Si Alloy, *Scripta Metall.*, 23, (1989), 113.

42. SKINNER D.J., ZEDALIS M.S. and PELTIER J., Anomalous Ductility Variation at Intermediate Temperatures in Rapidly Solidified Al-Base Alloys, *Dispersion Strengthened Aluminum Alloys*, Kim Y-W. and Griffith W.M., Eds., The Minerals, Metals & Materials Society, 1988, 71.
43. SKINNER D.J., ZEDALIS M.S. and GILMAN P.S., Effect of Strain Rate on Tensile Ductility for a Series of Dispersion-Strengthened Aluminum-Based Alloys, *Mat. Sci. Eng.*, All9, (1989), 81.
44. PHARR G.M., ZEDALIS M.S., SKINNER D.J. and GILMAN P.S., High Temperature Creep Deformation of a Rapid Solidified Al-Fe-V-Si Alloy, *Dispersion Strengthened Aluminum Alloys*, Kim Y-W. and Griffith W.M., Eds., The Minerals, Metals & Materials Society, 1988, 309.
45. BROWN A.M., SKINNER D.J., RAYBOULD D., DAS S.K., BYE R.L. and ADAM C.M., Crack Growth and Fracture Properties of Rapidly Solidified Al-Fe-V-Si Alloys, *Aluminum Alloys-Physical and Mechanical Properties*, E.A. Starke Jr and T.H. Sanders Jr, Eds., Emas, Charlottesville, 1986, 1029.
46. MIDSON S.P., BUCKLEY R.A. and JONES H., Aging Behaviour of Aluminium-Rich Al-Cr-Zr Alloy Solid Solutions Extended by Rapid Solidification, *Rapidly Quenched Metals*, Steeb S. and Warlimont H., Eds., Elsevier Science Publishers, Würzburg, 1985, 923.
47. TSAKIROPOULOS P., PRATT R.C., JONES H., RESTALL J.E. and GARDINER R.W., Development of Al-Cr-X and Al-Cr-Zr-X Alloys Rapidly Solidified from the melt, *Sixth Int. Conf. Rapidly Quenched Metals*, *Mat. Sci. Eng.*, 98, (1988), 143.
48. HUGHES I.R., MARSHALL G.J. and MILLER W.S., Production and Processing of Rapidly Solidified Aluminium Alloys, *Rapidly Quenched Metals*, Steeb S. and Warlimont H., Eds., Elsevier Science Publishers, Würzburg, 1985, 1743.
49. MARSHALL G.J., HUGUES I.R. and MILLER W.S., Effect of Consolidation Route on Structure and Property Control in Rapidly Solidified Al-Cr-Zr-Mn Powder Alloy for High Temperature Service, *Mat. Sci. Tech.*, 2, (1986), 394.
50. TANAGUCHI Y., FURUSHIRO N., TAI H. and HORI S., Precipitation Behavior During Aging in a Rapidly Solidified Al-1.8Cr-1.7Zr Alloy, *J. Japan Inst. Light Metals*, 37, (1987), 300.
51. MILLER W.S., HUGUES I.R., PALMER I.G., THOMAS M.P., SAINI T.S. and WHITE J., Production and Properties of Rapidly Solidified Aluminium-Chromium-Zirconium Alloys, *High Strength Powder Aluminum Alloys II*, Hildeman G.J. and Koczak M.J., Eds., The Metalurgical Society of AIME, Toronto, 1986, 311.
52. PALMER I.G., THOMAS M.P. and MARSHALL G.J., Development of Thermally Stable Al-Cr-Zr Alloys Using Rapid Solidification Technology, *Dispersion Strengthened Aluminum Alloys*, Kim Y-W. and Griffith W.M., Eds., The Minerals, Metals & Materials Society, 1988, 217.
53. OCTOR H. and NAKA S., Early Stage of  $\text{Al}_3\text{Zr}$  Precipitation in a Rapidly Solidified Al-Cr-Zr Alloy, *Phil. Mag.* 59, (1989), 229.
54. ZEDALIS M. and FINE M.E., Lattice Parameter Variation of Al (Ti,V,Zr,Hf) in Al-2at% (Ti,V,Zr,Hf) alloys, *Scripta Metall.*, 17, (1983), 1251.
55. ANGERS L., CHEN Y., FINE M.E., WEERTMAN J.R. and ZEDALIS M.S., Rational Design of High Temperature Alloys, *Aluminum Alloys - Physical and Mechanical Properties*, E.A. Starke Jr and T.H. Sanders Jr, Eds., Emas, Charlottesville, 1986, 321.
56. ZEDALIS M.S. and FINE M.E., Precipitation and Ostwald Ripening in Dilute Al Base-Zr-V Alloys, *Metall. Trans.*, 17A, (1986), 2187.
57. FINE M.E., Stability and Coarsening of Dispersoids in Aluminum Alloys, *Dispersion Strengthened Aluminum Alloys*, Kim Y-W. and Griffith W.M., Eds., The Minerals, Metals & Materials Society, 1988, 103.
58. CHEN Y.C., FINE M.E., WEERTMAN J.R. and LEWIS R.E., Coarsening behavior of L12 Structured  $\text{Al}_3(\text{Zr}_{1-x})$  Precipitates in Rapidly Solidified Al-Zr-V Alloy, *Scripta Metall.*, 21, (1987), 1003.
59. YANEY D.L., LEWIS R.E. and NIEH T.G., Microstructural Characterization of Rapidly Solidified Al-Zr-V Alloys, *Dispersion Strengthened Aluminum Alloys*, Kim Y-W. and Griffith W.M., Eds., The Minerals, Metals & Materials Society, 1988, 59.
60. HAWK J.A., ANGERS L.M. and WILSDORF H.G.F., High Volume Fraction P/M Aluminum Alloys - Stability and Strength at Elevated Temperatures, *Dispersion Strengthened Aluminum Alloys*, Kim Y-W. and Griffith W.M., Eds., The Minerals, Metals & Materials Society, 1988, 339.

61. FERNANDEZ RIVERA C., ARCADE P. and CHAMPIER G., Microstructure and Mechanical Properties of Al-3Cr-1Ce (at%) Alloy, *Int. Conf. Advanced Aluminium and Magnesium Alloys*, ASM Europe, Amsterdam, 20-22 June 1990, (sous presse).
62. ZAIDI A., ARCADE P. and CHAMPIER G., Mechanical Behaviour of Rapidly Solidified Al-3Cr-xMn (at%) Alloys, *Int. Conf. Advanced Aluminium and Magnesium Alloys*, ASM Europe, Amsterdam, 20-22 June 1990, (sous presse).

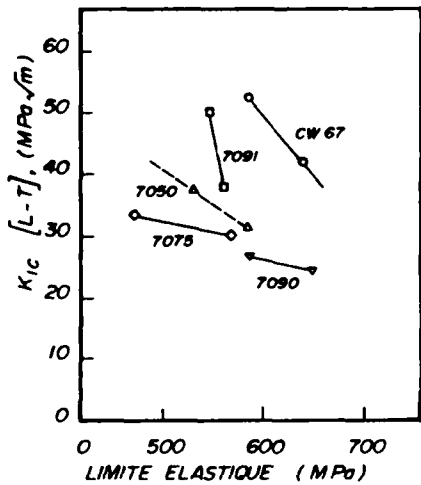


Fig. 1. Comparaison des combinaisons limite élastique-ténacité pour les alliages solidifiés rapidement (7090, 7091 et CW67) et les alliages conventionnels (7050 et 7075) [5].

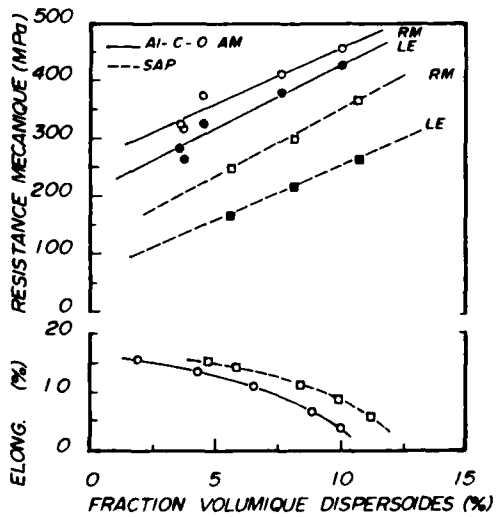


Fig. 2. Variations de la limite élastique, de la résistance mécanique et de l'élongation à la rupture en fonction de la fraction volumique des dispersoides dans l'alliage Al-C-O allié mécaniquement; comparaison avec l'alliage SAP[10].

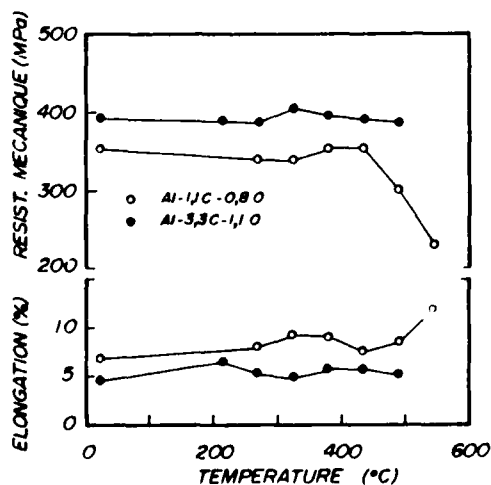


Fig. 3. Variations de la résistance mécanique et de l'élongation à la rupture mesurées à la température ordinaire des alliages Al-1.1C-0.8O et Al-3.3C-1.1O après un maintien de 100 heures à haute température [15].

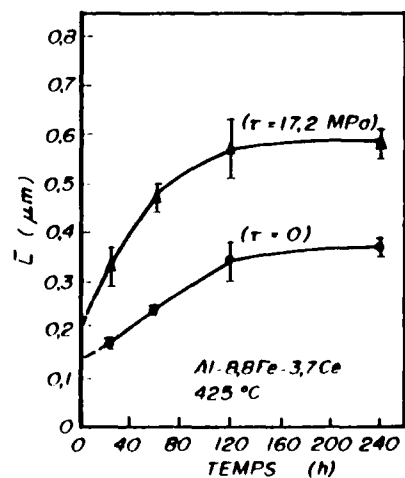


Fig. 5. Variation de la taille moyenne des précipités dans l'alliage Al-8.8Fe-3.7Ce pendant un maintien isotherme à 425°C sous une contrainte nulle et sous une contrainte de 17.2 MPa [24].

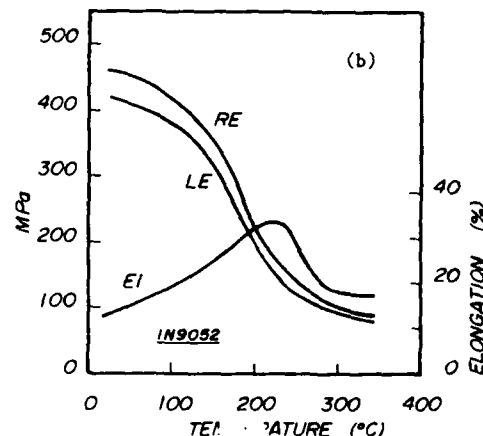
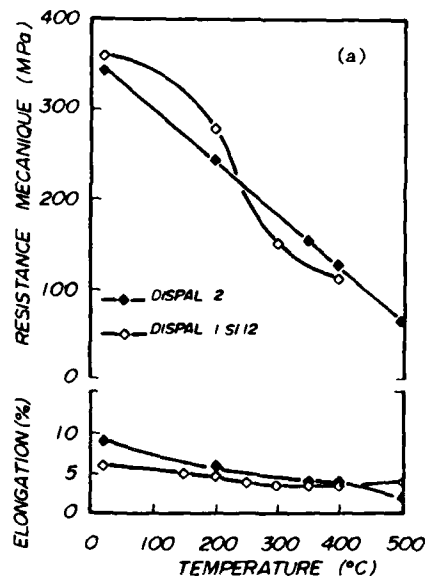


Fig. 4. Variations de la limite élastique, de la résistance mécanique et de l'elongation à la rupture (a) des alliages DISPAL 2 et DISPAL 1S112 [12] et (b) de l'alliage IN9052 [18].

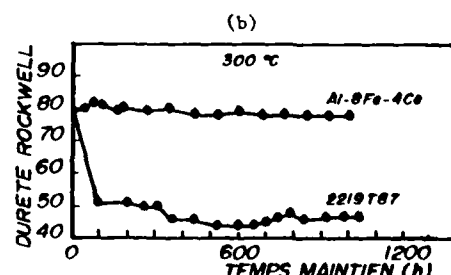
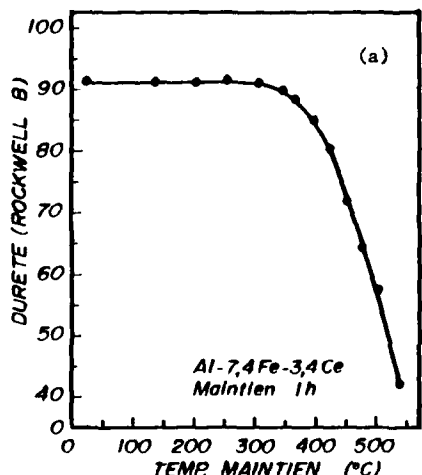


Fig. 6. Variation de la dureté mesurée à la température ordinaire (a) de l'alliage Al-7,4Fe-3,4Ce après un maintien de 1h à haute température [25], (b) de l'alliage Al-8Fe-4Ce après un maintien à 300°C; comparaison avec l'alliage conventionnel 2219-T87 [26].

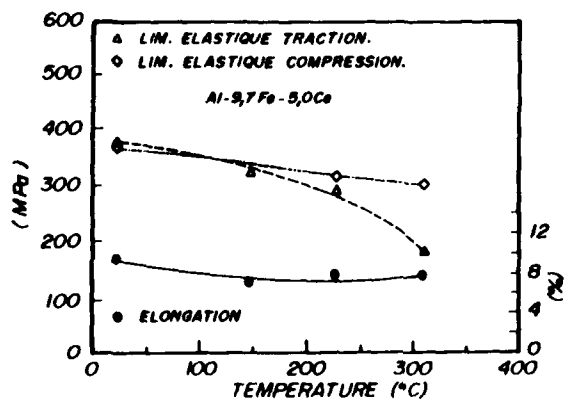


Fig. 7. Variations des limites élastiques en traction et en compression de l'alliage Al-9,7Fe-5,0Ce mesurées à la température ordinaire après un maintien de 1000 h à 149 et 232°C et de 100 h à 316°C [27,28].

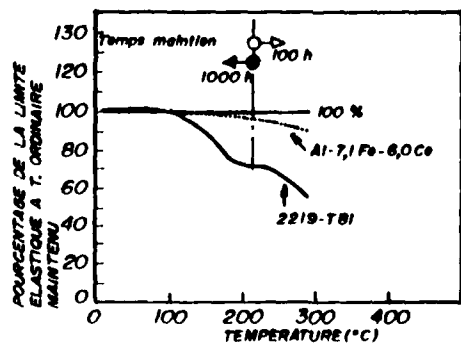


Fig. 8. Effet d'un maintien à haute température sur la limite élastique mesurée à la température ordinaire de l'alliage Al-7,1Fe-6,0Ce et de l'alliage conventionnel 2219-T81 [29].

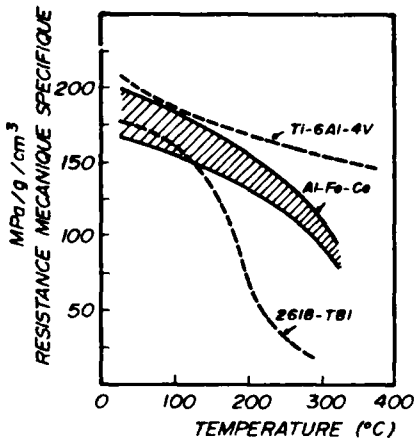


Fig. 9. Variation de la résistance mécanique spécifique en fonction de la température pour les alliages Al-Fe-Ce, l'alliage conventionnel 2618-T81 et l'alliage Ti-6Al-4V [21].

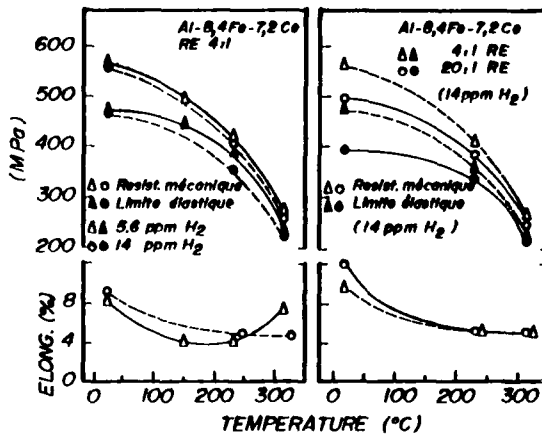


Fig. 10. Variations de la limite élastique, de la résistance mécanique et de l'élongation à la rupture en fonction de la température de l'alliage Al-8,4Fe-7,2Ce; (a) influence de la teneur en hydrogène; (b) influence du rapport d'extrusion [21].

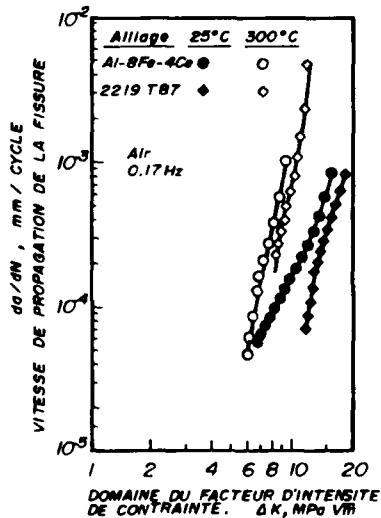


Fig. 11. Comparaison de la propagation de la fissure en fatigue de l'alliage Al-8Fe-4Ce et de l'alliage conventionnel 2219-T87 à 25 et 300°C [26].

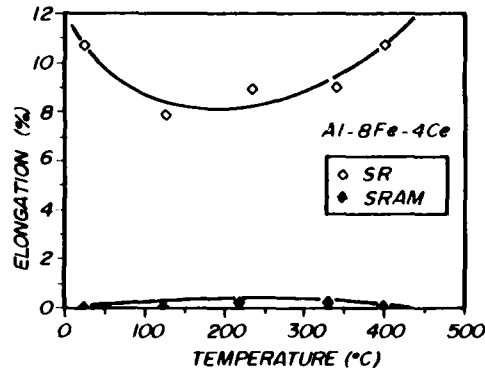


Fig. 13. Variation de l'élongation à la rupture de l'alliage Al-8Fe-4Ce solidifié rapidement (SR) puis allié mécaniquement (SRAM) en fonction de la température [31].

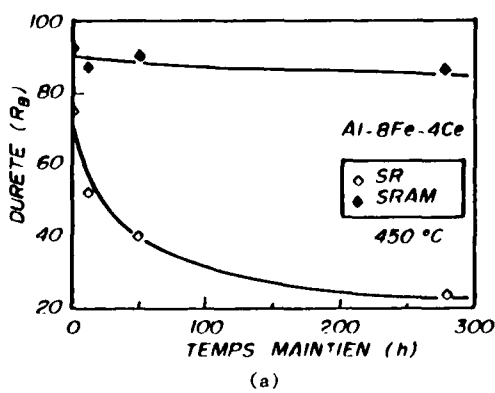
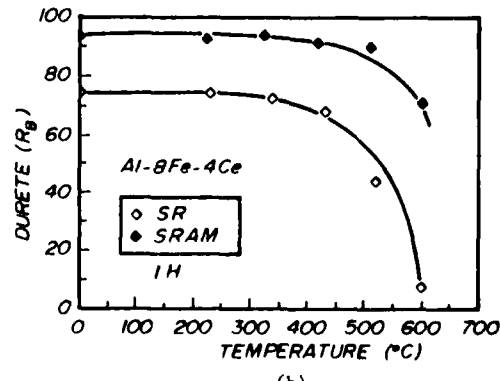


Fig. 12. Stabilité thermique de l'alliage Al-8Fe-4Ce solidifié rapidement (SR) puis allié mécaniquement (SRAM); variation de la dureté après un maintien : (a) à 450°C pendant un temps variable; (b) pendant une heure à différentes températures [31].



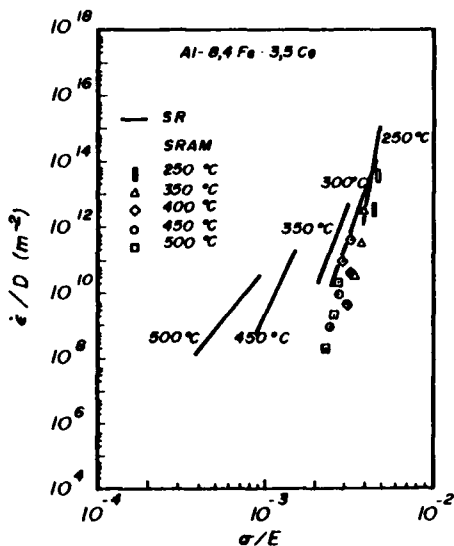


Fig. 14. Essai de compression à haute température de l'alliage Al-8,4Fe-3,5Ce solidifié rapidement (SR) puis allié mécaniquement (SRAM): vitesse de déformation rapportée au coefficient d'autodiffusion de l'aluminium en fonction de la valeur de la contrainte appliquée rapportée au module d'Young [33].

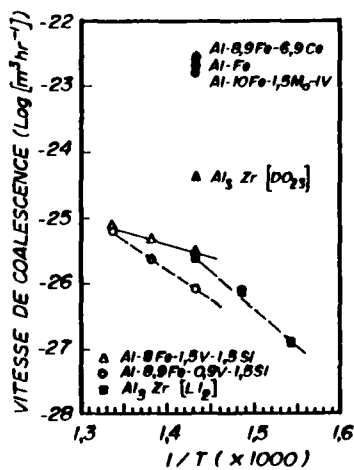


Fig. 15. Vitesse de coalescence des précipités des alliages Al-Fe-V-Si en fonction de la température; comparaison avec les précipités des alliages Al-Fe-X et avec Al<sub>3</sub>Zr pour ses deux structures D<sub>23</sub> et L<sub>12</sub> [37]

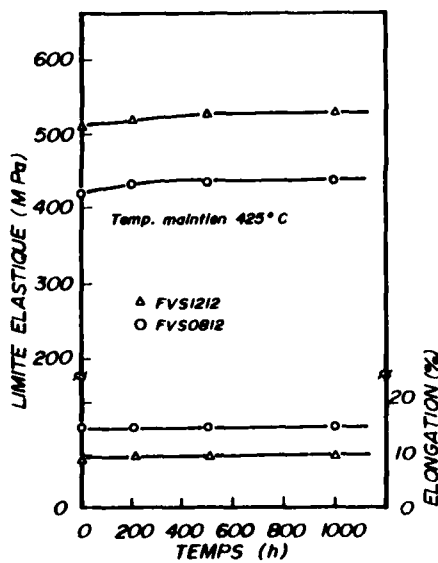


Fig. 16. Variations de la limite élastique et de l'élongation à la rupture des alliages Al-Fe-V-Si mesurée à la température ordinaire après un maintien à 524°C [36].

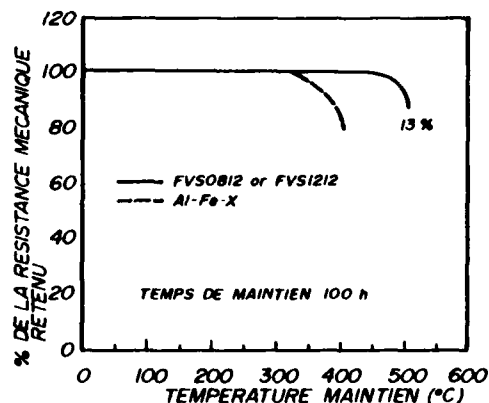


Fig. 17. Pourcentage retenu de la résistance mécanique des alliages Al-Fe-V-Si mesurée à la température ordinaire après un maintien de 100 heures à haute température; comparaison avec les alliages Al-Fe-X [36].

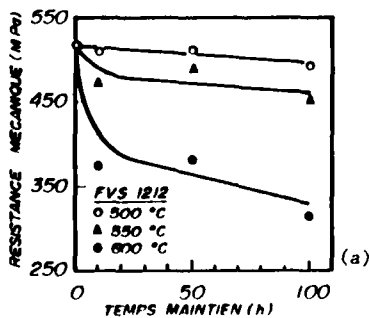
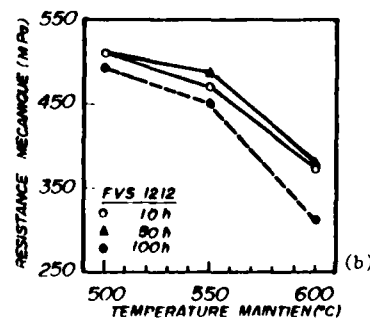
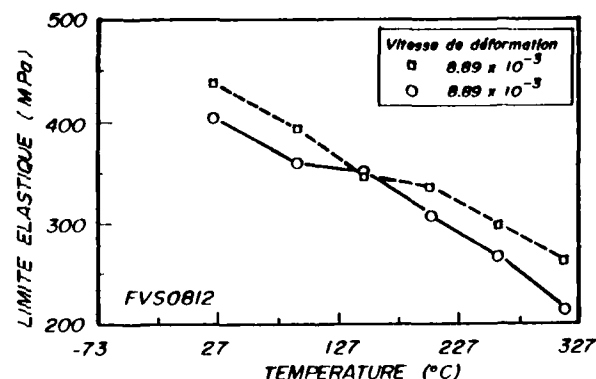
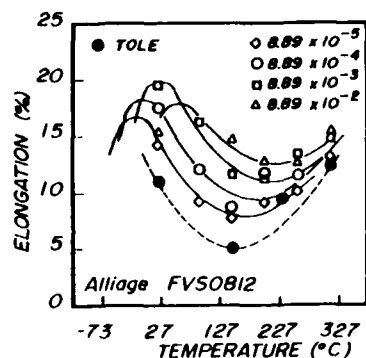


Fig. 18. Variation de la résistance mécanique de l'alliage Al-Fe-V-Si FVS1212 mesurée à la température ordinaire après un maintien (a) à 500, 550 et 600°C en fonction du temps, (b) de 10, 50 et 100 heures aux mêmes températures [41].





(a)



(b)

fig. 20. Variation (a) de la limite élastique et (b) de l'élongation à la rupture de l'alliage Al-Fe-V-Si FVS0812 en fonction de la température pour différentes vitesses de déformation [42,43].

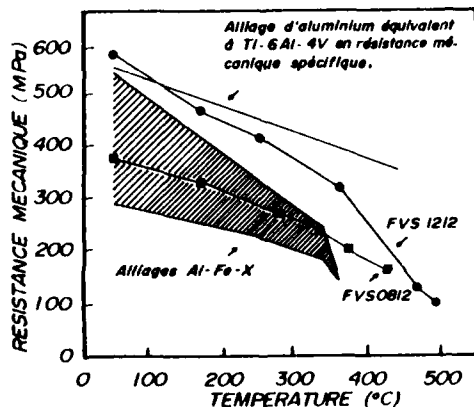


Fig. 19. Variations de la limite élastique des alliages Al-Fe-V-Si, FVS0812 et FVS1212, en fonction de la température; comparaison avec les alliages Al-Fe-X et l'alliage hypothétique d'aluminium qui aurait la même limite élastique spécifique que l'alliage Ti-6Al-4V [36].

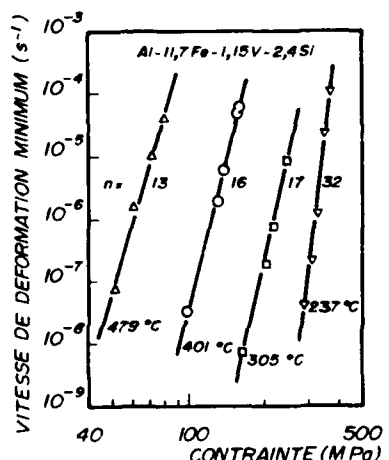


Fig. 21. Variation de la vitesse de déformation en fluage en fonction de la contrainte appliquée pour différentes valeurs de la température, alliage Al-11,7Fe-1,15V-2,4Si [44].

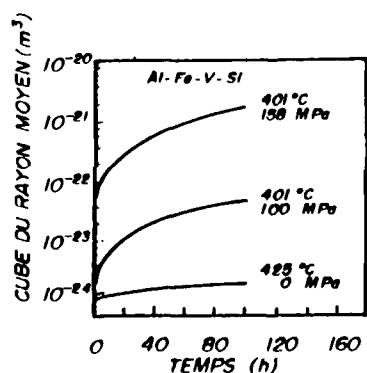
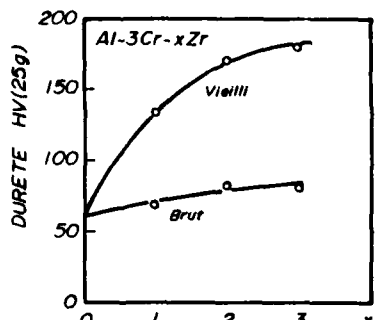
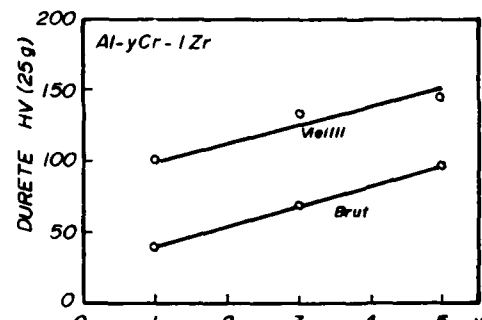


Fig. 22. Variation du volume des précipités des alliages Al-Fe-V-Si, FVS0812 et FVS1212, en fonction du temps; influence d'une contrainte appliquée [44].



(a)



(b)

fig. 23. Variation de la dureté (a) d'un alliage Al-3Cr-xZr en fonction de x et (b) d'un alliage Al-yCr-1Zr en fonction de y, d'une part à l'état brut de solidification rapide et d'autre part après vieillissement au maximum de la dureté [48,49].

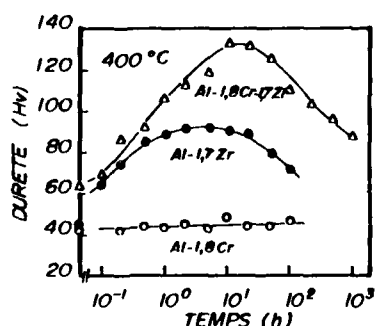


Fig. 24. Variation de la dureté des alliages Al-1.8Cr, Al-1.7Zr et Al-1.8Cr-1.7Zr au cours du vieillissement à 400°C [50].

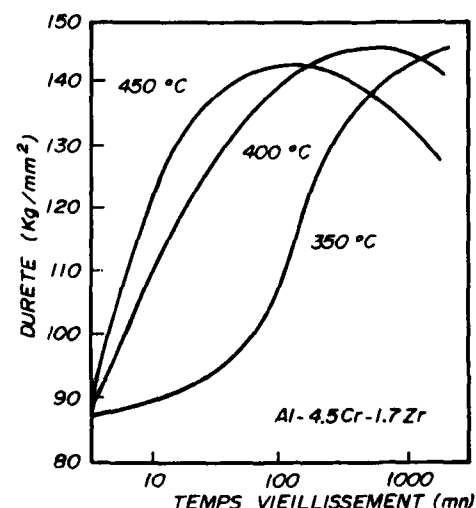


Fig. 25. Variation de la dureté de l'alliage Al-4.5Cr-1.7Zr au cours du vieillissement à 350, 400 et 450°C [49,51,52].

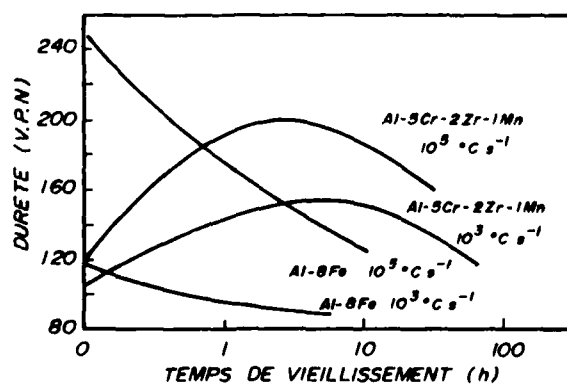


Fig. 26. Comparaison des valeurs obtenues pour la dureté des alliages Al-8Fe et Al-5Cr-2Zr-1Mn, solidifiés rapidement avec les vitesses de 10<sup>5</sup> et 10<sup>3</sup> °C/s, après un vieillissement à 400°C [52].

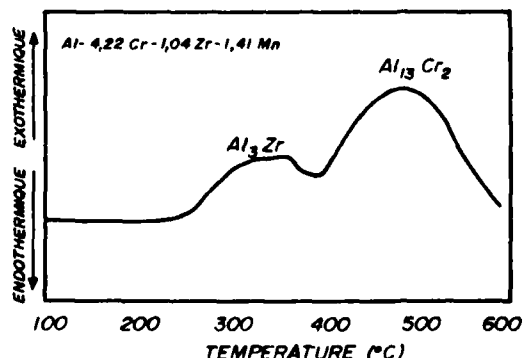


Fig. 27. Enregistrement de calorimétrie différentielle montrant la décomposition de la microstructure de la poudre d'alliage Al-4.22Cr-1.04Zr-1.41Mn [49].

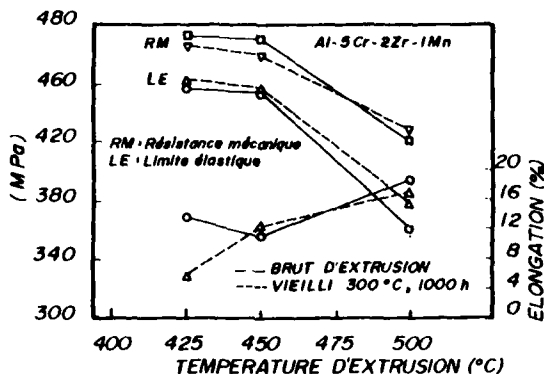


Fig. 28. Influence de la température d'extrusion et du vieillissement de 1000h à 300°C sur les propriétés mécaniques de l'alliage Al-5Cr-2Zr-1Mn pour un temps de préchauffage de 45 minutes [52].

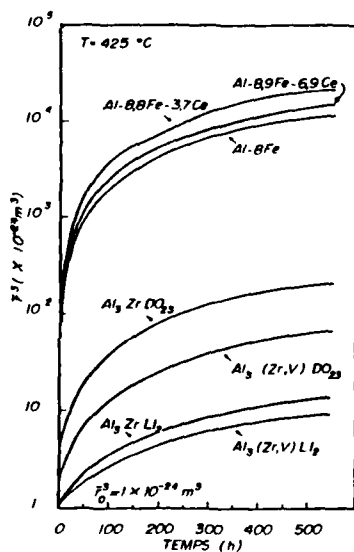


Fig. 30. Comparaison de l'accroissement de volume des précipités de différents alliages en fonction du temps de maintien à 425°C; influence de la composition et de la structure cristalline de ces précipités [55].

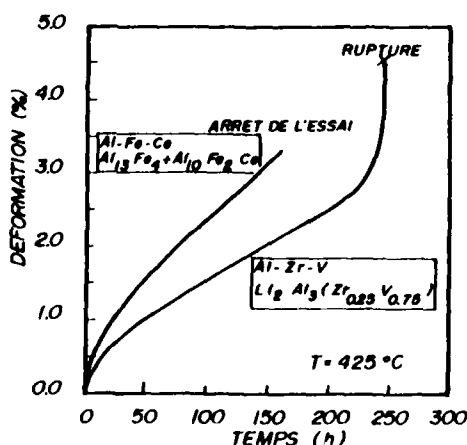


Fig. 31. Comparaison de la déformation en fluge des alliages Al-Fe-Ce et Al-Zr-V [57].

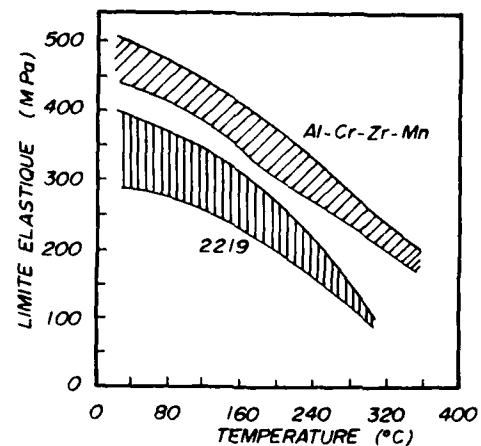


Fig. 29. Limite élastique de l'alliage Al-5,2Cr-1,9Zr-1Mn à haute température comparée à celle de l'alliage 2219 [52].

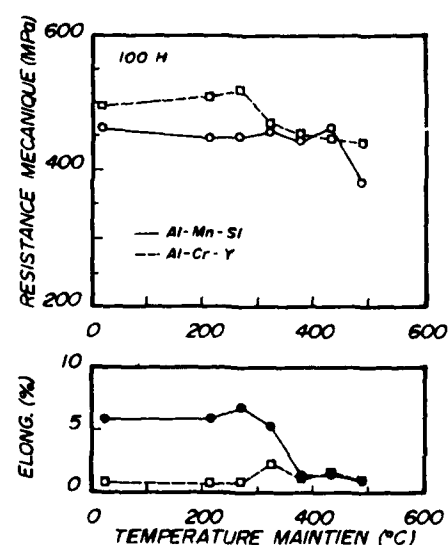


Fig. 32. Variations de la résistance mécanique et de l'élongation à la rupture des alliages Al-4,8Si-12,6Mn et Al-6,8Cr-5,1Y mesurées à la température ordinaire après un maintien de 100 heures à haute température [60].

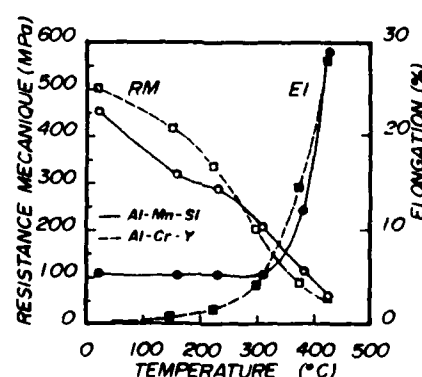


Fig. 33. Variations de la résistance mécanique et de l'élongation à la rupture des alliages Al-4,8Si-12,6Mn et Al-6,8Cr-5,1Y en fonction de la température [60].

## CAST AND RAPIDLY SOLIDIFIED MAGNESIUM ALLOYS

by  
 D J Bray  
 Materials and Structures Department  
 Royal Aerospace Establishment  
 Farnborough  
 Hampshire GU14 6TD UK

## SUMMARY

Recent developments in magnesium alloy technology will be described. The majority of applications for magnesium alloys in the aerospace industry are in castings. A range of yttrium containing alloys has been introduced for high temperature applications, and the corrosion resistance of Mg-Al-Zn cast alloys has been improved by increasing the alloy purity. Fluxless melting, to reduce the number of inclusions, is now common, and low pressure casting permits more complex, thin walled components to be made. For gearbox casings, a polyimide coating has been developed which resists attack by lubricating oils up to 225°C. Further development of magnesium alloys by ingot metallurgy is limited by the structure of the phase diagram of many magnesium alloy systems. To overcome these restrictions, attention is now turning to the rapid solidification of magnesium alloys and progress in this field will be reviewed.

## 1 INTRODUCTION

The principal attraction of magnesium alloys for aerospace applications is their low density. This can range from about 1.5 gcm<sup>-3</sup> for magnesium-lithium alloys to about 1.8 gcm<sup>-3</sup> for magnesium-rare earth alloys; ie approximately two thirds those of aluminium alloys. Despite these low values, the use of magnesium alloys is restricted by shortcomings in other properties, particularly in corrosion resistance, but also in mechanical properties and formability.

In Fig 1, the specific yield and tensile strengths of some wrought magnesium and aluminium alloys are compared. ZK60, AZ80 and ZCM711 are the highest strength commercial wrought magnesium alloys, but their tensile strengths are significantly lower than those of high strength aluminium alloys. Consequently, the advantage of a low density is somewhat reduced and the specific strengths of the magnesium alloys are no better than those of the aluminium alloys. Under a compressive load, the density advantage of magnesium alloys is reduced further because their compressive yield strengths are usually lower than their tensile yield strengths. In Fig 2, specific stiffnesses are compared. The magnesium alloys are equivalent to the aluminium-zinc alloy, 7075, but inferior to the aluminium-lithium alloy, 8090. However, where buckling resistance is required at low to moderate loads,  $E^{1/3}/\rho$  is the design criterion, E being the Young's modulus and  $\rho$  the density. A low density becomes the more dominant factor and on this criterion the magnesium alloys are superior to the aluminium alloys (Fig 3). Furthermore, in a component where minimum gauge is the design criterion, the least weight is achieved by using the lowest density material and here again magnesium alloys are more competitive.<sup>2</sup>

In the 1950s and 1960s these benefits were exploited to a greater extent than they are today. For example, magnesium alloy thin sheet was used for fuselage and wing skins, and extrusions were used for cabin floors and missile bodies.<sup>3,4</sup> However in many cases, severe corrosion problems were encountered and the use of wrought magnesium alloys was discontinued in favour of the steadily improving high strength aluminium alloys. In addition, the costs of wrought magnesium alloys are higher than for aluminium alloys. This is partly because the raw material is more expensive, but also because production costs are higher; for example, slower extrusion speeds must be used with magnesium alloys to prevent hot shortness.<sup>5</sup> Today practically all the applications for magnesium alloys in aerospace are in castings, typically in helicopter gearbox cases and cockpit canopy frames.<sup>6</sup>

The inherent corrosion resistance of magnesium alloys is poor in comparison with aluminium alloys.<sup>7</sup> Corrosion rates of commercial alloys measured by weight loss experiments can be several hundred times greater than those of aluminium alloys (Fig 4). In water, the naturally forming oxide film on the surface of magnesium converts to magnesium hydroxide ( $Mg(OH)_2$ ). This provides only limited protection. Unlike the alumina film on aluminium, the magnesium hydroxide film cracks and curls away from the surface. It is also slightly soluble in water and is attacked more rapidly in industrial and salt water environments. Furthermore, the large negative electrode potentials of magnesium alloys make them susceptible to galvanic corrosion when they are in contact with a more noble metal in the presence of an electrolyte.<sup>7,8</sup> Iron, copper and nickel alloys cause the most severe galvanic attack (Table I) while that caused by aluminium alloys depends on their composition. Those containing copper have the worst effect, but pure aluminium is almost compatible with magnesium. In practice, most corrosion problems associated with magnesium alloys in aircraft structures stem from joints to other metals. For example, when magnesium alloy skin was used, galvanic corrosion commonly occurred around the aluminium rivets which had to be used because magnesium rivets do not have sufficient formability.<sup>7</sup> To some extent, galvanic

corrosion can be overcome by careful design of joints to avoid water entrapment and by use of wet assembly techniques and sealing compounds.<sup>9</sup> Protective coatings have also been developed for magnesium alloys in aerospace applications,<sup>10</sup> but even when these are applied, concern over corrosion resistance results in the alloys being used only where they can be easily inspected.

The purpose of this paper is to review recent developments in magnesium alloy technology which have relevance to current or potential aerospace applications. Since cast alloys make up the bulk of current usage, developments in this field will be considered first. The latter part of the paper will describe progress in the field of rapidly solidified magnesium alloys, through which improvements in mechanical properties, corrosion resistance and formability are being sought to make magnesium alloys more competitive with other materials.

## 2 CAST ALLOYS

### 2.1 Alloy developments

The cast alloys which are currently used can be divided into two groups.<sup>11,12</sup> Firstly, there are the Mg-Al-Zn alloys, the most well known of which is AZ91 (9%Al-1%Zn). Secondly, and more widely used, are those which contain rare earth (RE) elements and are grain refined with zirconium, for example ZE41 (4%Zn-1%RE). Alloys in the first group are less expensive, but are more difficult to cast and are prone to stress corrosion cracking. Those in the second group have better casting qualities; a low melting point eutectic at the grain boundaries suppresses porosity, making it easier to obtain pressure tight castings than in Mg-Al-Zn alloys. Table II shows the tensile properties of some cast magnesium alloys. The Mg-Al-Zn alloys are limited to applications at less than 120°C, but alloys in the second group are able to operate at higher temperature. For example, the widely used alloy ZE41 is a medium strength alloy which retains its properties up to about 150°C. QE22 and EQ21 are high strength alloys containing silver which are used in applications up to 200°C.

The most recent development in the Mg-Al-Zn alloys, pioneered by the Dow Chemical Co. and AMAX Magnesium,<sup>13,14</sup> has been the trend towards high purity alloys. Standard purity alloys contain small, but significant amounts of metallic impurities. The levels of iron, copper and nickel are particularly important. These elements have low solid solubilities in magnesium, their electrode potentials are much more positive than that of magnesium (Table I) and they have low hydrogen overvoltages. When magnesium alloys corrode, the cathodic part of the process is the evolution of hydrogen. These elements form particles which are active sites for the cathodic reaction, thus increasing the general corrosion rate. The iron content can be partially controlled by the addition of manganese which helps iron particles to settle during melting and surrounds those which remain during solidification.<sup>15</sup> A more effective procedure is to reduce the total impurity content, which decreases the number of particles and leads to a reduction in the corrosion rate. This phenomenon was recognised in the 1950s,<sup>16</sup> but it is only in the last few years that high purity alloys have been produced on a commercial basis.

Work at the Dow Chemical Company defined the tolerance level of each element. The compositions of the standard AZ91C alloy and the high purity version, AZ91E, are compared in Table III. Typical corrosion rates are reported to be about 10 mpy (mils per year = thousandths of an inch per year) or 0.25mm/year. This is about a hundred times lower than that of the standard alloy (Fig 5). These improvements have been reported in gravity and pressure die castings.<sup>17</sup> Further reductions in corrosion rate to about 3 mpy (0.08mm/year) have been reported by increasing the purity of the basic AZ91 alloy still further.<sup>18</sup> These low values are comparable to the corrosion rates of some aluminium alloys, but it must be recognised that increasing the purity of the alloy does not make it less susceptible to galvanic corrosion. This inevitably restricts the number of applications where advantage can be taken of these improvements.

In the second group of alloys, that is those containing rare earth elements and grain refined with zirconium,<sup>11,12</sup> developments have been aimed at improving room and elevated temperature strength as well as corrosion resistance. Unlike the Mg-Al-Zn alloys, the corrosion rates of these alloys cannot be reduced to very low levels by increasing the alloy purity, for, even in the absence of iron, copper and nickel particles, deliberate alloying additions such as zirconium and silver will provide sites for the cathodic reaction. Corrosion resistance must therefore be improved through the addition of suitable alloying elements. The high strength alloys containing silver are used up to about 200°C. Alloys containing thorium, for example HZ32, can operate above 300°C, but their strengths are lower. Because thorium is a health hazard and necessitates precautions being taken when handling it, Mg-Th alloys are being phased out.<sup>5</sup>

The most recent alloys in the second group are those from the Mg-Y-Nd system which have been developed by Magnesium Elektron Ltd. Pure yttrium is expensive so the element is added as a lower grade material also containing 20-25% heavy rare earth (RE) elements.<sup>5</sup> The first alloy to be developed was WE54,<sup>19,20</sup> containing 5.0-5.5%Y, 1.5-2.0%Nd and 1.5-2.0% RE. When solution treated and aged, the following precipitation sequence was identified.<sup>20</sup> A  $\beta''$  precipitate formed at about 175°C, transforming to the  $\beta'$  phase at 200°C. This phase in turn converted to the equilibrium  $\beta$  phase above about 300°C. WE54 was aged at 250°C to encourage formation of the  $\beta'$  precipitate.<sup>5</sup> Improvements in yield strength, tensile strength (Fig 6) and thermal stability were achieved over the silver containing alloys. However, when the long term thermal stability was evaluated between 100 and 200°C, although tensile strength was unaffected,

there was a significant drop in the ductility after 1000-2000 hours, due to the formation of the metastable and embrittling  $\beta''$  precipitate. To overcome this problem the yttrium and neodymium contents were reduced, giving rise to the alloy WE43 which contains 3.75-4.25%Y, 2.0-2.5%Nd, 0.75-1.25%RE and 0.3%Zr.<sup>5</sup> Although this resulted in some loss of strength, the typical ductility of WE43 in the as-cast state is higher than that of WE54 and the reduction in room temperature ductility after long periods at elevated temperature at 150°C is not as great. The room temperature strength of WE43 is similar to that of the silver containing alloys (Fig 6), but WE43 is thermally more stable (Fig 7) and has improved creep properties (Fig 8).

Yttrium has a second beneficial effect in that it reduces the corrosion rate of the alloy. In weight loss tests, the corrosion rates of WE54 and WE43 were reported to be similar to those of the high purity AZ91 alloys (Fig 9). However, like the high purity alloys, the yttrium containing alloys are still susceptible to galvanic corrosion.

## 2.2 Developments in casting techniques

As well as alloy developments, foundry techniques have been refined to improve the properties of castings, to reduce the variability in properties and to make more complex components. The technique of fluxless melting is now widespread. It has been used in the die casting of magnesium for some time, but its use in sand casting where metal temperatures are higher is more recent. Instead of using a flux based on alkali and alkaline earth halides, a protective atmosphere of air, argon or carbon dioxide containing 0.5-2% sulphur hexafluoride is used to inhibit the oxidation of magnesium up to about 800°C. Melting losses are reduced and, in combination with filter systems, the use of fluxless melting reduces the number of inclusions trapped in the metal. Inclusions are frequently the sites of corrosion, so a reduction in their number leads directly to an improvement in the overall corrosion resistance.<sup>11</sup>

The use of cold setting, resin bonded sands for moulds and cores has allowed castings of more complex shape to be made. The finish on the cast surface and dimensional accuracy are improved.<sup>11</sup> Wall thicknesses of 3.5mm and casting tolerances of  $\pm 0.5\text{mm}$  are achievable, and passageways of at least 2mm diameter can be incorporated.<sup>21</sup> However, even thinner walls may be cast in aluminium alloys,<sup>22</sup> and so, despite their lower density, magnesium alloys may not always be competitive if sufficiently thin walls cannot be achieved. Therefore, methods for casting under low pressure, which have been used with aluminium alloys, are also being developed for magnesium alloys. The technique has been used for casting magnesium in permanent moulds, but is now being considered for sand casting because of improvements in mould and core making. The process is shown schematically in Fig 10. Either a positive pressure is applied to the crucible or the mould is evacuated. Under the low pressure difference created, the flow of metal into the mould can be controlled more easily than in gravity feeding giving more reproducible castings with microstructures and properties more consistent across different sections. Running and gating systems can be made simpler so there is less turbulence and thinner walled castings can be produced.

## 2.3 Protective coatings

Developments in coatings for magnesium alloys are as important as the alloys themselves because of their chemical reactivity. For airframe components the basic coating remains the chromate conversion coating sealed with epoxy resin. In the United Kingdom, the rules governing the protection of magnesium alloys are given in Specification DTD 911C.<sup>23</sup> A casting is first cleaned by fluoride anodising to remove contamination caused by abrasive blasting, etc. The fluoride film which remains is a poor base for subsequent coatings and is removed in chromic acid. A chromate conversion coating is then applied to provide a key for a layer of epoxy resin which is applied to seal the surface prior to painting. For very aggressive environments a hard anodising treatment is used to provide a thick, abrasion resistant coating. The coating itself is porous, giving insufficient corrosion resistance, and is therefore sealed with resin.

A new protective coating, based on a hard anodising treatment, has been developed for aeroengine gearbox cases. The use of magnesium alloys in this application is restricted to engines where the operating temperature of the lubricating oil is less than about 160°C. Above this temperature, chemical breakdown of the oil to a mixture of organic acids causes corrosive attack of the chromate based coating on magnesium alloys. A new system has been developed jointly by Rolls-Royce Ltd and Magnesium Elektron Ltd under a contract sponsored by the Corrosion Section at RAE Farnborough. This provides improved protection for magnesium alloys in systems where the oil temperature is greater than 200°C.<sup>24</sup>

Early investigation showed that a resin sealed Dow 17 hard anodised coating<sup>25</sup> was more resistant than a resin sealed, chromate pretreatment. Therefore a selection of epoxy, phenolic and polyimide resins were applied to test-pieces which had been given a Dow 17 pretreatment and each coating system was evaluated in static and dynamic oil immersion tests to discover which system gave the best protection. The corrosion rate was monitored by measuring the magnesium content of the oil. After 300 hours at 170°C, the standard coating of a chromate treatment sealed with an epoxy resin had broken down, whereas all the systems based on a Dow 17 pretreatment were unaffected.

At 225°C in the static oil immersion tests, the Dow 17/epoxy coating was satisfactory up to 200 hours, but after 300 hours the coating was damaged at the edge

of the test-piece. The Dow 17/ polyimide coating showed no visible signs of breakdown, although there was a slight increase in the magnesium content of the oil after 300 hours (Fig 11). In the dynamic oil immersion tests at 225°C, the conventional chromate/epoxy coating blistered after 50 hours, but the systems based on the Dow 17 pretreatment showed little change after 150 hours. After 250 hours, the phenolic resin coating blistered, followed by the epoxy system at 300 hours. The polyimide system showed no visible signs of attack after 350 hours.

The polyimide sealed Dow 17 coating may therefore be considered for future gearbox applications. The throwing power of the anodic pretreatment is such that satisfactory coatings can be produced over complex castings with internal passageways. Promising results were also obtained when the protective system was evaluated in high temperature salt spray corrosion tests, indicating that it may have potential applications in high temperature environments other than gearboxes.

### 3 RAPIDLY SOLIDIFIED MAGNESIUM ALLOYS

#### 3.1 Introduction

Further development of magnesium alloys by ingot metallurgy is limited by the structure of the equilibrium phase diagram of many magnesium alloy systems. The maximum solid solubility of the alloying element in magnesium is often low (Table IV). This can be explained in terms of the Hume-Rothery rules.<sup>26-28</sup> In some cases the diameters of the solute and magnesium atoms differ by more than 15%, which does not favour extended solid solubility. Also, magnesium is a very electropositive atom and when alloyed with elements which tend to complete their electron octet, such as silicon, compound formation is preferred. Finally, magnesium uses sp hybrid orbitals in its bonding. Consequently, it tends not to bond with elements which employ a large proportion of d-bonding, for example, mid-row transition elements.

These restrictions can only operate completely when an alloy is cooled slowly from the melt, as happens in a large ingot. To partly overcome them, and extend the scope for alloy development, interest is therefore increasing in the rapid solidification (RS) of magnesium alloys.<sup>29-33</sup> The advantages to be gained have been well documented.<sup>34</sup> Equilibrium microstructures predicted by phase diagrams can be avoided, solid solubilities of elements can be extended and new metastable structures can be produced. More uniform and refined microstructures can be achieved with smaller grain sizes and finer distributions of intermetallics. In comparison with aluminium alloys, the rapid solidification of magnesium alloys has received less attention, but some promising results have been achieved. A large fraction of the reported data has been on constitutional changes and on the formation of metallic glasses,<sup>35</sup> but the intention here is to concentrate on examples where engineering properties have been measured.

Magnesium powder alloys were first produced in the early 1950s using gas atomisation,<sup>36</sup> but the great interest in rapid solidification which followed the work of Duwez et al<sup>37</sup> in the 1960s left magnesium alloys somewhat neglected. In the last decade interest has been revived and other rapid solidification techniques have been used, including twin roller quenching, melt spinning and planar flow casting. The extent to which microstructures can be refined increases with increasing cooling rate. Those achievable by atomisation are up to  $10^5$  Ks<sup>-1</sup> and those from chill methods such as melt spinning are up to  $10^{10}$  Ks<sup>-1</sup>. An inert gas atmosphere is necessary to minimise oxidation of the powder particles or ribbon during solidification because of the reactivity of magnesium alloys. An additional problem with magnesium is its high vapour pressure, which can result in metal losses from the melt whilst achieving the required superheat if the liquidus temperature is high or if the dissolution rate of the element in magnesium is low. In gas atomisation, control of powder particle size is difficult because metal droplets are drawn out into ligaments which separate into a series of large and small particles.<sup>38,39</sup> The fraction of very fine particles which is generated can be highly flammable and difficult to handle. Liquid dynamic compaction has also been used to produce rapidly solidified (RS) magnesium alloys.<sup>40</sup> The cooling rates are about  $10^3$  Ks<sup>-1</sup>, so the degree of microstructural refinement is less than that achieved by other methods, but the need to handle powder is avoided. Consolidation of powder or ribbon is done preferably by extrusion to create the shear forces necessary to break up the oxide layer around each particle and promote metal to metal bonding. The usual extrusion temperatures for conventional magnesium alloys are in the range 300–450°C to make deformation easier, but RS alloys are usually extruded at less than 250°C to retain their metastable microstructures.

In the more advanced field of RS aluminium alloys, degassing prior to extrusion is considered necessary to ensure a fully dense product.<sup>41</sup> If the powder or ribbon is not degassed sufficiently then moisture or hydrogen released during heat treatment can cause blistering, and the pores so produced decrease the fracture toughness and the ductility. In the exploratory work on RS magnesium alloys described in this paper inclusion of a degassing step is not always reported. Joshi et al<sup>42</sup> investigated the degassing of Mg-Al-Zn-rare earth alloy ribbon and detected gaseous emissions at about 218°C and 305°C. The former was caused by the evolution of H<sub>2</sub>O, CO and CO<sub>2</sub> and the latter by the evolution of hydrocarbons. Nussbaum et al<sup>43</sup> studied the effect of degassing on RS AZ91 alloy ribbons. H<sub>2</sub>O was released between 250 and 350°C, and CO<sub>2</sub> and H<sub>2</sub> above 300°C. The ribbons were therefore extruded at 250°C or 350°C. Degassing was found to reduce the tensile properties in the longitudinal direction, but there was no evidence that it was a necessary step. However, it was noted that its effect on compressive strength and transverse properties needed to be investigated.

### 3.2 Improvements in mechanical properties

The limitations in the mechanical properties of magnesium alloys and the way rapid solidification is being used to extend them will now be considered. One of the main objectives is to increase the strengths of magnesium alloys. Several magnesium alloy systems can be age hardened,<sup>44</sup> for example, Mg-Zn, Mg-Al and Mg-Ag, but the response is significantly less than in aluminium alloys. Using rapid solidification the solid solubilities of elements in magnesium can be extended so that greater volume fractions of known precipitates may be obtained or completely new age hardening systems may be investigated. Furthermore, the grain sizes of RS alloys are smaller than those of ingot metallurgy alloys and therefore increased yield strengths may be expected because of the Hall-Petch effect.

The mechanical working of magnesium alloys is difficult because of the limited number of slip systems available in the hexagonal crystal structure.<sup>27</sup> At room temperature the only slip systems which can operate are the three in the basal plane in the  $\langle 11\bar{2}0 \rangle$  directions. Consequently, considerable stresses develop at boundaries between grains which are unfavourably orientated for slip and adjacent grains in which slip can occur more easily. This causes cracking. Twinning can also take place on the  $\{10\bar{1}2\}$  pyramidal planes. When stresses are parallel to the basal plane twinning occurs only in compression, and when stresses are perpendicular to the basal plane it occurs only in tension.<sup>45</sup> Extrusion and rolling of magnesium alloys at relatively low temperatures aligns the basal plane parallel to the extrusion direction or the rolling direction respectively. Since twinning occurs readily when compressive stresses are parallel to the basal plane, wrought magnesium alloys usually have a lower proof strength in compression than in tension. The ratio can be between 0.5 and 0.7, but increases with increasing temperature, because above about 225°C, additional slip systems begin to operate on the  $\{10\bar{1}1\}$  pyramidal planes, making twinning less important and deformation easier.

The reduction in grain size from using rapid solidification can therefore have two further beneficial effects on mechanical properties. Firstly, twinning becomes more difficult as the grain size decreases so that the ratio of compressive to tensile proof strength increases. Secondly, the stresses between grains of different orientation are less, thus reducing the risk of cracking during mechanical working. Another route being followed is to produce extended solid solutions containing elements which decrease the axial ratio of magnesium's hexagonal lattice. This makes slip on the  $\{10\bar{1}1\} \langle 11\bar{2}0 \rangle$  system easier and mechanical working is improved.<sup>30</sup>

Some experimental results can now be considered, beginning with those where commercially available alloys were rapidly solidified. Busk and Leontis<sup>36</sup> were the first to recognise the benefits of a refined microstructure on the mechanical properties of magnesium alloys. The grain size, dendrite size and scale of coring of an AZ31 alloy (3%Al-1%Zn) were much finer in gas atomised powder than in the equivalent cast billets, and the properties of the resulting extrusions were at least as good as, and usually better than, those of extruded cast billets (Fig 12). The most significant property improvement was in compressive yield strength, presumably because the smaller grain size made twinning more difficult.

Isserow and Rizzitano<sup>46</sup> produced powder of the commercial alloy ZK60A using the rotating electrode process. ZK60A contains nominally 6%Zn and 0.5%Zr and is one of the strongest conventional wrought magnesium alloys. The powder was extruded at room temperature, 65°C and 120°C using an extrusion ratio of 10:1. One of the best combinations of strength and ductility was obtained using an extrusion temperature of 65°C, followed by a heat treatment of 24 hours at 120°C. The tensile 0.2% proof stress was 40% higher, and the UTS 20% higher than the values for the conventionally cast and extruded alloy (Fig 13). The higher strength of the extruded powder was attributed principally to the very fine, elongated grains, about 1μm in diameter, and also to a fine distribution of Mg-Zn intermetallics and increased effectiveness of cold working. Results from Charpy impact tests were approximately three times higher than for the commercial alloy which was explained by an erratic crack path across the fibrous grain structure. The fracture surfaces of the tensile test pieces were also fibrous and Flemings and Mortensen<sup>47</sup> noted from this that the transverse properties of the alloy may have been poor. They therefore produced melt spun ribbon of the same ZK60A alloy and showed that the amount of shear taking place with an extrusion ratio of 10:1 was insufficient to fully consolidate the ribbon. However, using an extrusion ratio of 30:1 and extrusion temperature of 210°C, consolidation was improved and the fibrous fracture was replaced by a more ductile one. The tensile properties were again better than those of conventionally processed ZK60A alloy (Fig 13). The yield and tensile strengths were somewhat lower than those obtained by Isserow and Rizzitano,<sup>46</sup> but the elongation was higher; a yield stress of 365MPa, a UTS of 388MPa and an elongation of 19.6% were reported.

More recently Nussbaum et al<sup>43,48</sup> have investigated the effects of rapid solidification on the commercially available high purity version of AZ91 alloy. Ribbon was made by melt spinning, then cold compacted and extruded in the temperature range 200-350°C at extrusion ratios of between 12:1 and 30:1 and at ram speeds of 0.5-3mm s<sup>-1</sup>. The grains in the extruded specimens were about 1μm in diameter compared to 30μm in conventionally processed material, and equiaxed, showing that recrystallisation had occurred. Grain size increased with increasing extrusion temperature and extrusion speed. The highest strengths were reported for samples extruded at 0.5mm s<sup>-1</sup> and 200°C, using an extrusion ratio of 20:1. The tensile yield strength was 416MPa, the

UTS 486MPa and the total elongation 6% (Fig 14). The yield strength was 50% higher than that of the conventionally processed alloy A280 and moreover, the compressive and tensile yield strengths of the fine grained extruded RS alloys were equal. They considered the strengthening mechanisms in the alloy - solid solution strengthening, dispersion strengthening and grain size strengthening - and concluded that the reduction in grain size alone could account for the difference. The Hall-Petch coefficient for the alloy was estimated to be 210MPa  $\mu\text{m}$ . They noted that this was somewhat lower than values reported for conventional magnesium alloys (280-320MPa  $\mu\text{m}$ ), but nevertheless much higher than that for aluminium 68MPa  $\mu\text{m}$ ). This demonstrated the sensitivity to grain size of the yield strength of a hexagonal metal such as magnesium in comparison to a face centred cubic metal such as aluminium. Refinement of grain size by RS is applicable to both, but the effect is much greater in magnesium.

Alloys whose compositions lie outside the range of those of conventional ingot metallurgy have also been investigated by RS processing. Meschter<sup>49</sup> examined the properties of Mg-10%Al and Mg-12.5%Al-1.5%Si alloys made by twin roller quenching, followed by extrusion at 230-250°C. These alloys contained a greater percentage of aluminium than is normally present in cast alloys and the aim was to achieve a higher volume fraction of Mg<sub>17</sub>Al<sub>12</sub> strengthening precipitate. The grain size of the RS Mg-10%Al alloy was 7 to 10 times smaller than in extrusions of conventionally cast Mg-9%Al alloys, and that of the Mg-12.5%Al-1.5%Si alloy was further reduced by a factor of 4.6, because grain boundaries were pinned by Mg<sub>2</sub>Si dispersoids, impeding grain growth during extrusion and heat treatment. The Mg-10%Al alloys were solution treated and aged with and without a prior 2% stretch. In slowly cooled alloys precipitation of Mg<sub>17</sub>Al<sub>12</sub> is usually continuous, but the small grain size in the RS Mg-10%Al alloy caused almost complete discontinuous precipitation to form a lamellar structure. A 2% stretch prior to aging resulted in an increase in the volume fraction of continuous precipitate with a consequent increase in yield strength. For example, following a 2% stretch and aging for 64 hours at 140°C, a yield stress of 351MPa, a UTS of 430MPa and an elongation of 3.8% were achieved (Fig 14). A higher yield strength was measured for the finer grained Mg-12.5%Al-1.5%Si alloy, but the elongation was reduced to 1.4%.

Perhaps one of the most attractive alloying additions to magnesium is lithium. Not only does it reduce the density, but also by the addition of 11wt% lithium, the hexagonal crystal structure of magnesium is changed to a single phase, body centred cubic structure which is more ductile and easier to form. In the 1950s, magnesium-lithium alloys were thought to have considerable potential for aerospace applications, but this potential has never been realised. High strength Mg-Li alloys containing additions of Zn, Al, Cd or Ag were developed with 0.2% proof stresses of approximately 300MPa. However, these strong alloys overaged readily above about 65°C and were susceptible to creep when stressed at relatively low levels at room temperature and they had poor corrosion resistance.<sup>3</sup> The problems of overaging could not be overcome in the high strength alloys and the commercially available alloys developed, eg LA141, were of relatively low strength. The grain size of these alloys is quite large and Meschter and O'Neal<sup>50</sup> used rapid solidification by twin roller quenching to refine the grain size. A Mg-9%Li alloy was used with the addition of approximately 1% Ce or Si. These elements have low solid solubilities in magnesium and they form a fine dispersoid to stabilise the grain size. Mg-9%Li is a two phase  $\alpha/\beta$  alloy and the  $\alpha$  plate thickness and plate spacing were 10-30 times smaller than those in conventionally processed alloys. After 2 hours at 300°C, the  $\alpha/\beta$  microstructure of the RS Mg-Li flakes had coarsened slightly, that of the Mg-Li-Ce flakes had coarsened extensively, while that of the Mg-Li-Si flakes was unaffected. The combination of microstructural refinement and dispersion strengthening in the extruded Mg-Li-Si flake resulted in a yield strength 60% higher than that in a conventionally cast and extruded Mg-9%Li billet. Grensing and Fraser<sup>51</sup> examined the possibility of adding greater amounts of silicon to Mg-Li alloys to produce a metastable supersaturation of silicon which could be heat treated to form a fine dispersion of Mg<sub>2</sub>Si particles. However, the microstructure of a melt spun binary Mg-2.75%Si alloy was a coupled eutectic and the ribbons were very brittle.

The RS magnesium alloys which have received the most attention are the Mg-Al-Zn-Rare Earth alloys developed by Chang et al<sup>52,53</sup> at Allied Signal Inc. Initially, a series of Mg-Al-Zn-RE, Mg-Al-Zn-RE-Mn and Mg-Al-Zn-Si-Mn alloys were produced by planar flow casting and melt spinning, and extruded using an extrusion ratio of 18:1. The grain size of the as-spun ribbon in the Mg-Al-Zn-RE alloys was 0.36-0.7 $\mu\text{m}$  diameter and fine dispersoids, 0.04-0.07 $\mu\text{m}$  in diameter, were present. In the alloys containing Ce, Nd and Pr, the dispersoids were Mg<sub>3</sub>Ce, Mg<sub>3</sub>Nd and Mg<sub>3</sub>Pr respectively, whilst in the alloys containing yttrium the dispersoids were Mg<sub>17</sub>Y<sub>3</sub>. These dispersoids pinned the grain boundaries during subsequent consolidation. High yield strengths and tensile strengths were reported and two compositions were selected for further development because of their good combination of mechanical properties and corrosion resistance. The first contains 5%Al, 5%Zn and 4.9%Nd and is designated EA55RS, and the second contains 5%Al, 5%Zn and 5.9%Y and is designated EA65RS.<sup>54</sup> EA65RS is the stronger of the two alloys, but EA55RS is the more ductile (Fig 15). In common with other RS magnesium alloys the compressive yield strength is similar to the tensile yield strength because of the very small grain size. Fracture toughness results have also been reported for these alloys. In the as-extruded condition the values are low; that of EA55 is about 15MPa  $\sqrt{\text{m}}$ , but it has been increased to 17MPa  $\sqrt{\text{m}}$  by a T4 heat treatment, with an accompanying decrease in strength.<sup>55</sup> The low fracture toughness in the as-extruded condition is attributed to brittle particles which are aligned along

the extrusion direction. Some of these brittle particles are dissolved during heat treatment to improve the fracture toughness.

Joshi et al<sup>42,56</sup> produced a range of complex alloys containing Al, Li, Mn, Zn, Ce and Y. The melt spun ribbon of each alloy was cold pressed, hot pressed, then extruded between 250 and 350°C using an extrusion ratio of 20:1. An alloy containing 10.2%Al, 2.7%Mn, 3.2%Zn and 5.8%Ce had a yield strength of 431MPa, an ultimate tensile strength of 468MPa, a Young's modulus of 42.7GPa and an elongation to fracture of 14.9% (Fig 15). Once again the compressive yield strength was similar to the tensile yield strength because of the small grain size. An alloy containing 6.8%Al, 3.4%Li, 0.41%Li, 2.57%Zn and 3.55%Ce had a lower density, but the yield strength and ultimate tensile strength were also lower such that the specific properties were not as good as those of the first alloy.

Inevitably, the majority of results reported above are for tensile properties for these are usually the first to be obtained in any exploratory work. A systematic study of the effect of alloying additions on the Young's modulus of RS magnesium alloys has not been carried out. Theoretical calculations indicate that Al, Y, Mn, Ni and Fe should not significantly affect the specific modulus while Zn, Ca and Ce should reduce it slightly.<sup>31</sup> Only Si and Be are calculated to increase it, but RS Mg-Si alloys containing 3%Si are brittle and Be is only slightly soluble in molten magnesium. Whether improvements in mechanical properties alone would be acceptable for aircraft structures is questionable, for the greatest resistance to the use of magnesium alloys arises from their poor corrosion properties. Although a high strength rapidly solidified alloy could be given a protective coating, there would still be the risk that the coating could be damaged. Therefore, efforts are also being directed towards improving the corrosion resistance of magnesium alloys by rapid solidification.

### 3.3 Corrosion properties

There are three approaches which can be taken to improve the corrosion resistance of magnesium alloys. It was described earlier how the corrosion rates of magnesium alloys are often controlled by the presence of more noble second phase particles. The first approach is therefore to use the microstructural refining capabilities of RS to homogenise an alloy and slow down the cathodic reaction. Cotton and Jones<sup>57</sup> showed that an RS Mg-15%Al alloy was less sensitive to heavy metal impurities than a conventionally solidified alloy. Their explanation was that the distribution of Mg<sub>17</sub>Al<sub>12</sub> precipitates was much finer in the RS sample. Therefore, an iron rich particle in a slowly cooled sample could be surrounded by a region of only magnesium solid solution, whereas a similar particle in an RS alloy would be more likely to be surrounded by a fine mixture of magnesium solid solution and Mg<sub>17</sub>Al<sub>12</sub> precipitates. These fine, less active precipitates may have raised the overall corrosion potential of the area immediately surrounding the iron rich particles.

The second approach is to increase the electrode potential of magnesium by alloying it with a more noble element. This would reduce the potential difference between the resulting alloy and any more noble metal to which it was joined. Such a method could only be successful if the alloying element was in solid solution and if the solid solution was thermally stable. If precipitation occurred, the precipitate would inevitably be more noble than the matrix and many sites for the cathodic reaction would be created.

The third and most favoured approach is to alloy magnesium with elements which may cause a more protective film to form on the metal surface. If a thin film is formed on the surface of a corroding metal then anodic polarisation can occur, with a consequent reduction in the metal dissolution rate. Ideally, the film should be stable, self healing and have low ionic and electronic conductivity. It has already been stated that the naturally forming hydroxide film on magnesium causes some polarisation, but it tends to crack and is partially soluble in water and therefore does not give complete protection. Using rapid solidification it may be possible to develop a new magnesium alloy on whose surface a completely different and more protective surface film is formed.

When a binary alloy containing two elements A and B corrodes in water, there are a number of oxides or hydroxides which could form on the surface. Those of pure A and/or pure B may form and either may contain small amounts of the other cation. Alternatively, the two elements may combine together to form a mixed oxide. Thermodynamically, the oxide which is most likely to form is that which has the most negative free energy of formation. A list of these values is given in Table V. The values in the table refer to unit activities and they may be different in a binary alloy.

In practice, however, the formation of a particular oxide is controlled not only by thermodynamic considerations, but also by kinetic factors. Suppose that in a binary alloy, the oxide of the solute element has a much more negative free energy of formation than the oxide of the solvent metal. In theory the former should develop preferentially, but it may not do so if the atomic fraction of the solute element is too small, or if the solute element is unable to diffuse to the surface quickly enough. Furthermore, the thermodynamics and kinetics cannot predict if the oxide which forms will be porous or firmly adherent to the surface. To offer good protection, it must be adherent, non-porous and not dissolve in the electrolyte.

Clearly, with so many factors involved, it is difficult to predict the film

forming characteristics of any prospective RS magnesium alloy. It seems reasonable however that in choosing possible alloying additions, attention should turn to those elements whose oxides have more negative free energies of formation than MgO. Unfortunately MgO itself has a large negative free energy of formation and there are only a few elements below it in Table V. Beryllium is one such element and a small amount of beryllium (0.01%) does indeed improve the high temperature oxidation resistance of magnesium by forming a thin layer of BeO on the surface, as seen with the Magnox alloys used in the nuclear industry<sup>3</sup>. However, this does not occur at room temperature because the diffusion rate of beryllium is too low. Yttrium and the rare earth elements, cerium, neodymium and gadolinium, for example, and calcium also lie below magnesium in Table V and several examples of additions of these elements to RS magnesium alloys will be described later.

If the free energy of formation was the only factor involved then the choice of elements would be very limited. However, as stated earlier, the free energy of formation is only one indicator of the likelihood of a certain corrosion reaction taking place; it gives no information about the speed of the reaction. It is thus possible that two different oxide layers or a mixed oxide could form on the surface.<sup>58</sup> Suppose the oxide is formed by the outward movement of cations. If the mobilities of the cations in the initially formed oxide film are different, the more mobile cation could migrate towards the growing oxide surface, leaving the less mobile cation in the inner layers. In the limiting case, two distinct oxides will form. Alternatively, the cations could dissolve at different rates at the film/solution interface so that the surface film becomes enriched in the slower dissolving element. If either were to take place on a magnesium alloy, then initial formation of magnesium oxide or hydroxide could be followed by the formation of a second oxide, the latter controlling the corrosion rate. The chance of this happening would be greater if the oxide of the second element also had a large negative free energy of formation. A third possibility is the formation of a mixed oxide, for example the spinel MgAl<sub>2</sub>O<sub>4</sub>. This is inert to water and alkali solutions and has been shown to form on aluminium-magnesium alloys resulting in improved corrosion resistance.<sup>59</sup>

The benefits of alloying to produce a more protective film are well known for stainless steels. Chromium oxide has a more negative free energy of formation than iron oxide and creates a more passivating film. The surface film on stainless steels is enriched in chromium and when 12-18%Cr is added the passivating properties of chromium are approached.<sup>60</sup> A similar behaviour on a magnesium alloy is the desired objective in work using rapid solidification. All the elements which are being considered are likely to have their greatest effect on the composition of the surface film when they are retained in solid solution. An oxide film is more likely to be uniform, and hence more protective, if the distribution of elements beneath it, in its parent metal, is also more uniform. The ability of RS to achieve microstructural refinement and extend solid solubilities therefore makes it a particularly attractive route for investigating new alloys.

The experimental results which have been reported will now be described, beginning with investigations of the addition of yttrium and rare earth metals. The rare earths are a standard addition to conventional cast and wrought magnesium alloys to suppress porosity and to improve high temperature strength and creep resistance. They are not usually added to increase corrosion resistance, although the relatively low corrosion rates of the new high temperature alloys, WE54 and WE43,<sup>5</sup> are due in part to their yttrium content. The interest in rare earth additions to RS magnesium alloys stemmed from the results reported by Chang et al<sup>52,53</sup> at Allied Signals for their Mg-Al-Zn-RE alloys containing up to 6% yttrium, cerium, praseodymium or neodymium. The tensile properties of these alloys were reported earlier, but, in addition to having high strengths these alloys have low corrosion rates. The addition of yttrium, neodymium or praseodymium was found to be more beneficial than addition of cerium. Weight loss tests in aqueous 3% NaCl solution on extruded samples of EA55 and EA65 showed the corrosion rates of these alloys to be about 10mpy (0.25mm/year) which is comparable with that of the high purity version of AZ91 (Fig 16). This was attributed partly to the refined microstructure including the formation of (Fe,Mn)Al<sub>3</sub> which reduced the damaging galvanic effect of iron impurities, and partly to the inertness of the second phase particles containing rare earth elements which prevented pitting. It was also speculated that the rare earths altered the nature of the surface film in some way to make it more protective.

A more systematic study of the effects of yttrium and rare earths on the corrosion properties of magnesium has been carried out by Krishnamurthy et al.<sup>61-64</sup> Melt spinning and twin piston quenching were used to produce binary alloy ribbon and splats containing up to 26%Y, 20%Nd or 21%Ce. The maximum equilibrium solid solubilities of these elements in magnesium are 12.4%, 3.6% and 0.52% respectively, but RS has been used to form metastable solid solutions containing 25%, 6.1% and 3.5% respectively.<sup>65</sup> In the work of Krishnamurthy et al<sup>61-64</sup>, the splats were about 150μm thick and the ribbons about 50μm thick and the cooling rates achieved were not sufficient to prevent the formation of second phases. In the Mg-Nd alloys, the equilibrium phase Mg<sub>12</sub>Nd was formed, together with a metastable cubic phase Mg<sub>32</sub>Nd.

The corrosion properties of bulk alloys are frequently assessed by measuring the weight lost from the specimen after immersion in a salt solution or exposure to a salt spray for several days. This is impractical on ribbon and splats because they are so thin that perforation soon occurs. Short time weight loss experiments can be done on thicker splats, but often the corrosion properties are investigated using techniques

such as potentiodynamic polarisation and electrochemical impedance spectroscopy (EIS).<sup>66</sup> In the former, the potential of the specimen is varied by impressing on it a current which is equal to the difference between the anodic and cathodic current, to produce a curve of potential vs. current density. The corrosion rate can be found by extrapolation of the curves in the region of the corrosion potential and they also show, for example, whether the specimen undergoes an active-passive transition. In electrochemical impedance spectroscopy a sinusoidal voltage perturbation is imposed on the specimen, centred around the free corrosion potential. By measuring the response of the sample the corrosion resistance ( $R_{corr}$ ) can be found, which is inversely related to the corrosion rate. Care should be taken in interpreting the results of such tests for they are obtained in a much shorter time than weight loss results. Corrosion rates frequently decrease with time and corrosion rates measured by these techniques may be higher than those obtained by weight loss. However, Makar et al<sup>67</sup> obtained good correlation between EIS and weight loss results providing the corrosion was uniform, and such techniques help to gain a fundamental understanding of the corrosion processes taking place. They can also be used to identify in a short time potentially corrosion resistant alloys, although it cannot be assumed that any promising results on ribbons or splats will automatically be transferred to the extruded product for the micro-structure may change during consolidation.

Krishnamurthy et al<sup>61-64</sup> assessed the corrosion behaviour of their splats by obtaining potentiodynamic polarisation curves. The specimens were immersed in 0.01M NaCl solution and the most significant feature in the curves for the RS Mg-Nd and Mg-Y alloys was a region of pseudopassivation, which was absent from the curves for ingot cast alloy of the same composition (Fig 17). This occurred at potentials greater than about +0.4V and the effect was to reduce the current density by a factor of about ten in comparison to the ingot cast alloy. The reduction in current density associated with the pseudopassivation became greater as the neodymium content increased. The effect was attributed partly to the large negative electrode potential of the rare earth elements and partly to their enrichment in the surface film. The electrode potentials of the rare earth elements are slightly more negative than that of magnesium and hence the second phases containing rare earths were anodic to and therefore sacrificially protected the magnesium matrix during corrosion. Surface analysis of the Mg-20%Nd ribbon showed moderate enrichment of the  $Mg(OH)_2$  film in neodymium, and more significantly where the film had cracked there was a pronounced increase in the neodymium content, suggesting the formation of a second film. Additions of Y, Nd and Ce to rapidly solidified ZK60 magnesium alloy were then investigated and it was found that the pseudopassivation effect was also reproduced in these more complex alloys. Hehmann et al<sup>68</sup> investigated the corrosion properties of melt spun magnesium alloy ribbon containing 5.8 and 17.7%Y. The yttrium had a detrimental effect on corrosion rate when in solid solution, but when the samples were heat treated, to form the  $Mg_{25}Y_4$  precipitate, the corrosion rates were improved. It was suggested that these precipitates might give cathodic protection to the magnesium matrix.

A second element which has been investigated and found to improve the corrosion properties of magnesium is aluminium. Again, this is a standard addition to conventional cast and wrought magnesium alloys. Nussbaum et al<sup>43</sup> reported that the low corrosion resistance of high purity AZ91 (9%Al-1%Zn) could be retained in the rapidly solidified and extruded version described earlier. The maximum aluminium content of conventional magnesium alloys is about 9% whereas RS has also been used to investigate alloys with higher aluminium contents. In a systematic study of RS binary alloys, Joshi et al<sup>66,67</sup> produced melt spun ribbon containing 14.4%, 28% and 42.8%Al. The corrosion rates of the 20-50μm thick ribbons were measured in 0.05M sodium borate solution (pH 9.2) using electrochemical impedance spectroscopy. As the aluminium content was increased, the corrosion rate steadily decreased. Surface analysis of the air formed oxides on the ribbons showed that those containing 28% and 42.8%Al were enriched in aluminium. Ahmed et al<sup>69</sup> produced RS binary Mg-Al alloys containing up to 14.5%Al by twin piston splat quenching. Weight loss tests on the splats were carried out in 3%NaCl solution buffered to pH 10.4 with  $Mg(OH)_2$ . The tests were short, 4hr and 17hr, because the 100μm thick splats quickly perforated, but the results were in accord with those of Makar et al<sup>67</sup> in that aluminium decreased the corrosion rate. Further support for the beneficial effect of aluminium was obtained by Hehmann et al<sup>70</sup> who obtained potentiodynamic polarisation curves from binary Mg-Al ribbon containing 9.6-23.4%Al in 0.001M NaCl solution. The corrosion current of an RS alloy containing 9.6%Al was approximately three times lower than that of a chill cast alloy of the same composition. As the aluminium content of the ribbons was increased to 23.4% their corrosion rates continued to decrease by about two orders of magnitude. Furthermore, the potential at which pitting began increased as the aluminium content was increased from 17% to 23%.

The effect of aluminium on corrosion rate observed by these three groups is shown in Fig 18. The absolute values should not be compared because alloys of different purity were used and they were tested by different methods in different electrolytes, but the results demonstrate the beneficial effect of aluminium. It was generally agreed that there were two reasons for these beneficial effects. The first was the extension of solid solubility of aluminium in magnesium. Although Makar et al<sup>67</sup> detected some  $Mg_{17}Al_{12}$  precipitates in their ribbons, Hehmann et al<sup>70</sup> observed a single phase microstructure in the as-spun ribbon containing 21.6%Al, and Lu<sup>71</sup> has shown that the solubility can be extended to at least 24.5%.  $Mg_{17}Al_{12}$  is more noble than magnesium and its absence therefore removes any damaging galvanic action. The second reason was that the aluminium altered the nature of the surface film. Makar et al<sup>67</sup> analysed the air formed film on the ribbons and found it to be composed of a  $MgO$  top layer and an Al/Mg mixed oxide underlayer. The  $MgO$  layer became thinner as the aluminium content

was increased. Hehmann et al<sup>70</sup> analysed the variation with time of the composition of the electrolyte used in the polarisation tests of a Mg-23.4%Al alloy and found that initially only the magnesium dissolved and that further dissolution stopped after 2-5 minutes. This was interpreted as aluminium enrichment of the surface favouring the formation of a passive alumina based film. Baliga et al<sup>72</sup> made a detailed study of the corrosion products on the surface of RS Mg-3.5%Al alloy splats, but found no evidence of aluminium enrichment in the surface of this more dilute alloy.

Joshi et al<sup>56,67</sup> also studied the effect of up to 27.5%Zn, 39.3%Ca, 14%Li or 1.7%Si on the corrosion rate of magnesium, and Ahmed et al<sup>69</sup> studied the effect of up to 12.4%Zn. Both agreed that additions of zinc increased the corrosion rate (Fig 19). Themines<sup>73</sup> reported earlier that the equilibrium solid solubility of zinc in magnesium (8.4%) was not extended when cooling rates of 105 Ks<sup>-1</sup> were used. Ahmed et al<sup>69</sup> therefore assumed that in ribbon containing more zinc the corrosion rates would be increased by the presence of the galvanically active phase Mg<sub>7</sub>Zn<sub>3</sub>. Joshi et al<sup>56,67</sup> also found that additions of calcium, lithium and silicon increased the corrosion rate (Fig 19). The solid solubility of calcium was thought to have been extended from 1.3% to 11.3% and the air formed oxide films on Mg-Ca ribbons were enriched in calcium. Calcium oxide (CaO) has a lower free energy of formation than that of magnesium (Table V) and also has a more negative electrode potential (Table I). If CaO formed on the surface of magnesium in aqueous solution it would probably convert to the hydroxide Ca(OH)<sub>2</sub>. If this happened in preference to, or together with the formation of Mg(OH)<sub>2</sub>, then the corrosion rate might not be improved because the solubility of Ca(OH)<sub>2</sub> in water is greater than that of Mg(OH)<sub>2</sub><sup>74</sup>. However, Hehmann et al<sup>75</sup> found that the corrosion rates of magnesium alloy splats containing calcium were improved by a heat treatment and suggested that this might be due to the formation of a dispersion of calcium containing particles which cathodically protected the magnesium matrix.

The results described above are for binary alloys. In more complex alloys the effect of different elements is less clear. Ahmed et al<sup>69</sup> found that addition of up to 2.7%Ce increased the corrosion rate of RS Mg-Zn alloys, but decreased the rate of RS Mg-Al alloys. Addition of neodymium also reduced the corrosion rate of Mg-Al alloys and a Mg-4%Zn alloy, but increased the rate of a Mg-8%Zn alloy. Chang et al<sup>52,53</sup> found Y, Nd or Pr to be more effective than Ce in reducing the corrosion rate of Mg-Al-Zn-RE alloys. Similarly, Joshi et al<sup>56</sup> found Y and Nd to have a better effect than Ce in complex alloys containing different amount of Al, Li, Mn, Zn, Ce, Y and Nd. However, Makar et al<sup>67</sup> found Ce to be more beneficial after testing the same series of alloys. It was difficult to isolate the effect of individual elements when the composition of more than one element changed between samples. The effects are clearly complicated and as Ahmed et al<sup>69</sup> noted, it could depend on how much of each element was in solid solution. Further microstructural work and surface analysis would be valuable in clarifying the effects of individual elements.

There is more agreement over the beneficial effect of manganese. When up to 4% was added to RS Mg-Al and Mg-Zn alloys<sup>69</sup> and up to 2% to more complex alloys,<sup>67</sup> it consistently lowered the corrosion rate. A small amount of manganese (0.3%) is added to commercial alloys to control the iron content which has already been noted (Section 2.1), but the manganese additions to RS alloys are in excess of this. Again, the form in which the manganese is present would be important. Varich and Litvin<sup>76</sup> extended the solid solubility of manganese in magnesium to 5.4% and noted that the alloys were more resistant to etching as the manganese content increased.

From their investigation of a range of elements Joshi et al<sup>42,56</sup> placed them in order of their beneficial or detrimental effect. Y, Mn, Nd and Ce, in decreasing order were found to be the most beneficial and Si, Zn, Ca and Li, in decreasing order were found to be the most damaging. Although the beneficial effect of aluminium was discussed earlier, its effect was not as great as that of the rare earths so that large fractions had to be added before the effect was significant. Based on this information, three more complex alloys were investigated - Mg-6.8Al-3.4Li-0.41Mn-2.57Zn-3.55Ce, Mg-10.2Al-2.67Mn-3.18Zn-5.8Ce and Mg-11.1Al-2.44Zn-3.2Y. The high strengths of these alloys were reported in Section 3.2 and EIS results indicated that their corrosion rates were lower than commercial alloys. However, the corrosion rates of extruded samples calculated from weight loss after immersion in 0.05M sodium borate/3.5%NaCl were high (43-320mpy, 1.1-8.1mm/year). Corrosion was localised at prior particle boundaries and, therefore, corrosion rates calculated from weight loss were increased by the loss of individual particles. It was thought that the oxide around each particle was not broken up sufficiently during thermomechanical processing leaving regions of different chemical behaviour. Process development to hinder the formation of the oxide rich interfaces was expected to improve the salt water corrosion resistance.<sup>42</sup>

Reference has been made to the equilibrium phase diagrams of binary magnesium systems, which show that many elements have low solid solubility in magnesium. In addition, there are a number of systems, for example, Mg-Be, Mg-Fe, Mg-Cr and Mg-Ti which have large liquid immiscibility gaps. Clearly the investigation of these alloy systems is outside the capability of any melt quenching techniques. Mg-Fe and Mg-Ti composite alloys have been made by mechanical alloying to produce supercorroding alloys which react with sea water quickly and at controlled rates to provide heat sources.<sup>77</sup> For this purpose, the iron and titanium had to be separate phases embedded in the magnesium. However, by using ion implantation or physical vapour deposition, extended solid solutions of elements insoluble in molten magnesium can be produced. In ion implantation, a beam of energetic ions is used to inject chosen elements into the surface of the material to be treated. This provides the opportunity of extending

solid solubility limits, but the technique is limited to the modification of surface layers. Akavipat et al<sup>78,79</sup> implanted iron or boron ions into the surface of pure magnesium and the alloy AZ91C, and assessed the changes in corrosion properties of the alloys by obtaining potentiodynamic polarisation curves in 0.1% NaCl solution. The current densities of the implanted samples were lower than those of the unimplanted samples and the iron and boron also made the corrosion potential more noble. In addition, the implantation of iron into the surface of the AZ91C alloy altered the corrosion process. In the unimplanted sample, the magnesium matrix corroded around the more cathodic Mg<sub>17</sub>Al<sub>12</sub> particles, but in the iron implanted samples, the Mg<sub>17</sub>Al<sub>12</sub> particles themselves corroded and there was no severe attack of the solid solution regions between the islands. It was suggested that the iron altered the nature of the protective film thus changing the initial breakdown conditions.

Unlike ion implantation, physical vapour deposition is not limited to the modification of surface layers. At RAE, a process has been developed for the production of bulk aluminium alloy deposits up to 40mm thick,<sup>80</sup> and methods for producing bulk magnesium alloys are being investigated. When an atom condenses on a cold surface the time taken for it to reach equilibrium with the surface can be as short as 10-13 seconds.<sup>81</sup> Hence the capability to extend solid solubility limits is greater than in melt quenching techniques where the fastest cooling rates are about 10<sup>10</sup> K s<sup>-1</sup>. To explore the possibilities of developing vapour deposited magnesium alloys a series of binary Mg-Mn and Mg-Cr deposits were made. In the Mg-Cr deposits the solid solubility of chromium was extended to 29%, but in the Mg-Mn deposits, although there was some extension of solid solubility, particles of  $\alpha$ -Mn were also present at grain boundaries. The corrosion rates were calculated from weight loss measurements on 1mm thick samples immersed in 3% NaCl solution for one week. The results are shown in Fig 20. The corrosion rate of unalloyed vapour deposited magnesium was low because its purity was increased by the evaporation process. Chromium increased the corrosion rate compared to that of vapour deposited pure magnesium. Small additions of manganese may have decreased the corrosion rate, as found by Ahmed et al<sup>69</sup>, but when more manganese was added it increased again, possibly because of the large volume fraction of  $\alpha$ -Mn particles present. The ability to produce these alloys demonstrates the increased scope for alloy development presented by vapour deposition, and other alloy systems are under investigation.

### 3.4 Summary

In work aimed at improving the mechanical properties of magnesium alloys, it is apparent that the aspect of RS of which most advantage has been taken is microstructural refinement. Improvements in tensile yield strength have been attributed principally to a reduction in grain size and, therefore, increased strengthening through the Hall-Petch effect. Compressive yield strengths are also higher because twinning is more difficult. The fine grain size present in powder or ribbon is often stabilised during consolidation by the addition of a dispersion of intermetallics based on silicon or rare earth elements. There has been little work aimed at increasing the volume fraction of known age hardening precipitates or investigating new age hardening systems.

With regard to corrosion properties, the lowest corrosion rates in salt solution reported for RS magnesium alloys are for the Mg-Al-Zn-RE alloys, EA55 and EA65,<sup>54</sup> and RS high purity AZ91.<sup>43,48</sup> In the former, the improvement comes from the addition of rare earth elements and in the latter from the high purity of the alloy constituents. The target of a more protective, self healing surface film has not yet been achieved, although there is some evidence that an alumina based film may form on some Mg-Al alloys. Of the alloying elements investigated, yttrium, neodymium, cerium and manganese appear to be the most beneficial. It was suggested earlier that since the free energy of formation of the oxides of yttrium and the rare earth elements are more negative than that of magnesium (Table V) then these elements might cause a more protective film to form on the surface. This has not occurred in the alloy compositions so far investigated. There was some evidence that neodymium was enriched in the surface film of an alloy containing 20%Nd, but, in another example, even when 18%Y was present in solid solution it had a harmful effect on the corrosion properties. To consider adding more Y or Nd than this to alter the nature of the film becomes increasingly impractical because of the increasing cost and density of the alloy. Instead, most of the observed benefit of rare earth additions appears to come from the second phase particles which they form. These are anodic to, and sacrificially protect, the magnesium matrix. As more work on the microstructure of alloys and surface analysis of protective films is done, then our understanding of the corrosion processes should improve. The effect of alloying additions is mostly understood when the elements are present as a second phase and there is scope for more investigations of the effects of elements in solid solution. In this respect, the results of the ion implantation experiments were particularly encouraging. As Akavipat et al<sup>78</sup> remarked, iron is known for its particularly damaging effect when present as a second phase, but when implanted into the surface it had a beneficial effect.

In the introduction to this paper, the specific properties of conventional high strength magnesium alloys were compared with those of high strength aluminium alloys. A similar comparison can now be made between the properties of RS magnesium alloys and those of other materials in use or under development. From the alloys discussed in this section, EA55 from Allied Signal Inc,<sup>54</sup> RS AZ91 from Pechiney<sup>43,48</sup> and the MG-Al-Mn-Zn-Ce alloy from Lockheed<sup>42,56</sup> have the best combinations of strength and corrosion resistance and have been used to represent the magnesium alloys. EA55 is the alloy nearest to commercialisation.<sup>5</sup> The specific strengths of the RS alloys are

greater than those of conventional magnesium alloys and 7000 series aluminium alloys (Fig 21). They are comparable to or slightly higher than that of the Al-Li alloy 8090. Another class of material receiving considerable attention is particulate reinforced metal matrix composites (MMCs)<sup>82</sup> and the specific strength of one example of an aluminium based MMC has been included in Fig 21. It can be seen that the specific strengths reported for RS magnesium alloys are higher than for the composite. In Fig 22, specific stiffnesses are compared. Those of the RS magnesium alloys are no higher than those for the conventionally processed magnesium alloys. In fact, because the densities of the Mg-Al-Zn-RE alloys are increased without a proportional increase in stiffness, their specific stiffnesses are reduced a little (Fig 22). The Al-Li alloy and the aluminium based MMC have the highest specific stiffnesses. However, when specific buckling resistance ( $E^{1/3}/\rho$ ) is considered, it can be seen that the RS magnesium alloys compare well with the Al-Li alloy and the MMC, because a low density is the more important factor (Fig 23). The stiffness of magnesium alloys can also be increased further by the addition of ceramic particulate. The Young's modulus of cast and extruded AZ61 alloy containing 20% SiC particulate is reported to be 78GPa.<sup>83</sup> A review of magnesium based metal matrix composites is outside the scope of this paper, but one possible manufacturing route is to blend together and extrude a mixture of rapidly solidified powder with ceramic particulate. This could result in low density MMCs with even higher combinations of strength and stiffness. Even without reinforcement the comparisons made above demonstrate that RS magnesium alloys are potentially useful weight saving materials and worthy of further development and evaluation.

#### 4 CONCLUDING REMARKS

Despite their low densities, the use of magnesium alloys in aircraft structures is limited by shortcomings in corrosion resistance and mechanical properties. The principal use of magnesium alloys in aerospace is currently in castings. The two most recent developments are the trend towards high purity Mg-Al-Zn alloys with improved corrosion resistance and the introduction of Mg-Y-Nd alloys with improved room and elevated temperature properties combined with improved corrosion resistance.

The use of fluxless melting and resin bonded sands in the casting of magnesium is now widespread and, to help compete with cast aluminium alloys, low pressure casting is being introduced to enable wall thickness to be reduced and integrity to be improved. By applying a polyimide/Dow 17 coating, magnesium alloys can still be considered for gearbox applications where the oil temperature is up to 225°C.

Improvements in the mechanical properties and corrosion resistance of magnesium alloys have been achieved through the use of rapid solidification technology. Development is at an early stage and few alloy systems have been investigated, but already specific strengths greater than high strength aluminium alloys have been obtained, combined with improved corrosion resistance. The low density of magnesium alloys in comparison with aluminium alloys gives them an advantageous starting point from which to develop alloys with good specific properties.

Before any advanced magnesium alloy gains acceptance it will have to demonstrate that it can give satisfactory long term service. During the 1950s and 1960s magnesium alloys gained a reputation for corrosion problems, which could have been avoided in some cases if better precautions had been taken. If advanced magnesium alloys are put into service, the correct measures must be taken to guard against corrosion, so that in the long term, confidence in these alloys can be gained. Provided these precautions are taken, they have the potential to save weight in aerospace structures and the opportunities to exploit them should be fully explored.

#### REFERENCES

- 1 J C Ekwall, J E Rhodes and G G Wald, Methodology for evaluating weight savings from basic material properties, ASTM STP 761, P R Abelkis and C M Hudson, Eds, ASTM, 328-341, (1982).
- 2 G T Hudson, Designing with magnesium alloys, Proc. Conf. Magnesium Technology, London, Nov 1986, Institute of Metals, 60-65.
- 3 E F Emley, Principles of magnesium technology, Pergamon Press, 1966.
- 4 G B Evans, Reflections and Projections: thoughts on the use of magnesium alloys in airframes, Proc. 43rd World Magnesium Conf., Los Angeles, Jun 1986, 24-36.
- 5 J F King, The development of magnesium materials for advanced aerospace components, Proc. Conf., Metals Fight Back, London, Oct 1989, Shephard Press.
- 6 G B Evans, Applications of magnesium in aerospace, Ref 2, 103-109.
- 7 H P Goddard, The corrosion of light metals, Wiley, 1967, 257-311.
- 8 D L Hawke, Galvanic corrosion of magnesium, 14th Internat. Die Casting Congress, Toronto, Canada, May 1987.
- 9 D L Hawke, J E Hillis, W Unsworth, Preventative Practice for controlling the galvanic corrosion of magnesium alloys, International Magnesium Association, 7927 Jones Branch Drive, Lancaster Building, Suite 400, McLean, Virginia 22102, USA.

- 10 MEL Ltd, Surface treatments for magnesium alloys in aerospace and defence  
Magnesium Elektron Ltd, Regal House, London Road, Twickenham, TW1, 3QA, UK.
- 11 A Stevenson, Mg casting alloys for the aerospace challenge, J Metals, 39,  
(1987), 16-19.
- 12 W Unsworth, Developments in magnesium alloys for casting applications, Metals  
and Materials, 4, (1988), 83-86.
- 13 K N Reichek, K J Clark and J E Hillis, Controlling the salt water corrosion  
performance of magnesium AZ91 alloys, SAE Tech. Paper 850417.
- 14 D Magars, The potential for magnesium die castings in aerospace applications,  
Ref 4, 58-65.
- 15 C S Roberts, Magnesium and its alloys, Wiley, New York, 1960, Ch.8.
- 16 J D Hanawalt, C F Nelson and J A Peloubet, Corrosion studies of magnesium and  
its alloys, Trans. AIME, 147, (1942), 273-299.
- 17 K J Clarke, AZ91E magnesium sand casting alloy: the standard for excellent  
corrosion resistance, Ref 4, 37-41.
- 18 D J Zuliani, The improved corrosion resistance of ultra high purity magnesium  
alloy castings, Proc. 67th AGARD Conf., Mierlo, Netherlands, October 1988.
- 19 W Unsworth and J F King, New high performance casting alloy developed,  
Metallurgia, 53 (1986), 199-200.
- 20 W Unsworth and J F King, Recent casting alloy developments, Ref 2, 25-35.
- 21 N Zeumer, H Fuchs, G Betz, New developments in casting of magnesium, Ref 2  
18-24.
- 22 J Campbell, Thin wall castings, Mater. Sci. and Technol., 4, (1988), 194-204.
- 23 Specification DTD 911C, Protection of magnesium rich alloys against corrosion.
- 24 D Tawil and M Rendu, Improved protection of magnesium alloys against synthetic  
aviation lubricants at elevated temperatures, 24th Aerospace/Airline plating  
and metal finishing forum, Phoenix, Arizona, Apr 1988, SAE Tech. Paper 880869.
- 25 Specification MIL-M-45202, Anodic treatment of magnesium alloys.
- 26 L A Carapella, Fundamental alloying nature of magnesium, Metal Prog., 48, (1945),  
297-307.
- 27 G V Raynor, The physical metallurgy of magnesium and its alloys, Pergamon Press,  
London, 1959.
- 28 W Hume-Rothery, Factors affecting the stability of metallic phases, Proc. Conf.,  
Phase stability in metals and alloys, Geneva, Switzerland, March 1966,  
McGraw-Hill, 3-23.
- 29 F Hehmann and H Jones, The status and potential of rapid solidification of  
magnesium alloys, Proc. Conf., Rapidly solidified alloys and their mechanical  
and magnetic properties, Boston, Ma., USA, Dec 1985, Materials Research Soc.,  
259-274.
- 30 F Hehmann and H Jones, Rapid solidification processing of magnesium alloys,  
Ref 2, 83-96.
- 31 R E Lewis, Y W Kim and H Jones, Rapidly solidified magnesium alloys for high  
performance structural applications: a review, Proc. Conf., Processing of  
structural metals by rapid solidification, Orlando, USA, Oct 1986, ASM  
International, 367-378.
- 32 F H Froes, Y W Kim and F Hehmann, Rapid solidification of Al, Mg and Ti,  
J Metals, 39 (1987), 14-21.
- 33 H Jones, A Joshi, R G Rowe and F H Froes, The current status of rapid  
solidification of magnesium-base and titanium-base alloys, Internat. J.  
Powder Metall., 23, (1987), 13-24.
- 34 H Jones, Rapid solidification of metals and alloys, The Institution of  
Metallurgists monograph No 8, London, 1982.
- 35 H Jones, Rapid solidification of magnesium alloys: a bibliography 1950-1988,  
Internat. J. Rapid Solidification, 4, (1989), 297-315.
- 36 R S Busk and T E Leontis, Powdered magnesium alloys, Trans. AIME, 188, (1950),  
297-306.

- 37 P Duwez, R H Willens and W Klement, Continuous series of metastable solid solutions in silver-copper alloys, *J Appl. Phys.*, 31 (1960), 1136-1137.
- 38 R E Anderson, J W Simon and D R Clemens, Microstructural evaluation of RSR processed magnesium alloys, *Proc. Conf., PM Aerospace materials, Luzern, Nov 87*, 36.1-36.14.
- 39 A Unal, Production of rapidly solidified magnesium powders by gas atomisation, *Mater. Sci and Technol.*, 5, (1989), 1027-1033.
- 40 E J Lavernia, E Gomez and N J Grant, The structures and properties of Mg-Al-Zr and Mg-Zn-Zr alloys produced by liquid dynamic compaction, *Mater. Sci and Eng.*, 95, (1987), 225-236.
- 41 M J Koczak and M K Premkumar, High performance powder metallurgy aluminium alloys - an overview, *AGARD Conf. Proc. No 444, New light alloys*.
- 42 A Joshi, R E Lewis and H Jones, Selection, processing and properties of three rapidly solidified Mg-Al-Zn based alloys, *Internat. J. Rapid. Solidif.*, 4, (1989), 251-269.
- 43 G Nussbaum, H Gjestland and G Regazzoni, Rapid solidification of magnesium alloys, *Light Metal Age*, Aug 1988, 16-19.
- 44 G W Lorimer, Structure-property relationships in cast magnesium alloy, Ref 2, 47-53.
- 45 I J Polmear, *Light Alloys*, Edward Arnold, London, (1981), 127-161.
- 46 S Isserow and F J Rizzitano, Microquenched ZK60A alloy, *Internat. J. Powder Metall. and Powder Tech.*, 23, (1987), 13-24.
- 47 M C Flemings and A Mortensen, Rapid solidification processing of magnesium alloys, *Massachusetts Inst. of Tech.*, Sept 1984, Report No. AMMRC-TR-84-37, Gov't Acc. No AD-A150270.
- 48 G Nussbaum, P Samfort, G Ragazzoni and H Gjestland, Strengthening mechanisms in the rapidly solidified AZ91 magnesium alloy, *Scripta Metall.*, 23, (1989), 1079-1084.
- 49 P J Meschter, Microstructures and properties of rapidly solidified Mg-10Al and Mg-12.5Al-1.5Si alloys, *Metall. Trans. A*, 18A, (1987), 347-350.
- 50 P J Meschter and J E O'Neal, Rapid solidification processing of magnesium-lithium alloys, *Metall. Trans. A*, 15A, (1984), 237-240.
- 51 F C Grensing and H L Fraser, Microstructure and properties of rapidly solidified magnesium-lithium alloys, Ref 31, 429-435.
- 52 C F Chang, S K Das, D Raybould and A Brown, Corrosion resistant high strength magnesium alloys by RSP, *Metal Powder Rep.*, 41, (1986), 302-305 and 308.
- 53 C F Chang, S K Das and D Raybould, Rapidly solidified Mg-Al-Zn-Rare Earth alloys, *Proc. Conf., Rapidly solidified materials, San Diego, USA, Feb 1986, ASM*, 129-135.
- 54 F H Froes, W E Quist and S K Das, Advanced lightweight metals using rapid solidification, Ref 38, 16.1-16.29.
- 55 C F Chang, S K Das and D Raybould, The effect of heat treatment on the properties of rapidly solidified Mg-Al-Zn-RE alloys, Ref 31, 409-415.
- 56 A Joshi and R E Lewis, Role of RSP on microstructure and properties of magnesium alloys, *Proc. Conf., Advances in magnesium alloys and composites, Phoenix, Arizona, Jan 1988, TMS*, 89-103.
- 57 J D Cotton and H Jones, The Sensitivity of the aqueous corrosion rate of rapidly solidified Mg-15wt% Al extrusions to Fe impurity content, to be published in *Internat. J. Rapid Solidification*.
- 58 T P Hoar, On corrosion resistant materials. *J Electrochem. Soc.*, 117, (1970), 17C-22C.
- 59 W B Nowak and J Seyyedi, Corrosion resistant ion plated aluminium-magnesium alloy films, In: *Fundamental aspects of corrosion protection by surface modification*, E McCafferty, C R Clayton and J Oudar, Eds., *Electrochem. Soc.*, Pennington, New Jersey, USA, 89-96.
- 60 G Wranglen, An introduction to corrosion and protection of metals, Chapman and Hall, London, 1985.
- 61 S Krishnamurthy, E Robertson, F H Froes, Magnesium-neodymium alloys produced by rapid solidification, Ref 31, 399-408.

- 62 S Krishnamurthy, F H Froes and E Robertson, Investigation of rapidly quenched Mg-Ce alloys, Proc. Conf., Rapidly solidified materials: properties and processing, San Diego, California, USA, March 1988, 107-113.
- 63 S Krishnamurthy, E Robertson and F H Froes, Rapidly solidified magnesium alloys containing rare earth additions, Ref 56, 77-88.
- 64 S Krishnamurthy, M Khobaib, E Robertson and F H Froes, Corrosion behaviour of rapidly solidified Mg-Nd and Mg-Y alloys, Mater. Sci. and Eng., 99, (1988), 507-511.
- 65 F Hehmann, F Sommer and H Jones, Extension of solid solubility of yttrium and rare earth metals in magnesium by rapid solidification, Ref 31, 379-398.
- 66 M G Fontana, Corrosion Engineering, McGraw-Hill, New York 1987.
- 67 G L Makar, J Kruger and A Joshi, The effect of alloying elements on the corrosion resistance of rapidly solidified magnesium alloys, Ref 56, 105-121.
- 68 F Hehmann, R G J Edyvean, H Jones and F Sommer, Effect of rapid solidification processing on corrodability of magnesium alloys, Ref 30, 46.1-46.16.
- 69 D S Ahmed, R G J Edyvean, C M Sellars and H Jones, The effect of Mn, Ce, Nd and Si additions on the rate of dissolution of splat quenched Mg-Al and Mg-Zn alloys in 3% NaCl solution, to be published in Mater. Sci and Tech.
- 70 F Hehmann, F Sommer, H Jones, and R G J Edyvean, Corrosion inhibition in magnesium based alloys induced by rapid solidification processing, J. Mater. Sci., 24, (1989), 2369-2379.
- 71 H L Luo, CC Chao and P Duwez, Metastable solid solutions in aluminium-magnesium alloys, Trans AIME, 230, (1964), 1488-1490.
- 72 C B Baliga, P Tsakiroopoulos and J F Watts, Corrosion products formed on a rapidly solidified Mg-Al alloy, Internat. J. Rapid. Solidif., 4 (1989), 231-250.
- 73 D Themines, W Riehemann, W Henning and B L Mordike, Mechanical properties of rapidly solidified Mg-Zn alloys, Ref 29, 275-280.
- 74 R C Weast, Handbook of chemistry and physics, CRC Press, Boca Raton, Florida, USA.
- 75 F Hehmann, S Krishnamurthy, E Robertson, A G Jackson, S J Savage and F H Froes, Mechanical properties and corrosion behaviour of rapidly solidified Mg-Ca-Cu and Mg-Ca-Ni alloys, Proc. Conf., Horizons of powder metallurgy, Dusseldorf, July 1986, Vol. 2, 1001-1008.
- 76 N I Varich and B N Litvin, Study of Mg-Mn and Mg-Zr alloys prepared by quenching from the melt, Fiz. Metal. Metalloved., 4, (1963), 526-529.
- 77 S S Sergev, S A Black and J F Jenkins, US Patent No. 4264362, described in Materials synthesis by mechanical alloying, C C Koch, Annu. Rev. Mater. Sci., 19, (1989), 121-143.
- 78 S Akavipat, E B Hale, C E Habermann and P L Hagans, Effects of iron implantation on the aqueous corrosion of magnesium, Mater. Sci. and Eng., 69, (1985), 311-316.
- 79 S Akavipat, C E Habermann, P L Hagans and E B Hale, Electrochemical and auger measurements on boron implanted magnesium, Ref 59, 52-61.
- 80 R W Gardiner and M C McConnell, Production of advanced aluminium alloys by vapour deposition, Metals and Mater., 3, (1987), 254-258.
- 81 J P Hirth and G M Pound, Condensation and evaporation, Prog. Mater. Sci., Vol 11, Pergamon, (1963).
- 82 C J Peel, The relative performance of metals and composites in aerospace structures, Ref 5.
- 83 B A Mikucki, S O Shook, W E Mercer and W G Green, Magnesium matrix composites at Dow: status update, Ref 4, 13-23.
- 84 C J Smithells, Metals reference book, 5th Ed., Butterworths, London, (1976).

Metal	Ion	Standard electrode potential ( V )
Gold	Au <sup>3+</sup>	+1.42
Silver	Ag <sup>+</sup>	+0.799
Copper	Cu <sup>2+</sup>	+0.345
Hydrogen	H <sup>+</sup>	0.000
Nickel	Ni <sup>2+</sup>	-0.230
Iron	Fe <sup>2+</sup>	-0.409
Cadmium	Cd <sup>2+</sup>	-0.426
Chromium	Cr <sup>3+</sup>	-0.740
Zinc	Zn <sup>2+</sup>	-0.763
Aluminium	Al <sup>3+</sup>	-1.66
<b>Magnesium</b>	<b>Mg<sup>2+</sup></b>	<b>-2.38</b>
Calcium	Ca <sup>2+</sup>	-2.76
Lithium	Li <sup>+</sup>	-3.04

Table I Standard electrode potentials of some common elements.<sup>74</sup>

Alloy	Typical Composition ( wt% )					Tensile Properties		
	Zn	RE	Th	Ag	Zr	0.2%PS (MPa)	UTS (MPa)	%EI
ZE41	4.2	1.3	—	—	0.7	135	200	3
ZH62	5.5	—	1.8	—	0.7	155	255	5
EZ33	2.5	3.0	—	—	0.6	95	140	3
HZ32	2.2	—	3.0	—	0.7	85	185	5
QE22	—	2.0	—	2.5	0.6	175	240	2
EQ21	—	2.1	—	1.5	0.6	175	240	2

Table II Compositions and tensile properties of cast magnesium alloys (RE = rare earth elements). Tensile properties are specification minima in precipitation treated condition (from MEL data).

Element	AZ91C		AZ91E	
	%min	%max	%min	%max
Al	8.1	9.3	8.1	9.3
Zn	0.4	1.0	0.4	1.0
Mn	0.13	0.35	0.17	0.35
Fe		—		0.005
Si		0.30		0.20
Cu		0.10		0.015
Ni		0.01		0.001

Table III Compositions of AZ91C and high purity AZ91E alloys.<sup>5</sup>

Solubility (at%)	Solute Element
>25	Cd
5-25	<b>Al</b> , Dy, Er, Ho, In, <b>Lu</b> , Lu, Pb, Sc, Tl, Tm, <b>Zn</b>
1-5	<b>Ag</b> , Bi, Ga, Sn, Yb, <b>Y</b>
0.1-1	Au, Gd, La, <b>Mn</b> , <b>Nd</b> , Pd, Sm, <b>Th</b> , <b>Zr</b>
<0.1	Ba, <b>Ce</b> , Co, Cu, Ge, La, Ni, Pr, Sb, Si, Sr

Table IV Maximum equilibrium solid solubilities of elements in magnesium (from Froes et al<sup>32</sup>). Those in bold type are used in commercial alloys.

Formula of oxide	Free energy (kJ per mol O <sub>2</sub> )	Formula of oxide	Free energy (kJ per mol O <sub>2</sub> )
Ag <sub>2</sub> O	-22	ZrO <sub>2</sub>	-1028
PbO	-378	Al <sub>2</sub> O <sub>3</sub>	-1054
NiO	-426	<b>MgO</b>	<b>-1138</b>
CoO	-426	Nd <sub>2</sub> O <sub>3</sub>	-1140
CdO	-452	Gd <sub>2</sub> O <sub>3</sub>	-1153
FeO	-482	Ce <sub>2</sub> O <sub>3</sub>	-1154
V <sub>2</sub> O <sub>5</sub>	-568	BeO	-1162
ZnO	-636	Pr <sub>2</sub> O <sub>3</sub>	-1173
Cr <sub>2</sub> O <sub>3</sub>	-701	ThO <sub>2</sub>	-1174
MnO	-726	Dy <sub>2</sub> O <sub>3</sub>	-1182
SiO <sub>2</sub>	-856	CaO	-1208
TiO <sub>2</sub>	-862	Y <sub>2</sub> O <sub>3</sub>	-1211

Table V Free energies of formation of metal oxides.<sup>74,84</sup>

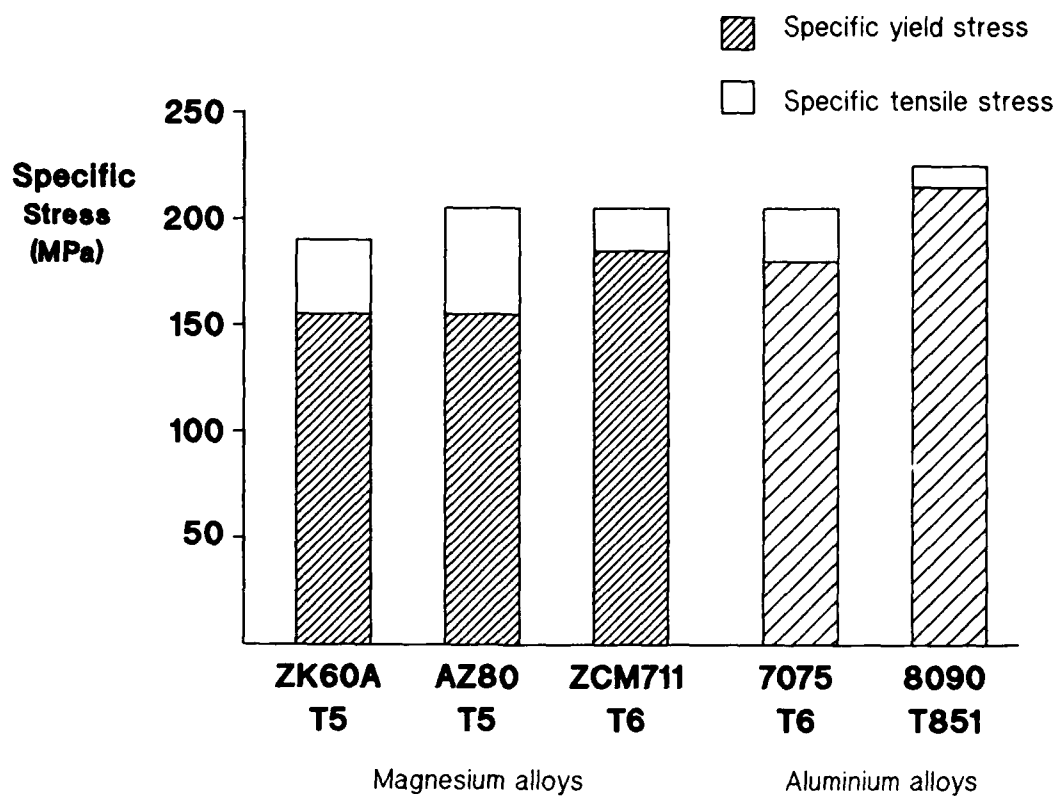


Fig.1 Specific strengths of some wrought magnesium and aluminium alloys (typical properties of extrusions).

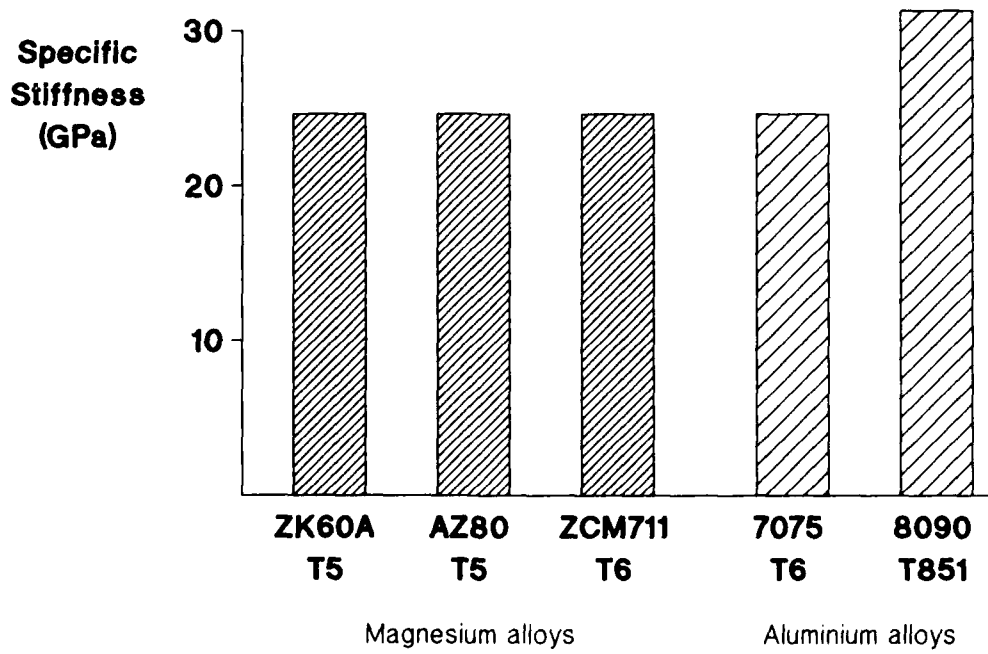


Fig.2 Specific stiffnesses of some wrought magnesium and aluminium alloys (typical properties of extrusions).

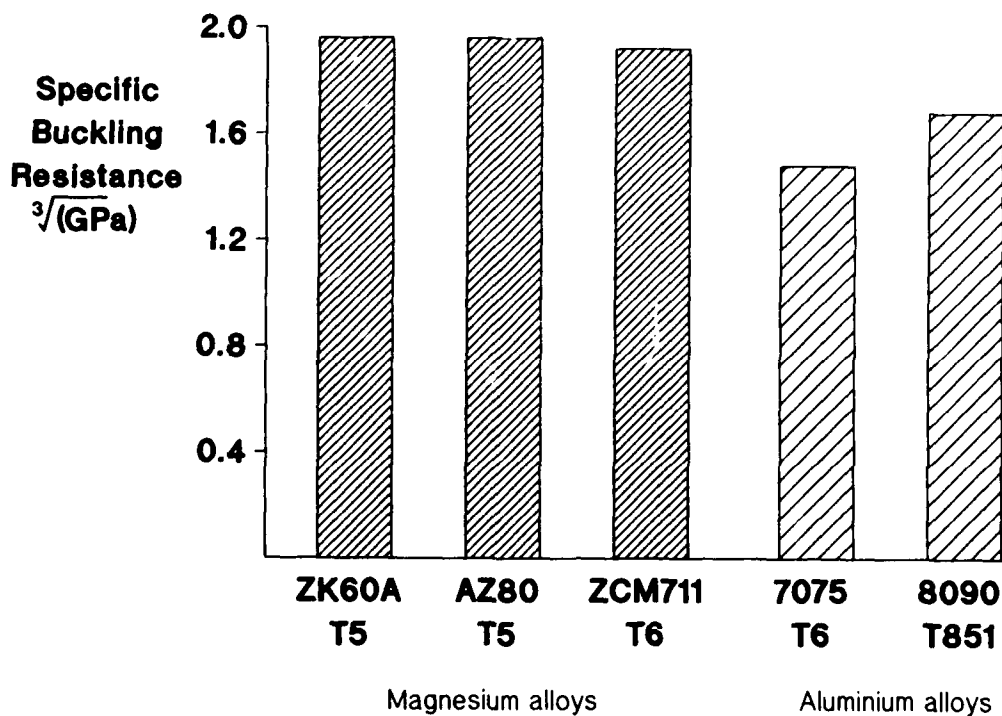


Fig.3 Specific buckling resistance ( $E^{\frac{1}{3}}/\rho$ ) of some wrought magnesium and aluminium alloys (typical properties of extrusions).

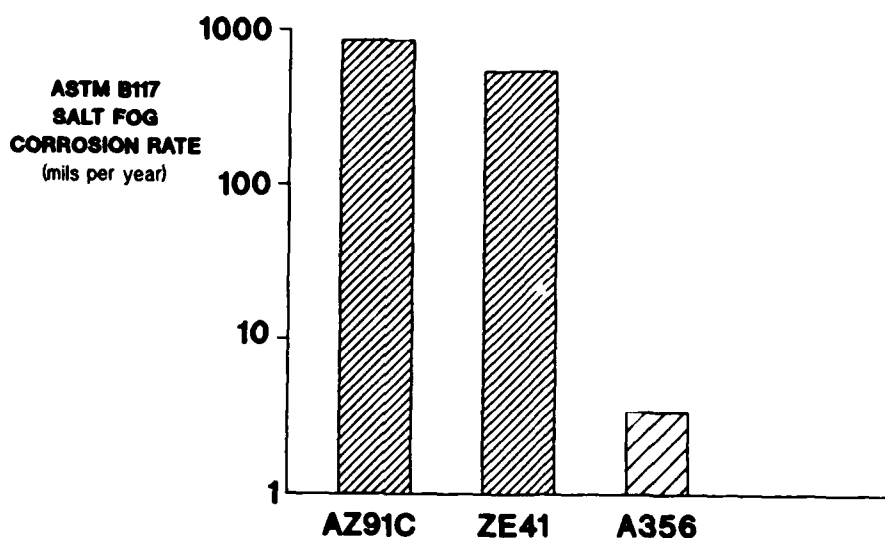


Fig.4 Corrosion rates of magnesium casting alloys AZ91C and ZE41, and aluminium casting alloy A356 (from King<sup>5</sup>).

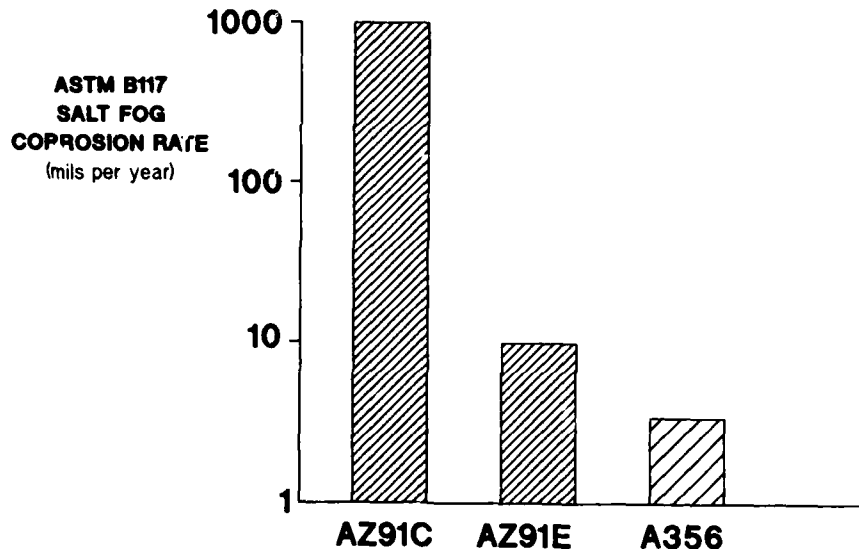


Fig.5 Corrosion rates of magnesium casting alloys AZ91C and high purity AZ91E, and aluminium casting alloy A356 (from King<sup>5</sup>).

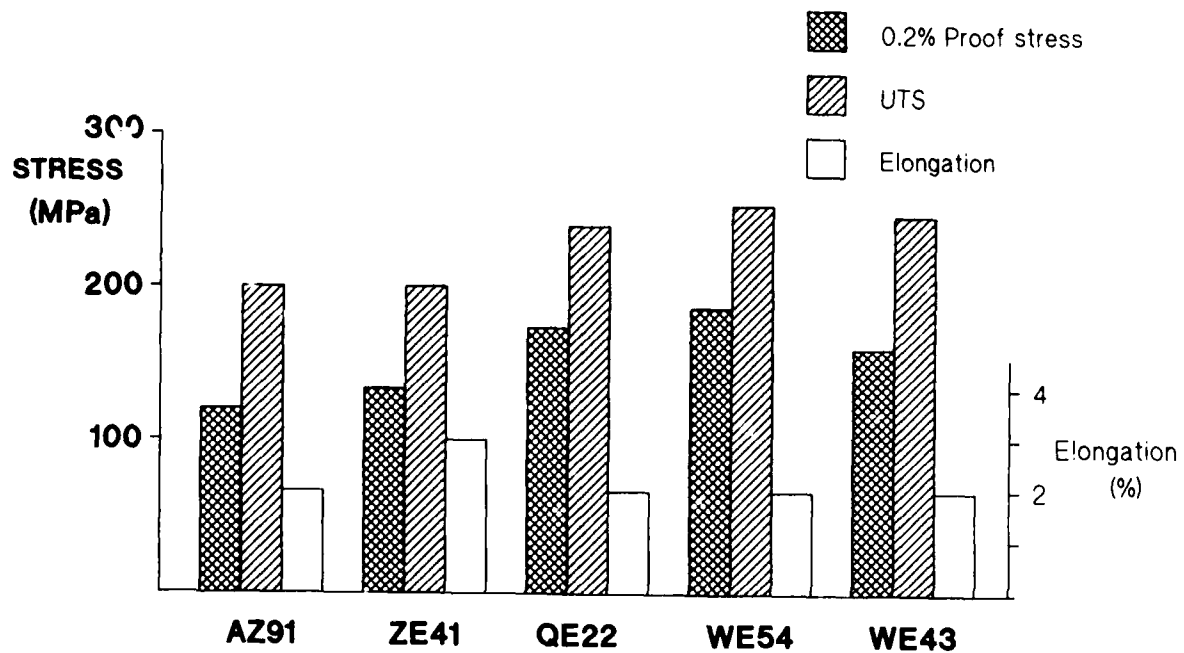


Fig.6 Minimum tensile properties of WE54, WE43 and other cast magnesium alloys in precipitation treated condition (MEL data).

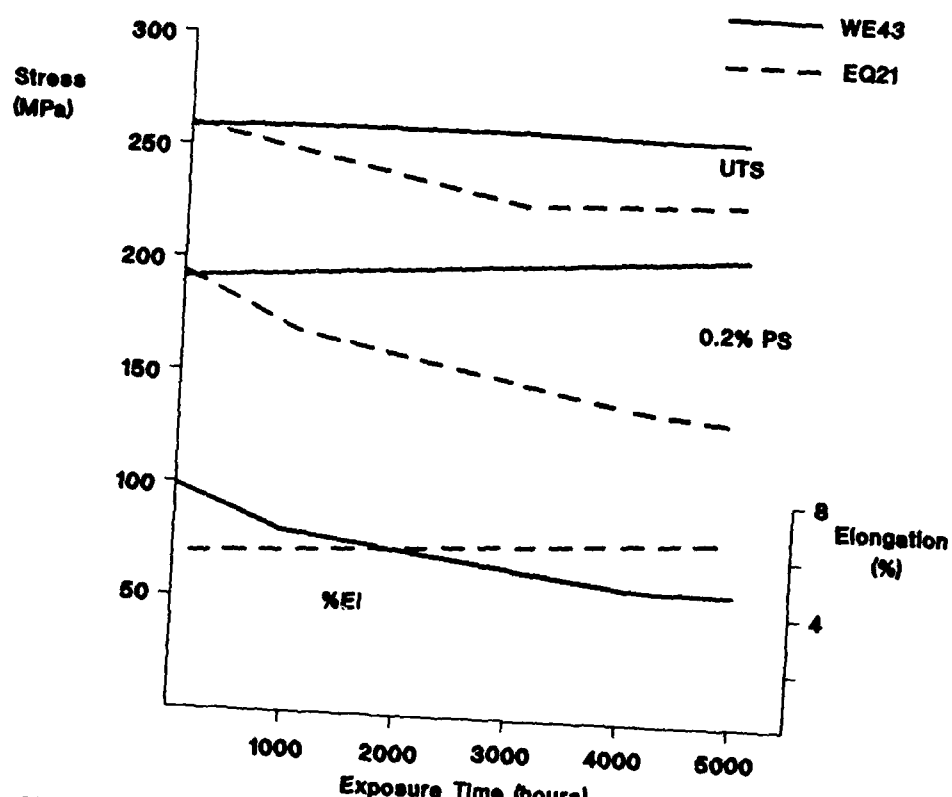


Fig. 7 Effect of exposure to 200°C on room temperature tensile properties of WE43 and EQ21 (from King<sup>5</sup>).

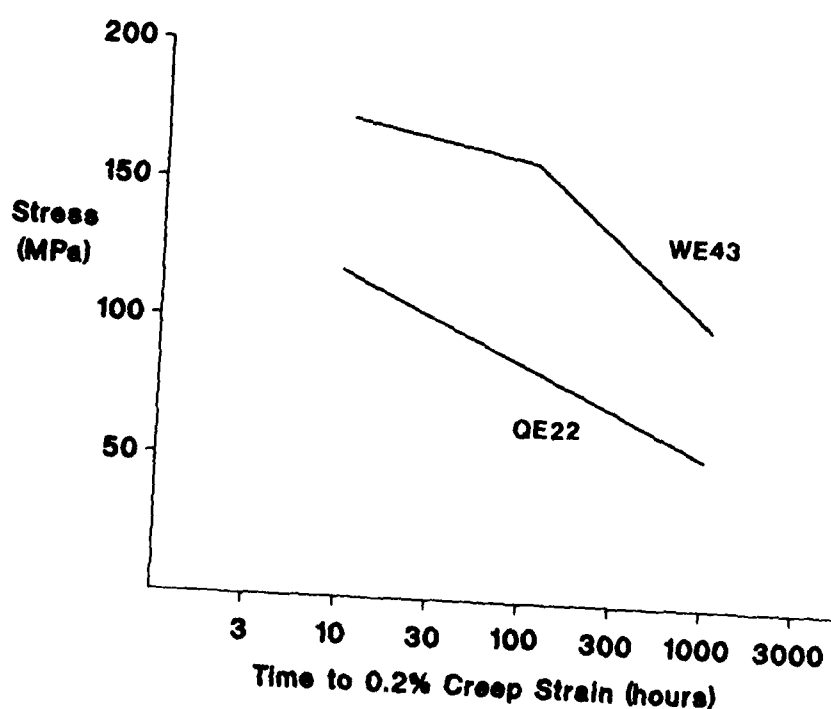


Fig. 8 Stress/time relationship for WE43 and QE22 at 200°C (from King<sup>5</sup>).

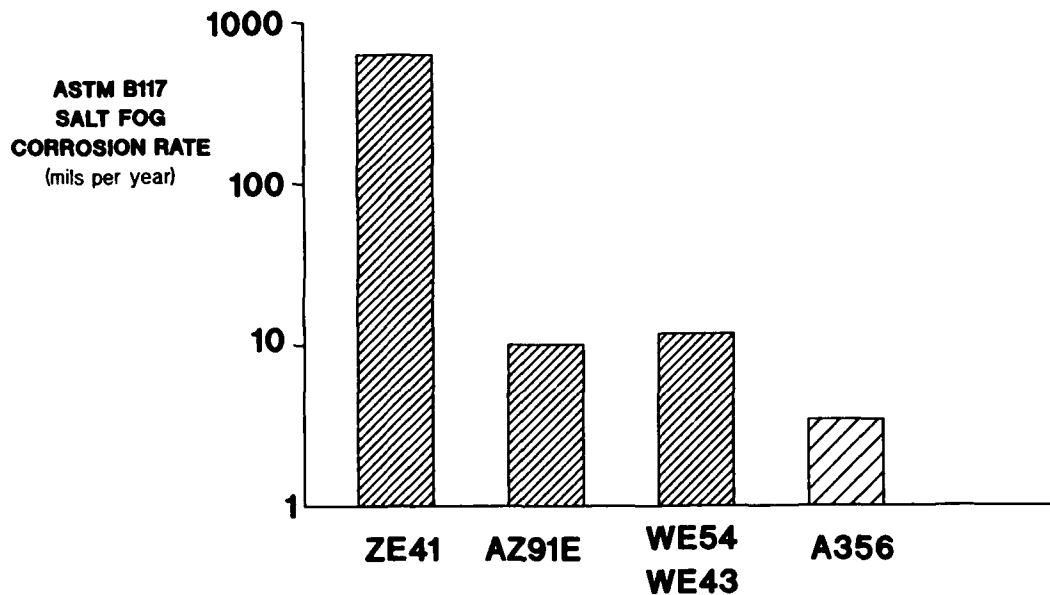


Fig.9 Corrosion rates of WE54, WE43 and other magnesium casting alloys, and aluminium casting alloy A356 (from King<sup>5</sup>).

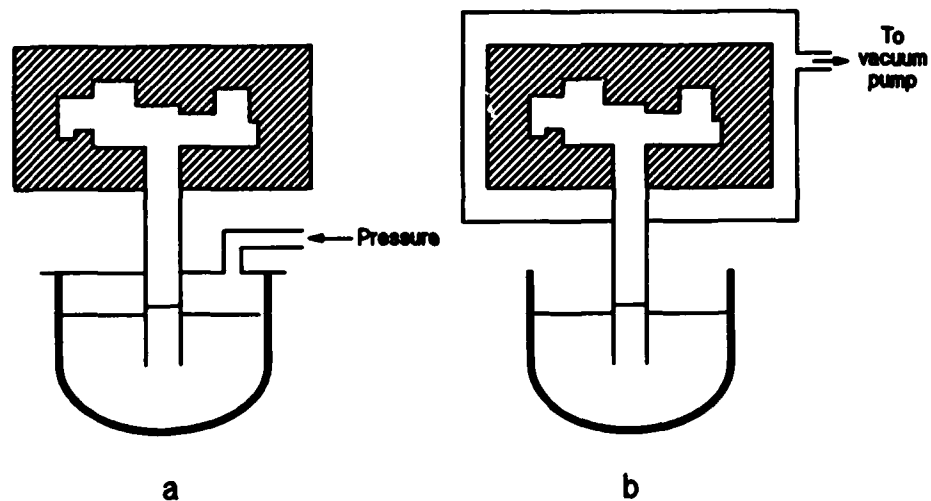


Fig.10 Schematic diagrams of low pressure casting techniques (a) pressurised crucible (from Zeumer et al<sup>21</sup>) (b) evacuated mould (from MEL).

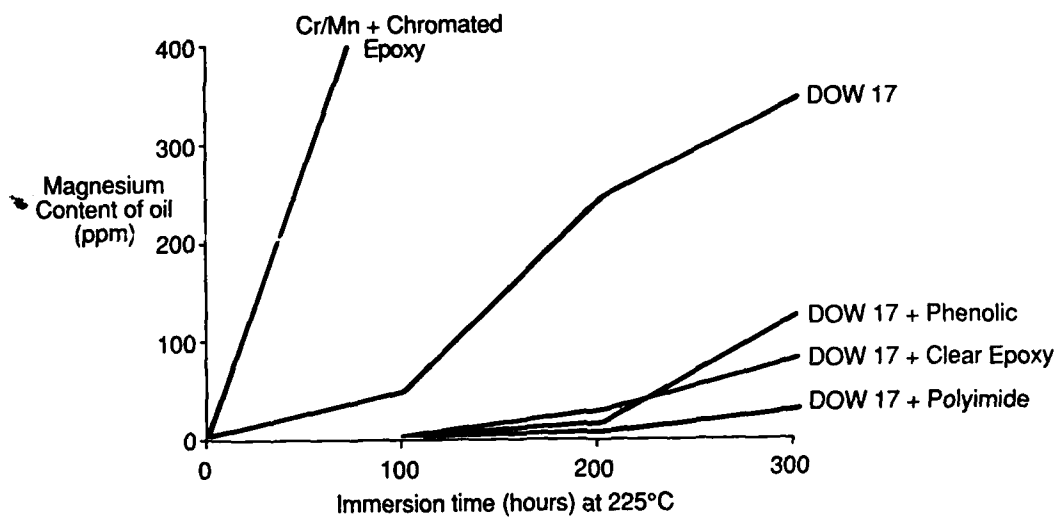


Fig.11 Comparative performance of different coatings in static lubricant immersion tests at 225°C (courtesy Rolls-Royce Ltd and MEL).

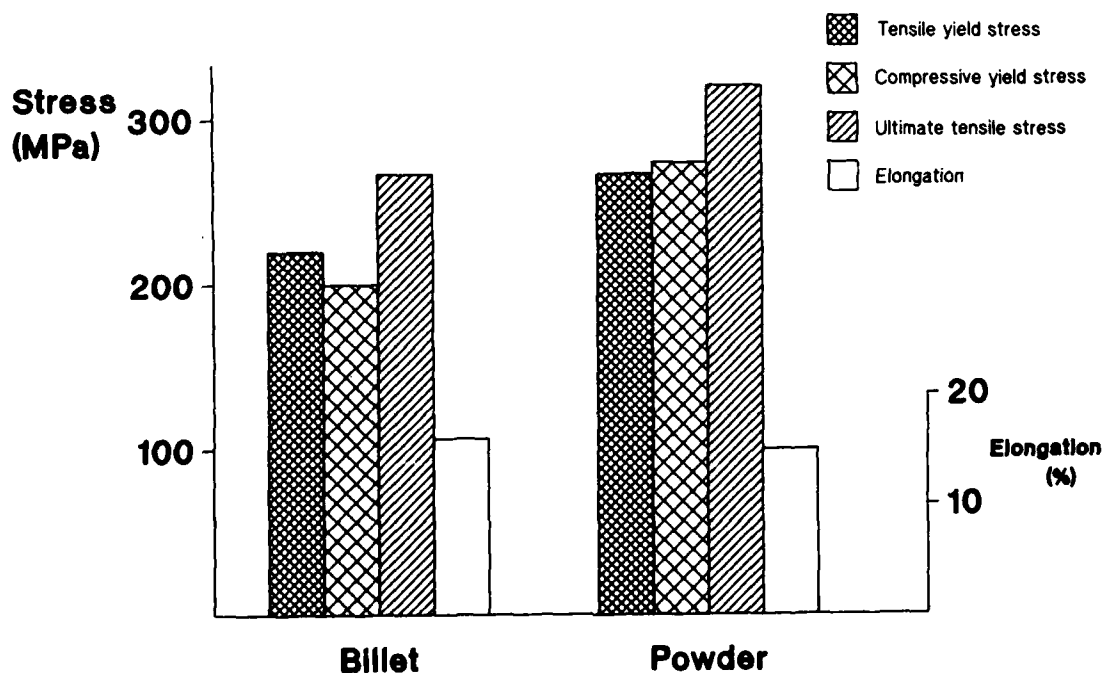


Fig.12 Comparison of tensile and compressive properties of extruded billet and powder of AZ31 alloy (from Busk and Leontis<sup>36</sup>).

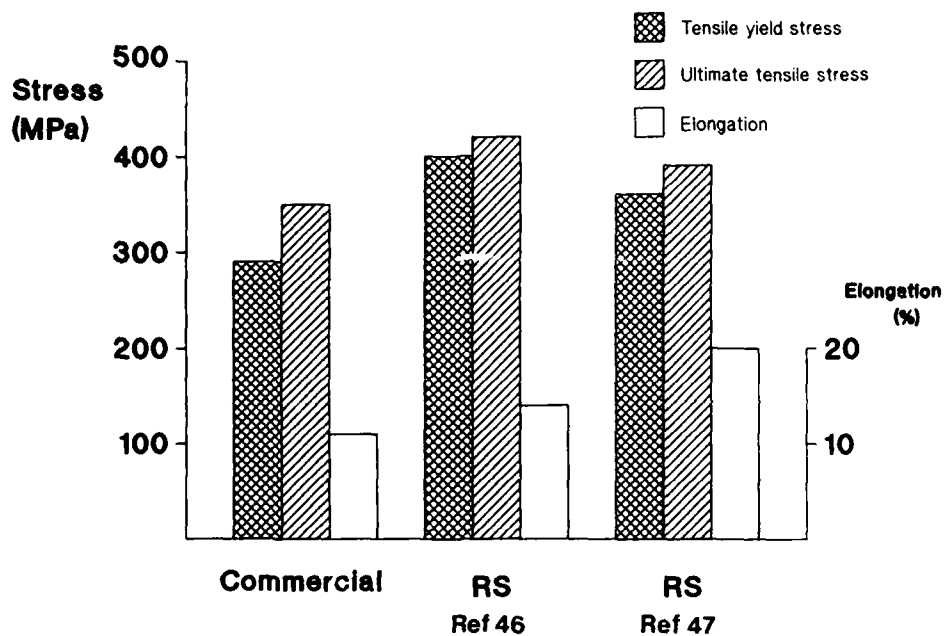


Fig.13 Comparison of tensile properties of extrusions of conventionally cast and rapidly solidified ZK60A magnesium alloy (from Isserow and Rizzitano<sup>46</sup> and Flemings and Mortensen<sup>47</sup>).

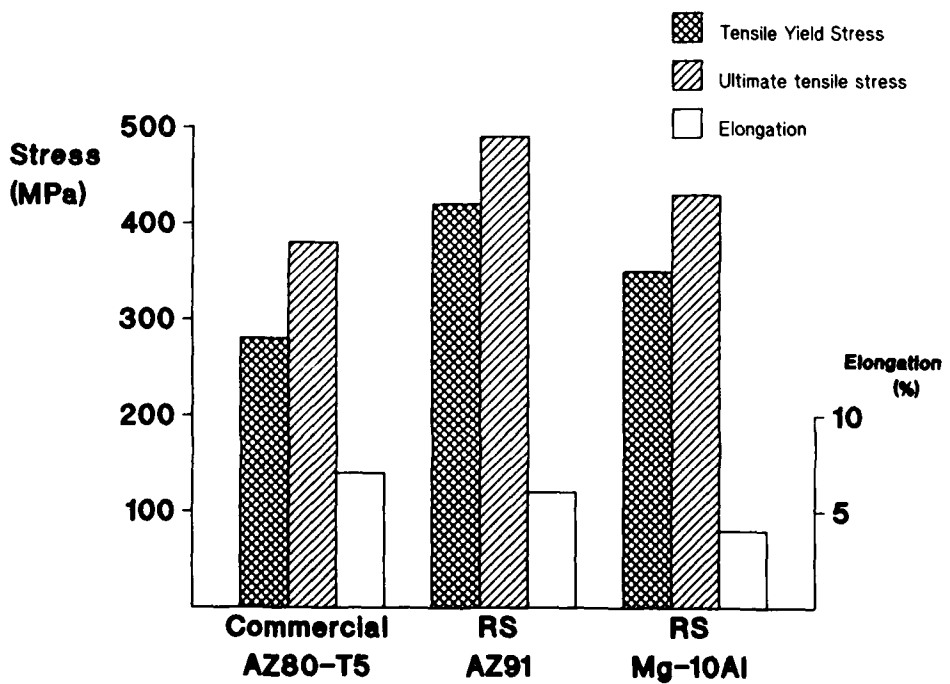


Fig.14 Tensile properties of extrusions of rapidly solidified AZ91 (from Nussbaum et al<sup>43</sup>) and Mg-10Al alloy (from Meschter<sup>49</sup>)

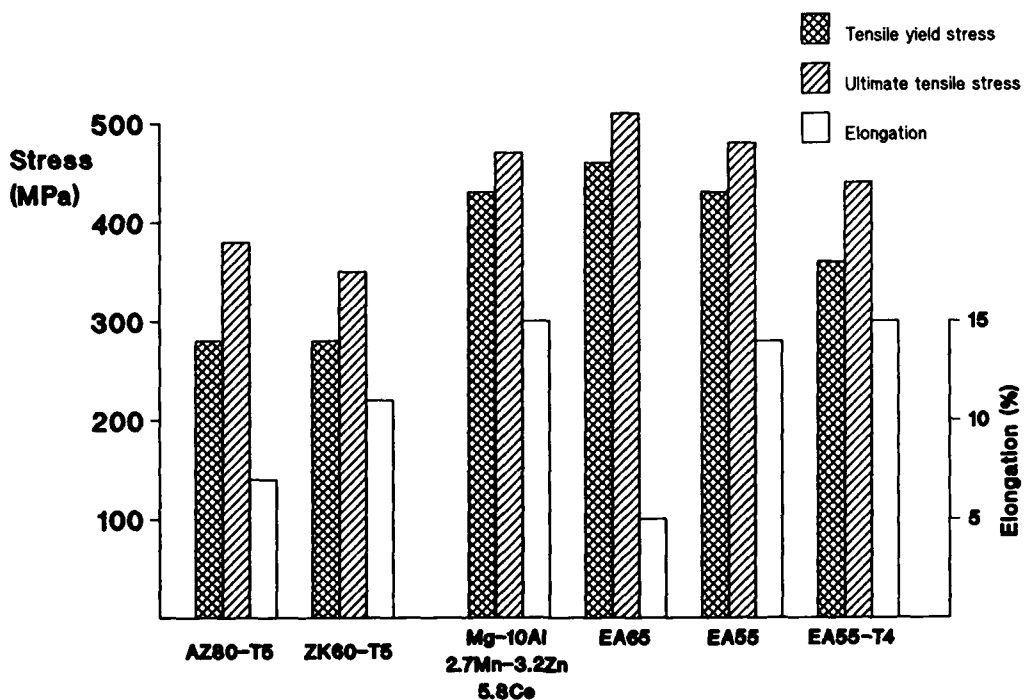


Fig.15 Tensile properties of extrusions of rapidly solidified Mg-10Al-2.7Mn-3.2Zn-5.8Ce alloy (from Joshi et al<sup>42</sup>) and EA55 and EA65 (from Froes et al<sup>54</sup>)

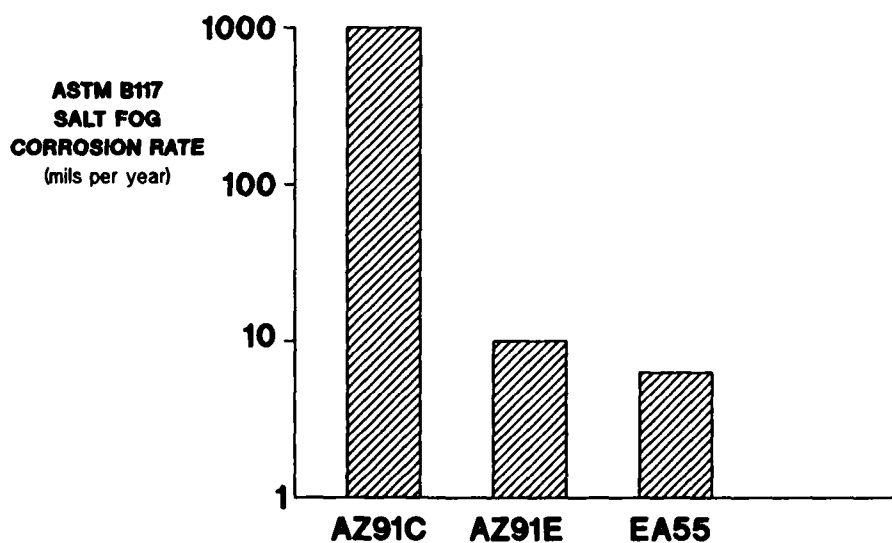


Fig.16 Corrosion rates of magnesium alloys AZ91C and AZ91E, and RS alloy EA55 (from MEL data)

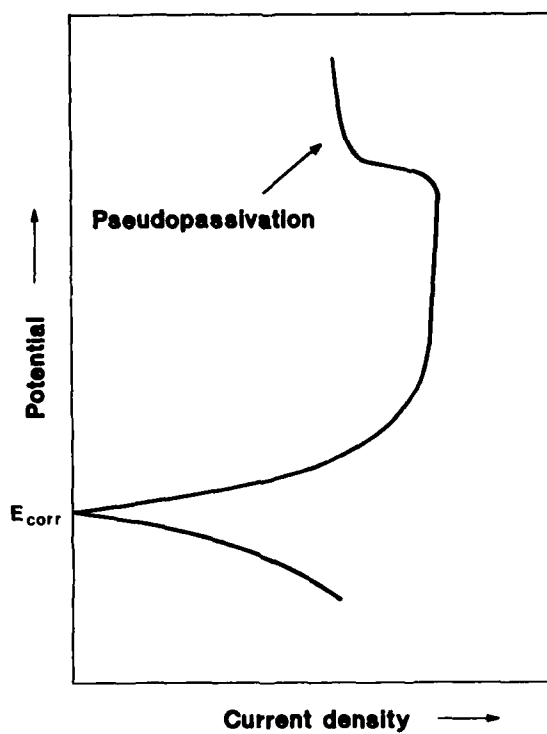


Fig.17 Simplified potentiodynamic polarisation curve showing pseudo-passivation effect in RS magnesium-rare earth alloys  
(from Krishnamurthy et al<sup>61</sup>)

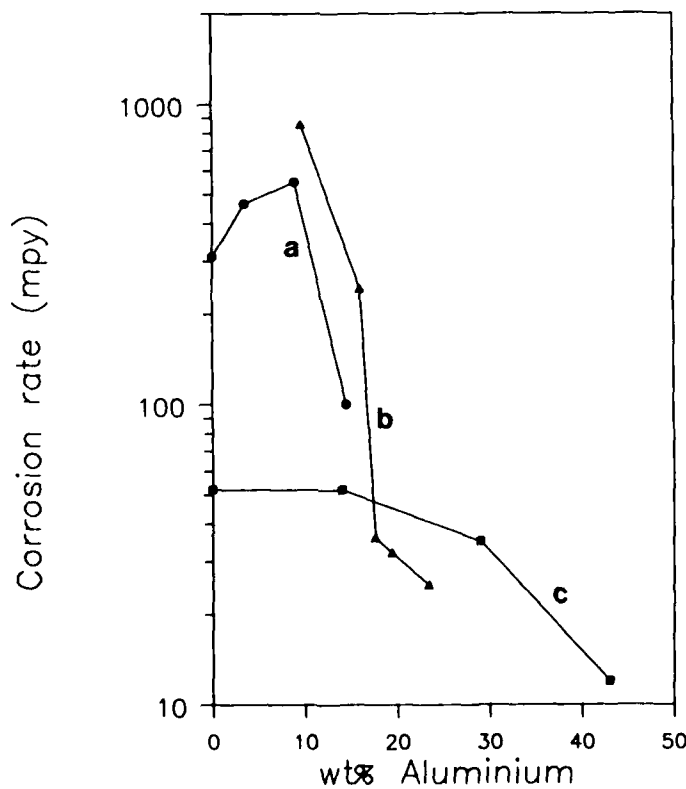
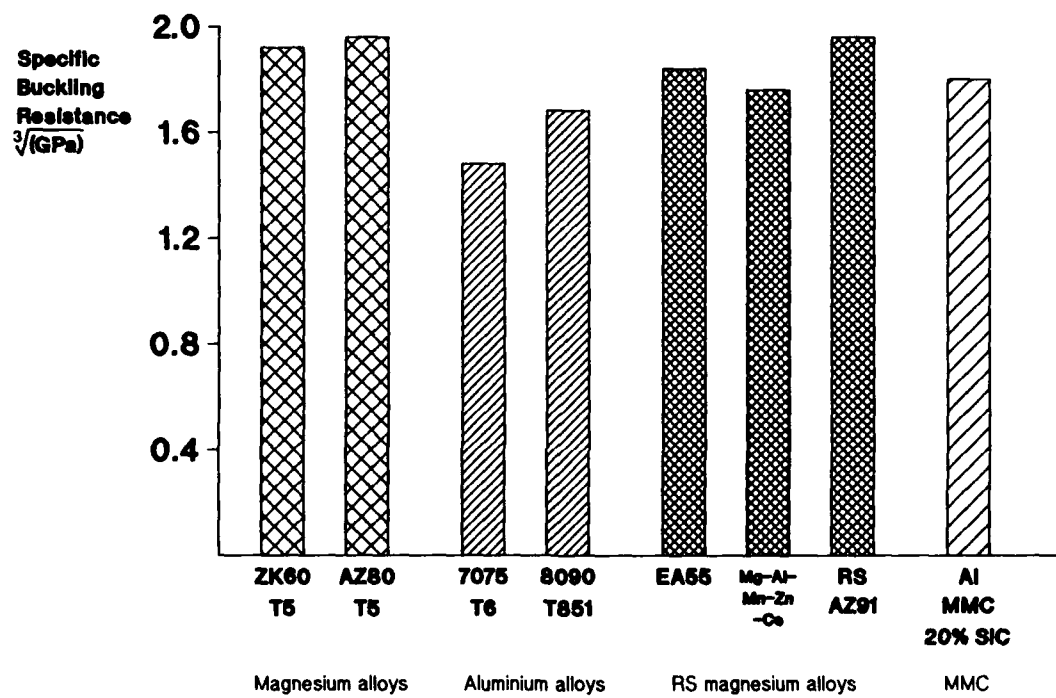


Fig.18 Effect of aluminium content on corrosion rates of RS Mg-Al alloys:  
(a) from Ahmed et al<sup>69</sup>; (b) from Hehmann et al<sup>70</sup>; (c) from Joshi et al<sup>56,67</sup>



**Fig.23** Specific buckling resistances of conventional magnesium and aluminium alloys, RS magnesium alloys and an aluminium based MMC (sources - as Fig.21)

REPORT DOCUMENTATION PAGE				
<b>1. Recipient's Reference</b>	<b>2. Originator's Reference</b>	<b>3. Further Reference</b>	<b>4. Security Classification of Document</b>	
	AGARD-LS-174	ISBN 92-835-0588-3	UNCLASSIFIED	
<b>5. Originator</b>	Advisory Group for Aerospace Research and Development North Atlantic Treaty Organization 7 rue Ancelle, 92200 Neuilly sur Seine, France			
<b>6. Title</b>	NEW LIGHT ALLOYS			
<b>7. Presented at</b>				
<b>8. Author(s)/Editor(s)</b> Various			<b>9. Date</b>	September 1990
<b>10. Author's/Editor's Address</b> Various			<b>11. Pages</b>	248
<b>12. Distribution Statement</b>	This document is distributed in accordance with AGARD policies and regulations, which are outlined on the Outside Back Covers of all AGARD publications.			
<b>13. Keywords/Descriptors</b>	<ul style="list-style-type: none"> <li>↳ Aluminium alloys ,</li> <li>Magnesium alloys ,</li> <li>Light alloys ,</li> <li>Aircraft panels ,</li> <li>Aerospace engineering ,</li> <li>Mechanical properties ,</li> <li>France (JS) ↳</li> </ul>			
<b>14. Abstract</b>	<p>The Lecture Series will review developments in research, manufacture and exploitation of new light alloys (based on Aluminium and Magnesium) for structural applications in aeronautics and space.</p> <p>These new alloys exhibit significant potential for reducing structural weight and are gaining recognition as competitive materials within the aerospace industries.</p> <p>Topics to be addressed in the lectures include: metal physics and processing aspects, properties of existing materials and prospects for future development and exploitation.</p> <p>This Lecture Series, sponsored by the Structures and Materials Panel of AGARD, has been implemented by the Consultant and Exchange Programme.</p>			

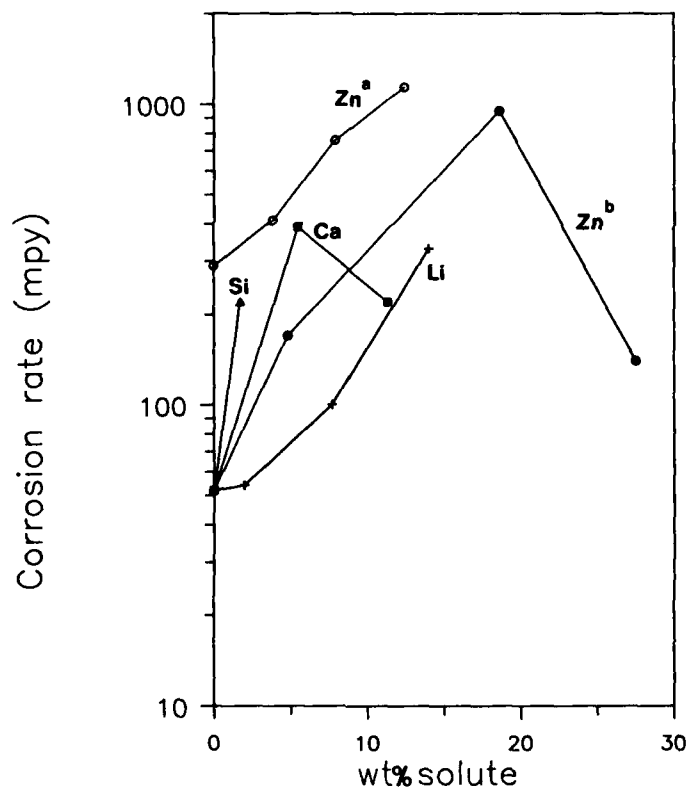


Fig.19 Effect of zinc content on corrosion rates of RS Mg-Zn alloys ((a) from Ahmed et al<sup>69</sup>; (b) from Joshi et al<sup>56,67</sup>) and effect of silicon, calcium and Lithium content on corrosion rates of RS Mg-Si, Mg-Ca and Mg-Li alloys (from Joshi et al<sup>56,67</sup>)

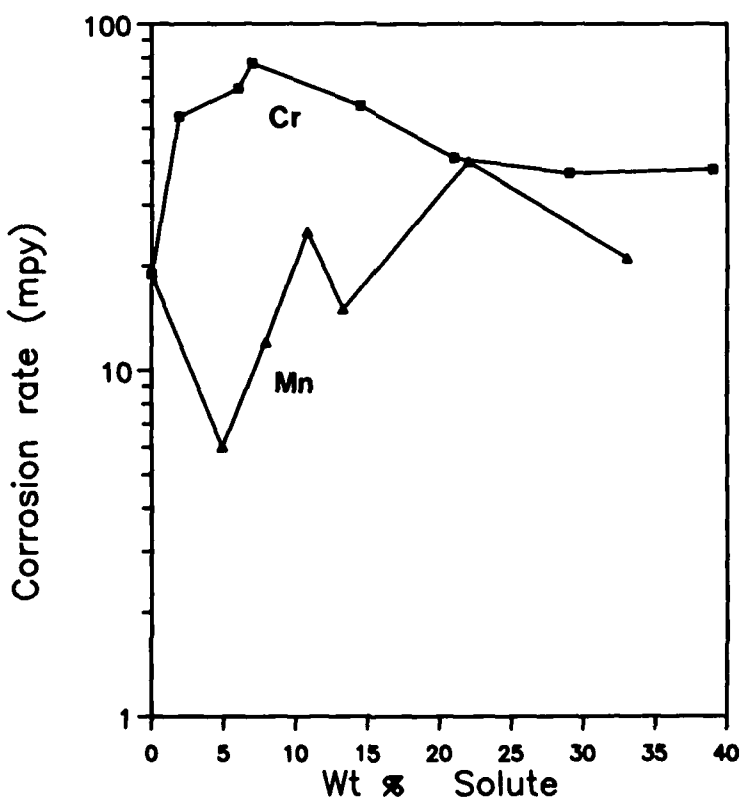


Fig.20 Effect of chromium and manganese content on corrosion rates of vapour deposited Mg-Cr and Mg-Mn alloys

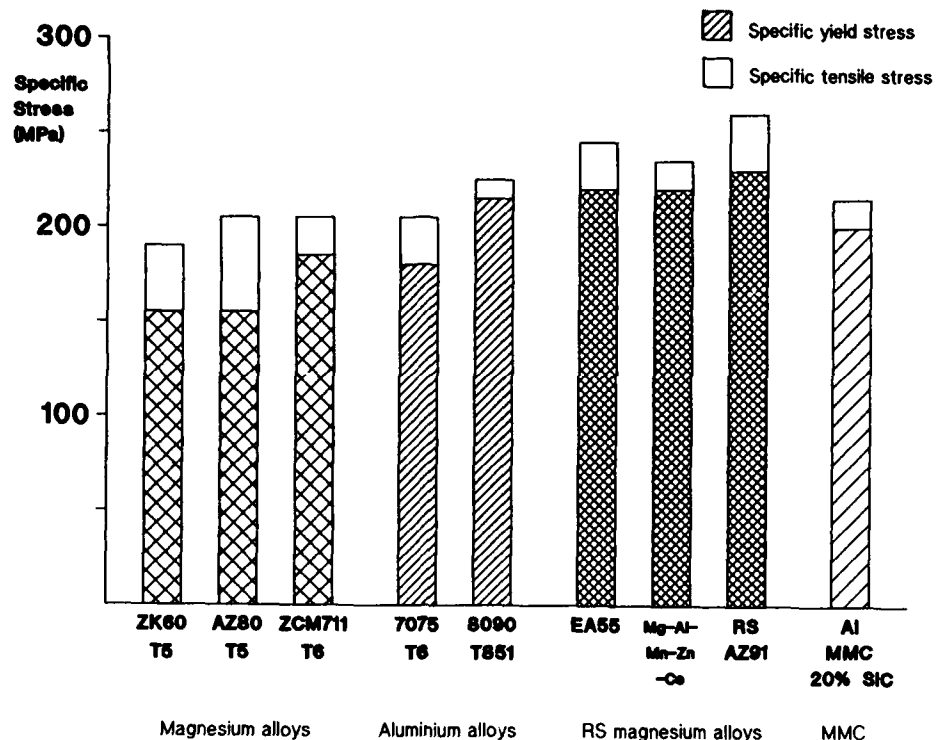


Fig.21 Specific strengths of conventional magnesium and aluminium alloys, RS magnesium alloys and an aluminium based MMC (typical properties of extrusions). (EA55 - from Froes et al<sup>54</sup>; Mg-Al-Mn-Zn-Ce - from Joshi et al<sup>42</sup>; RS AZ91 - from Nussbaum et al<sup>43</sup>; Al MMC - from Peel<sup>82</sup>).

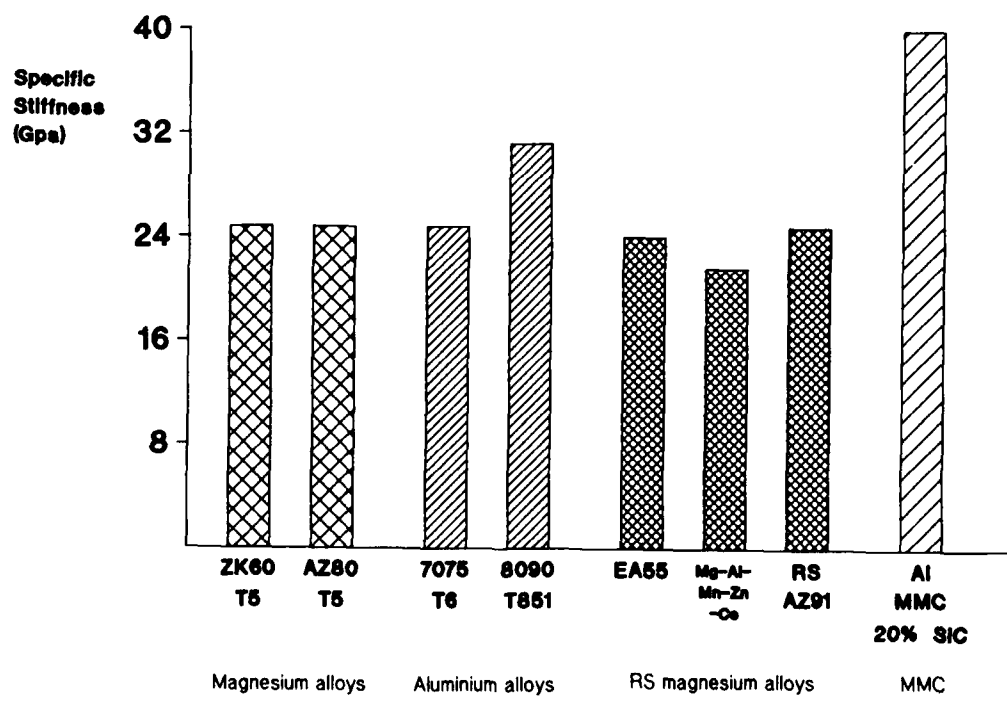


Fig.22 Specific stiffnesses of conventional magnesium and aluminium alloys, RS magnesium alloys and an aluminium based MMC (sources - as Fig.21)

AGARD Lecture Series No.174 Advisory Group for Aerospace Research and Development, NATO <b>NEW LIGHT ALLOYS</b> Published September 1990 248 pages	AGARD-LS-174 Aluminium alloys Magnesium alloys Light alloys Aircraft panels Aerospace engineering Mechanical properties	AGARD Lecture Series No.174 Advisory Group for Aerospace Research and Development, NATO <b>NEW LIGHT ALLOYS</b> Published September 1990 248 pages	The Lecture Series will review developments in research, manufacture and exploitation of new light alloys (based on Aluminium and Magnesium) for structural applications in aeronautics and space.  These new alloys exhibit significant potential for reducing structural weight and are gaining recognition as competitive materials within the aerospace industries.	P.T.O.	AGARD-LS-174 Aluminium alloys Magnesium alloys Light alloys Aircraft panels Aerospace engineering Mechanical properties
AGARD Lecture Series No.174 Advisory Group for Aerospace Research and Development, NATO <b>NEW LIGHT ALLOYS</b> Published September 1990 248 pages	AGARD-LS-174 Aluminium alloys Magnesium alloys Light alloys Aircraft panels Aerospace engineering Mechanical properties	AGARD Lecture Series No.174 Advisory Group for Aerospace Research and Development, NATO <b>NEW LIGHT ALLOYS</b> Published September 1990 248 pages	The Lecture Series will review developments in research, manufacture and exploitation of new light alloys (based on Aluminium and Magnesium) for structural applications in aeronautics and space.  These new alloys exhibit significant potential for reducing structural weight and are gaining recognition as competitive materials within the aerospace industries.	P.T.O.	AGARD-LS-174 Aluminium alloys Magnesium alloys Light alloys Aircraft panels Aerospace engineering Mechanical properties

<p>Topics to be addressed in the lectures include: metal physics and processing aspects, properties of existing materials and prospects for future development and exploitation.</p> <p>This Lecture Series, sponsored by the Structures and Materials Panel of AGARD, has been implemented by the Consultant and Exchange Programme.</p>	<p>Topics to be addressed in the lectures include: metal physics and processing aspects, properties of existing materials and prospects for future development and exploitation.</p> <p>This Lecture Series, sponsored by the Structures and Materials Panel of AGARD, has been implemented by the Consultant and Exchange Programme.</p>
<p>ISBN 92-835-0588-3</p>	<p>ISBN 92-835-0588-3</p>